

Dynamical coupled-channel models for hadron dynamics

Michael Döring^{a,b,*}, Johann Haidenbauer^c, Maxim Mai^{d,a,e}, Toru Sato^f

^a*Department of Physics, The George Washington University, 725 21st St, NW, Washington, 20052, District of Columbia, USA*
^b*Theory Center Thomas Jefferson National Accelerator Facility Newport News VA 23606 USA*

^c*Institute for Advanced Simulation (IAS-4), Forschungszentrum Jülich GmbH, Jülich, 52428, NRW, Germany*
^d*Albert Einstein Center for Fundamental Physics, Institute for Theoretical Physics, University of Bern, Sidlerstrasse 5, Bern, 3012, Switzerland*

^e*Helmholtz-Institut für Strahlen- und Kernphysik (Theorie) and Bethe Center for Theoretical Physics, Universität Bonn, Bonn, 53115, Germany*

^f*Research Center for Nuclear Physics (RCNP), Osaka University, 10-1 Mihogaoka, Ibaraki, 567-0047, Osaka, Japan*

Abstract

Dynamical coupled-channel (DCC) approaches parametrize the interactions and dynamics of two and more hadrons and their response to different electroweak probes. The inclusion of unitarity, three-body channels, and other properties from scattering theory allows for a reliable extraction of resonance spectra and their properties from data. We review the formalism and application of the ANL-Osaka, the Juelich-Bonn-Washington, and other DCC approaches in the context of light baryon resonances from meson, (virtual) photon, and neutrino-induced reactions, as well as production reactions, strange baryons, light mesons, heavy meson systems, exotics, and baryon-baryon interactions. Finally, we also provide a connection of the formalism to study finite-volume spectra obtained in Lattice QCD, and review applications involving modern statistical and machine learning tools.

Preprint: JLAB-THY-25-4298

Keywords: Dynamical coupled-channel approaches, Baryon spectroscopy, Meson spectroscopy, Amplitude analysis, S-matrix theory, Photoproduction reactions, Baryon-baryon interactions

Contents

1	Introduction	2
1.1	What are Dynamical Coupled-Channel approaches?	2
1.2	Brief overview of DCC approaches for the light baryon sector	4
2	Formalism of dynamical coupled-channel approaches	5
2.1	Scattering equation	5
2.2	ANL-Osaka model	6
2.2.1	Effective Hamiltonian and the method of unitary transformation	6
2.2.2	Model Hamiltonian	7
2.2.3	Scattering equation	8
2.3	Meson-baryon interactions in the JBW approach and its SU(3) structure	11
2.4	From interactions to scattering in the JBW approach	11
2.5	Partial-wave projection	13
2.6	Channels and transitions	14
2.6.1	The <i>u</i> -channel transitions and phenomenological contact terms	15
2.6.2	The <i>t</i> -channel transitions and correlated two-pion exchange	16
2.6.3	The <i>s</i> -channel transitions, two-potential formalism, and renormalization	16
2.7	Three-body unitarity and its implementation for the σN , ρN and $\pi\Delta$ channels	18
2.7.1	The S-matrix and its unitarity	18
2.7.2	Three-body channels in the ANL-Osaka and JBW models	21
2.8	Solving the scattering equation	21
2.8.1	Continuation to real momenta and triangle singularities	23

*Corresponding author

Email addresses: doring@gwu.edu (Michael Döring), j.haidenbauer@fz-juelich.de (Johann Haidenbauer), maxim.mai@faculty.unibe.ch (Maxim Mai), tsato@rcnp.osaka-u.ac.jp (Toru Sato)

2.8.2	Production reactions and “direct inversion”	24
2.9	Analytic continuation to complex energies	25
2.9.1	Analytic structure of the multi-channel scattering amplitude	26
2.9.2	Continuation for two-body channels	29
2.9.3	Continuation for three-body channels	30
2.10	Related approaches and aspects	32
2.10.1	The Bethe-Salpeter equation in coupled channels	32
2.10.2	Statistical aspects and machine learning tools	33
2.11	Finite-volume extensions	35
2.11.1	Two-body quantization condition and Lüscher formula	35
2.11.2	DCC approaches for two-body systems in finite volume	36
2.11.3	Connection of DCC approaches to three-body finite-volume systems	38
3	Light and strange baryons	39
3.1	Background	39
3.2	Meson-induced reactions	41
3.3	Photoproduction reactions	44
3.3.1	Overview of different analysis frameworks	44
3.3.2	Photoproduction in the JBW approach	46
3.3.3	The weak Λ decay parameter α_- from CLAS data	48
3.3.4	Photoproduction in the ANL-Osaka approach	48
3.3.5	Summary of the light baryon spectrum	49
3.3.6	Highlight: The S_{11} partial wave	50
3.3.7	Highlight: The P_{11} partial wave	52
3.4	Electroproduction reactions	54
3.5	Applications in neutrino physics	57
3.6	DCC approaches for strangeness systems	60
4	Three-meson systems: the ANL-Osaka and IVU models	62
4.1	A two-channel model for the $a_1(1260)$ meson	63
4.2	A unitary amplitude with pions and kaons	64
4.3	Triangle singularities as channel transitions in DCC approaches	67
5	Coupled-channel baryon-baryon systems	68
5.1	Baryon-baryon interaction in chiral effective field theory	69
5.2	Baryon-baryon interaction in the meson-exchange picture	70
5.3	The ΛN - ΣN system	71
5.4	Coupled channels with strangeness $S = -2$	75
5.4.1	The H -dibaryon	75
5.4.2	ΞN scattering	76
5.5	Other coupled baryon-baryon systems	77
6	Heavy sector	78
6.1	The DN interaction and the charm counterpart of the $\Lambda(1405)$	78
6.2	XYZ and pentaquark states	81
6.2.1	Hidden-charm pentaquarks	82
6.2.2	Hidden-charm pentaquarks with strangeness	84
6.2.3	Other heavy systems	86
7	Summary and outlook	87

1. Introduction

1.1. What are Dynamical Coupled-Channel approaches?

Scattering processes, including production reactions in which final states re-scatter, represent one of the few avenues to experimentally access the properties of the sub-atomic world. Together with the study of decay processes they allow to study strong interactions, or the response of strongly interacting systems to electroweak probes. Often, the desired output extracted from scattering consists in partial-wave projected amplitudes and the hadronic resonance spectrum contained therein, that allow for comparison with theory and models. This includes quark models, unitarized chiral approaches,

Dyson-Schwinger, and other functional methods. Some theory approaches, including modern Lattice QCD-based hadron spectroscopy efforts (for reviews see [1–6]), allow in some cases to directly compare to amplitudes, while other models might only predict the spectrum of hadronic resonances, but not their widths or branching ratios.

Amplitude analyses aim to reconstruct scattering and production amplitudes, resonances, and their properties from experimental data to allow for such comparisons. S-matrix principles, unitarity and analyticity, help constrain this endeavor, which often requires the parametrization of the amplitude in kinematic variables like energy, sub-energies, and scattering angles. Dynamical coupled-channel (DCC) approaches are a class of amplitude parametrizations formulated in terms of mesons and baryons as degrees of freedom that are stable under strong interactions (see Sect. 2 for the formalism). The “coupled-channel” aspect refers to the fact that strongly interacting systems can transform back and forth to different states as allowed by conserved quantum numbers. Conversely, the coupled-channel framework enables one to synthesize independent sources of information of a strongly interacting system manifested in its different decay channels and excitation mechanisms.

The “dynamical” part of DCC approaches is less well defined. Historically it is attributed to the explicit meson and baryon exchanges in the included interactions in all three Mandelstam variables s , t , and u , or other kinematic variables for reactions involving more than two-body systems. This is to be seen in contrast to modern approaches guided by the idea of scale separation [7] in which, at a given order, some particle exchange processes could be explicitly included while others are simply absorbed into contact terms. Although the explicit modeling of strong interactions through exchange processes undoubtedly forms an aspect of DCC approaches, the use of contact terms is common practice, as well. Explicit particle exchange is also a necessity in terms of unitarity once three-body channels are considered as discussed in Sect. 2.7.1. In that sense, the dynamical exchange of mesons and baryons is less a model ingredient and more a requirement of S-matrix properties.

A technical aspect of “dynamical” concerns the relativistic scattering equation of DCC approaches that always involves at least one explicit momentum integration, rendering it a genuine integral equation. For two-body systems one can restrict the driving interaction to on-shell kinematics, simplifying the integral equation to an algebraic “K-matrix”(-like) expression. After all, only on-shell quantities are accessible experimentally and off-shell extensions are ambiguous, as discussed in Sect. 2.10. However, for three-body channels the integration over a “spectator” momentum is always required even if the two-body sub-channels can still be expressed in terms of the on-shell amplitudes, see Sects. 2 and 2.7.1 for a discussion. In that case one is stuck with an integral equation.

Indeed, many DCC approaches were formulated for systems including three-body states because the DCC parametrization allows to relatively easily incorporate coupled-channel two- and three-body unitarity, at least in principle. The prime example is the pion-nucleon (πN) sector with the ubiquitous $\pi\pi N$ channel into which all excited baryon resonances except for the $\Delta(1232)$ decay¹. The three-body aspect of DCC approaches is discussed in depth in Sects. 2.7.1 and 4.

Sometimes, the only aspect kept from DCC approaches for three-body physics is the unitarity structure and the pertinent particle exchange processes, while the two-body sub-amplitudes, referred to as “isobars”, can be provided in any parametrization respecting two-body unitarity. In such cases, no attempts are made to understand interactions in terms of microscopic exchange processes (except for processes required by unitarity). Instead, DCC approaches serve for a relatively clean amplitude parametrization to analyze large data sets for the purpose of determining the spectrum of excited states and their properties.

Indeed, since DCC approaches have a substantial theoretical underpinning, they are often used to analyze meson-baryon scattering (Sect. 3.2), real-photon induced reactions (Sect. 3.3), virtual-photon induced reactions (Sect. 3.4), neutrino-induced reactions (Sect. 3.5), multi-meson production reactions (Sect. 4), and lattice QCD data (Sect. 2.11). There are also baryon-baryon systems where coupled-channel aspects play an important role, for example for the ΛN - ΣN interaction (Sect. 5). And coupled-channel dynamics is one of the starting points for interpreting and explaining the various structures observed in the heavy sector, i.e., in systems that involve charmed and bottom hadrons, the XYZ states and pentaquarks (Sect. 6).

While DCC approaches are extensively applied for data analysis and respect S-matrix principles, their origin lies in the field-theoretical description of particle interactions. In their original formulation, an effective Lagrangian using meson and baryon degrees of freedom is expanded to provide the vertices for exchange processes that are then re-summed. We start this discussion in Sect. 2.2 that is focused on the ANL-Osaka formulation and subsequently compare it to the Juelich model formulation in Sect. 2.3. These two approaches are highlighted throughout this review, but there are many more approaches pursued in the last decades as summarized in Sect. 1.2.

Finally, we note that despite the advantages mentioned above DCC approaches require substantial formal and computational resources to unite aspects of field theory with a plethora of coupled channels and different excitations of the strongly interacting system by hadrons and/or electroweakly interacting particles. Such models are then used to analyze tens of thousands of data of different final states. Therefore, DCC approaches tend to be refined over many years meaning that there is also a historical aspect to this class of approaches discussed in the next subsection. Statistical aspects are discussed in Sect. 2.10.2 and extensions to finite-volume physics relevant for lattice QCD in Sect. 2.11.

¹The PDG notation includes the spin-parity assignment J^P in resonance names that we often omit for better readability.

As for notation, the total energy of the produced baryon-meson, meson-meson, or baryon-baryon systems is traditionally named differently. Throughout this review, we use

$$E = \sqrt{s} = W = z \quad (1.1)$$

except for Sect. 2.9.1 where z stands for an uniformization variable. The notation E refers to the energy in the context of quantum mechanics, \sqrt{s} is the Mandelstam invariant, W is traditionally used in baryon spectroscopy for the center-of-mass (c.m.) energy, and z is sometimes used when the range of the energy is extended to complex values.

1.2. Brief overview of DCC approaches for the light baryon sector

The concept of coupled channels has a rich history and broad scope of applications [8, 9]. While the term “dynamical coupled channel approaches” was coined in Refs. [10, 11], earliest examples for DCC approaches in the literature are studies of the $\bar{K}N$ interaction [12–16]. In those works the coupling to the $\pi\Sigma$ and (in some cases) also to $\pi\Lambda$ channels were included. Note, however, that initially separable potentials were used. Only in later works [15, 16] the dynamics is based on the meson-exchange picture. In Ref. [15] separable potentials as well as meson exchange are considered.

Regarding the πN system an early example for a study in the spirit of the DCC approach is an off-shell isobar model from 1985 that includes the coupling to ηN and to effective two-body channels representing $\pi\pi N$ [17]. See also the dynamical model including pion photoproduction of Ref. [18]. The Dubna-Mainz-Taipei (DMT) model also builds on a long history [19–21]. It was extended to include the ηN channel besides the πN channel, plus imaginary parts for resonance propagators modeling decay into other channels [22]. The analysis was extended up to F -waves and a center-of-mass (c.m.) energy of $\sqrt{s} \approx 2$ GeV. The DMT partial waves were analytically continued to complex scattering energies to extract resonance poles and residues [23]. In the same paper, this direct determination of resonance singularities was compared to approximate methods relying on information on the real-energy axis, like speed plots [24] and the regularization method [25].

While the relativistic πN model of Gross and Surya is restricted to the elastic πN channel [26], its treatment of unitarized dynamics retaining the Dirac structure of the amplitude allows for the gauge invariant coupling of the photon [27]. One of the surprising findings of Ref. [26] is that setting the pion on its mass shell and iterating the nucleon exchange once produces a good approximation of the box and crossed box Feynman diagrams. This is taken as motivation for the three-dimensional reduction of the four-dimensional Bethe-Salpeter equation (BSE) using a prescription of Pearce and Jennings [28]. In the latter work, different reduction schemes are compared. See also Ref. [21] for a systematic investigation of different reduction schemes. Similarly, the covariant πN model of Pascalutsa and Tjon [29] is based on the solution of a dimensionally reduced (quasipotential) Bethe-Salpeter equation, later expanded to electroproduction reactions [30]. A more thorough discussion on the different schemes for the three-dimensional reduction of the BSE, leading to scattering equations like the ones by Blankenbecler-Sugar [31], Kadyshhevsky [32], or Thomson [33] that are commonly used in studies of meson-baryon and/or baryon-baryon interactions, can be found in Refs. [34–36].

Solving the full, four-dimensional BSE is necessary to avoid dependence on reduction schemes or when including the πN amplitude in a bigger setting of, e.g., photoproduction amplitude while maintaining unitarity and gauge invariance at the same time [37–43] although gauge invariance can be reconstructed [44]. So far, such four-dimensional BSE have been solved analytically when using only contact terms [38, 39] or with non-local terms using Wick rotation [45]. In both approaches, the complexity of overlapping singularities due to u -channel baryon exchange has been circumvented for the price of giving up exact three-body dynamics. In Sect. 2.7.1 we discuss one reduction scheme of the BSE in more detail for illustration.

Starting point of the Juelich-Bonn coupled-channel meson-baryon interaction is the simple πN potential by Schütz et al. [46, 47] where, as the main new aspect, the phenomenological σ - and ρ -exchanges were eliminated and the corresponding contributions in the scalar-isoscalar (0^+) and vector-isovector (1^-) channels were fixed from a microscopic evaluation of correlated 2π -exchange. It was derived within relativistic time-ordered perturbation theory (TOPT), in close analogy to the famous Bonn potential for nucleon-nucleon (NN) scattering [48]. The range of validity was up to $p_{\text{lab}} \approx 500$ MeV/c ($\sqrt{s} \approx 1.35$ GeV). In the next step [49] the ηN channel and effective $\pi\pi N$ channels (in the form of σN and $\pi\Delta$) were added and the dynamical origin of the $N(1535)$ and $N(1440)$ resonances were investigated. Specifically, it was argued that there are strong hints that the $N^*(1535)$ is a genuine resonance in the sense of the quark model while the $N(1440)$ is very likely dynamically generated. The energy range was still limited, reaching up to $\sqrt{s} \approx 1.4$ GeV in general and up to $\sqrt{s} \approx 1.6$ GeV for specific partial waves like S_{11} and the P_{11} , in the common notation L_{2I2J} with orbital angular momentum L (S, P, D, \dots), isospin I and total angular momentum J .

In the work of Krehl et al. [50, 51] some theoretical refinements were implemented and the dynamics of the $N^*(1440)$ (Roper resonance) was examined thoroughly. In that model, besides two physical channels ($\pi N, \eta N$), now three effective channels were included ($\sigma N, \rho N, \pi\Delta$) in order to represent the physics of the $\pi\pi N$ channels. Finally, in Ref. [52] further improvements in the treatment of the dynamics were made. Specifically, a consistent description of the πN phase shift in the S_{11} partial wave and of the $\pi N \rightarrow \eta N$ transition cross section near the threshold was achieved. Later milestones in the development of the Juelich-Bonn model included the extension to channels with strangeness [53], photoproduction [54–57],

and inclusion of the ωN channel [58]. The extension to electroproduction reactions [59–61] is referred to as Juelich-Bonn-Washington model (JBW). In this review, we often refer to all different sub-approaches as “JBW” for simplicity. Related formalisms were used to explore the nature of states with hidden charm [62–64].

The ANL-Osaka DCC model shares some but also differs in some construction principles from the JBW model. In the ANL-Osaka model, a Hermitian effective Hamiltonian that is independent of the scattering energy is constructed from a field theoretical model Lagrangian. Because of the energy-independent Hamiltonian, unitarity of the scattering amplitude is almost trivially satisfied within the Fock space in which one works.

The method to obtain the Hermitian Hamiltonian was first developed for nuclear potentials by Fukuda et al. [65], Okubo [66] and Nishijima [67, 68] (FST-Okubo-Nishijima). In this method, the Fock space is truncated to only nucleons by eliminating the meson degrees of freedom. This allows one not only to determine the Hamiltonian but also the electroweak currents of the system. A consistent application of the model for all generators and currents produces approximate Lorentz invariance of the form factors and currents conservation [69, 70]. This transformation method can be understood as a systematic way of a three-dimensional reduction of the Bethe-Salpeter amplitude [71] similar to the Folded Diagram Method [72]. However, the straightforward application of the FST-Okubo-Nishijima method gives singular non-static two-boson exchange potential in momentum space. In the ANL-Osaka model, a modified FST-Okubo-Nishijima method, the “unitary transformation method” [73, 74], is utilized to construct a Hermitian Hamiltonian which describes the system below and above the meson production threshold.

The first application of the method was the analysis of single pion photoproduction and electroproduction around the Δ resonance region [10, 75]. In addition to the magnetic transition form factor, electric and Coulomb quadrupole form factors of $N\Delta$ transition were predicted within the dynamical model. The cross sections were found to agree well with the experimental data. The accumulated precise $p(e, e'\pi)N$ data was then re-analyzed and $N\Delta$ transition form factors were revised [76]. The coupled channel dynamics was studied extending the approach for the $KY \oplus \pi N$ DCC model of the $\gamma p \rightarrow KY$ reaction [77].

To investigate the meson production reactions beyond the $\Delta(1232)$ energy region, the effective Hamiltonian and scattering equations for the two-body states $\pi N, \eta N, \pi\Delta, \sigma N, \rho N$ and the three-body state $\pi\pi N$ were formulated in Ref. [11]. The DCC model for πN scattering up to $\sqrt{s} < 2$ GeV including S -, P -, D - and F -waves was first studied in Ref. [78] (JLMS model). Using the meson-induced reaction model, the helicity amplitudes of $\gamma N \rightarrow N^*$ were extracted from the analysis of the photoproduction (γ, π) [79] data for $\sqrt{s} < 1.65$ GeV. Then, the Q^2 dependence of helicity amplitudes for S_{11} , P_{11} and D_{13} were obtained by analyzing electroproduction $p(e, e'\pi)N$ [80] data. The validity of the model for the inelastic processes was tested by the analyses of $\pi N \rightarrow \eta N$ [81], $\pi N \rightarrow \pi\pi N$ [82] and $\gamma N \rightarrow \pi\pi N$ [83]. The results indicated a reasonable description of those processes, but suggested a need for the improvement in the higher energy region. Meanwhile, the analytic structure of the scattering amplitude, the way to access the unphysical Riemann sheets, and the characterization of resonances through their pole positions and residues within the DCC model were studied in Refs. [84, 85], while poles of the P_{11} resonances were examined in Ref. [86].

Later, the JLMS model was extended to (1) include $K\Lambda$ and $K\Sigma$ channels and to (2) perform a combined analysis of pion and photon-induced reactions on the proton [87] for $\sqrt{s} < 2$ GeV, which is the basis of the current ANL-Osaka model. The pole positions, residues of the scattering amplitudes, and electromagnetic helicity amplitudes of $\gamma p \rightarrow N^*$ were extracted in Ref. [87]. The helicity amplitude of $\gamma n \rightarrow N^*$ are provided in Ref. [88, 89] allowing one to separate the iso-scalar and iso-vector helicity amplitudes. The elementary photoproduction reactions and meson-baryon scattering amplitudes also served as input for the calculation of η photoproduction on the deuteron [90]. The DCC model was extended for the weak vector and axial vector currents for $Q^2 < 3$ $(\text{GeV}/c)^2$ [91, 92], which provides cross sections for neutrino physics. The Q^2 dependencies of the helicity amplitudes in the ANL-Osaka model were reported in Ref. [93]. The model was also extended to $\bar{K}N$ reactions for studying hyperon resonances [94, 95].

2. Formalism of dynamical coupled-channel approaches

2.1. Scattering equation

Many approaches have been developed to extract the spectrum and properties of nucleon resonances from pion, photon and electron-induced meson production reactions. Dynamical coupled channel approaches provide a particularly suitable reaction framework to analyze the pertinent data. The scattering amplitudes of the meson production reactions are obtained by solving a three-dimensional relativistic Lippmann-Schwinger equation of two- and three-particle states with the model interactions. The particles and their interactions are usually introduced via a model Lagrangian in relativistic quantum field theory. The form of the Lagrangian is constrained by the symmetries, such as Lorentz invariance, flavor and chiral symmetry, and their breaking where applicable. The two approaches discussed in the following reflect two different approaches of how to cast this framework in a practical applications. In the implementations some differences exist between them.

Approach I: The Argonne-Osaka/ANL-Osaka assumes that in the 'medium' energy region only 'few-body' degrees of freedom are active and that they must be treated explicitly instead of solving the field theory which is an intrinsic many body problem. The effects due to the many-body states are included as an effective interaction calculated perturbatively in coupling constants. The Fock-space of the model consists of "bare" resonances, two-body meson-baryon, and $\pi\pi N$ three-body states. The interactions among the particles are obtained by applying a unitary transformation perturbatively on the field theoretical Hamiltonian. A feature of the approach is that the resulting interactions do not depend on the scattering energy \sqrt{s} and the single nucleon state decouples from meson-baryon scattering state. The scattering equation of the meson-baryon systems are obtained by applying the projection operator technique.

Approach II: Juelich-Bonn-Washington/JBW approach is based on relativistic time-ordered perturbation theory (TOPT), with the effective interaction derived from the Wess-Zumino Lagrangian and from explicit Lagrangians for excited baryons states. In this approach retardation effects from the exchange diagrams are retained and as a consequence the interaction depends explicitly on the energy. The resulting pseudo-potential is iterated in a Lippman-Schwinger type scattering equation, ensuring unitarity. There is also a renormalization program for the nucleon bound state. The approach shares many properties with the ANL-Osaka approach as a comparison of the scattering equations below shows [Eq. (2.21) vs. Eq. (2.57)].

2.2. ANL-Osaka model

2.2.1. Effective Hamiltonian and the method of unitary transformation

To illustrate the unitary transformation method, we consider the simplest phenomenological Hamiltonian of N, N^* and π ,

$$H = H_0 + H_I . \quad (2.1)$$

Here, H_0 is free energy of particles. The interaction H_I describes pion production or absorption $B \leftrightarrow B' + \pi$, where (B, B') are (N, N) , (N, N^*) or (N^*, N) . In this section, both the excited baryons of isospin $I = 1/2(N^*)$ and $I = 3/2(\Delta)$ are represented by N^* while Δ represents the $\Delta(1232)3/2^+$ resonance.

The essence of the unitary transformation method is to extract an effective Hamiltonian in a "few-body" space defined by a unitary operator U , such that the resulting scattering equations can be solved in practice,

$$H' = UHU^\dagger . \quad (2.2)$$

In the approach of Ref. [73], the first step is to decompose the interaction Hamiltonian H_I into two parts,

$$H_I = H_I^P + H_I^Q , \quad (2.3)$$

where H_I^P defines the process which can take place in free space. In this model, H_I^P describes the process $N^* \rightarrow N + \pi$. H_I^Q defines the virtual process, which cannot occur in free space because of energy-momentum conservation. H_I^Q includes $N \rightarrow N + \pi$ and $N \rightarrow N^* + \pi$. The virtual processes are eliminated by choosing an appropriate unitary transformation U . This can be done systematically by using a perturbative expansion of U in powers of coupling constants. As a result the effects of "virtual processes" appear as effective interactions in the transformed Hamiltonian. Defining the first transformation $U = \exp(-iS^{(1)})$ by a Hermitian operator $S^{(1)}$ and expanding $U = 1 - iS^{(1)} + \dots$, the transformed Hamiltonian can be written as

$$H' = UHU^\dagger = H_0 + H_I^P + H_I^Q + [H_0, iS^{(1)}] + [H_I^P, iS^{(1)}] + \frac{1}{2!} [[H_0, iS^{(1)}], iS^{(1)}] + \dots . \quad (2.4)$$

The virtual processes H_I^Q which are of first-order in the coupling constant are eliminated from Eq. (2.4) by imposing

$$H_I^Q + [H_0, iS^{(1)}] = 0 . \quad (2.5)$$

Since H_0 is a diagonal operator in the Fock space, Eq. (2.5) clearly implies that $iS^{(1)}$ must have the same operator structure as H_I^Q and is first order in the coupling constant. By using Eq. (2.5), Eq. (2.4) can be written as

$$H' = H_0 + H_I^P + [H_I^P, iS^{(1)}] + \frac{1}{2} [H_I^Q, iS^{(1)}] + \text{higher order terms} . \quad (2.6)$$

In this example, the effective Hamiltonian includes decay and production of N^* (the second term H_I^P) and s- and u-channel baryon-exchange, non-resonant $\pi B - \pi B'$ potentials (the third and the fourth terms). The backward propagation of hadrons, for example, pair production, is also included in H_I^Q and therefore taken into account as part of the effective

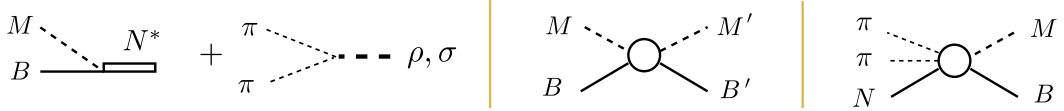


Figure 1: Basic mechanisms of the model Hamiltonian defined in Eq. (2.11).

potential. It is informative to quote the matrix element of the πN potential with s-channel nucleon exchange in this approach,

$$\langle \pi(\mathbf{p}') N(-\mathbf{p}') | V | \pi(\mathbf{p}) N(-\mathbf{p}) \rangle = \Gamma(p') \frac{1}{2} \left(\frac{1}{E_N(\mathbf{p}') + \omega_\pi(\mathbf{p}') - M_N} + \frac{1}{E_N(\mathbf{p}) + \omega_\pi(\mathbf{p}) - M_N} \right) \Gamma(p), \quad (2.7)$$

where $\Gamma(p)$ is the πNN vertex, $E_N(\mathbf{p}) = \sqrt{\mathbf{p}^2 + M_N^2}$ and $\omega_\pi(\mathbf{p}) = \sqrt{\mathbf{p}^2 + m_\pi^2}$. In TOPT, the corresponding matrix element of the driving term is given as

$$\langle \pi(\mathbf{p}') N(-\mathbf{p}') | V | \pi(\mathbf{p}) N(-\mathbf{p}) \rangle = \Gamma(p') \frac{1}{E - M_N} \Gamma(p), \quad (2.8)$$

where E is scattering energy. Eq. (2.7) and Eq. (2.8) coincide at the on-energy shell matrix element. Note that up to the same order Eq. (2.4) should have an additional term which is the one-pion-loop contribution to the single nucleon state. Such a mass renormalization term is dropped in practice, since it is part of the physical nucleon mass in the resulting effective Hamiltonian. The interaction $MB \rightarrow \pi\pi N$ is obtained by applying the next order unitary transformation $U' = \exp(iS^{(2)})$.

The effective electromagnetic current or weak current which should be used together with the Hamiltonian H' is obtained by applying the same transformation U as

$$J_{\text{eff}}^\mu = U J^\mu U^\dagger. \quad (2.9)$$

Here J^μ represents electromagnetic current J_{EM}^μ or weak charged/neutral current J_{CC}^μ/J_{NC}^μ . The effective current gives, for example, $J_{em}^\mu + N \rightarrow \pi N$ or $J_{em}^\mu + N \rightarrow N^*$ processes. They are used to describe meson photo-, electroproduction and neutrino reactions.

In summary, a feature of the method is that the effective Hamiltonian is hermitian and independent on the scattering energy \sqrt{s} . As a result, the unitarity relation of the scattering amplitude is almost trivially satisfied. Another feature which is convenient for the phenomenological description is that the effective Hamiltonian is parametrized in terms of the 'physical' nucleon. The single nucleon state is diagonalized in the effective Hamiltonian and has no coupling with the πB Fock space. Analytic properties of the reaction amplitudes based on the ANL-Osaka model and the relation to the three-dimensional reduction of the BSE and TOPT are discussed in Refs. [74, 96].

2.2.2. Model Hamiltonian

Towards a realistic model, the starting point is a set of Lagrangians describing the interactions between mesons ($M = \pi, \eta, \rho, \omega, \sigma, K$) and baryons ($B = N, \Lambda, \Sigma, \Delta, N^*$). We start from the Hamiltonian density \mathcal{H} of the meson-baryon system, which is derived by the standard quantization procedure from the model Lagrangian density \mathcal{L} ,

$$\mathcal{H} = \sum_j \dot{\Phi}_j \Pi_j - \mathcal{L}, \quad (2.10)$$

where Π_j is the conjugate momentum of Φ_j given by $\Pi_j = \frac{\delta \mathcal{L}}{\delta \dot{\Phi}_j}$, and we set equal time commutation relation between the field and its conjugate momentum.

By applying the unitary transformation method briefly explained in the previous section, we obtain the effective Hamiltonian for the 'bare' excited baryon states $P_1 = N^*$, the meson-baryon states $P_2 = \pi N, \eta N, \pi \Delta, \rho N, \sigma N, K \Lambda, K \Sigma$ and the $Q = \pi \pi N$ state. The Fock space of the model Hamiltonian consists of $P + Q$ with $P = P_1 + P_2$.

The effective Hamiltonian of the model derived from the starting Lagrangian is given as [11, 87]

$$H_{\text{eff}} = H_0 + V. \quad (2.11)$$

H_0 is the free energy operator. For example, $\langle \alpha(\mathbf{p}) | H_0 | \alpha(\mathbf{p}) \rangle = \sqrt{m_\alpha^2 + \mathbf{p}^2} = E_\alpha(\mathbf{p})$ for particle α with mass m_α . The interaction Hamiltonian is

$$V = \Gamma_V + \sum_{M'B', MB} v_{M'B', MB} + \left(\sum_{MB} v_{\pi\pi N, MB} + (\text{h.c.}) \right). \quad (2.12)$$

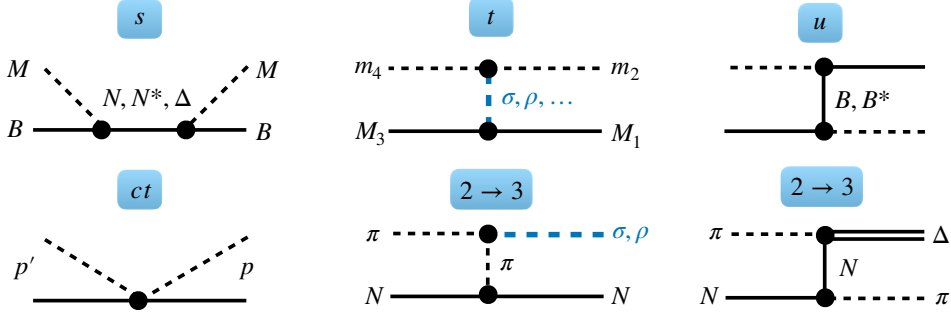


Figure 2: Meson (M) baryon (B) transitions through s -, t -, u -channel, and contact (ct) processes. Also, the $2 \rightarrow 3$ processes to populate the effective σN , ρN , and $\pi\Delta$ channels are shown. The figure also labels incoming (outgoing) c.m. momenta p (p') and baryon (meson) masses M_1 , M_3 (m_2 , m_4).

Here $h.c.$ denotes the hermitian conjugate. The interaction Γ_V connects Fock-spaces $P_1 \leftrightarrow P_2$ and $P_2 \leftrightarrow Q$ given as

$$\Gamma_V = \left(\sum_{N^*, MB} \Gamma_{N^* \rightarrow MB} + \sum_{M^*=\rho, \sigma} h_{M^* \rightarrow \pi\pi} \right) + (h.c.) . \quad (2.13)$$

The resonances associated with the *bare* excited baryon states N^* and meson states $M^* = \rho, \sigma$ are induced by the interactions $\Gamma_{N^* \rightarrow MB}$ and $\Gamma_{M^* \rightarrow \pi\pi}$. These interactions are illustrated in Fig. 1 (a). The masses $M_{N^*}^0$ and $m_{M^*}^0$ of those bare states N^* and M^* are the parameters of the model which will be determined by fitting the πN and $\pi\pi$ scattering data.

The non-resonant meson-baryon interactions $v_{MB', MB}$ and $MB \rightarrow \pi\pi N$ interaction $v_{\pi\pi N, MB}$ are illustrated in Fig. 1(b) and Fig. 1(c), respectively. All of these interactions are defined by the tree-diagrams generated from the considered Lagrangians. The mechanism of the meson-baryon interaction consist of the u - and s - channel baryon exchange, t -channel meson exchange and the contact interaction shown in Fig. 2. Here, as an example, the πN potential $v_{\pi N, \pi N}$ with s -channel nucleon exchange is given:

$$\langle \pi(\mathbf{k}', i), N(\mathbf{p}', s') | v_{\pi N, \pi N} | \pi(\mathbf{k}, j), N(\mathbf{p}, s) \rangle = \frac{1}{(2\pi)^3} \sqrt{\frac{M_N}{E_N(p')}} \sqrt{\frac{M_N}{E_N(p)}} \frac{1}{\sqrt{2\omega_\pi(k') 2\omega_\pi(k)}} \times \left(\frac{f_{\pi NN}}{m_\pi} \right)^2 \bar{u}_{s'}(p') \not{k}' \gamma_5 \tau_i \frac{1}{2} \left[\frac{1}{\not{k}' + \not{p}' + M_N} + \frac{1}{\not{k} + \not{p} + M_N} \right] \not{k} \gamma_5 \tau_j u(p)_s \quad (2.14)$$

where $k^\mu = (\omega_\pi(k), \mathbf{k})$, $p^\mu = (E_N(p), \mathbf{p})$. In Eq. (2.14), nucleon propagator is similar to the covariant propagator except time component of the momentum. The u -channel nucleon exchange potential is expressed in a similar form. The explicit expressions of all interactions in Eq. (2.12) can be found in Refs. [11, 87].

The non-resonant interaction $v_{\pi\pi N, MB}$ is calculated from Eq. (2.6). The mechanisms for $v_{\pi\pi N, \pi N}$ are shown in Fig. 3 together with the mechanisms of $v_{\pi\pi N, \gamma N}$.

2.2.3. Scattering equation

Our next task is to derive a set of dynamical coupled-channel equations for describing $\pi N, J^\mu N \rightarrow MB, \pi\pi N$ reactions within the model space $N^* \oplus MB \oplus \pi\pi N$.

The starting point is the Lippmann-Schwinger equation for the T-matrix,

$$T(E) = V + V \frac{1}{E - H_0 + i\epsilon} T(E) , \quad (2.15)$$

where $E = \sqrt{s}$ is the total energy. The interaction V is defined from the effective Hamiltonian in Eq. (2.12). The unitarity condition is given as

$$T(E) - T^\dagger(E) = -2\pi i T^\dagger(E) \delta(E - H_0) T(E) . \quad (2.16)$$

This relation is satisfied since our model interaction does not depend on the scattering energy E . V does not have discontinuities.

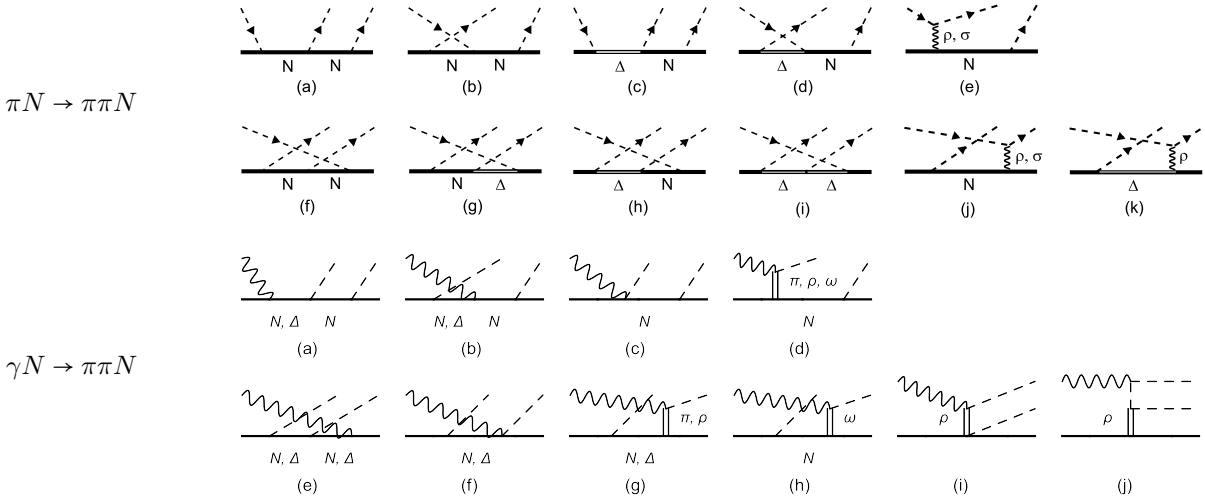


Figure 3: The mechanisms for $v_{\pi\pi N, \pi N}$ and $v_{\pi\pi N, \gamma N}$

$$Z_{M'B',MB}(E) = \Delta(1232) \xrightarrow{\text{---}} \pi + \rho, \sigma \xrightarrow{\text{---}} \pi$$

Figure 4: One-particle-exchange interactions $Z_{\pi\Delta, \pi\Delta}(E)$, $Z_{\pi\Delta, \rho N}(E)$ and $Z_{\pi\Delta, \sigma N}(E)$.

We cast Eq. (2.15) into a more convenient form for practical calculations. Applying the standard projection operator techniques [97], the coupled equations of P space (N^* and MB) and Q space ($\pi\pi N$) are given as

$$T_{PP}(E) = \bar{V}_{PP}(E) + \bar{V}_{PP}(E) \frac{P}{E - H_0 + i\epsilon} T_{PP}(E) , \quad (2.17)$$

$$T_{QP}(E) = V_{QP} \left[1 + \frac{P}{E - H_0 + i\epsilon} T_{PP}(E) \right] , \quad (2.18)$$

$$\bar{V}(E) = V_{PP} + V_{PQ} \frac{Q}{E - H_0 + i\epsilon} V_{QP} . \quad (2.19)$$

Here, for example, $T_{QP} = QTP$, and $V_{QP} = QVP$ using projection operators P and Q of the Fock-spaces P and Q. The effective interactions for N^* and MB \bar{V}_{PP} become energy dependent due to the channel coupling. The eliminated $\pi\pi N$ intermediate states generate the energy dependent particle exchange interaction $Z_{\beta,\alpha}(E)$ shown in Fig. 4 and the self-energies of unstable particles for the $\pi\Delta$, ρN and σN Green's functions. The P space in the above equation contains N^* and MB. The equation for the two-body MB T-matrix is obtained by eliminating N^* components or, equivalently, by the two-potential formula of Eq. (2.61) for the JBW approach. The full description of the coupled-channels equation is given in Appendix B of Ref. [11].

The partial wave T-matrix of $M(\mathbf{p}) + B(-\mathbf{p}) \rightarrow M'(\mathbf{p}') + B'(-\mathbf{p}')$ is given as

$$T_{\beta,\alpha}(p', p; E) = t_{\beta,\alpha}(p', p; E) + t_{\beta,\alpha}^R(p', p; E) , \quad (2.20)$$

where α, β represent the MB states $\pi N, \eta N, \rho N, \sigma N, \pi\Delta$, in addition, external current JN for α and angular momentum and isospin. The first term in Eq. (2.20) is defined by the following coupled-channels equation of non-resonant interaction (non-pole term),

$$t_{\beta,\alpha}(p', p; E) = \bar{V}_{\beta,\alpha}(p', p; E) + \int_C dq q^2 \sum_{\gamma} \bar{V}_{\beta,\gamma}(p', q; E) G_{\gamma}(q; E) t_{\gamma,\alpha}(q, p; E) , \quad (2.21)$$

where $\bar{V}_{\beta,\alpha}(p', p; E)$ is defined as

$$\bar{V}_{\beta,\alpha}(p', p; E) = v_{\beta,\alpha}(p', p) + Z_{\beta,\alpha}(p', p; E) . \quad (2.22)$$

Here, the energy dependent particle exchange interaction $Z_{\beta,\alpha}(p', p; E)$ is due to the coupling of MB states with the $\pi\pi N$ states. The integration path C , in principle ranging from $q = 0$ to ∞ , will be discussed later.

The meson-baryon Green's function for the stable particles ($\pi N, \eta N, K\Lambda, K\Sigma$) and unstable particles ($\pi\Delta, \rho N, \sigma N$)

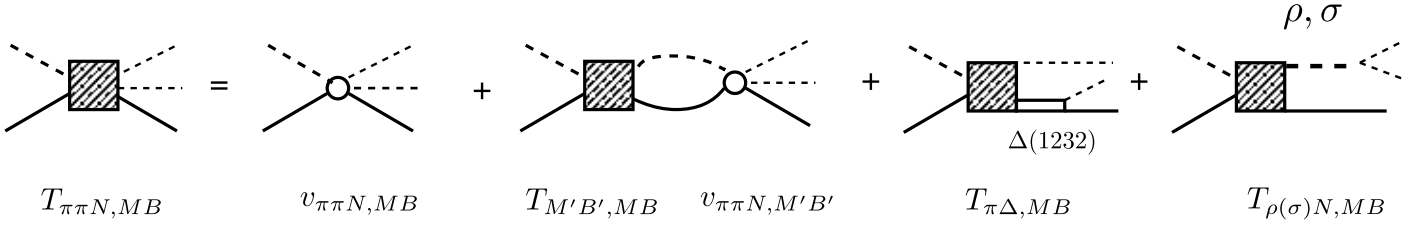


Figure 5: Graphical representations of $T_{\pi\pi N, MB}$ defined by Eq. (2.30).

is given by

$$G_{MB}(q; E) = \frac{1}{E - \omega_M(q) - E_B(q) + i\epsilon} , \quad (2.23)$$

$$G_{MB}(q; E) = \frac{1}{E - \omega_M(q) - E_B(q) - \Sigma(q; E)} , \quad (2.24)$$

respectively. For example, the self-energy for $MB = \pi\Delta$ is given as

$$\Sigma_\Delta(p; E) = \int_{C'} \frac{dq q^2 \Gamma_{\Delta, \pi N}^2(q)}{E - \omega_\pi(p) - [(\omega_\pi(q) + E_N(q))^2 + p^2]^{1/2}} . \quad (2.25)$$

The second term, the resonant T -matrix is given as

$$t_{\beta, \alpha}^R(p'; p; E) = \sum_{i,j} \bar{\Gamma}_{\beta, i}(p'; E) [G_{N^*}(E)]_{i,j} \bar{\Gamma}_{\alpha, j}(p; E), \quad (2.26)$$

with

$$[G_{N^*}^{-1}]_{i,j}(E) = (E - m_{N_i^*}) \delta_{i,j} - \Sigma_{i,j}(E) . \quad (2.27)$$

Here i, j denote the bare N^* states defined in the Hamiltonian. $m_{N_i^*}$ are their masses. In general, the bare states mix with each other through the off-diagonal matrix elements of the self-energies. The dressed vertices and the energy shifts of the second term in Eqs. (2.26)-(2.27) are defined by

$$\bar{\Gamma}_{\alpha, j}(p; E) = \Gamma_{\alpha, j}(p) + \int_C dq q^2 \sum_\gamma t_{\alpha, \gamma}(p, q; E) G_\gamma(q; E) \Gamma_{\gamma, j}(q) , \quad (2.28)$$

$$\Sigma(E)_{i,j} = \int_C dq q^2 \sum_\gamma \Gamma_{\gamma, i}(q) G_\gamma(q; E) \bar{\Gamma}_{\gamma, j}(q) , \quad (2.29)$$

where $\Gamma_{\alpha, i}(p)$ defines the coupling of the i -th bare N^* state to channel α .

The amplitudes $T_{M'B', MB} = t_{M'B', MB} + t_{M'B', MB}^R$ defined by Eq. (2.20) can be used directly to calculate the cross sections of the $\pi N \rightarrow MB$ and the $JN \rightarrow MB$ reactions. They are also the input to the calculations of the two-pion production amplitudes. The two-pion production amplitudes are illustrated in Fig. 5. They can be cast into the following form

$$T_{\pi\pi N, MB}(E) = T_{\pi\pi N, MB}^{\text{dir}}(E) + T_{\pi\pi N, MB}^{\pi\Delta}(E) + T_{\pi\pi N, MB}^{\rho N}(E) + T_{\pi\pi N, MB}^{\sigma N}(E) , \quad (2.30)$$

with

$$T_{\pi\pi N, MB}^{\text{dir}}(E) = \sum_{M'B'} v_{\pi\pi N, M'B'} [\delta_{M'B', MB} + G_{M'B'}(E) T_{M'B', MB}(E)] , \quad (2.31)$$

$$T_{\pi\pi N, MB}^{\pi\Delta}(E) = \Gamma_{\Delta \rightarrow \pi N}^\dagger G_{\pi\Delta}(E) T_{\pi\Delta, MB}(E) ,$$

$$T_{\pi\pi N, MB}^{\rho N}(E) = h_{\rho \rightarrow \pi\pi}^\dagger G_{\rho N}(E) T_{\rho N, MB}(E) ,$$

$$T_{\pi\pi N, MB}^{\sigma N}(E) = h_{\sigma \rightarrow \pi\pi}^\dagger G_{\sigma N}(E) T_{\sigma N, MB}(E) . \quad (2.32)$$

The $\pi\pi N$ state is mainly produced through the unstable $\pi\Delta$, ρN , and σN states illustrated in Fig. 5. Each term has contributions from the non-resonant amplitude $t_{M'B', MB}(E)$ and the resonant term $t_{M'B', MB}^R(E)$. The mechanism of non-resonant interactions $v_{\pi\pi N, \pi N}$ and $v_{\pi\pi N, \gamma N}$ are shown in Fig. 3.

2.3. Meson-baryon interactions in the JBW approach and its SU(3) structure

The interaction of mesons and baryons in the Juelich-Bonn (JB) approach is parametrized through the Wess-Zumino effective Lagrangian [98]. Chiral symmetry of QCD is one of the guiding principles for its construction. The interaction also contains vector mesons. While there are general guiding principles to include them [99, 100], the JB approach adopts the version of Ref. [98]. The starting point is the nucleon and the pion field in a nonlinear σ model. Vector mesons are then included by gauging the chirally invariant Lagrangian, i.e., by requiring the Lagrangian to be invariant under local transformations, leading to vector and axial gauge fields. The $\rho\pi\pi$ coupling strength is related to f_π via the KSFR relation [101]. The Wess-Zumino Lagrangian provides πNN , ρNN , $\rho\pi\pi$, and $a_1\rho\pi$ interactions; there are also contact terms that contribute. See Appendix B of Ref. [53] for a list.

The SU(3) extension of the approach is achieved by relating these interactions to other hadrons via flavor symmetry [53], based on Ref. [102]. The coupling of a given meson nonet with the octet baryon current $8_B \otimes 8_B$ yields two products, namely $8_B \otimes 8_B \otimes 1_M$ and $8_B \otimes 8_B \otimes 8_M$. The coupling to the meson octet 8_M depends on two parameters, g_1, g_2 , corresponding to the symmetric and antisymmetric representations of $8_B \otimes 8_B$. They can be re-written in terms of a coupling constant g and a mixing parameter α in the notation of Ref. [102] that is used in the JBW as well,

$$g = \frac{\sqrt{30}}{40} g_1 + \frac{\sqrt{6}}{24} g_2, \quad \alpha = \frac{\sqrt{6}}{24} \frac{g_2}{g}. \quad (2.33)$$

Here g_1 and g_2 can be also expressed in terms of the standard D and F axial couplings [103]:

$$D = \frac{\sqrt{30}}{40} g_1, \quad F = \frac{\sqrt{6}}{24} g_2, \quad (2.34)$$

leading to $\alpha = F/(D + F)$. The coupling of the baryon octets to the meson singlet 1_M involves a further independent coupling constant. For the transitions $MB \rightarrow MB$, with the $J^P = 0^-$ octet mesons M and the $J^P = 1/2^+$ octet baryons B , the JB model includes the full set of diagrams required by SU(3) symmetry. This applies to the classes of diagrams of the exchange of $J^P = 1^-$ vector mesons, $J^P = 1/2^+$ baryons, and $J^P = 3/2^+$ baryons. In particular, non-diagonal transitions such as $\eta N \rightarrow KY$ ($Y = \Lambda, \Sigma$) are considered. See Appendix B2 of Ref. [53] for further details.

The same reference also provides information on how several processes not covered by SU(3) symmetry are modeled. For example, the coupling of scalar mesons to nucleons, σNN , and among themselves, $\sigma\sigma\sigma$, is described by Lagrangians with couplings strengths fit to data. Similarly, $\pi\Delta\Delta$ and $\rho\Delta\Delta$ interaction are allowed for, with interaction strength fixed from fits to data or external information. The physical ω and ϕ states are defined by ideal mixing of ω_1 and ω_8 states.

Effective Lagrangians for higher spin nucleon and Δ excited states with $J \leq 3/2$ are listed in Appendix B of Ref. [104]. Resonance interactions with total spin $J \geq 5/2$ are not described by corresponding Lagrangians but their decay vertices are related to those of lower spin with additional powers of momentum ensuring the correct centrifugal barriers. In general, s -channel resonances are allowed to couple to the MB (pseudo-scalar octet, baryon octet) channels πN , ηN , $K\Lambda$ and $K\Sigma$ with independent coupling strength not related through SU(3) symmetry. Additionally, resonances can couple to $\pi\Delta$ and ρN states, but not to σN . The argument is that, as long as the JBW model does not analyze $\pi\pi N$ data, there is no need to populate each possible $\pi\pi N$ three-particle states. There is usually more than one independent way to combine spin and angular momentum of ρ , N or π , Δ to a given J^P (see Table 1), but the JB model uses only one resonance Lagrangian suitably projected into different $\pi\Delta$ and ρN channels, with only one coupling constant, for simplicity.

2.4. From interactions to scattering in the JBW approach

For the construction of interactions from Lagrangians, the JB group uses TOPT [105]. The resulting pseudo-potentials are combined into s -, t -, and u -channel diagrams which are summed up by solving a three-dimensional integral equation of Lippmann-Schwinger type with relativistic kinematics. Such a three-dimensional scattering equation leads to a simplified singularity structure, as compared to that of a four-dimensional treatment in the context of the Bethe-Salpeter equation (BSE) discussed in Sect. 2.7.1, although even in a three-dimensional formalism using TOPT one has “moving” singularities in exchange processes that depend on the incoming and outgoing momenta and the energy. More details are provided in Sect. 2.8.

Through the Legendre transformation (2.10) the Wess-Zumino Lagrange density [98] is converted to a Hamilton density \mathcal{H} that is decomposed as

$$\mathcal{H} = \mathcal{H}^0 - \mathcal{L}_{\text{int}} + \mathcal{H}_{\text{ct}} \quad (2.35)$$

with a non-interacting part \mathcal{H}^0 , an interacting part, and contact interactions \mathcal{H}_{ct} . The latter originate if the interaction part contains explicit time derivatives of fields, or non-dynamical zero-components of vector fields [106]. Then, the contact terms restore the on-shell equivalence between the time-ordered and the covariant formalism. In practical terms, it is

straightforward to construct the contact terms at the diagrammatic level as the difference of the covariant Feynman expression and both time orderings,

$$V_{\text{ct}} = V_{\text{Feyn}} - V_{\text{TOPT}}^{\text{1st TO}} - V_{\text{TOPT}}^{\text{2nd TO}} . \quad (2.36)$$

The Hamiltonian is obtained by integrating \mathcal{H} over the spatial coordinates and can, again, be written in terms of a free and an interacting part, $H = H_0 + H_I$. In terms of the Hamiltonian, the scattering operator reads

$$S = \lim_{\substack{t \rightarrow \infty \\ t_0 \rightarrow -\infty}} \hat{U}(t, t_0) , \quad (2.37)$$

where $\hat{U}(t, t_0) = e^{iH_0 t} e^{-iH(t-t_0)} e^{-iH_0 t_0}$ is the evolution operator in the interaction picture. The (onshell) T-matrix has the quantum mechanical normalization

$$S_{fi} =: \delta_{fi} - i(2\pi)\delta(E_f - E_i)\mathcal{T}_{fi} , \quad (2.38)$$

where $i(f)$ denote initial (final state) and E_i, E_f are the respective energies. The on-energy shell T-matrix operator can be written as

$$\mathcal{T} = H_I + H_I \frac{1}{E - H + i\epsilon} H_I = H_I + H_I \frac{1}{E - H_0 - H_I + i\epsilon} H_I . \quad (2.39)$$

One can expand \mathcal{T} in a power series in H_I ,

$$\mathcal{T} = H_I \frac{1}{1 - \mathcal{G}H_I} = H_I + H_I \mathcal{G}H_I + \dots \quad (2.40)$$

with the Green's function of the free particle states,

$$\mathcal{G} = \frac{1}{E - H_0 + i\epsilon} = \oint_n \frac{|n\rangle \langle n|}{E - E_n + i\epsilon} . \quad (2.41)$$

The sum/integral over the right-hand side formally extends over all multi-particle states allowed, and n is a composite index for continuous and discrete variables. The next step towards writing a scattering equation consists in representing the perturbation series of Eq. (2.40) through matrix elements obtained from diagrams derived from H_I through TOPT rules that are similar to standard Feynman rules. The main differences consists in the occurrence of non-covariant TOPT contact terms that arise in addition to contact terms from the vector mesons from the Wess-Zumino Lagrangian itself as mentioned before. In the Green's function, one can explicitly separate 2-particle intermediate states off the rest, $\mathcal{G} = \tilde{\mathcal{G}} + \mathcal{G}^{(2)}$, arriving at

$$\mathcal{T} = \mathcal{V} + \mathcal{V}\mathcal{G}^{(2)}\mathcal{T} \quad (2.42)$$

with an effective potential

$$\mathcal{V} = H_I \frac{1}{1 - \tilde{\mathcal{G}}H_I} , \quad (2.43)$$

that contains the intermediate states with more than two particles. Furthermore, both the potential \mathcal{V} and the \mathcal{T} -matrix can be generalized to the off-shell case $E \neq E_i \neq E_f$,

$$\mathcal{T}_{fi} = \mathcal{V}_{fi} + \oint_j \frac{\mathcal{V}_{fj}\mathcal{T}_{ji}}{E - E_j - \omega_j + i\epsilon} , \quad (2.44)$$

for initial, final, and intermediate two-body states. The index j indicates the sum over discrete quantum numbers like particle spins, two-body channels, and continuous three-momenta \mathbf{q}_1 and \mathbf{q}_2 with states normalized as $\langle \mathbf{q} | \mathbf{q}' \rangle = \delta(\mathbf{q} - \mathbf{q}')$ and baryon and meson energies

$$E_j = \sqrt{M_B^2 + \mathbf{q}_1^2} , \quad \omega_j = \sqrt{m_M^2 + \mathbf{q}_2^2} , \quad (2.45)$$

where M_B and m_M are the baryon and meson masses, respectively. In the center-of mass frame where the momenta of initial and final particles fulfill $\mathbf{p}_1 + \mathbf{p}_2 = \mathbf{p}_3 + \mathbf{p}_4$, the matrix elements of $\mathcal{A} \in \{\mathcal{T}, \mathcal{V}\}$ can be written in terms of $A \in \{T, V\}$ as

$$\langle \mathbf{p}_3, \mathbf{p}_4, \lambda_3, \lambda_4, \mu, I, I_3 | \mathcal{A}(E) | \mathbf{p}_1, \mathbf{p}_2, \lambda_1, \lambda_2, \nu, I, I_3 \rangle = \delta(\mathbf{p}_3 + \mathbf{p}_4 - \mathbf{p}_1 - \mathbf{p}_2) A_{\mu\nu}^I(E, \mathbf{p}', \lambda', \mathbf{p}, \lambda) , \quad (2.46)$$

where $\mathbf{p} = \mathbf{p}_1$, $\mathbf{p}' = \mathbf{p}_3$, μ and ν are channel indices (πN , ηN , $K\Lambda$, $K\Sigma$, $\omega N, \dots$), and I is the total isospin. Furthermore, $\lambda = \lambda_1 - \lambda_2$ and $\lambda' = \lambda_3 - \lambda_4$ are helicity indices for the helicities of incoming and outgoing states [107]. With these simplifications, Eq. (2.44) reads

$$T_{\mu\nu}^I(\mathbf{p}', \lambda', \mathbf{p}, \lambda; E) = V_{\mu\nu}^I(\mathbf{p}', \lambda', \mathbf{p}, \lambda; E) + \sum_{\kappa, \lambda''} \int d^3q V_{\mu\kappa}^I(\mathbf{p}', \lambda', \mathbf{q}, \lambda''; E) \frac{1}{E - E_\kappa(q) - \omega_\kappa(q) + i\epsilon} T_{\kappa\nu}^I(\mathbf{q}, \lambda'', \mathbf{p}, \lambda; E) , \quad (2.47)$$

which formally resembles a Lippmann-Schwinger equation with relativistic energies. Note that this is similar to the Thompson equation [33, 35, 36]. Three-body states can then be re-inserted as individual channels instead of effective potentials, ordered by quantum numbers. This is discussed in Sect. 2.7.2. Note that the above equation is identical to the one of the ANL-Osaka approach in Eq. (2.14). If one aims at obtaining the interactions V from Lagrangians leading to a vertex \bar{V} by using TOPT rules, one has to insert a conversion factor [46],

$$A(\mathbf{p}', \mathbf{p}) = \frac{1}{(2\pi)^3} \sqrt{\frac{M_3}{E_3(\mathbf{p}')}} \sqrt{\frac{M_1}{E_1(\mathbf{p})}} \frac{1}{\sqrt{2\omega_4(\mathbf{p}')}} \frac{1}{\sqrt{2\omega_2(\mathbf{p})}} \bar{A} , \quad (2.48)$$

where, again, A stands for V or T and $\omega_2(\omega_4)$ are the incoming (outgoing) meson energies and analogously for baryon energies $E_1(E_3)$. This corresponds to the normalization [46]

$$S_{fi} = \delta_{fi} - i(2\pi)^{-2}\delta^4(P_f - P_i) \sqrt{\frac{M_3}{E_3}} \sqrt{\frac{M_1}{E_1}} \frac{1}{\sqrt{2\omega_4}} \frac{1}{\sqrt{2\omega_2}} \bar{T}_{fi} , \quad (2.49)$$

which implies that

$$\bar{V}(E, \mathbf{p}', \lambda', \mathbf{p}, \lambda) = \bar{u}(\mathbf{p}', \lambda') \Gamma u(\mathbf{p}, \lambda) \quad (2.50)$$

with Dirac spinors normalized to $\bar{u}u = 1$ and Γ containing the entire spin and isospin structure of the transition. These \bar{V} are related to the transition potentials quoted as \mathcal{V} in the Appendix of Ref. [53] according to

$$\mathcal{V} = \sqrt{\frac{M_3}{E_3}} \sqrt{\frac{M_1}{E_1}} \bar{V} . \quad (2.51)$$

Note that separation of the identity and interacting part (the reaction amplitude T) from the S-matrix differ vastly in the literature. For example, in many meson-baryon studies (see, e.g., Ref. [39, 42, 43, 108–110]) canonical Höhler nomenclature [111] defines $\hat{S} = \mathbb{1} + i\hat{T}$ on the level of operators and then utilizes spinors normalized as $\bar{u}_f(p)u_i(p) = 2M_N\delta_{fi}$ while defining the general Lorentz invariant and parity conserving T-matrix element for a meson-baryon transition $M(q)B(p) \rightarrow M(q')B(p')$ as

$$M_{fi} = \frac{1}{8\pi\sqrt{s}} \bar{u}_f(p') \left(A(s, t) + \frac{\not{q}' + \not{q}}{2} B(s, t) \right) u_i(p) . \quad (2.52)$$

Ultimately, the scalar quantities A, B are used to define partial-wave amplitudes, relating also to observable quantities like phase-shifts or cross sections.

2.5. Partial-wave projection

Dynamical coupled-channel models deal with s -channels containing spin-1/2 nucleons but also the spin-3/2 Δ and spin-1 vector mesons (ρ, ω). The partial-wave projection of $A \in \{V, T\}$ in the scattering equation (2.47) is a two-step process; as helicity and angular momentum commute, one can expand the helicity eigenstates in terms of eigenstates of total angular momentum. In particular, with incoming (outgoing) helicities λ_1, λ_2 (λ_3, λ_4), the quantity A as written in the states $|\mathbf{p}', \lambda_3, \lambda_4\rangle$ and $|\mathbf{p}, \lambda_1, \lambda_2\rangle$ can be decomposed as [107, 112]

$$\langle \mathbf{p}', \lambda' | A | \mathbf{p}, \lambda \rangle = \frac{1}{4\pi} \sum_J (2J+1) D_{\lambda\lambda'}^{J*}(\Omega_{\mathbf{p}'\mathbf{p}}, 0) \langle p', \lambda' | A^J | p, \lambda \rangle , \quad (2.53)$$

that depends only on the helicity differences $\lambda := \lambda_1 - \lambda_2$ and $\lambda' := \lambda_3 - \lambda_4$. Here, D are the Wigner-D functions with $\Omega_{\mathbf{p}'\mathbf{p}}$ the solid angle between \mathbf{p} (incoming nucleon) and \mathbf{p}' (outgoing nucleon). We choose $\Omega_{\mathbf{p}'\mathbf{p}} = (\phi_0, \theta_0)$ in the specific geometry where particle 1 (nucleon) comes in along the $+z$ -direction and particle 3 (nucleon) leaves at angles ϕ_0 and θ_0 [112]. Note that in some papers one can find a slightly different PWA expression, with the connection to the above one discussed in Sect. IIE of Ref. [113]. The inverse is given by

$$\langle p', \lambda' | A^J | p, \lambda \rangle = 2\pi \int_{-1}^1 d(\cos\theta) d_{\lambda\lambda'}^J(\theta) \langle \mathbf{p}', \lambda' | A | \mathbf{p}, \lambda \rangle , \quad (2.54)$$

for which $\mathbf{p} = (0, 0, p)^\top$ and $\mathbf{p}' = (p' \sin \theta, 0, p' \cos \theta)^\top$ is usually chosen for simplicity. The second step concerns the transformation from helicity to JLS basis. For total spin J with third component M one has

$$|JM\lambda_1\lambda_2\rangle = \sum_{LS} \langle JMLS|JM\lambda_1\lambda_2\rangle |JMLS\rangle \quad (2.55)$$

with orbital angular momentum L and total spin S that is the sum of the individual spins. For example, the ρN states can have $S = 1/2$ or $S = 3/2$. The transformation matrix is given by Clebsch-Gordan coefficients [112],

$$\langle J'M'LS|JM\lambda_1\lambda_2\rangle = \sqrt{\frac{2L+1}{2J+1}} \langle L0S\lambda|J\lambda\rangle \langle S_1\lambda_1 S_2 - \lambda_2|S\lambda\rangle \delta_{JJ'}\delta_{MM'} , \quad (2.56)$$

where, again, $\lambda = \lambda_1 - \lambda_2$. After these transformations, the partial-wave projected scattering equation in the c.m. frame, for given isospin I and spin-parity J^P , reads [51, 52, 104, 114, 115]

$$T_{\mu\nu}(p', p; E) = V_{\mu\nu}(p', p; E) + \sum_{\kappa} \int_0^{\infty} dq q^2 V_{\mu\kappa}(p', q; E) G_{\kappa}(q; E) T_{\kappa\nu}(q, p; E) , \quad (2.57)$$

where $p' \equiv |\mathbf{p}'|$ ($p \equiv |\mathbf{p}|$) is the modulus of the outgoing (incoming) three-momentum that may be on- or off-shell, $E = \sqrt{s}$ is the scattering energy, and μ, ν, κ are channel indices. In Eq. (2.57), the propagator for a stable meson and a stable baryon is given by

$$G_{\kappa} = \frac{1}{E - E_{\kappa}(q) - \omega_{\kappa}(q) + i\epsilon} , \quad (2.58)$$

with energies from Eq. (2.45). The propagators for unstable channels are more complicated as discussed in Sect. 2.7.2. Note that there are different possibilities for the $\pi\Delta$ and ρN channels to couple to a given J^P , that are counted as individual channels. The complete coupling scheme (applying to s -, t -, and u -channel exchanges) is shown in Table 1. There, the total spin $S = |\mathbf{S}_N + \mathbf{S}_{\rho}|$ is given by the sum of the ρ spin and the nucleon spin, and L is the orbital angular momentum.

2.6. Channels and transitions

Both the ANL-Osaka and the JB models include two-body channels with stable hadrons, πN , ηN , $K\Lambda$, $K\Sigma$, and ωN , as well as $\pi\Delta$, σN , and ρN . The unstable “isobars” in the latter three channels stand for two-body sub-channels with sub-energy-dependent amplitude rather than simple resonances, see Sect. 2.7.2. The extension of the original JBW model to include the $K\Lambda$ and $K\Sigma$ channels was carried out in Ref. [104], while the ωN channel was added only recently by Wang et al. [58]. In the same work, to make the dynamics of the $K\Sigma$ system complete, the exchange of a_0 was added for the $K\Lambda \rightarrow K\Sigma$ and $K\Sigma \rightarrow K\Sigma$ transitions. For a summary of exchange diagrams see Fig. 2 and Table 2, Ref. [53], or the supplementary material of Ref. [58] for the current status.

In the ANL-Osaka model [78, 87], the meson-baryon interaction is constructed as described in Sect. 2.2.3. The hadron exchange mechanisms of this model are also summarized Table 2. $K\Lambda$ and $K\Sigma$ channels are included in [87]. Here, the

Table 1: Angular momentum structure of the coupled channels in isospin $I = 1/2$ up to $J = 9/2$. The $I = 3/2$ sector is similar up to obvious isospin selection rules.

μ	$J^P =$	$\frac{1}{2}^-$	$\frac{1}{2}^+$	$\frac{3}{2}^+$	$\frac{3}{2}^-$	$\frac{5}{2}^-$	$\frac{5}{2}^+$	$\frac{7}{2}^+$	$\frac{7}{2}^-$	$\frac{9}{2}^-$	$\frac{9}{2}^+$
1	πN			S_{11}	P_{11}	P_{13}	D_{13}	D_{15}	F_{15}	F_{17}	G_{17}
2	$\rho N(S = 1/2)$			S_{11}	P_{11}	P_{13}	D_{13}	D_{15}	F_{15}	F_{17}	G_{17}
3	$\rho N(S = 3/2, J - L = 1/2)$			—	P_{11}	P_{13}	D_{13}	D_{15}	F_{15}	F_{17}	G_{17}
4	$\rho N(S = 3/2, J - L = 3/2)$			D_{11}	—	F_{13}	S_{13}	G_{15}	P_{15}	H_{17}	D_{17}
5	ηN			S_{11}	P_{11}	P_{13}	D_{13}	D_{15}	F_{15}	F_{17}	G_{17}
6	$\pi\Delta(J - L = 1/2)$			—	P_{11}	P_{13}	D_{13}	D_{15}	F_{15}	F_{17}	G_{17}
7	$\pi\Delta(J - L = 3/2)$			D_{11}	—	F_{13}	S_{13}	G_{15}	P_{15}	H_{17}	D_{17}
8	σN			P_{11}	S_{11}	D_{13}	P_{13}	F_{15}	D_{15}	G_{17}	F_{17}
9	$K\Lambda$			S_{11}	P_{11}	P_{13}	D_{13}	D_{15}	F_{15}	F_{17}	G_{17}
10	$K\Sigma$			S_{11}	P_{11}	P_{13}	D_{13}	D_{15}	F_{15}	F_{17}	G_{17}

Table 2: The t - and u -channel transitions in the JBW and ANL Osaka models. Both models also include s -channel poles and contact interactions that are not listed here. Black entries show common transitions, blue (green) transitions indicate processes only contained in the JBW model but not the ANL-Osaka model (ANL-Osaka model but not JBW model). The particle type implies which interaction channel (t or u) is meant. Abbreviations used: Δ for $\Delta(1232)3/2^+$, σ for $f_0(500)$, κ for $K_0^*(700)$, ρ for $\rho(770)$, a_0 for $a_0(980)$, f_0 for $f_0(980)$, Σ^* for $\Sigma(1385)3/2^+$, Ξ^* for $\Xi(1530)3/2^+$, and C for contact term. The $(\pi\pi)_\sigma$ and $(\pi\pi)_\rho$ entries correspond to correlated two-pion exchange that is treated differently in both approaches.

μ	πN	ηN	$K\Lambda$	$K\Sigma$	ωN	$\pi\Delta$	σN	ρN
πN	$N, \Delta,$ $(\pi\pi)_\sigma, \sigma, f_0$	a_0, N	$K^*, \Sigma,$ Σ^*, κ	$K^*, \Lambda,$ Σ, Σ^*, κ	ρ, N	ρ, N, Δ	π, N	$\pi, \omega,$ a_1, N, Δ, C
ηN		N, f_0	$K^*, \Lambda,$ κ	$K^*, \Sigma,$ Σ^*, κ	ω, N		N	N
$K\Lambda$			$\omega, f_0, \phi,$ Ξ, Ξ^*	$\rho, a_0,$ Ξ, Ξ^*	$K, K^*,$ Λ			
$K\Sigma$				$\rho, \omega, \phi,$ $f_0, a_0,$ Ξ, Ξ^*	$K, K^*,$ Σ, Σ^*			
ωN					σ, N			
$\pi\Delta$						ρ, N, Δ		π, N
σN							σ, N	N
ρN								$\rho, N,$ Δ, C

interaction in channels involving unstable particles $\pi\Delta$, σN and ρN includes Z -diagrams discussed in section 2.2.3. The ωN channel was added to the ANL-Osaka model in Ref. [116].

DCC approaches provide channel transitions through s -, t -, and u -channel exchanges as well as contact terms (see Fig. 2). The interaction V in Eq. (2.57) can be separated into different pieces according to

$$V_{\mu\nu} = V_{\mu\nu}^{\text{NP}} + \underbrace{\sum_{i=1}^n \frac{\gamma_{\mu;i}^a \gamma_{\nu;i}^c}{E - M_i^b}}_{V_{\mu\nu}^P} + \underbrace{\frac{\gamma_\mu^{\text{CT};a} \gamma_\nu^{\text{CT};c}}{M_N}}_{V_{\mu\nu}^{\text{CT}}} . \quad (2.59)$$

The first term, V^{NP} , contains non-separable t - and u -channel exchanges (see Fig 2). The second term, V^P , contains separable s -channel resonance contributions, with n being the number of bare s -channel states in a given partial wave. To simplify the notation, the explicit dependence on momenta and energy are omitted here and in the following. In Eq. (2.59), γ^c (γ^a) are the bare resonance creation (annihilation) vertices, indicated by the subscript c (a), of the s -channel states of bare mass M_i^b .

2.6.1. The u -channel transitions and phenomenological contact terms

The t - and u -channel exchanges included by the ANL-Osaka and JBW approaches are shown and compared in Table 2.

The u -channel exchanges (or Z-diagrams) involve the exchange of a baryon. For exchanged octet states, the JBW model employs TOPT nucleon propagators. For spin-3/2 propagators in u -channel transitions the choice

$$P^{\mu\nu}(k) = \frac{\not{k} + M_\Delta}{k^2 - M_\Delta^2 + i\epsilon} \left[-g^{\mu\nu} + \frac{\gamma^\mu \gamma^\nu}{3} + \frac{2k^\mu k^\nu}{3M_\Delta^2} - \frac{k^\mu \gamma^\nu - k^\nu \gamma^\mu}{3M_\Delta} \right] \quad (2.60)$$

is made that suppresses off-mass-shell terms [28]. The u -channel exchange plays a special role in the context of three-body channels that are included both in the ANL-Osaka and JBW models. As discussed in Sect. 2.7.2 three-body unitarity in the JBW approach requires u -channel exchange contributions in the potential V leading to moving singularities that depend both on incoming and outgoing momenta and energy. Correspondingly, the solution of the integral equation (2.47) requires a tailored treatment discussed in Sect. 2.9.1. Figure 2 illustrates the nucleon u -channel exchange in the $\pi N \rightarrow \pi\Delta$ transition as one of several processes required by unitarity. In the ANL-Osaka model, the u -channel exchange processes which develop $\pi\pi N$ cut are only the Z diagrams shown in Fig. 4. The other u -channel exchange mechanisms are included

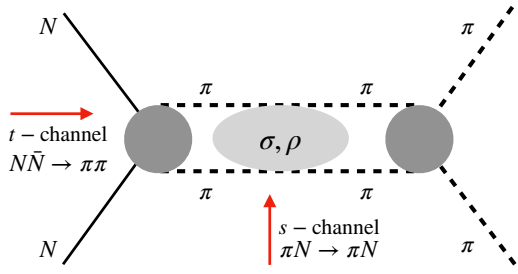


Figure 6: Scalar-isoscalar and vector-isovector exchanges in the t -channel, determined by using dispersion techniques, crossing symmetry, and a fit to quasi-empirical data of the $N\bar{N} \rightarrow \pi\pi$ reaction. Figure adapted from Ref. [46].

in the potential $v_{M'B',MB}$ of Eq. (2.12) with no $\pi\pi N$ cut. The pion production processes associated with the πNN vertex are included in $v_{\pi\pi N,MB}$ of Eq. (2.12).

The third term of Eq. (2.59), V^{CT} , contains phenomenological contact terms that are added to the interaction in a given partial wave [55]. These interactions are separable both in channel and momentum space; the correct threshold behavior is built into the γ^{CT} for each channel μ . These contact terms absorb contributions beyond the ones explicitly included in the model. As discussed in Sect. 2.4, there are also contact terms arising at the Lagrangian level or from the TOPT formalism requiring on-shell equivalence with Feynman formalism. These terms are associated with V^{NP} .

2.6.2. The t -channel transitions and correlated two-pion exchange

In the JBW model, the t -channel exchanges are, on one hand, given by the exchange of scalar and vector mesons. As explained in the supplementary material of Ref. [58] the exchange of the vector meson and scalar meson nonet except for the κ -meson is included. They provide realistic meson-baryon interactions that contribute to all partial waves simultaneously.

Second, there are t -channel pion exchanges for non-diagonal transitions such as $\pi N \rightarrow \rho N$ or $\pi N \rightarrow \sigma N$. Unlike other t -channel exchanges, these nondiagonal transitions go on-shell in the inelastic physical region $\sqrt{s} > 2m_\pi + M_N$ as required by unitarity, similar to the above-discussed u -channel exchanges (see Sect. 2.7.1).

Third, in the JBW model the most prominent t -channel exchanges in πN scattering, namely the scalar-isoscalar and the vector-isovector channels, are not mediated via explicit meson fields but by correlated $\pi\pi$ exchange as introduced in Ref. [46]. The correlated two-pion exchange is related to the $N\bar{N} \rightarrow \pi\pi$ amplitude as schematically indicated in Fig. 6. The idea [46] is to relate a model that describes “quasi-empirical” data of the $N\bar{N} \rightarrow \pi\pi$ and $\pi\pi$ amplitudes to the $\pi N \rightarrow \pi N$ reaction through crossing symmetry. The $N\bar{N} \rightarrow \pi\pi$ were obtained by analytic continuation of πN and elastic $\pi\pi$ data into the unphysical region below the $N\bar{N}$ threshold [111, 117, 118]. The amplitudes $f_\pm^0(t)$ and $f_\pm^1(t)$ describing them are related to the partial-wave projected invariant $A_\sigma^{(+)}, B_\sigma^{(+)}$ and $A_\rho^{(-)}, B_\rho^{(-)}$ amplitudes, respectively, where the upper index labels isoscalar (+) and isovector (-) amplitudes. For the Dirac structures associated with A and B , see Eq. (2.52). The invariant amplitudes can be related to the T matrix that can then be continued in different kinematic variables to the crossed reaction. See Ref. [46] for more details of the calculation, including a discussion of how to avoid double-counting of processes generated through iteration of the Lippmann-Schwinger equation.

It should be emphasized that the correlated two-pion exchange is implemented at the level of the interaction V and not the s -channel unitarized amplitude T . More sophisticated dispersive treatments consider crossing symmetry at the amplitude level (Roy Steiner equations) [119–121] and have been recently continued to complex energies to, e.g., extract the pole of the Roper resonance [122].

2.6.3. The s -channel transitions, two-potential formalism, and renormalization

The s -channel processes play a special role as they are separable and allow for the separation into a “pole part” and a “non-pole” part through the two-potential formalism. This is illustrated for the ANL-Osaka model in Sect. 2.2.3. For the JBW model, a very similar separation is discussed in Ref. [53]. In DCC approaches, the backwards-going parts of s -channel processes and channel propagation are usually neglected, but their role has been quantified for a mesonic systems some time ago [123]. In the ANL-Osaka model, the pair production processes are included in the potential as discussed on Eq. (2.14), while the backwards-going propagation of the bare excited baryons are not included.

On the one hand, resonance poles in the T-matrix can arise from solving the nonlinear scattering equation with only t - and u -channel exchanges. Such states are usually referred to as “dynamically generated”. In the JBW model, this occurs, e.g., for the Roper resonance [51]. On the other hand, and in most of the cases, resonances are accounted for by explicit s -channel exchanges. These are simple singularities of V in energy $E = \sqrt{s}$ that move into the complex energy plane once they are unitarized in the Lippmann-Schwinger equation (2.47). In the JBW model, s -channel baryonic states are included via Lagrangians up to spin $J = 3/2$, see, e.g., Table B.8 of Ref. [104]. For higher spin, resonances are related to

their lower-spin pendants by adding suitable barrier factors [104]. With this input, the partial-wave projected resonance creation and annihilation vertices γ_μ^a and γ_ν^c of Eq. (2.59) are calculated containing coupling constants to be fit to data.

In the following we discuss the “two-potential formalism” in the JB model that allows one to separate off s -channel exchanges. In the ANL-Osaka model a similar decomposition is performed as given in Eqs. (2.20), (2.21) and (2.26).

The full scattering T-matrix of Eq. (2.57) can be written as the sum of “pole” and “non-pole” part [53],

$$T_{\mu\nu} = T_{\mu\nu}^P + T_{\mu\nu}^{NP}, \quad (2.61)$$

which is the same decomposition as the one into the “resonant” and ”non-resonant” part in the ANL-Osaka formulation of Eq. (2.20). First, all t - and u -channel contributions, V^{NP} from Eq. (2.59), are unitarized in the non-pole part,

$$T_{\mu\nu}^{NP} = V_{\mu\nu}^{NP} + \sum_\kappa V_{\mu\kappa}^{NP} G_\kappa T_{\kappa\nu}^{NP}, \quad (2.62)$$

in operator notation implying integration over the second term. This part can actually develop poles that are dynamically generated through the non-linearity in V^{NP} . An example is given by the Roper resonance discussed in Sec. 3.3.7. Contributions from the s -channel exchanges, the pole part T^P , can be evaluated from the non-pole part T^{NP} given in Eq. (2.62). For this, we define the following quantities using the bare vertices of Eq. (2.59):

$$\Gamma_{\mu;i}^c = \gamma_{\mu;i}^c + \sum_\nu \gamma_{\nu;i}^c G_\nu T_{\nu\mu}^{NP}, \quad \Gamma_{\mu;i}^a = \gamma_{\mu;i}^a + \sum_\nu T_{\mu\nu}^{NP} G_\nu \gamma_{\nu;i}^a, \quad \Sigma_{ij} = \sum_\mu \gamma_{\mu;i}^c G_\mu \Gamma_{j;\mu}^a, \quad (2.63)$$

where Γ^c (Γ^a) are the “dressed resonance creation (annihilation) vertices” and Σ is the “self-energy”. The indices i, j label the s -channel state in the case of multiple resonances. For the two-resonance case with bare masses m_1 and m_2 , the pole part reads explicitly [124]

$$T_{\mu\nu}^P = \Gamma_\mu^a D^{-1} \Gamma_\nu^c, \quad (2.64)$$

where

$$\Gamma_\mu^a = (\Gamma_{\mu;1}^a, \Gamma_{\mu;2}^a), \quad \Gamma_\mu^c = \begin{pmatrix} \Gamma_{\mu;1}^c \\ \Gamma_{\mu;2}^c \end{pmatrix}, \quad D = \begin{pmatrix} E - m_1^b - \Sigma_{11} & -\Sigma_{12} \\ -\Sigma_{21} & E - m_2^b - \Sigma_{22} \end{pmatrix}, \quad (2.65)$$

with inverse propagator D , from which the one-resonance case follows immediately. This decomposition is widely used in the literature, see, e.g., Refs. [11, 45, 125, 126]. The non-pole part T^{NP} is sometimes referred to as *background*, although the unitarization of Eq. (2.62) may lead to dynamically generated poles in T^{NP} . In turn, T^P contains constant and other terms beyond the pole contribution of the Laurent expansion [114]. This demonstrates that a decomposition into resonant and non-resonant contribution according to the two-potential formalism is not identical to terms of the Laurent expansion, showing that this separation is not unique, and that it is difficult to attribute physical properties to them in a model-independent way.

However, there is a numerical advantage to this separation: All s -, t -, and u - channel exchanges have free fit parameters to be matched to data. Some parameters come through the form factors in t -, u - channel exchanges while others, the pole parameters, come through resonances coupling to the photon and hadronic channels. The two-potential formalism allows for hierarchical fit structures: One starts by evaluating T^{NP} once, with a given set of t -, and u -channel “slow” parameters. Evaluating V^{NP} is the numerical bottleneck because it requires the partial-wave projection of all matrix elements in momentum and channel space. Once these transitions are evaluated, one optimizes all pole parameters plus the separable contact terms discussed in Sect. 2.6.1. Indeed, due to their separable form, the latter can be organized in a structure very similar to the two-potential formalism for resonances [55] discussed before. Once these fast-evaluating parts of the amplitude are optimized, the next optimization step of slow parameters takes place, involving another evaluation of V^{NP} .

There is one special s -channel exchange that accounts for the nucleon itself. Its spin-parity of $J^P = 1/2^+$ corresponds to the P_{11} partial wave that also hosts the Roper resonance $N(1440)$ and higher-lying states. Parameterizing the nucleon pole in terms of an s -channel singularity, $V \sim (f_N^b)^2/(E - M_N^b)$ makes it apparent that the bare πNN coupling f_N^b and bare mass M_N^b undergo a renormalization such that the pole of the fully dressed T-matrix is at the physical nucleon mass, M_N , and its residue equals the residue induced by the physical πNN coupling, $f_{\pi NN}$. The renormalization depends on the included number of channels, the non-pole (i.e., t -, u -and contact) interactions, and the regularization. In principle, one could numerically ensure the physical nucleon mass and coupling by fitting M_N^b and f_N^b to M_N and $f_{\pi NN}$.

It is also possible (and realized in the JBW model [53]) to perform the renormalization analytically by separating the nucleon s -channel contributions from t - and u -channel contributions through the discussed two-potential formalism [45, 127]. Following Eq. (2.65), the pole part T^P in the one-resonance, one-channel (πN) case, with an s -channel nucleon exchange of bare mass M_N^b , can be written as

$$T^P = \frac{\Gamma^a \Gamma^c}{E - M_N^b - \Sigma(E)}. \quad (2.66)$$

We require that T^P has a pole at the physical nucleon mass M_N or, equivalently, that

$$M_N = M_N^b + \Sigma(M_N) . \quad (2.67)$$

To derive an expression for M_N^b that respects the renormalization condition (2.67) we expand the nucleon self-energy about $E = M_N$,

$$\Sigma(E) = \Sigma(M_N) + (E - M_N) \frac{\partial \Sigma(E)}{\partial E} \Big|_{E=M_N} + \mathcal{O}(E - M_N)^2 , \quad (2.68)$$

and define the reduced quantities $\tilde{\Sigma}$ and $\tilde{\Gamma}^{a,c}$ using that the bare coupling $f_N^b = x f_{\pi NN}$ can be factorized off Σ and Γ ,

$$\begin{aligned} \Sigma &= (f_N^b)^2 \Sigma^{\text{red}} = x^2 f_{\pi NN}^2 \Sigma^{\text{red}} = x^2 \tilde{\Sigma} , \\ \Gamma^{a,c} &= f_N^b \Gamma^{\text{red};a,c} = x f_{\pi NN} \Gamma^{\text{red};a,c} = x \tilde{\Gamma}^{a,c} . \end{aligned} \quad (2.69)$$

In Eq. (2.69), $\tilde{\Sigma}$ is the nucleon self-energy calculated with the physical nucleon coupling $f_{\pi NN}$, instead of the bare coupling. The same applies to $\tilde{\Gamma}^{a,c}$, and T^P from Eq. (2.66) reads now

$$T^P = \frac{1}{E - M_N} \left(\frac{x^2 \tilde{\Gamma}^a \tilde{\Gamma}^c}{1 - x^2 \partial_E \tilde{\Sigma}} \right)_{E=M_N} + \mathcal{O}(E - M_N)^0 . \quad (2.70)$$

To determine the bare coupling f_N^b , x is calculated: the physical residue of the nucleon pole in energy E is given by

$$(a_{-1})_{\pi N \rightarrow \pi N} = \tilde{\gamma}^a \tilde{\gamma}^c , \quad (2.71)$$

where $\tilde{\gamma}^{a,c}$ are the bare nucleon vertices calculated at $E = M_N$ with the physical nucleon coupling $f_{\pi NN}$ instead of the bare coupling (cf. Appendix B.1. of Ref. [104]). The residue in Eq. (2.71) has to agree with the residue of T^P from Eq. (2.70) at the pole position:

$$\left(\frac{x^2 \tilde{\Gamma}^a \tilde{\Gamma}^c}{1 - x^2 \partial_E \tilde{\Sigma}} \right)_{E=M_N} = (a_{-1})_{\pi N \rightarrow \pi N} , \quad (2.72)$$

leading to

$$\frac{1}{x^2} = \left(\partial_E \tilde{\Sigma} + \frac{\tilde{\Gamma}^a \tilde{\Gamma}^c}{\tilde{\gamma}^a \tilde{\gamma}^c} \right)_{E=M_N} . \quad (2.73)$$

The bare mass M_N^b is then

$$M_N^b = M_N - x^2 \tilde{\Sigma}(M_N) . \quad (2.74)$$

This matching procedure is valid for the nucleon in case it couples only to the πN channel. In Ref. [51], the renormalization for one bare s -channel state coupling to more than one channel is developed. In Ref. [53] the renormalization procedure in presence of an additional s -channel state, that may couple to all channels, is derived. This version is implemented in all versions of the JBW model thereafter. While the nucleon pole gets renormalized no attempt is made for a similar, self-consistent treatment of the nucleon appearing in exchange potentials $V_{\mu\nu}$ or the propagation functions G_κ of Eq. (2.57). Instead, the physical nucleon mass is used in these instances.

In the ANL-Osaka approach, the single nucleon state does not couple with MB states by construction and the nucleon state only appears in the u - and s -channel potential and Z-diagrams, where the *physical* nucleon mass is used. The introduction of a bare nucleon state within the model is examined in Ref. [128] for the analysis of the P_{11} partial-wave amplitude.

2.7. Three-body unitarity and its implementation for the σN , ρN and $\pi \Delta$ channels

2.7.1. The S-matrix and its unitarity

We illustrate how unitarity relates imaginary parts of the isobar-spectator propagation to imaginary parts of their interaction via u -channel processes. For the ANL-Osaka and the JBW models, the isobars refer to the resonant πN channel P_{33} for the Δ and to the σ and ρ quantum numbers for the two-pion amplitudes as discussed in Sect. 2.7.2. For three-meson systems (Sect. 4), there are resonant channels but also non-resonant isobars [113], for example the repulsive $3\pi^+$ system that does not host any resonances [129].

For simplicity, the argument in this subsection is outlined in terms of spinless particles and isobars following Ref. [130]. A relativistic, infinite-volume three-body scattering amplitude was formulated in Ref. [130] following much earlier work by Aaron, Amado and Young [131]. It can be expressed in terms of on-shell, two-body unitary $2 \rightarrow 2$ amplitudes (the isobars), complex exchange processes, and genuine three-body interactions containing the microscopic dynamics, which are forced to be real-valued by three-body unitarity. In the following we collect only the main results of the derivation, relevant for this review, and refer the reader for details to the original work [130].

The central quantity of most theoretical approaches to the properties of excited hadrons is the S-matrix, introduced in the first half of 20th century, see, e.g., Refs. [132, 133]. It relates asymptotically free states in the far past to those in the distant future. Consider n incoming and m outgoing spinless states with three-momenta $\{\mathbf{p}\} = \{\mathbf{p}_1, \dots, \mathbf{p}_n\}$ and $\{\mathbf{p}'\} = \{\mathbf{p}'_1, \dots, \mathbf{p}'_m\}$, respectively. The operators for the S- and T-matrix are

$$\langle \{\mathbf{p}'\} | \hat{S} | \{\mathbf{p}\} \rangle = \langle \{\mathbf{p}'\} | (\mathbb{1} + i\hat{T}) | \{\mathbf{p}\} \rangle. \quad (2.75)$$

The crucial point is that this allows one to formalize otherwise abstract principles of scattering theory in mathematical properties of the S-matrix. In particular, the S-matrix obeys *crossing symmetry*, *analyticity* and *unitarity*, see for more details Ref. [1] and references therein. In view of DCC approaches for hadron spectroscopy, analyticity and unitarity are of paramount importance. To be more specific, the S-matrix elements ($\in \mathbb{C}$) are analytic (holomorphic) functions of $(3m+3n-10)$ kinematic variables ($\in \mathbb{C}$). At the boundary of physical kinematics ($\in \mathbb{R}$), the S-matrix elements are, indeed, related to the physical/observable quantities, such as, e.g., phase shifts $\delta_\ell = \arg S_\ell/(2i)$ for the $n = m = 2$ case, projected to the ℓ -th partial wave. The unitarity of the S-matrix,

$$\hat{S}\hat{S}^\dagger = \mathbb{1} \Leftrightarrow \hat{T} - \hat{T}^\dagger = i\hat{T}^\dagger\hat{T}, \quad (2.76)$$

puts another constraint on the imaginary parts of matrix elements and invariant matrix elements (\mathcal{M})

$$\mathcal{M}_{\{\mathbf{p}\} \rightarrow \{\mathbf{p}'\}} = (2\pi)^4 \delta^{(4)} \left(\sum_{i=1}^n p_i - \sum_{i=1}^m p'_i \right) \langle \{\mathbf{p}'\} | \hat{T} | \{\mathbf{p}\} \rangle. \quad (2.77)$$

In the case of one particle type (scalar with mass m) this unitarity constraint reads

$$\begin{aligned} \langle \{\mathbf{p}'\} | (\hat{T} - \hat{T}^\dagger) | \{\mathbf{p}\} \rangle &= i \int \prod_{i=1}^N \frac{d^4 k_i}{(2\pi)^4} (2\pi) \delta^+(k_i^2 - m^2) \langle \{\mathbf{p}'\} | \hat{T}^\dagger | \{\mathbf{k}\} \rangle \langle \{\mathbf{k}\} | \hat{T} | \{\mathbf{p}\} \rangle, \\ \mathcal{M}_{\{\mathbf{p}\} \rightarrow \{\mathbf{p}'\}} - \mathcal{M}_{\{\mathbf{p}'\} \rightarrow \{\mathbf{p}\}}^* &= i \int \prod_{i=1}^N \frac{d^4 k_i}{(2\pi)^4} (2\pi) \delta^+(k_i^2 - m^2) (2\pi)^4 \delta^{(4)} \left(P - \sum_{i=1}^N k_i \right) \mathcal{M}_{\{\mathbf{p}'\} \rightarrow \{\mathbf{k}\}}^* \mathcal{M}_{\{\mathbf{p}\} \rightarrow \{\mathbf{k}\}}. \end{aligned} \quad (2.78)$$

Here, $\delta^+(k_i^2 - m^2)$ selects the positive energy solution only and P denotes the total four momentum of the system. The first observation is that putting N intermediate particles on-shell requires the system to have at least $E \geq N \cdot m$ total energy. The second observation is that when some set of intermediate particles can go on-shell, a discontinuity of the T-matrix elements is manifested along the real energy-axis – a branch cut – often referred to as the unitarity cut or right-hand cut.

In the following the $3 \rightarrow 3$ case of the above unitarity condition is considered for identical, spinless particles of mass m and out- and in-going four-momenta p'_1, p'_2, p'_3 and p_1, p_2, p_3 , respectively. The T-matrix consists of a fully connected (\hat{T}_c) and a once-disconnected piece (\hat{T}_d), related to the isobar-spectator scattering amplitude T and isobar-propagator τ as

$$\begin{aligned} \langle p'_1, p'_2, p'_3 | \hat{T} | p_1, p_2, p_3 \rangle &= \langle p'_1, p'_2, p'_3 | \hat{T}_c | p_1, p_2, p_3 \rangle + \langle p'_1, p'_2, p'_3 | \hat{T}_d | p_1, p_2, p_3 \rangle \\ &= \frac{1}{3!} \sum_{n=1}^3 \sum_{m=1}^3 v(p'_n, p'_{\bar{n}}) \left(\tau(\sigma(p'_n)) T(p'_n, p_m; s) \tau(\sigma(p_m)) - 2E_{p'_n} \tau(\sigma(p'_n)) (2\pi)^3 \delta^3(\mathbf{p}'_n - \mathbf{p}'_m) \right) v(p_{\bar{m}}, p_{\bar{m}}), \end{aligned} \quad (2.79)$$

where P is the total four-momentum of the system, $s = E^2 = P^2$. All four-momenta p_1, p'_1, \dots are on-mass-shell, and the square of the invariant mass of the isobar reads

$$\sigma(p') := (P - p')^2 = s + m_S^2 - 2\sqrt{s}E_{p'} \quad (2.80)$$

for spectator of mass $m_S = m$ and energy $E_{p'}$. We work in the total center-of-mass frame where $\mathbf{P} = \mathbf{0}$. The dissociation vertex $v(p, p')$ of the isobar decaying in asymptotically stable particles, e.g., $\rho(p+p') \rightarrow \pi(p)\pi(p')$, is chosen to be cut-free in the relevant energy region, which is always possible. The notation is such that, e.g., for a spectator momentum p_n , the isobar decays into two particles with momenta $p_{\bar{n}}$ and $p_{\bar{n}}$.

Consider again the connected isobar-spectator amplitude T from Eq. (2.79). It appears twice on the right-hand side of the unitarity relation (2.78) as schematically depicted in Fig. 7 (a). The blue highlighted area shows the three stable

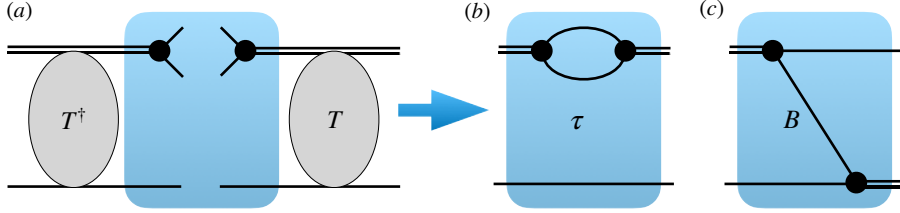


Figure 7: (a) Unitarity relation for stable particles (single lines) with intermediate isobars (double lines). The on-shell, three-body, intermediate state is populated by decaying isobars (shaded highlights) in two distinct ways: (b) by combining the isobar decay products to form a “self energy” or one can (c) combine a spectator with one of the isobar decay products. Next, one formulates a BSE ansatz for T and realizes combinations (b) and (c), leading to 8 terms. In Sect. 2.10.1 we quote the BSE in a different context. Equating these terms to 8 diagrammatically equivalent terms on the left-hand side of Eq. (2.78) translates into 3 conditions: for the imaginary parts of τ^{-1} , imaginary parts of B , while also putting the intermediate spectator on the energy-shell, reducing the BSE to a three-dimensional scattering equation that is manifestly unitary. The second condition leads through the use of an un-subtracted dispersion relation to

$$B(p', p; s) = \frac{-\lambda^2}{2E_{p'+p}(E - E_{p'} - E_p - E_{p'+p} + i\epsilon)}, \quad (2.81)$$

where $E = \sqrt{s}$, $E_{p'+p}^2 = m^2 + (\mathbf{p} + \mathbf{p}')^2$ etc., and p and p' denote the on-shell four-momenta of the in- and outgoing spectator, respectively. In addition, the dissociation vertex is chosen to be of simple scalar form, $v(p, p') := \lambda$.

The first condition, on $\text{Im } \tau^{-1}$, leads to the following form of the isobar propagator [130] using a twice subtracted dispersion relation,

$$\frac{1}{\tau(\sigma(q))} = \sigma(q) - M_0^2 - \int \frac{d^3 k}{(2\pi)^3} \frac{\lambda^2}{2E_k(\sigma(q) - 4E_k^2 + i\epsilon)}, \quad (2.82)$$

where M_0 is a free parameter that can be used to fit (together with λ and cutoff) the two-body amplitude corresponding to the considered isobar, $T_{22} := v\tau v$. We refer to the exchange process in Eq. (2.81) as B -term in the following, and to the integral term in Eq. (2.82) as self-energy. This formulation of two-body scattering for the isobars is used in both the ANL-Osaka and JBW approaches, see Eq. (2.24) and the next subsection. It should be emphasized that there is no need for τ to be of this specific form. For S -wave isobars, an amplitude τ' with $\text{Im } (\tau')^{-1} = \text{Im } v^2/\tau$ can also be used, removing v factors from the B -term suitably. For p -wave isobars, a slightly different matching has to be performed because there is a genuine angular dependence in the decay vertices v [113, 134, 135].

Finally, the last condition which puts the spectator on its energy-shell reduces the four-dimensional BSE to a three-dimensional scattering equation,

$$T(p', p; s) = B(p', p; s) + C(p', p; s) - \int \frac{d^3 q}{(2\pi)^3} (B(p', q; s) + C(p', q; s)) \frac{\tau(\sigma(q))}{2E_q} T(q, p; s). \quad (2.83)$$

Here we have added an additional real-valued term C which does not impact the three-body unitarity constraints, parameterizing the so-called three-body force. Recently, the determination of this quantity through use of lattice QCD and Effective Field Theory became quite an active field of research [129, 136–145]. Note however that C is not an observable quantity, meaning that it will always depend on the details of the integral equation and its regularization. Note also that the distribution of signs in Eqs. (2.81) and (2.83) is owed to the convention $\hat{S} = \mathbb{1} + i\hat{T}$ in Ref. [130]. In the JBW model for baryons, the “Infinite-volume unitary” (IVU) model for mesons discussed in Sect. 4), as well as the ANL-Osaka model, the convention $\hat{S} = \mathbb{1} - i\hat{T}$ is adopted.

In the ANL-Osaka approach, expressions of the full amplitudes satisfying unitarity are given in [11]. In the actual numerical analysis, the scattering amplitudes given in section 2.2.3 is used with the perturbative approximation of $v_{\pi\pi N, MB}$, i.e., the direct two-pion production mechanism. Apart from this, to satisfy three-body unitarity, the interaction Z in Eq. (2.22) illustrated in (c) of Fig. 7 and the self-energy $\Sigma(q, E)$ in Eq. (2.24) illustrated in (b) of Fig. 7 play a crucial role. The unitarity of the model is tested numerically.

Finally, we also note that even if explicit isobar (or dimer) fields are used to parametrize the 2-body subsystem, the isobar formulation is not an approximation but a re-parametrization of the full two-body amplitude as shown in Ref. [146] and also discussed in Ref. [147]. There are some mandatory requirements on the two-body amplitude, though:

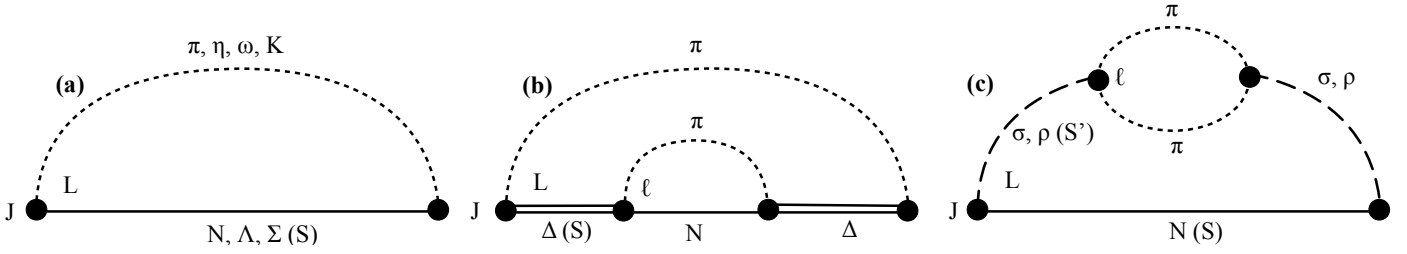


Figure 8: (a) Two-body channels, (b) $\pi\Delta$ channel, (c) $\pi\sigma$, $\pi\rho$ channels included in both the ANL-Osaka and JBW models. See text for further details.

it should be formulated in terms of the Lorentz scalar σ because its center of mass is not at rest in the three-body system; another requirement is obviously two-body unitarity; in addition, absence of poles or cuts on the first Riemann sheet as required by causality [148], and, in close connection to this, a regular behavior in the sub-threshold region. The latter two requirements are also connected to the contour deformation method for the SMC that extends to these regions as will be discussed in Sect. 2.9.3 in relation to Fig. 18.

2.7.2. Three-body channels in the ANL-Osaka and JBW models

Both the ANL-Osaka [87, 149] and JBW approaches [53] incorporate three-body channels with the effective quantum numbers of $f_0(500)N$, $\rho(770)N$, and $\pi\Delta(1232)3/2^+$, in short, called σN , ρN , and $\pi\Delta$. As the ρ , Δ , and nucleon have non-zero spin, some of these channels can couple to a given, overall spin-parity J^P in more than one way as shown in Table 1. The isobars are shown in Fig. 8. The total angular momentum is indicated with J , the orbital angular momentum between isobar and spectator with L , the baryon spin with S , and the meson isobar spin (for the ρ only) with S' . The orbital angular momentum between the isobar decay products, forming the self-energy Σ , is indicated with ℓ .

On the one hand, unitarity requires the inclusion of the complex isobars shown in Fig. 8. These structures simply express the physical process of realizing three particles $\pi\pi N$. The three-body Green's function G_κ for $\kappa \in \{\sigma N, \rho N, \pi\Delta\}$ is obtained by first fitting the isobar dissociation process v to the respective two-body phase shifts. For the σ and Δ quantum numbers in the JBW approach this was performed in Ref. [49]. The ρ isobar was fit to $\pi\pi$ phase shifts in Ref. [51]. The Green's functions G_κ of the JBW are very similar to the ones of the ANL-Osaka approach. See Eq. (2.24) and Refs. [49, 51] for explicit expressions, i.e., they are parametrized with an isobar propagator and a re-summed self energy as in Eq. (2.82).

On the other hand, as discussed in Sect. 2.7.1, the on-shell condition for $\pi\pi N$ must also be realized through complex-valued $3 \rightarrow 3$ exchanges of isobar decay products. This reflects the fact that all three particles can go on-shell simultaneously in the exchange process, if the energy is large enough. These transitions are shown in Fig. 4. In the context of the ANL-Osaka model, they are referred to as Z -diagrams; in the JBW model, these transitions are calculated using time-ordered perturbation theory, and in both approaches they provide the necessary imaginary parts. In both models, s -channel and t -channel exchanges can be added to the amplitude to model the microscopic interactions as described in Sect. 2.6. There are also $2 \rightarrow 3$ transitions required by unitarity in the JBW approach, as shown in the last two diagrams of Fig. 2. In particular, there is an important pion exchange populating the σ and ρ isobars, and a nucleon exchange to populate the $\pi\Delta$ state. In Sect. 2.9.3 we discuss how the 3-body singularities from exchange processes require special care when continuing the amplitude to complex energies to search for resonance poles.

For the meson-exchange models discussed in Sect. 4, three-body unitarity is guaranteed. Coupled-channel two-body unitarity is strictly fulfilled in the JBW model for light baryons, but only approximately for the three-body channels. On the one hand, the included nucleon u -channel diagram develops an imaginary part above $E = 2m_\pi + M_N$, but the corresponding isobar-spectator channel (with quantum numbers πP_{11}) is neglected in the inelastic region. On the other hand, form factors are used that at, large momenta, deviate from unity to guarantee the convergence of the scattering equation. For unitarity, these form factors should appear consistently in the corresponding isobar self energies. Indeed, covariant form factors can be constructed for that purpose [134].

2.8. Solving the scattering equation

The integral equation (2.57) can be solved along a complex spectator momentum contour (SMC) to avoid three-body singularities from particle exchange processes, as well as two-body singularities. This is a common solution strategy for the ANL-Osaka, JBW, and also the IVU approaches for excited baryons and mesons, respectively. For generic particles of mass m_a and m_b , the two-body singularities are given as the solution of $\sqrt{s} = E_a(p) + E_b(p)$,

$$p_{\text{cm}} = \frac{1}{2E} \sqrt{(E^2 - (m_a - m_b)^2)(E^2 - (m_a + m_b)^2)} . \quad (2.84)$$

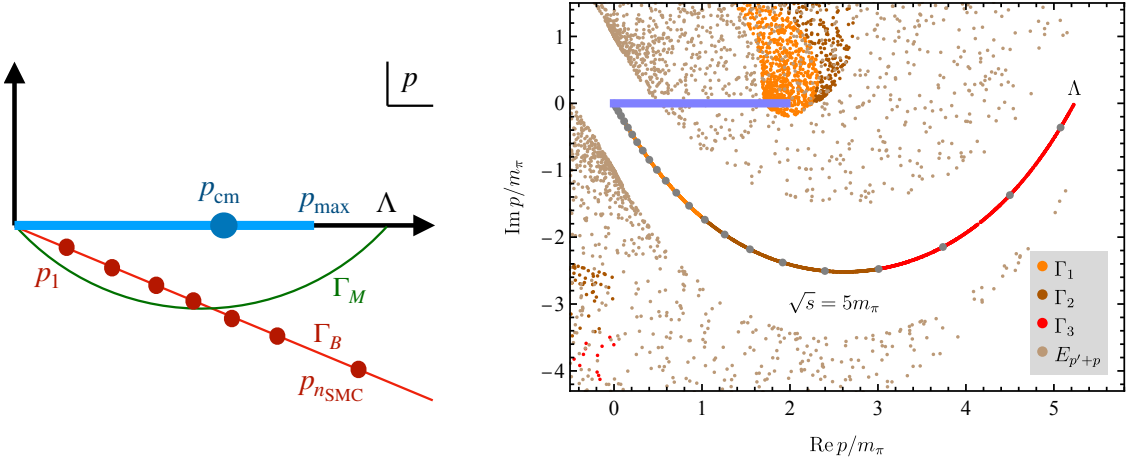


Figure 9: Left: Complex spectator momentum plane showing an integration contour (SMC) Γ_M for regularization by cutoff Λ , and another SMC Γ_B with form factor regularization implying $\Lambda \rightarrow \infty$. Also shown are the integration mesh points $\{p_1, \dots, p_{n_{SMC}}\}$, the on-shell point for two-body channels of stable particles, p_{cm} , and the on-shell region for three-body channels, $p \in [0, p_{\max}]$. Right: Situation of three-body singularities (dots) color coded for the corresponding parts of the SMC following a path Γ_M for cutoff regularization. See text for further explanations.

To solve the integral equation, the complex contour is discretized into a suitable set of mesh points $\{p_i\}$ and integration weights, $dp \rightarrow w_i$. With p , p' , and q sampled at the same momenta $\{p_i\}$, the integral equation becomes a set of linear equations. The solution is then known along a set of complex momenta for fixed \sqrt{s} . This is sufficient if one is only interested in searching for resonance poles. For phase shifts and observables, however, one needs to know the solution for real on-shell momenta $p = p_{cm}(\sqrt{s})$ in case of stable two-body channels κ . For this, the set of mesh points is enlarged, $\{p_i\} \rightarrow \{p_i, p_{cm}\}$ which provides on-shell↔off-shell and the physical on-shell→on-shell transitions [150]. For n_κ channels of two stable particles and n_{SMC} mesh points, the dimension of the numerical T-matrix is then $n_\kappa \cdot (n_{SMC} + 1)$. In reduction to one channel, it is easy to see that with matrix elements $T_{lk}^I = T(p_l, p_k; E)$ with momenta from $\{p_i, p_{cm}\}$ and, analogously, V_{lk} , together with the discretized propagator matrix containing integration weights w_i ,

$$G^I = \text{diag} \left(\frac{w_1 p_1^2}{E - E_\kappa(p_1) - \omega_\kappa(p_1)}, \dots, \frac{w_{n_{SMC}} p_{n_{SMC}}^2}{E - E_\kappa(p_{n_{SMC}}) - \omega_\kappa(p_{n_{SMC}})}, 0 \right), \quad (2.85)$$

the T-matrix is obtained by matrix inversion of $T^I = V + VG^IT^I$, with the physical on-shell to on-shell scattering given by its $(n_{SMC} + 1), (n_{SMC} + 1)$ matrix element. The generalization to n_κ coupled channels is obvious. The superscript I serves to indicate the solution on the first Riemann sheet, in contrast to the solution on other sheets discussed in Sect. 2.9.2. See also Ref. [151] for the role of contour deformations of Lorentz-invariant scattering equations.

In Fig. 9 to the left, some commonly used contours are shown. The JBW model uses regularization through form factors, allowing for a straight integration path Γ_B into the lower p plane as the integral back to the real axis at infinity vanishes (red line). An alternative to render the integrand convergent (allowing for an integration path to infinity) is by over-subtracting the dispersive propagation amplitude τ making it automatically convergent, see Eq. (14) in Ref. [130]. Similarly, unitarity only determines the imaginary part of the particle exchange B from Eq. (2.81), and over-subtracting it preserves unitarity while simultaneously guaranteeing the solution of the scattering equation [130].

One can also use a hard cutoff as shown with the green line Γ_M and realized in Refs. [113, 142] for excited meson systems (IVU model). The cutoff has to be large enough to not cut into the physically allowed state space, for all two- and three-body channels [142]. In any case, the cutoff Λ has to be chosen beyond all physically realizable momenta of the two-body and three-body channels [113, 142], symbolized with the blue dot and blue line in Fig. 9 to the left. The former stands for the two-body singularities at p_{cm} , while the latter indicates the range $[0, p_{\max}]$ of physically allowed spectator momenta in three-body channels.

The right-hand side of Fig. 9 shows the solution $p(p', \cos \theta)$ of $B^{-1} = 0$ with the exchange term B from Eq. (2.81) in the notation of momenta

$$\sqrt{s} - E_{p'} - E_p - E_{p'+p} = 0. \quad (2.86)$$

It is given by [113]

$$p_\pm(m_1, m_3, m_u, x) = \frac{p' x (q'^2 - \alpha^2 + m_u^2 - m_1^2) \pm \alpha \sqrt{(\beta - m_1)^2 - m_u^2 + p'^2 (x^2 - 1)} \sqrt{(\beta + m_1)^2 - m_u^2 + p'^2 (x^2 - 1)}}{2\beta^2}, \quad (2.87)$$

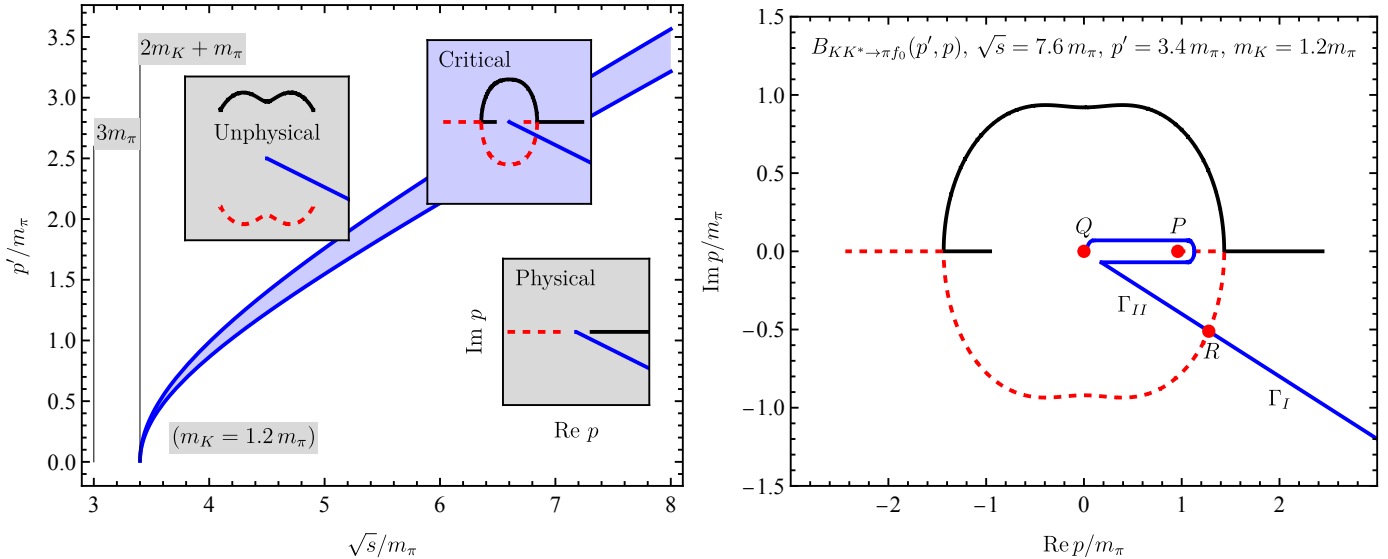


Figure 10: Left: Singularity structures in the s, p, p' variables. The insets show the position of three-body cuts in $p(p', x)$ for three different (\sqrt{s}, p') regions (physical, critical, and unphysical), for $x \in [-1, 1]$ for solutions p_+ (black lines) and p_- (red dashed lines) according to Eq. (2.87), for the kaon exchange in the triangle-singularity reaction $KK^* \rightarrow \pi f_0$. The insets also show a typical complex integration path with blue solid lines. The position of the insets corresponds to the regions in the (\sqrt{s}, p') plane. Right: Illustration of the integral path in the "critical region" for fixed outgoing p' , shown in the complex plane of incoming momentum p . The integration starts at the origin on the first Riemann sheet. Then, it goes around the logarithmic singularity at P , passing through the cut down onto the second Riemann sheet, and back to Q , that indicates the origin on the second Riemann sheet. From there, the integration follows the original SMC Γ with a smooth analytic transition of B at R from second sheet, B^{II} , back to the first sheet, B^I .

where

$$\alpha = \sqrt{s} - \sqrt{m_3^2 + p'^2}, \quad \beta^2 = \alpha^2 - p'^2 x^2 \quad (2.88)$$

for incoming (outgoing) spectator of mass m_1 (m_3) and exchanged mass m_u . The color coding to the right in Fig. 9 indicates from which p' of the SMC the solutions $p_{\pm}(p', \cos \theta)$ originate, while the brown points arise analogously from the pre-factor $E_{p+p'} = 0$ in the B -term. The chosen kinematics corresponds to pion spectators in incoming and outgoing states together with pion exchange. The figure demonstrates that the integration along Γ_M is numerically stable because none of the solutions p_{\pm} intersects with Γ_M , which would produce a pole in B . However, the figure also shows that one cannot simply add an on-shell point like in the previously discussed case of two stable propagating particles: Indeed, the region of real, on-shell spectator momenta, shown with the blue horizontal line, intersects with the p_{\pm} . This is not a coincidence and cannot be circumvented with a simple modification of Γ_M . Instead, it represents a genuine problem requiring nontrivial solutions discussed in the following.

2.8.1. Continuation to real momenta and triangle singularities

To discuss the problem of continuation of the three-body amplitude to real spectator momenta, consider the case of a real-valued contour $\Gamma = \{p | p \in [0, \Lambda]\}$. The solutions p_{\pm} for this case are shown to the left in Fig. 10, for the unequal-mass case. For small values of p' (inset "Physical"), the singularities lie on the real axis, but a complex integration contour starting at $p = 0$ (blue solid lines in insets) can easily avoid them. For intermediate values of p' (inset "critical" of Fig. 10), called "critical region" in Ref. [113], there is no way for an integration contour to "escape" the closed cut. For p' outside of the physical region, $p' > p_{\max}$, the cut opens again and the integration contour can avoid the three-body singularities (inset "Unphysical").

The problem of closed cut structure in the critical region can be solved by analytically continuing the B -term to the second sheet and an additional path deformation as shown in Fig. 10 to the right, for the process $KK^* \rightarrow \pi f_0$ as indicated. This method proposed by Cahill and Sloan [152, 153] was also applied recently in Ref. [154], see also Ref. [155]. The caption of Fig. 10 describes the path on first (Γ_I) and second (Γ_{II}) Riemann sheets with smooth transitions between them at P and R . In particular, the logarithmic singularity at P is exactly canceled in the chosen path which renders this method stable. Note that to perform this contour deformation, one first needs to know the solution on the interval $0 < p < P$, which is usually possible because it corresponds to values of p' below the critical region. One can then simply use a complex path as shown in the lower right inset in Fig. 10 to the left. See Ref. [113] for more detailed explanations.

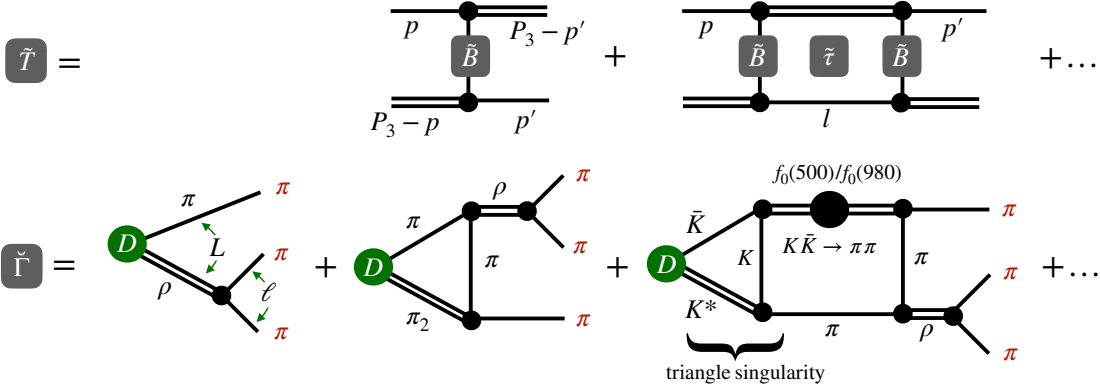


Figure 11: Upper row: The rescattering series \tilde{T} of isobars (double lines) and spectators (single lines) interacting through particle exchanges \tilde{B} , followed by propagation $\tilde{\tau}$. The amplitude $\tilde{T}(s, p', p)$ depends on the total Mandelstam $s = P_3^2$ and the incoming (outgoing) spectator momentum p (p'), while the isobar propagation depends on $\sigma = (P_3 - p)^2$, i.e., $\tilde{\tau}(\sigma(l))$ for the internal propagation shown. This series forms the final-state interaction in the production reaction $\tilde{\Gamma}(s, p')$ in the lower row. For $\tilde{\Gamma}(s, p')$, some coupled channels are indicated that contribute to a three-pion final state, as well as the orbital angular momentum L and isobar spin ℓ . Triangle singularities are naturally included in this rescattering series as indicated in an example.

However, for certain mass combinations, the lower end of the critical region, p'_{\min} , is to the left of P , located at

$$p_P = p_-(m_1, m_3, m_u, -1) \quad (2.89)$$

with p_- from Eq. (2.87), i.e., $p'_{\min} < p_P$. In Ref. [155] and in Ref. [156], a path for this case is discussed. It passes right through the point where both solutions p_\pm touch each other as shown to the right of point P in Fig. 10.

Note also the special kinematics when P coincides with the quasi-on-shell momentum p_{cm} from Eq. (2.84) of an adjacent channel (e.g., $KK^*(892)$) that contains a narrow resonance. At the corresponding \sqrt{s} , the exchanged particle, the spectator and the very narrow resonance are all on-shell, leading to a “triangle singularity”. Unitarized triangle singularities have been investigated in Ref. [157], see also references therein for further information on this kinematic phenomenon. Sakthivasan et al. [157] also compare the Cahill and Sloan method with a direct extrapolation of the amplitude at complex momenta to the real ones through continued fractions. We summarize the findings in Sect. 4.3.

2.8.2. Production reactions and “direct inversion”

The method by Cahill and Sloan discussed in the previous section is stable and computationally inexpensive. However, in the form presented here it only allows for continuation to real momenta of one of the two momenta of T for $3 \rightarrow 3$ scattering (either incoming or outgoing). It can still be used in the phenomenologically relevant $2 \rightarrow 3$ kinematics of the reaction πN to $\pi\pi N$, though. It can also be used in production reactions in which T provides the final-state interaction. The production reaction is referred to as $\tilde{\Gamma}$ as shown in Fig. 11. It is obtained by multiplying the “amputated” production reaction $\tilde{\Gamma}^T$ with the propagator of the final isobar $\tilde{\tau}$ and its decay \check{v}_j [113], with sums over identical channel indices implied,

$$\check{\Gamma}_j(s, p') = \check{v}_j(\sigma(p')) \tilde{\tau}_{jk}(\sigma(p')) [\tilde{\Gamma}_k(s, p') + D_k(s, p')] =: \check{v}_j(\sigma(p')) \tilde{\tau}_{jk}(\sigma(p')) \tilde{\Gamma}_k^T(s, p') \quad (2.90)$$

with a new quantity $\tilde{\Gamma}^T$ consisting of a “disconnected” part $\check{v}\tilde{\tau}D$ and the rescattering part $\tilde{\Gamma}$. The latter fulfills

$$\tilde{\Gamma}_j^T(s, p') = D_j(s, p') + \int_0^\Lambda \frac{dq q^2}{(2\pi)^3 2E_q} \tilde{B}_{ji}(s, p', q) \tilde{\tau}_{ik}(\sigma(q)) \tilde{\Gamma}_k^T(s, q) \quad (2.91)$$

for channels i, j, k , outgoing spectator momenta p' , and exchange process \tilde{B} similar to the expression given in Eq. (2.81). For simplicity, contact terms are chosen $C = 0$ in Ref. [113]. For the “tilde” notation and further details see Sect. 4.2. Note also the appearance of a second index in τ owing to the possibility of sub-channel transitions in the isobar itself, e.g., $\pi\pi \leftrightarrow K\bar{K}$ as illustrated in Fig. 11 to the lower right.

One disadvantage of the contour deformation method by Cahill and Sloan is the dependence of the contour on the spectator masses (e.g., the position of point P) which can become complicated in the multichannel case with unequal masses (although this problem was solved in Ref. [157]).

An alternative method is discussed in Ref. [153], based on the original reference [158]. We refer to it as direct inversion (DI) as compared to the contour deformation method (CD) discussed before. Its advantage is the independence from

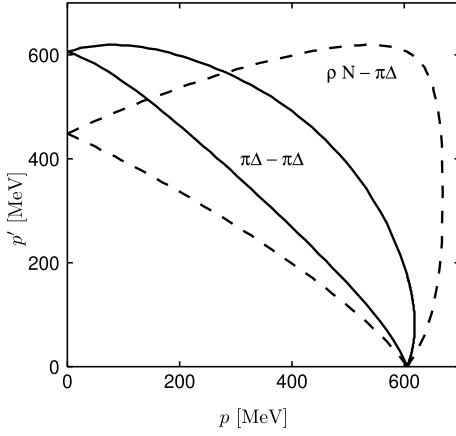


Figure 12: Logarithmically divergent regions of the matrix elements of $Z(p', p; E)$ for the $\pi\Delta - \pi\Delta$ and $\rho N - \pi\Delta$ transitions shown in Fig. 4.

channel masses. The main idea is that the solution $\tilde{\Gamma}^T$ is suitably discretized in q by a finite set of real $q_i \in [0, \Lambda]$, which can be well approximated by an interpolating polynomial connecting the discrete $\tilde{\Gamma}^T(q_i)$ (channel index and index s omitted),

$$\tilde{\Gamma}^T(q) \approx \sum_{i=1}^N \tilde{\Gamma}^T(q_i) H_i(q) , \quad (2.92)$$

using a set of interpolating polynomials H_i , e.g., Lagrange polynomials. Inserting this Ansatz into Eq. (2.91) immediately yields that the integral equation decouples into an algebraic equation, with the complicated three-body cut structure moved to integrals. The latter can be evaluated with standard numerical methods that are robust to the presence of logarithmic singularities.

Alternatively to the use of Lagrange polynomials, one can approximate $\tilde{\Gamma}^T$ by splines of a given order, which requires a certain care in choosing appropriate grid points [11].

In the ANL-Osaka approach, a crucial point of numerical calculation is how to choose the integration path C, C' and grid points of momentum in Eq. (2.21) and Eq. (2.25). The coupled integral equation is solved by using the matrix inversion method in momentum space. In order to calculate observables, the integration paths C and C' are chosen from zero to infinity on the real axis without any contour deformation. When only $v_{\beta,\alpha}$ in Eq. (2.22) contributes, the choice of the grid points of momentum is well known. Including the on-shell momentum of the two-body Green's function, the integrand of principal value integral is replaced by adding the subtraction term to obtain smooth momentum dependence and stabilize the numerical integration [159]. The particle exchange interaction $Z(p', p; E)$ has logarithmic singularity above the $\pi\pi N$ three-body breakup threshold. The logarithmically divergent moon-shape region is shown in Fig. 12. The imaginary part is non-zero inside the moon-shape region, which corresponds to the on-shell momentum for the two-body Green's function. The singularity depends on both p' and p , which makes it difficult to solve the integral equation. To overcome the difficulty, one writes the unknown half-off shell t-matrix in terms of an interpolation function $S_i(p)$ and chooses appropriate grid points $\{p_i\}$,

$$t_{\beta,\alpha}(p, p_0; E) = \sum_i S_i(p) t_{\beta,\alpha}(p_i, p_0; E) . \quad (2.93)$$

Then, the required integration can be carried out as precisely as necessary using the known function $S_i(p)$. Splines are chosen as interpolation functions, which depend locally on the grid points and which are known to be less oscillating compared to the polynomial interpolation. Hermitian splines are used that only have the first derivative continuous. Both the first and the second derivatives are continuous for natural splines. Furthermore, the appropriate choice of the grid points is explained in Refs. [11, 160] using the Amado model [161], as an example. As a fast numerical calculation, one can use a contour C in the complex momentum plane as will be discussed in Sect. 2.9 to calculate observables for the two-body final states.

2.9. Analytic continuation to complex energies

Resonance poles are situated at complex energies $E = \sqrt{s}$ and, in sub-channels, at complex sub-energies or invariant masses $\sqrt{\sigma}$. Phenomenologically relevant poles are the ones close to the physical axis, situated on the analytically continued amplitude in the lower \sqrt{s} half-plane. Technically, the analytic continuation to complex \sqrt{s} with negative imaginary part can be achieved, for example, by a complex contour deformation [86, 115, 142, 162, 163] of the integration

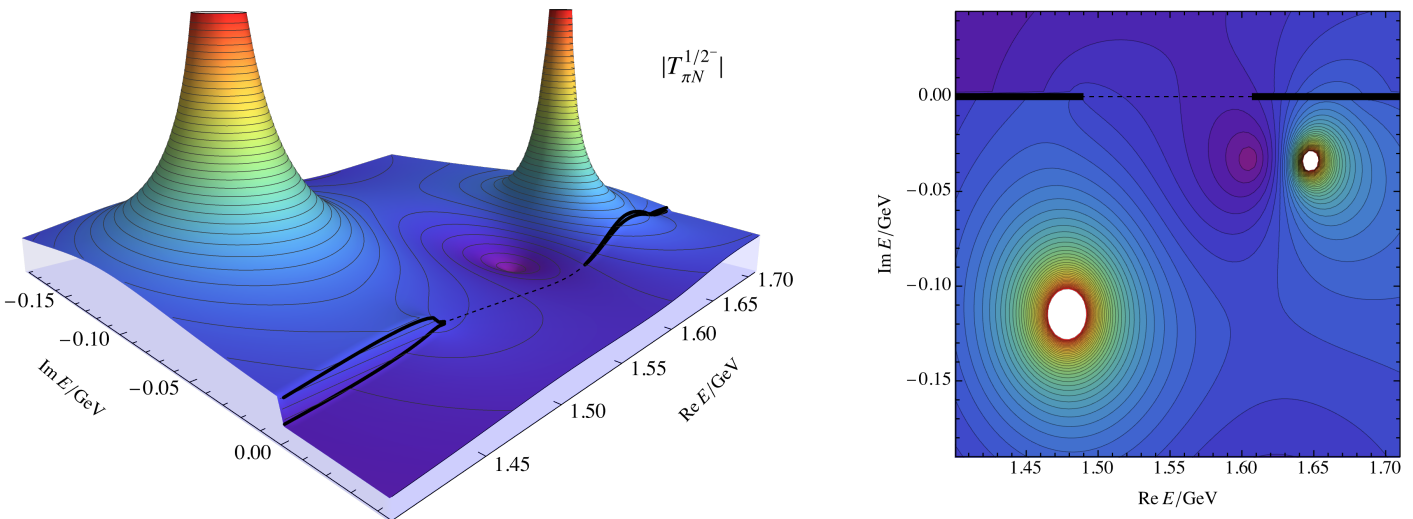


Figure 13: Example of Riemann sheets $[++++++]$ and $[- - + ++]$ with respect to $\{p\pi^0, n\pi^+, p\eta, \Lambda K^+, \Sigma^0 K^+, \Sigma^- K^0\}$ meson-baryon two-particle channels. Both Riemann sheets are connected along the real energy axis between $p\eta$ and ΛK^+ thresholds. The amplitude is taken from Ref. [39] corresponding to πN scattering for $I = 1/2$, $J^P = 1/2^-$. The poles correspond to the $N(1535)$ and a $N(1650)$ resonances.

momentum running inside the loop integrals. Mesonic resonance poles in three-body amplitudes were only extracted recently [135, 142, 164, 165], while the extraction of excited baryon resonance poles, including three-body channels, has been carried out by various groups since a long time [86, 115]. The first extraction of a mesonic resonance pole, the $a_1(1260)$, from data, with a three-body unitary amplitude, was achieved in Ref. [142], including a quantification of the noticeable effect from the inclusion of particle exchange as required by unitarity. First Lattice-QCD-based determinations of pole positions of three-body resonances have also been pioneered recently, for the $a_1(1260)$ [164] and the $\omega(782)$ [135]. For the mesonic amplitude discussed in Secs. 4.1 and 4.2, one can directly follow Ref. [142]. We summarize the main ideas of that study in the following.

2.9.1. Analytic structure of the multi-channel scattering amplitude

The analytic structure of the scattering amplitude is characterized by resonance/bound state poles and branch points. Zeros of the amplitude are related to poles [166]; their interplay in the meson-baryon sector has been illustrated in Ref. [124]. In addition, there can be triangle singularities [148, 167]. In general, each branch point is associated with one or more cuts. Some branch points and cuts exist in the plane-wave amplitude (right and left-hand cut), but some cuts arise only after partial-wave projection, like the circular cut and the short nucleon cut [118]. Resonance poles and branching ratios have been related in Ref. [168].

The multi-valuedness of the T-matrix, discussed in the previous section, leads to the concept of single-valued Riemann sheets [118] which, together, form the multi-valued Riemann surface. Any measured (experimentally or as a result of a numerical lattice calculation) values are located on the real energy-axis of the so-called physical sheet, denoted most commonly by $[+ \dots +]$ referring to $\text{Sgn}(\text{Im}(q_i(s)))$ in each two-body channel where q_i indicates the c.m. momentum in channel i according to Eq. (2.84). The physical axis in the Mandelstam variable s lies at $s + ie$ to make it clear that it is situated above the “right-hand cut”. Generalizing this notation, we denote all sheets by the same type of sequence, see, e.g., Ref. [1]. Specifically, the unphysical sheet connected to the physical one along the right-hand cut, between the first and second threshold, is denoted as $[- + \dots +]$, the one connected to the physical sheet between the second and third threshold by $[- - + \dots +]$ etc.. An example of Riemann sheets for a meson-baryon system is depicted in Fig. 13.

There is a broad $N(1535)$ pole and a narrower $N'(1650)$ pole. Note that the latter is “hidden” behind the $K\Lambda$ threshold (hence the prime notation). It is a replica of the actual $N(1650)$ resonance pole on the $[- - - + +]$ sheet (not shown). Indeed, poles often repeat on different Riemann sheets. In particular, if the pole residue to a given channel is small the pole repeats at almost the same complex energy E on the two sheets corresponding to that channel.

The example of the S_{11} partial wave is also illuminating because the other resonance in that partial wave, $N(1535)$, is located close to the ηN channel opening at $E \approx 1486$ MeV, and it couples *strongly* to that channel. This leads usually to an enhancement of threshold cusps [124] as further discussed in Sec. 3.3.6. Another example is the large cusp in the ΛN cross section at the opening of the ΣN channel which is due to the appearance of an (unstable) ΣN bound state close to the ΣN threshold [169].

The analytic structure of the P_{11} partial wave is discussed in the following to illustrate three-body aspects of the analytic structure. More phenomenological aspects of that partial wave are discussed in Sect. 3.3.7. The P_{11} wave

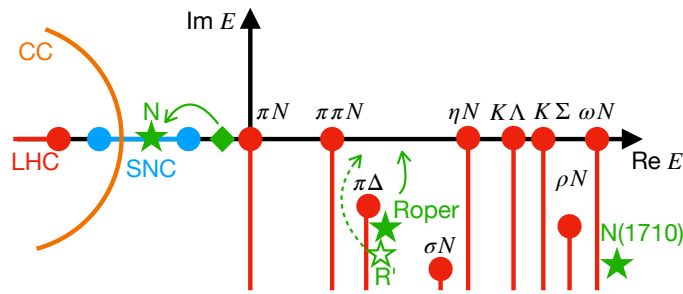


Figure 14: Analytic structure of the P_{11} partial wave, for complex scattering energies $E = \sqrt{s}$. The circular cut is labeled “CC”, the left-hand cut “LHC”. The nucleon is labeled as N . See text for further explanations.

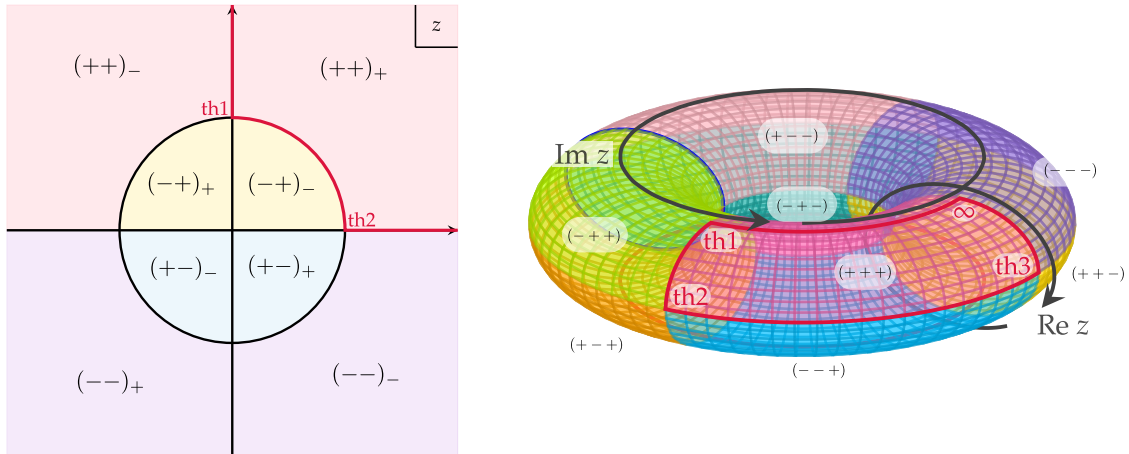


Figure 15: Left: Riemann sheet of a two-channel system in terms of the uniformization variable z . The subscript of the Riemann sheets denotes either the positive or negative complex half plane of the latter. Right: representation of a 3-channel system on a torus. The corresponding two-body thresholds are denoted by “th”.

($J^P = 1/2^+$) is particularly interesting because it hosts the nucleon as a bound state. Its analytic structure is displayed in Fig. 14. Channels of two stable particles (πN , ηN , ...) have branch points (thresholds) on the real-energy axis. Each of these two-body channels is associated with one right-hand cut. The figure also shows the $\pi\pi N$ branch points on the real axis and in the complex plane from the $\pi\Delta$, σN , and ρN channels as discussed in Sect. 2.9.3. To search for poles on the most relevant Riemann sheets, the cuts are chosen to be oriented from the threshold openings into the negative imaginary E -direction as indicated in the figure. In addition, the figure shows the sub-threshold short nucleon cut (SNC), circular cut (CC) and left-hand cut (LHC). The structure of some of these cuts and branch points is discussed in Ref. [118], see also [115].

The (green) stars indicate the positions of the physical poles. The nucleon appears as a bound state pole on the first Riemann sheet in the amplitude, right on top of the SNC. The gray cross indicates the bare nucleon pole that moves to the physical position after renormalization (see Sect. 2.6.3). There are two Roper poles on different $\pi\Delta$ sheets, labeled as $N(1440)$ and $N'(1440)$. This two-pole structure is found in several analyses, such as GWU/SAID [170], EBAC [86], and JB [53]. It is due to the fact that poles can repeat on different sheets as discussed previously for the case of the $N(1535)$ and $N(1650)$. In addition, the proximity of the complex $\pi\Delta$ branch point to the resonance poles leads to a non-standard shape of the Roper resonance that is not of the Breit-Wigner type. Another reason for the unusual shape is the strong influence of the σN channel. All three particles π , π , N are in relative S -waves for P_{11} . The absence of any centrifugal barriers then, indeed, leads to a large inelasticity at low energies, strongly distorting the Roper resonance shape. In addition, other resonances ($N(1710)1/2^+$ and $N(1750)1/2^+$) have been reported in some analyses as the figure indicates. The role of the $N(1710)1/2$ is further discussed in Sect. 3.3.7.

Recently, a model-independent approach that incorporates the resonant and threshold behavior was proposed by Morimatsu and Yamada [171]. This approach is a tool for a data driven methodology extracting the resonance information without referring to a specific model. The starting point is that one can unfold the Riemann surface choosing the appropriate variable called uniformization variable z in place of energy \sqrt{s} (in all other parts of this review, except for this subsection, z stands for \sqrt{s} according to Eq. (1.1)). For the single channel case, $z = p = \sqrt{s - \epsilon^2}/2$ with threshold

energy ϵ . For the two-channel case, the uniformization variable is given as [172, 173],

$$z = \frac{p_1 + p_2}{\Delta} , \quad (2.94)$$

where $p_i = \sqrt{s - \epsilon_i^2}/2$, $\epsilon_i = (m_i + m'_i)$ and $\Delta = \sqrt{\epsilon_2^2 - \epsilon_1^2}/2$. Fig. 15 shows the Riemann surface of the two-channel case with respect to z which represents four sheets $[++]$, $[-+]$, $[+-]$ and $[--]$. The red line corresponds to the real scattering energy \sqrt{s} and the subscript (\pm) indicates the sign of the imaginary part of \sqrt{s} . The lower(higher) threshold is at $z = i(z = 1)$.

The scattering amplitude \mathcal{A} and the S-matrix become a single-valued function of uniformization variable z . The meromorphic function can be expressed by the sum of pole terms and an entire function, which is the Mittag-Leffler(ML) expansion [174–176]. In the uniformized ML expansion approach, the scattering amplitude is expressed as

$$\mathcal{A}(z) = \sum_{n=1} \left(\frac{c_n}{z - z_n} - \frac{c_n^*}{z + z_n^*} \right). \quad (2.95)$$

Here from the symmetry property of the S-matrix, the amplitude is expressed as a sum of the pair of the poles at z_n and $-z_n^*$. The symmetry imposes the series to obey the proper threshold behaviors. The method is applied to study the pole properties of the $\Lambda(1405)$ [177] from the analysis of the invariant mass distribution of $\pi\Sigma$ in the $\gamma p \rightarrow K^+\pi\Sigma$ and K^-p cross sections. The data are well fitted as seen in Ref. [177] with three pair of poles. The central values of the poles are $z_1 = 0.524 + i0.316$ ($\sqrt{s_1} = (1.42 - i0.048)$ GeV), $z_2 = 1.640 - i1.04$ ($\sqrt{s_2} = (1.428 - i0.07)$ GeV) and $z_3 = 2.323 - 0.068i$ ($\sqrt{s_3} = 1.51 - i0.007$ GeV). The conjugate poles are at $-z_1^*, -z_2^*$ and $-z_3^*$. Pole 1 is on the $[-+]$ sheet just below the $\bar{K}N$ threshold and pole 2 and 3 are on the $[--]$ sheet. The broad peak between $\pi\Sigma$ and $\bar{K}N$ is sufficiently explained by the pair of poles 1 + 1^* .

The method is also applied to demonstrate the manifestation of S-matrix poles in the physical amplitude near an inelastic threshold [178]. The left panel of Fig. 16 shows six positions, A-F, of a pole near an inelastic two-body threshold. The right panel shows imaginary parts of the pole-pair contribution of the normalized amplitude given as

$$f(z; z_p, \phi_p) = -\frac{1}{\pi} \text{Im} \left[\frac{\exp(i\phi_p)}{z - z_p} - \frac{\exp(-i\phi_p)}{z + z_p^*} \right]. \quad (2.96)$$

The pole z_p is expressed as $z_p = r_p \exp(i\theta_p)$. The two cases of the phase of the residue, $\phi_p = \phi_0$ and $\phi_p = \phi_0 - \pi/2$ are shown. ϕ_0 is chosen as $\phi_0 = \theta_p - \pi/2$, $\text{Arg}(z_p - 1) - \pi/2$ and 0 for $[-+]$, $[+-]$ and $[--]$ sheet respectively. See Ref. [178] for details. The quantity e is a normalized energy variable given as

$$e = \frac{s - \epsilon_1^2}{\epsilon_2^2 - \epsilon_1^2}. \quad (2.97)$$

The transition of the spectrum is continuous as the pole moves from A to F crossing the boundaries of Riemann sheets when the pole position is sufficiently close to the threshold in the z plane. The pole near the inelastic threshold exists irrespective of which Riemann sheet it is on, and the amplitude shows a peak shape. Since there is no essential difference on the shape of the spectrum, for example B $[-+]_+$, C $[+-]_+$, D $[+-]_+$ and E $[--)_-$, high precision data will be needed to determine to which Riemann sheet the pole belongs. It is noticed, poles C, D with positive imaginary part of the energy are close to the upper threshold, while the conjugate poles are far from the upper threshold in z plane. The argument suggests that the peak near $\bar{D}D^*$ threshold found in the analysis of the HAL QCD [179, 180] is most likely due to the existence of pole near $\bar{D}D^*$ threshold.

The uniformization variable z itself has been used to analyze the relation between the poles and the shape of the $\Lambda-N$ cross section [181] and the movement of poles in a two-channel Breit-Wigner formula [84]. An interesting observation of Ref. [172] is that, for the two-channel case, the minimum number of the set of poles is two at z_1 and z_2 and the positions of the two poles satisfy $|z_1 z_2| = 1$. Therefore, one of the poles is inside the unit circle of z , i.e., the $[+-]$ or $[-+]$ sheet and the other pole is outside the circle on the $[--]$ sheet. One can also rewrite the Flatté formula [182] in the form of Eq. (2.95) with two pairs of poles, whose explicit form is given in [178]. In general, the use of the uniformization variable can help understand the pole movement with respect to some internal parameters of the theory such as, e.g., interaction strength or quark mass in Lattice QCD calculations, see Refs. [183–185].

Clearly, one might be intrigued to extend this approach to the three-channel case. For that case, there are eight Riemann sheets. Note that the topological structure of the Riemann surface for two channels is equivalent to that of a sphere, whereas for three-channels it is equivalent to a torus [186], see also a corresponding discussion in Ref. [1]. The explicit construction of the uniformization variable and the description of the Riemann surface is for the first time provided in Ref. [187]. It reads

$$z = \frac{1}{4K(1/\gamma^2)} \text{sn}^{-1}(\gamma, z_{12}, 1/\gamma^2). \quad (2.98)$$

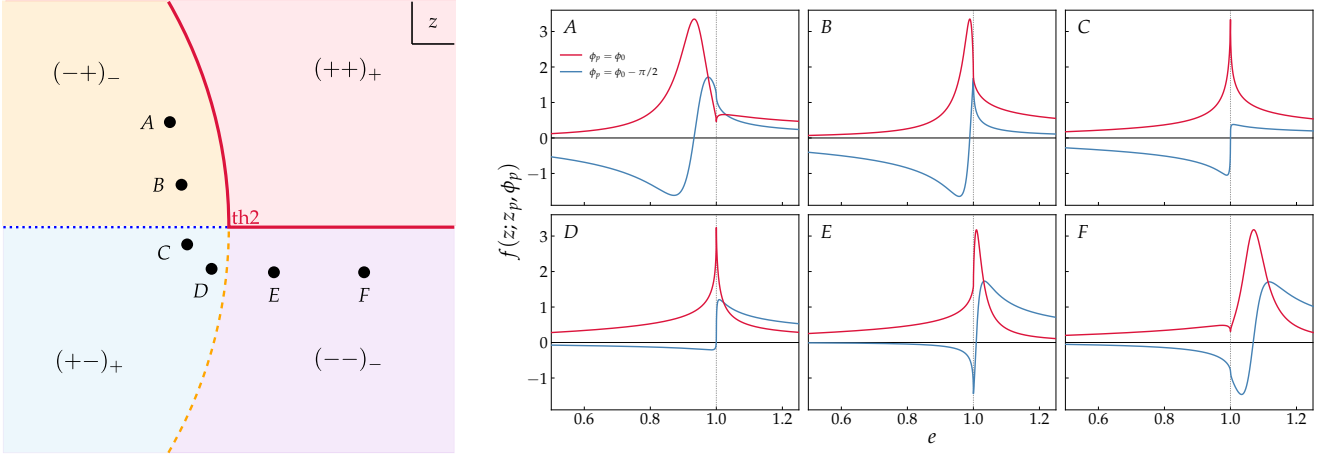


Figure 16: S-matrix pole close to the upper threshold(th2) in z plane and the shape of the spectrum. On the left, the pole positions $A \rightarrow \dots \rightarrow F$ are shown, which also includes poles (C, D) being located on the more distant $[+-]_+$ Riemann sheet. The effect of the pole on the imaginary part of the scattering amplitude for real energies (2.97) is depicted in the right panel.

Here, z_{12} is the uniformization variable of channels 1 and 2, and sn is the Jacobian elliptic function. The constants γ and K are given as

$$\gamma = \frac{\Delta_{13} + \Delta_{23}}{\Delta_{12}}, \quad K(k) = \int_0^1 \frac{ds}{\sqrt{(1-s^2)(1-k^2 s^2)}}. \quad (2.99)$$

With this uniformization variable, the ML expansion of the amplitude is given as

$$\mathcal{A}(z) = \sum_i [r_i(\zeta(z - z_i) + \zeta(z_i)) - r_i^*(\zeta(z + z_i^*) + \zeta(-z_i^*))], \quad (2.100)$$

where $\zeta(z)$ is Weierstraß's zeta function. The use of the ML expansion is demonstrated with a simple example of nonrelativistic effective field theory with contact interactions for the $0^+, \Lambda\Lambda - N\Xi - \Sigma\Sigma$ coupled-channel problem.

2.9.2. Continuation for two-body channels

As discussed, resonance poles are situated on the unphysical sheet in the lower $\sqrt{s} \in \mathbb{C}$ half plane that is analytically connected to the physical axis [148]. To find resonance poles in \sqrt{s} one cannot simply dial in complex energies because the resulting amplitude on the physical sheet has a right-hand unitarity cut along the real \sqrt{s} axis that separates the lower \sqrt{s} half plane from the physical axis at $\sqrt{s} + i\epsilon$. To illustrate this consider the integration path of Eq. (2.57) or Eq. (2.91).

For one channel of two stable particles with masses m_a and m_b , there is a two-body singularity given by Eq. (2.84) at $p = p_{\text{cm}}$ that has to be avoided in the integration. Complex paths in the lower momentum plane as shown in Fig. 9 achieve this as \sqrt{s} develops a negative imaginary part, $\sqrt{s} \rightarrow \sqrt{s'}$. Such a deformation allows to smoothly (“analytically”) continue into the lower $\sqrt{s'}$ plane onto the unphysical sheet, as long as $\text{Im } \sqrt{s}$ does not become too negative making $p_{\text{cm}}(\sqrt{s})$ cross the integration contour. This situation is shown in Fig. 17 to the left. The right-hand side of the figure illustrates an alternative: instead of deforming the path for analytic continuation, one can add the residue (given by the closed circle) to the integral of Eqs. (2.57) and proceed with a path along real momenta because the integrations along the vertical direction cancel [115]:

$$T_{\mu\nu}(E, p', p) = V_{\mu\nu}(E, p', p) + \sum_{\kappa} \int_0^{\infty} dq q^2 V_{\mu\kappa}(E, p', q) G_{\kappa}(E, q) T_{\kappa\nu}(E, q, p) + \sum_{\kappa} \delta G_{\kappa},$$

$$\delta G_{\kappa} = -\theta(E - m_{\kappa} - M_{\kappa}) V_{\mu\kappa}(E, p', q_{\text{cm}}) \frac{2\pi i q_{\text{cm}} E_{\kappa}(q_{\text{cm}}) \omega_{\kappa}(q_{\text{cm}})}{E} T_{\kappa\nu}(E, q_{\text{cm}}, p), \quad (2.101)$$

with $\text{Im } E < 0$, q_{cm} from Eq. (2.84), on-shell baryon and meson energies $E_{\kappa}(q_{\text{cm}})$, $\omega_{\kappa}(q_{\text{cm}})$, and the θ function ensuring that the continuation to the second sheet occurs only above the respective thresholds. Equivalently, one can say that this corresponds to rotating the right-hand cuts into the negative imaginary E -direction, see Fig. 14. Adding the residue is, of course, equivalent to adding the discontinuity along the real axis. In a discretized matrix scheme for the integral

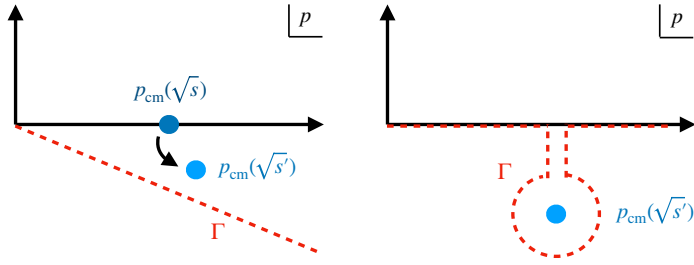


Figure 17: Left: Analytic continuation in \sqrt{s} by deforming the integration contour Γ (adapted from Ref. [142]). The figure indicates the position of the two-body singularity at p_{cm} as the energy develops a negative imaginary part, $\text{Im } \sqrt{s'} < 0$. Right: Alternatively, one can integrate along the real axis and add the residue to the integral as contributions along the vertical parts of Γ cancel (adapted from Ref. [115]).

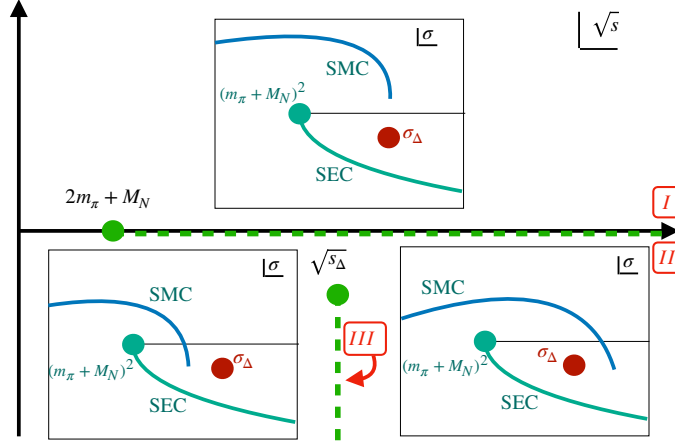


Figure 18: The inelastic cut connecting sheets I and II, and the complex branch point at $\sqrt{s_\Delta}$ inducing sheet III, for the example of the $\pi\Delta$ channel (figure adapted from Ref. [142]). Corresponding to their location in the \sqrt{s} plane, the insets show the squared sub-energy plane σ for different values of \sqrt{s} . They contain the $\Delta(1232)$ pole at σ_Δ , the rotated two-body cut (SEC), and the spectator momentum contour (SMC) that avoids the SEC. The branch point at $\sqrt{s_\Delta}$ occurs when the SMC, mapped to the σ -plane, starts at σ_Δ .

equation, the residue term can simply be added to G^I of Eq. (2.85) leading to a new second-sheet propagator,

$$G_{lk}^{II} = \begin{cases} -\frac{2\pi i q_{\text{cm}} E(q_{\text{cm}}) \omega(q_{\text{cm}}) \theta(E-m_\pi-M_N)}{E} & \text{for } l=k=n_{\text{SMC}}+1 \\ G_{lk}^I & \text{otherwise.} \end{cases} \quad (2.102)$$

The prescription of Eq. (2.101) (adapted to possible differences in the normalization of the T-matrix) is often used in chiral unitary approaches [39, 124, 183, 188], while contour deformation has the advantage that it can simultaneously work for two- and three-body channels if the path is chosen accordingly. The disadvantage of contour deformation is that the solution is only known along complex momenta on Γ ; this is less relevant when searching for resonance, but one can still add the (now complex) “on-shell” point p_{cm} of Eq. (2.84) to a discretized integration scheme as discussed at the beginning of Sect. 2.8. This is required when calculating pole residues related to branching ratios [104].

Also, for various channels with different masses, the contour deformation into the lower momentum plane allows to analytically continue the amplitude for all channels at once. In addition, it automatically ensures the continuation to the sheet closest to the physical axis in a given segment of \sqrt{s} between two thresholds (see next section).

2.9.3. Continuation for three-body channels

For three-body channels, the contour deformation method can be generalized by taking into account the additional cuts, poles, and branch points from the three-body dynamics [86, 115, 142, 162, 163]. Instead of two stable particles, there is now a stable “spectator” and a two-body sub-amplitude called “isobar” or “dimer”. That isobar may contain a resonance – in the JBW and ANL-Osaka models, that is the case for the $\pi\Delta(1232)$, $f_0(500)N$ (usually called “ $\sigma N'$ ”), and $\rho(770)N$ channels as discussed in Sect. 2.7.2. In case of mesonic amplitudes, the IVU model [113, 129, 130, 143, 189] contains the $f_0(500)$, $f_0(980)$, $\rho(770)$, $K_0^*(700)$ (“ κ ”), and $K^*(892)$ resonances (apart from non-resonant, repulsive isobars) as discussed in Sect. 4.

In the following we first discuss the continuation in the JBW approach and then in the ANL-Osaka approach, pointing out the similarities even if the variables differ. For complex energies \sqrt{s} , the SMC in the JBW approach still has to avoid

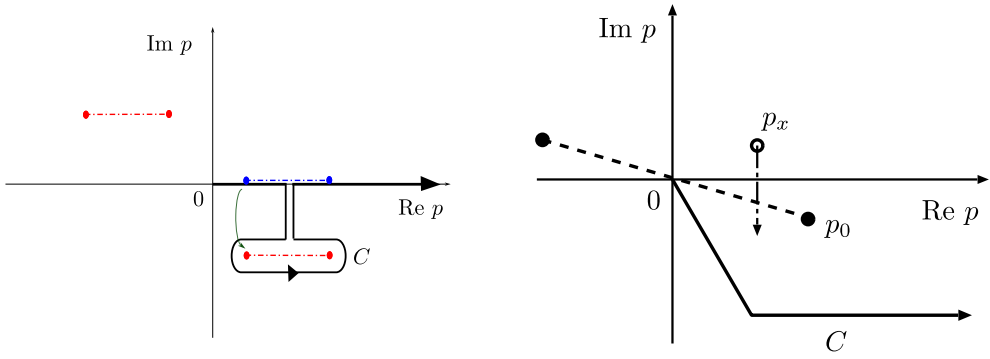


Figure 19: Integration contour C . Left: logarithmic singularity of $Z(p', p; E)$ for fixed p' from [196]. Right: Singularity of $G_{\pi\Delta}(p; E)$ from [85].

the three-body cuts in the exchange diagrams as shown to the right in Fig. 9 which is one constraint on its form. A new constraint arises by inspecting the sub-energy plane σ given by Eq. (2.80). The insets in Fig. 18 show the SMC in the σ plane for different \sqrt{s} according to the approximate location of the insets. The additional constraint for the SMC arises from the threshold at $m_\pi + M_N$ and the associated right-hand cut that has to be avoided. Sometimes, for example in the JBW model, resonant two-body sub-amplitudes are parametrized with s -channel propagators and self-energies [113], see Sect. 2.7.2. The latter can be evaluated with a selfenergy contour (SEC). In other instances, the isobar amplitude is expressed by the Inverse Amplitude Method [190–192] as in Refs. [129, 143], or by chiral unitary amplitudes [193, 194] or simple contact terms as in Ref. [113], that all can generate two-body resonances through the two-body unitarization. In all cases, one chooses the right-hand cut to be rotated into the lower σ half plane as shown because the SMC contour starts at a σ with negative imaginary part if \sqrt{s} has a negative imaginary part. Once both of the discussed constraints are fulfilled for the SMC, the amplitude is automatically continued from sheet I to sheet II as indicated in the figure, just as in case of two stable particles discussed before.

There are two occasions in which the SMC cannot avoid non-analyticities in the σ plane: If $\sqrt{s} = \sqrt{s_\Delta} = m_\pi + \sqrt{\sigma_\Delta}$ the SMC, mapped to the σ variable, starts at the resonance pole at σ_Δ . This induces a branch point at $\sqrt{s_\Delta}$ and an associated cut connecting the amplitude to a new Riemann sheet III as indicated in the figure. As one aims at searching for poles on the sheets most closely connected to the physical axis, one intends to rotate that cut into the negative imaginary direction as shown.

The second case occurs when the SMC starts at $\sqrt{\sigma} = m_\pi + M_N$. This induces the branch point at $\sqrt{s} = 2m_\pi + M_N$ as expected. Depending on the orbital angular momentum between isobar and spectator, L , and the decay angular momentum of the isobar, ℓ , the barrier factors at the branch points can be calculated [195].

For a more technical discussion of analytic continuation see Ref. [113]. For the JBW model an approximation to the discussed contour deformation method is taken as discussed in Ref. [115]. In short, the amplitude on the unphysical sheet II is evaluated by adding the discontinuity along the righthand cut to sheet I (with the naming as shown in Fig. 18), just as it can be done for the case of two stable particles discussed in Sect. 2.9.2. The approximation consists in replacing the momentum-dependent nature of this process (for three-body channels) by choosing approximate on-shell momenta assuming the σ , ρ and Δ resonances are stable. The resulting amplitude on sheet II still exhibits the full analytic structure with complex and real branch points discussed before. Ref. [115] contains also suitable prescriptions for integration paths to continue to sheet III. In practical terms the poles are searched in the upper \sqrt{s} planes on the corresponding sheet which is equivalent due to Schwartz' reflection principle [115].

In the ANL-Osaka model, all the right hand cuts in Fig. 14 are parallel to the real axis. Analytic continuation of the T-matrix to the unphysical sheet is performed by deforming the integral contour. For stable meson-baryon (MB) channels such as $\pi N, \eta N, KY$, only the potential $v_{\beta,\alpha}(p', p)$ contributes. For the T-matrix on unphysical sheet, the integration contour C in Eq. (2.21) is deformed so that the on-shell momentum does not cross C in a similar way to the left panel of Fig. 17. For unstable MB such as $\pi\Delta, \rho N, \sigma N$, the contour C is chosen by taking into account the $\pi\pi N$ discontinuity of $Z(p', p; E)$ [196, 197] and the singularity of the MB Green's function (2.24) [85]. For real energy E , $Z(p', p; E)$ develops a logarithmic singularity along the real p axis for fixed p' as illustrated with the blue dotted line in the left panel of Fig. 19. For E with negative imaginary part, the singularity moves and becomes the red dotted line, and one can access the T-matrix of the nearest Riemann sheet across the $\pi\pi N$ cut by deforming the contour as C , similar to the stable MB case. Since p' is also varying on C , the allowed path C is similar to the one in right panel of Fig. 9. One has to also take into account the singularity of the Green's function. As an example, $G_{\pi\Delta}(p; E)$ has a pole corresponding "on-shell" momentum p_x (right panel of Fig. 19) given as

$$E - \omega_\pi(p_x) - E_\Delta(p_x) - \Sigma_\Delta(p_x, E) = 0 . \quad (2.103)$$

In the JBW approach, p_x corresponds to the Δ -pole in the σ variable at σ_Δ , discussed above. The Green's function also has a discontinuity associated with $\pi\pi N$ through the self-energy indicated with the dashed line in the right panel of Fig. 19, that has to be avoided by the contour. Note that the integration contour C' of Eq. (2.25) has to be deformed [85]. In the JBW approach, the self-energy contour (SEC) is similarly deformed as indicated in Fig. 18. For unstable MB, the contour C is determined by the singularity of $Z(p', p; E)$ and $G_{MB}(p; E)$ simultaneously.

2.10. Related approaches and aspects

The challenge to construct coupled-channel scattering amplitudes from general properties of the scattering S-matrix has received much interest in recent years as reviewed, e.g., by Oller [198], JPAC [199] and, and Mai et al. [1]. In the following we discuss a particular approaches related to the previously introduced DCC models and point out similarities and differences.

2.10.1. The Bethe-Salpeter equation in coupled channels

We start the discussion with the general Bethe-Salpeter equation (BSE) from which most DCC approaches arise through different schemes for three-dimensional reductions as discussed in Sec. 2.7.1.

In the following we sketch a coupled-channel, chiral unitary formalism (UCHPT) which is related to DCC approaches but relies on chiral Lagrangians and is *not* reduced to three dimensions. Various versions of UCHPT formalisms exist which differ in the form and iteration prescription of the chiral potential, for a review see [200]. Here we demonstrate the methodology [38, 39, 201] which is most closely related to an expansion in Feynman diagrams allowing, e.g., for extensions of the approach to manifestly gauge-invariant photoproduction amplitudes [38, 42, 202].

The formalism relies on the fully covariant BSE [203]. We denote the in- and outgoing meson momenta by q_1 and q_2 , and the overall four-momentum by $p = q_1 + p_1 = q_2 + p_2$, where p_1 and p_2 are the momenta of in- and out-going baryon, respectively. For the meson-baryon scattering amplitude $T(\not{q}_2, \not{q}_1; p)$ and chiral kernel $V(\not{q}_2, \not{q}_1; p)$ the integral equation to solve reads

$$T(\not{q}_2, \not{q}_1; p) = V(\not{q}_2, \not{q}_1; p) + i \int \frac{d^d l}{(2\pi)^d} V(\not{q}_2, \not{l}; p) S(\not{p} - \not{l}) \Delta(l) T(\not{l}, \not{q}_1; p), \quad (2.104)$$

where S and Δ represent the baryon (of mass m) and the meson (of mass M) propagator respectively, that are given by $iS(\not{p}) = i/(\not{p} - m + i\epsilon)$ and $i\Delta(k) = i/(k^2 - M^2 + i\epsilon)$. Note that, in contrast to the rest of this review and more in line with baryon CHPT, baryon (mesons) masses are indicated with lowercase m (capitalized M) in this subsection. The suppressed channel indices in the above formulas include all relevant (meson-baryon) coupled channels, such that T , V , S and Δ are matrices in channel space. For strangeness $S = 0$ and electric charge $Q = +1$ one is left with the following channels: $\{p\pi^0, n\pi^+, p\eta, \Lambda K^+, \Sigma^0 K^+, \Sigma^+ K^0\}$.

The interaction kernel to be iterated in Eq. (2.104) includes only the contact-term contributions from leading and next to leading order (NLO) chiral Lagrangians. Baryon exchange diagrams (Born terms) are omitted in this approach for technical reasons. Clearly, this is a limitation of the approach, rooted in the fact that Born terms are required by three-body unitarity, see Sect. 2.7.1. Still, this procedure provides the only way to treat chiral NLO corrections in the covariant BSE, without making use of the on-shell approximation or S -wave projection of the chiral potential, so that also a P -wave can be iterated. Separating the momentum space from channel space structures the chiral potential considered here takes the form:

$$V(\not{q}_2, \not{q}_1; p) = \underbrace{A_{WT}(q_1 + q_2)}_{\text{leading order CHPT}} + \underbrace{A_{14}(q_1 \cdot q_2) + A_{57}[q_1, q_2] + A_M(q_1 \cdot q_2) + A_{811}(\not{q}_2(q_1 \cdot p) + \not{q}_1(q_2 \cdot p))}_{\text{next-to-leading order CHPT (local terms)}}, \quad (2.105)$$

where the first matrix (A_{WT}) only depends on the meson decay constants F_π , F_K , F_η , whereas A_{14} , A_{57} , A_{811} and A_M also depend on the NLO low-energy constants as specified in the appendix of Refs. [42, 202]. The loop diagrams appearing in the BSE Eq. (2.104) are in general divergent and require renormalization. In case of a strict chiral perturbation expansion, the terms can be renormalized in a quite straightforward way, order by order, including, at a given order, all the counterterms absorbing the loop divergencies. On the other hand, the treatment of the divergencies of the BSE is known to be a complicated issue, see, e.g., Refs. [38, 204] which is why here the loops are regularized by treating the regularization scale as a fitting parameter.

Finally, to solve the BSE one embraces the fact that the invariant Dirac-structures of Eq. (2.105) induce a closed set (under iterations) of Dirac-structures. Thus, the iteration through the BSE can be solved exactly embedding the T-matrix in the latter space as

$$T(\not{q}_2, \not{q}_1; p) = \sum_{i=1}^{20} \mathbf{x}_i \cdot \mathbf{T}_i, \quad V(\not{q}_2, \not{q}_1; p) = \sum_{i=1}^{20} \mathbf{x}_i \cdot \mathbf{V}_i, \quad (2.106)$$

where the coefficients T_i and V_i are 6×6 matrices in channel space, which only depend on the c.m. energy \sqrt{s} after fixing the low-energy constants, and $\aleph := (\psi_1, \psi\psi_1, \psi_2\psi\psi_1, \psi_2\psi_1, \psi\psi_1(q_2 \cdot p), \psi_1(q_2 \cdot p), \psi_2(q_1 \cdot p), \psi_2\psi_1, (q_1 \cdot p)(q_2 \cdot p), \psi(q_1 \cdot p)(q_2 \cdot p), (q_1 \cdot p), \psi(q_1 \cdot p), (q_2 \cdot q_1), \psi\psi_2, \psi_2, \psi(q_2 \cdot p), (q_2 \cdot p), \mathbf{1}, \psi)$ is a vector in the 20-dimensional space of invariant structures. Note that the scalar products are listed here as independent structures because we include the full off-shell dependence of the chiral potential in the BSE, which prevents us from writing them as simple functions of the Mandelstam variables s and t . Reinserting now the latter decomposition into the BSE (2.104) and collecting all $T_i(s)$ on the r.h.s. one obtains the following expression

$$\sum_{i=1}^{20} V_i \aleph_i(q_2, q_1; p) = \sum_{i=1}^{20} \left(\aleph_i(q_2, q_1; p) - \sum_{j=1}^{20} V_j \left(i \int \frac{d^d l}{(2\pi)^d} \frac{\aleph_j(q_2, l; p)(\psi - l + m)}{(l^2 - M^2 + i\epsilon)((p-l)^2 - m^2 + i\epsilon)} \right) \right) T_i(s), \quad (2.107)$$

where V is expressed as coefficients of the vector elements of \aleph . The term in the inner parentheses has the crucial property that, due to Lorentz invariance, it is also an element of the Dirac-momentum subspace spanned by the elements of the vector \aleph ,

$$\forall_{a \in \aleph(q_2, l; p), b \in \aleph(l, q_1; p)} : \exists_{C \in \mathbb{C}^{20}} \quad \int \frac{d^d l}{(2\pi)^d} \frac{a(\psi - l + m)b}{((p-l)^2 - m^2)(l^2 - M^2)} = \sum_{k=1}^{20} C_k \aleph_k(q_2, q_1; p). \quad (2.108)$$

The coefficients C_i are here complex-valued functions of scalar quantities only, i.e., s, M, m and scalar loop integrals determined utilizing Passarino-Veltman reduction. Consequently, the r.h.s. of Eq. (2.107) can be rewritten as

$$\sum_{i=1}^{20} V_i \aleph_i(q_2, q_1; p) = \sum_{i=1}^{20} \sum_{j=1}^{20} \left(\delta_{ij} - \tilde{C}_{ij} \right) T_j(s) \aleph_i(q_2, q_1; p),$$

where the coefficients \tilde{C}_{ij} are matrices in channel space, obtained from Eq. (2.108) replacing $a = V$ and $b = \aleph_i$. In fact, the latter expression is a system of 20 coupled linear equations which we can rewrite in an even more elegant way as

$$\mathbf{X}_i^j T_j(s) = V_i, \quad (2.109)$$

where we have utilized the Einstein summation convention for $i, j \in [1, 20]$ and $\mathbf{X} \in Mat^{20 \times 20}$, whereas each element is a complex valued channel space matrix defined by $\mathbf{X}_{ij} = (\delta_{ij} - \tilde{C}_{ij})$.

If one is interested in scattering quantities, one can solve equation (2.109) for all 20 structures reducing them in the final step to two on-shell structures $\{\psi, \mathbf{1}\}$, c.f., Eq. (2.52), ultimately reducing to partial-wave amplitudes etc. [42]. In Sect. 3.3.6 we discuss such an application.

2.10.2. Statistical aspects and machine learning tools

The interpretation of near-threshold enhancement phenomena is one of the central issues of resonance searches. Common procedures, sometimes referred to as top-to-bottom approaches, start from a model such as UCHPT, or DCC which include symmetry assumptions. Then, comparing the model to the data or fitting free parameters and performing analytic continuation to complex energies, resonance parameters are extracted, see Sect. 2.9.1 or Ref. [205] for an introductory and historical review. Alternatively, one can ask if observed line shapes actually encode some information about the nature of the enhancement inducing resonances as, e.g., virtual, resonance, or bound states. Recently, there has been notable progress in this direction, sometimes referred to as bottom-to-top approaches, often relying on the development of machine learning tools. The general workflow is that minimal assumptions are made for the form of the amplitude producing a large set of synthetic data, being variations of line shapes with known resonance pole class, training a neural network. A trained network can recognize pattern in the line shapes associated with the pole category. It is then applied to the real experimental data providing probabilities for the presence of a resonance, bound states, etc..

A program utilizing deep neural networks (DNN) was carried out in Ref. [206]. There, a deep feed-forward neural network (for a schematic representation of the latter see Fig. 20) in classifying objects was utilized and shown to have high level of accuracy ($> 90\%$) which however can drop with sizable background effects. DNN were also explored by JPAC [208]. In this proof of concept study, a neural network was trained on a synthetic data set containing 10^5 line shapes produced with a generic form of an amplitude for $J/\psi - p$ scattering. Each of these line shapes was labeled by the characteristics of the pole being a virtual or bound state, and the corresponding Riemann sheets. Through this (including the necessary validation procedures), the DNN learned how the nature of the state is related to the details of the pertinent line shape. Applying this so-called DNN classifier to the experimental data one can, indeed, obtain a probability for the nature of the state as favored by the data. This was done for the LHCb data for the $P_c(4312)$ signal, leading to a virtual state interpretation favored also by the previous traditional amplitude study [209]. Studies of coupled-channel effects within DNN-type approaches can be found in Refs. [210], see also Refs. [211–213] for further

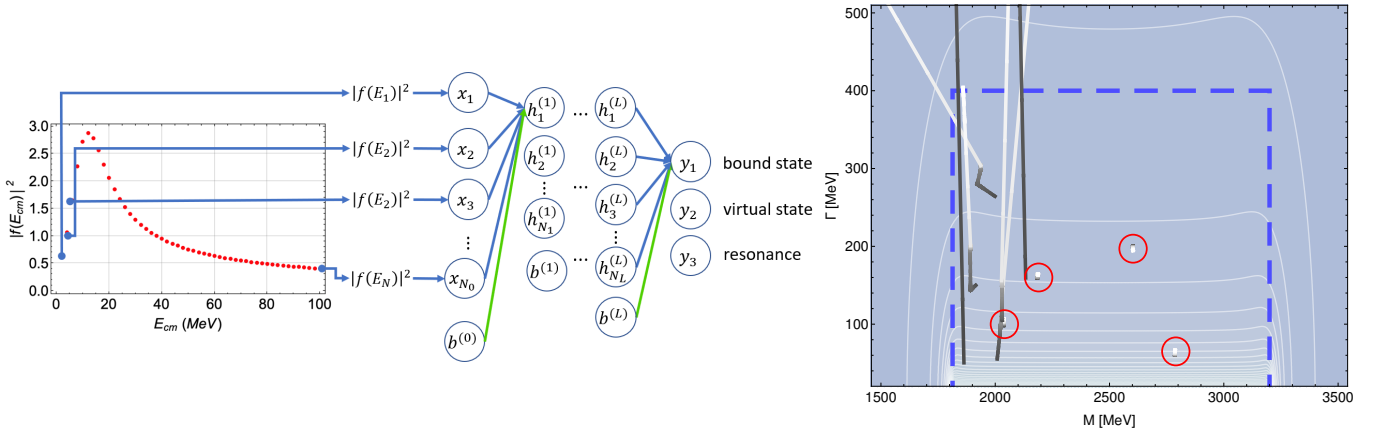


Figure 20: **Left:** Schematic picture of a deep neural network for S-matrix pole classification. Figure adapted from Ref. [206]. **Right:** Resonance trajectories (thick solid lines) in the M/Γ -plane as function of the penalty parameter λ penalizing an over-structured amplitude. The very short trajectories of significant resonances are highlighted by red circles. Some extra resonances are initially present in the chosen mass/width window, describing insignificant fluctuations leading to an improved χ^2 . Once the penalty is increased, the spurious resonances are pushed far into the complex plane, as the long trajectories show, while the data description does not suffer significantly. Figure adapted from Ref. [207].

applications and Ref. [214] for an example of how detector effects can be removed from the identification of multi-particle final states. Related approaches [215, 216] aim at distinguishing kinematic triangle singularities (see Sect. 2.8.1) from genuine resonance effects. For related reviews see Refs. [199, 217].

In the context of spectroscopy, there are various “blindfolded” ways to test new resonances, without the need of manual intervention. These methods are robust in the sense that they allow for a relative model comparison even if the overall χ^2 is not excellent. Bayesian inference to determine the resonance spectrum was introduced into baryon spectroscopy by the Ghent group [218, 219]. In a related context, the necessary precision of data to discriminate models was determined in Ref. [220]. Another method for the partial-wave analysis of mesonic systems was presented in Ref. [221], see also Ref. [222]. The Least Absolute Shrinkage and Selection Operator (LASSO) allows one to generate a series of models with varying partial-wave content, for an application at COMPASS, see Ref. [223]. Ideally, LASSO tests all combinations of partial waves for all numbers of partial waves. Realistically, this is not achieved as fits are usually nonlinear, have different local minima etc. The non-convexity of the problem tied to this has been recently addressed in Ref. [224] in connection with ways to make pole searches in partial waves more efficient. The best model among all the ones generated by LASSO can then be selected in an additional step through cross validation or various criteria from information theory (BIC, AIC, ...) [225, 226].

Specifically, in Ref. [207] the procedure was applied to the $\bar{K}N \rightarrow K\Xi$ world data base, including polarized and unpolarized differential cross sections, to determine the minimally needed set of resonances to describe the data. For photoproduction data in Ref. [227], minimal models compatible with data were automatically identified with the same technique, minimizing the number of significant partial waves and the number of parameters within the nonzero waves. The basic idea is to provide a very flexible model based on general properties of scattering theory allowing for a very large number of resonances, but penalizing overfitting data fluctuations through unphysical resonances. Several scenarios are also tested on synthetic data providing more certainty in these novel techniques. As an example, in one of the approaches [207] the penalty procedure smoothly “pushed” the resonances not necessarily demanded by the data, out of the relevant mass/width window as depicted in the right panel of Fig. 20. Related forms of penalty functions are utilized in Refs. [228, 229] in combination with LASSO, Ridge regression and other methods for kaon photoproduction reactions. In Ref. [230] Genetic Algorithms (evolution inspired update framework) are applied within a realistic Lagrangian model of the pion photoproduction reaction. This may, indeed, have an advantage over traditional χ^2 minimization methodology when multiple local minima are present.

On a more general footing, machine learning tools aim at replacing microscopic models by data driven methods extracting some fundamental characteristics of underlying dynamics. Clearly, this procedure is very much sensitive to the quality and quantity of data, and it suffers under possible systematic uncertainties in the data. An example of possible pitfalls is given in Ref. [231] using kaon photoproduction data with a Λ -baryon in the final state. In this regard, the famous d’Agostini bias is worth mentioning, which systematically favors smaller model values when a normalization error in the experimental data is implemented in the naive way [232]. See also Ref. [233] in which a way is discussed to avoid bias when fitting multiple normalization constants from different experiments.

As a forward-looking perspective for necessary development we emphasize that besides controlled systematics –such as choice of architecture– a major challenge is the question of how to include symmetries in machine learning approaches. The use of observed symmetries is, indeed, what helped particle physics to achieve a high level of predictability in the first place. In DCC models this is addressed through implementation of phenomenological Lagrangians. In some idealized physics

problems neural networks can indeed learn symmetries by themselves [234, 235]. Still the question is how to implement this in a more data-sparse, realistic scenario for the example of meson-photoproduction off the nucleon discussed in this review. Perhaps one practical approach is to “bake-in” the symmetries directly into the architecture [236, 237] possibly by utilizing existing techniques of DCC models.

2.11. Finite-volume extensions

2.11.1. Two-body quantization condition and Lüscher formula

Lattice QCD provides information about the spectrum, structure, and interactions of hadrons as they emerge from quark-gluon dynamics. This numerical approach relies on Monte-Carlo sampling of correlation functions on Euclidean space-time evaluated in a finite (space-time) volume. Due to this, real-time observables such as scattering amplitudes cannot be accessed directly. Instead, as pioneered by Lüscher for two-body systems [238–240], the dependence of energy eigenvalues on the volume size can be used to single out dynamics of the system for not too small volumes. In this section, we briefly motivate the Lüscher method suitable for two-body systems and discuss how it is related to DCC approaches. Then we show the connection between DCC models and the Finite-Volume Unitarity (FVU) approach for three-body systems. For specialized reviews on the topic see Refs. [1, 6, 241, 242].

Lattice QCD calculations are performed in a finite volume because of the finiteness of computational resources. This necessitates the need for boundary conditions, for simplicity most frequently periodic boundary conditions are chosen equating wave functions $\psi(x) = \psi(x + L)$ in each space dimension. The system, therefore, exhibits a discrete set of real energy eigenvalues. An equation which maps the latter to complex-valued infinite-volume scattering amplitudes is referred to as *quantization condition*.

To illustrate this in an example of two-to-two scattering, we follow the simplified derivation of Ref. [243]. Consider two stable scalar particles interacting through some potential V projected to the S -wave. Suppressing for the following discussion the momentum dependence of the potential, $V = V(E^2)$, the scattering amplitude can be obtained as a solution of the scattering equation,

$$T = V + VGT = \frac{1}{V^{-1} - G} \quad \text{for} \quad G = \int_{|\mathbf{q}| < q_{\max}} \frac{d^3\mathbf{q}}{(2\pi)^3} \frac{1}{2\omega_1(\mathbf{q})\omega_2(\mathbf{q})} \frac{\omega_1(\mathbf{q}) + \omega_2(\mathbf{q})}{E^2 - (\omega_1(\mathbf{q}) + \omega_2(\mathbf{q}))^2 + i\epsilon}, \quad (2.110)$$

for total energy E and particle masses m_1, m_2 with corresponding energies $\omega_{1,2}(\mathbf{q}) = \sqrt{m_{1,2}^2 + \mathbf{q}^2}$. Here the two-particle loop integral is regularized with some sharp cutoff q_{\max} . We note that the loop function G is a relativistic form of the integral over the non-relativistic Green’s function $1/(E - H_0)$ and thus $T \sim 1/(E - H)$. The imaginary part of the loop function is given by $\text{Im } G = -q_{\text{cm}}/(8\pi\sqrt{s})$ with q_{cm} from Eq. (2.84). This amplitude fulfills two-body unitarity and can be written in terms of the phase-shift as

$$T = \frac{-8\pi E}{q_{\text{cm}} \cot \delta - iq_{\text{cm}}} \quad \text{for} \quad q_{\text{cm}} \cot \delta = -8\pi E(V^{-1} - \text{Re } G). \quad (2.111)$$

Consider now the same system in a finite volume or, more specifically, a 3-dimensional cube with side length L with periodic boundary conditions. In that system momenta become discretized, i.e., $\mathbf{q} \in \mathbb{R}^3 \rightarrow \mathbf{q} \in \mathfrak{X}_L := \{(2\pi/L)\mathbf{n} | \mathbf{n} \in \mathbb{Z}^3\}$ such that the loop function in Eq. (2.110) becomes

$$G \rightarrow \tilde{G} = \frac{1}{L^3} \sum_{\mathbf{q} \in \mathfrak{X}_L} \frac{1}{2\omega_1(\mathbf{q})\omega_2(\mathbf{q})} \frac{\omega_1(\mathbf{q}) + \omega_2(\mathbf{q})}{E^2 - (\omega_1(\mathbf{q}) + \omega_2(\mathbf{q}))^2}. \quad (2.112)$$

Note that \tilde{G} is a real but singular function, with poles emerging whenever the on-shell condition $E = \omega_1(\mathbf{q}) + \omega_2(\mathbf{q})$ is fulfilled for any $\mathbf{q} \in \mathfrak{X}_L$. Furthermore, the above equation explicitly provides the volume dependence of \tilde{G} . In contrast to the Green’s function G , the interaction V does not contain any configurations in which the two-particle system is on-shell, i.e., $V \in \mathbb{R}$ in the physical region. In fact, this is a prerequisite for two-body unitarity. Therefore, the infinite-volume interaction equals the finite-volume interaction, $V \approx \tilde{V}$ up to small contributions. One can think of V containing, e.g., tadpole loops for which the integration is replaced by a summation in finite volume, or t -channel exchange of off-shell particles. In contrast to G , these off-shell terms do not exhibit poles in the physical region; the sum that replaces the integral, therefore, approximates the integral well. The differences are *exponentially suppressed* according to the regular summation theorem, $\sim e^{-ML}$ where M is the characteristic energy scale of the problem, e.g., the pion mass.

With this information we can use the finite-volume loop function \tilde{G} to define a finite-volume quantity \tilde{T}

$$T \rightarrow \tilde{T} = \frac{-8\pi E}{q_{\text{cm}} \cot \delta - (-8\pi E)G_L} \quad \text{with} \quad G_L = \tilde{G} - \text{Re } G, \quad (2.113)$$

with a real-valued, volume-dependent function G_L . Just like in the infinite volume, the discrete energy eigenstates $\{E_L\}$ of the Hamiltonian correspond to poles of $\tilde{T} \sim 1/(E - H)$ except for the modified boundary conditions. Consequently, for an energy eigenvalue E^* the phase shift at this energy is obtained as

$$q_{\text{cm}}(E^*) \cot \delta(E^*) = (-8\pi E^*) G_L(E^*) \quad \text{for } E^* \in \{E_L\} \quad (2.114)$$

\uparrow
Experiment
Effective Field Theories
 \dots

\downarrow
lattice QCD

and $\hat{q} = q_{\text{cm}}(E^*)L/(2\pi)$. It is notable that the right-hand side is proportional to the Lüscher zeta-function \mathcal{Z}_{00} up to regular and, thus, exponentially suppressed terms e^{-ML} ,

$$(-8\pi E^*) G_L(E^*) = \frac{2}{\sqrt{\pi}L} \mathcal{Z}_{00}(1, \hat{q}^2) + \mathcal{O}(e^{-ML}), \quad (2.115)$$

see Refs. [243, 244] for an explicit derivation. The quantization condition (2.114) allows one to either predict the finite volume spectrum provided knowledge of the phase shift (e.g., from experiment or an effective theory), or, given a set of eigenenergies $\{E_L\}$ determined by lattice QCD, to calculate a set of phase shifts at these energies as schematically indicated by the arrows in Eq. (2.114). Note that there is no ultraviolet divergence for G_L as $q_{\text{max}} \rightarrow \infty$. If one operates with an explicit cutoff regularization the integrand/summand is usually smoothed to make the cutoff effect exponentially suppressed with the volume [243].

The present discussion skips the special role of the angular momenta leading in the finite volume to the decomposition into irreducible representations of the cubic group, and we also skip extensions to multichannel systems. For more details on this we refer the reader to Refs. [243, 245–252]. The key takeaway point of the above discussion is, however, that unitarity identifies all on-shell configurations of two particles which then allows one to single out volume independent terms connecting quantities accessible on the lattice and the infinite volume/experiment. This methodology is also at the core of the FVU approach in deriving the three-body quantization condition proposed in Ref. [253] and described in Sect. 2.11.3.

2.11.2. DCC approaches for two-body systems in finite volume

Before turning to three-body systems we summarize the findings of Ref. [254] on DCC approaches in the finite volume. This is closely related to the previous introductory discussion in that it also relies on explicit two-body unitarity. In addition, we discuss different boundary conditions and higher angular momentum potentials. Starting with the partial-wave projected DCC equation in the meson-baryon normalization (2.57) and replacing the integral with a sum as in Eq. (2.112), one obtains the scattering equation in discretized momentum space,

$$T^{(\text{BC})}(E, p', p) = V(E, p', p) + \frac{2\pi^2}{L^3} \sum_{i=0}^{\infty} \vartheta^{(\text{BC})}(i) \frac{V(E, p', q_i) T^{(\text{BC})}(E, q_i, p)}{\sqrt{s} - E(q_i) - \omega(q_i)}, \quad q_i = f^{\text{BC}}(i), \quad (2.116)$$

where q_i is the distance from the origin to the i -th neighbors, called “shell”, depending on the imposed boundary conditions (BC). All quantities in this equation are real and the potential V automatically contains the correct threshold behavior due to its partial-wave projection. The $\vartheta^{(\text{BC})}$ are the BC-dependent multiplicities counting the number of lattice points on shell $i+1$. In comparison to Eq. (2.57), the integration measure is replaced as $dqq^2 \rightarrow 2\pi^2 \vartheta^{(\text{P})}(i)/L^3$ in the finite volume. For periodic (P) boundary conditions, the $\vartheta^{(\text{P})}$ series (1,6,12,...) is given by the coefficients of the Taylor expansion around $x = 0$ of the function $g^{(\text{P})}(x) = [\vartheta_3(0, x)]^3$,

$$g^{(\text{P})}(x) = \sum_{i=0}^{\infty} \vartheta^{(\text{P})}(i) x^i, \quad \text{where} \quad \vartheta_3(0, x) = \sum_{k=-\infty}^{\infty} x^{k^2}, \quad (2.117)$$

denoting the elliptic ϑ function [255]. The distance to shell i is simply $f^{\text{P}}(i) = 2\pi\sqrt{i}/L$. Another choice is given by antiperiodic (A) boundary conditions [243]. In that case, the multiplicities, $\vartheta^{(\text{A})} = 8, 24, 24, \dots$ are given by the coefficients of the Taylor expansion [cf. Eq. (2.117)] around $x = 0$ of the function $g^{(\text{A})}(x) = [\vartheta_2(0, \sqrt{x})]^3 x^{-3/8}$, where ϑ_2 is the elliptic ϑ function [255]

$$\vartheta_2(0, \sqrt{x}) = 2 x^{1/8} \sum_{k=0}^{\infty} x^{k(k+1)/2}, \quad (2.118)$$

and the distance from origin to shell i is now given as $f^{\text{A}}(i) = \frac{2\pi}{L} \sqrt{\frac{8i+3}{4}}$ with $i = 0, 1, \dots$, provided that the origin is now in the center of a momentum cell and no longer at the edge as for periodic BC.

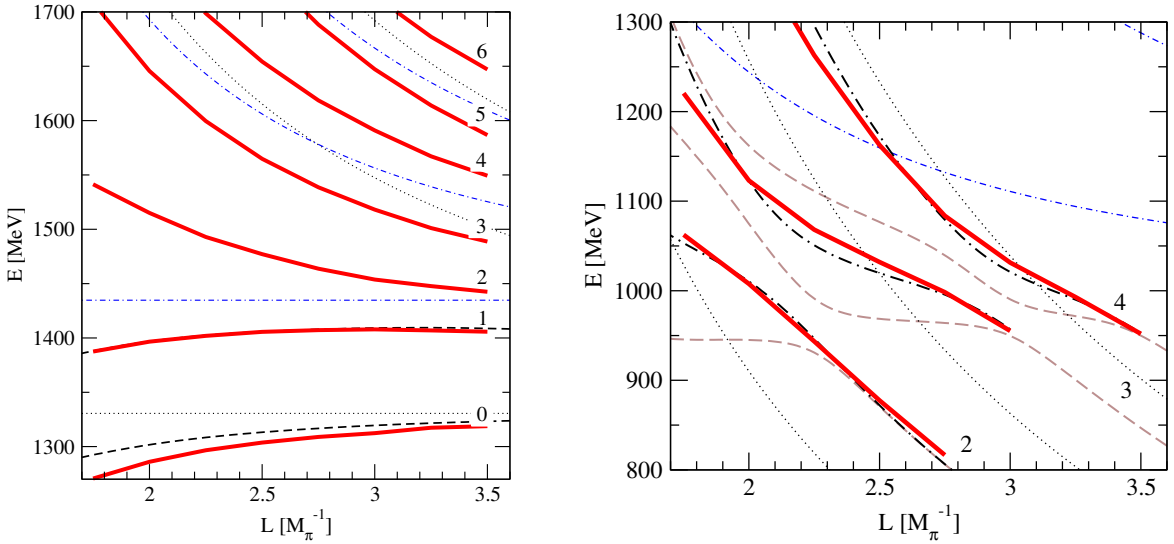


Figure 21: **Left:** Spectrum $E(L)$ of the $I = 0, S = -1, J^P = \frac{1}{2}^-$ meson-baryon sector [$\Lambda(1405)$] for periodic boundary conditions in the $G_{1u}(0)$ irrep. Solid lines: results for the $\bar{K}N$ DCC Juelich model [16, 276]. Dashed lines: For comparison, the first two levels as obtained from the chiral unitary approach of Ref. [277]. Dotted (dash-dotted) lines: free $\pi\Sigma(\bar{K}N)$ levels. **Right:** Finite-volume spectrum of the scalar-isoscalar sector with anti-periodic boundary conditions ($\theta = \pi$) in the $\bar{K}K$ channel, for the DCC model of Refs. [278, 279] (solid lines). For comparison, the result with anti-periodic boundary conditions for the chiral unitary approach of Ref. [193] is shown with thick dash-dotted lines. Also, the result with periodic boundary conditions in the A_1^+ irrep is shown (dashed lines). Dotted (thin dash-dotted) lines: free $\pi\pi$ (free anti-periodic $\bar{K}K$) levels.

Comparing Eq. (2.116) and Eq. (2.113) we note that the former allows for explicit momentum dependence in V while the latter does not, rendering the scattering equation algebraic. In fact, if V is derived from a Langrangian, its momentum is replaced by the on-shell momentum, $p \rightarrow p_{\text{cm}}$ for this purpose. We conclude that this replacement of putting momenta on-shell changes both the amplitude in the infinite volume and the energy spectrum in the finite volume. However, the difference between both formalisms, when it comes to mapping between finite and infinite volume, is exponentially suppressed as the approaches coincide on-shell. As exponentially suppressed contributions are model-dependent, anyway, there is no advantage of one formalism over the other. An exception is the case of a close-by left-hand cut. Such structures can be built explicitly into DCC approaches with their full momentum dependence. See Refs. [256–258] for related approaches.

Technically, the solution of Eq. (2.116) proceeds just like the solution of the infinite-volume scattering equation (2.57) by discretization as explained in Sect. 2.8. In fact, the only difference lies in the distribution of sample points and integration weights, that are replaced by multiplicities.

Note also that the situation radically changes when considering three-body systems discussed in Sect. 2.11.3. Then, the momentum dependence of V is compulsory due to three-body unitarity, and there is a whole range of on-shell momenta. In that case, the scattering equation can never be recast as a geometric series and remains a true integral equation. As a last remark, the determination of the two-body finite-volume spectrum from a Hamiltonian discussed here resembles the effective Hamiltonian approach for the same purpose [259–262].

In the following, two predictions from Ref. [254] of the finite-volume spectrum from existing DCC approaches are presented, for the $\Lambda(1405)$ (baryonic) and for the $f_0(500)$ (mesonic) quantum numbers and the respective irreps $G_{1u}(0)$ and A_1^+ . For the $\Lambda(1405)$ and the f_0 several lattice QCD collaborations have produced data and finite-volume analyses leading to the first determinations of the respective resonance poles from QCD, see Refs. [184, 260, 263–268] and Refs. [185, 251, 269–275], respectively.

To produce the finite-volume spectra in the $I = 0, S = -1$ meson-baryon sector shown to the left in Fig. 21, the dynamical coupled-channel model of Refs. [16, 276] is considered. It includes the channels $\pi\Lambda$, $\pi\Sigma$, and $\bar{K}N$. The attraction in coupled channels is so strong that the $\Lambda(1405)$ appears dynamically generated. In this approach, also the channels $\bar{K}\Delta$, \bar{K}^*N , and $\bar{K}^*\Delta$ are included. However, these channels contribute only effectively to the direct $\bar{K}N$ interaction in form of box diagrams [16]. Below the three-body thresholds, these channels are physically closed, the box diagrams are real, and one can refrain from explicitly discretizing the integrals related to these box diagrams; the three-body system is more intricate, anyway, as outlined below. The level structure below the $\bar{K}N$ threshold is interesting because of a conjectured two-pole structure of the $\Lambda(1405)$ [280, 281]. Indeed, also the hadron-exchange approach of Ref. [16], considered here, predicts two poles below the $\bar{K}N$ threshold [276]. The two different approaches both predict an attractive $\pi\Sigma$ threshold level (level 0) and another level close to but below the $\bar{K}N$ threshold (level 1). The non-interacting threshold levels are given by the horizontal lines. Note that while both amplitudes contain two $\Lambda(1405)$ poles,

the latter are not manifested in additional energy eigenvalues.

For the scalar-isoscalar finite-volume spectrum shown to the right in Fig. 21, the interaction potential developed in Refs. [278, 279] is used for which the coupling between the $\pi\pi$ (or $\pi\eta$) and $\bar{K}K$ channels is taken into account. The $\sigma \equiv f_0(500)$, $f_0(980)$, and $a_0(980)$ resonances all appear dynamically generated, i.e., without the need of corresponding s -channel exchanges. On the other hand, the model does include also a genuine resonance in form of an s -channel pole diagram, tentatively called $f_0(1400)$ in Ref. [278], whose bare mass is at 1520 MeV. The finite-volume spectrum exhibits a characteristic avoided level crossing at around 980 MeV shown with the dashed lines. In general, avoided level crossing is not only a signal for a resonance but also for S -wave thresholds. Here the $f_0(980)$ coincides with the $K\bar{K}$ threshold, making it difficult to disentangle both effects. It is, therefore, useful to modify the BC to obtain more information on the system. Using the multiplicities ϑ^A and shell radii f^A quoted above, the resulting energy eigenvalues are shown with the thick red solid lines. Indeed, the avoided level crossing disappears with anti-periodic BC [243, 282].

To conclude this part, it should be mentioned that chiral unitary approaches in which the full, four-dimensional BSE (2.104) is solved, can also be matched to the finite volume, allowing for predictions or data analyses. This has been demonstrated in Ref. [283]: For various coupled channels, extensions to twisted boundary conditions, and different hadron masses, the spectrum of the $N(1535)$ and $N(1650)$ was predicted.

2.11.3. Connection of DCC approaches to three-body finite-volume systems

Since a few years, it has become possible to calculate three-body systems from LQCD due to two closely intertwined factors. First, increased computational capacities and algorithmic developments have made the implementation of multi-hadron operators possible, see Refs. [135, 138, 140, 143, 164, 284–295] for recent studies including lattice calculations. Such programs provide a discrete finite-volume energy spectrum, which encodes the full QCD dynamics. Relating this spectrum to the infinite-volume (coupled-channel) amplitude is accomplished by the previously introduced Quantization Conditions (QCs). See Refs. [241, 242] for dedicated reviews in the three-hadron sector and Ref. [164] for a first application to a three-body resonance using two channels. As mentioned in Sect. 4, there are also recent extensions to unequal masses and coupled channels [138, 290, 296] in the context of an alternative approach.

Here, we discuss the connection of three-body quantization conditions in form of the FVU approach to DCC approaches. The infinite-volume aspect of three-body unitarity (IVU) [130] is reviewed in Sect. 2.7.1. The FVU approach was developed in Ref. [253]. Following these works, the three-body scattering amplitude of identical spinless particles, $\Phi\Phi\Phi \rightarrow \Phi\Phi\Phi$, is given by Eq. (2.79) as the sum of a connected piece and a once-disconnected piece. The connected piece contains the three-dimensional isobar-spectator re-scattering piece T that obeys Eq. (2.83), which resembles a Lippmann-Schwinger equation with relativistic kinematics. The re-arrangement interaction B is complex-valued as demanded by unitarity and given in Eq. (2.81). Together with a real-valued term C they determine the dynamics of the three-body scattering.

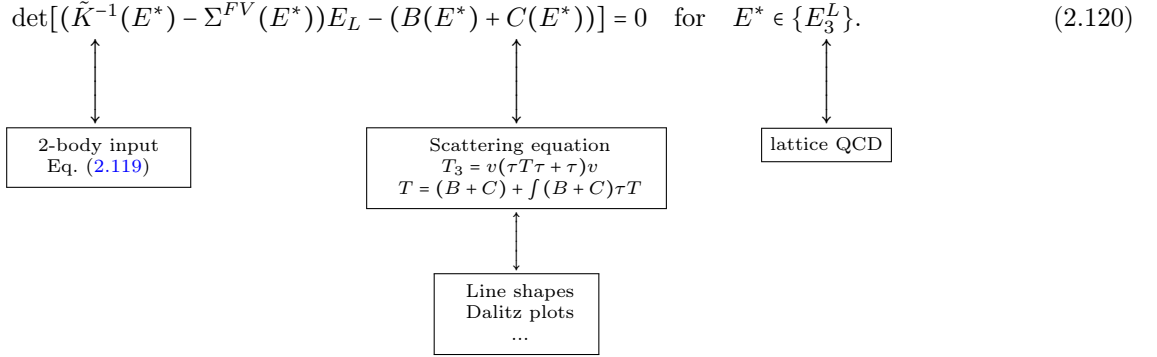
The two-body Green's function is given in Eq. (2.82). We rewrite it in a slightly more general form using a K-matrix-like \tilde{K} as

$$\tau(\sigma_p) = \frac{1}{\tilde{K}^{-1}(\sigma_p) - N_2 \underbrace{\int \frac{dk k^2}{E_k} \frac{v(k, P-k)v^*(k, P-k)}{\sigma_p - 4E_k^2}}_{=: \Sigma}} \quad \text{for } N_2, N_3, v, C, \tilde{K} \in \mathbb{R}. \quad (2.119)$$

The normalization constants (N_2, N_3) address possible isospin or other combinatorial coefficients while v carries angular dependence of the isobar decaying to the asymptotically stable final states. Neither of these have free parameters which can all be absorbed into the remaining unspecified real-valued terms C, \tilde{K} . Since τ is proportional to the two-body scattering amplitude $\Phi\Phi \rightarrow \Phi\Phi$ up to angular factors, one can, indeed, exactly relate $\tilde{K} \sim q_{cm} \cot \delta_{\phi\phi \rightarrow \phi\phi}$. Similarly, one could hope to identify also C with some sort of three-body K-matrix, see, e.g., Refs. [297]. However, this is in general not possible since any three-body observables can only be obtained from the knowledge of the C -term via the integral equation (2.83) plugged into Eq. (2.79). Thus, this relation will always depend on the details of the integration like cutoff-dependence, which, for example, leads to a cycling behavior of this three-body force becoming infinite at specific choices of the cutoff [147, 298, 299]. Therefore, this term has more analogy with a coupling constant than a K-matrix.

In view of the relation between the finite-volume spectrum accessible in lattice QCD calculations and observables such as line shapes or Dalitz plots, the key point of identifying on-shell configurations is accomplished by invoking unitarity, leading to on-shell configurations not only in the isobar-spectator propagation but also in the particle exchange interaction. This enables one to follow the same steps as used in deriving the two-body quantization condition Eq. (2.114) and replace all (intermediate) momenta as $\mathbf{q} \in \mathbb{R} \rightarrow \mathbf{q} \in \mathbb{X}_L := \{(2\pi/L)\mathbf{n} | \mathbf{n} \in \mathbb{Z}^3\}$. In the denominator of Eq. (2.119) this induces a sum over relative momenta in the two-body subsystem ($\Sigma \rightarrow \tilde{\Sigma}$) similarly to Eq. (2.112). This transforms the integral equation Eq. (2.83) to a real-valued matrix equation with singularities located at the eigen-energies (set $\{E_3^L\}$) of the Hamiltonian in the finite volume borrowing the same logic as the one used to derive two-body quantization condition before. Overall, and noting that for any matrix the singularities are given by the zeros of the determinant, we obtain the

FVU three-body quantization condition



Here, the determinant is taken with respect to all possible momentum configurations. This is an infinite-dimensional space \aleph_L since the spectator can take on any of these momenta. Similarly to Eq. (2.114), we ignore here the angular momentum decomposition and the corresponding decomposition into the irreducible representations of the cubic group in the finite volume. In any case, the methodology of relating lattice determined energy eigenvalues to observable scattering quantities is here not one-to-one one as in Eq. (2.114). Instead, the energy eigenvalues determine the roots of the above equation, thus, constraining the volume-independent quantities C and \tilde{K} . In fact, C is fit to the three-body energies E_3^L , while input from the two-body lattice QCD system enters through \tilde{K} . It is only in the second step, by putting these quantities in the corresponding infinite-volume scattering equation, that the experimentally accessible quantities (line shapes, Dalitz plots, pole positions) can be retrieved as indicated in Eq. (2.120). This is of course valid for all currently available and employed approaches to the three-body quantization condition [147, 253, 297].

The discussion above serves as an anchor point relating methods central to this review with results of modern lattice QCD approaches. Most technical details are left out for the sake of clarity. For more dedicated reviews on this topic we refer the reader to Refs. [1, 6, 241, 242]. In summary, DCC approaches can be extended to tackle finite-volume multi-hadron systems. The main connection, to, e.g., the FVU approach in the finite volume becomes, however, clear when considering three-body systems. Indeed, three-body unitarity serves as the prime tool to identify on-shell configurations in interaction and propagation, both guiding the construction of infinite-volume amplitudes but also finite-volume quantization conditions. First Lattice QCD based studies of resonant three-meson systems are available in Ref. [164] for the $a_1(1260)$ and in Ref. [135] for the $\omega(782)$. Extensions of the method to excited baryon systems are underway [300].

3. Light and strange baryons

3.1. Background

The determination of the light baryon spectrum, its properties, and its interpretation has received increased attention in the past two decades. Situated in the intermediate energy region between low and high-energy QCD, light baryonic resonances represent the excited states of the proton and neutron, making them a bridge between matter as we know it, and the regime where QCD is understood perturbatively [301, 302].

Theory predictions from quark models, dynamical quark and gluon approaches/functional methods, effective field theories, and lattice QCD were and are tested in large experimental campaigns at facilities like JLab, ELSA, MAMI, LEPS and other experiments around the world. So much experimental and theoretical work has been invested in the study of light baryons that we can only aim at providing a complete overview of reviews on the topic, with an incomplete list of papers tied to particular issues, in addition.

The canonical literature for meson-baryon scattering and resonances contains the book by Bransden and Moorhouse [303]. The book by Höhler includes a technical discussion of (pion-nucleon) scattering theory [304] and is a widely used reference. Similarly, the book by Ericson and Weise [305] contains many aspects on pion-nucleon scattering, and the lecture series by Levi-Setti and Lasinski [306] has many derivations of commonly used formulas in scattering with spin. An introductory work to K-matrix formalism was written by Chung et al. [307]. A lecture series by Dalitz was published in Ref. [308] discussing hadronic reactions and resonances, together with an introduction to dispersion theory. See also a monograph [309] containing different contributions on “Electromagnetic interactions and hadronic structure”.

First reviews on meson-baryon scattering often highlighted aspects of duality, see, e.g., Rosner [310], Donnachie’s review on partial-wave analysis [311], and a discussion by Dalitz [312], “What is resonance?” A more recent review covering both experimental aspects but also models and theories for light baryons was published by Klempert and Richard 15 years ago [313]. This review is a good starting point for the topic of light baryons; it also contains a pedagogic introduction to quark models, see also Ref. [314] by Richard. An introduction to quark models was provided by Eichmann recently, as well, containing aspects of the flavor structure of baryons and functional methods, in addition [315] (see also an update

in Ref. [316]). Mai recently provided a pedagogical introduction to resonances in Ref. [205] following a major review on the same topic as a key to understanding QCD [1]. See also a discussion summary in Ref. [317].

Quark models for excited baryons and other hadrons [318, 319, 319–323] were discussed in a dedicated review by Capstick 20 years ago [324]. Over the years, the approach has been further refined in relativistic quark models with instanton-induced quark forces [325–328], quark-diquark models [329–332], hypercentral constituent quark models [333–336], in covariant models [337–343] with predictions of electromagnetic properties including timelike form factors [344]. Few-quark dynamics was even extended to five-body systems [345]. See also Refs. [346–350] for other quark models and related approaches for excited baryons. A recent review [351] by Peña and Ramalho is dedicated to form factors, their parametrization [352, 353] and their connection to quark models. Hadronic reactions have been described in the framework of suitably extended constituent quark models, as well [354–361], including even photoproduction reactions of baryon resonances [362, 363]. The $1/N_c$ expansion of baryons and its role in spectroscopy was discussed in Refs. [364–374] and reviewed in Ref. [375] by Matagne.

The relativistic light-front quark model [376–381] and its application to electroproduction reactions was reviewed by Azauryan and Burkert [382] and by Aznauryan, Bashir, Braun, Brodsky, and Burkert in Ref. [378]. See also Sect. 3.4 that contains a more detailed introduction to electroproduction reactions with its own literature overview. We mention here only the short reviews by Carman and Mokeev [383, 384], and also by Dai, Haidenbauer, and Meißner for timelike form factors [385]. New perspectives of exploring hadron structure through transition GPDs were recently summarized in a whitepaper [386].

Holographic QCD is an approach with extra spatial dimensions to model hadrons, as explained in an introductory text by Erlich [387]. A suggestive example of a particle propagating in a compact extra dimension is provided to illustrate that excited hadrons can be interpreted as Kaluza-Klein modes. Holographic QCD for baryon resonances has been proposed in Refs. [388, 389], see also Refs. [390, 391]. The approach of Ref. [389] is highly successful in organizing the hadron spectrum, although it underestimates the spin-orbit separations of the $L = 1$ orbital states. In Ref. [392] a two-parameter mass formula from quark-diquark correlations emerging from AdS/QCD was derived which reproduces the baryon mass spectrum with surprising precision. In Ref. [393] this and related approaches were reviewed by Brodsky, de Teramond, Dosch, and Erlich.

Dyson-Schwinger approaches and functional methods have been developed to understand hadrons as reviewed by Roberts and Maris already 20 years ago [394, 395]. These methods were recently reviewed by Ding, Roberts, and Schmidt [396], following reviews by Roberts, Richards, Horn, and Chang [397], Burkert and Roberts [398], and Bashir et al. [399] reflecting the progress in the baryon sector [400–402] including the prediction of Transition Form Factors (TFFs) [403–406], see Sect. 3.4 of this review. Furthermore, there is the review by Cloët and Roberts [407] with emphasis on the connection of the Schwinger-Dyson formalism to observables like form factors of pion and nucleon, and TFFs of excited baryons.

There are reviews by Fischer and Eichmann [316, 408, 409] for functional methods, and Refs. [410–417] in the context of excited baryons. The role of diquarks was reviewed by Barabanov et al. [332], see also Refs. [418, 419] for connections to Lattice QCD.

(Excited) Meson and (excited) baryon degrees of freedom form the basis for Chiral Perturbation Theory (CHPT) approaches [420] to excited baryons [110, 421–436]. See, for example, the reviews by Bernard, Kaiser, and Meißner [437], by Pascalutsa, Vanderhaeghen, and Yang [438] on the $\Delta(1232)$ resonance, and by Bernard [439].

Through the unitarization of a chiral (or other) interactions to a given order [440], light baryons [15, 39, 108, 188, 441–460] or light-strange baryons [183, 184, 201, 277, 280, 281, 461–470] can emerge (see remarkable progress for unifying these sectors in Ref. [471]). Their description as dynamically generated states can be tested by coupling the photon to the constituents [38] and predicting electromagnetic properties [41–43, 124, 472–488]. Analogously, coupling vector mesons to constituents allows for predictions of the corresponding reaction cross sections [489–491]. Rescattering through chiral unitary potentials can be extended to three particles [492–499]. There are reviews on coupled-channel scattering by Oller [500] and Oset et al. [200, 501–503] with emphasis on chiral unitary methods and, at least partially, covering light baryons. In this context, one has to mention the role of anomalous thresholds [504] and their effect in unitarization. In certain kinematic regions they becomes so strong that even the dynamical generation of P -wave resonances becomes possible [505]. Compositeness criteria to assess the nature of light baryons in terms of meson and baryon components were formulated and applied in Refs. [266, 506, 507]. Some baryonic resonances/structures in specific reactions have also been explained as enhancements due to triangle singularities [508–511].

The Roy-Steiner set of equations were applied to the πN and other sectors in Ref. [119, 120, 512, 513] and also used to extract resonance pole parameters including the $\Delta(1232)$ and Roper resonances [122]. Furthermore, the authors confirm a sub-threshold singularity on the unphysical sheet in S_{11} close to the circular cut, see Sect. 3.3.6 for a more detailed discussion.

As for lattice QCD approaches for baryon spectroscopy, see Refs. [514–519] and approaches in which phase shifts, scattering lengths and other properties are extracted [263, 264, 284, 520–524], as well as pioneering studies on higher excited baryons [261, 262, 286, 525–532]. We refer to dedicated reviews and whitepapers for more details [6, 533, 534]. For the extraction of Low Energy Constants from global fits to baryon lattice QCD data, see Refs. [535, 536] as well as

the dedicated sections in the FLAG report [537].

The phenomenology and experimental aspects of baryon spectroscopy were reviewed by Crede and Roberts in 2013 [538], including also aspects of heavy baryons, quark models, and a discussion of the impact of modern experiments on the baryon spectrum, especially from photoproduction reactions.

Most recently, in 2022, Thiel, Afzal, and Wunderlich [539] reviewed the light baryon spectrum including a consistent compendium of experimental results, discussion of complete experiments, different analysis frameworks (including DCC approaches), and impact on the baryon spectrum and its properties. Notably, this review provides also short introductions to theories and models for baryons like lattice QCD, quark models, Dyson-Schwinger methods etc. and represents a good starting point to obtain an overview of these methods.

There are also specialized reviews on the data aspects, specific reactions, and specific resonances in light baryons spectroscopy. This includes a 2019 overview by Ireland, Pasyuk, and Strakovsky [540], an older review by Schadmand and Krusche on meson photoproduction from 2003 [541], an η physics handbook from 2002 [542], and an updated review on η and η' production on nucleons and nuclei by Krusche from 2014 [543]. One of the most prominent states of the baryon spectrum, the Roper resonance, $N(1440)1/2^+$, was reviewed by Burkert and Roberts in Ref. [398], especially regarding the evidence of this resonance being the first radially excited state of the nucleon itself [417]. See also Ref. [544] by Álvarez Ruso for a short review on the Roper resonance and Refs. [545–547] for examples of the Roper resonance appearing in other reactions than πN and γN -induced ones, including measurements and partial-wave analyses from BESIII.

Regarding the role of amplitude analysis and high-energy parametrizations for light baryons, we mention work from JPAC and others [548–556] for aspects of S-matrix theory, their connection to Regge theory, finite-energy sum rules, and the formulation of new reaction amplitudes guided by these principles, as reviewed by JPAC in Ref. [199]. In the context of amplitude analysis for resonance physics, the review by Yao, Dai, Zheng, and Zhou [557] discusses the role of chiral effective field theory and dispersion relations in the determination of partial waves and their resonance content, for a wide range of systems including πN .

Finally, we mention the role of meson-baryon dynamics in related contexts. Meson and photon-induced reaction are discussed in depth in the following because DCC approaches have been developed for their analysis. However, light excited baryons and, sometimes, their timelike electromagnetic form factors were also measured in pp -induced reactions at experiments like HADES [558–560] and COSY-TOF [561–563] and were analyzed by the Bonn-Gatchina (BnGa) group, Sibirtsev et al., and others [344, 484, 564–577]. See the review by Salabura [578].

Laget reviewed exclusive meson photoproduction at high energies in the so-called partonic non-perturbative regime [579] that is particularly relevant for current and future experiments at JLab and the EIC. The in-medium properties of excited baryons were reviewed by Lenske [580], and, in close relation, by Metag [581]. Hadronic reactions close to thresholds have simple kinematics and allow for tests of different models as reviewed by Moskal [582], see also Ref. [583]. Photoproduction reactions at low energies was reviewed in Ref. [584]. The field of light-strange baryons, including the $\Lambda(1405)$ is vast; the contribution from DCC approaches in discussed in Sect. 3.6 and we mention here only the reviews by Hyodo [503, 585], Mai [200], Meiñner on two-pole structures [502], and Tolos [586].

3.2. Meson-induced reactions

Meson beams are versatile probes for hadron spectroscopy. Elastic pion-nucleon scattering was the first reaction providing access to the baryon spectrum in the classical partial-wave analyses by Höhler, Koch, and Cutkoski leading to the establishment of many states by the 90’s [118, 127, 587–589]. See also the analysis by Manley et al. that includes elastic πN scattering and the $\pi\pi N$ final state [590, 591] and the Carnegie-Mellon-Berkeley (CMB) model by Vrana, Dytman, and Lee [592] and by the Zagreb group [593–596].

The analyses of πN scattering including the reaction $\pi N \rightarrow \eta N$ and pion photoproduction on proton and neutron have been further refined to this day by the GWU/SAID analysis group [170, 597–616]. The SAID pion and photon-induced formalisms were unified into a Chew-Mandelstam parametrization in Ref. [605]. The partial-wave dispersion relations by Frazer and Fulco [617] derived from the Mandelstam representation [618] provided useful constraints for many of the πN analyses. Notably, all other modern partial-wave analysis efforts rely on the SAID or other analyses for elastic pion scattering, although the ANL-Osaka analysis [78] follows a two-step procedure: (1) SAID input is used to locate the range of the parameters of the model; (2) The obtained parameters are refined and confirmed by directly comparing with the original πN -scattering data.

In Ref. [619] the covariance matrices between different partial waves of the SAID Single-Energy Solutions (SES) were provided, that allow, in principle, to reconstruct a meaningful χ^2 representing the actual underlying data. However, this means one implicitly accepts the correction of systematic errors as applied by SAID. Systematic uncertainties and their correction are not small, at all, due to the problematic data situation of elastic πN scattering. It is, therefore, better (albeit much more tedious) to fit the underlying πN data base with a procedure to correct for various normalization factors [233] as practiced in Ref. [119] in which the $\pi\pi \rightarrow \bar{N}N$ process is related to the s -channel $\pi N \rightarrow \pi N$ reaction.

Meson-induced reactions are central in any modern analysis aiming at a complete data description, but the available data are problematic. In Ref. [620] a case for new measurements using meson beams was made with minor updates

regarding the planned Electron Ion Collider in Ref. [621]. Historically, the argument for using photons in the discovery of excited baryons (instead of meson beams) was the sensitivity to states that couple only weakly to πN . A resonance that couples substantially to the photon but weakly to the πN channel could be easier to detect in photoproduction reactions. Reactions like $\gamma N \rightarrow \eta N, K\Lambda, K\Sigma, \dots$ are ideal for this purpose. The downside of photoproduction is the larger number of amplitudes. In general, a resonance with given spin-parity J^P couples to both an electric and a magnetic multipole, i.e., more degrees of freedom are present in photoproduction reactions than in pion-induced reactions. This substantially increases the number of necessary measurements to determine an amplitude. See next section for a discussion on “complete experiments”.

In addition, modern baryon spectroscopy analysis frameworks add the real or virtual photon to an existing hadronic rescattering part in one way or another [11, 27, 54–57, 59–61, 79, 81, 149, 622–626] as discussed in Sect. 3.3. The rescattering part itself is constrained from pion-induced reactions. In that, any data problems in pion-induced reactions will have consequences for the analysis of photon-induced reactions, especially when it comes to resonances that are tied to the strongly interacting rescattering part. This is particularly the case for pion-induced inelastic reactions such as $\pi N \rightarrow \eta N, K\Lambda, K\Sigma, \omega N$ or three-body channels. On one hand, data in these reactions are known to be problematic as discussed below. On the other hand, new resonances coupling weakly to πN are still more visible in these reactions than in elastic πN scattering. Summarizing, there are four reasons why re-measuring inelastic, pion-induced reactions can significantly contribute to an improved and more quantitative understanding of the excited baryon spectrum, and the discovery of new states: (a) the poor data situation, (b) reducing the bias for photoproduction analysis, (c) fewer amplitudes than in $\gamma^{(*)}$ -induced reactions, and (d) sensitivity to channels other than πN (for inelastic reactions).

Of the possible final states, the reactions $\pi N \rightarrow \eta N, K\Lambda$ and $\pi^+ p \rightarrow K^+ \Sigma^+$ have to be highlighted because they isospin filter $I = 1/2$ N^* ’s [53] and Δ ’s [104], respectively. The reactions $\pi N \rightarrow K\Lambda$ and $\pi N \rightarrow K\Sigma$ provide unique information in that the outgoing baryon is self-analyzing allowing for an easy access to spin observables. Take, for example, the reaction $\pi^+ p \rightarrow K^+ \Sigma^+$ measured in Ref. [627]. The measurements cover a substantial angular and energy range, and they include data on differential cross sections and recoil polarization P . Together with much less precise data on the spinrotation parameter β from Ref. [628] the set of observables is almost complete (see, e.g., the discussion in Ref. [313]).

Regarding the overall data situation, an overview of inelastic pion-induced reactions is provided in Table 3. The table is taken from Ref. [57] and amended by the available $\pi N \rightarrow \omega N$ data collected and analyzed in Ref. [58]. The number of data points should be compared to the tens of thousands of data available in photoproduction reactions [57], or the hundreds of thousands of data in electroproduction [61].

In addition, the pion-induced reaction data often carry large uncertainties and are, in many cases, contradictory due to underestimated systematic effects. This leads to notoriously large χ^2 values in global fits, making the application of traditional statistical criteria to, e.g., assess the significance of a signal for a new resonance, very difficult. The aim of a new pion-induced experiment would not only be to provide more data, but, for the first time, provide *consistent* data. This is indeed possible: for example, the EPECUR experiment has drastically improved the data situation in elastic pion-nucleon scattering [630] (see, e.g., Fig. 4 in Ref. [621]). See also Ref. [631] for a demonstration how drastically the measurements of the $K^+ \Sigma^+$ final state can be improved with modern experimental techniques. Planned reactions with meson beams at J-PARC are discussed in Ref. [632]; for the study of pion-induced reactions at HADES, see Ref. [633].

The situation for the inelastic reactions is illustrated in Fig. 22. The differential cross section data demonstrates that the systematic problems are not just given by simple multiplicative factors that might be adjustable [233] –the shapes of the cross sections do not match. The plot of the spinrotation parameter β demonstrates how few data are available for this most valuable experimental quantity; and the right-hand plot shows the typical quality for polarization data (that are supposed to be limited to $|P| \leq 1$).

The total cross sections shown in Fig. 23 exhibit similar problems, i.e., clearly contradictory data. For example, the total cross section of the reaction $\pi^- p \rightarrow K^+ \Sigma^-$ is almost impossible to describe due to a supposed structure around a scattering energy of $E = z \approx 2$ GeV, which is, however, only due to one or two data points. Having more conclusive data

Table 3: Inelastic pion-induced reaction data. The quantity β is the spinrotation parameter. A full list of references to the different experimental publications can be found online [629].

Reaction	Observables (# data points)	Total
$\pi^- p \rightarrow \eta n$	$d\sigma/d\Omega$ (676)	755
$\pi^- p \rightarrow K^0 \Lambda$	$d\sigma/d\Omega$ (814)	1358
$\pi^- p \rightarrow K^0 \Sigma^0$	$d\sigma/d\Omega$ (470)	590
$\pi^- p \rightarrow K^+ \Sigma^-$	$d\sigma/d\Omega$ (150)	150
$\pi^+ p \rightarrow K^+ \Sigma^+$	$d\sigma/d\Omega$ (1124)	1682
$\pi N \rightarrow \omega N$	$\sigma(54)$	178
	$d\sigma/d\Omega$ (124)	

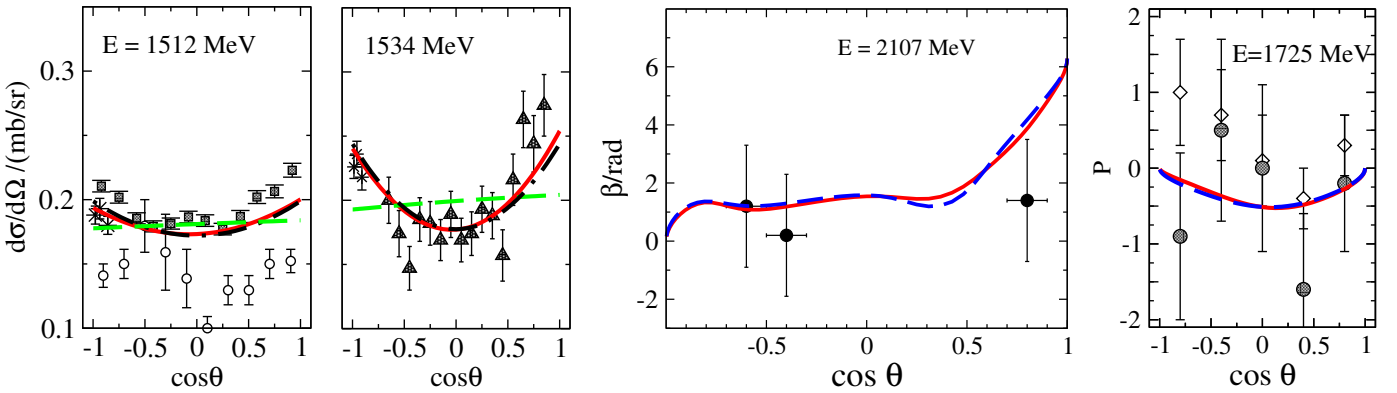


Figure 22: Left two figures: Differential cross section of the reaction $\pi^- p \rightarrow \eta n$ at different scattering energies E . The u-shape in fits and data reveals the S - D -wave interference of $N(1535)1/2^+$ and $N(1520)3/2^-$. Central figure: Spin-rotation parameter β for $\pi^+ p \rightarrow K^+ \Sigma^+$. Right figure: Polarization P for the reaction $\pi^- p \rightarrow K^0 \Sigma^0$. Solid red (dashed blue) lines: JBW solutions A (B) from Ref. [53]. For data references see Ref. [53].

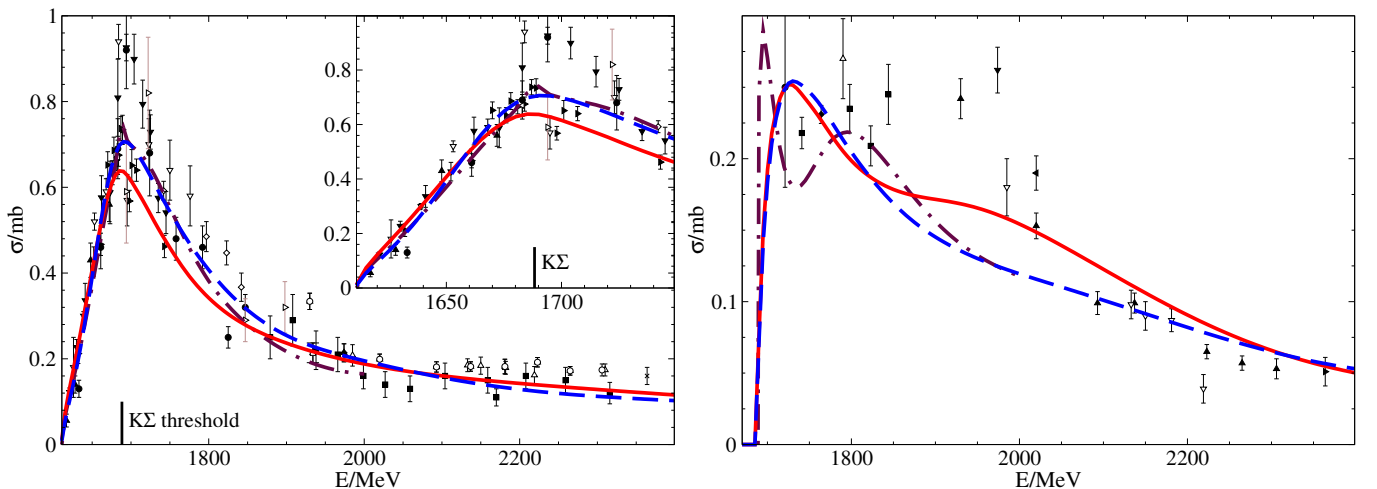


Figure 23: Total cross sections of the reactions $\pi^- p \rightarrow K^0 \Lambda$ (left) and $\pi^- p \rightarrow K^+ \Sigma^-$ (right). Red solid (blue dashed) lines: JBW solutions A (B) from Ref. [53]. Dash-dotted dark brown lines: ANL-Osaka solution from Ref. [149]. See Ref. [53] for data references.

would be particularly valuable because this reaction does not allow for t -channel meson exchange and is, thus, of special interest to study hadron dynamics. There is no polarization available for this reaction, at all.

The $\pi N \rightarrow \pi\pi N$ reaction also provides valuable information on the baryon spectrum and its few-body decays. Such reactions have been considered in the ANL-Osaka DCC approach as described below. Although the $\pi N \rightarrow \pi\pi N$ data are few and similarly problematic as the data discussed before, new experimental efforts are being made at J-PARC in the E45 experiment to drastically increase the data base [634, 635]. Inelastic reactions like $\pi N \rightarrow \pi\eta N$ have also been used to gain information on the dynamical nature of resonances like $\Delta(1700)$ [485], see also recent progress by JPAC/GlueX/COMPASS [636–639] in the context of searching for exotic mesons in this reaction.

The $\pi\pi N$ states are known to have strong couplings with most of the high-mass nucleon resonances and, thus, are relevant for spectroscopy. They are not directly included in the analysis of the nucleon resonances in the ANL-Osaka model. As a first step of a complete analysis to include two-body and three-body final states for the pion and photon induced reactions, the $\pi N \rightarrow \pi\pi N$ [82, 634] and $\gamma N \rightarrow \pi\pi N$ [83] reactions are studied within the DCC model [78, 87]. The situation of the theoretical approaches and the experimental data on $\pi N \rightarrow \pi\pi N$ are briefly summarized in Ref. [82].

With the approximation of $T_{\pi\pi N, \pi N}^{dir}$ (Eq.(2.31)) neglecting the final state interaction on the mechanisms (f)-(k) of $v_{\pi\pi N, \pi N}$ in Fig. 3 [82], the $\pi N \rightarrow \pi\pi N$ cross section is calculated using information of the ANL-Osaka model [78, 87] with no additional parameters. The total cross sections for five channels are compared with the data as shown in Fig. 24. The red solid curves are from a recent version of the ANL-Osaka approach [87] while the green dotted curves are from the previous JLMS model [78]. Both the magnitude and the energy dependence of the data for five 2π production can be reproduced to a very large extent. The direct mechanism $T_{\pi\pi N, \pi N}^{dir}$ plays an important role especially for $\pi^+ p \rightarrow \pi^+ \pi^+ n$ and $\pi^- p \rightarrow \pi^- \pi^0 p$. In the low-energy region $W < 1.4$ GeV, the calculation is comparable to the calculation of chiral perturbation theory. This suggests that the model of $v_{\pi\pi N, \pi N}$ is reasonable and the discrepancies with the data in the higher W region are more likely results from the uncertainties in the contribution for $\pi\Delta, \rho N$ and σN transitions.

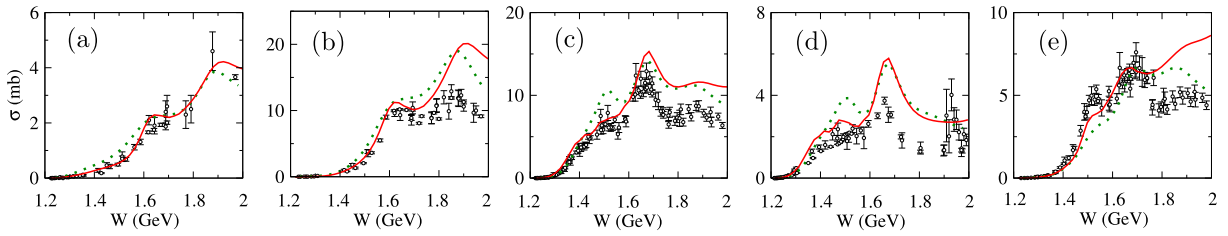


Figure 24: The $\pi N \rightarrow \pi\pi N$ total cross section predicted by the ANL-Osaka models from Refs. [87] (red solid) and [78] (green dotted lines) as a function of energy $E = W$. The reaction channels are (a) $\pi^+ p \rightarrow \pi^+ \pi^+ n$, (b) $\pi^+ p \rightarrow \pi^+ \pi^0 p$, (c) $\pi^- p \rightarrow \pi^+ \pi^- n$, (d) $\pi^- p \rightarrow \pi^0 \pi^0 n$, and (e) $\pi^- p \rightarrow \pi^- \pi^0 p$.

The $\pi\pi$ and πN invariant mass distributions at $W = 1.79$ GeV and the contributions of each of the $\pi\Delta, \rho N, \sigma N$ channels are shown in Fig. 25. The DCC model is able to reproduce the main features of the data. The DCC model shows the strong interference among those channels for the invariant mass distributions. Future measurements of the $\pi N \rightarrow \pi\pi N$ reactions are important for the extraction of higher-mass nucleon resonances and for an improved description of the $N^* \rightarrow \pi\Delta, \rho N, \sigma N$ couplings.

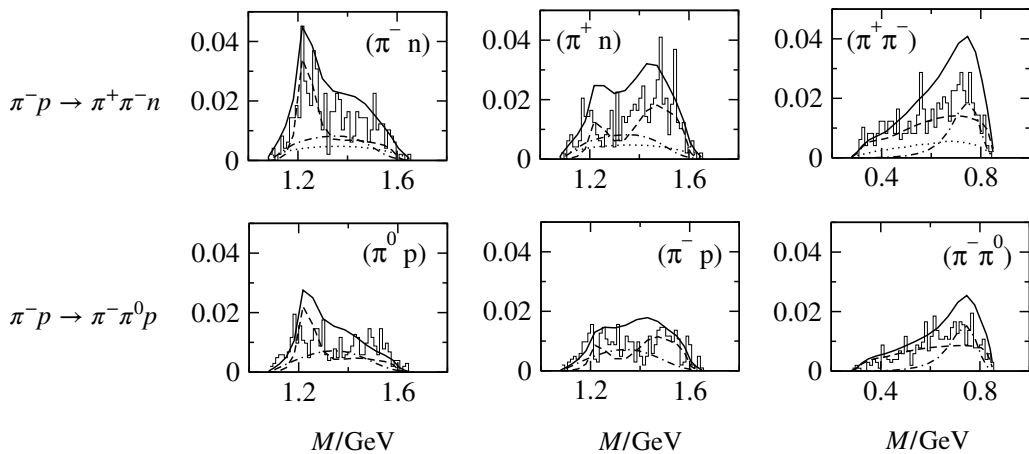


Figure 25: Predicted contributions from the $\pi\Delta$ (dashed), σN (dotted), and ρN (dot-dashed) channels to the invariant mass distributions of $\pi^- p \rightarrow \pi\pi N$ at $W = 1.79$ GeV. The data are from Arndt [640], with magnitudes determined by normalizing them to the total $\pi N \rightarrow \pi\pi N$ cross section.

In summary, inconsistencies dominate the data uncertainties for pion-induced reactions. This has severe consequences for baryon spectroscopy affecting the reliability of determining the spectrum, especially when it comes to hard statistical criteria. Indirectly, these problems also affect the analysis of photoproduction reactions, in which so much experimental and analysis effort has been invested in the past decades. Having a large set of consistent data on pion-induced reactions, especially inelastic ones, would allow one to take advantage of the inherent upsides of meson beams: Fewer amplitudes than in photoproduction (for single-meson final states), easier to achieve “complete experiment”, larger cross sections and, to some extent, still having sensitivity to resonances that couple only weakly to πN . The $\pi\pi N$ final states were predicted by the ANL-Osaka approach demonstrating that DCC models can analyze these states. The impact of new data on different analyses, such as J-PARC E45 [641], once available, could be quantified in common efforts across different analysis groups as practiced in Ref. [610] for photoproduction.

3.3. Photoproduction reactions

3.3.1. Overview of different analysis frameworks

In the last three decades, a plethora of final states, differential cross sections, and spin observables were measured in photoproduction reactions at JLAB/CLAS [609, 642–646], CB-ELSA/TAPS [511, 647–653] (continued at the new BGOOD detector [654–661]), MAMI/A2/CrystalBall [611, 662–666], LEPS [667–670], ELPH/FOREST [671], GRAAL [480, 672], and other facilities. Sometimes observables are tied to specific choices of reference frames that are not unique across different experiments and analyses. The “Rosetta Stone Paper” provides an overview [673].

The data and their analyses provided unprecedented information on baryonic resonances, not only for their electromagnetic properties, but also for the spectrum itself. Indeed, many new states were added to the Particle Data Book [103]

in the photoproduction era. States found before that were promoted in the PDG star rating while a few other ones descended or disappeared, see, e.g., Table 9 of Ref. [538]. In the reviews [313, 538–540], comprehensive compilations of data and their features can be found. We do not aim at replicating these works here and just pick out some interesting findings in the context of DCC approaches and general hadron dynamics, see Sects 3.3.6 and 3.3.7. There are other topics beyond the scope of this review like the efforts to experimentally confirm the GDH sum rule [615, 666, 674] or Compton scattering reviewed by Grießhammer, McGovern, Phillips, and Feldman [675], including the role of the $\Delta(1232)$ [676] in the low-energy chiral expansion.

There are also extended discussions on specific structures that have attracted much attention such as a peak in η photoproduction on the neutron at around $W = 1675$ MeV that is absent at the proton target [649, 663]. This has been interpreted as an interference effect [677], a coupled-channel effect [479], or a new resonance [678], possibly a pentaquark [679]. The need for a new narrow resonance was disputed in Ref. [680] by BnGa, and the Giessen group did not find new narrow states for photoproduction on the proton [681].

The extraction of multipoles from photoproduction data is a challenge. There are continuous and discrete ambiguities [682]. Due to the presence of electric and magnetic multipoles, the extraction requires in general more observables than in reactions induced by spinless mesons. Such questions tied to “complete experiments” have been discussed in Refs. [683–688] by Wunderlich et al.. There are two variants of this issue: How many measurements are needed to determine the amplitude at a given energy and scattering angle [689], and, second, the “truncated partial-wave” complete experiment [685, 686, 690] that is somewhat more relevant when it comes to baryon spectroscopy of resonances with given J^P . See Refs. [691, 692] for recent comparisons of these types of complete experiment and a discussion of the role of uncertainties. In relation to this, one of the tasks in spectroscopy is to determine which partial waves actually contribute in a given kinematic region. This question has been addressed in Ref. [693] for the baryon sector and in Ref. [227] as a problem for which machine learning techniques can be used.

In practice, one needs assumptions on the amplitude to extract energy-dependent multipoles to reconstruct resonances and their electromagnetic properties. Assumptions on the smoothness of multipoles in energy are indeed mandatory as the set of observables is never complete in all kinematic regions. Starting from such energy-dependent solutions, single-energy solutions (SES) can be derived in which the solutions are allowed to vary in an energy bin describing only the data in that bin. One needs subsidiary conditions for this such as fixing multipole phases to avoid the SES to vary uncontrolled from bin to bin. This allows to scan for narrow structures and can also help detect systematic shortcomings of the global parametrization. See Refs. [694–698] for recent progress in this direction using the Laurent-Pietarinen expansion, as well as Refs. [699, 700] in which t -channel analyticity and unitarity have been used to constrain the determination of single-energy solutions. Resonance pole parameters in the complex plane can be determined by fitting them with meromorphic functions [697]. The Mittag-Leffler expansion is used in [171, 701] by introducing the uniformization variable discussed in section 2.9.1.

Many frameworks have been developed for the analysis of meson photoproduction reactions - sometimes, the efforts are bundled, e.g., to study the impact of new polarization data on the different analysis frameworks [610]. We discuss here only approaches that do *not* fall into the DCC category. The ANL-Osaka and JBW approaches have been discussed in depth in this review, while other DCC approaches have been summarized in Sect. 1.2. Furthermore, we discuss here approaches that, in many cases, not only analyze photoproduction but also pion-induced reactions.

The SAID group including Arndt, Briscoe, Schmidt, Strakovsky, Workman et al. developed one of the earlier approaches for the analysis of photoproduction on the proton [603, 604, 616, 664, 702] but also neutron [612–614] as reviewed in Ref. [703]. For the latter case, mostly referring to photoproduction on the deuteron, there are strong corrections (Fermi motion and final state interactions) that have to be taken into account [704, 705]. As discussed in Sect. 3.2, the photoproduction and pion-induced reactions were formulated in a unified SAID framework in Ref. [605].

The MAID unitary isobar approach to meson photoproduction has also evolved over time. After initial studies using effective Lagrangian approaches [706, 707] and fixed- t dispersion relations [708], Drechsel, Hanstein, Kamalov, Tiator et al. developed the unitary isobar MAID framework in Ref. [622] for pion photoproduction. In another single-channel analysis, the framework was extended to η photo and electroproduction [709] with a reggeized version for the background presented in Ref. [710]. Kaon photoproduction was studied in KAON-MAID [711, 712] by Bennhold, Haberzettl, Lee, Mart, and Wright, within a tree-level model that incorporates hadronic form factors consistent with gauge invariance. The MAID 2007 approach is a unified analysis of pion photo and electroproduction [624] using suitably unitarized Breit-Wigner forms for the resonances. The paper also contains an overview of the historic evolution of the MAID approach. See also Sect. 3.4 for a more specific literature review on electroproduction and the respective analysis frameworks. An analysis of low-energy $\gamma^{(*)}$ -induced data with chiral perturbation theory was performed under the chiral MAID label in Refs. [713, 714]. An update on η and η' photoproduction was published in Ref. [715]. Finally, Ref. [716] summarizes the legacy of MAID and points towards future developments of the approach.

In the BnGa approach both pion and photon-induced reactions are analyzed simultaneously [717], like in the ANL-Osaka and JBW approaches. While electroproduction reactions are not yet considered, the range of analyzed photoproductions is larger than in the DCC approaches. Apart from the reactions analyzed in the mentioned DCC approaches, the BnGa group analyzes also three-body final states of reactions like $\gamma p \rightarrow \pi^0 \eta p$ or $\pi^0 \pi^0 p$ [652, 718, 719]. See also recent

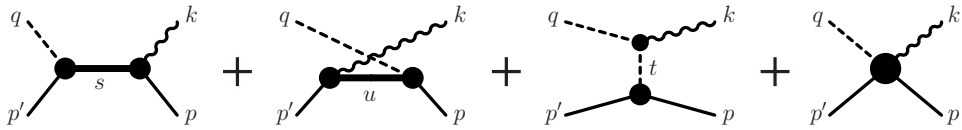


Figure 26: Generic structure of the pion photoproduction current M^μ for $\gamma N \rightarrow \pi N$. Time proceeds from right to left. Nucleons and pions are depicted by solid and dashed lines, respectively, and the photon is shown as a wavy line. The first three diagrams depict the s -, u -, and t -channel pole diagrams M_s^μ , M_u^μ , and M_t^μ , respectively. The last diagram shows the contact-type interaction current. Figure taken from Ref. [44].

effort on two-pion photoproduction by the JPAC group [720–723] and Haberzettl [724], as well as tests of chiral unitary models in two-meson photoproduction [477, 487] and other two-meson isobar models [725–728].

The BnGa amplitude was formulated in Ref. [623] with main results published in Ref. [625], which have been updated based on new data and reactions over the years [651, 729, 730], such as ω photoproduction [731, 732]. Evidence for several new excited baryons and new decay channels of known baryons was found [718, 733–739] leading to substantial updates of the Particle Data Book, for example for a $N(1900)3/2^+$ [740, 741] and a $N(1895)1/2^-$ [653]. The case of the latter resonance is particularly intriguing due to the closeness of the $\eta' p$ threshold [653]. In Ref. [742] BnGa explored the region of high-lying states and found evidence for four new states by performing mass scans. In this technique, resonances are inserted into the amplitude as Breit-Wigner forms with their masses held fixed and other parameters allowed to re-adjust with the data. The χ^2 is plotted as a function of the mass, preferably for different final states. Simultaneous minima of the χ^2 for different final states are taken as a signal for a new resonance at that mass. The four new states were interpreted in light of the general mass ordering expected in quark models from the spin-flavor symmetry leading to the group SU(6) that is decomposed into 70-plets etc., which can then further be decomposed into different SU(3) groups with different spin multiplicities. An organization of states in spin doublets and quartets is plausible. If that is the case, “the diquark hypothesis - which freezes one pair of quarks into a quasi-stable S -wave flavor diquark - is ruled out as explanation of the missing resonance problem” [743]. Dynamical diquarks behave differently [332, 402].

The Giessen coupled-channel approach by Lenske, Mosel, Penner, Shklyar et al. employed a coupled-channel K-matrix formalism for the combined analysis of pion and photon-induced reactions [677, 681, 744–749] including vector meson and $\pi\pi N$ final states in form of the partial-wave results by Manley [591]. The Kent state analyses by Manley et al. addressed a variety of final states including πN [591, 750–752] but also inelastic, pion and photon-induced reactions [750], using a product S-matrix approach. Single-energy solutions [753] provide additional insight into structures not uncovered by global, energy-dependent multi-channel fits.

Effective Lagrangian or Regge plus resonance approaches have also served as a tool to extract information on excited baryons from photoproduction reactions by Kim, Mart, Petrellis, Skoupil, Wang, Xie, and many others [229, 231, 526, 754–785], see also the work by the Ghent group [218, 219] in combination with statistical tools as discussed in Sect. 2.10.2. In addition, effective Lagrangian approaches have been used to analyze related reactions simultaneously [786] exploiting the universality of resonance couplings. For such approaches the question of maintaining gauge invariance becomes relevant; Regge amplitudes with gauge invariance have been discussed by Haberzettl [787, 788] and JPAC [789]; a related issue is the construction of gauge invariant form factors [790, 791]. See also Refs. [553, 792, 793] for π^0 , η , and η' photoproduction at high energies using Regge theory and finite-energy sum rules, in connection with the first GlueX experiments [794].

3.3.2. Photoproduction in the JBW approach

The interaction of the photon with the hadronic interactions is constrained by gauge invariance in terms of the Ward-Takahashi identity [37, 724, 795, 796]. Based on the formalism of Refs. [797, 798], single meson photoproduction was studied within the JBW approach by Huang et al. in Ref. [44]. The hadronic part of the JBW model was taken as final state interaction for a gauge invariant coupling scheme of the photon to s , t , and u -channel processes, as well as a generalized, gauge-restoring contact term, to compute the pion photoproduction current M^μ . This is indicated in Fig. 26. The starting point is the topology of the πNN vertex with the photon coupling to all legs. In addition, the photon can couple to the internal components of the complicated rescattering part which is parametrized with the contact term taking into account the internal structure. One obtains a tower of coupled non-linear Dyson-Schwinger-type equations that can only be solved iteratively. In practice, it is subject to a gauge-invariant truncation for the dressed nucleon current and the contact-type five-point current [44]. For this purpose, the non-covariant normalization of the scattering equation (2.47) is transformed into the Kadyshevsky equation [32] which is a covariant three-dimensional reduction of the Bethe-Salpeter equation that preserves elastic unitarity. The photoproduction current is then constructed within the same covariant, three-dimensional reduction. With an efficient parametrization of the contact term in terms of a few parameters, neutral and charged pion photoproduction data were fitted up to $E = 1.65$ GeV because only resonances up to spin $J = 3/2$ were included in Ref. [44]. Some coupling constants were taken from the literature, and only about 40 parameters (most of them resonance couplings to the photon) were varied to obtain an excellent description of differential cross sections and

photon spin-asymmetry data on a proton as well as a neutron target [44]. This demonstrates that gauge invariance is not only a theoretical requirement but can be helpful in guiding the construction of efficiently parametrized amplitudes.

In subsequent analyses of photoproduction reactions, the JBW amplitude was technically simplified by switching to a partial-wave-wise parametrization. The photoproduction multipole amplitude in terms of a photoproduction kernel $V_{\mu\gamma}$ is given by [54]

$$M_{\mu\gamma}(q, E) = V_{\mu\gamma}(q, E) + \sum_{\kappa} \int_0^{\infty} dp p^2 T_{\mu\kappa}(q, p; E) G_{\kappa}(p, E) V_{\kappa\gamma}(p, E) . \quad (3.1)$$

Here, the index γ is used exclusively for the γN channel. Note that in the second term $V_{\kappa\gamma}$ produces a meson-baryon pair in channel κ with off-shell momentum p that rescatters via the hadronic (partial-wave projected) half-offshell T-matrix from Eq. (2.57), producing the final πN state (more generally, channel μ) with momentum q . The meson-baryon propagator G_{κ} is defined in Eq. (2.58) for two-body intermediate state; for three-body intermediate states see Sect. 2.7.2. The photoproduction kernel can be written as

$$V_{\mu\gamma}(p, E) = \alpha_{\mu\gamma}^{\text{NP}}(p, E) + \sum_i \frac{\gamma_{\mu;i}^a(p) \gamma_{\gamma;i}^c(E)}{E - M_i^b} . \quad (3.2)$$

Here, $\alpha_{\mu\gamma}^{\text{NP}}$ represents the photon coupling to t - and u -channel diagrams and to contact diagrams. These diagrams together form the non-pole part of the full photoproduction kernel as can be seen from field-theoretical considerations [796]. Note that the form of the photoproduction kernel allows one to vary the strength of resonances and background independently without violating Watson's theorem [799]. The summation in Eq. (3.2) is over the resonances i in a multipole, and the $\gamma_{\gamma;i}^c$ are the real-valued tree-level γNN_i^* and $\gamma N\Delta_i^*$ photon couplings. It is crucial that the resonance annihilation vertex γ^a in Eq. (3.2) is precisely the same as in the hadronic part of Eq. (2.59) so that the explicit singularity at $E = M_i^b$ cancels.

The two-potential formalism allows one to rewrite the photoproduction amplitude M as

$$\begin{aligned} M_{\mu\gamma} &= \alpha_{\mu\gamma}^{\text{NP}} + \sum_{\kappa} T_{\mu\kappa}^{\text{NP}} G_{\kappa} \alpha_{\kappa\gamma}^{\text{NP}} + \Gamma_{\mu;i}^a (D^{-1})_{ij} \Gamma_{\gamma;j}^c \\ \Gamma_{\gamma;j}^c &= \gamma_{\gamma;j}^c + \sum_{\kappa} \Gamma_{\kappa;j}^c G_{\kappa} \alpha_{\kappa\gamma}^{\text{NP}} \end{aligned} \quad (3.3)$$

with the dressed resonance propagator D from Eq. (2.65) and with the dressed resonance-creation photon-vertex $\Gamma_{\gamma;j}^c$ which is a vector in resonance space, like the strong dressed vertex $\Gamma_{\mu;i}^c$ in Eq. (2.65). This standard result has been derived, e.g., in Ref. [124]. In the form of Eq. (3.3) it becomes apparent that in $M_{\mu\gamma}$ all singularities due to the bare resonance propagators of Eq. (3.2) have canceled.

Alternatively, one can write the amplitude simply in terms of the full hadronic T-matrix as

$$M_{\mu\gamma} = \sum_{\kappa} (1 - VG)^{-1}_{\mu\kappa} V_{\kappa\gamma} . \quad (3.4)$$

In principle, any of the forms (3.1), (3.3), or (3.4) can be used in practical calculations. In the form of Eq. (3.4), which resembles the one of Ref. [800], the similarity with the CM12 Chew-Mandelstam parameterization of the SAID group [605] becomes apparent, in which the hadronic kernel $\bar{K}_{\kappa\nu}$ of their hadronic T-matrix,

$$T_{\mu\nu} = \sum_{\kappa} (1 - \bar{K}C)^{-1}_{\mu\kappa} \bar{K}_{\kappa\nu} , \quad (3.5)$$

is replaced by a photoproduction kernel, $\bar{K}_{\kappa\gamma}$,

$$M_{\mu\gamma} = \sum_{\kappa} (1 - \bar{K}C)^{-1}_{\mu\kappa} \bar{K}_{\kappa\gamma} . \quad (3.6)$$

Here, C is the complex Chew-Mandelstam function that guarantees two-body unitarity and even the complex thresholds for effective three-body channels [605]. While Eq. (3.6) is formally identical to Eq. (3.4), there is a practical difference: Eq. (3.4) implies an integration over intermediate off-shell momenta, while the quantities \bar{K} and C in Eq. (3.6) factorize. In both approaches the dispersive parts of the intermediate loops G and C are maintained. In the JBW approach, the terms $\alpha_{\mu\gamma}^{\text{NP}}$ and $\gamma_{\gamma;i}^c$ in Eq. (3.2) are approximated by polynomials P ,

$$\alpha_{\mu\gamma}^{\text{NP}}(p, E) = \frac{\tilde{\gamma}_{\mu}^a(p)}{\sqrt{M_N}} P_{\mu}^{\text{NP}}(E) , \quad \gamma_{\gamma;i}^c(E) = \sqrt{M_N} P_i^{\text{P}}(E) , \quad (3.7)$$

where $\tilde{\gamma}_{\mu}^a$ is a vertex function equal to $\gamma_{\mu;i}^a$ but stripped of any dependence on the resonance number i . Equation (3.7) means that one has $n+m$ polynomials per multipole with n resonances i and m hadronic channels μ . With this parameterization,

non-analyticities from left-hand cuts, like the one from the pion-pole term, are approximated. As the distance to the physical region is quite large, such an approximation can be justified. Note in this context that even for the $\gamma\gamma \rightarrow \pi\pi$ reaction that has a very close-by left-hand cut, the Born contributions can be effectively parameterized by a linear polynomial [801]. In any case, it is clear that in this multipole-wise parametrization one needs substantially more fit parameters than in the plane-wave approach of Ref. [44] in which gauge invariance was used to guide the parametrization.

This review is focused on summarizing and explaining the formal aspect of DCC approaches. Therefore, we keep the discussion of applications of the JBW model to photoproduction very short. Pion photoproduction on the proton up to an energy of $E \approx 2.3$ GeV was analyzed in Ref. [54], including also isospin breaking at low energies due to hadronic mass differences within the pion and nucleon multiplets. About 20,000 data for differential cross sections and all polarization observables available at that time were analyzed, with some exclusion of data in the extreme forward direction because the approach was truncated at a total angular momentum of $J = 9/2$. Photocouplings were extracted at the resonance poles and compared to values of the SAID and BnGa approaches. Notably, these helicity amplitudes are complex and not real as they would be for a Breit-Wigner formulation. In the pole definition, photocouplings are, by definition, independent of the final state because coupled-channel amplitude factorize at resonance poles. The photoproduction data of the ηN , $K\Lambda$, and $K\Sigma$ final states were successively added in the respective analysis updates in Refs. [55], [56], and [57], with an accumulated data set of more than 70,000 points. All fit results to all data (pion- and photon-induced) are documented on a web site [629]. Results of electroproduction fits are collected on a different, interactive website [802], see Sect. 3.4. Many resonance pole positions, branching ratios, and electromagnetic couplings determined in the JBW approach are quoted in the PDG “above the line” [103].

3.3.3. The weak Λ decay parameter α_- from CLAS data

For reactions with Λ and Σ final states, it should be noted that in experimental analyses the weak asymmetry parameter α_- scales the values of polarization observables. The value of this fundamental constant was questioned through new experimental evidence at BESIII [803]. In Ref. [804], Ireland and JBW independently determined α_- using photoproduction data in combination with Fierz identities,

$$O_x^2 + O_z^2 + C_x^2 + C_z^2 + \Sigma^2 - T^2 + P^2 = 1 \quad (3.8)$$

$$\Sigma P - C_x O_z + C_z O_x - T = 0. \quad (3.9)$$

As all observables in Eqs. (3.8) and (3.9) were measured by CLAS [642, 643, 805], these Fierz identities can be used to estimate the calibration parameters l , c , and a , where l and c are the relative systematic uncertainties of the linear and circular photon polarization, while a varies the value of the weak decay parameter α_- . It is known that O_x , O_z , T scale with al , C_x and C_z scale with ac , Σ scales with l , and P with a . If one has sufficiently many measurements, this set of scaling conditions together with the Fierz identities of Eqs. (3.8, 3.9) allow to extract the scaling factor a , and, hence, a re-determination of α_- . Special care has to be paid to statistical aspects as this problem bears a few intricacies: the Fierz identities are to be fulfilled in a statistical sense; the estimation of normalization factors is notoriously prone to biases that have to be avoided; and the distribution of the systematic uncertainties for linear and circular polarization are unknown. Using different priors for these distributions, a new value of $\alpha_- = 0.721(6)(5)$ was found which is close to, but not compatible with, the new BESIII value of $\alpha_- = 0.750(9)(4)$. In contrast, the previous PDG value [806] of $\alpha_- = 0.642(13)$ had been accepted and used for over 40 years, affecting all hyperon polarization data. The results are summarized in Fig. 27. In Ref. [804], the data affected by the change in α_- data were re-fitted with the JBW approach. The re-analysis shows that the lowest χ^2 is indeed obtained with the α_- value obtained from CLAS data, pointing towards internal consistency of the new value, that is now quoted in the PDG “above the line” [103].

3.3.4. Photoproduction in the ANL-Osaka approach

The partial wave T-matrix element for the meson photoproduction $\gamma(\mathbf{p}) + N(-\mathbf{p}) \rightarrow M'(\mathbf{p}') + B'(-\mathbf{p}')$ is given by Eq. (2.20) with $\alpha = \gamma N$, J , λ_γ , λ_N and $\beta = M'B', LSJ$. In the following, we simply write $\alpha = \gamma N$ and $\beta = M'B'$ to make clear the Fock-space component of the states. The photoproduction amplitude is given by a non-resonant and a resonant part,

$$T_{M'B',\gamma N}(p', p; E) = t_{M'B',\gamma N}(p', p; E) + t_{M'B',\gamma N}^R(p', p; E). \quad (3.10)$$

In the following, we assume only the first order term of the electromagnetic coupling constant e and the processes which need higher order terms like the $\gamma - \gamma$ amplitude of Compton scattering or $\gamma - Z$ amplitude of parity violating processes are not considered here. The non-resonant photoproduction T-matrix $t_{M'B',\gamma N}(p', p; E)$ is given as follows by rewriting Eq. (2.21),

$$t_{M'B',\gamma N}(p', p; E) = v_{M'B',\gamma N}(p', p) + \int_C dq q^2 \sum_{M''B''} t_{M'B',M''B''}(p', q; E) G_{M''B''}(q; E) v_{M''B'',\gamma N}(q, p), \quad (3.11)$$

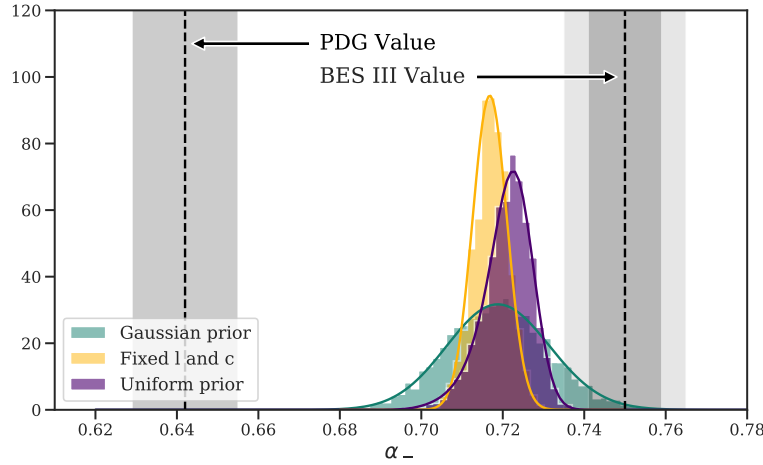


Figure 27: Posterior densities for the weak Λ decay parameter α_- from different priors for the beam polarization calibration constants P_C^γ (scaling parameter c) and P_L^γ (scaling parameter l), as indicated with the colored histograms/lines [804]. The gray vertical bands represent statistical uncertainty for the old PDG [806] and the new BESIII [803] values. Figure taken from Ref. [804].

which includes all order of the strong interaction within the model and the first order electromagnetic interaction $v_{MB,\gamma N}$. The potential $v_{MB,\gamma N}$ is constructed by the s -, t -, and u -channels hadron exchange processes applying Eq. (2.9). The resonant T-matrix $t_{M'B',\gamma N}^R(p', p; E)$ is given by Eq. (2.26) with the dressed electromagnetic helicity amplitude $\bar{\Gamma}_{\gamma N,j}(p; E)$ of N_j^* as

$$t_{M'B',\gamma N}^R(p', p; E) = \sum_{i,j} \bar{\Gamma}_{M'B',i}(p'; E) [G_{N^*}(E)]_{i,j} \bar{\Gamma}_{\gamma N,j}(p; E). \quad (3.12)$$

The dressed helicity amplitude $\bar{\Gamma}_{\gamma N,j}$ is given as

$$\bar{\Gamma}_{\gamma N,j}(p; E) = \Gamma_{\gamma N,j}(p) + \int_C dq q^2 \sum_{MB} \Gamma_{MB,j}(q) G_{MB}(q; E) t_{MB,\gamma N}(q, p; E). \quad (3.13)$$

This formula corresponds to Eq. (3.3) of the JBW model. Due to the non-resonant electromagnetic meson production process $t_{MB,\gamma N}$, the bare helicity amplitude $\Gamma_{\gamma N,j}$ is dressed $\bar{\Gamma}_{\gamma N,j}$ as illustrated in Fig. 28. The contribution of non-resonant processes is called the “meson cloud effect”.

The pion photoproduction reactions are investigated up to the second resonance region $1.1 < W < 1.6$ GeV in Ref. [79]. Starting from the strong interaction model JLMS [78] of the pion induced reaction, the bare resonance helicity amplitudes are the only free parameters adjusted to describe the data of pion photoproduction. Large effects of coupled channel in the second resonance region are found. The Q^2 dependence of the meson could effects are studied, which are important in the low- Q^2 region.

The current ANL-Osaka DCC model [87] is an extension of the JLMS model [78]. In the extension (1) $K\Lambda$ and $K\Sigma$ states are included in addition to the $\pi N, \eta N, \pi\pi N$ and $\pi\Delta, \rho N, \sigma N$ states, (2) a unified analysis of πN and γN reactions is performed, (3) the analysis is extended to include higher-energy $\sqrt{s} < 2.1$ GeV reactions. The single energy solutions of the SAID partial wave amplitudes are fitted up to $\sqrt{s} < 2.3$ GeV while πN and γN reactions are analyzed below $\sqrt{s} < 2.1$ GeV. Lists of the fitted observables and the number of data points are given in Ref. [87]. The bare helicity amplitudes $A_\lambda^{N^*}$ are parametrized using magnetic $M_{l\pm}^{N^*}$ and electric $E_{l\pm}^{N^*}$ multipole amplitudes as

$$A_{3/2}^{N^*} = \frac{\sqrt{l(l+2)}}{2} [-M_{l+}^{N^*} + E_{l+}^{N^*}], \quad A_{1/2}^{N^*} = -\frac{1}{2} [lM_{l+}^{N^*} + (l+2)E_{l+}^{N^*}] \quad \text{for } j = l + 1/2 \quad (3.14)$$

$$A_{3/2}^{N^*} = -\frac{\sqrt{(l-1)(l+1)}}{2} [M_{l-}^{N^*} + E_{l-}^{N^*}], \quad A_{1/2}^{N^*} = \frac{1}{2} [(l+1)M_{l-}^{N^*} - (l-1)E_{l-}^{N^*}] \quad \text{for } j = l - 1/2. \quad (3.15)$$

In Ref. [87], $M_{l\pm}^{N^*}$ and $E_{l\pm}^{N^*}$ are parametrized by the low-energy photon momentum dependence of the magnetic and electric multipole amplitudes and include a damping factor for the large momentum behavior. The bare helicity amplitudes were treated as constant in the previous analysis [79]. The results of the model for observables and the multipole amplitudes can be found on a web site [807].

3.3.5. Summary of the light baryon spectrum

In Fig. 29 the baryon spectrum is shown as determined by the ANL-Osaka [87] and the JBW [57] approaches. The upper set of pictures shows the pole positions with uncertainties ordered by isospin and parity. The two lower pictures

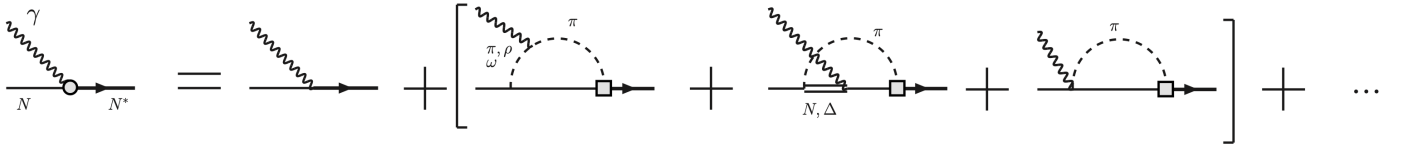


Figure 28: Graphical illustration of the contribution of the πN intermediate state to the dressed $\gamma N \rightarrow N^*$ [76] transition. The term in brackets illustrates the meson-cloud effect.

display similar information in bar plots, but with PDG states in addition. Here, the heights of the bars correspond to the resonance widths. The resonance spectrum in the JBW approach has changed over the years, with an example discussed in Sect. 3.3.7.

Overall, both approaches exhibit a similar spectrum although there are remarkable differences, especially for some of the widths. Other than S_{11} and P_{11} , both approaches find two N^* with $J^P = 3/2^+$, but the heavier one differs in mass and width. For $J^P = 1/2^-$ and $J^P = 3/2^-$, the JBW approach has only one Δ resonance, while the ANL-Osaka has two. For the positive parity $J^P = 3/2^+$, both approaches have, of course, the $\Delta(1232)$. The JBW approach has a $\Delta(1600)$ and a very wide, heavy Δ resonance. It is debatable how stable such wide resonances are under re-parameterizations of the amplitude, which is why the ANL-Osaka approach only quotes states up to 400 MeV width. See also Sect. 2.10.2 where stability tests for resonance signals are discussed. Another question is the bias induced by fitting to the SAID partial-wave analysis. Like in many other analyses, information from SAID on elastic πN scattering is contained in both analyses, and many states of the SAID analysis are also quoted in the PDG. This might induce a confirmation bias. The solution lies in directly fitting the elastic πN data. However, this is complicated because of a very inhomogeneous data set with systematic uncertainties that are often unknown. See Sect. 3.2 for a discussion.

3.3.6. Highlight: The S_{11} partial wave

The $J^P = 1/2^-$ partial wave features the excited states $N(1535)$, $N(1650)$ and, possibly, an $N(1895)$. As Fig. 29 shows, the ANL-Osaka and JBW approaches find the first two resonances but not the third state. The latter state has been found in the BnGa analysis that also contains the $\eta'N$ channel [653] (it is also found in the Kent State analysis [751]). Once the DCC approaches contain this channel, a need for that state may arise.

Theoretical interest in studying the first state, $N(1535)$, roots in the fact that it is heavier than the second state of the parity-partner channel P_{11} , the Roper resonance $N(1440)$, which challenges the expectation from quark models [318, 319, 326]. Furthermore, inelastic meson-baryon thresholds (ηN , $K\Lambda$, and $K\Sigma$) are located close to the first two $J^P = 1/2^-$ states, such that coupled channel effects need to be taken into account. In Ref. [808] it was argued that the $N(1535)$ couples even stronger to the $K\Lambda$ than to the ηN channel by examining BES data, see also Ref. [809].

Within chiral unitary models, it was realized early [460] that low-lying S_{11} resonances might not be a three-quark (pre-existing) states but rather be generated by strong channel dynamics, with a substantial $K\Sigma - K\Lambda$ component in their wave functions. This idea was extended in Ref. [188], where within certain approximations the effects of 3-body $\pi\pi N$ channels were also included. In Ref. [457], the S_{11} phase shift was fitted from threshold to about $\sqrt{s} \approx 2$ GeV together with cross section data for $\pi^- p \rightarrow \eta n$ and $\pi^- p \rightarrow K^0 \Lambda$ in the respective threshold regions. This led to a satisfactory description of the S_{11} phase. Two poles were found corresponding to the $S_{11}(1535)$ and the $S_{11}(1650)$ resonances together with a close-by unphysical pole on the first Riemann sheet. More recently, it was pointed out in a meson-exchange model that there is indeed strong resonance interference between the two S_{11} resonances, as each of these resonances provides an energy-dependent background in the region of the other [115].

In Sect. 2.10.1 a scheme to solve the four-dimensional Bethe-Salpeter equation with chiral LO and NLO contact terms was discussed. The resulting coupled-channel, chiral unitary amplitude was derived in Ref. [39], and the low-energy constants were fitted to the SAID partial waves providing a compelling picture of a dynamically generated $N(1535)$ as a pole on the second Riemann sheet shown in Fig. 13. Additionally, a second pole is recorded outside of the fitted energy region. It is quite tempting to assume this to be a prediction of the $N(1650)$ state from chiral dynamics and coupled-channel unitarity.

Coupled-channel dynamics is an integral aspect of the $N(1535)$, irrespective of its nature. This resonance is located very closely to the ηN threshold to which it also couples very strongly [103]. As resonance poles usually repeat on different Riemann sheets (see discussion in Sec. 2.9.1), one has here the situation of a regular $N(1535)$ and a hidden $N'(1535)$ on a different sheet that, together, generate the particular ηN cusp structure of the S_{11} partial wave as illustrated in Fig. 30.

It should be noted that this is not what is usually referred to as “two-pole nature” of a resonance. In the limit of vanishing coupling of a resonance to an inelastic two-body channel, it (trivially) repeats on both sheets of that channel at the exact same position. If the channel coupling is stronger, as it is the case for the $N(1535)$ and the ηN channel, the poles repeat at substantially different positions. In contrast, the $\Lambda(1405)$, which is believed to have a true two-pole nature, has both its poles on the same Riemann sheet [280, 281].

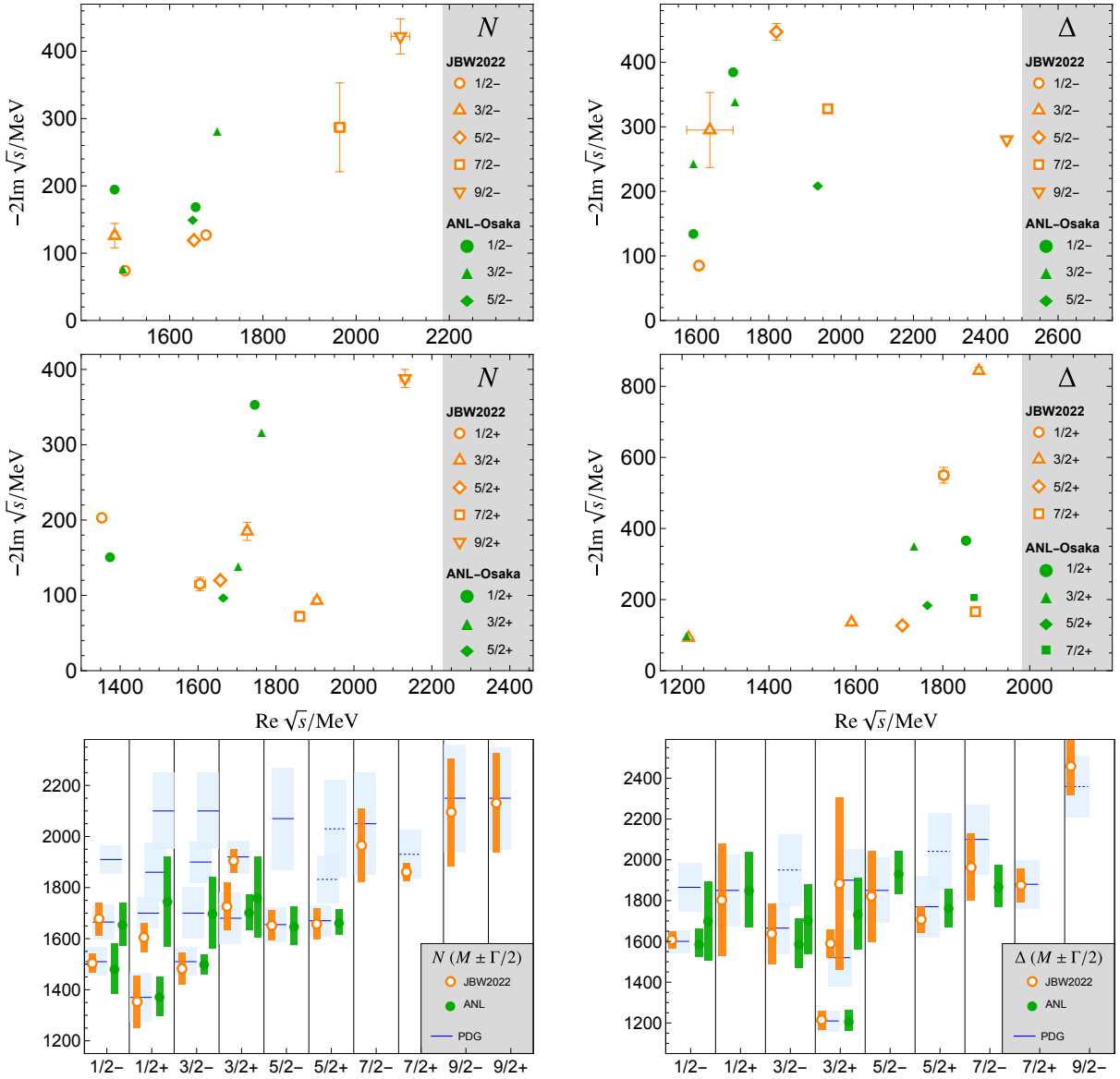


Figure 29: Summary of results for the baryon parameters obtained in the ANL-Osaka [87] and JBW [57] approaches. The error bars in the upper four plots show uncertainties, the lengths of the bars in the two lower plots correspond to the resonance widths. For these cases, PDG information [103] is displayed in blue. Note that for the ANL-Osaka model, only resonances up to 2 GeV in mass and 400 MeV in width are quoted.

To the right in Fig. 30, the real part of S_{11} from the fit of Ref. [124] is shown (dark red). In addition we show the “pole approximations” (PA) of the $N(1535)$ and the hidden $N'(1535)$ with the solid and dotted blue line as indicated in the figure. These curves are given by $a_{-1}/(E - E_0)$ where a_{-1} is the residue of the pole at $E = E_0$. Consequently, the dotted curve only shows the “shoulder” of the hidden $N'(1535)$. Indeed, the shapes of these two PA’s explain the cusp quantitatively. Still the PA’s of the $N(1535)$ and $N(1650)$ show a large offset with the actual partial wave - this reflects the fact that each of these resonances provides a substantial background for the other one.

In addition to these PA’s, there is another PA from a virtual state (VS) at $E_0 = (1031 - i 203)$ MeV shown with the dashed line, that explains the sharp rise of the S_{11} partial wave at threshold. While that state was found in Ref. [124] in 2009, no claims for its existence were made as it is located far from the physical axis and the amplitude parametrization of Ref. [124] was rather simple. However, this state has recently received substantial interest. In Ref. [810] (see also Ref. [811]), Wang et al. discovered it at $E_0 = (861 \pm 53) - i(130 \pm 75)$ MeV using the general Peking University (PKU) representation [812–815] in connection with relativistic baryon chiral perturbation theory to estimate the contributions from the left-hand cut. In Ref. [816] the sub-threshold singularity was found again at $E_0 = (918 \pm 3) - i(163 \pm 9)$ MeV in a Roy-Steiner analysis that was checked numerically with the previous framework of Hoferichter et al. [119]. Resonance poles in the latter analysis were searched in Ref. [122]. Apart from a determination of the $\Delta(1232)$ and Roper poles, the subthreshold pole at $E_0 = (913.9 \pm 1.6) - i(168.9 \pm 3.1)$ MeV was found again. There have also been dispersive studies of low-energy pion photoproduction [817, 818] extracting the photocoupling of that state which was found to be substantial.

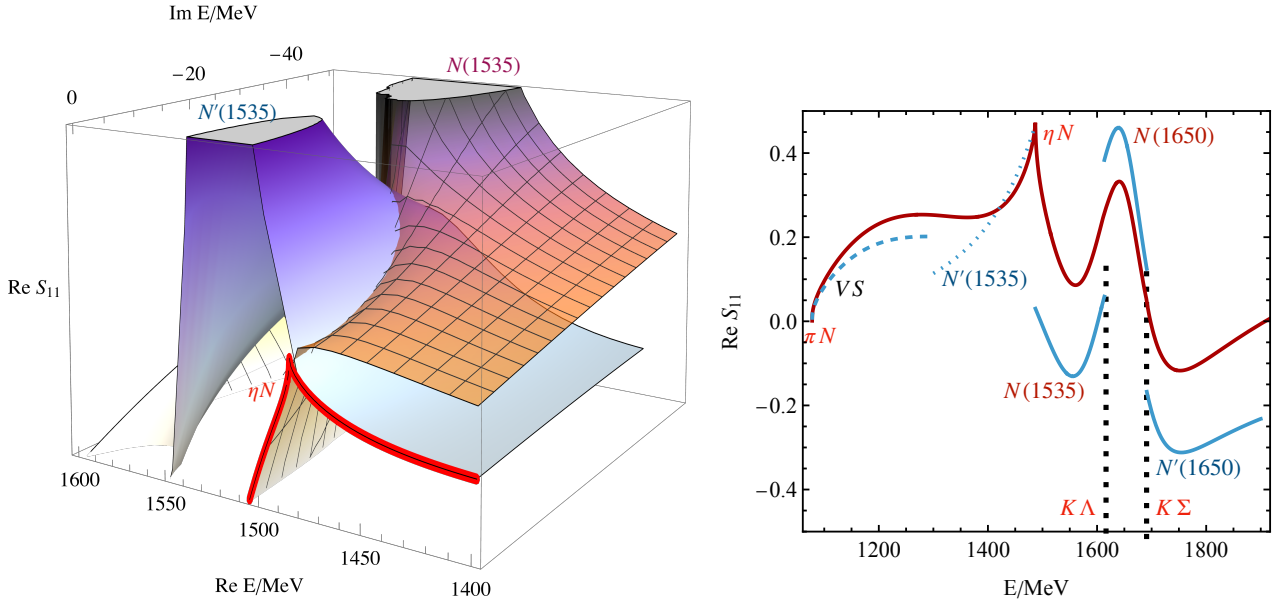


Figure 30: **Left:** In orange, the $N(1535)$ on the sheet connected to the physical axis (red line) above the ηN cusp; in blue, a hidden replica $N'(1535)$ on the sheet connected to the physical axis below the ηN cusp. Together, they generate the particular cusp structure and unusual $N(1535)$ shape of the S_{11} amplitude (red solid line). See also Fig. 16 for a discussion on cusp structures. **Right:** The real part of the S_{11} amplitude (dark red) with two-body thresholds and residue terms $a_{-1}/(E - E_0)$ where a_{-1} is the residue of the pole at $E = E_0$ (blue dashed, dotted, and solid lines). The enhancement of $\text{Re } S_{11}$ at the πN threshold is due to a virtual state (VS) as the blue dashed line shows. See text for further explanations. Figures adapted from Ref. [124].

The pole trajectory of the state with pion mass has been studied in a linear σ model [819]. While there are now strong indications for this state, “the physical interpretation of this singularity is far from obvious, as its position, far in the complex plane, casts doubts on its relevance for observables in the physical region” [122].

3.3.7. Highlight: The P_{11} partial wave

In the nucleon channel $J^P = 1/2^+$, the properties, interactions, and nature of the $N(1440)$ or Roper resonance [597, 820] have been discussed extensively. The reversed mass pattern between $N(1535)$ and $N(1440)$ appeared as a puzzle in quark models [318, 319, 326]. A proper description in the constituent quark model can be achieved by including Goldstone bosons as effective degrees of freedom [821]. Note that most recent functional methods do indeed reproduce the right ordering [410]. For further details see the review [398].

Phenomenological analyses reveal an intricate analytic structure of the Roper [115, 170, 544] including strong coupling to the three-body channels. Indeed, the P_{11} partial wave has an early and strong onset of inelasticity [170]. This is related to the fact that for the $J^P = 1/2^+$ quantum numbers three particles π, π, N can all be in a relative S -wave, i.e., there is no centrifugal barrier that could suppress the influence of three-body channels in the σN channel (and other effective two-body channels such as a πN system with $J^P = 1/2^-$ and a third pion). In addition, the Roper pole is close to the complex $\pi\Delta$ branch point as shown in Fig. 14. As poles repeat on different sheets, there is a complicated interaction of two poles and a complex branch point as first noted by the SAID group [170]. On the physical axis, this leads to the unusual, non-Breit-Wigner shape of the Roper. As discussed before, one would *not* refer to this as a two-pole resonance like the $\Lambda(1405)$, since for the latter both poles lie on the same Riemann sheet.

As there is a σN channel in relative S -wave, where σ stands for the $f_0(500)$, the “threshold” of that pseudo-two-body system lies, indeed, around the Roper $N(1440)$ mass. Dynamically generated states are often situated close to two-body S -wave thresholds, and, indeed, the Roper resonance has been found as dynamically generated from this channel in the JB approach without a qqq core [49, 51]. Mass trajectories in specific amplitude parametrization, that fit QCD lattice eigenvalues, seem to support the dynamical generation [525]. A substantial ingredient in this picture is also the renormalized nucleon pole that has a pole part reaching to energies above the πN threshold (see Sect. 2.6.3 and Fig. 38 in Ref. [53]). The Roper resonance was also dynamically generated in the multichannel model of Refs. [822, 823] in which quark model predictions were used to fix coupling constants.

In the ANL-Osaka model, the Roper resonance appears from dressing a bare state (“genuine resonance”) through coupled channels [86]. In fact, even the next-higher state, the $N(1710)1/2^+$ originates from the same bare state as shown in Fig. 31 to the left. The corresponding trajectories are obtained by slowly switching on the bare pole self energies in the different channels. While both pictures of the Roper are intriguing and allow for their own interpretation, they also demonstrate the dependence of the interpretations (of the same data) on the underlying parametrization. In

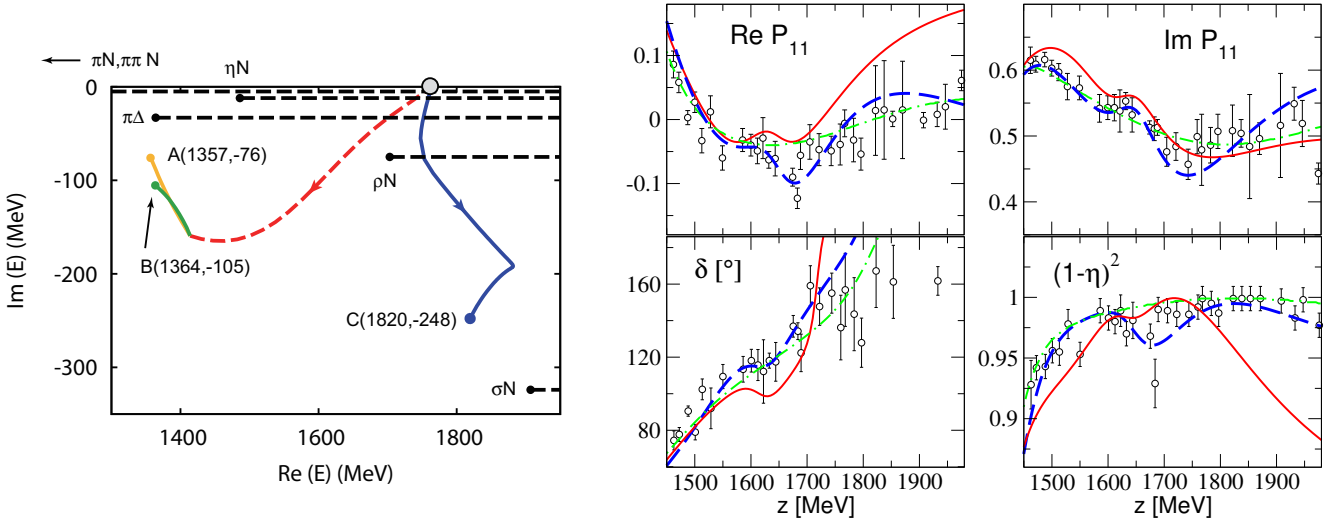


Figure 31: **Left:** The Roper poles A, B and the $N(1710)$ pole C in the ANL-Osaka parametrization of Ref. [86], on different Riemann sheets. The trajectories are obtained by slowly switching off the self energies of a genuine s -channel state showing that, in this parametrization, the resonances originate from the same bare state. Here, the cuts are run into the real-energy direction in contrast to Fig. 14 where they are run into the negative $\text{Im } E$ direction. **Right:** Detail of the partial-wave amplitude (top) and phase shift/inelasticity (bottom) of the elastic $\pi N \rightarrow \pi N$ P_{11} wave in the JB solution of 2012 [53], as a function of energy $z = E$. Shown are fit A (solid red lines) and fit B (dashed blue lines) that represent fits to the energy-dependent GWU/SAID solution [170] (dash-dotted green lines). The single-energy solution [170] (data points) is *not* included in the fitting procedure but predicted. Figures taken from Refs. [53, 86].

Fig. 43 of Ref. [53] the dependence of the bare mass on the bare resonance couplings and included channels was studied. It was shown that one can obtain very similar descriptions of the $\Delta(1620)$ amplitude in the S_{31} wave for variations of the bare mass over more than a GeV (with corresponding variations of bare couplings). In contrast, as expected, resonance residues change very little.

The dependence of the extracted resonance parameters on the reaction model and the accuracy of the empirical partial wave amplitude are commonly investigated issues. In the ANL-Osaka model, the analytic structure of the P_{11} amplitude near the nucleon pole is rather different from the JBW model. In Ref. [128], a bare nucleon state is included with mass and vertex renormalization. Then, the SAID amplitude is re-fitted and the CMB amplitude is examined for comparison. The results indicate that the pole structure of the Roper resonance is rather insensitive to the analytic structure below the πN threshold. In addition, the study showed the need for more accurate data in the $\sqrt{s} > 1.6$ GeV region for precise extraction of poles.

Many attempts have also been made to tackle the Roper channel through Lattice QCD, but no definite conclusions have been drawn despite significant efforts [515, 517, 824–828]. More sophisticated lattice studies [284, 285] followed later, consistently ruling out the exclusive qqq interpretation of the Roper-resonance. Instead the sizable coupling to the five-quark operators (meson-baryon states) is noted in Ref. [285]. In a recent lattice calculation, a multi-two-body-channel model was set up to extend the energy range up to the next excited state beyond the Roper [525]. Owing to different available pion masses, resonance pole trajectories were mapped out.

Notably, there is a missing level [284, 829, 830] when comparing to the expectation from elastic πN scattering alone. There are also further attempts based on Hamiltonian effective field theory (HEFT) [530] to interpret the measured finite-volume spectrum [284]. The clean solution to analyzing the finite-volume spectrum of the Roper resonance lies in correctly including the three-body dynamics in form of the $\pi\pi N$ inelastic channels, see Ref. [831] for progress in this direction. For progress of finite-volume three-body physics in general, see Sect. 2.11.3 and reviews [200, 241].

In Fig. 31 to the right, the region around $\sqrt{s} = E \approx 1.7$ GeV is displayed in more detail. The figure shows, apart from solutions A and B from the 2012 JBW analysis [53], the energy-dependent P_{11} partial wave from Ref. [170] that was fitted (green dash-dotted lines). The SES (data) were *not* fitted. Nonetheless, fit B, and to some extent also A, do exhibit the structure of the SES from Ref. [170] as the $N(1710)$ moved to that position. In the 2012 JB analysis, the inclusion of the $N(1710)$ became necessary for an entirely different reason, i.e., to improve the description of the $\pi^- p \rightarrow K^0 \Lambda$ differential cross section and polarization data. In Ref. [53], the unexpected repercussion for elastic πN scattering was taken as strong evidence for a resonance at this energy, and as a powerful demonstration how DCC approaches connect different reactions.

The existence of the $N(1710)$ resonance has also been advocated for based on ηN data [595]. While the existence of this resonance is well established, nowadays the P_{11} partial wave around that energy has served as a testing ground to discuss the role of complex threshold openings from three-body channels in baryon spectroscopy [195]. The starting point of this exercise is the smooth, energy-dependent P_{11} amplitude from SAID or an older version of the JBW amplitude that

both do not contain an $N(1710)$ pole, but which both *do* contain the complex threshold opening of the ρN channel (see Fig. 14) at around the same energy, $E = M_N + E_\rho$ where E_ρ is the complex $\rho(770)$ pole position. This amplitude is then fit with an early version of the Carnegie-Mellon-Berkeley type model developed by the Zagreb group [593–596] which does not contain this branch point, but which does contain resonances to fit amplitude structures. Indeed, the fit demands a resonance at $E = (1698 - i130)$ MeV which simulates the branch point missing in that model. The exercise demonstrates the need to explicitly include known non-analyticities like complex threshold openings in amplitude parametrizations, to avoid false positives in baryon detection.

3.4. Electroproduction reactions

Electromagnetic probes of strongly interacting matter provide independent access to emergent phenomena of QCD such as resonances. Photoproduction reactions have been used to determine the spectrum and properties of excited baryons [539, 540] as analyzed by different groups [54, 87, 605, 624, 625, 746, 752]. These analyses allow for a comparison to theory like lattice QCD [265, 516–518, 832–838] or quark models [321, 323, 326, 329, 333, 821, 839–842]. See Ref. [1] for a review. Notably, first calculations of meson-baryon scattering amplitudes in lattice QCD have appeared recently, some of them containing the $\Delta(1232)3/2^+$ resonance [520–522, 843, 844]. Complementary to photoproduction reactions, radiative decays of excited baryons, such as measured by CLAS [845–851], can reveal information about the nature of the $\Delta(1700)$ resonance [483] and the $\Lambda(1405)$ and $\Lambda(1520)$ hyperons [482, 486].

In addition, the momentum transfer of the probe can be tuned once the photon is allowed to become virtual, testing strong interactions at different scales. Indeed, electroproduction reactions are a prime tool to study the structure of excited baryons [351, 383, 384, 852, 853], but they also serve to discover new baryonic states [854] as discussed below. One cannot directly test the response of a resonance to a virtual photon, but determine transition form factors (TFFs) in the electro-excitation of the resonance from the nucleon. One can also map out the transverse charge density by using electromagnetic form factors [855]. The Q^2 -dependent multipoles can also be used to test calculations within chiral perturbation theory [856–863] and unitary extensions [200, 478, 481], chiral resonance calculations [864, 865], quark models [337, 341, 359, 376, 866–871] and other theory predictions [872–875]. Notably, a chiral unitary framework for kaon electroproduction was developed in Ref. [38] and extended later [42, 43]. Transition form factors also serve as point of comparison for dynamical quark calculations referred to as Dyson-Schwinger approaches [402–405, 410, 417, 876–878]. In this context, remarkable agreement of the lower-lying baryon spectrum with predictions has been achieved [410, 878], showing little evidence for a “missing resonance” problem at lower energies. See Refs. [315, 378, 382, 399, 409] for reviews. Methods to study the Q^2 -dependence of resonance couplings in lattice QCD were proposed in Ref. [879]. A pioneering lattice calculation was carried out recently in the meson sector [880].

Transition form factors have been defined in different ways [382], but the only reaction-independent definition is given in terms of Q^2 -dependent couplings at the resonance pole, to be determined by an analytic continuation of electroproduction multipoles [881]. We review the steps taken in the JBW model towards determining TFFs at resonance poles.

The multipoles themselves are determined by analyzing the exclusive electroproduction of one or more mesons. The advantage of simultaneously analyzing different final states in a coupled-channel approach lies in the factorization of the amplitude at the pole, i.e., the fact that the resonance TFF is the same for any final state, by construction.

Single-channel analyses of single-meson electroproduction data have a long history; one of the first approaches is MAID for pion photo- and electroproduction [624, 882], later complemented by a chiral-MAID approach at low energies [714]. There is also the etaMAID2001 analysis on eta electroproduction [709]. See Ref. [883] for a review. The CLAS collaboration extracted helicity amplitudes for several resonances from their experiment using two different methods, namely a unitary isobar model and an amplitude constructed with fixed-t dispersion relations, developed by Aznauryan [379, 884–886]. One of the findings was the unusual zero in the $A_{1/2}$ Roper form factor. See also the analysis of Refs. [887–889] on the extraction of TFFs and their role in different reactions. See also Refs. [758, 768, 890–892] for electroproduction analyses using tree-level effective Lagrangian frameworks.

Questions on efficient parametrizations of electroproduction amplitudes and transition form factors are discussed in Refs. [352, 893–895]. The two-pion electroproduction reaction has also been measured at CLAS [896–901] and analyzed with the JM reaction model [854, 887, 902, 903], see also Ref. [904]. Consistent results on N^* electroexcitation amplitudes obtained from independent studies of two major exclusive meson electroproduction channels in the resonance region, with different non-resonant contributions πN and $\pi^+ \pi^- p$, support the reliable extraction of these quantities.

In Ref. [854] the existence of a second $N(1720)3/2^+$ is claimed which would be the first resonance exclusively discovered in electroproduction. Notably, much higher Q^2 values for resonance transition form factors become accessible in ongoing CLAS12 experiments [378, 905]. Most relevant for the present analysis of $K\Lambda$ electroproduction is KAON-MAID [712, 906], an analysis using an effective Lagrangian approach [892], and the more recent analyses using a Regge-plus-resonance amplitude [218, 907]. See Ref. [908] for an overview of kaon electroproduction reactions and Refs. [553, 783, 784, 788, 791, 909, 910] for related analyses and theoretical developments by JPAC and others.

The data situation in electroproduction reactions is more challenging than in photoproduction. On the one hand, this is due to the presence of another kinematic variable in addition to the energy W , namely the virtuality of the photon

$Q^2 = -q^2$, where q is the transferred four-momentum of the photon. Even though the number of data points is larger in electro- than in photoproduction, the data are still sparser due to this additional variable. On the other hand, there are longitudinal multipoles to be determined from data, in addition to the electric and magnetic ones that parametrize the photoproduction amplitudes. While there are in principle more spin observables than in photoproduction [706], fewer have been measured than in photoproduction.

However, the data situation is improving rapidly through new measurements with the CLAS12 detector [905, 911, 912]. CLAS12 is the only available facility in the world capable of extending information on the evolution of the N^* electroexcitation amplitudes towards $Q^2 = 10 \text{ (GeV}/c)^2$. The first measurements with the CLAS12 of inclusive $(e, e'X)$ cross sections [913] have revealed the presence of resonance structure in the second and third resonance regions, suggesting promising prospects for the extraction of N^* electroexcitation amplitudes within the range of $Q^2 \leq 10 \text{ (GeV}/c)^2$. The development of coupled channel approaches capable of extracting N^* electroexcitation amplitudes within that range represents an important and very needed direction in theory support of these ongoing experimental efforts.

The related question of how many measurements are necessary to determine a truncated partial-wave expansion of the electroproduction amplitude is discussed in Refs. [687, 690].

The sparse data situation is another motivation for the simultaneous analysis of $\pi N, \eta N, K\Lambda, K\Sigma$ electroproduction data, apart from the above mentioned property of amplitudes factorizing at resonance poles, improving the reaction-independent extraction of TFFs. The available world data consists mostly of cross sections but includes also some polarization observables. A summary of the data is provided in the table in Fig. 32, most of them being included in the latest JBW analysis [61]. Sometimes structure functions are extracted from cross sections in which case JBW analyzes only the underlying cross sections. There are also data on $K\Sigma$ electroproduction [846, 848, 850, 914], but they are not yet included in the JBW analysis.

The JBW group analyzed πN [59], ηN [60], and, most recently, the combined πN , ηN , and $K\Lambda$ electroproduction data base [61]. Each time the maximal energy was increased requiring the inclusion of more and more partial waves, currently up to F -waves. The approach represents the first coupled-channel electroproduction analysis, while data at the photon point ($Q^2 = 0$) are also included as a boundary condition from the JBW approach to pion [54], eta [55], and $K\Lambda$ [56] photoproduction [57] and pion-induced reactions [53, 104]. Specifically, the JBW electroproduction multipoles are constructed in close analogy to the photoproduction multipoles of Eq. (3.1),

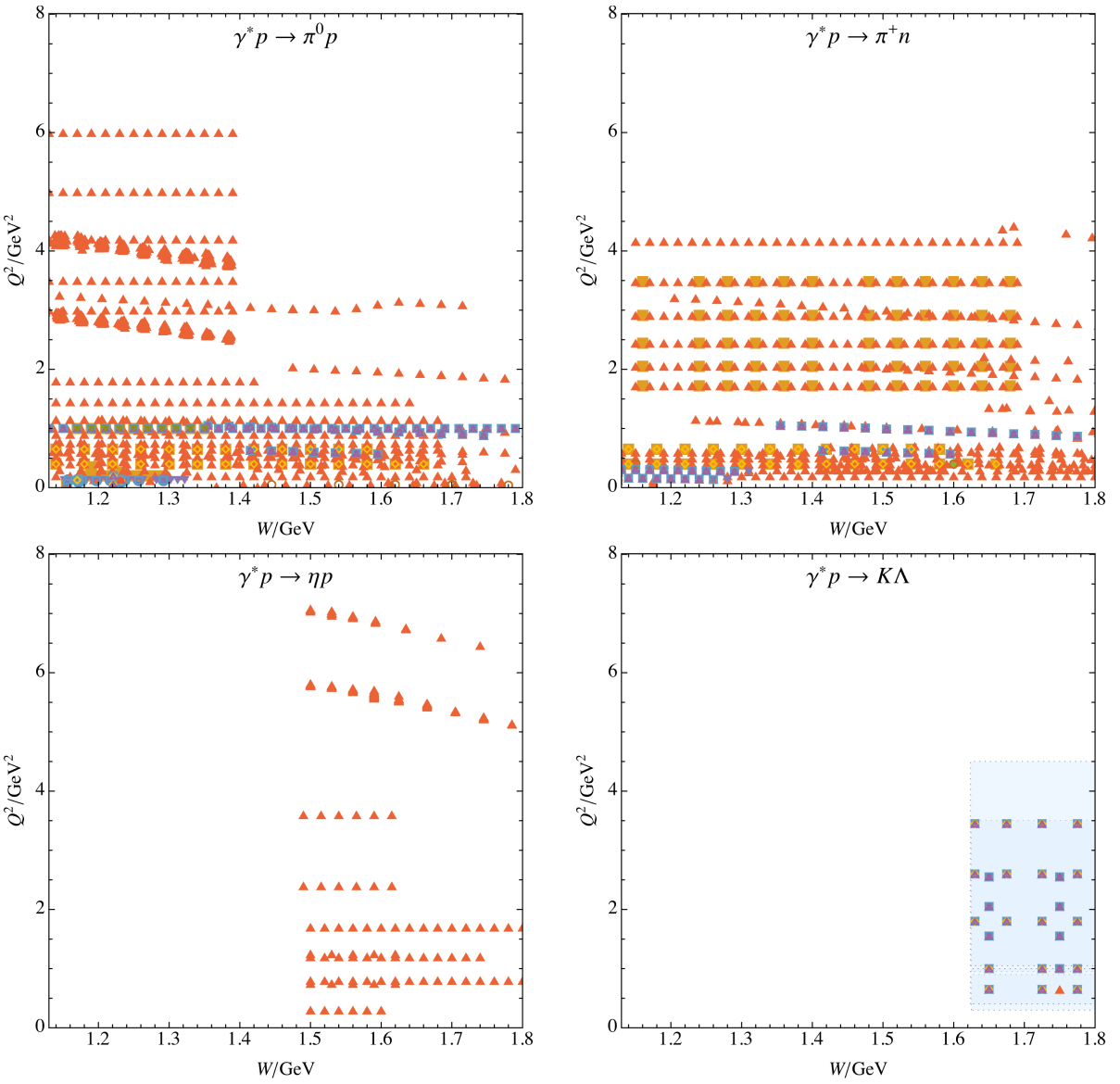
$$\mathcal{M}_{\ell,\mu\gamma^*}(p', E, Q^2) = R_{\ell'}(\lambda, q/q_\gamma) \left(V_{\ell,\mu\gamma^*}(p', E, Q^2) + \sum_{\kappa} \int_0^\infty dq q^2 T_{\ell,\mu\kappa}(p', q; E) G_\kappa(q, E) V_{\ell,\kappa\gamma^*}(q, E, Q^2) \right), \quad (3.16)$$

for outgoing meson momentum p' , total energy $E = \sqrt{s}$, and $\kappa, \mu, \nu \in \{\pi N, \eta N, K\Lambda, \pi\Delta, \rho N\}$ meson baryon channels. Note that there are no real or virtual photon couplings to the $K\Sigma$, σN states included, while the hadronic rescattering encoded in T does contain these channels. As no $K\Sigma$ electroproduction data are analyzed yet, the input from the photoamplitude is taken from Ref. [56] which does not contain the analysis of $K\Sigma$ photoproduction, either. The multipoles in Eq. (3.16) are formulated for a given angular momentum ℓ , $\mathcal{M}_{\ell,\mu\gamma^*} \in \{E_\ell, M_\ell, L_\ell\}$ are the electroproduction multipoles. The G_κ are meson-baryon propagators (see Sects. 2.5 and 2.7.2); R'_ℓ is a barrier factor ensuring correct threshold behavior while taming its high-momentum behavior. It depends on the photon momentum q and $q_\gamma = q(Q^2 = 0)$ [61]. For the connection of ℓ and ℓ' see also Ref. [61]. The $V_{\mu\gamma^*}$ are the Q^2 -dependent photon transitions such that for $Q^2 = 0$ they exactly match the JB2017 photoproduction solution [56]. Note that longitudinal multipoles cannot be matched to photoproduction data. Instead, a valuable constraint is provided through the long-wavelength limit encoded in the so-called Siegert's condition [969, 970].

Apart from π and η electroproduction data, the JBW analyses [59–61] fit cross section data for $\gamma^* p \rightarrow K\Lambda$ from CLAS. Notably, the data base was recently enlarged through the addition of beam-recoil transfer polarization data from CLAS [914]. This data is confronted (no fit) with the predictions of the JBW approach in Ref. [61], demonstrating the need for further analysis. While the comparison of data and fit solutions of pion- and real-photon-induced reactions with JB have been collected on a website [629], the JBW electroproduction solutions are collected on another interactive website [802].

After adjusting the amplitude parameters in the simultaneous to πN , ηN , and $K\Lambda$ electroproduction data, results for TFFs can be calculated. In the JBW coupled-channel approach, twelve N^* and Δ transition form factors at the pole were extracted recently in Ref. [626] using data with the center-of-mass energy from πN threshold to 1.8 GeV, and the photon virtuality $0 \leq Q^2/(\text{GeV}/c)^2 \leq 8$. For the $\Delta(1232)$ and $N(1440)$ states, the results are in qualitative agreement with previous studies, while the transition form factors at the poles of some higher excited states are estimated for the first time. Since quarks are charged, the electroproduction probe can provide a spatial scan of the charge density ρ of, e.g., $p \rightarrow N^*$ transition in a certain reference frame [351, 971, 972]. This is shown in Fig. 33.

In the ANL-Osaka model the electroproduction data are analyzed by extending the model of the pion- and photon-induced reactions. The parameters for this analysis are the Q^2 dependence of the bare helicity amplitudes $\Gamma_{\gamma N,j}$ of Eq. (3.13) and the new parameters on the transition charge form factors $S_{l\pm}^{N^*}$. The first analysis addressed the pion electroproduction reaction around the $\Delta(1232)$ resonance region [75]. Analyzing the available data at that time for



Type	$N_{\text{data}}^{\pi^0 p}$	$N_{\text{data}}^{\pi^+ n}$	$N_{\text{data}}^{\eta p}$	$N_{\text{data}}^{K\Lambda}$
• ρ_{LT}	45 [915, 916]	—	—	—
■ $\rho_{LT'}$	2768 [917–921]	5068 [922, 923]	—	—
◆ σ_L	—	2 [924]	—	—
▲ $d\sigma/d\Omega$	48135 [918, 919, 925–946]	44266 [923, 930, 945, 947–959]	3665 [960–963]	2055 [846, 850]
▼ $\sigma_T + \epsilon\sigma_L$	384 [915, 918, 925, 925, 939, 940, 964–966]	182 [948, 953]	—	204 [846, 850]
○ σ_T	30 [943]	2 [924]	—	—
□ σ_{LT}	373 [915, 918, 925, 925, 939, 940, 964–966]	138 [948, 953]	—	204 [846, 850]
◇ $\sigma_{LT'}$	214 [917, 939, 964, 965]	208 [917]	—	156 [847, 850]
△ σ_{TT}	327 [925, 925, 939, 940, 965, 966]	123 [948, 953]	—	204 [846, 850]
▽ K_{D1}	1527 [919]	—	—	—
● P_Y	—	2 [967, 968]	—	—
Total	53804	49989	3665	2823

Figure 32: World data and data types for meson-electroproduction process. The kinematical region covered by the recent beam-recoil transferred polarization measurement of Ref. [914] is represented by the blue shaded area. Figure and table adapted from Ref. [61].

$Q^2 = 2.8$ and $Q^2 = 4$ (GeV/c) 2 [929], three transition form factors G_M, G_E, G_C , which are related to the helicity amplitudes, were obtained. The magnitude of the Coulomb quadrupole coupling G_C at $Q^2 = 0$ was obtained from G_E assuming the relation between the electric and Coulomb form factors in the long wave length limit, i. e., Siegert's theorem. The model predicted a characteristic enhancement of form factors due to the meson cloud illustrated in Fig. 28. These predictions were later confirmed in the low- Q^2 region. The extensive data on pion electroproduction from CLAS in the $\Delta(1232)$ region are re-analyzed in Ref. [76]. Based on the $\pi N, \eta N, \pi\Delta, \sigma N$ and ρN coupled-channel JLMS model [78], single pion

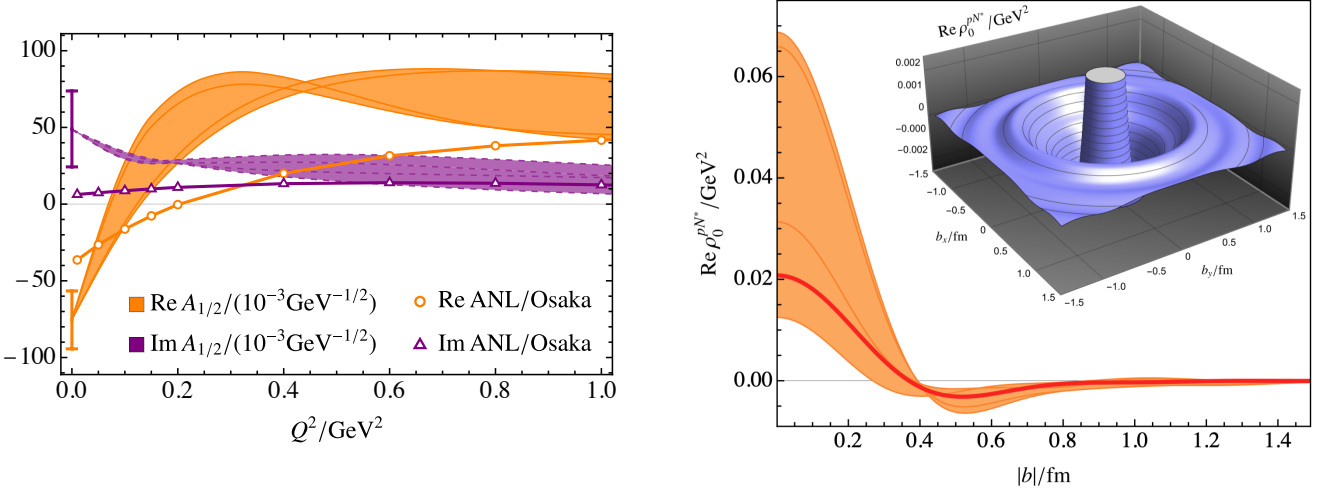


Figure 33: **Left:** $N(1440)$ transition form factors at small Q^2 from the JBW analysis [626] in comparison with the ANL-Osaka solutions [93]. The error bars at $Q^2 = 0 \text{ GeV}^2$ depict the uncertainties of the photoproduction solution at the pole from Ref. [56]. A zero in the real part of the TFF is observed. **Right:** Unpolarized transverse charge density ρ_0^{pN*} of the $p \rightarrow N(1440)$ transition as a function of the transverse position b in the xy -plane from Refs. [61, 626]. The orange band (thick red line) depicts the uncertainty band of the determination (the result using the MAID 2007 helicity couplings [624]). The inset shows the corresponding representation in position space.

electroproduction data for $\sqrt{s} < 1.6 \text{ GeV}$ and $Q^2 < 1.45 (\text{GeV}/c)^2$ are studied in Ref. [80]. The $\gamma^* N \rightarrow N^*$ helicity amplitudes for $P_{33}, P_{11}, S_{11}, D_{13}$ resonances are extracted and their Q^2 dependence and meson cloud effects are discussed.

In Ref. [85], $\gamma N \rightarrow N^*$ helicity amplitudes are studied as the residue of the scattering amplitude for the first time at finite Q^2 . In terms of the pole expansion of the Green's function, helicity amplitudes can be understood as nucleon to resonance transition form factor $\langle N^* | J_\mu^{EM}(Q) | N \rangle$. Within the JLMS model, the helicity amplitudes are extracted for the $P_{33}(1232), D_{13}(1521), P_{11}(1357), P_{11}(1820)$ resonances up to $Q^2 < 1.45 (\text{GeV}/c)^2$. Using the ANL-Osaka model [87], N^* helicity amplitudes are determined in Ref. [92] for the $Q^2 < 3 (\text{GeV}/c)^2$ region. The parametrization of the bare helicity amplitudes of the vector current are given in Appendix C of Ref. [92]. In this analysis, all available data of the single pion electroproduction data and also empirical parametrization of the structure function W_1^{em}, W_2^{em} [973] are used. The data on η and K electroproduction are not included in the analysis. The model is constructed for the neutrino reaction which is supposed to cover the resonance region below the DIS region. The model including two-pion production is reasonably consistent with the nucleonic PDF at $x \sim 0.45$ (where $\sqrt{s} \sim 2 \text{ GeV}$), as shown in Fig. 34 taken from Ref. [974]. The extracted helicity amplitudes $A_{1/2}, A_{3/2}$ of the $P_{33}(1232), D_{13}(1520)$ resonances from the ANL-Osaka model agree reasonably well with those from the JLMS model for $Q^2 < 1.45 (\text{GeV}/c)^2$ [975]. The $A_{1/2}$ helicity amplitude of the Roper resonance reported in Ref. [93] is shown in Fig. 33.

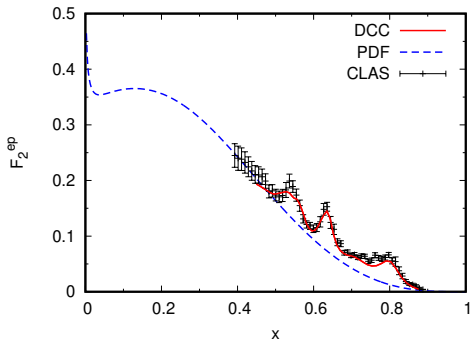


Figure 34: The proton structure function F_2 for inclusive electron-proton scattering at $Q^2 = 2.425(\text{GeV}/c)^2$ with the ANL-Osaka model (red solid curve) and with the nucleonic PDF (blue dashed curve). The horizontal axis shows the Bjorken scaling variable x . The data are from Ref. [976].

3.5. Applications in neutrino physics

Neutrino-induced reactions have recently received much attention in the context of long base-line experiments such as T2K, HK, DUNE [977–979] and atmospheric neutrino data. To extract neutrino properties such as CP violation and the

neutrino mixing angle, the precise understanding of neutrino reactions in the GeV neutrino energy range plays a crucial role [974, 980–982]. For neutrino energies from around 1 GeV to a few GeV, meson production is the main mechanism of the neutrino-nucleus reaction.

Isobar models provide simple and useful parametrizations of neutrino reactions in the resonance region. The Rein-Sehgal model [983, 984] has often been used in neutrino reaction generators. In this model, the amplitude is constructed using Breit-Wigner forms for nucleon resonances with the masses, widths, and branching ratios from the PDG. Coupling constants have been estimated with a relativistic quark model. Theoretical analyses from the 1970’s, mainly for the $\Delta(1232)$ region using isobar models and dispersion theory, are summarized in Ref. [985].

The model of Hernández et al. [986–988] (HNV model) includes the $\Delta(1232)$ and non-resonant mechanisms from the chiral Lagrangian. The vector form factors of the resonances are determined from the analysis of electron scattering data. The model is improved to satisfy the requirement of unitarity using Watson’s theorem for the single-pion production region [989]. Several extensions of HNV including higher resonances such as $N(1535)1/2^-$, $N(1440)1/2^+$ and $N(1520)3/2^-$ were developed, for a detailed discussion see Ref. [990]. The model of neutrino-induced single-pion production [991] is a hybrid model based on the HNV approach for the low- W region and a reggeized, non-resonant amplitude based on the chiral Lagrangian for the higher $W > 2$ GeV region.

For energies above the $\Delta(1232)$, many meson-baryon channels such as $\pi N, \pi\pi N, \eta N, K\Lambda, K\Sigma$ open up, rendering the construction of a model for the multi-resonance and multi-channel neutrino reaction very challenging. The coupled-channel approach is a way to construct such a model, which is constrained by the extensive data of pion-, photo- and electro-production data. The first attempt along this line was made in Refs. [992, 993] for the Δ resonance region, and then the model was extended for $W < 2$ GeV and $Q^2 < 3(\text{GeV}/c)^2$ in Refs. [91, 92] based on the ANL-Osaka model. A coupled-channel approach has also been used to study the strangeness-changing production of $\Lambda(1405)$ in antineutrino-proton interactions [994]. Below, we briefly review the current status of the ANL-Osaka coupled-channel model for neutrino reactions in the resonance region for strangeness-conserving processes.

In the Standard Model, the hadronic weak charged current (CC) and neutral current (NC) together with the electromagnetic current (EM) are given in terms of the vector (V_μ) and axial (A_μ) currents as

$$J_\mu^{\text{CC}}(x) = V_{ud}(V_\mu^\pm(x) - A_\mu^\pm(x)) , \quad (3.17)$$

$$J_\mu^{\text{NC}}(x) = (V_\mu^3(x) - V_\mu^s(x)) - (A_\mu^3(x) - A_\mu^s(x)) - 2 \sin^2 \theta_W J_\mu^{\text{EM}}(x) , \quad (3.18)$$

$$J_\mu^{\text{EM}}(x) = V_\mu^3(x) + V_\mu^{\text{IS}}(x) , \quad (3.19)$$

where the superscript \pm indicates the isospin raising (lowering) current, ‘3’ is the third component of the isovector, and ‘IS’ is the isoscalar current. In the model, strange currents V^s and A^s are not taken into account.

The starting point of the neutrino-nucleon reaction model [92] is the ANL-Osaka model [87]. There, all model parameters that govern hadronic interactions are determined through the analysis of pion-, photon-, and electron-induced meson-production reactions. The contributions of the individual isovector and isoscalar vector currents are obtained from the analysis of the proton and deuteron reactions [88]. However, one still needs to fix the remaining unknown axial current. The non-resonant axial current can be derived from a chiral Lagrangian on which the πN interaction potentials are based. By construction, the non-resonant axial current and the πN potentials are related by the PCAC relation at $Q^2 = 0$. The neutrino-induced forward reactions for various meson production channels, which are related to the $\pi N \rightarrow X$ reaction are studied in Ref. [91]. The axial $N-N^*$ transition strengths at $Q^2 = 0$ are related to the corresponding πNN^* couplings via the PCAC relation. The advantage of the approach is that one can uniquely fix not only the axial coupling strengths but also their phases. The Q^2 dependencies of the axial couplings are difficult to determine because of the lack of experimental information. Here, one assumes that all of the axial couplings have the dipole Q^2 dependence of $1/(1 + Q^2/M_A^2)^2$ with $M_A = 1.026$ GeV.

The total cross sections of ν_μ induced CC single pion production on proton and neutron of the ANL-Osaka model and the HNV model are shown in Fig. 35 in comparison with the ANL [995, 996] and BNL [997] data. The final state of $\nu p \rightarrow l^- \pi^+ p$ is a purely isospin $3/2$ amplitude, therefore, a large part of the cross section is due to the $\Delta(1232)$, while $\nu n \rightarrow l^- \pi^+ n$ and $\nu n \rightarrow l^- \pi^0 p$ contain the contribution of the $I = 1/2$ amplitude. Both models agree reasonably well, while they both lie slightly above the data in the 1–2 GeV region. For $\nu n \rightarrow l^- \pi^+ n$, the discrepancies between the two models are larger in the high-energy region. The experimental data are obtained from the analysis of νd reactions. Effects of the final state interaction and deuteron wave function within the ANL-Osaka model are studied in Refs. [998, 999], and are found to enhance the cross section at the quasi-elastic peak by 10% to 30% for the $\nu n \rightarrow \mu^- \pi^+ n$ channel.

The mechanism of pion production can be closely examined by the angular distribution of the pion. In the massless lepton limit, the formula of the neutrino-induced pion production can be written in a similar way as pion electroproduction,

$$\frac{d\sigma_{\text{CC}}}{d\Omega' dE'_l d\Omega_\pi^*} = \frac{|\mathbf{k}'|}{|\mathbf{k}|} \frac{G_F^2}{4\pi^2} (A^* + B^* \cos \phi_\pi^* + C^* \cos 2\phi_\pi^* + D^* \sin \phi_\pi^* + E^* \sin 2\phi_\pi^*) . \quad (3.20)$$

Here, the pion angular distribution is expressed in the πN center of mass system and ϕ_π^* is the angle between the lepton scattering plane and the πN production plane. Comparing with the well known formula for pion electroproduction, we

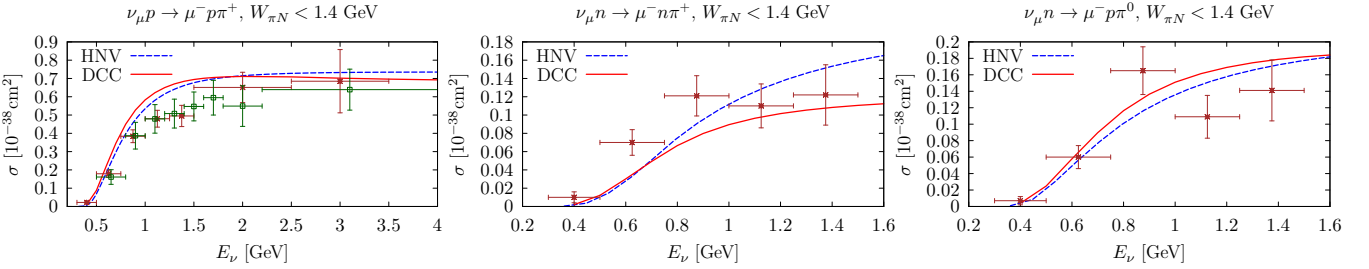


Figure 35: The $\nu_\mu N \rightarrow \mu^- \pi N$ total cross section as a function of the neutrino energy. The experimental data have been taken from the reanalysis of old ANL (crosses) and BNL (open square) data [997] done in Ref. [996]. The $W_{\pi N}$ cut is $W_{\pi N} < 1.4$ GeV.

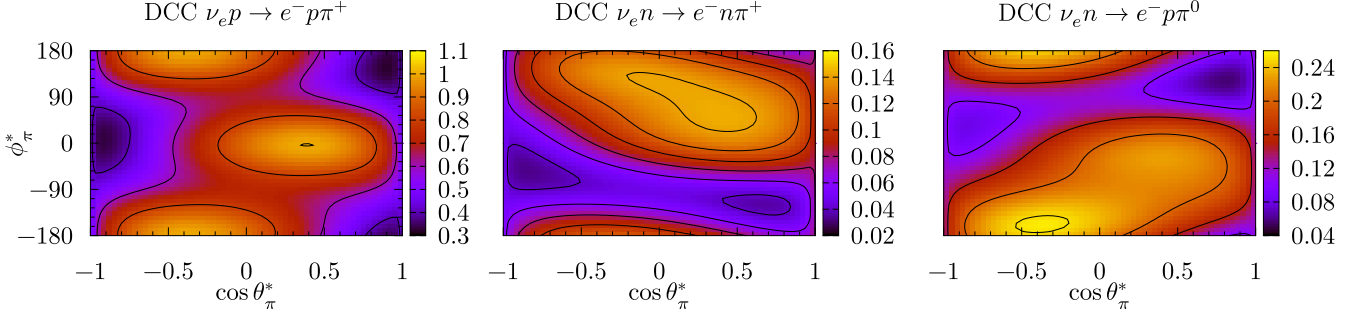


Figure 36: Neutrino-nucleon cross section $d\sigma/dQ^2/dW_{\pi N}/d\Omega_{\pi}^*$ in units of $10^{-38}\text{cm}^2/\text{GeV}^3$ for $E_\nu = 1\text{ GeV}$, $W_{\pi N} = 1.23\text{ GeV}$, and $Q^2 = 0.1\text{ GeV}^2$.

note that there is no E^* term in electron scattering. In Fig. 36, the contour plot of the neutrino-nucleon cross section at $W_{\pi N} = 1.232\text{ GeV}$ is shown. The cross section is calculated with the ANL-Osaka model. The parity violation effect $d\sigma(\phi_{\pi}^*) \neq d\sigma(-\phi_{\pi}^*)$ is apparent. Therefore, the D^* and E^* terms should have a similar size as the A^*, B^*, C^* terms.

The excitation spectrum of the neutrino-induced single-pion production reaction $d\sigma/dW_{\pi N}$ is shown in Fig. 37. The data are taken from the CERN bubble chamber BEBC [1000]. For comparison, the cross section is calculated using the ANL-Osaka model at $E_\nu = 50\text{ GeV}$ and the normalization is adjusted for the $\nu_\mu p \rightarrow \mu^- \pi^+ p$ reaction. The reaction $\nu_\mu p \rightarrow \mu^- \pi^+ p$ is dominated by the $\Delta(1232)$, while for the other reactions isospin $I = 1/2$ structures are important in the high $W_{\pi N}$ region. Also note that for the $\nu_\mu n \rightarrow \mu^- \pi^+ n$ channel, the strength of N^* resonances is significant.

Inclusive double-differential cross sections $d\sigma/dW/dQ^2$ for the neutron target carry important physical information. The result is shown in Fig. 38. There, the prominent peak due to the $\Delta(1232)$ has a long tail toward the high Q^2 region. Contributions of the second resonance region are also seen in the single-pion production cross section. A similar contour plot is shown for double-pion productions. The situation looks very different from the single-pion production case. The main contributions are from the second and the third resonance region.

The ANL-Osaka model of the neutrino-induced meson production reaction is constrained from the experimental data of pion-, photon-, and electron-induced reactions as far as possible. However, there is a limitation on the axial vector current to data-driven phenomenological models because of the lack of experimental data. Except for the $\Delta(1232)$ region, all of the existing models for the neutrino-induced meson production reactions use assumptions on the Q^2 dependence of the axial vector current such as the dipole form factor discussed before. The predicted CC structure functions F_i for high Q^2 of the reaction model are known to miss strength in comparison with the parton model even though the model predicts reasonably well for EM structure functions. Possible effects to improve the situation by modifying the axial form factors are discussed in Ref. [990]. Further progress in the theoretical modeling of weak meson production reactions

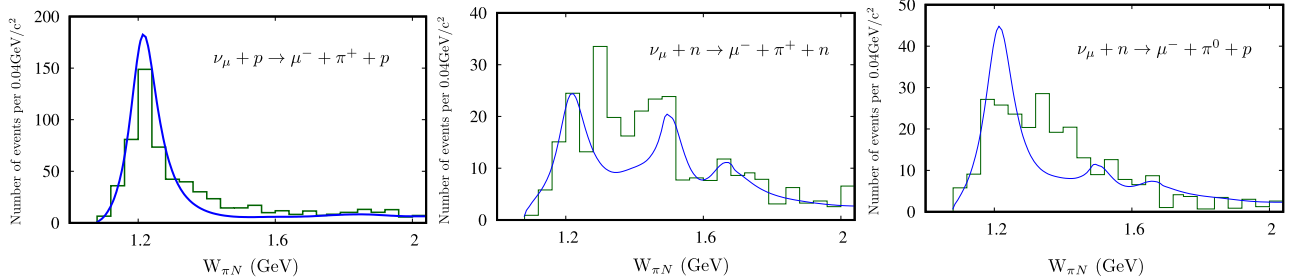


Figure 37: Cross section $d\sigma/dW_{\pi N}$ of the single-pion production reaction.

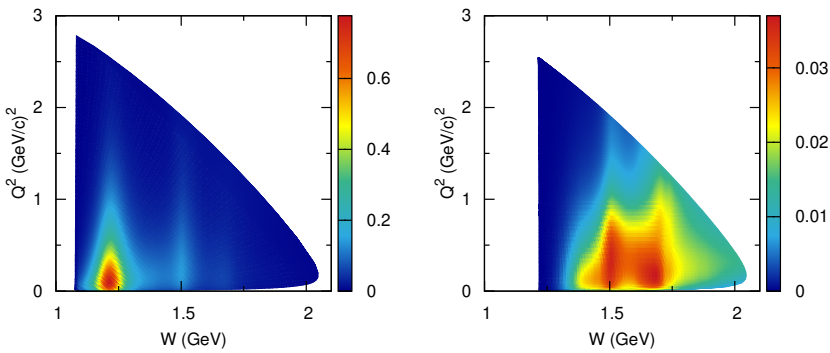


Figure 38: Contour plots of $d\sigma/dW/dQ^2$ for $\nu_\mu n \rightarrow \mu^- \pi N$ (left) and $\nu_\mu n \rightarrow \mu^- \pi^+ \pi^- p$ (right) at $E_\nu = 2$ GeV.

requires new measurement of (anti)neutrino inelastic scattering on hydrogen and deuterium targets.

3.6. DCC approaches for strangeness systems

Generally, the spectrum of excited hyperons (Y^*) is much less known than that of non-strange excited nucleons (N^* and Δ). This is mostly owed to the fact that experiments with open strangeness are harder to conduct because the reaction participants decay quickly. However, some options exist, such as using secondary Kaon beams, as proposed for example in the upcoming KLF experiment [1001], and in ongoing and planned experiments at J-PARC [632, 1002, 1003]. Regarding the latter, for example, spectroscopy of Ξ hyperons (P97), of Ω baryons (P86), access to the region below $\bar{K}N$ threshold ($\Lambda(1405)$) [1004] (E31), measurements of a missing-mass spectrum near the ΣN threshold (“ ΣN cusp”) [1005] (E90), as well as a study of the $\eta\Lambda$ final state [1006] (E72) are on the agenda. Future measurements in this direction are also discussed for the AMBER experiment [1007, 1008] and as an opportunity for SIS100@FAIR [1009]. Another alternative is to use photo-induced reactions and separating a third particle (spectator) carrying one unit of strangeness away as in the CLAS experiment [1010]. Also, multi-step decays of charmed states as in the Belle analysis of the $\Xi^- \pi^+$ invariant mass spectrum [1011] carry new information. See the recent review by Crede and Yelton [1012]. There is also the femtoscopic methodology employed for example by the ALICE collaboration [1013], see the review [586]. In the latter cases the theoretical analysis is complicated by the less known systematics in the creation mechanism of the open-strangeness configurations. For a critical discussion see Ref. [1014]. Obviously, the situation becomes even more complicated if one is interested in higher-strangeness states, and even less is known there regarding the resonance spectrum. For more details and other options see recent reviews [200, 503, 585, 1015].

Theoretically, the by far largest interest in this field was generated from chiral perturbation theory and unitarization techniques such as described in Sect. 3.3.6. Specifically, CHPT is derived from QCD by integrating out heavy degrees of freedom. Interaction patterns of this Effective Field Theory for the meson-baryon scattering are used then in a unitarized approach to extend the region of applicability to a resonance region. Overall, the inclusion of chiral symmetry and S-matrix principles constrains the amplitudes such that predictions can be made outside of the data region leading for example to a prediction of the second isoscalar pole of the $\Lambda(1405)$, for more details see reviews [200, 585, 1015]. We restrict ourselves in the following to the context of DCC models only.

Most of the past partial wave analyses for investigating Y^* resonances were performed using the Breit-Wigner parametrization. An analysis aiming at the extraction of the poles and their residue of the partial wave amplitudes was presented only more recently [1016]. In the multi-channel K-matrix method, the $K^- p$ reactions were analyzed in Refs. [1017, 1018] (KSU). In Ref. [1019], the amplitudes of Refs. [1017, 1018] are used to extract resonance parameters. The Bonn-Gatchina (BnGa) group analyzed the strangeness sector with their K-matrix approach, describing not only two but also three-body final states. Resonance parameters were extracted in Refs. [1020–1022].

In DCC approaches, two-body meson-baryon interactions consist of s -, t - and u -channel hadron exchange mechanism as described in section Sect. 2. The data on $K^- p$ reactions were analyzed by the Juelich group [16, 276] and, recently, by the ANL-Osaka group [94, 95]. In the Juelich approach to the KN [1023, 1024] and $\bar{K}N$ [16] interactions, most of the parameters of the model are constrained from SU(3) flavor symmetry. Additional parameters are fixed from the analysis of KN and $\bar{K}N$ elastic and inelastic cross section data that existed at the time. The channels included for negative strangeness are $\pi\Lambda$, $\pi\Sigma$, and $\bar{K}N$. The three-body channels $\bar{K}\Delta$, \bar{K}^*N , and $\bar{K}^*\Delta$ are perturbatively included in the form of box diagrams. The $\Lambda(1405)$ is predicted as a $\bar{K}N$ quasi-bound state and exhibits a two-pole structure [276] similar to that observed in works performed in chiral unitary approaches [200]. The validity of the model is limited to energies below the $\Lambda(1520)$ resonance.

In the ANL-Osaka model [94, 95], coupled channel equations for the two-body states $MB = \bar{K}N, \pi\Sigma, \pi\Lambda, \eta\Lambda, K\Xi, \pi\Sigma^*, \bar{K}^*N$ and the three-body states $\pi\pi\Lambda$ and $\pi\pi\Sigma$ are formulated as given in Sect. 2. The data used in the analyses of the

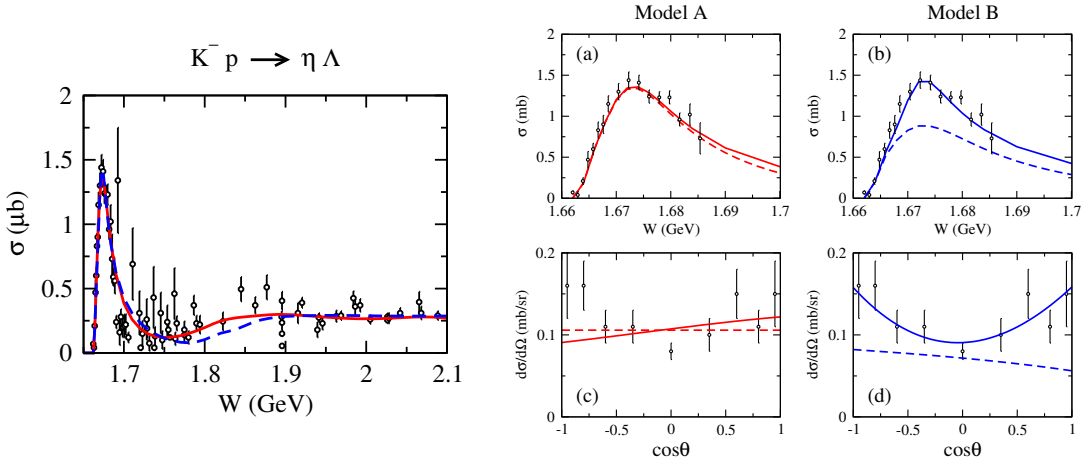


Figure 39: Total cross section for $K^- p \rightarrow \eta \Lambda$ (left). Total cross section near the threshold (right top) and differential cross section (right bottom) at $\sqrt{s} = 1672$ MeV for $K^- p \rightarrow \eta \Lambda$ (right). Red (blue) curves are results of model A (B) in the ANL-Osaka approach [94]. Solid curves are the full results, while the dashed curves are results obtained by turning off the P_{03} partial wave.

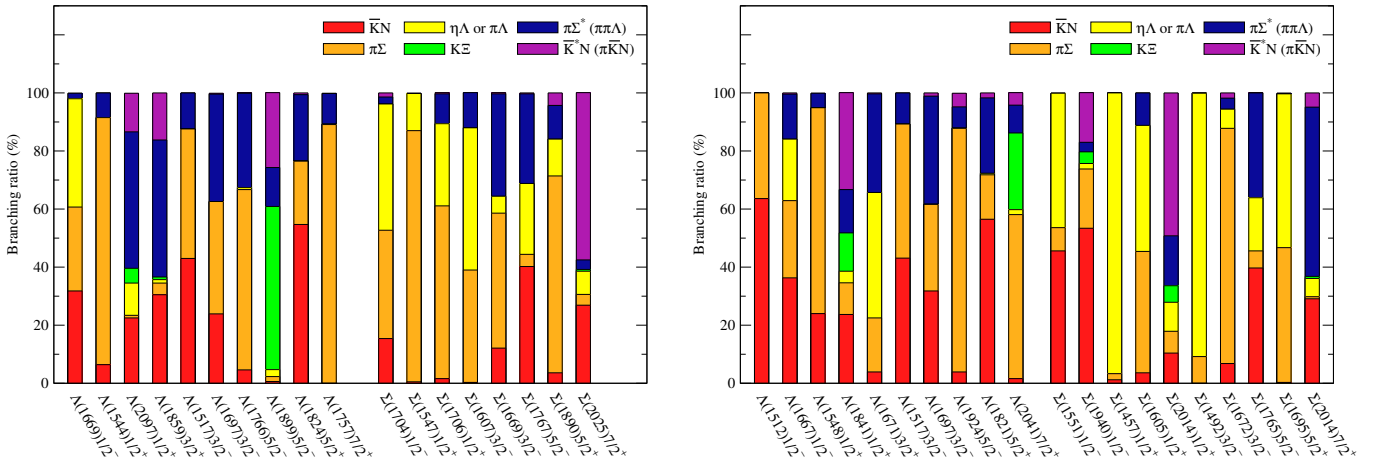


Figure 40: Branching ratio for the decay of Λ^* and Σ^* in model A (left) and model B (right). Figure adapted from Ref. [95].

ANL-Osaka model [94] and the KSU model [1017] are unpolarized differential and total cross sections and polarization observables of the $K^- p \rightarrow \bar{K}N, \pi\Sigma, \pi\Lambda, \eta\Lambda, K\Sigma$ reactions. In addition, the ANL-Osaka group also studied strangeness production on the deuteron [1025]. In Ref. [1022] by the BnGa group, $\omega\Lambda$ and the three-body final states $K^- p \rightarrow \pi^0\pi^0\Lambda, \pi^0\pi^0\Sigma$ are included in the fits as well. In the work of the ANL-Osaka group [94], two solutions (model A and model B) have been obtained which have quite different values for the model parameters, while both models fitting the $K^- p$ data only have similar quality of data description. Results for the energies of Y^* resonances from model A, B [95] and KSU [1017] show excellent agreement for several states. However, in some cases large discrepancies are also seen, mirroring the fact that the existing $K^- p$ data are not yet sufficient to constrain the mass spectrum of Y^* . The $S_{01}(1/2^-)$ resonance around 1.67 GeV has a large contribution to the total cross section of $K^- p \rightarrow \eta\Lambda$ as shown in the left panel of Fig. 39. The situation is similar to the total cross section of $\pi^- p \rightarrow \eta n$ and the role of $S_{11}(1535)$. Around the $\eta\Lambda$ threshold region, model B additionally predicts a narrow P -wave resonance $P_{03}(3/2^+)$ at $E = 1671^{+2}_{-8} - i(5^{+11}_{-2})$ MeV. This resonance couples strongly with $\eta\Lambda$. About 40% of the peak of the total cross section is due to this P_{03} resonance in model B, while the $S_{01}(1670)$ resonance dominates the peak of the cross section in model A. The difference between the model A and model B shows up in the angular distribution of $\eta\Lambda$ as shown in Fig. 39 suggesting that the data of angular distribution seems to favor the p -wave contribution and resonance in model B.

For both models also the branching ratios of the Y^* resonances are determined. They are depicted in Fig. 40. The results show large branching ratios to $\pi\Sigma^*$ and \bar{K}^*N states for higher-energy resonances, suggesting the importance to establish those resonance from the data of three-body reactions $KN \rightarrow \pi\pi\Lambda, \pi\bar{K}N$. For some cases, see, e.g., the lowest Λ $1/2^-$ or $1/2^+$ states, both models predict not only similar masses but also similar coupling to different channels. Less pronounced agreement in some other cases indicates the need for more precise data to pin down the properties of the hyperons. This again emphasizes the importance of experimental updates [1001, 1007–1009] discussed at the beginning of this section.

4. Three-meson systems: the ANL-Osaka and IVU models

The previous discussion of excited baryons has shown that the elastic energy window is usually small, making it necessary to consider coupled channels and three or more body dynamics. Indeed, already the first excited state of the nucleon, the Roper-resonance $N^*(1440)1/2^+$, is above the $\pi\pi N$ threshold, decaying substantially into effective three-body channels $f_0(500)N$ and $\pi\Delta$ causing the unusual line shape of that resonance [53, 496, 544, 598]. Some resonances like the $a_1(1260)$ meson decay overwhelmingly into three particles [103]. The same is expected for the lightest meson with exotic spin-parity quantum numbers, $J^{PC} = 1^{-+}$, the $\pi_1(1600)$ that was found by COMPASS [1026]. This state is currently a subject of extensive experimental and theoretical investigations [1027, 1028], see also Refs. [199, 1029] for recent reviews. Three-body effects can also be relevant for the other exotic candidates, like the $X(3872)$ [1030], the $Y(4260)$ [1031], or the $T_{cc}^+(3875)$ [1032, 1033] observed in the charmonium spectrum close to various three-body thresholds.

In experimental analyses, the description of three-body final states with unitary isobar amplitudes has made substantial progress recently. See Refs. [123, 126, 130, 1034–1041] for formal developments. In close conceptual connection to Refs. [134, 142] highlighted in this section, in Ref. [1042] a three-body unitary coupled-channel framework was used to analyze $K_SK_S\pi^0$ Dalitz plot pseudodata for the $J^{PC} = 0^{-+}$ amplitude in the $J/\psi \rightarrow \gamma K_SK_S\pi^0$ decay related to the controversial $\eta(1405/1475)$, extracting also the associated resonance poles. That framework is conceptually related to the pioneering work by the ANL-Osaka group [1043, 1044]. The final-state interaction of three pions in the decays of $a_1(1260), \pi_2(1670), \pi_2(2100)$ and D^0 and also the photon-induced three pion production is investigated in DCC. The role of particle-exchange interaction (Z diagram) needed for three-body unitarity is demonstrated for the Dalitz plot, the phase of the decay amplitudes, and the extraction of resonance pole and residue. See also Refs. [165, 1040] for other unitary three-body coupled-channel applications. Ref. [165] is an attempt of a unified description of the various final states in $e^+e^- \rightarrow c\bar{c}$ similar to the N^* analysis with DCC.

Three-body rescattering effects can also be quantified using Khuri-Treiman (KT) equations and in similar frameworks by the Bonn group, JPAC, and others for light meson decays [126, 1034, 1036, 1045–1065]. Faddeev-type arrangements of chiral two-body amplitudes were used to predict resonance states and to study known ones [496, 499, 1066–1069]. See also Ref. [1070] for a pedagogical introduction into dispersive methods and Ref. [1071] for connections between Khuri-Treiman equations and three-body unitary methods. We also highlight Ref. [1072] in which KT and Omnès-functions for the two-body part were used to study $\pi\rho$ rescattering in close relation to the physical systems discussed in this review.

In experiments producing excited baryons there is often a well-defined initial state such as πN , $\bar{K}N$, or $\gamma^{(*)}N$. This usually simplifies modeling the production mechanisms. For example, in elastic πN scattering or pion-induced meson-baryon production, there is no need to model the production mechanism separately from the coupled-channel rescattering, at all. Sometimes, however, the production mechanism is not fully known as in the study of excited mesons with three-body channels. In some cases, like semi-leptonic τ decays, the production via a highly virtual gauge boson filters quantum numbers of the three-meson system, like in case of the a_1 [134]. In high-energy experiments, on the other hand, many partial waves are simultaneously excited through complicated production mechanisms. One way of dealing with the dependence of results on the production mechanism is to kinematically divide it and check if the results depend, e.g., on the Mandelstam variable t bins [1073]. See Ref. [223] for a review on COMPASS physics.

In the pertinent experimental analyses of three-body final states, the traditional “isobar model” employs line shapes (isobars) for the final 2-body correlations in the decay, without explicit three-body rescattering effects, e.g., at Crystal Barrel [1074] (includes coupled channels), BESIII [1075], Belle [1076], and LHCb [1077]. Diagrammatically, this would correspond (but not be equal) to the first term in the second line of Fig. 11: There is a complex “partial-wave amplitude” that is fit to events, and that couples to spectators and isobars which subsequently decay into asymptotically stable states - no explicit final-state interaction and no coupled channels. Both effects are, at least partially, absorbed into the complex partial wave. Recently, the COMPASS collaboration significantly advanced the analysis of the three-pion spectrum [223, 1073] by performing independent partial-wave decompositions in sub-energy bins of the two-pion subsystems, i.e., without using fixed isobar line shapes [1078]. If the isobar is “freed” in this way, the amplitude is general enough that three-body effects like rescattering and coupled channels can be accommodated. In contrast, the three-body methods discussed in this review parametrize these effects explicitly, with the consequence that the production vertex D (see Fig. 11) is always real and does not contain physical resonance information by itself.

From a theoretical point of view one can argue that manifestly implementing coupled channels and unitarity corrections in the amplitude allows for a better understanding of these effects, and, in the future, these amplitudes might even be used to analyze data directly. In addition, there are kinematic effects like triangle singularities (TS) which cannot easily be accommodated in simple isobar models. However, these effects naturally arise as coupled-channel effect (with unequal masses) in DCC approaches [157] as illustrated in the last diagram of Fig. 11. We briefly review recent developments in this respect in Sect. 4.3.

In this review, we report on the development and applications of unitary DCC amplitude with explicit rescattering and coupled channels related in concept and formalism to the previously discussed DCC approaches. The previously discussed baryonic JBW models focus on phenomenological aspects and data analysis from experiment by starting from some phenomenological Lagrangian. In contrast to this, mesonic three-body DCC approaches are sometimes related

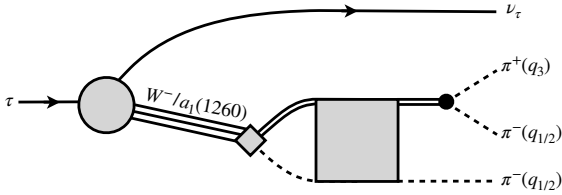


Figure 41: Factorization of the (weak) production mechanism and (hadronic) final state three-body interaction in semileptonic τ decays. Full-directed, dashed, and double lines denote leptons, mesons and auxiliary ρ fields, respectively. The initial production mechanism is shown by a shaded circle and diamond. The three-body unitary isobar-spectator interaction in the gray square corresponds to \tilde{T} from Eq. (4.5). Note that there is also a “disconnected” production of the final isobar-spectator pair in the IVU parametrization as indicated in Fig. 11. The Figure is taken from Ref. [142].

to finite-volume methods for the mapping of lattice-QCD energy eigenvalues to the physical scattering amplitudes in infinite volume. In particular, the Finite-Volume Approach (FVU) discussed in Sect. 2.11.3 uses the concept of three-body unitarity [130] discussed in Sect. 2.7.1 to construct a finite-volume amplitude in which spurious singularities cancel systematically in an interplay of disconnected and connected contributions, and exchange singularities with propagation singularities [253]. We, therefore, call the corresponding amplitudes discussed here infinite-volume unitary (IVU) approaches. While finite-volume physics is not the focus of this review [241, 242, 1079], it should be mentioned that alternative method exists, referred to as the RFT approach [258, 1080]. Here, several three-body systems of excited mesons were formulated [1081, 1082] including the unequal mass case of Refs. [138, 294] and Ref. [296] ($\eta\pi\pi$ and $K\bar{K}\pi$ channels), as well the solution of integral equations in this context [290].

In Sect. 4.1 we report the two-channel approaches of Refs. [142, 164] in which, for the first time, a three-body resonance pole was extracted from data with a unitary amplitude. In Sect. 4.2 a recent extension to the unequal mass case is discussed for a nine-channel amplitude containing pions and kaons [113]. The unequal-mass case can also lead to the formation of so-called triangle singularities in the physical region. While this is a long-known issue evaluated at the one-loop level, triangle singularities can also be understood as off-diagonal channel transitions of a three-body unitarized amplitude. Recent developments in this direction are discussed in Sect. 4.3.

4.1. A two-channel model for the $a_1(1260)$ meson

A DCC amplitude with manifest three-body unitarity (referred to as infinite-volume unitary, IVU) was developed in Ref. [134] for the two coupled partial waves $(\pi\rho)_S$ and $(\pi\rho)_D$ to study the $a_1(1260)$ resonance. This amplitude was later reformulated for the finite volume to perform the first extraction of a three-body resonance from lattice QCD data [164]. The analytic continuation of the amplitude to the $a_1(1260)$ resonance pole was explained in detail in Ref. [142] and, for the first time, the pole of that resonance was determined from experimental data using the continuation techniques discussed in Sect. 2.9.3.

See also Ref. [1083] for an extraction of the $a_1(1260)$ resonance pole with an approximately unitarity amplitude. The $a_1(1260)$ resonance can also decay to the $\pi\sigma$ channel and the branching ratio to this subdominant channel was estimated in Ref. [1084]. Different parametrizations for the a_1 meson and consequences for observables were studied in Ref. [1085]. A model that systematically includes S - and P -wave isobars and also strangeness channels was formulated in Ref. [113] and is discussed in Sect. 4.2, but it has not yet been applied to a physical system.

Coming back to the $a_1(1260)$ resonance, it couples to three-pion states in the $I^G(J^{PC}) = 1^-(1^{++})$ channel that can be decomposed as $\pi\rho$ in S/D -wave, $\pi\sigma$ and $\pi(\pi\pi)_{I=2}$ in P -waves and other channels. Phenomenologically, the channel $(\pi\rho)_S$ is dominant [1086], with the branching ratios into other channels being quite uncertain [103]. The semileptonic τ decay leading to the a_1 formation is shown in Fig. 41. The starting point to formulate the hadronic final-state interaction is, again, the connected production amplitude $\tilde{\Gamma}$ from Eq. (2.8.2) plus the disconnected part D_j that we refer to as a “bare” production mechanism in the sense that it is a real, energy and momentum-dependent function in the physical region. The index j stands for the two channels $(\pi\rho)_S$ and $(\pi\rho)_D$. The production vertices D_j contain a regular piece and a first-order pole in the three-body energy \sqrt{s} [142], similar to Eq. (3.2) for photoproduction. That pole cancels with a corresponding zero in the rescattering part just like for the photoproduction case. Also, there is now a nonzero contact term in rescattering, C from Eq. (2.83). It contains the same singularity. This corresponds to V^P in baryon amplitudes, see Eq. (2.59). Together, the matching singularities in D and C provide a flexible way to parametrize the $a_1(1260)$. Also, both D and C contain regular, real-valued terms that can depend on three-body energy \sqrt{s} and spectator momentum p . All these parts contain fit parameters that can be adjusted to data. Note the formal similarity of the overall amplitude to the photo and electroproduction amplitude in DCC model, see Eq. (3.16). In particular, the production amplitude has the same structure as the “dressed resonance creation vertex” in Eq. (2.63), consisting of a direct/disconnected piece and a rescattering/connected piece.

To connect the production amplitude to the observable $\pi^-\pi^-\pi^+$ state in τ decays, the angular dependence is introduced into the production process $\check{\Gamma}$ related to Eq. (2.90) with the help of Wigner-D functions,

$$\Gamma_{\Lambda\lambda}(\mathbf{q}_1, \mathbf{q}_2, \mathbf{q}_3) = \sqrt{\frac{3}{4\pi}} \mathfrak{D}_{\Lambda\lambda}^{1*}(\phi_1, \theta_1, -\phi_1) U_{L'\lambda'}^T \check{\Gamma}_{L'L}(q_1) U_{L\lambda} v_\lambda(\mathbf{q}_2, \mathbf{q}_3), \quad (4.1)$$

with transformation matrices U between helicity and JLS basis [112] implying sums over λ' , L , and L' and where $\mathfrak{D}_{\Lambda'\lambda}^J(\phi_1, \theta_1, -\phi_1)$ are the capital Wigner-D function with angles θ_1 and ϕ_1 giving the polar and azimuthal angles of \mathbf{q}_1 . Note the explicit appearance of the last isobar decay vertex v_λ here that contains an additional angular dependence due to the P -wave decay of the ρ (defined in its rest frame). For consistency, it should be mentioned that in Eq. (2.90) and in Ref. [113] that vertex is absorbed in the definition of $\check{\Gamma}$ while in $\hat{\Gamma}$ of Eq. (4.1) it is not, following the notation of Ref. [142].

Finally, the amplitude has to be symmetrized to account for indistinguishable particles. The amplitude $\hat{\Gamma}_{\Lambda\lambda}$, describing the decay of the axial $a_1(1260)$ -resonance at rest with helicity Λ measured along the z -axis into a π^- and a $\rho_\lambda^0 \rightarrow \pi^+ \pi^-$ with helicity λ , is given by

$$\hat{\Gamma}_{\Lambda\lambda}(\mathbf{q}_1, \mathbf{q}_2, \mathbf{q}_3) = \frac{1}{\sqrt{2}} [\Gamma_{\Lambda\lambda}(\mathbf{q}_1, \mathbf{q}_2, \mathbf{q}_3) - (\mathbf{q}_1 \leftrightarrow \mathbf{q}_2)], \quad (4.2)$$

where \mathbf{q}_1 , and \mathbf{q}_2 are outgoing π^- momenta, and \mathbf{q}_3 is the outgoing π^+ momentum, see also Fig. 41.

In Ref. [134] the connection of $\hat{\Gamma}$ to different observables is evaluated: The most detailed information is contained in Dalitz plots at a fixed three-body energy \sqrt{s} ; there are Dalitz plot projections, and there is the line shape that is the integral over the full phase space as a function of \sqrt{s} ,

$$\mathcal{L}(\sqrt{s}) = N(m_\tau^2 - s)^2 \int \frac{d^3 q_1}{(2\pi)^3} \frac{d^3 q_2}{(2\pi)^3} \frac{d^3 q_3}{(2\pi)^3} \frac{(2\pi)^4 \delta^4(P_3 - q_1 - q_2 - q_3)}{8E_{q_1} E_{q_2} E_{q_3}} \left(\left| \sum_\lambda \hat{\Gamma}_{-1\lambda} \right|^2 + \frac{m_\tau^2}{s} \left| \sum_\lambda \hat{\Gamma}_{0\lambda} \right|^2 + \left| \sum_\lambda \hat{\Gamma}_{+1\lambda} \right|^2 \right), \quad (4.3)$$

with arbitrary normalization N . See also Ref. [1083] for the derivation of the weak decay part. The Monte-Carlo integration over phase space and other numerical details are explained in Ref. [134]. Note that the analytic continuation of the amplitude to real spectator momenta using Padé approximants, as proposed in that paper, is less rigorous than the exact methods explained in Sects. 2.8.1 and 2.8.2. The line shape fit from Ref. [142] is shown together with data and fit residuals in Fig. 42 to the left. As the line shape data themselves have been extracted from raw data, they contain correlations that are included in the fit. The cutoff Λ refers to the production amplitude in Eq. (2.91).

As for the analytic continuation to complex energies onto the unphysical Riemann sheet, see Sect. 2.9.3. The resulting pole positions and their variations under changes of the parametrization are shown in Fig. 42 to the right. The $\pi\rho$ branch point is outside the shown area. The most probable pole position is shown with the red dot. Data resampling results in the small blue dots that can be used to determine an error ellipse shown in light blue, even though the fit problem is obviously not very linear (i.e., the most probable value is not in the center but at the margin of the ellipse). Systematic uncertainties, shown with the light green rectangle, were determined by varying the cutoff Λ in a wide range while re-fitting all other parameters. This shows that the parametrization is consistent and cutoff changes can be well absorbed in changing the contact C -terms.

In Ref. [142] the role of the pion exchange term was also tested (see also Eq. (4.8) below). The fit quality without this term changes little, but the most probable pole position, shown with the open red circle in Fig. 42, changes significantly compared to the uncertainties. This demonstrates that the exchange process, demanded by three-body unitarity [130], does have an influence and should be taken into account when determining resonance poles from data.

4.2. A unitary amplitude with pions and kaons

Reference [113] builds on these works and allows for pions and kaons in the amplitude. Nine channels are included that not only contain canonical S - and P -wave resonances in the two-body subsystems –the $f_0(500)$ “ σ ”, $f_0(980)$, $\rho(770)$, $K_0^*(700)$ “ κ ”, $K^*(892)$ – but also repulsive $\pi\pi$ (“ π_2 ”) and πK (“ $K_{3/2}$ ”) subsystems at maximal isospin. Amplitude transitions are formulated for both G -parities η_G and all total isospins $I \in \{0, \dots, 3\}$ with zero overall strangeness. An overview of the channel space is shown in Table 4. The last row shows the partial waves for the a_1 quantum numbers. Other total angular momenta are easily obtained following Sec. 2.5.

All channels contribute to total isospin $I = 1$, but only some would contribute to isospins $I = 0$, $I = 2$, and $I = 3$. Note that positive/negative G -parity requires the channels containing kaons to be combined according to

$$\eta_+ = \frac{1}{\sqrt{2}} (\bar{K}_{I_I} K + K_{I_I} \bar{K}) \quad \eta_- = \frac{1}{\sqrt{2}} (\bar{K}_{I_I} K - K_{I_I} \bar{K}), \quad (4.4)$$

where K_{I_I} stands for the S -wave or P -wave isobars in isospin $I_I = 1/2$ or $I_I = 3/2$. In Table 4, we indicate the combinations η_- as KK^* , $K\kappa$, or $KK_{3/2}$. The included channels represent all possible isobars up to P -wave, except for a very small

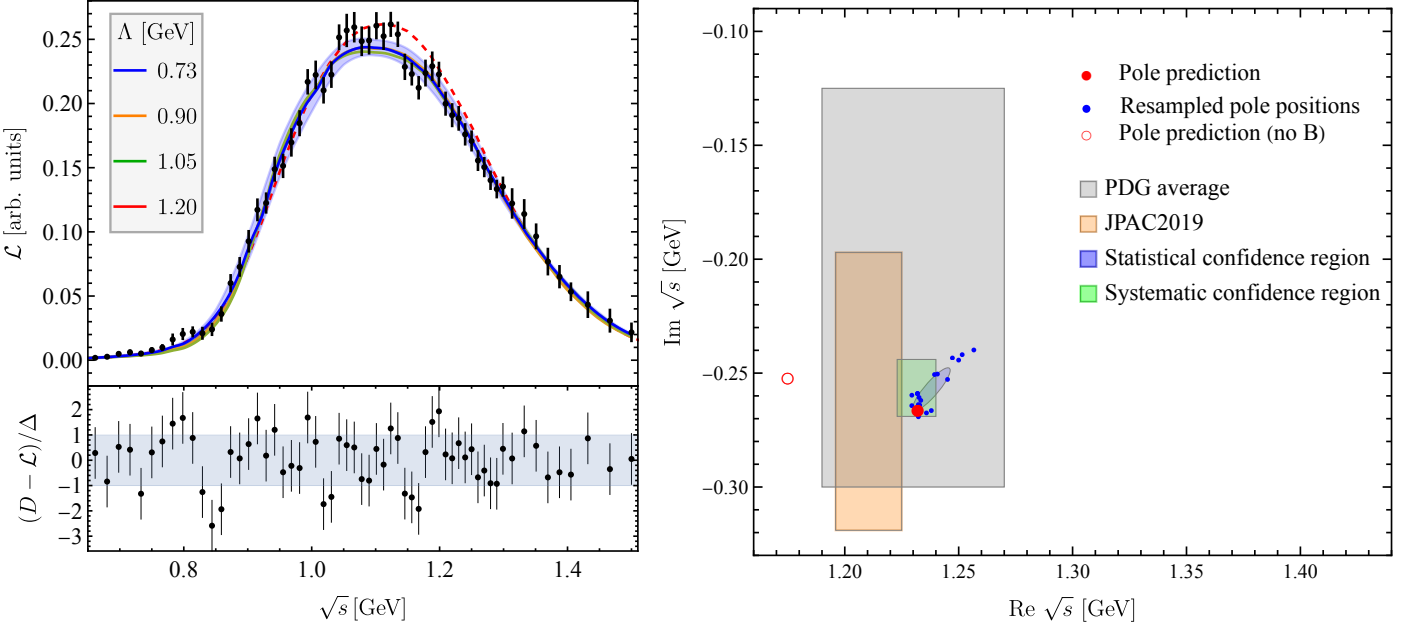


Figure 42: **Left:** Fit to the line shape data from the ALEPH experiment [1087] for different cutoff values (top) and the normalized residuals for the $\Lambda = 0.73$ GeV case (bottom), where $D - \mathcal{L}$ is a given residual and Δ the pertinent data uncertainty. In the upper figure, the blue band shows the statistical uncertainties of the $\Lambda = 0.73$ GeV fit, multiplied by ten for visibility. The red dashed line shows the $\Lambda = 0.73$ GeV fit with all D-wave terms set to 0. **Right:** Compilation of pole positions determined in Ref. [142] including statistical and systematic uncertainties. For convenience, the PDG [103] average and a result by JPAC [1083] are quoted as well. See text for further explanations. Figures taken from Ref. [142].

P -wave $I = 3/2$, πK isobar and an S -wave, $I = 1$, $K\bar{K}$ isobar. There are 11 partially redundant channels in the helicity basis (HB) and 9 channels in the standard JLS basis. The transformations are carried out via the partial-wave projection discussed in Sect. 2.5.

The projected scattering equation reads

$$\tilde{T}_{ji}(s, p', p) = \tilde{B}_{ji}(s, p', p) + \int_{\Gamma} \frac{dq q^2}{(2\pi)^3 2E_q} \tilde{B}_{jk}(s, p', p) \tilde{\tau}_{kk'}(\sigma(q)) \tilde{T}_{k'i}(s, q, p) \quad (4.5)$$

with block-diagonal isobar-spectator propagation $\tilde{\tau}_{kk'}$ allowing for channel transitions during the isobar propagation, see also Eq. (2.91) for the corresponding production amplitude. Currently, these transitions are only allowed for the f_0 isobar quantum numbers with $\pi\pi \leftrightarrow K\bar{K}$ as illustrated in Fig. 11. In the above equation, the \tilde{B} are the exchange (“rearrangement”) processes that become complex above the three-meson thresholds as required by unitarity, see Sect. 2.7.1. The \tilde{T} -matrix serves as input for the production reaction according to

$$\tilde{\Gamma}_j(s, p') = \int_{\Gamma} \frac{dp p^2}{(2\pi)^3 2E_p} \tilde{T}_{ji}(s, p', p) \tilde{\tau}_{ik}(\sigma(p)) D_k(s, p), \quad (4.6)$$

but $\tilde{\Gamma}$ plus the disconnected piece D can also be obtained via Eq. (2.91) without the need to solve for \tilde{T} first. The full production amplitude is obtained from Eq. (2.90).

In the previous equations as well as in Ref. [113], a “tilde” notation for \tilde{B} , $\tilde{\tau}$, and \tilde{T} is introduced to allow for a clear separation of the isospin structure associated with the exchange \tilde{B} from the propagation $\tilde{\tau}$, cast into simple isospin

Table 4: Channels for $\eta_G = -1$ from Ref. [113]. The spin ℓ and isospin I_I of the isobar is indicated in the first line for clarity. The second line shows the eleven channels in helicity basis (HB). The third line indicates the nine channels in the JLS basis for total angular momentum $J = 1$. The outermost subscripts indicate the relative angular momentum L between isobar and spectator. The abbreviation π_2 stands for the S -wave isospin $I_I = 2$ repulsive $\pi\pi$ channel and $K_{3/2}$ for the repulsive S -wave $I_I = 3/2$ πK channel.

Isobar (ℓ, I_I)	(1, 1)		(1, 1/2)		(0, 0)		(0, 2)	(0, 1/2)	(0, 3/2)
HB basis (11 Ch.)	$\pi\rho_{\lambda=\pm 1,0}$		$KK_{\lambda=\pm 1,0}^*$		$\pi\sigma$	$\pi(K\bar{K})_S$	$\pi\pi_2$	$K\kappa$	$KK_{3/2}$
JLS basis (9 Ch.)	$(\pi\rho)_S$	$(\pi\rho)_D$	$(KK^*)_S$	$(KK^*)_D$	$(\pi\sigma)_P$	$(\pi(K\bar{K})_S)_P$	$(\pi\pi_2)_P$	$(K\kappa)_P$	$(KK_{3/2})_P$

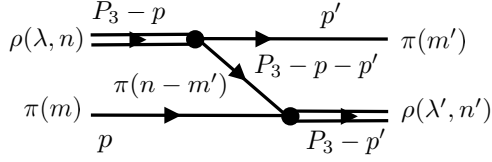


Figure 43: The $\pi\rho \rightarrow \pi\rho$ transition. The labels $n^{(\prime)}$, $m^{(\prime)}$ stand for third components of isospin of the incoming (outgoing) states.

recoupling factors for both quantities. This is in contrast to previous IVU works for excited mesons [134, 142, 164] but also the previously discussed JBW approach for excited mesons. There, Lagrangians were used to calculate isospin coefficients for transitions B that partly contain an isospin structure from the isobar propagation τ , see the discussion in Appendix A of Ref. [113]. In particular, the isospin coefficients in Ref. [113] are obtained simply by

$$\tilde{I}_F = \sum_{\substack{m,n \\ m',n'}} (I_{In} I_{Sm} | II_3) (I_{I'n'} I_{S'm'} | II_3) (I_{xn} - m' I_{Sm} | I_{I'n'}) (I_{xn} - m' I_{S'm'} | I_{In}), \quad \text{for } \pi\pi\pi \text{ only}, \quad (4.7)$$

where I_I ($I_{I'}$) is the isospin of the incoming (outgoing) isobar, I_S ($I_{S'}$) is the isospin of the incoming (outgoing) spectator, and I_x is the isospin of the exchanged particle. Figure 43 shows the label assignments for the example of $\pi\rho \rightarrow \pi\rho$ transition. The calculation is slightly more intricate in the presence of kaons as one has to adopt a convention of how particles with strangeness are ordered. The logic of Eq. (4.7) can be illustrated as follows. The two-body input of the current formalism are isobar amplitudes in the isospin basis. To construct the particle exchange, one needs to first “unfold” these amplitudes to the particle/charge basis (third and fourth coefficient). One then has to sum over all possible particle exchanges. Finally, one needs to construct total isospin states (first and second coefficient). The particle phases [102] associated with π^+ and ρ^+ always cancel in the process. To demonstrate the angular dependence of isobars with spin, the exchange transitions with the labeling of Fig. 43 read in the helicity basis:

$$\tilde{B}_{ji}(s, \mathbf{p}', \mathbf{p}) = \frac{(\tilde{\mathbf{I}}_F)_{ji} v_j^*(p, P_3 - p - p') v_i(p', P_3 - p - p')}{2E_{p'+p}(\sqrt{s} - E_p - E_{p'} - E_{p'+p}) + i\epsilon} \quad \text{for } i, j \in \text{HB}, \quad (4.8)$$

with the angular structures of P - and S -wave isobars,

$$v_i(p, q) = \begin{cases} g_i (p - q)^\mu \epsilon_\mu(\mathbf{p} + \mathbf{q}, \lambda) & \text{for } \ell = 1 \text{ isobars,} \\ 1 & \text{for } \ell = 0 \text{ isobars,} \end{cases} \quad (4.9)$$

with polarization state vectors ϵ , for exact definitions see Ref. [112]. Note that the presence of the vector meson coupling to pseudoscalar mesons, g_i , is due to the particular representation of the two-body amplitude with explicit isobars [113]. In contrast, the $\ell = 0$ isobars are not parametrized with isobars. While the same is possible for $\ell = 1$ isobars, the angular dependence of the vector isobar channel is always moved inside the definition of \tilde{B} because that is the object undergoing partial-wave projection according to Sect. 2.5.

Another issue concerns symmetry factors as explained in Sect. II D of Ref. [113]. The amplitude entering the propagation $\tilde{\tau}$, together with the adjacent angular structure in case of P -wave isobars corresponds to the full, plane-wave, 2-body amplitude that no longer absorbs any symmetry factors in its definition. This is potentially an issue, because it is often customary (e.g., in many chiral unitary approaches) to absorb symmetry factors from the two-body propagation of identical particles – pions count as identical in the isospin basis – into the definition of two-body states (e.g., Ref. [194]), or the partial-wave projected amplitudes in case of the Inverse Amplitude Method (e.g., Ref. [191]). In contrast, note that the self-energy integral of Eq. (2.82) explicitly contains the symmetry factor of 1/2 for identical particles, where it belongs. The detailed procedure to match different two-body amplitudes from the literature to $\tilde{\tau}$ as input for three-body calculations is given in Ref. [113].

The next step in the amplitude construction consists in determining the isobars from two-body scattering data. In the scalar-isoscalar (f_0) channel, there are not only data for the $\pi\pi$ phase shifts, but also for the $\pi\pi \rightarrow K\bar{K}$ transition and the inelasticity η_0^0 that determine the coupled-channel isobar amplitude. With all input available the integral equation for the production amplitude can be calculated either by direct inversion (Sect. 2.8.2), contour deformation (Sect. 2.8), or continued fractions [157]. For contour deformation, one needs to analytically continue the amplitude to real spectator momenta as described in Sect. 2.8.1. In Ref. [113] it is checked that this method and direct inversion lead to the same result.

In Fig. 44 the production amplitude $\tilde{\Gamma}$ from Eq. (2.90) is shown for different choices of “bare” production vertices D in different channels. The blue highlighted regions correspond to the “critical region” shown in Fig. 10 to the left. The fact that the amplitude exhibits a smooth behavior and transition to the noncritical region demonstrates the validity of the Cahill and Sloan method discussed in Sect. 2.8.

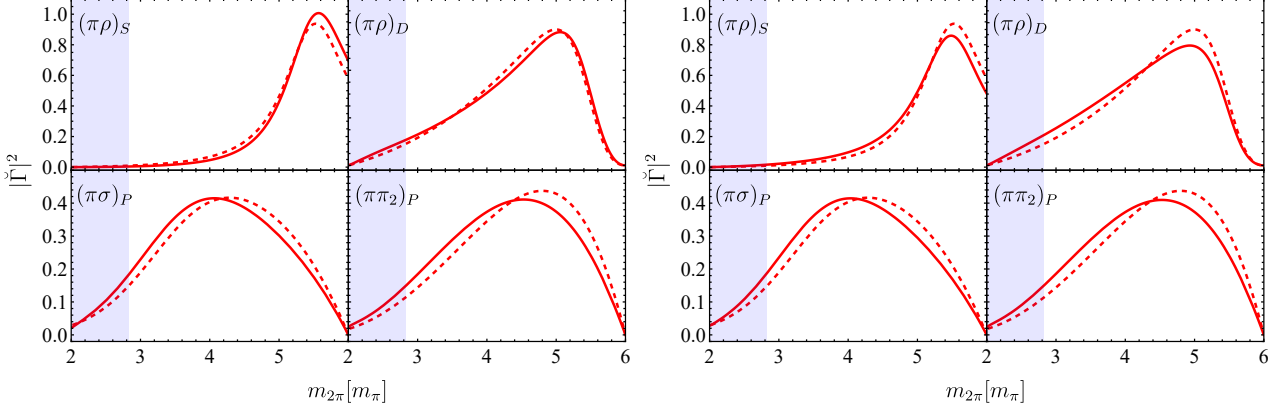


Figure 44: Production amplitude $|\tilde{\Gamma}|^2$ (unitless for all channels) in terms of the isobar invariant mass. The left figure shows the result with the standard choice for the production vertex D , while the right figure corresponds to modified input. The red dashed lines show the disconnected contributions that correspond to traditional isobar amplitudes/line shapes, while the red solid lines correspond to the full, three-body unitary amplitude including coupled channels and meson exchanges. The areas under all curves are normalized to one to facilitate the comparison of the line shapes. The light blue area indicates the critical region, see the discussion of Fig. 10 for further explanations. Figure taken from Ref. [113].

In Fig. 44, to the left, we show the complete production amplitude $\tilde{\Gamma}$ from Eq. (2.90) including the disconnected part, the final isobar propagation, and its decay. Consequently, one observes the ρ and σ line shapes, but not the $f_0(980)$ line shape, due to the chosen energy being $\sqrt{s} = 7m_\pi$. The dashed lines show the disconnected part alone. This would correspond to the traditional isobar model, in which line shapes are related to two-body scattering amplitudes only. The solid lines show the full, three-body unitary amplitude $|\tilde{\Gamma}|^2$, including coupled channels and rescattering. There is a noticeable modification of the line shapes by these effects, at some invariant masses. We observe a distortion of the σ meson towards smaller invariant masses and similarly moderate changes for the other channels.

If one chooses the input for the production vertex D_f differently, one obtains different line shapes as shown in Fig. 44 to the right. Of course, there is additional freedom in the amplitude that will further modify the line shapes. This refers to the isobar-spectator contact terms C in Eq. (2.83). These terms encode three-body resonance dynamics [142] and other QCD effects, and they have all been set to zero in Ref. [113] for simplicity. In summary, the work from Ref. [113] demonstrates how rescattering, coupled channels, three-body forces C , and the relative strengths of the production processes D all lead to modifications of the traditional isobar line shapes.

4.3. Triangle singularities as channel transitions in DCC approaches

Three-body effects can be enhanced by a kinematical effect known as triangle singularity (TS) [167]. It sometimes occurs in the decay of a resonance to an intermediate resonance and a spectator. In a specific kinematic region one of the decay products of the intermediate resonance can ‘‘catch up’’ with the spectator. This on-shell condition produces a bump in the invariant mass spectrum of these two particles, without any resonance being responsible for it [1088–1092]. See also Refs. [1093, 1094] for the conceptual treatment of TS. The $a_1(1420)$, was at first claimed to be a new resonance while posterior analyses suggested that a TS effect can take place in the decay chain $a_1(1260) \rightarrow K^* \bar{K} \rightarrow K \bar{K} \pi \rightarrow f_0 \pi \rightarrow 3\pi$ resulting in a peak in the 3π mass 0.2 GeV above the nominal a_1 mass [167, 1095, 1096], see also Refs. [167, 1094, 1097, 1098] for general discussions. See Refs. [1099–1101] for further examples of TS. The exact position of the TS can also be used to determine the mass of an exotic state close to a three-body threshold when the decay channel of the exotic particle is mediated by a TS [1102, 1103].

In the context of DCC approaches, triangle singularities are nothing but enhanced hadron exchanges between channels of unequal masses. An example is given by the diagram in Fig. 11 to the lower right: In a system of pions and kaons that interact strongly, the above-mentioned $K^* \bar{K} \rightarrow K \bar{K} \pi \rightarrow f_0 \pi$ transition is clearly visible as kaon exchange in an infinite rescattering series. Qualitatively, at around $\sqrt{s} \approx 1.42$ GeV the quasi-on-shell K^* and the kaon spectator are on-shell at the momentum of the exchanged kaon flying in backwards direction, thus being able to ‘‘catch up’’ with the kaon spectator and form an f_0 as if it were a classical kinematic process. That kinematic point is given as p_P from Eq. (2.89). This enhancement of processes that are allowed in classical kinematics is referred to as Coleman-Norton theorem [1088].

The role of TS in dynamical coupled channel approaches has been recently discussed in depth in Ref. [157]. Using the IVU formalism [130] the question was studied whether the appearance of triangle singularities is affected by an infinite series of rescattering of final two- and three-body final states. It was found that the position of the triangle singularity is not affected through the final-state rescattering. This is in full agreement with the argument provided by the generalization of the Landau equations [1090, 1104, 1105] to include rescattering effects. Specifically, it was found

that inclusion of higher topologies (triangle \times box, triangle \times box \times box etc.) leads either to non-singular configurations or provides a sub-leading singularity through a factorization into the triangle diagram and the rest that is non-singular. A first estimate of the size of the effect due to rescattering was carried out and found to be quite small. Clearly, some approximations were made, neglecting the full spin/isospin structure for the $a_1(1420)$ system, but the driving effect for the smallness of the rescattering effect seems to lie in the particular size of the coupling constants, fixed mostly by the mass and the width of the K^* and $f_0(980)$ resonances. This explains a different observation of Ref. [1042] where the rescattering effects for the $\eta(1405/1475)$ are found to be more important. It seems that the general path forward is to always include all rescattering effects and let data decide whether rescattering is relevant or not.

5. Coupled-channel baryon-baryon systems

The by far best studied baryon-baryon (BB) system, experimentally as well as theoretically, is the nucleon-nucleon (NN) system. However, in most theoretical investigations coupled-channel effects do not really play a role. It has to do with the fact that the threshold of the next BB channel ($N\Delta(1232)$) is separated by roughly 300 MeV, see Fig. 45. Moreover, there is no coupling between S -wave states. Such a coupling can only occur with the $\Delta\Delta$ channel whose threshold is another 300 MeV higher up. Indeed, the first channels that opens is that of the three-body system $NN\pi$ and πd at about 140 MeV. Near threshold a perturbative treatment of the π production is possible [1106] because at low momenta the πN interaction is weak due to constraints from chiral symmetry. However, at intermediate energies one faces the challenge of treating the $NN\pi$ three-body system (and eventually the $NN\pi\pi$ system) and its coupling to NN rigorously [1107, 1108]. Thus, most of the NN potentials in the literature are designed to describe and reproduce the NN scattering data only up to the pion-production threshold. Nonetheless, there is a considerable number of NN potentials where the Δ resonance is included as explicit degree of freedom and where the coupling to the $N\Delta$ and/or $\Delta\Delta$ systems is taken into account, for example in Refs. [1109–1112]. An extensive overview and references to the pertinent literature is given in Ref. [1113]. In some of the potentials established within the meson-exchange approach Δ 's are only included in order to achieve more realistic values for model parameters like the meson-baryon coupling constants [48], whereas in others the motivation is indeed to describe NN phenomenology up to and even beyond the thresholds involving the Δ resonance [1109, 1110, 1114]. As a matter of facts, the influence of the coupling of the NN system to the $N\Delta$ channel on some NN phase shifts like the 1D_2 or 3F_3 has been long established by phase-shift analyses but also by model calculations.

Also in modern approaches to the BB interaction like chiral effective field theory (EFT) the inclusion of the Δ has been considered from the very beginning [1115]. Among others, it has been found to improve the convergence in peripheral NN phases [1116, 1117]. But like in some phenomenological NN potentials mentioned above, Δ 's are not an active degree of freedom and the calculations are restricted to energies below the $NN\pi$ threshold. Anyway, the dynamics around the $N\Delta$ threshold and possible coupled-channels effects are beyond the validity of the present chiral potentials and cannot be addressed.

The kinematical situation is different for BB systems involving strange baryons. In case of strangeness $S = -1$ there are two channels involving octet baryons, ΛN and ΣN , while for $S = -2$ there are even four channels, $\Lambda\Lambda$, ΞN , $\Lambda\Sigma$ and $\Sigma\Sigma$. In the limit of SU(3) flavor symmetry their thresholds coincide. SU(3) symmetry is, of course, broken, but even for physical masses the separation between the thresholds remains small as can be seen from the overview provided in Fig. 45. Thus, for a realistic description of the dynamics of YN systems the explicit inclusion of the channel coupling is indispensable. Indeed, already in the first attempts to establish a potential for the $S = -1$ sector the coupling between ΛN and ΣN was taken into account [1118]. An early review on the hyperon-nucleon interaction is provided in Ref. [1119]. An overview of the work of the Nijmegen group can be found in Ref. [1120], while the tools for describing the YN interaction within chiral EFT, pursued by the Juelich-Bonn group, are summarized in Ref. [1121].

Contrary to the meson-baryon systems discussed above, excited hadrons in form of conventional $q\bar{q}$ or qqq states cannot occur in BB systems. However, it is possible to find exotic hadrons, the so-called dibaryons. Historically, one has tried to distinguish between genuine (compact) $6q$ states, with masses well below the lowest BB threshold, and bound states/resonances close to the physical region and generated by the (coupled-channel) dynamics. Whether that distinction is meaningful on a practical level is a matter of belief. In any case, predictions like the H -dibaryon (a state with $S = -2$, $J = 0$, $I = 0$) [1122] have definitely stimulated the interest in the $S = -2$ sector for decades. In recent times there has been some excitement about a dibaryon in the NN sector, the $d^*(2380)$ discovered at the COSY facility in Juelich [1123], which is associated with a possible $\Delta\Delta$ bound state (with $J = 3$, $I = 0$). For a detailed discussion of this state, and a more general review of dibaryons, see Ref. [1124].

The next two subsections provide an introduction to the theoretical frameworks most commonly applied for constructing the interactions in the BB system, chiral EFT and meson-exchange. In Sect. 5.3 the ΛN - ΣN system is discussed. An overview of results for the Λp , $\Sigma^- p$, and $\Sigma^+ p$ channels is given. These are the channels which are experimentally reasonably well explored. In addition, the situation regarding a possible bound state (dibaryon) near the ΣN threshold in the 3S_1 - 3D_1 partial wave is examined. Its appearance and structure is closely related with the strength of the ΛN - ΣN re-channel coupling. Sect. 5.4 is devoted to the $S = -2$ sector. One of the aspects summarized is the present situation re-

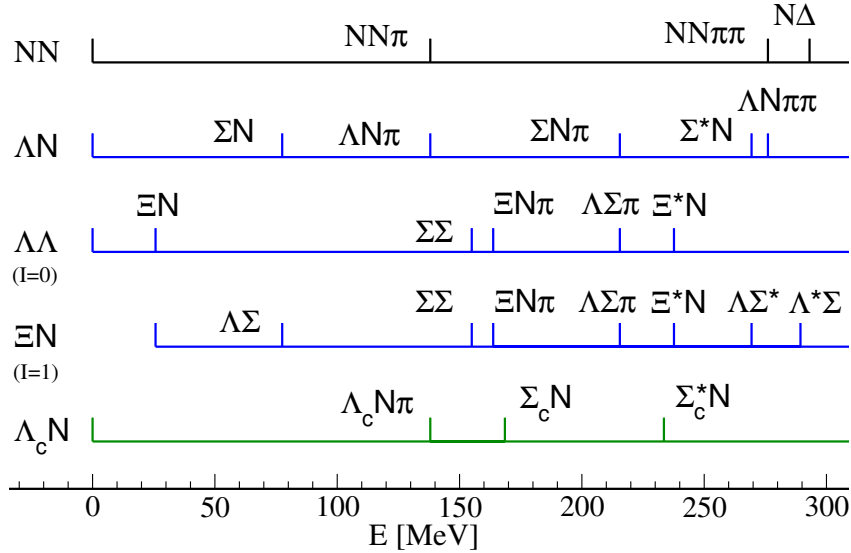


Figure 45: Thresholds of baryon-baryon systems with strangeness $S = 0, -1, -2$ and with charm. E is the kinetic energy relative to the lowest threshold. Σ^* , Λ^* , Ξ^* , and Σ_c^* refer to the $\Sigma^*(1385)$, $\Lambda^*(1405)$, $\Xi^*(1530)$, and $\Sigma_c^*(2520)$ resonances.

garding the H -dibaryon. Furthermore the overall experimental situation is discussed and results for recent measurements of two-particle momentum correlation functions are shown. Those allow conclusions on the properties of the $\Lambda\Lambda$ and $\Xi^- p$ interaction. Finally, in Sect. 5.5 the situation in other BB systems is briefly reviewed.

5.1. Baryon-baryon interaction in chiral effective field theory

The application of chiral EFT to the NN system is thoroughly documented in various reviews, see e.g. [1125, 1126]. Potentials up to the fifth order in the chiral expansion have been presented [1127, 1128]. Chiral potentials for the BB interaction involving strange baryons are so far available up to the third order [1129]. Details on the derivation of the chiral BB potentials for the strangeness sector at leading order (LO) using the Weinberg power counting and assuming approximate SU(3) flavor symmetry can be found in Refs. [1130] and [1131], and for up to next-to-leading order (NL0) in Ref. [1132]. Here we provide only a brief summary of the essential features.

The LO potential consists of four-baryon contact terms without derivatives and of one-pseudoscalar-meson exchanges, see Fig. 46 (top). As described in Ref. [1130], imposing SU(3) symmetry there are six independent contact interactions at LO whose strength can be given in terms of six corresponding low-energy coefficients (LECs). Not surprisingly, the number of terms corresponds to the number of irreducible representations of SU(3) for the octet baryons: $8 \times 8 = 27 + 10 + 10^* + 8_s + 8_a + 1$ [102]. The LECs contribute to the 1S_0 and 3S_1 partial waves (using the standard partial-wave notation ${}^{2S+1}L_J$ for BB systems) and need to be determined by a fit to experimental data.

The lowest order $SU(3)_f$ invariant pseudoscalar-meson–baryon interaction Lagrangian with the appropriate symmetries was discussed in [1130, 1132]. It leads to a one-pseudoscalar-meson-exchange potential similar to the static one-pion-exchange potential in [1133] (recoil and relativistic corrections give higher order contributions),

$$V_{B_1 B_2 \rightarrow B'_1 B'_2} = -f_{B_1 B'_1 P} f_{B_2 B'_2 P} \frac{(\sigma_1 \cdot \mathbf{q})(\sigma_2 \cdot \mathbf{q})}{\mathbf{q}^2 + m_P^2}, \quad (5.1)$$

where m_P is the mass of the exchanged pseudoscalar meson. The transferred and average momentum, \mathbf{q} and \mathbf{k} , are defined in terms of the final and initial c.m. momenta of the baryons, \mathbf{p}' and \mathbf{p} , as $\mathbf{q} = \mathbf{p}' - \mathbf{p}$ and $\mathbf{k} = (\mathbf{p}' + \mathbf{p})/2$. Assuming $SU(3)_f$ symmetry imposes specific relations between the coupling constants $f_{B_i B'_i P}$ so that they can be expressed in terms of a coupling constant f and the $F/(F+D)$ -ratio α [102]. Here $f \equiv g_A/2f_0$ where f_0 is the pseudoscalar-meson decay constant in the chiral limit, g_A is the axial-vector strength measured in neutron β -decay, and F and D are coupling constants which satisfy the relation $F+D=g_A \approx 1.26$. In the YN potentials of the Juelich-Bonn group f_0 is fixed to the weak pion decay constant, $f_\pi = 92.4$ MeV. In the extension to next-to-next-to-leading order (N^2LO) the explicit $SU(3)$ breaking of the decay constant was taken into account by using the empirical values for f_π , f_K , and f_η [1129]. For the $F/(F+D)$ -ratio the $SU(6)$ value ($\alpha=0.4$) was adopted in all BB studies.

In next-to-leading order (NLO), contributions from (non-iterative) two-pseudoscalar-meson exchange diagrams arise [1132, 1134]. Those involve the leading meson-baryon Lagrangian which describes a (Weinberg-Tomozawa) vertex between two baryons and two mesons. Explicit expressions for the resulting NLO potential can be found in the appendix of

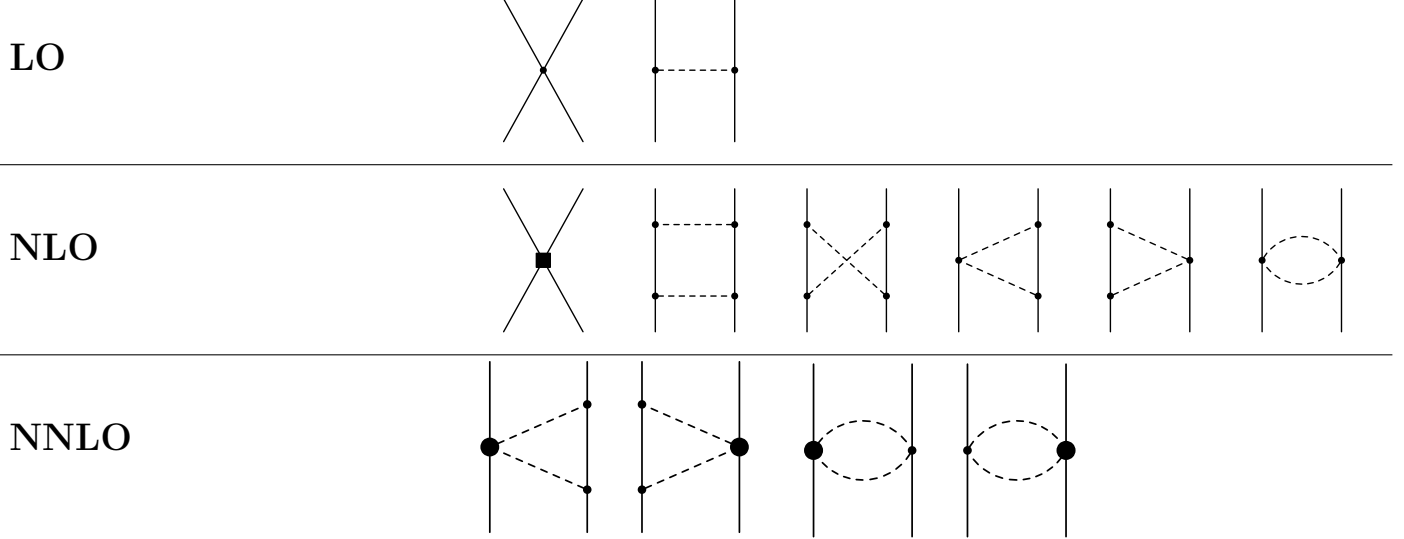


Figure 46: Diagrams contributing at LO (top), NLO (center), and N^2 LO (bottom) in chiral EFT. Solid and dashed lines denote octet baryons and pseudoscalar mesons, respectively.

Ref. [1132]. A graphical representation of the contributions is provided in the middle line of Fig. 46 and consists of (irreducible) planar box, crossed box, triangle, and football diagrams. In addition there are four-baryon contact terms with two derivatives, involving additional LECs. Performing a partial wave projection for the latter and imposing again $SU(3)_f$ symmetry one finds that in case of the YN interaction there are ten new coefficients entering the S waves and S - D transitions, respectively, and eight coefficients in the P -waves [1132]. Finally, at N^2 LO contributions involving the subleading meson-baryon Lagrangian [1129] arise. Those are depicted at the bottom of Fig. 46.

The reaction amplitudes are obtained in a DCC approach by solving a coupled-channel Lippmann-Schwinger (LS) equation for the interaction potentials:

$$T_{\rho''\rho'}^{\nu''\nu',J}(p'',p';E) = V_{\rho''\rho'}^{\nu''\nu',J}(p'',p') + \sum_{\rho,\nu} \int_0^\infty \frac{dp p^2}{(2\pi)^3} V_{\rho'\rho}^{\nu''\nu,J}(p'',p) \frac{2\mu_\nu}{q_\nu^2 - p^2 + i\eta} T_{\rho\rho'}^{\nu\nu',J}(p,p';E). \quad (5.2)$$

The label ν indicates the particle channels and the label ρ the partial wave. The pertinent reduced mass is denoted by μ_ν . The on-shell momentum in the intermediate state, q_ν , is defined by $E = E_{B_{1,\nu}} + E_{B_{2,\nu}} = \sqrt{M_{B_{1,\nu}}^2 + q_\nu^2} + \sqrt{M_{B_{2,\nu}}^2 + q_\nu^2}$. Relativistic kinematics is used for relating the laboratory energy T_{lab} of the hyperons to the c.m. momentum. In principle, one could also use a relativistic propagator like in Eq. (2.47), which in fact has been done in the first YN potential developed in Juelich [1135]. However, then one can no longer straightforwardly apply the potentials in standard few-body calculations of hypernuclei [1136–1138] or in nuclear matter studies [1139, 1140], which all require non-relativistic kinematics.

The LS equation is solved in the particle basis, in order to incorporate the correct physical thresholds. Depending on the specific values of strangeness and charge up to six baryon-baryon channels can couple. For the $S = -1$ sector where a comparison with scattering data is possible the Coulomb interaction is taken into account appropriately. The potentials in the LS equation are cut off with a regulator function, $\exp[-(p'^4 + p^4)/\Lambda^4]$, in order to remove high-energy components of the baryon and pseudoscalar meson fields [1134]. Cut-off values in the range 500, ..., 650 MeV are considered, similar to what was used for chiral NN potentials [1134]. In the extension to N^2 LO [1129] a novel scheme is used, called semilocal momentum-space (SMS) regularization [1127].

Alternative chiral EFT approaches to the BB interaction involving strange baryons have been pursued in Ref. [1141], where the so-called Kaplan-Savage-Weise (KSW) resummation scheme [1142] has been applied, and in Refs. [1143–1145] where calculations are performed in covariant chiral EFT, but so far only at LO.

5.2. Baryon-baryon interaction in the meson-exchange picture

For a long time investigations of the BB interactions have been done primarily within phenomenological meson-exchange potentials such as the Juelich [1135, 1146, 1147], Nijmegen [1120, 1148, 1149], or Ehime [1150, 1151] potentials. Below we give a brief introduction to these type of models.

Conventional meson-exchange models of the YN interaction are usually also based on the assumption of $SU(3)$ flavor symmetry for the occurring coupling constants, and in some cases even on the $SU(6)$ symmetry of the quark model, see

Refs. [1135, 1146]. In the derivation of the meson-exchange contributions one follows essentially the same procedure as outlined in the previous subsection, for the case of pseudoscalar mesons. Besides the lowest pseudoscalar-meson multiplet also the exchanges of vector mesons (ρ , ω , K^*), of scalar mesons (σ ($f_0(500)$), ...), or even of axial-vector mesons ($a_1(1260)$, ...) [1120, 1149] are included. The spin-space structure of the corresponding meson-baryon Lagrangians differ from that for pseudo-scalar mesons and, accordingly, the final expressions for the corresponding contributions to the YN interaction potentials differ as well. Details can be found in Refs. [1120, 1135, 1148]. We want to emphasize that even for pseudoscalar mesons the final result for the interaction potentials differs, in general, from the expression given in Eq. (5.1). Contrary to the chiral EFT approach, recoil and relativistic corrections are often kept in meson-exchange models because no power counting rules are applied. Moreover, in case of the Juelich potential pseudoscalar coupling is assumed for the meson-baryon interaction Lagrangian for the pseudoscalar mesons instead of the pseudovector coupling dictated by chiral symmetry. Note that in some YN potentials of the Juelich group [1135, 1146] contributions from two-meson exchanges are included. The ESC08 and ESC16 potentials [1120, 1149] include likewise contributions from two-meson exchange, in particular, so-called meson-pair diagrams analog to the last three diagrams shown in the center of Fig. 46. Moreover, there are some YN potentials which include the coupling to channels with decuplet baryons ($\Sigma^* N$, $\Lambda\Delta$, $\Sigma\Delta$) [1135, 1146, 1152].

The major conceptual difference between the various meson-exchange models consists in the treatment of the scalar-meson sector. This simply reflects the fact that, unlike for pseudoscalar and vector mesons, so far there is no general agreement about what are the actual members of the lowest lying scalar-meson SU(3) multiplet. See for example a review [1153] about the long debated $f_0(500)$ resonance. Therefore, besides the question of the masses of the exchange particles it also remains unclear whether and how the relations for the coupling constants should be specified. As a consequence, different prescriptions for describing the scalar sector, whose contributions play a crucial role in any BB interaction at intermediate ranges, were adopted by the various authors who published meson-exchange models of the YN interaction. For example, the Nijmegen group views this interaction as being generated by genuine scalar-meson exchange. In their models NSC97 [1148] and ESC08 (ESC16) [1120, 1149] a scalar SU(3) nonet is exchanged - namely, two isospin-0 mesons (an $\epsilon(760)$ and the $f_0(980)$) an isospin-1 meson ($a_0(980)$) and an isospin-1/2 strange meson κ with a mass of 1000 MeV. In the initial YN models of the Juelich group [1135, 1146] a σ meson with a mass of ≈ 550 MeV is included which is viewed as arising from correlated $\pi\pi$ exchange. In practice, however, the coupling strength of this fictitious σ to the baryons is treated as a free parameter and fitted to the data. In the latest meson-exchange YN potential presented by the Juelich group [1147] a microscopic model of correlated $\pi\pi$ and $K\bar{K}$ exchange [1154] is utilized to fix the contributions in the scalar-isoscalar (σ) and vector-isovector (ρ) channels.

Let us mention for completeness that meson-exchange models are typically equipped with phenomenological form factors in order to cut off the potential for large momenta (short distances). For example, in case of the YN models of the Juelich group the interaction is supplemented with form factors for each meson-baryon-baryon vertex, c.f., [1135, 1146] for details. Those form factors are meant to take into account the extended hadron structure and are parametrized in the conventional monopole or dipole form. In the case of the Nijmegen potentials, a Gaussian form factor is used. In addition, there is some intricate short-range phenomenology that controls the interaction at short distances [1120, 1149]. Finally, we note that realistic models for the YN interaction have been also established within the constituent quark model [1155].

5.3. The ΛN - ΣN system

Let us first focus on two channels of the ΛN - ΣN coupled-channel system, namely on Λp , on the one hand, which couples to the $\Sigma^+ n$ and $\Sigma^0 p$ channels, and $\Sigma^- p$, which couples to Λn and $\Sigma^0 n$. This choice is dictated by the fact that for those systems scattering data for low momenta are available. Indeed, in case of $\Sigma^- p$ besides the cross section for elastic scattering also the transition cross sections to the other two channels have been established. It should be noted that there are data for $\Lambda p \rightarrow \Sigma^0 p$ too [1157], which are, however, incompatible with the measurements for $\Sigma^- p \rightarrow \Lambda n$ when considering isospin symmetry and the principle of detailed balance. Moreover, there are data on the $\Sigma^0 p$ two-particle momentum correlation function [1158] which, however, suffer from low statistics. There are also data on $\Sigma^+ p$, which, however, is an isospin $I = 3/2$ state and does not couple to ΛN . Thus, we do not discuss the pertinent results here and refer the interested reader to the original works [1129, 1132, 1148, 1156]. Nonetheless, it should be emphasized that the interaction in the $I = 3/2$ channel is not disconnected from the results for the other ones. Because of the underlying isospin symmetry the potentials for $\Sigma^- p$, $\Sigma^0 p$, etc. are combinations of the $I = 1/2$ and $I = 3/2$ components.

Cross sections are presented in Fig. 47 for a selection of YN potentials. In case of the chiral potentials from 2019 [1156] bands are shown which reflect the residual cutoff dependence, i.e., the variation of the results for $\Lambda = 500, \dots, 650$ MeV [1156]. For completeness, we list also results for the effective range parameters in Table 5. As one can see from the figure the data at low energy are rather well reproduced, though one should certainly keep in mind that those data are the ones included in the fitting procedure to determine the free parameters of the interaction. The channel coupling, i.e., its effect on Λp , is easily recognizable by the large cusp-like structure at the ΣN threshold which is predicted by all considered potentials and, actually, in all coupled-channel treatments which provide a realistic description of the Λp and $\Sigma^- p$ data

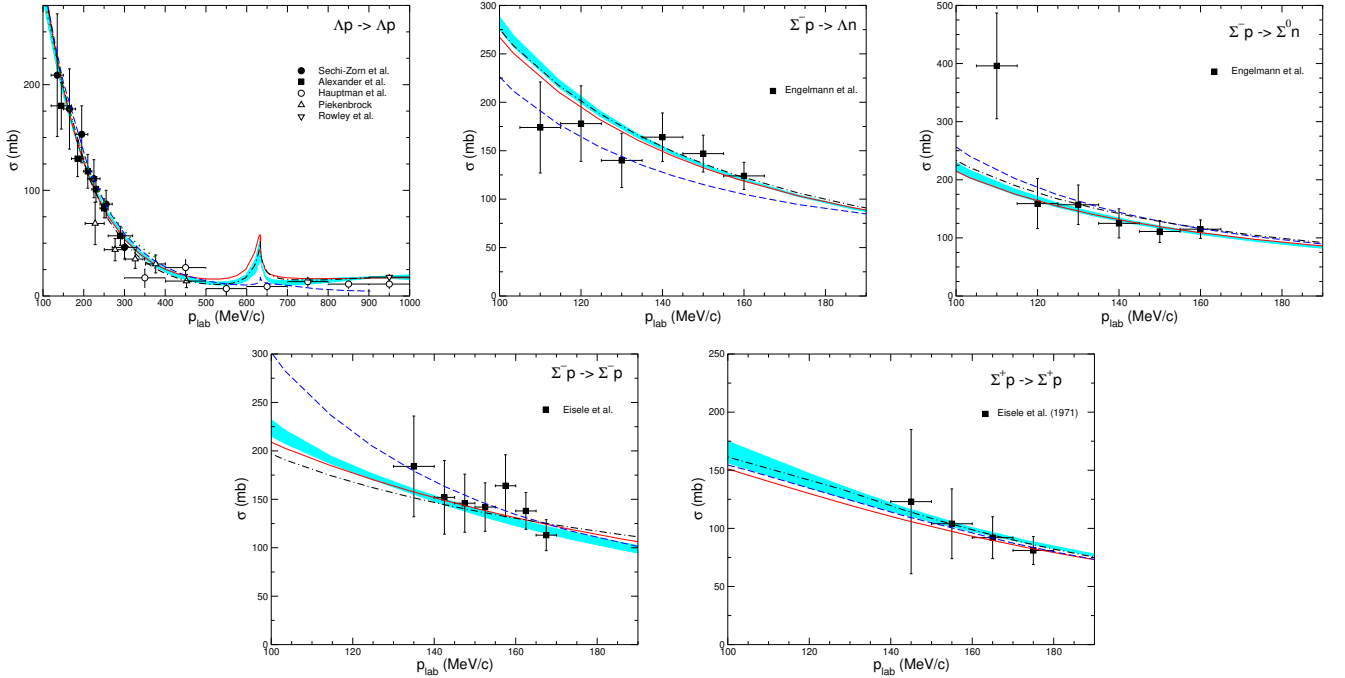


Figure 47: Λp , $\Sigma^- p$, and $\Sigma^+ p$ cross sections. Results are shown for the chiral YN potentials NLO19 [1156] (cyan band) and SMS N²LO (550) [1129] (red line). In addition cross sections of meson-exchange potentials by the Juelich group (Juelich '04 [1147], dashed blue line) and the Nijmegen group (NSC97f [1148], dash-dotted black line) are included.

including the $\Sigma^- p$ capture ratio at rest. Unfortunately, the few Λp data points available in the pertinent momentum region suffer from low statics and poor momentum resolution and do not allow any conclusions.

Nonetheless, there is solid information on the existence of a threshold effect from measurements of the Λp invariant-mass spectrum in reactions like $K^- d \rightarrow \pi^- \Lambda p$, $\pi^+ d \rightarrow K^+ \Lambda p$, or $pp \rightarrow K^+ \Lambda p$, but also from studies of the Λp two-particle momentum correlation function in high energy pp collisions. Indeed, the first evidence for a cusp-like structure was

Table 5: Scattering lengths (a) and effective ranges (r) for singlet (s) and triplet (t) S -waves (in fm), for ΛN , ΣN with isospin $I = 1/2, 3/2$. The results are for the chiral YN potentials NLO13 [1132], NLO19 [1156], and SMS NLO (500) and N²LO (550) [1129]. Results from the meson-exchange potentials by the Juelich group (Juelich '04 [1147]), and the Nijmegen group (NSC97f [1148]) are included too.

	SMS NLO	SMS N ² LO	NLO13	NLO19	Juelich '04	Nijmegen
Λ [MeV]	550	550	600	600		NSC97f
$a_s^{\Lambda N}$	-2.79	-2.79	-2.91	-2.91	-2.56	-2.60
$r_s^{\Lambda N}$	2.72	2.89	2.78	2.78	2.74	3.05
$a_t^{\Lambda N}$	-1.57	-1.58	-1.54	-1.41	-1.67	-1.72
$r_t^{\Lambda N}$	2.99	3.09	2.72	2.53	2.93	3.32
$\text{Re } a_s^{\Sigma N} (I=1/2)$	1.15	1.12	0.90	0.90	0.90	1.16
$\text{Im } a_s^{\Sigma N}$	0.00	0.00	0.00	0.00	-0.13	0.00
$\text{Re } a_t^{\Sigma N} (I=1/2)$	2.42	2.38	2.27	2.29	-3.83	1.68
$\text{Im } a_t^{\Sigma N}$	-2.95	-3.26	-3.29	-3.39	-3.01	-2.35
$a_s^{\Sigma N} (I=3/2)$	-4.05	-4.19	-4.45	-4.55	-4.71	-6.11
$r_s^{\Sigma N}$	3.89	3.89	3.68	3.65	3.31	3.24
$a_t^{\Sigma N} (I=3/2)$	0.47	0.44	0.44	0.43	0.29	-0.29
$r_t^{\Sigma N}$	-4.74	-4.96	-4.59	-5.27	-11.6	-16.7

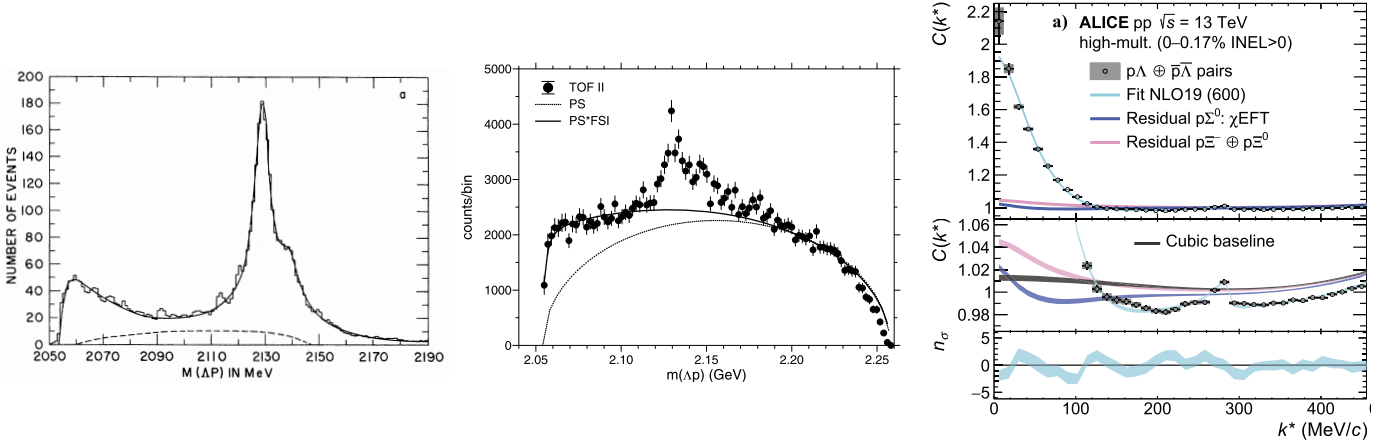


Figure 48: Cusp-like structure at the ΣN threshold seen in the invariant-mass spectra of the reactions $K^-d \rightarrow \pi^-\Lambda p$ [1159] (left), $pp \rightarrow K^+\Lambda p$ [1160] (middle), and in the Λp two-particle momentum correlation function measured in high energy pp collisions [1161] (right). The results on the right-hand side are shown as function of the Λp center-of-mass momentum k^* .

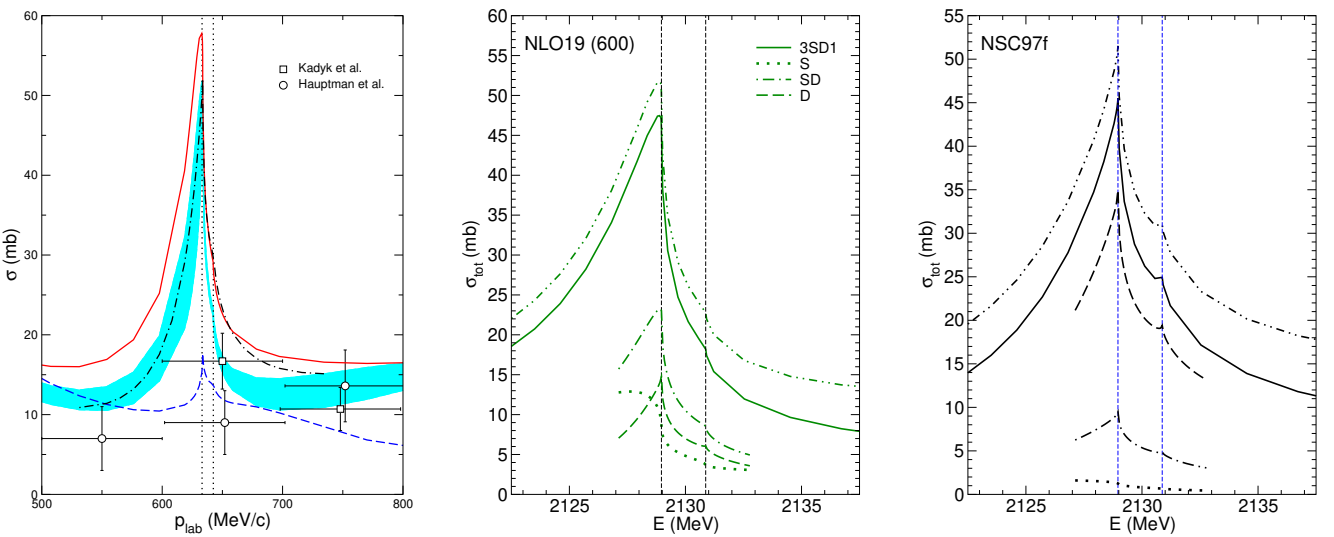


Figure 49: A detailed view on the cusp-like structure at the ΣN threshold. On the left the Λp cross section for selected YN potentials is shown as a function of p_{lab} . Same description of curves as in Fig. 47. In the other two graphs a break down of individual partial waves for the chiral YN potential NLO19 with cutoff $\Lambda = 600$ MeV and the Nijmegen NSC97f potential is presented as a function of the total energy. The dashed-dotted lines are the full results, including the 1S_0 and P - and D -waves.

already reported as early as 1961 [1162], but the first convincing signal and still one of the most prominent examples is from the measurement of the reaction $K^-d \rightarrow \pi^-\Lambda p$ by Tan in 1969 [1159]. A review of other early observations can be found in Ref. [1163] and an overview of later measurements is provided by Machner et al. [1164]. More recent examples for the presence of a ΣN threshold effect, in the reaction $pp \rightarrow K^+\Lambda p$, can be found in Refs. [561, 1160, 1165]. Very recently evidence of the threshold structure has been also observed in measurements of the Λp correlation function in pp collisions at $\sqrt{s} = 13$ GeV by the ALICE Collaboration [1161]. For illustration we present a selection of measurements in Fig. 48. Note that there are plans at J-PARC for performing a dedicated experiment to pin down the threshold cusp more quantitatively [1005].

As already mentioned in the introduction to this section, the interesting question is, of course, whether the observed threshold effect is a signal for a dibaryon - in form of a deuteron-like ΣN bound state - or whether it is simply a regular cusp that is enhanced due to the presence of a near-by virtual state. In the latter case there would be a sharp peak directly at the ΣN threshold while in the former ideally one expects to see a peak below (and well separated from) the threshold. However, there are two issues that complicate any calculation/interpretation. First, while there are only two channels in isospin space there are three in the physical world and, thus, there are two ΣN thresholds, namely those of Σ^+n and Σ^0p . Second, and more important, because of the tensor coupling in the 3S_1 - 3D_1 partial wave there are three amplitudes that are responsible for generating the threshold effect, namely the S - and D wave and also the $S \leftrightarrow D$ transition. The two aspects are illustrated in Fig. 49. On the left hand side is a close-up of the Λp cross section around

the ΣN thresholds predicted by the considered potentials. One can see that in all cases the peak of the produced cusp-like structure coincides with the lower ($\Sigma^+ n$) threshold. At the $\Sigma^0 p$ threshold there is only a kink. On the right hand side one can see the different partial-wave contributions to the Λp cross section around the ΣN thresholds.

Anyway, given the experimental situation, in the past the possibility of a dibaryon was discussed predominantly in the context of the reaction $K^- d \rightarrow \pi^- \Lambda p$ owing to the prominent experimental signal [1163, 1166–1172]. While initial investigations were more or less inconclusive, in the latest works [1169, 1171, 1172] the unanimous conclusion has been drawn that a ΣN bound state does not exist near the ΣN threshold. However, one must keep in mind that in those studies simplified models of the YN interaction were employed. Specifically, with regard to the 3S_1 - 3D_1 partial wave where a possible dibaryon occurs, the tensor coupling mediated by the long-ranged one-pion exchange was ignored and usually only the S -wave component was taken into account. Realistic YN potentials suggest that the $\Lambda N \rightarrow \Sigma N$ transition occurs predominantly from the ΛN 3D_1 state [1130, 1132, 1135, 1146–1148, 1156, 1173, 1174]. Furthermore, in those early works often no constraints from SU(3) flavor symmetry were implemented. Though SU(3) symmetry is certainly broken, presumably on the level of 20 - 30 % [1175], it is likely to end up with unrealistic results if one ignores it altogether.

In Ref. [1164] a systematic but purely phenomenological attempt was made to determine the position of the peak. In that work a combined analysis of the structure as seen in the older data from $K^- d \rightarrow \pi^- \Lambda p$ with the new measurements of $pp \rightarrow K^+ \Lambda p$ was performed. For that as tools a Breit-Wigner parameterization as well as a Flatté approach was employed to determine the position of the peak. Values that agree quite well for the various measurements were found and the reported mean value amounts to 2128.7 ± 0.3 MeV, which pretty much coincides with the threshold energy of the $\Sigma^+ n$ channel. The authors concluded that the structure should be interpreted as a genuine cusp, signaling an inelastic virtual state in the 3S_1 - 3D_1 partial wave of the ΣN $I = 1/2$ channel.

An entirely different strategy was followed in the works of [181] and [169]. Those studies focused on the ΛN - ΣN system itself and explored directly the pole structure of the coupled-channel amplitude in the 3S_1 - 3D_1 partial wave in the region of the ΣN threshold, see also the more educational analysis that has been presented in Ref. [1176]. Though there is no useful empirical information on the Λp cross section around the ΣN threshold, as mentioned above, in principle the threshold region is well constrained by cross section data on the $\Sigma^- p$ elastic and inelastic channels. In addition the so-called capture ratio at rest has been determined with high precision [1177, 1178]. The latter is defined by [1118]

$$r_R = \frac{1}{4} \frac{\sigma_s(\Sigma^- p \rightarrow \Sigma^0 n)}{\sigma_s(\Sigma^- p \rightarrow \Lambda n) + \sigma_s(\Sigma^- p \rightarrow \Sigma^0 n)} + \frac{3}{4} \frac{\sigma_t(\Sigma^- p \rightarrow \Sigma^0 n)}{\sigma_t(\Sigma^- p \rightarrow \Lambda n) + \sigma_t(\Sigma^- p \rightarrow \Sigma^0 n)},$$

where σ_s (σ_t) is the total reaction cross section in the singlet 1S_0 (triplet 3S_1 - 3D_1) partial wave. The cross sections are the ones at zero momentum, but in calculations it is common practice [1148] to evaluate the cross sections at a small non-zero momentum, namely $p_{\text{lab}} = 10$ MeV/c. The essential question is, of course, in how far those data pin down the coupled-channel amplitude and, in turn, allow one to determine the location of the poles reliably.

In Ref. [181] a variety of meson-exchange potentials of the Nijmegen group has been explored, NSC97f [1148] being the most modern one at that time. The poles were searched in the complex planes of the relative momenta in the ΛN and ΣN channels, $q_{\Lambda N}$ and $q_{\Sigma N}$, respectively. It turned out that for two of the considered potentials the poles are on the second quadrant of the $q_{\Sigma N}$ plane while for the other two they are on the third quadrant. (For details on various conventions used for the classification of the pole structure we refer to [9, 1176].) In the first case this should indicate an unstable (dibaryon-like) bound state while the second implies an inelastic virtual state. The resulting shape of the ΛN cross section around the ΣN threshold is also illustrated in [181] and should consist of a round peak, similar to a Breit-Wigner form, below the threshold in the first case, and a sharp peak (cusp) at the threshold in the second case, according to text-book knowledge [1179]. However, as is obvious from the concrete results reported in Ref. [181] for the considered potentials, not all show the idealized shape. In particular, for NSC97f that produces an unstable bound state, in the nomenclature of Ref. [9], the resulting shape is ambiguous [181], see also Fig. 49.

In Ref. [169] the poles and the resulting structure were investigated more systematically by considering a larger set of potentials, including the new chiral YN potentials, and by performing the calculations not only in isospin basis but also for the charge $Q = 1$ ($\Lambda p - \Sigma^+ n - \Sigma^0 p$) as well as for the $Q = 0$ ($\Lambda n - \Sigma^0 n - \Sigma^- p$) coupled-channel systems. The found pole positions are summarized in Fig. 50. One can see that most of the poles are located in the 2nd quadrant (sheet II). The few exceptions where the poles are either in the 3rd quadrant (sheet IV) or very close to it concern potentials that do not describe the near-threshold $\Sigma^- p$ data well, as emphasized in Ref. [169]. For example, the Juelich '04 potential (blue inverted triangle in the left plot) fails to reproduce the capture ratio and it also underestimates the $\Sigma^- p \rightarrow \Lambda n$ cross section, see Fig. 47.

As one can see in Fig. 50 the poles are in the lower half of the 2nd quadrant, i.e., $\text{Im } q_{\Sigma N} \leq |\text{Re } q_{\Sigma N}|$. A Breit-Wigner type signal can be only expected, however, when the poles are sufficiently close to the ΣN threshold and specifically close to the negative or positive $\text{Im } q_{\Sigma N}$ axis. Obviously, the second condition is not fulfilled by any of the YN potentials. Thus, one is far from the mentioned ideal case and that means, citing Pearce and Gibson [1176], in “a gray area where it is not obvious whether the effect will be cusp or peak”.

Anyway, the conclusion drawn from the analysis in Ref. [169] is that, if one takes the presently available low-energy ΣN data serious and aims at their best possible reproduction, then the appearance of a deuteron-like dibaryon in form of a

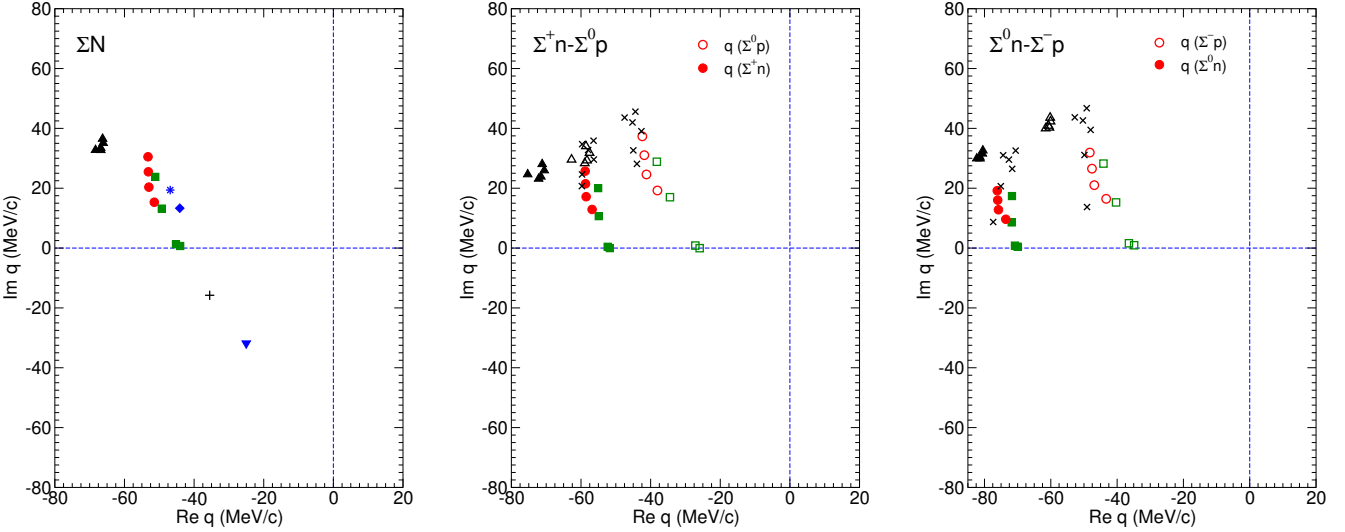


Figure 50: Pole positions for the Nijmegen NSC97f model (triangles), and the chiral YN potentials NLO13 (squares) and NLO19 (circles), and the SMS potentials from Ref. [1129] (crosses) in the complex q plane. Results are presented for the isospin $I = 1/2$ channel and for the $\Lambda p - \Sigma^+ n - \Sigma^0 p$ and $\Lambda n - \Sigma^0 n - \Sigma^- p$ systems. In the latter cases the poles for the two ΣN channels are shown in the same plot. In case of isospin averaged masses also results for the Juelich meson-exchange potentials '04 [1147], $\bar{\Lambda}$ [1146] (blue diamond), and A [1135] (blue star), and for the Nijmegen potential ND [1173] (plus) are included.

(unstable) ΣN bound state close to the ΣN threshold seems to be practically unavoidable. On the other hand, there is also strong evidence that it might be wishful thinking to expect a truly convincing and unambiguous signal for a strangeness $S = -1$ dibaryon, i.e., a peak that is well separated from the (and unambiguously below the) ΣN threshold.

5.4. Coupled channels with strangeness $S = -2$

As one can see from Fig. 45 the strangeness $S = -2$ sector is extremely rich as far as coupled channels are concerned. Moreover, the separation of the thresholds is, in general, fairly small, with the ones between $\Lambda\Lambda$ and ΞN being just about 25 MeV. However, contrary to the strangeness $S = -1$ sector discussed above experimental information on BB channels with $S = -2$ is really very much limited. Indeed for many of the reactions only upper limits on the cross sections have been established. A summary of available data is provided in Ref. [1180]. Recently, a new source of information has opened up by measurements of two-particle momentum correlation functions by the ALICE and STAR collaborations. So far data on the $\Lambda\Lambda$ [1181, 1182] and $\Xi^- p$ [1183–1185] channels have been published.

5.4.1. The H -dibaryon

Certainly the most interesting aspect related to the $S = -2$ sector and one of the main motivations for pertinent investigations has been the possible existence of the H -dibaryon. Initially proposed as a deeply bound 6-quark state with $J = 0$ and $I = 0$ by Jaffe, based on the bag model [1122], it has been suggested as a dark-matter candidate in recent times [1186, 1187]. Given its quantum numbers it should couple to the $\Lambda\Lambda - \Xi N - \Sigma\Sigma$ system. With its proposed energy of 2150 MeV it would lie around 80 MeV below the $\Lambda\Lambda$ threshold.

None of the past experimental searches for the H -dibaryon has let to convincing signals, see e.g. [1188]. However, in 2010 the interest in that state was revitalized by evidence for a bound H -dibaryon based on lattice QCD calculations [1189–1191]. The calculations were performed for quark masses that correspond to unphysical meson and baryon masses, specifically to pion masses of 230 and 389 MeV in case of the NPLQCD Collaboration and 469–1171 MeV by the HAL QCD Collaboration. The most recent lattice calculations of the H are from the Mainz group [1192] for $m_\pi \approx 420$ MeV and the HAL QCD calculation near the physical point [1193]. The latter work concludes that the $\Lambda\Lambda$ attraction is too weak to generate a bound or resonant dihyperon, see the discussion below. In the former work and in [1194] one can also find a review of earlier lattice calculations. A compilation of available predictions for the H -dibaryon is given in Fig. 51. As shown in this figure (from Ref. [1192]), systematics due to continuum extrapolations also may play an important role in identifying this illusive state from QCD.

Immediately after the publication of the lattice results several attempts have been made to extrapolate those results to the physical pion mass. Those extrapolations, performed with different methods and under different assumptions suggested that the H -dibaryon could be either loosely bound or move into the continuum [1194, 1195]. In Ref. [1196, 1197] chiral EFT at leading order was employed to study the fate of the H -dibaryon for physical masses. In that work not only

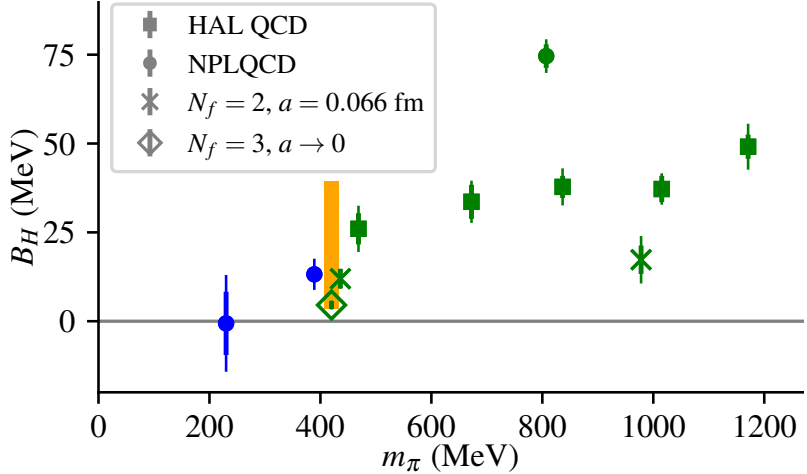


Figure 51: Lattice QCD results for the H-dibaryon binding energy, by the NPLQCD and HAL QCD Collaborations and the Mainz group. The variation of lattice spacing from the calculations of Ref. [1192] is shown by the orange band. The figure is taken from Ref. [1192].

the effect of the pion mass dependence of the interaction (which at LO consists of pion exchange and a contact term) was explored, but also the influence of the baryon masses which depend likewise on the quark mass and which enter the scattering or bound-state equations (5.2). It was found that the mass dependence of the latter has a much more dramatic effect on the binding energy of the H than the pion-mass dependence of the potential. The effect is caused by the relative shift of the three thresholds $\Lambda\Lambda$, $\Sigma\Sigma$ and ΞN due to the SU(3) breaking in the masses. Specifically, with physical values the binding energy of the H is reduced by as much as 60 MeV as compared to a calculation based on degenerate (i.e. SU(3) symmetric) BB thresholds. Translating this observation to the situation in the HAL QCD calculation, implied that the bound state should disappear at the physical point. For the case of the NPLQCD calculation, a resonance in the $\Lambda\Lambda$ system might survive.

Of course, nowadays lattice calculations at (almost) the physical point ($m_\pi \simeq 146$ MeV, $m_K \simeq 525$ MeV) are available, thanks to the work of the HAL QCD Collaboration [1193]. Their results for the $\Lambda\Lambda$ phase-shift in the 1S_0 partial wave are shown in Fig. 52 for the $t/a = 12$ case with t the sink-source time separation and a the lattice spacing. In that calculation no bound state (nor a resonances) was found around the $\Lambda\Lambda$ threshold. However, as one can see in the figure, there is still a remnant of the H -dibaryon, in form of a virtual state in the ΞN channel close to its threshold. It produces a sizable cusp-like structure in the $\Lambda\Lambda$ phase. Interestingly, the chiral potential at NLO, established a few years earlier by the Juelich group [1180], produces such a cusp too. (More details of that interaction will be discussed below.) On the other hand, the results of both groups indicate that the actual location of the virtual state is still uncertain. For example, in the calculation with the chiral potential the large cusp appears only when solving the coupled-channel equations with isospin averaged ΞN masses (left side). Once the mass difference between the Ξ^0 and Ξ^- is taken into account, i.e., the splitting between the thresholds for $\Xi^0 n$ and $\Xi^- p$, the virtual state is no longer close to either of the thresholds and the cusp structure is strongly reduced (right side).

5.4.2. ΞN scattering

For illustrating the experimental situation in the $S = -2$ sector, as examples $\Xi^- p$ elastic and inelastic cross sections are presented in Fig. 53. The theory results for the ΞN cross sections are based on a ΞN potential established within chiral EFT in 2019 [1198]. Again the bands reflect the residual cutoff dependence. In the construction of the potential constraints from the $\Lambda\Lambda$ scattering length in the 1S_0 state together with experimental upper bounds on the cross sections for ΞN scattering and for the transition $\Xi N \rightarrow \Lambda\Lambda$ have been exploited. This allowed to fix the additional LECs that arise in the $\{1\}$ irreducible representation of SU(3) [1180], which contribute only to the BB interaction in the $S = -2$ sector. Furthermore, the consideration of those empirical constraints necessitated to add SU(3) symmetry breaking contact terms in other irreps ($\{27\}$, $\{10\}$, $\{10^*\}$, $\{8_s\}$, $\{8_a\}$), with regard to those determined from the ΛN and ΣN data. This is anyway expected and fully in line with the power counting of SU(3) chiral EFT, as discussed in Ref. [1199]. It is interesting to see that the theory predicts coupled-channel effects at the opening of the $\Lambda\Sigma$ channel. But these are just standard (moderate) cusp structures and it will be difficult to verify their existence experimentally. Note that the recent BESIII data [1200] shown in Fig. 54 (middle) are for $\Xi^0 n \rightarrow \Xi^- p$, and actually deduced from the $\Xi^0 + {}^9\text{Be}$ reaction.

At present, the only more quantitative test for the ΞN interaction is provided by two-particle momentum correlations. For $\Xi^- p$, correlation functions have been measured recently by the ALICE Collaboration in p -Pb collisions at 5.02 TeV [1183] and in pp collisions at 13 TeV [1184]. There are also new and still preliminary results from Au+Au collisions at

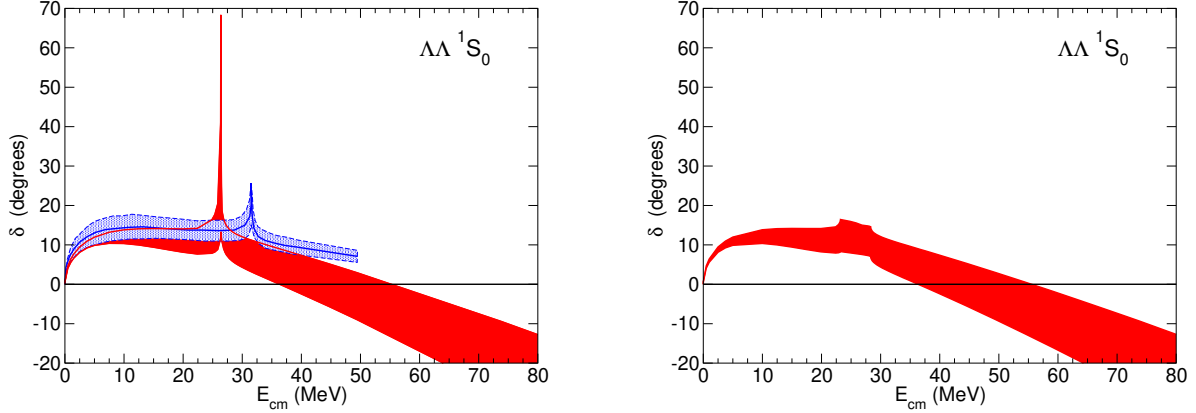


Figure 52: Phase shift for the $\Lambda\Lambda$ 1S_0 partial wave. The results are from the lattice simulation by the HAL QCD Collaboration [1193] (blue band) and the chiral NLO potential [1180] (red band). The former calculation corresponds to (meson and baryon) masses which are slightly larger than the physical ones and, therefore, the ΞN threshold appears at a higher energy. The curves on the left are for isospin averaged masses, while on the right-hand side physical masses have been used.

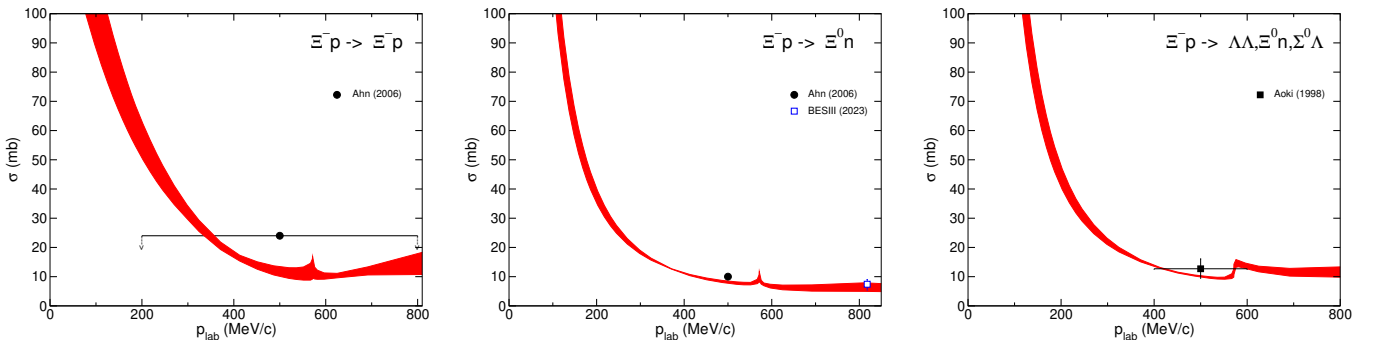


Figure 53: Results for the ΞN cross sections of the NLO potential [1198]. Data are from Refs. [1200–1202].

200 GeV by the STAR Collaboration [1185]. In Fig. 54 predictions for $C(k)$ for the chiral $S = -2$ interaction from [1198] are presented. Details on the evaluation of such correlation functions can be found, e.g., in Refs. [1203, 1204]. Clearly, the correlation functions, evaluated for the source radii R taken from the corresponding pp fits by ALICE [1182] (1.43 fm for 5.02 TeV and 1.18 fm for 13 TeV), agree nicely with the measurements. For a more thorough discussion on the choice of R and of the other parameters that enter into the calculation, see the work of Kamiya et al. [1204]. In this context, note also the critics on the “universality assumption” for the source (radius) in Ref. [1014]. Comparable results have been also achieved by Liu et al. [1205] based on a full coupled-channel potential ($\Lambda\Lambda$, ΞN , $\Lambda\Sigma$, $\Sigma\Sigma$) established within covariant chiral EFT, whose LECs were fitted to the $\Lambda\Lambda$ and ΞN phase shifts of the HAL QCD potential [1193].

For completeness, results for the correlation function in the $\Lambda\Lambda$ channel are shown too. Exploratory calculations [1203, 1204] suggested that there could be a pronounced threshold effect at the opening of the ΞN channel, cf. Fig. 52. However, the data from ALICE themselves do not exhibit any structure, though admittedly the statistics is low and the momentum resolution too poor.

5.5. Other coupled baryon-baryon systems

The interaction of octet baryons in BB channels with strangeness $S = -3, -4$ have been studied in the meson-exchange picture [1206] and in chiral EFT [1207, 1208] by exploiting the underlying SU(3) symmetry. However, there are large variations/ambiguities in the predictions. First but still limited experimental constraints have emerged only recently for the $\Lambda\Xi^-$ system, again in form of momentum correlation functions [1209]. The present statistics is not sufficient to see any coupled-channel effects, say in form of a structure at the opening of the $\Sigma\Xi$ channels. There are also results from lattice QCD simulations by the HAL QCD collaboration for quark masses close to the physical point [1210]. Finally, there are some results on the $N\Omega$ interaction from lattice QCD [1211] and empirical correlation functions [1184, 1212]. This channel couples to $\Xi\Lambda$ and $\Xi\Sigma$.

Regarding BB systems with charmed baryons, there are studies on the $\Lambda_c^+ N - \Sigma_c N$ system. Again there are results from lattice QCD simulations by the HAL QCD collaboration [1213, 1214], though in this case the masses are still away

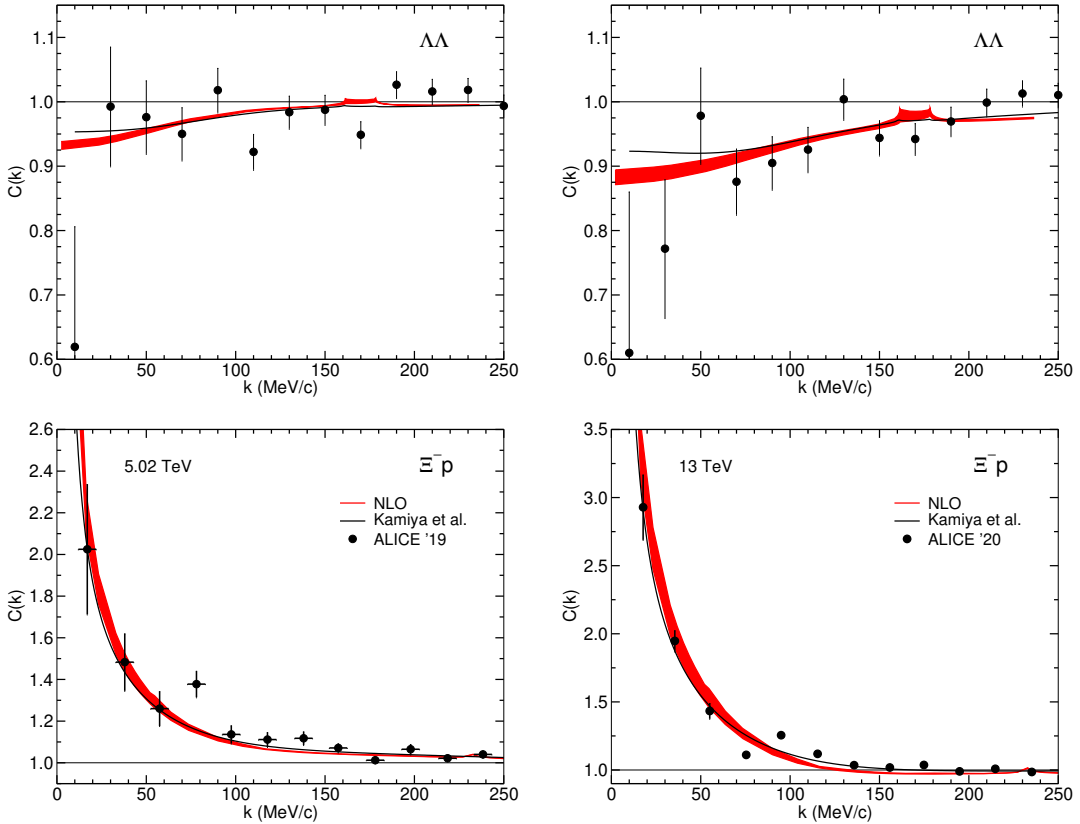


Figure 54: $\Lambda\Lambda$ and Ξ^-p two-particle momentum correlation function calculated from the NLO potential [1198] (red bands). Results for the HAL QCD potential, taken from Ref. [1204], are shown by the solid (black) line. Data from $p\text{Pb}$ collisions at 5.02 TeV (left) and pp collisions at 13 TeV (right) are by the ALICE Collaboration [1182–1184].

from the physical point. An extrapolation to the physical point based on (conventional as well as covariant) chiral EFT has been attempted [1215–1217] - with in part contradictory results. There are also attempts to construct potential models based on meson exchange relying on the assumption of SU(4) flavor symmetry [1218, 1219]. In any case, as one can see from Fig. 45, the thresholds in the charm sector are farther apart and actually the $\Lambda_c^+ N\pi$ threshold lies below that of $\Sigma_c N$. Thus, more pronounced coupled-channel effects are unlikely to occur, specifically if the overall strength of the interaction is in the order of magnitude as suggested by the HAL QCD lattice simulations.

6. Heavy sector

6.1. The DN interaction and the charm counterpart of the $\Lambda(1405)$

In 1993 first evidence for the $\Lambda_c(2595)^+$ resonance was reported by the CLEO collaboration [1220] and its mass was subsequently confirmed by other experiments [1221–1223]. It is now generally believed that this resonance is the charm counterpart of the $\Lambda(1405)$ [103]. As discussed in Sect. 3.6, there is strong theoretical evidence that the $\Lambda(1405)$ is a $\bar{K}N$ bound state (molecule) and very likely even has a two-pole structure [200, 502, 585]. This circumstance triggered several studies under the premise that the $\Lambda_c(2595)^+$ could be likewise a dynamically generated state. Those studies build again on flavor symmetry and on chiral symmetry, and several of them also on heavy-quark spin symmetry (HQSS). In addition, in most of the works, the experimentally known mass of the $\Lambda_c(2595)^+$ resonance has been utilized as constraint for fixing inherent parameters of the interaction.

The connection between the $\bar{K}N$ and DN interactions can be easily established within chiral unitary (and related) approaches, by extending the scheme from SU(3) to SU(4) in flavor space. Thereby, in analogy to the $\Lambda(1405)$ resonance, states in the corresponding charm sector are generated by the dynamics in the coupled-channel system that involves channels like $\pi\Lambda_c^+$, $\pi\Sigma_c$, or DN , i.e., where the strange quark in the hadrons is simply replaced by the one with charm [276, 1225–1232]. There is some dispute on the question how one should deal with the flavor and chiral symmetries in detail and what additional symmetries should be imposed. In the simplest extension based on the SU(3) subgroup one has again an octet of pseudoscalar mesons and an octet (nonet) of ($J^P = 1/2^+$) baryons. The number of channels that couple is then comparable to those in the strangeness $S = -1$ sector. When keeping only Goldstone bosons in the chiral SU(3)

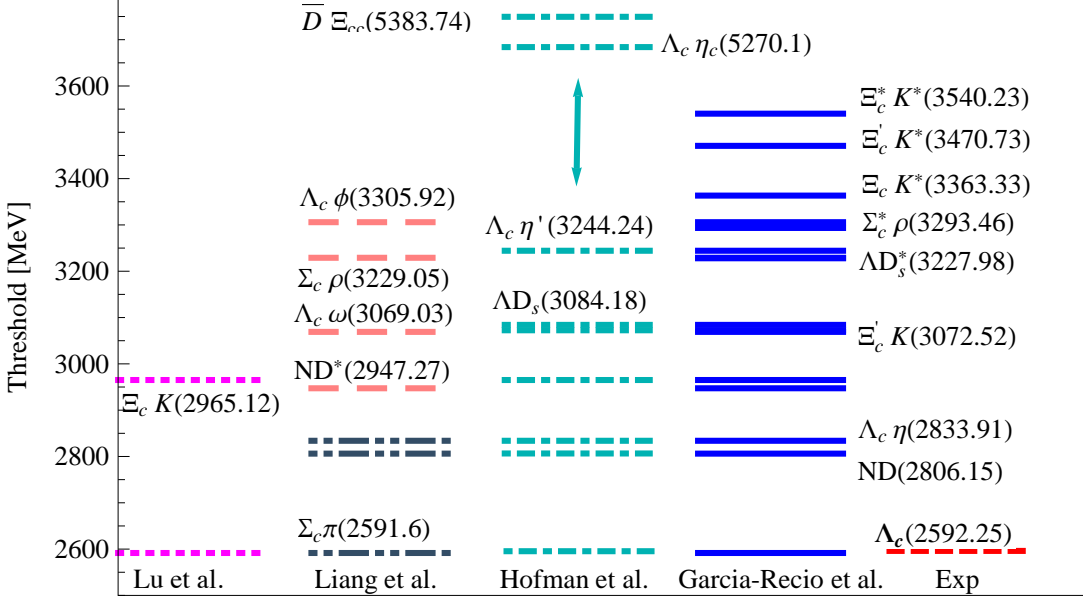


Figure 55: Thresholds of channels included in different studies: Lu et al. [1224], Liang et al. [1225], Hofmann et al. [1226], Garcia-Recio et al. [1227]. The figures is adapted from Ref. [1224].

Lagrangian, potentially important channels like DN are excluded [1224, 1228]. On the other hand, when implementing also HQSS [1227, 1232], vector mesons and also $J^P = 3/2^+$ baryons enter so that the number of coupled channels increases significantly. Then one has also D^*N , $D^*\Delta$, $\omega\Lambda_c$, etc. – in fact a total of 16 channels for $I = 0$ and 22 for $I = 1$ that all couple to DN [1227]. Channels involving vector mesons appear also in the extended local hidden gauge approach followed in Ref. [1225]. A visual impression of the situation is provided in Fig. 55. Clearly, with the increasing number of channels there is a simultaneous increase in the number of dynamically generated states, as spelled out in Ref. [1224]: “it seems that the number of states generated is proportional to the number of coupled channels considered”. It should be noted that most of the states found in the calculations have so far not been confirmed experimentally.

In the aforementioned approaches the dynamics is provided by vector-meson exchange [1226, 1231], by the Weinberg-Tomozawa (WT) term [1228–1230], or by an extension of the WT interaction to an SU(8) spin-flavor scheme [1227, 1232]. The model presented in Ref. [276] is derived within the conventional meson-exchange picture. There, besides contributions from vector-meson exchanges also scalar-mesons are considered. The included channels are $\pi\Lambda_c^+$, $\pi\Sigma_c$, DN but also D^*N , $D\Delta$, and $D^*\Delta$, in close analogy to the Juelich $\bar{K}N$ potential model [16] which forms the basis for the extension to the charm sector via SU(4) symmetry.

There are also additional works which focus on specific aspects. For example, Refs. [1233, 1234] consider mainly the physics around the $\Sigma_c(2800)$ resonance, which is located close to the DN threshold. A recent overview of the various investigations can be found in Ref. [1235].

Let us review in more detail the situation for the $\Lambda_c(2595)^+$ and the $\Sigma_c(2800)$. First, we want to emphasize that there is an essential difference between the situation for the $\Lambda(1405)$ and for the $\Lambda_c(2595)^+$: The former is located about 30 MeV below the $\bar{K}N$ threshold while the latter is about 200 MeV below the DN threshold. Thus, if the $\Lambda_c(2595)^+$ is indeed a DN bound state it would be rather deeply bound. Accordingly, the interactions have to be fairly strong. Since the mass of the $\Lambda_c(2595)^+$ is commonly used as input, as mentioned above, it is in usually well reproduced in such studies. There is a bit more variation when it comes to the width Γ , where the present experimental value is 2.6 ± 0.6 MeV [103]. The theoretical predictions range from 0.6 MeV [1227] to 4.8 MeV [276]. However, given the delicate situation that the $\Lambda_c(2595)^+$ coincides with the $\pi\Sigma_c$ thresholds and in view of the fact that the three-body decay channel $\pi\pi\Lambda_c^+$ is not included in any of the calculations the agreement is still remarkably good. Anyway, one has to keep in mind that in calculations typically the pole position is determined whereas the experimental value is the result of a Breit-Wigner type fit.

One of the characteristic features of the $\Lambda(1405)$ in chiral unitary approaches is its two-pole structure, see, e.g., the review by Mai [200]. Indeed such a two-pole structure is also found for the $\Lambda(2595)^+$ in several studies, notably in Refs. [276, 1225, 1227, 1229, 1232]. In the majority of the calculations, the second pole is very close to that of the $\Lambda(2595)^+$, say within 10 to 15 MeV but with a considerably larger width. The latter reflects the fact that the second pole is already well above the $\pi\Sigma_c$ threshold and it is dominated by the $\pi\Sigma_c$ component. Compared to the $\bar{K}N$ ($\Lambda(1405)$) case, there is even less concrete experimental evidence for the partner state. Initial works in the chiral unitary approach

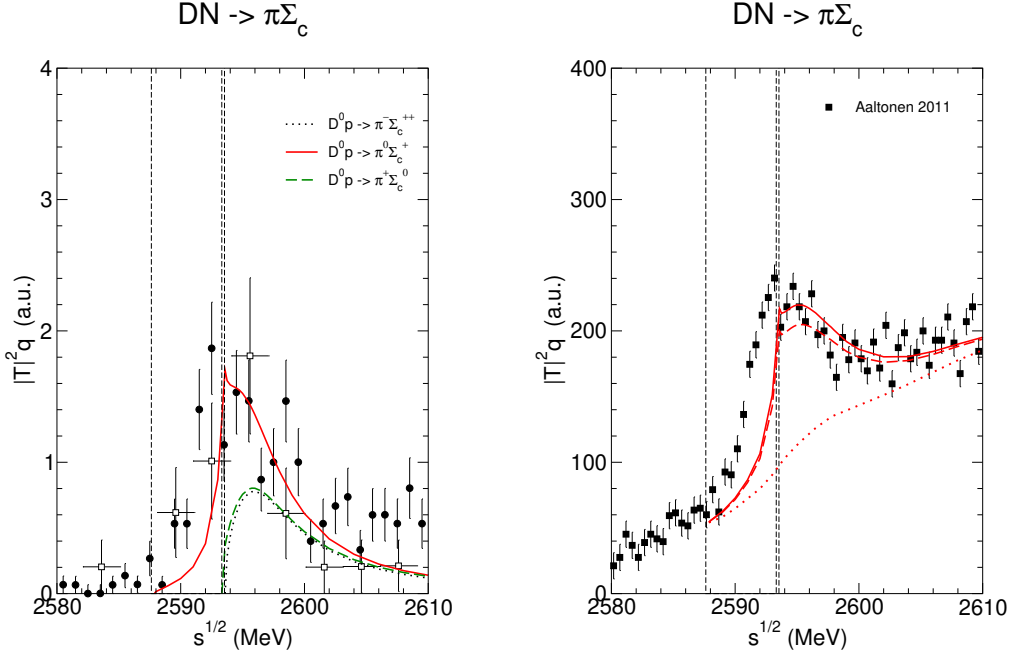


Figure 56: $\pi\Sigma_c$ invariant-mass spectrum predicted by the DN potential of the Juelich group [276]. For comparison experimental information on the $\pi^+\pi^-\Lambda_c^+$ mass distribution in the $\Lambda_c(2593)^+$ region is shown. The data are from ARGUS [1222] (open squares), Zheng (CLEO) [1236] (circles) and CDF [1223] (filled squares). The nominal thresholds of the $\pi^0\Sigma_c^+$, $\pi^+\Sigma_c^0$, and $\pi^-\Sigma_c^{++}$ channels are indicated by vertical lines.

associated the second pole with the $\Lambda_c(2625)^+$ but the predicted width is much too large as compared to the experiment. Anyway, the latter is now commonly assumed to be a $J^P = 3/2^-$ state, i.e., the counterpart of the $\Lambda(1520)$.

Predictions for the $\pi\Sigma_c$ invariant-mass spectrum in the region of the $\Lambda_c(2595)^+$ resonance were presented in Ref. [276], obtained from the $\pi\Sigma_c \rightarrow \pi\Sigma_c$ and $DN \rightarrow \pi\Sigma_c$ reaction amplitudes multiplied with the appropriate phase-space factors. Since there is no qualitative difference between the two cases, we reproduce here only the results for the latter, see Fig. 56. The invariant-mass distributions are given in arbitrary units but the relative normalization between the different charge channels as predicted by the model has been kept fixed. Then the drastic effect due the splitting of the thresholds in the $\pi\Sigma_c$ channels caused by the mass differences between π^\pm and π^0 and between the Σ_c 's is preserved. Indeed, the threshold of the $\pi^0\Sigma_c^+$ channel is about 6 MeV lower than those of the other two charge channels and, as a consequence, the predicted invariant-mass distribution is about twice as large. Moreover, there is a clear cusp in the $\pi^0\Sigma_c^+$ amplitude at the opening of the $\pi^+\Sigma_c^0$ channel. The threshold of $\pi^-\Sigma_c^{++}$ is just about 0.3 MeV above the one for $\pi^+\Sigma_c^0$. This produces a noticeable kink in the $\pi^0\Sigma_c^+$ invariant-mass distribution.

For illustration, the experimental $\pi^+\pi^-\Lambda_c^+$ mass distributions where the signal for the $\Lambda_c(2595)^+$ is seen [1222, 1236] are also displayed in the left panel of the Fig. 56. The results for the $D^0 p \rightarrow \pi^0\Sigma_c^+$ channel resemble very much the measured signal and one can imagine that smearing out the results by the width of the Σ_c^+ , which is around 2.3 MeV [103], could further improve the already good agreement with the data. However, experimentally it was found that the $\Lambda_c(2595)^+$ decays predominantly into the $\pi^+\Sigma_c^0$ and $\pi^-\Sigma_c^{++}$ channels with a combined branching fraction in the range of 50% [103]. Smearing out the corresponding results with the widths of the Σ_c^0 and Σ_c^{++} , which are likewise around 2 MeV [103], would still leave a large fraction of the events found below the nominal $\pi^+\Sigma_c^0$ and $\pi^-\Sigma_c^{++}$ threshold unexplained, especially for the data from Ref. [1236]. Thus, it seems that the position of the $\Lambda_c(2595)^+$ resonance being so close to or even below the nominal $\pi^+\Sigma_c^0/\pi^-\Sigma_c^{++}$ thresholds and the found large branching ratios into those channels are difficult to reconcile. In any case, one has to keep in mind that there is also a branching fraction of 20% directly into the three-body channel $\pi^+\pi^-\Lambda_c^+$ [103], which is not included in the theoretical curve. For a dedicated study of the situation of the $\Lambda_c(2595)^+$ being so close to the $\pi\Sigma_c$ threshold see [1237].

A comparison with the data from the CDF experiment [1223] is provided in the right panel of Fig. 56. In this case a background contribution has been established/added in the analysis of the data (cf. dotted line) and we add this contribution to the $\pi\Sigma_c$ invariant-mass spectrum evaluated in Ref. [1223]. Once that is done, there is again a fairly good agreement with the experimental spectrum, but again an underestimation below the nominal $\pi^+\Sigma_c^0$ and $\pi^-\Sigma_c^{++}$ thresholds.

Concerning the actual structure of the $\Lambda_c(2595)^+$ the conclusions drawn from the various studies remain ambiguous. While there is consent that the resonance contains a large meson-baryon component, it remains unclear which of those components might be the dominant one. Actually, it seems that the compositeness depends strongly on the number of considered coupled channels and also on the regularization schemes employed in the course of the unitarization [1224].

Specifically, in approaches where only (approximate) flavor symmetry is imposed one finds either a dominant $\pi\Sigma_c$ component or a dominant DN component. On the other hand, models that implement also HQSS often find a large D^*N component. For example, in the SU(8) spin-flavor scheme of Ref. [1227] the $\Lambda_c(2595)^+$ becomes predominantly a D^*N quasi-bound state – though still with important additional binding effects from the DN channel. Finally, in a recent work by Nieves et al. [1238] even the analogy between the $\Lambda_c(2595)^+$ and the $\Lambda(1405)$ is called into question. The study is based on the standard Weinberg-Tomozawa (WT) term and incorporates HQSS. However, it addition, it includes also the exchange of resonances from the constituent quark model in the s -channel.

Now to the $\Sigma_c(2800)$, a state which is located very close to the DN threshold and whose quantum numbers are still not determined [103]. The Juelich potential predicts a dynamically generated S -wave state with mass 2797 MeV [276] and isospin $I = 1$, and it is quite tempting to identify it with the $\Sigma_c(2800)$ [103]. However, there is a caveat because the predicted width is with just about 12 MeV significantly smaller than the value of roughly 75 ± 20 MeV given by the PDG. Since that resonance decays primarily to $\pi\Lambda_c^+$ the failure to reproduce the width could be an indication that the $DN \rightarrow \pi\Lambda_c^+$ transition potential is too small in that model. Most of the other studies do not find states with suitable quantum number in that region. Actually, the majority of the predictions suggest masses around or even below 2700 MeV for S -wave states with $I = 1$. Only in [1231] an isovector state with 2800 MeV is predicted, interestingly with t -channel vector-meson exchange as driving force just as in the Juelich model, and again with a somewhat too small width.

In this context, let us mention that recently evidence against the bound-state nature of the $\Sigma_c(2800)$ was reported by Wang et al. [1234], who studied the state within chiral EFT to NLO, including, however, only the DN and D^*N channels. In contrast to that, a theoretical analysis of the D^0p invariant-mass spectrum, measured by the LHCb Collaboration in the reaction $\Lambda_b \rightarrow \pi^- D^0 p$ [1239], supports the existence of a bound state right below the D^0p threshold [1240]. In that work also the DN scattering lengths were extracted. Interestingly, but not really surprising, the obtained values are fairly close to those predicted by the Juelich model [276], thus, giving support to the strength of the DN interaction generated by that potential.

6.2. XYZ and pentaquark states

DCC approaches play also an essential role in studies of the structure of the so-called XYZ states and of possible pentaquark states, see the reviews [167, 440, 1028, 1241–1249]. Many of the new states seen in the charm or bottom sectors, which do not fit into the standard quark-antiquark or three-quark classification, have been observed close to thresholds. The first and perhaps still most famous one is the $\chi_{c1}(3872)$, formerly known as $X(3872)$ [1250], whose mass coincides with the $D\bar{D}^*/D^*\bar{D}$ threshold within the experimental uncertainty. Indeed channel coupling and aspects associated with it like threshold anomalies have been revisited in various works since they are considered as possible explanation for the nature and structure of some XYZ and other exotic states, see, e.g., Refs. [1251, 1252] and the review [167] for very recent examples.

Since the focus of the present review are DCC approaches we do not have the ambition and the space to provide an adequate overview over the vast amount of studies and publications dedicated to exotic states in the heavy sector. Anyway, as mentioned above, there are already various excellent and comprehensive reviews available. Accordingly, here we want to highlight a few specific and illustrative systems/works, selected by the criterion that channel coupling plays a decisive role for the physical conclusions drawn in those studies. Accordingly, our emphasis will be on specific meson-baryon systems involving heavy hadrons where potentially many channels are coupled. In this context the (approximate) heavy-quark spin symmetry (HQSS) [1253], a symmetry which requires the dynamics of heavy hadrons to become independent of the spin of the constituent heavy quark ($Q = c, b$) in the limit $m_Q \rightarrow \infty$, plays an important role in a two-fold way. On the one hand side, it results in mass splittings $\bar{D}^* - \bar{D}$, $\Sigma_c^* - \Sigma_c$, etc. that are significantly smaller than those between the strange counterparts $K^* - K$ and $\Sigma^* - \Sigma$,

$$\begin{aligned} M_{K^*} - M_K &= 396 \text{ MeV} & M_{D^*} - M_D &= 141 \text{ MeV} & M_{B^*} - M_B &= 45 \text{ MeV} \\ M_{\Sigma^*} - M_\Sigma &= 191 \text{ MeV} & M_{\Sigma_c^*} - M_{\Sigma_c} &= 65 \text{ MeV} & M_{\Sigma_b^*} - M_{\Sigma_b} &= 19 \text{ MeV} \end{aligned} \quad (6.1)$$

so that the thresholds of the meson-baryon channels that can be formed are much closer together. In addition it provides constraints on the interaction between the pertinent hadrons and it singles out the relevant channels, which would all have degenerate thresholds in the strict HQSS limit.

DCC approaches in the heavy sector are characterized by the intention to interpret observed exotic states in terms of bound states, commonly referred to as molecules or dynamically generated states. This strategy is motivated by the fact that many of the exotic states seen in experiments are located conspicuously close to thresholds, as mentioned above, which suggests that their nature could be analogous to that of the deuteron. The coupling between channels whose thresholds are fairly close together enhances effectively the overall strength of the interaction in the system, and specifically in channels where the underlying direct interaction is attractive, and, consequently, favors the formation of bound states. For a specific review from a molecular perspective see Ref. [440].

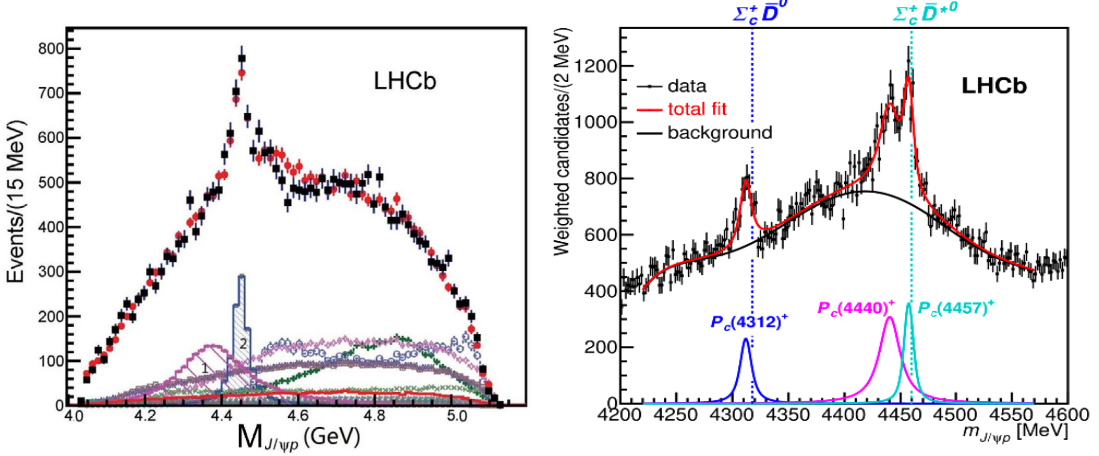


Figure 57: Hidden-charm pentaquarks established by the LHCb Collaboration in the $\Lambda_b^0 \rightarrow J/\psi p K^-$ decays in 2015 [1254] (left) and (2019) [1255] (right). Left: Squares represent the data and circles the result of a fit. The histograms labeled “1” and “2” indicate the contributions from the $P_c(4380)$ and $P_c(4450)$ states. Right: The fit to the data is based on a sixth-order polynomial background and three Breit-Wigner functions representing the pentaquark candidates.

6.2.1. Hidden-charm pentaquarks

First evidence for two possible pentaquark candidates, the $P_c(4380)$ and $P_c(4450)$ ($P_{c\bar{c}}$ in the new convention by the PDG [103]), were reported by the LHCb Collaboration in 2015 based on a measurement of the $J/\psi p$ invariant mass spectrum via the weak decay $\Lambda_b^0 \rightarrow J/\psi p K^-$ [1254]. Four years later the LHCb Collaboration presented new results by exploiting a much larger data sample [1255]. In that work a new structure, the $P_c(4312)$, was found and, in addition, the (former) $P_c(4450)$ resolved into two fairly narrow states, the $P_c(4440)$ and $P_c(4457)$, respectively. The mass spectra from the two LHCb publications are shown in Fig. 57 while the properties of the states are summarized in Tab. 6, together with there theoretically favored quantum numbers. Another state, the $P_c(4338)$, was identified in the decay $B_s^0 \rightarrow J/\psi p\bar{p}$ [1256]. Note that a detailed overview on pentaquarks, by Karliner and Skwarnicki, is included in the latest review of the PDG [103].

The plot on the right-hand side of Fig. 57 reveals already the most interesting aspect, the $P_c(4312)$, $P_c(4440)$ and $P_c(4457)$ are just below the $\bar{D}^0 \Sigma_c^+$ and $\bar{D}^{*0} \Sigma_c^+$ thresholds of 4318 and 4460 MeV, respectively. Those channels are two of the four primary channels, $\bar{D}\Sigma_c$, $\bar{D}\Sigma_c^*$, $\bar{D}^*\Sigma_c$, and $\bar{D}^*\Sigma_c^*$, which are closely connected by HQSS. Other channels of relevance are $\bar{D}\Lambda_c^+$ and $\bar{D}^*\Lambda_c^+$, and the hidden-charm channels $\eta_c N$ and specifically $J/\psi N$, since the latter system is the one whose invariant mass spectrum was measured in the LHCb experiments.

Besides those obvious channels, further and also more special channels have been considered. For example, $\bar{D}\Lambda_c(2595)^+$ could be of relevance because its threshold, at 4457 MeV, coincides exactly with the mass of one of the LHCb pentaquarks [1258–1260]. Of course, since the $\Lambda_c(2595)^+$ has $J^P = \frac{1}{2}^-$, then the $\bar{D}\Lambda_c(2595)^+$ S-wave state can couple only to P-wave states of $J/\psi N$ and of the primary channels mentioned above and the pentaquark in question should have $J^P = \frac{1}{2}^+$ instead of $\frac{1}{2}^-$ or $\frac{3}{2}^-$. There have been also speculations about the role of the $\chi_{c1} p$ channel whose threshold is at 4449 MeV, i.e., right in the pentaquark region [1261]. Also in this case the S-wave is in $J^P = \frac{1}{2}^-$, just like for the $D\Lambda_c(2595)^+$ channel. Another unusual channel is considered in the work of Wu et al. [1260]. Here, the $P_c(4457)$ pentaquark is interpreted as a $J^P = 1/2^+$ state in the $\bar{D}^0 \Lambda_c(2595)^+ - \pi^0 P_c(4312)$ DCC system. Finally, let us mention that, in principle, there are also three-body channels like $\bar{D}\Lambda_c^+\pi^-$ that open in the relevant energy region.

While by far the majority of the works on the pentaquarks that have been published list only the poles, there

Table 6: Properties of the $P_c(4312)$, $P_c(4440)$, $P_c(4457)$ [1255], the $P_c(4380)$ [1254], and the $P_c(4338)$ [1256] (in MeV). The $I(J^P)$ quantum numbers are the theoretically favored ones; experimentally they are not yet established. Adapted from Ref. [1257].

States	Mass	Width	Threshold	Binding energy	$I(J^P)$
$P_c(4312)$	$4311.9 \pm 0.7^{+6.8}_{-0.6}$	$9.8 \pm 2.7^{+3.7}_{-4.5}$	$\Sigma_c^+ \bar{D}^0$	$-5.83 \pm 0.7^{+6.8}_{-0.6}$	$\frac{1}{2} \left(\frac{1}{2}^- \right)$
$P_c(4440)$	$4440.3 \pm 1.3^{+4.1}_{-4.7}$	$20.6 \pm 2.7^{+8.7}_{-10.1}$	$\Sigma_c^+ \bar{D}^{*0}$	$-19.45 \pm 1.3^{+4.1}_{-4.7}$	$\frac{1}{2} \left(\frac{1}{2}^- \right)$
$P_c(4457)$	$4457.3 \pm 0.6^{+4.1}_{-1.7}$	$6.4 \pm 2.0^{+5.7}_{-1.9}$	$\Sigma_c^+ \bar{D}^{*0}$	$-2.45 \pm 0.6^{+4.1}_{-1.7}$	$\frac{1}{2} \left(\frac{3}{2}^- \right)$
$P_c(4380)$	$4380 \pm 8 \pm 29$	$205 \pm 18 \pm 86$	$\Sigma_c^{*+} \bar{D}^0$	$-2.33 \pm 8 \pm 29$	$\frac{1}{2} \left(\frac{3}{2}^- \right)$
$P_c(4338)$	4337^{+7+2}_{-4-2}	29^{+26+14}_{-12-14}			

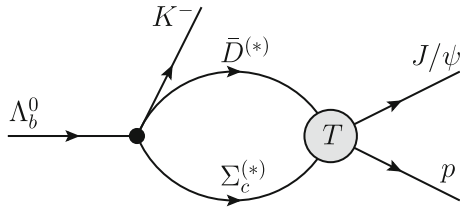


Figure 58: Illustration of the treatment of the reaction $\Lambda_b^0 \rightarrow J/\psi p K^-$ in Refs. [1262, 1263] and [64].

are a few which provide results for the $J/\psi p$ invariant-mass spectrum which then can be compared directly with the measurements [63, 64, 1262, 1263]. We will focus on those works in the following, starting with a discussion of the publication of Du et al. [1263]. In their study, all four $\bar{D}^{(*)}\Sigma_c^{(*)}$ channels are included. Their thresholds are all close to the discovered P_c states and they are all related by HQSS so that their consistent inclusion is anyway demanded by that symmetry. Those are called elastic channels by Du et al. In addition, $J/\psi N$ is included as so-called inelastic channel [1262] and, in Ref. [1263], also $\eta_c N$ and $\bar{D}^{(*)}\Lambda_c^+$. The latter step is necessary from a HQSS perspective since $(\eta_c, J/\psi)$ form likewise a heavy quark spin doublet, just as (\bar{D}, \bar{D}^*) . In the actual calculations three different schemes are considered [1263]. In scheme I the leading-order (LO) contact potentials in the $\bar{D}^{(*)}\Sigma_c^{(*)}$ channels are taken into account and in the same way the coupling to the S - and D -wave $J/\psi N$ and $\eta_c N$ channels. In scheme II, the contributions from one pion exchange (OPE) are added. The OPE potential is derived in line with chiral effective field theory and the involved coupling constants are fixed from the measured width of the decay $D^{*+} \rightarrow D^0 \pi^+$ on one hand side, and from results by lattice QCD calculations regarding the coupling to the $\Sigma_c^{(*)}$ s [1264]. Furthermore, an NLO S - D contact term for the $\bar{D}^{(*)}\Sigma_c^{(*)}$ channels is added to absorb undesired artifacts from the regularization of the OPE potential [1265, 1266]. Finally, in scheme III, the coupling to the $\bar{D}^{(*)}\Lambda_c^+$ channels is added.

The evaluation of the $J/\psi p$ invariant mass is illustrated schematically in Fig. 58. Its calculation involves the reaction amplitudes (T-matrices) for the meson-baryon channels, which are obtained by solving a Lippmann-Schwinger type equation. As indicated in the figure, in the intermediate state only the elastic channels are kept. The free parameters of the different schemes are fixed in a fit to the $J/\psi N$ invariant mass reported by the LHCb collaboration. In fact, that work contains three sets of $m_{J/\psi p}$ distributions, one that includes all m_{Kp} events, one where only events with $m_{Kp} > 1.9$ GeV are included, and a third set where $\cos\theta_{P_c}$ -dependent weights are applied to each event candidate [1255] so that the P_c signals are enhanced. In Ref. [1263] Du et al. present a variety of fits, based on the different schemes and for the different data sets, where all of them reproduce the data with fairly similar quality (i.e. similar χ^2). For illustration, we pick out the one in scheme II and for the $\cos\theta_{P_c}$ weighted case, see Fig. 59 (right side). One can see that the mass spectrum is very well reproduced, including the structure associated with the P_c states. Note that besides the theoretical $J/\psi p$ invariant-mass distribution, evaluated via the mechanism displayed in Fig. 58, a smooth incoherent background has to be added. The latter is indicated by the dotted line.

Exploring the pole structure of the reaction amplitude, the authors found a total of seven P_c states, for all fits/schemes considered, and in line with other investigations where HQSS was imposed on the employed interaction models [1267]. To be concrete, they identified three states with $J^P = \frac{1}{2}^-$, three states with $J^P = \frac{3}{2}^-$, and one with $J^P = \frac{5}{2}^-$. The lowest one corresponds to the $P_c(4312)$ with $\frac{1}{2}^-$ and is a $\bar{D}\Sigma_c$ bound state. There are two $\bar{D}^*\Sigma_c$ bound states, with $\frac{1}{2}^-$ and $\frac{3}{2}^-$, respectively, which in the solution shown in Fig. 59 correspond to a reversed order for $P_c(4457)$ and $P_c(4440)$. It should be said that in scheme I the “theoretically favored” ordering $P_c(4440)$, $P_c(4457)$, see Table 6, can be realized too [1262, 1263]. In addition, there is a pole around 4380 MeV, with a dominant $\bar{D}\Sigma_c^*$ component. This mass is close to the structure reported in the first LHCb paper [1254], however, it is much narrower than the state reported by LHCb. Finally, there are three P_c states (with $\frac{1}{2}^-$, $\frac{3}{2}^-$, and $\frac{5}{2}^-$, respectively) which are $\bar{D}^*\Sigma_c^*$ bound states and which are located close to the threshold of that channel. Their interpretation is unclear so far, since the mass spectrum from the LHCb measurement does not show any unambiguous structure in that invariant-mass region.

The other study of the LHCb pentaquarks reviewed here is performed by members of the Juelich-Bonn (JB) group [63, 64], who likewise presented results for the $J/\psi p$ invariant mass. This DCC study is performed within the traditional meson-exchange picture and can be viewed as an extension of the JB model [53] (see Sect. 2.3) to the heavy sector. It includes six channels, namely $\bar{D}\Lambda_c^+$, $\bar{D}\Sigma_c$, $\bar{D}^*\Lambda_c^+$, $\bar{D}^*\Sigma_c$, $\bar{D}\Sigma_c^*$, and $J/\psi N$. The potentials acting in the various channels are derived from an effective interaction based on the Lagrangians of Wess and Zumino [98] using time-ordered perturbation theory. They consist of contributions from t -channel meson-exchange processes and also from u -channel baryon exchanges. The former comprise the pseudoscalar mesons π , η , η' and the vector mesons ρ , ω , depending on the quantum numbers of the involved charmed mesons and baryons. The transition $\bar{D}^{(*)}\Sigma_c^{(*)}, \bar{D}^{(*)}\Lambda_c^+ \rightarrow J/\psi N$ is mediated by \bar{D} and \bar{D}^* exchanges. The coupling constants at the various meson-meson-meson- and baryon-baryon-meson vertices are fixed by assuming SU(3) and SU(4) flavor symmetry. The free parameters in the model are the cutoff masses associated with the phenomenological form factors that are attached to each vertex. Some of them are determined in the fitting procedure

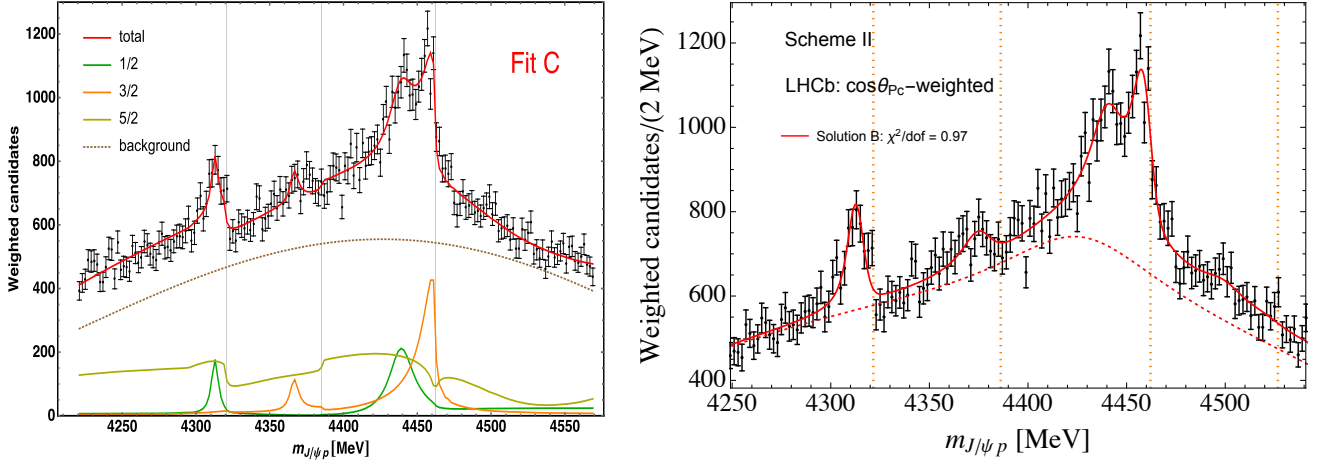


Figure 59: $J/\psi p$ invariant-mass spectrum measured by the LHCb Collaboration [1255]. Left: Calculation taken from Ref. [64]. Right: Calculation taken from Ref. [1263]. The vertical lines indicate the $\bar{D}\Sigma_c$, $\bar{D}\Sigma_c^*$, $\bar{D}^*\Sigma_c$, and $\bar{D}^*\Sigma_c^*$ thresholds, respectively, from left to right.

while others are kept fixed, see Table 5 in Ref. [64] for details.

The evaluation of the $J/\psi p$ invariant mass is similar to that of Du et al. described above, see also Fig. 58. Again, the employed reaction amplitudes for the meson-baryon channels are obtained by solving a Lippmann-Schwinger type equation. And again only $\bar{D}^{(*)}\Sigma^{(*)}$ are kept in the intermediate state. Finally, as in [1263] different solutions are found which describe the $J/\psi p$ invariant-mass spectrum almost equally well. Out of the three fits presented in Ref. [64] we show here exemplary Fit C, see the left-hand side of Fig. 59.

As one can see from the figure, also here a smooth incoherent background was added, which is indicated by the brown solid line. In addition the contributions from the different partial waves are shown, specifically those for $J = \frac{1}{2}$ (green), $\frac{3}{2}$ (orange), and $\frac{5}{2}$ (olive). Evidently, the three P_c states from the recent LHCb measurement are reproduced where the $P_c(4312)$ appears as a $\bar{D}\Sigma_c$ bound state with $J^P = \frac{1}{2}^-$ and the $P_c(4440)$ and $P_c(4457)$ are states with $\frac{1}{2}^-$ and $\frac{3}{2}^-$, respectively, associated mainly with the $\bar{D}^*\Sigma_c$ channel. Interestingly, (and different from Fit A and B) in Fit C the pole for the latter is above the threshold, a situation similar to that observed for a possibly strange dibaryon in the $\Lambda N-\Sigma N$ system [169], see Sect. 5.3. The pole around 4366 MeV with $\frac{3}{2}^-$, a $\bar{D}\Sigma_c^*$ bound state, is in line with the structure reported in the first LHCb paper, but again it is much narrower than what has been deduced by the experimentalists. Note that, besides the states discussed here, the JB model predicts many more states, from $\frac{1}{2}^-$ up to $\frac{7}{2}^-$, however, with fairly large widths. Future and more precise experiments might shed light on the question whether these exist or not.

As already said above, there are many more theoretical studies of the LHCb pentaquarks employing various approaches. However, as far as we could see, they are all restricted to the determination of the poles and no comparison with the observed $J/\psi p$ mass spectrum is provided. Moreover, several of those works are not performed in a factual coupled-channel framework. Nonetheless, we want to mention selectively some of them, namely two of the earliest works [36, 1268], published well before experimental evidence for pentaquark candidates were found, the studies of Meng et al. [1269], where the interaction is derived within chiral perturbation theory, including contact terms, and one-pion and two-pion exchange, a calculation by Xiao et al. [1270], performed with a dynamical input obtained from an extension of the local hidden gauge approach, and the works of Wu et al. [1271] and of Zhang [1272], which is based on the conventional meson-exchange approach and where predictions for $\gamma p \rightarrow J/\psi p$ are provided. Interesting are also works like Ref. [1257] where hidden-charm pentaquarks are considered and predictions for hidden-bottom pentaquarks are given, see Fig. 60. For yet other prediction of hidden-bottom pentaquarks, see e.g., Ref. [1273].

6.2.2. Hidden-charm pentaquarks with strangeness

First experimental evidence for a hidden-charm pentaquark candidate with strangeness, the $P_{cs}(4459)^0$ ($P_{c\bar{c}s}$ in the new convention by the PDG [103]), was reported by the LHCb Collaboration in 2020 from an analysis of $\Xi_b^- \rightarrow J/\psi \Lambda K^-$ decays [1274]. The state is located about 18 MeV below the $\bar{D}^{*0}\Xi_c^0$ threshold (4477 MeV) and about 15 MeV above the one of the $\bar{D}\Xi'_c$ channel (4444 MeV). Two years later a second candidate was identified, the $P_{cs}(4338)$, in $B^- \rightarrow J/\psi \Lambda \bar{p}$ decays [1275]. It is located basically at the $\bar{D}\Xi_c$ threshold. Very recently, the $P_{cs}(4459)^0$ was also observed by the Belle Collaboration [1276], in inclusive decays of $\Upsilon(1S, 2S)$ to $J/\psi \Lambda$. The $J/\psi \Lambda$ invariant-mass spectrum measured by LHCb, where the $P_{cs}(4459)^0$ was identified, is reproduced in Fig. 61. As one can see from the figure, besides the single-pentaquark solution (left), the LHCb Collaboration explored also the possibility that there are two states (right), inspired by corresponding model predictions of a calculation based on chiral effective field theory up to the next-to-leading order [1277]. The masses suggested from that analysis for the pentaquark candidates are 4454.9 ± 2.7 MeV and

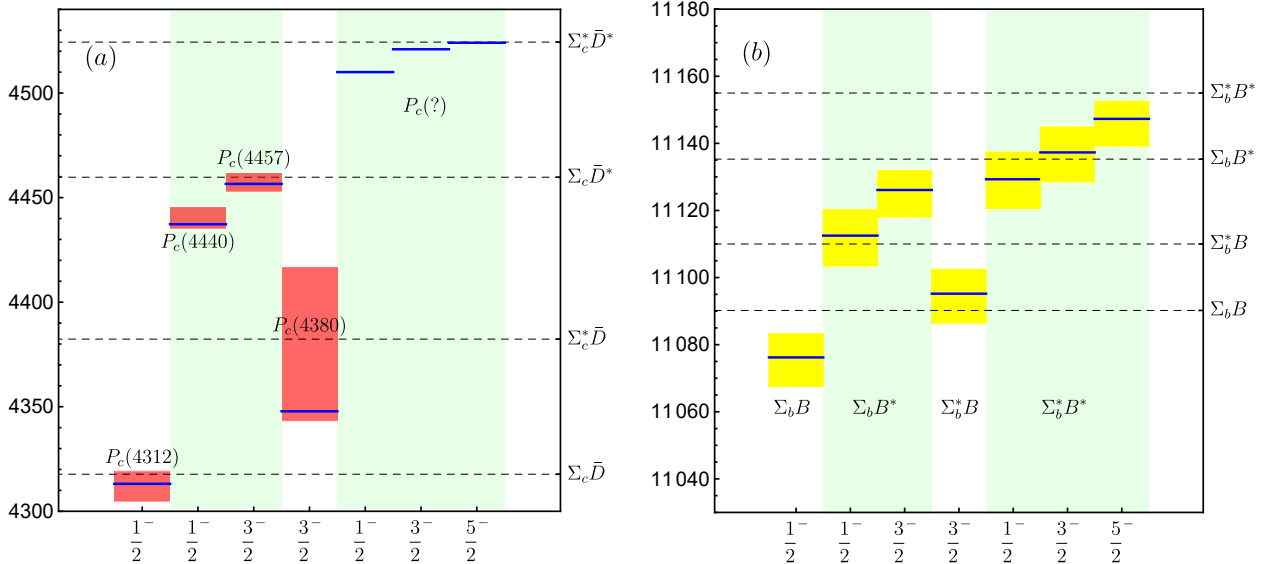


Figure 60: Hidden-charm (a) and hidden-bottom (b) pentaquarks. Results are taken from [1257]. Experimentally established hidden-charm states are indicated by the red bands. The yellow bands for the hidden-bottom predictions are an estimate of the theoretical uncertainty.

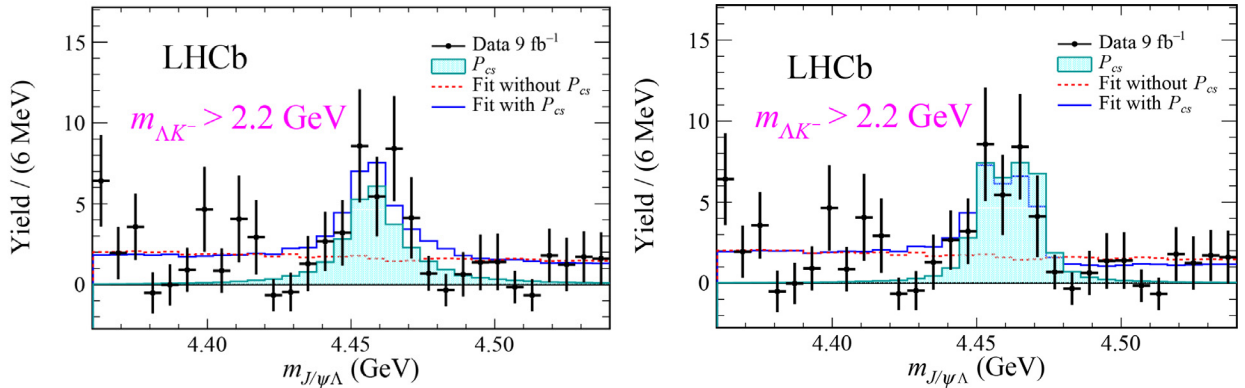


Figure 61: Hidden-charm pentaquark(s) with strangeness established by the LHCb Collaboration in the $\Xi_b^- \rightarrow J/\psi \Lambda K^-$ decays [1274]. Interpretation of the data in terms of one (left) or two (right) pentaquarks are shown.

4467.8 ± 3.7 MeV, respectively. The quantum numbers predicted by theory [1277] are $J^P = \frac{1}{2}^-$ and $\frac{3}{2}^-$, respectively.

A first study of the nature of the $P_{cs}(4459)^0$ within a DCC approach was presented by Du et al. [1278]. Besides $J/\psi \Lambda$, out of the many $\bar{D}^{(*)}\Xi_c^{(*)}$ and $\bar{D}^{(*)}\Xi'_c$ open-charm channels only those whose thresholds are close to the observed structure were taken into account, namely $\bar{D}\Xi'_c$ and $\bar{D}^*\Xi_c$. The calculation was performed in a leading-order EFT-type ansatz with the potentials represented by constant terms. For the considered channels constraints from HQSS were implemented. The reaction amplitude is established in the on-shell factorization approximation where the one-loop two-point Green's function is evaluated in the dimensional regularization scheme [1278]. The 8 parameters of the model, three that specify the interaction in the $\bar{D}\Xi'_c$ and $\bar{D}^*\Xi_c$ channels, two for the coupling of those channels to $J/\psi \Lambda$, and three related to the elementary decay (production) vertices, are fitted to the mass spectrum. The result is shown in Fig. 62 (right). One can see that the potential considered by Du et al. leads indeed to a two-state structure of the observed pentaquark. Both are dominated by the $\bar{D}^*\Xi_c$ channel, where the lower state corresponds to $\frac{1}{2}^-$ and the higher one to $\frac{3}{2}^-$. Note that the greenish area indicates the fitting region. It should be mentioned that in Ref. [1278] some other scenarios are discussed too, with just two coupled channels, and in some only a single structure appears. In addition the authors considered a perturbative treatment of the $\bar{D}\Xi'_c$ channel.

DCC results for the invariant-mass spectrum were also presented by Zhu et al. [1279]. In that study a total of nine coupled channels are considered: $J/\psi \Lambda$, $\bar{D}^{(*)}\Xi'_c$, $\bar{D}^{(*)}\Xi_c$, $\bar{D}^{(*)}\Xi_c^*$, $\bar{D}_s^{(*)}\Lambda_c^+$. The work is performed within the conventional meson-exchange picture, where the exchanges of pseudoscalar (π, η) and vector (ρ, ω) mesons are considered, and in addition a scalar-isoscalar (σ) meson. Furthermore, the transition to the $\bar{D}_s^{(*)}\Lambda_c^+$ channels is mediated by K and K^* exchange and the one to the $J/\psi \Lambda$ channel by D, D^* and D_s, D_s^* exchanges, respectively. The coupling constants for all pseudoscalar and vector mesons are fixed assuming SU(4) symmetry. The reaction amplitude is obtained by solving a LS-type equation for the coupled-channel potentials, where the latter are furnished with Gaussian form factors. Their

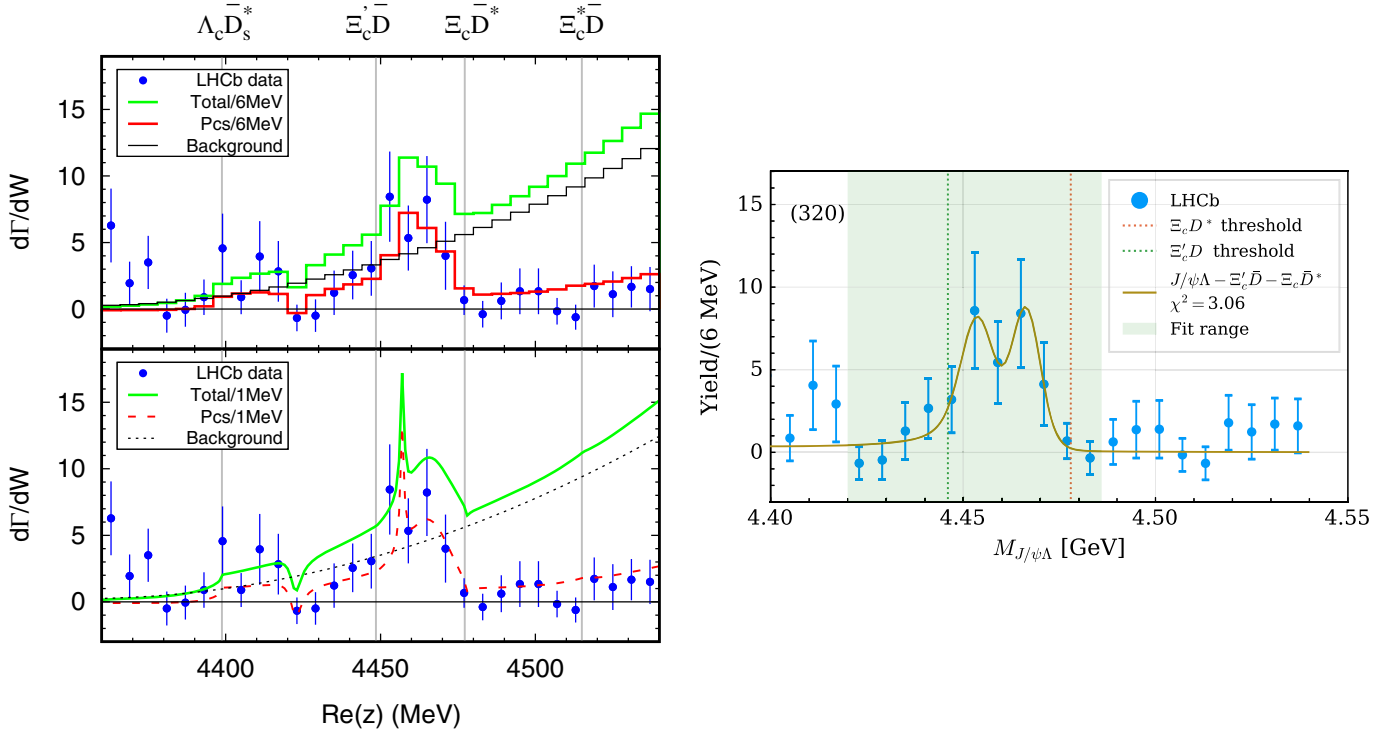


Figure 62: Results for the $J/\psi\Lambda$ invariant-mass spectrum, taken from Refs. [1278] (right) and [1279] (left). Data are by the LHCb Collaboration from the $\Xi_b^- \rightarrow J/\psi\Lambda K^-$ decays [1274].

cutoff masses (one for the light mesons and one for $D^{(*)}$, $D_s^{(*)}$) are free parameters. The other free parameters are related to the elementary decay (production) vertices; there is one for the $J = 1/2$ channel and one for $3/2$. Note that in this work the invariant-mass spectrum is evaluated in the Migdal-Watson approximation [1280, 1281], i.e., it is assumed to be proportional to the square of the meson-baryon reaction amplitudes times the phase space factor.

The resulting invariant-mass spectrum is shown in Fig. 62 (left). In the upper panel the outcome of the calculation is adapted to the experimental bin width of 6 MeV, while in the lower panel a bin width of only 1 MeV is assumed. In both cases from the full calculation (green curves) a background is subtracted (black curves) so that the resonance signals can be isolated and a comparison with the LHCb data can be made [1279]. Zhu et al. report four poles in the energy region displayed in Fig. 62, namely at 4423 MeV ($\bar{D}\Xi'_c$, $\frac{1}{2}^-$), at 4457 MeV ($\bar{D}^*\Xi_c$, $\frac{3}{2}^-$), at 4465 MeV ($\bar{D}^*\Xi_c$, $\frac{1}{2}^-$), and at 4512 MeV ($\bar{D}\Xi_c^*$, $\frac{3}{2}^-$), where the dominant channel is indicated in the brackets. Obviously, the experimental signal of the $P_{cs}(4459)$ pentaquark is primarily reproduced by the $\frac{1}{2}^-$ state with 4465 MeV. The near-by $\frac{3}{2}^-$ state predicted by this model is too narrow to be seen when the bin width is 6 MeV. The same is true for the $\frac{1}{2}^-$ state with 4423 MeV. Note that the potential of Zhu et al. produces also a pole around 4336.5 MeV, dominated by the strong coupling between $\bar{D}_s\Lambda$ and $\bar{D}\Xi_c$, which could be identified with the $P_{cs}(4338)$ pentaquark of the LHCb collaboration.

In Ref. [1282] another coupled-channel calculation based on dynamics generated by one-boson exchange can be found. The channels included are $\bar{D}^{(*)}\Xi_c'^{(*)}$, $\bar{D}^{(*)}\Xi_c^{(*)}$. The interaction is deduced from the one for $\bar{D}^{(*)}\Sigma_c^{(*)}$ by using heavy quark symmetry and SU(3) flavor symmetry, where the latter is fixed from a fit to the P_c states established by LHCb. Only poles are reported but no $J/\psi\Lambda$ invariant-mass distribution. Results for the resonance spectrum are shown in Fig. 63. A similar coupled-channel study has been presented in Ref. [1283] very recently. Finally, in Ref. [1284] one can find a coupled-channel calculation performed with a dynamical input obtained from an extension of the local hidden gauge approach. Also here there are no predictions for the invariant-mass distribution.

6.2.3. Other heavy systems

Channel coupling plays also a role in the interpretation of the exotic XYZ states and the doubly charmed tetraquark state T_{cc}^+ , observed in meson-meson systems. Most studies in this field are based on the chiral unitary approach or comparable formalisms and exploit the on-shell factorization to simplify the calculations. However, whenever vector mesons like K^* , D^* , or B^* are involved pion exchange is possible and generates a long-ranged interaction that couples the different channels. In particular, the strong tensor force induced by pion exchange leads to a coupling between the S -wave (where molecules/bound states are primarily expected) and the D -wave. These aspects are considered only in a small number of works because it requires a much more elaborate and tedious computational treatment.

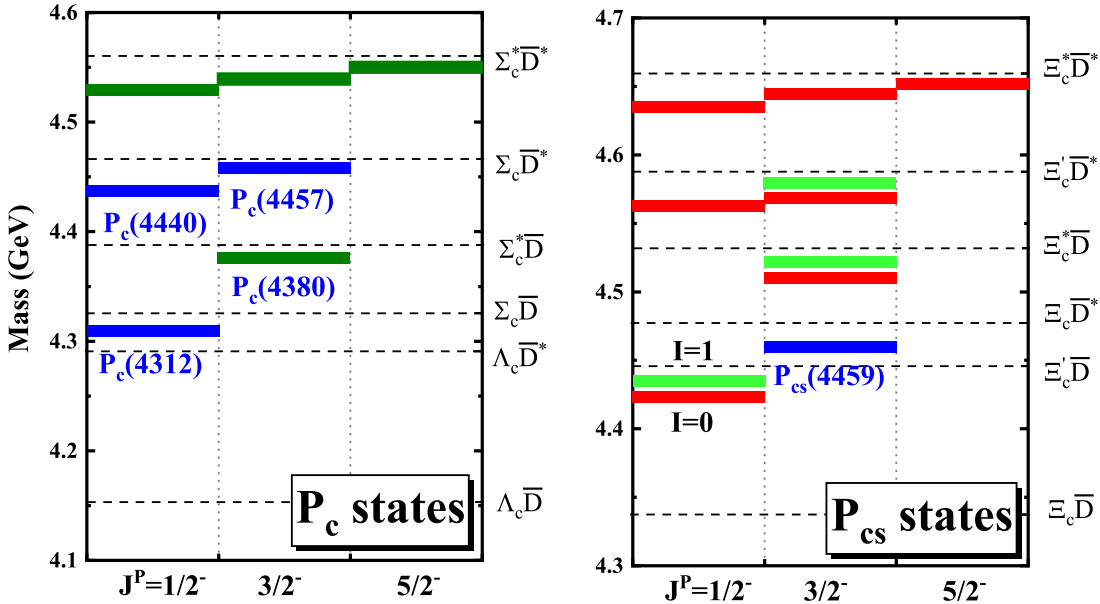


Figure 63: Hidden-charm open-strange pentaquarks predicted in Ref. [1282] based on an interaction established in the hidden-charm sector. Experimentally established states are indicated by blue bars.

One state where pion exchange plays an essential and delicate role is the aforementioned $\chi_{c1}(3872)$ [1250], discovered in the $\pi^+\pi^-J/\psi$ channel, and located extremely close to the $\bar{D}^{*0}D^0$ threshold. Since the D^{*0} mass itself is very close to the $D^0\pi^0$ threshold, a pion exchanged in the coupled $D\bar{D}^*$ - $D^*\bar{D}$ system can go on shell, in other words the $D\bar{D}\pi$ channel opens right in the crucial region where the bound state is located. This makes a proper inclusion of the three-body $D\bar{D}\pi$ unitarity cuts mandatory if one wants to obtain reliable results [1030]. See also the discussion in Sect. 2.7.

Pion exchange plays likewise an important role in case of the tetraquark candidate T_{cc}^+ , observed in the $D^0D^0\pi^+$ spectrum [1285]. The structure is located just about 300 keV below the $D^{*+}D^0$ threshold. Also here the exchanged pion can go on shell so that it is necessary to include three-body effects [295, 1032].

Regarding systems involving the bottom mesons $B^{(*)}$, $\bar{B}^{(*)}$ the overall conditions are similar but differ in important details. Here, the $Z_b(10610)$ and $Z_b(10650)$ states have been observed by Belle in the invariant-mass distributions of the $\Upsilon(nS)\pi^\pm$ ($n = 1, 2, 3$) and $h_b(mP)\pi^{pm}$ ($m = 1, 2$) subsystems of the dipion transitions from $\Upsilon(10860)$ [1286]. They are located close to the $B\bar{B}^*$ and $B^*\bar{B}^*$ thresholds. Since the separation between the $B\bar{B}$, $B\bar{B}^*$ - \bar{B}^*B , \bar{B}^*B^* channels is smaller than the pion mass, see Eqs. (6.1), the opening of three-body channels involving the pion does not play a role. On the other hand, the coupling between $\bar{B}B$ and $\bar{B}B^*$ - \bar{B}^*B to \bar{B}^*B^* becomes more important as compared to the charmed counterpart. Various aspects of the coupled-channel dynamics like the role of pion exchange (and also η exchange) and the coupling between S - and D -waves were addressed in Refs. [1265, 1287].

Another state where coupled-channel dynamics has been advocated for explaining its structure, is the $X(6900)$ observed in the invariant-mass spectrum of J/ψ pairs, produced in proton-proton collisions [1288]. In the study of Dong et al. [1289] the channels $J/\psi - J/\psi$, $\psi(2S) - J/\psi$, and $\psi(3770) - J/\psi$ are considered, motivated by the observation that the $\psi(2S) - J/\psi$ threshold (6783 MeV) coincides with the dip seen in the invariant mass while the $\psi(3770) - J/\psi$ threshold is close to the sharp peak in the experimental spectrum. It should be said, however, that the dynamics considered in this work is restricted to a pure contact coupled-channel short-range potential. Note that there is a recent update [1290], where additional new from ATLAS [1291] and CMS [1292] were considered in combination with the previous LHCb results.

Finally, let us point to the work of Malabarba et al. [492], where hidden-charm states with a possible three-body nature have been studied by considering the $N\bar{D}D^*$ - $ND^*\bar{D}$ systems within a Faddeev-type approach based on the fixed center approximation. Thereby the dynamics in the DN system, discussed in Sect. 6.1, is combined with the assumption that the $D\bar{D}^*$ - $D^*\bar{D}$ subsystems form bound states corresponding to the $\chi_{c1}(3872)$ and the $Z_c(3900)$ states.

7. Summary and outlook

Dynamical coupled-channel approaches are a versatile tool to study hadron dynamics in different context. Historically, they arose as data in wide kinematic ranges and for different reactions became available, calling for a unified analysis and interpretation of different data within one overarching formalism. Uniting principles of S-matrix theory with the option to incorporate microscopic dynamics of underlying theories (strong and electroweak interactions), they became a universal tool in baryon spectroscopy and beyond. As discussed, they allow to describe hadronic reactions with known initial

states such as pions, real and virtual photon probes, but also neutrino-induced reactions and baryon-baryon interactions. They also allow to parametrize the final-state interaction in the mesonic sector with three-body decays. Owing to their formulation, DCC approaches are particularly suited to incorporate full three-body dynamics while maintaining three-body unitarity.

In this review the emphasis lies on two out of several DCC approaches, the ANL-Osaka and the Juelich-Bonn-Washington approach (JBW). They have been used in the analysis of light baryons, but they are both members of a larger family of DCC approaches addressing mesons with two and three-body dynamics and baryon-baryon interactions (light, strange, and heavy), as well as the exotic XYZ and pentaquark states, that often require to map out complicated threshold dynamics. DCC approaches also allow to describe and predict hadronic phenomena such as cusps, three-body thresholds, triangle singularities and dynamical resonance generation, all of which have been discussed in this review.

DCC approaches become a bridge connecting various areas of hadron spectroscopy bundling searches for new excited states across different initial states, or studies of electromagnetic transition form factors across different final states. They also connect to functional methods, or, most recently, infinite volume mappings of finite volume spectra obtained in Lattice QCD.

With new experiments being commissioned exploring various strangeness sectors and higher photon virtualities at BE-SIII, CERN (AMBER, COMPASS), ELSA, Jefferson Lab, J-PARC, MAMI, SIS100, and other facilities, DCC approaches are well positioned for coming decades exploring the transition region from perturbative to non-perturbative QCD, and the interplay with electroweak probes, with the option to match to low-energy effective QCD and with perspectives to connect even larger data sets across different flavor sectors.

DCC approaches deal with new data coming from high-precision modern facilities but, also, include data from decades ago, often with unknown systematic effects. This calls for utilization of modern statistical tools beyond χ^2 minimization. The input from Bayesian statistics and machine learning for DCC approaches will help in analyzing the large, inhomogeneous data sets that DCC approaches usually deal with. Planned experiments with, e.g., meson beams will substantially help in this endeavor and provide further analysis opportunities for DCC approaches.

The neutrino interaction in the N^* region plays crucial role in neutrino physics, especially for the analysis of long base line neutrino experiments. DCC models well constrained from the electromagnetic reactions are in a good position to describe the electroweak reactions in the N^* region. With further theoretical or experimental inputs on the axial vector response of nucleon, such as parity-violating asymmetry of electron scattering, DCC approaches will play an important in neutrino physics.

When data becomes more and more abundant, novel data driven machine learning and AI tools – ranging from hands-on tools like LASSO or information criteria, to neural networks or more involved architectures such as transformers – become more relevant. Application of such techniques and integration thereof into dynamical coupled channel formalisms is an exciting avenue for future explorations.

Acknowledgment

The authors thank Luis Álvarez Ruso, Vadim Baru, Evgeny Epelbaum, Jeremy Green, Feng-Kun Guo, Hiroyuki Kamano, T.-S. H. Lee, Terry Mart, Ulf-G. Meißner, Viktor Mokeev, Osamu Morimatsu, Satoshi Nakamura, Fernando Romero-López, Deborah Rönchen, Denny Sombillo, Ron Workman, and Wren Yamada for useful discussions and for pointing out literature. The work of MD is supported by the National Science Foundation under Grant No. PHY-2310036. The work of MD is also supported by the U.S. Department of Energy grant DE-SC0016582 and DOE Office of Science, Office of Nuclear Physics under contract DE-AC05-06OR23177. This work contributes to the aims of the U.S. Department of Energy ExoHad Topical Collaboration, contract DE-SC0023598. The work of MM was supported through the Heisenberg Programme (project number: 532635001) and by the Deutsche Forschungsgemeinschaft (DFG, German Research Foundation), the NSFC through the funds provided to the Sino-German Collaborative Research Center CRC 110 “Symmetries and the Emergence of Structure in QCD” (DFG Project-ID 196253076 - TRR 110, NSFC Grant No. 12070131001). The work of TS was supported by the JSPS KAKEMHI Grant No. 24K07062.

References

- [1] M. Mai, U.-G. Meißner, C. Urbach, Towards a theory of hadron resonances, *Phys. Rept.* 1001 (2023) 1–66. [arXiv:2206.01477](https://arxiv.org/abs/2206.01477), [doi:10.1016/j.physrep.2022.11.005](https://doi.org/10.1016/j.physrep.2022.11.005).
- [2] S. Aoki, et al., Review of lattice results concerning low-energy particle physics, *Eur. Phys. J. C* 77 (2) (2017) 112. [arXiv:1607.00299](https://arxiv.org/abs/1607.00299), [doi:10.1140/epjc/s10052-016-4509-7](https://doi.org/10.1140/epjc/s10052-016-4509-7).
- [3] S. Prelovsek, Lattice QCD review of charmonium and open-charm spectroscopy, in: 6th International Workshop on Charm Physics, 2013. [arXiv:1310.4354](https://arxiv.org/abs/1310.4354).
- [4] D. Mohler, Review of lattice studies of resonances, PoS LATTICE2012 (2012) 003. [arXiv:1211.6163](https://arxiv.org/abs/1211.6163), [doi:10.22323/1.164.0003](https://doi.org/10.22323/1.164.0003).
- [5] H.-W. Lin, Review of Baryon Spectroscopy in Lattice QCD, *Chin. J. Phys.* 49 (2011) 827. [arXiv:1106.1608](https://arxiv.org/abs/1106.1608).
- [6] R. A. Briceño, J. J. Dudek, R. D. Young, Scattering processes and resonances from lattice QCD, *Rev. Mod. Phys.* 90 (2) (2018) 025001. [arXiv:1706.06223](https://arxiv.org/abs/1706.06223), [doi:10.1103/RevModPhys.90.025001](https://doi.org/10.1103/RevModPhys.90.025001).

- [7] S. Weinberg, Nuclear forces from chiral Lagrangians, Phys. Lett. B 251 (1990) 288–292. [doi:10.1016/0370-2693\(90\)90938-3](https://doi.org/10.1016/0370-2693(90)90938-3).
- [8] J. A. Oller, Coupled-channel formalism (1 2025). [arXiv:2501.10000](https://arxiv.org/abs/2501.10000).
- [9] A. M. Badalian, L. P. Kok, M. I. Polikarpov, Y. A. Simonov, Resonances in Coupled Channels in Nuclear and Particle Physics, Phys. Rept. 82 (1982) 31–177. [doi:10.1016/0370-1573\(82\)90014-X](https://doi.org/10.1016/0370-1573(82)90014-X).
- [10] T. Sato, T.-. S. H. Lee, Meson exchange model for πN scattering and $\gamma N \rightarrow \pi N$ reaction, Phys. Rev. C 54 (1996) 2660–2684. [arXiv:nucl-th/9606009](https://arxiv.org/abs/nucl-th/9606009), [doi:10.1103/PhysRevC.54.2660](https://doi.org/10.1103/PhysRevC.54.2660).
- [11] A. Matsuyama, T. Sato, T. S. H. Lee, Dynamical coupled-channel model of meson production reactions in the nucleon resonance region, Phys. Rept. 439 (2007) 193–253. [arXiv:nucl-th/0608051](https://arxiv.org/abs/nucl-th/0608051), [doi:10.1016/j.physrep.2006.12.003](https://doi.org/10.1016/j.physrep.2006.12.003).
- [12] M. A. Alberg, E. M. Henley, L. Wilets, Theory of Kaonic Atoms, Annals Phys. 96 (1976) 43–87. [doi:10.1016/0003-4916\(76\)90111-1](https://doi.org/10.1016/0003-4916(76)90111-1).
- [13] E. M. Henley, M. A. Alberg, L. Wilets, THE K- NUCLEON INTERACTION AND THE K- NUCLEUS OPTICAL POTENTIAL. (TALK), Nukleonika 25 (1980) 567–576.
- [14] R. H. Landau, The $K^- p$ Bound State With Coupling to Hyperon Channels, Phys. Rev. C 28 (1983) 1324. [doi:10.1103/PhysRevC.28.1324](https://doi.org/10.1103/PhysRevC.28.1324).
- [15] P. B. Siegel, W. Weise, Low-energy K^- Nucleon Potentials and the Nature of the Λ (1405), Phys. Rev. C 38 (1988) 2221–2229. [doi:10.1103/PhysRevC.38.2221](https://doi.org/10.1103/PhysRevC.38.2221).
- [16] A. Mueller-Groeling, K. Holinde, J. Speth, $K^- N$ interaction in the meson exchange framework, Nucl. Phys. A 513 (1990) 557–583. [doi:10.1016/0375-9474\(90\)90398-6](https://doi.org/10.1016/0375-9474(90)90398-6).
- [17] R. S. Bhalerao, L. C. Liu, OFF-SHELL MODEL FOR THRESHOLD PIONIC ETA PRODUCTION ON A NUCLEON AND FOR ETA N SCATTERING, Phys. Rev. Lett. 54 (1985) 865–868. [doi:10.1103/PhysRevLett.54.865](https://doi.org/10.1103/PhysRevLett.54.865).
- [18] S. Nozawa, B. Blankleider, T. S. H. Lee, A Dynamical Model of Pion Photoproduction on the Nucleon, Nucl. Phys. A 513 (1990) 459–510. [doi:10.1016/0375-9474\(90\)90395-3](https://doi.org/10.1016/0375-9474(90)90395-3).
- [19] C.-C. Lee, S.-N. Yang, T. S. H. Lee, Meson exchange πN model and neutral pion photoproduction from protons near threshold, J. Phys. G 17 (1991) L131–L137. [doi:10.1088/0954-3899/17/8/003](https://doi.org/10.1088/0954-3899/17/8/003).
- [20] C.-T. Hung, S.-N. Yang, T. S. H. Lee, A Relativistic meson exchange model of pion nucleon scattering, J. Phys. G 20 (1994) 1531–1536. [doi:10.1088/0954-3899/20/9/021](https://doi.org/10.1088/0954-3899/20/9/021).
- [21] C.-T. Hung, S. N. Yang, T. S. H. Lee, Meson exchange πN models in three-dimensional Bethe-Salpeter formulation, Phys. Rev. C 64 (2001) 034309. [arXiv:nucl-th/0101007](https://arxiv.org/abs/nucl-th/0101007), [doi:10.1103/PhysRevC.64.034309](https://doi.org/10.1103/PhysRevC.64.034309).
- [22] G. Y. Chen, S. S. Kamalov, S. N. Yang, D. Drechsel, L. Tiator, Nucleon resonances in πN scattering up to energies $s^{1/2} < 2.0$ GeV, Phys. Rev. C 76 (2007) 035206. [arXiv:nucl-th/0703096](https://arxiv.org/abs/nucl-th/0703096), [doi:10.1103/PhysRevC.76.035206](https://doi.org/10.1103/PhysRevC.76.035206).
- [23] L. Tiator, S. S. Kamalov, S. Ceci, G. Y. Chen, D. Drechsel, A. Švarc, S. N. Yang, Singularity structure of the πN scattering amplitude in a meson-exchange model up to energies $W \leq 2.0$ GeV, Phys. Rev. C 82 (2010) 055203. [arXiv:1007.2126](https://arxiv.org/abs/1007.2126), [doi:10.1103/PhysRevC.82.055203](https://doi.org/10.1103/PhysRevC.82.055203).
- [24] G. Höhler, A. Schulte, Determination of πN resonance pole parameters from speed plots, PiN Newslett. 7 (1992) 94–128.
- [25] S. Ceci, J. Stahov, A. Švarc, S. Watson, B. Zauner, Resolution of the multichannel anomaly in the extraction of S-matrix resonance-pole parameters, Phys. Rev. D 77 (2008) 116007. [arXiv:hep-ph/0609236](https://arxiv.org/abs/hep-ph/0609236), [doi:10.1103/PhysRevD.77.116007](https://doi.org/10.1103/PhysRevD.77.116007).
- [26] F. Gross, Y. Surya, Unitary, relativistic resonance model for πN scattering, Phys. Rev. C 47 (1993) 703–723. [doi:10.1103/PhysRevC.47.703](https://doi.org/10.1103/PhysRevC.47.703).
- [27] Y. Surya, F. Gross, Unitary, gauge invariant, relativistic resonance model for pion photoproduction, Phys. Rev. C 53 (1996) 2422–2448. [doi:10.1103/PhysRevC.53.2422](https://doi.org/10.1103/PhysRevC.53.2422).
- [28] B. C. Pearce, B. K. Jennings, A Relativistic meson exchange model of pion - nucleon scattering, Nucl. Phys. A 528 (1991) 655–675. [doi:10.1016/0375-9474\(91\)90256-6](https://doi.org/10.1016/0375-9474(91)90256-6).
- [29] V. Pascalutsa, J. A. Tjon, Pion nucleon interaction in a covariant hadron exchange model, Phys. Rev. C 61 (2000) 054003. [arXiv:nucl-th/0003050](https://arxiv.org/abs/nucl-th/0003050), [doi:10.1103/PhysRevC.61.054003](https://doi.org/10.1103/PhysRevC.61.054003).
- [30] G. L. Caia, L. E. Wright, V. Pascalutsa, A Dynamical model for pion electroproduction on the nucleon, Phys. Rev. C 72 (2005) 035203. [arXiv:nucl-th/0506006](https://arxiv.org/abs/nucl-th/0506006), [doi:10.1103/PhysRevC.72.035203](https://doi.org/10.1103/PhysRevC.72.035203).
- [31] R. Blankenbecler, R. Sugar, Linear integral equations for relativistic multichannel scattering, Phys. Rev. 142 (1966) 1051–1059. [doi:10.1103/PhysRev.142.1051](https://doi.org/10.1103/PhysRev.142.1051).
- [32] V. G. Kadyshevsky, Quasipotential type equation for the relativistic scattering amplitude, Nucl. Phys. B 6 (1968) 125–148. [doi:10.1016/0550-3213\(68\)90274-5](https://doi.org/10.1016/0550-3213(68)90274-5).
- [33] R. H. Thompson, Three-dimensional bethe-salpeter equation applied to the nucleon-nucleon interaction, Phys. Rev. D 1 (1970) 110–117. [doi:10.1103/PhysRevD.1.110](https://doi.org/10.1103/PhysRevD.1.110).
- [34] R. M. Woloshyn, A. D. Jackson, Comparison of three-dimensional relativistic scattering equations, Nucl. Phys. B 64 (1973) 269–288. [doi:10.1016/0550-3213\(73\)90626-3](https://doi.org/10.1016/0550-3213(73)90626-3).
- [35] K. Erkelenz, Current status of the relativistic two nucleon one boson exchange potential, Phys. Rept. 13 (1974) 191–258. [doi:10.1016/0370-1573\(74\)90008-8](https://doi.org/10.1016/0370-1573(74)90008-8).
- [36] J.-J. Wu, T. S. H. Lee, B. S. Zou, Nucleon Resonances with Hidden Charm in Coupled-Channel Models, Phys. Rev. C 85 (2012) 044002. [arXiv:1202.1036](https://arxiv.org/abs/1202.1036), [doi:10.1103/PhysRevC.85.044002](https://doi.org/10.1103/PhysRevC.85.044002).
- [37] C. H. M. van Antwerpen, I. R. Afnan, A Gauge invariant unitary theory for pion photoproduction, Phys. Rev. C 52 (1995) 554–567. [arXiv:nucl-th/9407038](https://arxiv.org/abs/nucl-th/9407038), [doi:10.1103/PhysRevC.52.554](https://doi.org/10.1103/PhysRevC.52.554).
- [38] B. Borasoy, P. C. Bruns, U.-G. Meißner, R. Nißler, A Gauge invariant chiral unitary framework for kaon photo- and electroproduction on the proton, Eur. Phys. J. A 34 (2007) 161–183. [arXiv:0709.3181](https://arxiv.org/abs/0709.3181), [doi:10.1140/epja/i2007-10492-4](https://doi.org/10.1140/epja/i2007-10492-4).
- [39] P. C. Bruns, M. Mai, U. G. Meißner, Chiral dynamics of the S11(1535) and S11(1650) resonances revisited, Phys. Lett. B 697 (2011) 254–259. [arXiv:1012.2233](https://arxiv.org/abs/1012.2233), [doi:10.1016/j.physletb.2011.02.008](https://doi.org/10.1016/j.physletb.2011.02.008).
- [40] P. C. Bruns, A formalism for the study of $K^+ \pi \Sigma$ photoproduction in the $\Lambda^*(1405)$ region (12 2020). [arXiv:2012.11298](https://arxiv.org/abs/2012.11298).
- [41] P. C. Bruns, A. Cieplý, M. Mai, Testing chiral unitary models for the $\Lambda(1405)$ in $K+\pi\Sigma$ photoproduction, Phys. Rev. D 106 (7) (2022) 074017. [doi:10.1103/PhysRevD.106.074017](https://doi.org/10.1103/PhysRevD.106.074017).
- [42] M. Mai, P. C. Bruns, U.-G. Meißner, Pion photoproduction off the proton in a gauge-invariant chiral unitary framework, Phys. Rev. D 86 (2012) 094033. [arXiv:1207.4923](https://arxiv.org/abs/1207.4923), [doi:10.1103/PhysRevD.86.094033](https://doi.org/10.1103/PhysRevD.86.094033).
- [43] D. Ruić, M. Mai, U.-G. Meißner, η -Photoproduction in a gauge-invariant chiral unitary framework, Phys. Lett. B 704 (2011) 659–662. [arXiv:1108.4825](https://arxiv.org/abs/1108.4825), [doi:10.1016/j.physletb.2011.09.090](https://doi.org/10.1016/j.physletb.2011.09.090).
- [44] F. Huang, M. Döring, H. Haberzettl, J. Haidenbauer, C. Hanhart, S. Krewald, U. G. Meißner, K. Nakayama, Pion photoproduction in a dynamical coupled-channels model, Phys. Rev. C 85 (2012) 054003. [arXiv:1110.3833](https://arxiv.org/abs/1110.3833), [doi:10.1103/PhysRevC.85.054003](https://doi.org/10.1103/PhysRevC.85.054003).
- [45] A. D. Lahiff, I. R. Afnan, Solution of the Bethe-Salpeter equation for pion nucleon scattering, Phys. Rev. C 60 (1999) 024608. [arXiv:nucl-th/9903058](https://arxiv.org/abs/nucl-th/9903058), [doi:10.1103/PhysRevC.60.024608](https://doi.org/10.1103/PhysRevC.60.024608).

- [46] C. Schütz, J. W. Durso, K. Holinde, J. Speth, Role of correlated two pion exchange in pi N scattering, Phys. Rev. C 49 (1994) 2671–2687. [doi:10.1103/PhysRevC.49.2671](https://doi.org/10.1103/PhysRevC.49.2671).
- [47] C. Schütz, K. Holinde, J. Speth, B. C. Pearce, J. W. Durso, A Dynamical model for correlated two pion exchange in the pion - nucleon interaction, Phys. Rev. C 51 (1995) 1374–1383. [arXiv:nucl-th/9411022](https://arxiv.org/abs/nucl-th/9411022), [doi:10.1103/PhysRevC.51.1374](https://doi.org/10.1103/PhysRevC.51.1374).
- [48] R. Machleidt, K. Holinde, C. Elster, The Bonn Meson Exchange Model for the Nucleon Nucleon Interaction, Phys. Rept. 149 (1987) 1–89. [doi:10.1016/S0370-1573\(87\)80002-9](https://doi.org/10.1016/S0370-1573(87)80002-9).
- [49] C. Schütz, J. Haidenbauer, J. Speth, J. W. Durso, Extended coupled channels model for pi N scattering and the structure of N*(1440) and N*(1535), Phys. Rev. C 57 (1998) 1464–1477. [doi:10.1103/PhysRevC.57.1464](https://doi.org/10.1103/PhysRevC.57.1464).
- [50] O. Krehl, C. Hanhart, S. Krewald, J. Speth, What does 'rho exchange' in pi N scattering mean?, Phys. Rev. C 60 (1999) 055206. [arXiv:nucl-th/9906090](https://arxiv.org/abs/nucl-th/9906090), [doi:10.1103/PhysRevC.60.055206](https://doi.org/10.1103/PhysRevC.60.055206).
- [51] O. Krehl, C. Hanhart, S. Krewald, J. Speth, What is the structure of the Roper resonance?, Phys. Rev. C 62 (2000) 025207. [arXiv:nucl-th/9911080](https://arxiv.org/abs/nucl-th/9911080), [doi:10.1103/PhysRevC.62.025207](https://doi.org/10.1103/PhysRevC.62.025207).
- [52] A. M. Gasparyan, J. Haidenbauer, C. Hanhart, J. Speth, Pion nucleon scattering in a meson exchange model, Phys. Rev. C 68 (2003) 045207. [arXiv:nucl-th/0307072](https://arxiv.org/abs/nucl-th/0307072), [doi:10.1103/PhysRevC.68.045207](https://doi.org/10.1103/PhysRevC.68.045207).
- [53] D. Rönchen, M. Döring, F. Huang, H. Haberzettl, J. Haidenbauer, C. Hanhart, S. Krewald, U.-G. Meißner, K. Nakayama, Coupled-channel dynamics in the reactions $\pi N \rightarrow \pi N$, ηN , $K\Lambda$, $K\Sigma$, Eur. Phys. J. A 49 (2013) 44. [arXiv:1211.6998](https://arxiv.org/abs/1211.6998), [doi:10.1140/epja/i2013-13044-5](https://doi.org/10.1140/epja/i2013-13044-5).
- [54] D. Rönchen, M. Döring, F. Huang, H. Haberzettl, J. Haidenbauer, C. Hanhart, S. Krewald, U.-G. Meißner, K. Nakayama, Photocouplings at the Pole from Pion Photoproduction, Eur. Phys. J. A 50 (6) (2014) 101, [Erratum: Eur.Phys.J.A 51, 63 (2015)]. [arXiv:1401.0634](https://arxiv.org/abs/1401.0634), [doi:10.1140/epja/i2014-14101-3](https://doi.org/10.1140/epja/i2014-14101-3).
- [55] D. Rönchen, M. Döring, H. Haberzettl, J. Haidenbauer, U.-G. Meißner, K. Nakayama, Eta photoproduction in a combined analysis of pion- and photon-induced reactions, Eur. Phys. J. A 51 (6) (2015) 70. [arXiv:1504.01643](https://arxiv.org/abs/1504.01643), [doi:10.1140/epja/i2015-15070-7](https://doi.org/10.1140/epja/i2015-15070-7).
- [56] D. Rönchen, M. Döring, U.-G. Meißner, The impact of $K^+\Lambda$ photoproduction on the resonance spectrum, Eur. Phys. J. A 54 (6) (2018) 110. [arXiv:1801.10458](https://arxiv.org/abs/1801.10458), [doi:10.1140/epja/i2018-12541-3](https://doi.org/10.1140/epja/i2018-12541-3).
- [57] D. Rönchen, M. Döring, U.-G. Meißner, C.-W. Shen, Light baryon resonances from a coupled-channel study including $K\Sigma$ photoproduction, Eur. Phys. J. A 58 (2022) 229. [arXiv:2208.00089](https://arxiv.org/abs/2208.00089), [doi:10.1140/epja/s10050-022-00852-1](https://doi.org/10.1140/epja/s10050-022-00852-1).
- [58] Y.-F. Wang, D. Rönchen, U.-G. Meißner, Y. Lu, C.-W. Shen, J.-J. Wu, Reaction $\pi N \rightarrow \omega N$ in a dynamical coupled-channel approach, Phys. Rev. D 106 (9) (2022) 094031. [arXiv:2208.03061](https://arxiv.org/abs/2208.03061), [doi:10.1103/PhysRevD.106.094031](https://doi.org/10.1103/PhysRevD.106.094031).
- [59] M. Mai, M. Döring, C. Granados, H. Haberzettl, U.-G. Meißner, D. Rönchen, I. Strakovsky, R. Workman, Jülich-Bonn-Washington model for pion electroproduction multipoles, Phys. Rev. C 103 (6) (2021) 065204. [arXiv:2104.07312](https://arxiv.org/abs/2104.07312), [doi:10.1103/PhysRevC.103.065204](https://doi.org/10.1103/PhysRevC.103.065204).
- [60] M. Mai, M. Döring, C. Granados, H. Haberzettl, J. Hergenrather, U.-G. Meißner, D. Rönchen, I. Strakovsky, R. Workman, Coupled-channels analysis of pion and η electroproduction within the Jülich-Bonn-Washington model, Phys. Rev. C 106 (1) (2022) 015201. [arXiv:2111.04774](https://arxiv.org/abs/2111.04774), [doi:10.1103/PhysRevC.106.015201](https://doi.org/10.1103/PhysRevC.106.015201).
- [61] M. Mai, J. Hergenrather, M. Döring, T. Mart, U.-G. Meißner, D. Rönchen, R. Workman, Inclusion of $K\Lambda$ electroproduction data in a coupled channel analysis, Eur. Phys. J. A 59 (12) (2023) 286. [arXiv:2307.10051](https://arxiv.org/abs/2307.10051), [doi:10.1140/epja/s10050-023-01188-0](https://doi.org/10.1140/epja/s10050-023-01188-0).
- [62] C.-W. Shen, D. Rönchen, U.-G. Meißner, B.-S. Zou, Exploratory study of possible resonances in heavy meson - heavy baryon coupled-channel interactions, Chin. Phys. C 42 (2) (2018) 023106. [arXiv:1710.03885](https://arxiv.org/abs/1710.03885), [doi:10.1088/1674-1137/42/2/023106](https://doi.org/10.1088/1674-1137/42/2/023106).
- [63] Z.-L. Wang, C.-W. Shen, D. Rönchen, U.-G. Meißner, B.-S. Zou, Resonances in heavy meson-heavy baryon coupled-channel interactions, Eur. Phys. J. C 82 (5) (2022) 497. [arXiv:2204.12122](https://arxiv.org/abs/2204.12122), [doi:10.1140/epjc/s10052-022-10462-2](https://doi.org/10.1140/epjc/s10052-022-10462-2).
- [64] C.-W. Shen, D. Rönchen, U.-G. Meißner, B.-S. Zou, Y.-F. Wang, Exploration of the LHCb P_c states and possible resonances in a unitary coupled-channel model, Eur. Phys. J. C 84 (7) (2024) 764. [arXiv:2405.02626](https://arxiv.org/abs/2405.02626), [doi:10.1140/epjc/s10052-024-13139-0](https://doi.org/10.1140/epjc/s10052-024-13139-0).
- [65] N. Fukuda, K. Sawada, M. Taketani, On the construction of potential in field theory, Prog. Theor. Phys. 12 (2) (1954) 156–166. [doi:10.1143/PTP.12.156](https://doi.org/10.1143/PTP.12.156).
URL <https://doi.org/10.1143/PTP.12.156>
- [66] S. Okubo, Diagonalization of Hamiltonian and Tamm-Dancoff Equation, Prog. Theor. Phys. 12 (1954) 603. [doi:10.1143/PTP.12.603](https://doi.org/10.1143/PTP.12.603).
- [67] K. Nishijima, On the adiabatic nuclear potential, i, Prog. Theor. Phys. 6 (5) (1951) 815–828.
- [68] K. Nishijima, On the Adiabatic Nuclear Potential, II, Prog. Theor. Phys. 6 (6) (1951) 911–924. [doi:10.1143/ptp/6.6.911](https://doi.org/10.1143/ptp/6.6.911).
URL <https://doi.org/10.1143/ptp/6.6.911>
- [69] T. Sato, K. Tamura, T. Niwa, H. Ohtsubo, Relativistic Bound State Problem of One-dimensional System, J. Phys. G 17 (1991) 303–318. [doi:10.1088/0954-3899/17/3/012](https://doi.org/10.1088/0954-3899/17/3/012).
- [70] K. Tamura, T. Niwa, T. Sato, H. Ohtsubo, Relativistic effects on electron scattering of deuteron, Nucl. Phys. A 536 (1992) 597–636. [doi:10.1016/0375-9474\(92\)90115-Z](https://doi.org/10.1016/0375-9474(92)90115-Z).
- [71] Y. Nambu, Force potentials in quantum field theory, Prog. Theor. Phys. 5 (1950) 614–633.
- [72] M. B. Johnson, Theory of Meson Exchange Potentials for Nuclear Physics, Annals Phys. 97 (1976) 400–451. [doi:10.1016/0003-4916\(76\)90042-7](https://doi.org/10.1016/0003-4916(76)90042-7).
- [73] M. Kobayashi, T. Sato, H. Ohtsubo, Effective interactions for mesons and baryons in nuclei, Prog. Theor. Phys. 98 (1997) 927–951. [doi:10.1143/PTP.98.927](https://doi.org/10.1143/PTP.98.927).
- [74] B. Julia-Díaz, H. Kamano, T.-S. H. Lee, A. Matsuyama, T. Sato, N. Suzuki, On the Methods for Constructing Meson-Baryon Reaction Models within Relativistic Quantum Field Theory, Chin. J. Phys. 47 (2009) 142–158. [arXiv:0902.3200](https://arxiv.org/abs/0902.3200).
- [75] T. Sato, T. S. H. Lee, Dynamical study of the Δ excitation in $N(e, e'\pi)$ reactions, Phys. Rev. C 63 (2001) 055201. [arXiv:nucl-th/0010025](https://arxiv.org/abs/nucl-th/0010025), [doi:10.1103/PhysRevC.63.055201](https://doi.org/10.1103/PhysRevC.63.055201).
- [76] B. Julia-Díaz, T.-S. H. Lee, T. Sato, L. C. Smith, Extraction and Interpretation of $\gamma N \rightarrow \Delta$ Form Factors within a Dynamical Model, Phys. Rev. C 75 (2007) 015205. [arXiv:nucl-th/0611033](https://arxiv.org/abs/nucl-th/0611033), [doi:10.1103/PhysRevC.75.015205](https://doi.org/10.1103/PhysRevC.75.015205).
- [77] B. Julia-Díaz, B. Saghai, T.-S. H. Lee, F. Tabakin, Dynamical coupled-channel approach to hadronic and electromagnetic production of kaon-hyperon on the proton, Phys. Rev. C 73 (2006) 055204. [arXiv:nucl-th/0601053](https://arxiv.org/abs/nucl-th/0601053), [doi:10.1103/PhysRevC.73.055204](https://doi.org/10.1103/PhysRevC.73.055204).
- [78] B. Julia-Díaz, T.-S. H. Lee, A. Matsuyama, T. Sato, Dynamical coupled-channel model of πN scattering in the $W \leq 2$ GeV nucleon resonance region, Phys. Rev. C 76 (2007) 065201. [arXiv:0704.1615](https://arxiv.org/abs/0704.1615), [doi:10.1103/PhysRevC.76.065201](https://doi.org/10.1103/PhysRevC.76.065201).
- [79] B. Julia-Díaz, T.-S. H. Lee, A. Matsuyama, T. Sato, L. C. Smith, Dynamical coupled-channels effects on pion photoproduction, Phys. Rev. C 77 (2008) 045205. [arXiv:0712.2283](https://arxiv.org/abs/0712.2283), [doi:10.1103/PhysRevC.77.045205](https://doi.org/10.1103/PhysRevC.77.045205).
- [80] B. Julia-Díaz, H. Kamano, T. S. H. Lee, A. Matsuyama, T. Sato, N. Suzuki, Dynamical coupled-channels analysis of $p(e, e'\pi)N$ reactions, Phys. Rev. C 80 (2009) 025207. [arXiv:0904.1918](https://arxiv.org/abs/0904.1918), [doi:10.1103/PhysRevC.80.025207](https://doi.org/10.1103/PhysRevC.80.025207).
- [81] J. Durand, B. Julia-Díaz, T.-S. H. Lee, B. Saghai, T. Sato, Coupled-channels study of the $\pi^- p \rightarrow \eta n$ process, Phys. Rev. C 78 (2008) 025204. [arXiv:0804.3476](https://arxiv.org/abs/0804.3476), [doi:10.1103/PhysRevC.78.025204](https://doi.org/10.1103/PhysRevC.78.025204).

- [82] H. Kamano, B. Julia-Díaz, T.-S. H. Lee, A. Matsuyama, T. Sato, Dynamical coupled-channels study of $\pi N \rightarrow \pi\pi N$ reactions, Phys. Rev. C 79 (2009) 025206. [arXiv:0807.2273](#), [doi:10.1103/PhysRevC.79.025206](#).
- [83] H. Kamano, B. Julia-Díaz, T. S. H. Lee, A. Matsuyama, T. Sato, Double and single pion photoproduction within a dynamical coupled-channels model, Phys. Rev. C 80 (2009) 065203. [arXiv:0909.1129](#), [doi:10.1103/PhysRevC.80.065203](#).
- [84] N. Suzuki, T. Sato, T. S. H. Lee, Extraction of Resonances from Meson-Nucleon Reactions, Phys. Rev. C 79 (2009) 025205. [arXiv:0806.2043](#), [doi:10.1103/PhysRevC.79.025205](#).
- [85] N. Suzuki, T. Sato, T. S. H. Lee, Extraction of Electromagnetic Transition Form Factors for Nucleon Resonances within a Dynamical Coupled-Channels Model, Phys. Rev. C 82 (2010) 045206. [arXiv:1006.2196](#), [doi:10.1103/PhysRevC.82.045206](#).
- [86] N. Suzuki, B. Julia-Díaz, H. Kamano, T. S. H. Lee, A. Matsuyama, T. Sato, Disentangling the Dynamical Origin of P-11 Nucleon Resonances, Phys. Rev. Lett. 104 (2010) 042302. [arXiv:0909.1356](#), [doi:10.1103/PhysRevLett.104.042302](#).
- [87] H. Kamano, S. X. Nakamura, T. S. H. Lee, T. Sato, Nucleon resonances within a dynamical coupled-channels model of πN and γN reactions, Phys. Rev. C 88 (3) (2013) 035209. [arXiv:1305.4351](#), [doi:10.1103/PhysRevC.88.035209](#).
- [88] H. Kamano, S. X. Nakamura, T. S. H. Lee, T. Sato, Isospin decomposition of $\gamma N \rightarrow N^*$ transitions within a dynamical coupled-channels model, Phys. Rev. C 94 (1) (2016) 015201. [arXiv:1605.00363](#), [doi:10.1103/PhysRevC.94.015201](#).
- [89] S. X. Nakamura, Extraction of $\gamma n \rightarrow \pi N$ observables from deuteron-target data, Phys. Rev. C 98 (4) (2018) 042201. [arXiv:1808.02773](#), [doi:10.1103/PhysRevC.98.042201](#).
- [90] S. X. Nakamura, H. Kamano, T. Ishikawa, Low-energy η -nucleon interaction studied with η photoproduction off the deuteron, Phys. Rev. C 96 (4) (2017) 042201. [arXiv:1704.07029](#), [doi:10.1103/PhysRevC.96.042201](#).
- [91] H. Kamano, S. X. Nakamura, T. S. H. Lee, T. Sato, Neutrino-induced forward meson-production reactions in nucleon resonance region, Phys. Rev. D 86 (2012) 097503. [arXiv:1207.5724](#), [doi:10.1103/PhysRevD.86.097503](#).
- [92] S. X. Nakamura, H. Kamano, T. Sato, Dynamical coupled-channels model for neutrino-induced meson productions in resonance region, Phys. Rev. D 92 (7) (2015) 074024. [arXiv:1506.03403](#), [doi:10.1103/PhysRevD.92.074024](#).
- [93] H. Kamano, Electromagnetic N^* Transition Form Factors in the ANL-Osaka Dynamical Coupled-Channels Approach, Few Body Syst. 59 (3) (2018) 24. [doi:10.1007/s00601-018-1345-3](#).
- [94] H. Kamano, S. X. Nakamura, T. S. H. Lee, T. Sato, Dynamical coupled-channels model of $K^- p$ reactions: Determination of partial-wave amplitudes, Phys. Rev. C 90 (6) (2014) 065204. [arXiv:1407.6839](#), [doi:10.1103/PhysRevC.90.065204](#).
- [95] H. Kamano, S. X. Nakamura, T. S. H. Lee, T. Sato, Dynamical coupled-channels model of $K^- p$ reactions. II. Extraction of Λ^* and Σ^* hyperon resonances, Phys. Rev. C 92 (2) (2015) 025205, [Erratum: Phys. Rev. C 95, 049903 (2017)]. [arXiv:1506.01768](#), [doi:10.1103/PhysRevC.92.025205](#).
- [96] T. Sato, T.-S. H. Lee, Dynamical Models of the Excitations of Nucleon Resonances, J. Phys. G 36 (2009) 073001. [arXiv:0902.3653](#), [doi:10.1088/0954-3899/36/7/073001](#).
- [97] H. Feshbach, Theoretical nuclear physics: nuclear reactions, John Wiley & Sons, Inc., New York, New York, 1992.
- [98] J. Wess, B. Zumino, Lagrangian method for chiral symmetries, Phys. Rev. 163 (1967) 1727–1735. [doi:10.1103/PhysRev.163.1727](#).
- [99] U.-G. Meißner, Low-Energy Hadron Physics from Effective Chiral Lagrangians with Vector Mesons, Phys. Rept. 161 (1988) 213. [doi:10.1016/0370-1573\(88\)90090-7](#).
- [100] B. Borasoy, U.-G. Meißner, Chiral Lagrangians for baryons coupled to massive spin 1 fields, Int. J. Mod. Phys. A 11 (1996) 5183–5202. [arXiv:hep-ph/9511320](#), [doi:10.1142/S0217751X96002376](#).
- [101] K. Kawarabayashi, M. Suzuki, Partially conserved axial vector current and the decays of vector mesons, Phys. Rev. Lett. 16 (1966) 255. [doi:10.1103/PhysRevLett.16.255](#).
- [102] J. J. de Swart, The Octet model and its Clebsch-Gordan coefficients, Rev. Mod. Phys. 35 (1963) 916–939, [Erratum: Rev. Mod. Phys. 37, 326–326 (1965)]. [doi:10.1103/RevModPhys.35.916](#).
- [103] S. Navas, et al., Review of particle physics, Phys. Rev. D 110 (3) (2024) 030001. [doi:10.1103/PhysRevD.110.030001](#).
- [104] M. Döring, C. Hanhart, F. Huang, S. Krewald, U.-G. Meißner, D. Rönchen, The reaction $\pi^+ p \rightarrow K^+ \Sigma^+$ in a unitary coupled-channels model, Nucl. Phys. A 851 (2011) 58–98. [arXiv:1009.3781](#), [doi:10.1016/j.nuclphysa.2010.12.010](#).
- [105] S. S. Schweber, An introduction to relativistic quantum field theory, Dover Books on Physics, Dover Publications, Mineola, NY, 2005.
- [106] S. Weinberg, The Quantum Theory of Fields, Cambridge University Press, 1995.
- [107] M. Jacob, G. C. Wick, On the General Theory of Collisions for Particles with Spin, Annals Phys. 7 (1959) 404–428. [doi:10.1016/0033-4916\(59\)90051-X](#).
- [108] M. Mai, P. C. Bruns, B. Kubis, U.-G. Meißner, Aspects of meson-baryon scattering in three and two-flavor chiral perturbation theory, Phys. Rev. D 80 (2009) 094006. [arXiv:0905.2810](#), [doi:10.1103/PhysRevD.80.094006](#).
- [109] T. Becher, H. Leutwyler, Baryon chiral perturbation theory in manifestly Lorentz invariant form, Eur. Phys. J. C 9 (1999) 643–671. [arXiv:hep-ph/9901384](#), [doi:10.1007/PL00021673](#).
- [110] T. Becher, H. Leutwyler, Low energy analysis of $\pi N \rightarrow \pi N$, JHEP 06 (2001) 017. [arXiv:hep-ph/0103263](#), [doi:10.1088/1126-6708/2001/06/017](#).
- [111] G. Höhler, E. Pietarinen, The ρNN Vertex in Vector Dominance Models, Nucl. Phys. B 95 (1975) 210–230. [doi:10.1016/0550-3213\(75\)90042-5](#).
- [112] S. U. Chung, SPIN FORMALISMS (3 1971). [doi:10.5170/CERN-1971-008](#).
- [113] Y. Feng, F. Gil, M. Döring, R. Molina, M. Mai, V. Shastry, A. Szczepaniak, A unitary coupled-channel three-body amplitude with pions and kaons, Phys. Rev. D 110 (2024) 094002. [arXiv:2407.08721](#), [doi:10.1103/PhysRevD.110.094002](#).
- [114] M. Döring, C. Hanhart, F. Huang, S. Krewald, U.-G. Meißner, The Role of the background in the extraction of resonance contributions from meson-baryon scattering, Phys. Lett. B 681 (2009) 26–31. [arXiv:0903.1781](#), [doi:10.1016/j.physletb.2009.09.052](#).
- [115] M. Döring, C. Hanhart, F. Huang, S. Krewald, U.-G. Meißner, Analytic properties of the scattering amplitude and resonances parameters in a meson exchange model, Nucl. Phys. A 829 (2009) 170–209. [arXiv:0903.4337](#), [doi:10.1016/j.nuclphysa.2009.08.010](#).
- [116] M. W. Paris, Dynamical coupled channel calculation of pion and omega meson production, Phys. Rev. C 79 (2009) 025208. [arXiv:0802.3383](#), [doi:10.1103/PhysRevC.79.025208](#).
- [117] H. Nielsen, G. C. Oades, Consistency between the low-energy pion-pion interaction and pion-nucleon scattering, Nucl. Phys. B 49 (1972) 586–609. [doi:10.1016/0550-3213\(72\)90621-9](#).
- [118] G. Höhler, Methods and Results of Phenomenological Analyses / Methoden und Ergebnisse phänomenologischer Analysen, Vol. 9b2 of Landolt-Bornstein - Group I Elementary Particles, Nuclei and Atoms, Springer, 1983. [doi:10.1007/b19946](#).
- [119] M. Hoferichter, J. Ruiz de Elvira, B. Kubis, U.-G. Meißner, Roy-Steiner-equation analysis of pion-nucleon scattering, Phys. Rept. 625 (2016) 1–88. [arXiv:1510.06039](#), [doi:10.1016/j.physrep.2016.02.002](#).
- [120] M. Hoferichter, J. Ruiz de Elvira, B. Kubis, U.-G. Meißner, Matching pion-nucleon Roy-Steiner equations to chiral perturbation theory, Phys. Rev. Lett. 115 (19) (2015) 192301. [arXiv:1507.07552](#), [doi:10.1103/PhysRevLett.115.192301](#).
- [121] J. Ruiz de Elvira, M. Hoferichter, B. Kubis, U.-G. Meißner, Extracting the σ -term from low-energy pion-nucleon scattering, J. Phys. G

- 45 (2) (2018) 024001. [arXiv:1706.01465](https://arxiv.org/abs/1706.01465), doi:10.1088/1361-6471/aa9422.
- [122] M. Hoferichter, J. R. de Elvira, B. Kubis, U.-G. Meißner, Nucleon resonance parameters from Roy–Steiner equations, Phys. Lett. B 853 (2024) 138698. [arXiv:2312.15015](https://arxiv.org/abs/2312.15015), doi:10.1016/j.physletb.2024.138698.
- [123] X. Zhang, C. Hanhart, U.-G. Meißner, J.-J. Xie, Remarks on non-perturbative three-body dynamics and its application to the $K\bar{K}\bar{K}$ system, Eur. Phys. J. A 58 (2) (2022) 20. [arXiv:2107.03168](https://arxiv.org/abs/2107.03168), doi:10.1140/epja/s10050-021-00661-y.
- [124] M. Döring, K. Nakayama, The Phase and pole structure of the $N^*(1535)$ in $\pi N \rightarrow \pi N$ and $\gamma N \rightarrow \pi N$, Eur. Phys. J. A 43 (2010) 83–105. [arXiv:0906.2949](https://arxiv.org/abs/0906.2949), doi:10.1140/epja/i2009-10892-4.
- [125] I. R. Afnan, B. Blankleider, Unified Theory of NN and πD Scattering, Phys. Rev. C 22 (1980) 1638–1649. doi:10.1103/PhysRevC.22.1638.
- [126] M. Mikhasenko, Y. Wunderlich, A. Jackura, V. Mathieu, A. Pilloni, B. Ketzer, A. P. Szczepaniak, Three-body scattering: Ladders and Resonances, JHEP 08 (2019) 080. [arXiv:1904.11894](https://arxiv.org/abs/1904.11894), doi:10.1007/JHEP08(2019)080.
- [127] R. Koch, Improved πN Partial Waves Consistent With Analyticity and Unitarity, Z. Phys. C 29 (1985) 597. doi:10.1007/BF01560295.
- [128] H. Kamano, S. X. Nakamura, T. S. H. Lee, T. Sato, Extraction of P11 resonances from pi N data, Phys. Rev. C 81 (2010) 065207. [arXiv:1001.5083](https://arxiv.org/abs/1001.5083), doi:10.1103/PhysRevC.81.065207.
- [129] M. Mai, M. Döring, Finite-Volume Spectrum of $\pi^+\pi^+$ and $\pi^+\pi^+\pi^+$ Systems, Phys. Rev. Lett. 122 (6) (2019) 062503. [arXiv:1807.04746](https://arxiv.org/abs/1807.04746), doi:10.1103/PhysRevLett.122.062503.
- [130] M. Mai, B. Hu, M. Döring, A. Pilloni, A. Szczepaniak, Three-body Unitarity with Isobars Revisited, Eur. Phys. J. A 53 (9) (2017) 177. [arXiv:1706.06118](https://arxiv.org/abs/1706.06118), doi:10.1140/epja/i2017-12368-4.
- [131] R. Aaron, R. D. Amado, J. E. Young, Relativistic three-body theory with applications to πN scattering, Phys. Rev. 174 (1968) 2022–2032. doi:10.1103/PhysRev.174.2022.
- [132] J. A. Wheeler, On the Mathematical Description of Light Nuclei by the Method of Resonating Group Structure, Phys. Rev. 52 (1937) 1107–1122. doi:10.1103/PhysRev.52.1107.
- [133] W. Heisenberg, THE 'OBSERVABLE QUANTITIES' IN THE THEORY OF ELEMENTARY PARTICLES (1943).
- [134] D. Sadasivan, M. Mai, H. Akdag, M. Döring, Dalitz plots and lineshape of $a_1(1260)$ from a relativistic three-body unitary approach, Phys. Rev. D 101 (9) (2020) 094018, [Erratum: Phys.Rev.D 103, 019901 (2021)]. [arXiv:2002.12431](https://arxiv.org/abs/2002.12431), doi:10.1103/PhysRevD.101.094018.
- [135] H. Yan, M. Mai, M. Garofalo, U.-G. Meißner, C. Liu, L. Liu, C. Urbach, ω Meson from Lattice QCD, Phys. Rev. Lett. 133 (21) (2024) 211906. [arXiv:2407.16659](https://arxiv.org/abs/2407.16659), doi:10.1103/PhysRevLett.133.211906.
- [136] S. M. Dawid, Z. T. Draper, A. D. Hanlon, B. Hörl, C. Morningstar, F. Romero-López, S. R. Sharpe, S. Skinner, QCD predictions for physical multimeson scattering amplitudes (2 2025). [arXiv:2502.14348](https://arxiv.org/abs/2502.14348).
- [137] S. Noh, A. Park, H. Yun, S. Cho, S. H. Lee, The inevitable quark three-body force and its implications for exotic states, Phys. Lett. B 862 (2025) 139278. [arXiv:2408.00715](https://arxiv.org/abs/2408.00715), doi:10.1016/j.physletb.2025.139278.
- [138] Z. T. Draper, A. D. Hanlon, B. Hörl, C. Morningstar, F. Romero-López, S. R. Sharpe, Interactions of πK , $\pi\pi K$ and $KK\pi$ systems at maximal isospin from lattice QCD, JHEP 05 (2023) 137. [arXiv:2302.13587](https://arxiv.org/abs/2302.13587), doi:10.1007/JHEP05(2023)137.
- [139] J. Baeza-Ballesteros, J. Bijnens, T. Husek, F. Romero-López, S. R. Sharpe, M. Sjö, The isospin-3 three-particle K-matrix at NLO in ChPT, JHEP 05 (2023) 187. [arXiv:2303.13206](https://arxiv.org/abs/2303.13206), doi:10.1007/JHEP05(2023)187.
- [140] M. Garofalo, M. Mai, F. Romero-López, A. Rusetsky, C. Urbach, Three-body resonances in the φ^4 theory, JHEP 02 (2023) 252. [arXiv:2211.05605](https://arxiv.org/abs/2211.05605), doi:10.1007/JHEP02(2023)252.
- [141] R. Brett, C. Culver, M. Mai, A. Alexandru, M. Döring, F. X. Lee, Three-body interactions from the finite-volume QCD spectrum, Phys. Rev. D 104 (1) (2021) 014501. [arXiv:2101.06144](https://arxiv.org/abs/2101.06144), doi:10.1103/PhysRevD.104.014501.
- [142] D. Sadasivan, A. Alexandru, H. Akdag, F. Amorim, R. Brett, C. Culver, M. Döring, F. X. Lee, M. Mai, Pole position of the $a_1(1260)$ resonance in a three-body unitary framework, Phys. Rev. D 105 (5) (2022) 054020. [arXiv:2112.03355](https://arxiv.org/abs/2112.03355), doi:10.1103/PhysRevD.105.054020.
- [143] A. Alexandru, R. Brett, C. Culver, M. Döring, D. Guo, F. X. Lee, M. Mai, Finite-volume energy spectrum of the $K^-K^-K^-$ system, Phys. Rev. D 102 (11) (2020) 114523. [arXiv:2009.12358](https://arxiv.org/abs/2009.12358), doi:10.1103/PhysRevD.102.114523.
- [144] P. Capel, D. R. Phillips, H. W. Hammer, Simulating core excitation in breakup reactions of halo nuclei using an effective three-body force, Phys. Lett. B 825 (2022) 136847. [arXiv:2008.05898](https://arxiv.org/abs/2008.05898), doi:10.1016/j.physletb.2021.136847.
- [145] H. Kamada, Four-Body Scattering Equations Including Three-Body Force, Few Body Syst. 60 (2) (2019) 33. doi:10.1007/s00601-019-1501-4.
- [146] P. F. Bedaque, H. W. Grießhammer, Quartet S wave neutron deuteron scattering in effective field theory, Nucl. Phys. A 671 (2000) 357–379. [arXiv:nucl-th/9907077](https://arxiv.org/abs/nucl-th/9907077), doi:10.1016/S0375-9474(99)00691-0.
- [147] H.-W. Hammer, J.-Y. Pang, A. Rusetsky, Three particle quantization condition in a finite volume: 2. general formalism and the analysis of data, JHEP 10 (2017) 115. [arXiv:1707.02176](https://arxiv.org/abs/1707.02176), doi:10.1007/JHEP10(2017)115.
- [148] V. Gribov, Cambridge monographs on particle physics, nuclear physics and cosmology: Strong interactions of hadrons at high energies: Gribov lectures on theoretical physics series number 27, Cambridge monographs on particle physics, nuclear physics and cosmology, Cambridge University Press, Cambridge, England, 2012.
- [149] H. Kamano, T. S. H. Lee, S. X. Nakamura, T. Sato, The ANL-Osaka Partial-Wave Amplitudes of πN and γN Reactions (9 2019). [arXiv:1909.11935](https://arxiv.org/abs/1909.11935).
- [150] J. H. Hetherington, L. H. Schick, Exact Multiple-Scattering Analysis of Low-Energy Elastic K-d Scattering with Separable Potentials, Phys. Rev. 137 (1965) B935–B948. doi:10.1103/PhysRev.137.B935.
- [151] G. Eichmann, P. Duarte, M. T. Peña, A. Stadler, Scattering amplitudes and contour deformations, Phys. Rev. D 100 (9) (2019) 094001. [arXiv:1907.05402](https://arxiv.org/abs/1907.05402), doi:10.1103/PhysRevD.100.094001.
- [152] R. T. Cahill, I. H. Sloan, Theory of neutron-deuteron break-up at 14.4 MeV, Nucl. Phys. A 165 (1971) 161–179, [Erratum: Nucl.Phys.A 196, 632–632 (1972)]. doi:10.1016/0375-9474(72)90798-1.
- [153] E. Schmid, H. Ziegelmann, The Quantum Mechanical Three-body Problem, Vieweg tracts in pure and applied physics, Pergamon Press, Oxford, 1974.
URL <https://books.google.es/books?id=DEaEwQEACAAJ>
- [154] J.-Y. Pang, R. Bubna, F. Müller, A. Rusetsky, J.-J. Wu, Lellouch-Lüscher factor for the $K \rightarrow 3\pi$ decays, JHEP 05 (2024) 269. [arXiv:2312.04391](https://arxiv.org/abs/2312.04391), doi:10.1007/JHEP05(2024)269.
- [155] Z.-H. Zhang, T. Ji, X.-K. Dong, F.-K. Guo, C. Hanhart, U.-G. Meißner, A. Rusetsky, Predicting isovector charmonium-like states from X(3872) properties, JHEP 08 (2024) 130. [arXiv:2404.11215](https://arxiv.org/abs/2404.11215), doi:10.1007/JHEP08(2024)130.
- [156] A. Fix, H. Arenhövel, Three-body calculation of incoherent $\pi 0$ photoproduction on a deuteron, Phys. Rev. C 100 (3) (2019) 034003. [arXiv:1904.04557](https://arxiv.org/abs/1904.04557), doi:10.1103/PhysRevC.100.034003.
- [157] A. S. Sakthivasan, M. Mai, A. Rusetsky, M. Döring, Effects of final state interactions on Landau singularities, JHEP 10 (2024) 246. [arXiv:2407.17969](https://arxiv.org/abs/2407.17969), doi:10.1007/JHEP10(2024)246.

- [158] F. Sohre, H. Ziegelmann, Numerical solution of the faddeev-amado integral equation without deformation of contours, Phys. Lett. B 34 (1971) 579–580. [doi:10.1016/0370-2693\(71\)90141-9](https://doi.org/10.1016/0370-2693(71)90141-9).
- [159] M. I. Haftel, F. Tabakin, NUCLEAR SATURATION AND THE SMOOTHNESS OF NUCLEON-NUCLEON POTENTIALS, Nucl. Phys. A 158 (1970) 1–42. [doi:10.1016/0375-9474\(70\)90047-3](https://doi.org/10.1016/0375-9474(70)90047-3).
- [160] A. Matsuyama, A Three-body Calculation of the πd Scattering Amplitude by the Spline Method, Phys. Lett. B 152 (1985) 42–46. [doi:10.1016/0370-2693\(85\)91135-9](https://doi.org/10.1016/0370-2693(85)91135-9).
- [161] R. D. Amado, Soluble Problems in the Scattering from Compound Systems, Phys. Rev. 132 (1) (1963) 485. [doi:10.1103/PhysRev.132.485](https://doi.org/10.1103/PhysRev.132.485).
- [162] S. M. Dawid, M. H. E. Islam, R. A. Briceño, Analytic continuation of the relativistic three-particle scattering amplitudes, Phys. Rev. D 108 (3) (2023) 034016. [arXiv:2303.04394](https://arxiv.org/abs/2303.04394), [doi:10.1103/PhysRevD.108.034016](https://doi.org/10.1103/PhysRevD.108.034016).
- [163] S. M. Dawid, M. H. E. Islam, R. A. Briceño, A. W. Jackura, Evolution of Efimov states, Phys. Rev. A 109 (4) (2024) 043325. [arXiv:2309.01732](https://arxiv.org/abs/2309.01732), [doi:10.1103/PhysRevA.109.043325](https://doi.org/10.1103/PhysRevA.109.043325).
- [164] M. Mai, A. Alexandru, R. Brett, C. Culver, M. Döring, F. X. Lee, D. Sadasivan, Three-Body Dynamics of the a1(1260) Resonance from Lattice QCD, Phys. Rev. Lett. 127 (22) (2021) 222001. [arXiv:2107.03973](https://arxiv.org/abs/2107.03973), [doi:10.1103/PhysRevLett.127.222001](https://doi.org/10.1103/PhysRevLett.127.222001).
- [165] S. X. Nakamura, X. H. Li, H. P. Peng, Z. T. Sun, X. R. Zhou, Global coupled-channel analysis of $e^+e^- \rightarrow c\bar{c}$ processes in $\sqrt{s} = 3.75 - 4.7$ GeV (12 2023). [arXiv:2312.17658](https://arxiv.org/abs/2312.17658).
- [166] J. A. Oller, E. Oset, N/D description of two meson amplitudes and chiral symmetry, Phys. Rev. D 60 (1999) 074023. [arXiv:hep-ph/9809337](https://arxiv.org/abs/hep-ph/9809337), [doi:10.1103/PhysRevD.60.074023](https://doi.org/10.1103/PhysRevD.60.074023).
- [167] F.-K. Guo, X.-H. Liu, S. Sakai, Threshold cusps and triangle singularities in hadronic reactions, Prog. Part. Nucl. Phys. 112 (2020) 103757. [arXiv:1912.07030](https://arxiv.org/abs/1912.07030), [doi:10.1016/j.ppnp.2020.103757](https://doi.org/10.1016/j.ppnp.2020.103757).
- [168] L. A. Heuser, G. Chanturia, F. K. Guo, C. Hanhart, M. Hoferichter, B. Kubis, From pole parameters to line shapes and branching ratios, Eur. Phys. J. C 84 (6) (2024) 599. [arXiv:2403.15539](https://arxiv.org/abs/2403.15539), [doi:10.1140/epjc/s10052-024-12884-6](https://doi.org/10.1140/epjc/s10052-024-12884-6).
- [169] J. Haidenbauer, U.-G. Meißner, On the structure in the ΛN cross section at the ΣN threshold, Chin. Phys. C 45 (9) (2021) 094104. [arXiv:2105.00836](https://arxiv.org/abs/2105.00836), [doi:10.1088/1674-1137/ac0e89](https://doi.org/10.1088/1674-1137/ac0e89).
- [170] R. A. Arndt, W. J. Briscoe, I. I. Strakovsky, R. L. Workman, Extended partial-wave analysis of piN scattering data, Phys. Rev. C 74 (2006) 045205. [arXiv:nucl-th/0605082](https://arxiv.org/abs/nucl-th/0605082), [doi:10.1103/PhysRevC.74.045205](https://doi.org/10.1103/PhysRevC.74.045205).
- [171] W. Yamada, O. Morimatsu, New method to extract information of near-threshold resonances: Uniformized Mittag-Leffler expansion of Green's function and T matrix, Phys. Rev. C 102 (5) (2020) 055201. [arXiv:2005.07022](https://arxiv.org/abs/2005.07022), [doi:10.1103/PhysRevC.102.055201](https://doi.org/10.1103/PhysRevC.102.055201).
- [172] M. Kato, Analytical properties of two-channel S-matrix, Annals Phys. 31 (1) (1965) 130–147. [doi:10.1016/0003-4916\(65\)90235-6](https://doi.org/10.1016/0003-4916(65)90235-6).
- [173] R. G. Newton, SCATTERING THEORY OF WAVES AND PARTICLES, 1982.
- [174] J. Humblet, L. Rosenfeld, Theory of nuclear reactions: I. resonant states and collision matrix, Nuclear Physics 26 (4) (1961) 529–578.
- [175] H. M. Nussenzveig, Causality and dispersion relations, Vol. 95, Academic Press, New York, London, 1972.
- [176] D. F. Ramírez Jiménez, N. G. Kelkar, Different manifestations of S-matrix poles, Annals Phys. 396 (2018) 18–43. [arXiv:1802.09467](https://arxiv.org/abs/1802.09467), [doi:10.1016/j.aop.2018.07.001](https://doi.org/10.1016/j.aop.2018.07.001).
- [177] W. A. Yamada, O. Morimatsu, Application of the uniformized Mittag-Leffler expansion to $\Lambda(1405)$, Phys. Rev. C 103 (4) (2021) 045201. [arXiv:2101.10029](https://arxiv.org/abs/2101.10029), [doi:10.1103/PhysRevC.103.045201](https://doi.org/10.1103/PhysRevC.103.045201).
- [178] W. A. Yamada, O. Morimatsu, T. Sato, K. Yazaki, Near-threshold spectrum from a uniformized Mittag-Leffler expansion: Pole structure of the $Z(3900)$, Phys. Rev. D 105 (1) (2022) 014034. [arXiv:2108.11605](https://arxiv.org/abs/2108.11605), [doi:10.1103/PhysRevD.105.014034](https://doi.org/10.1103/PhysRevD.105.014034).
- [179] Y. Ikeda, The tetraquark candidate $Z_c(3900)$ from dynamical lattice QCD simulations, J. Phys. G 45 (2) (2018) 024002. [arXiv:1706.07300](https://arxiv.org/abs/1706.07300), [doi:10.1088/1361-6471/aa9af9](https://doi.org/10.1088/1361-6471/aa9af9).
- [180] Y. Ikeda, S. Aoki, T. Doi, S. Gongyo, T. Hatsuda, T. Inoue, T. Iritani, N. Ishii, K. Murano, K. Sasaki, Fate of the Tetraquark Candidate $Z_c(3900)$ from Lattice QCD, Phys. Rev. Lett. 117 (24) (2016) 242001. [arXiv:1602.03465](https://arxiv.org/abs/1602.03465), [doi:10.1103/PhysRevLett.117.242001](https://doi.org/10.1103/PhysRevLett.117.242001).
- [181] K. Miyagawa, H. Yamamura, S-matrix poles near the ΛN and ΣN thresholds in the coupled $\Lambda N-\Sigma N$ system, Phys. Rev. C 60 (1999) 024003. [doi:10.1103/PhysRevC.60.024003](https://doi.org/10.1103/PhysRevC.60.024003).
- [182] S. M. Flatte, Coupled Channel Analysis of the $\pi\eta$ and $K\bar{K}$ Systems Near $K\bar{K}$ Threshold, Phys. Lett. B 63 (1976) 224–227. [doi:10.1016/0370-2693\(76\)90654-7](https://doi.org/10.1016/0370-2693(76)90654-7).
- [183] A. Cieplý, M. Mai, U.-G. Meißner, J. Smejkal, On the pole content of coupled channels chiral approaches used for the $\bar{K}N$ system, Nucl. Phys. A 954 (2016) 17–40. [arXiv:1603.02531](https://arxiv.org/abs/1603.02531), [doi:10.1016/j.nuclphysa.2016.04.031](https://doi.org/10.1016/j.nuclphysa.2016.04.031).
- [184] F.-K. Guo, Y. Kamiya, M. Mai, U.-G. Meißner, New insights into the nature of the $\Lambda(1380)$ and $\Lambda(1405)$ resonances away from the SU(3) limit, Phys. Lett. B 846 (2023) 138264. [arXiv:2308.07658](https://arxiv.org/abs/2308.07658), [doi:10.1016/j.physletb.2023.138264](https://doi.org/10.1016/j.physletb.2023.138264).
- [185] M. Döring, B. Hu, M. Mai, Chiral Extrapolation of the Sigma Resonance, Phys. Lett. B 782 (2018) 785–793. [arXiv:1610.10070](https://arxiv.org/abs/1610.10070), [doi:10.1016/j.physletb.2018.05.042](https://doi.org/10.1016/j.physletb.2018.05.042).
- [186] H. A. Weidenmüller, Studies of many-channel scattering, Annals Phys. 28 (1) (1964) 60–115. [doi:10.1016/0003-4916\(64\)90143-5](https://doi.org/10.1016/0003-4916(64)90143-5).
- [187] W. A. Yamada, O. Morimatsu, T. Sato, Analytic Map of Three-Channel S Matrix: Generalized Uniformization and Mittag-Leffler Expansion, Phys. Rev. Lett. 129 (19) (2022) 192001. [arXiv:2203.17069](https://arxiv.org/abs/2203.17069), [doi:10.1103/PhysRevLett.129.192001](https://doi.org/10.1103/PhysRevLett.129.192001).
- [188] T. Inoue, E. Oset, M. J. Vicente Vacas, Chiral unitary approach to S wave meson baryon scattering in the strangeness S = O sector, Phys. Rev. C 65 (2002) 035204. [arXiv:hep-ph/0110333](https://arxiv.org/abs/hep-ph/0110333), [doi:10.1103/PhysRevC.65.035204](https://doi.org/10.1103/PhysRevC.65.035204).
- [189] M. Mai, M. Döring, C. Culver, A. Alexandru, Three-body unitarity versus finite-volume $\pi^+\pi^+\pi^+$ spectrum from lattice QCD, Phys. Rev. D 101 (5) (2020) 054510. [arXiv:1909.05749](https://arxiv.org/abs/1909.05749), [doi:10.1103/PhysRevD.101.054510](https://doi.org/10.1103/PhysRevD.101.054510).
- [190] T. N. Truong, Chiral Perturbation Theory and Final State Theorem, Phys. Rev. Lett. 61 (1988) 2526. [doi:10.1103/PhysRevLett.61.2526](https://doi.org/10.1103/PhysRevLett.61.2526).
- [191] A. Gomez Nicola, J. R. Pelaez, Meson meson scattering within one loop chiral perturbation theory and its unitarization, Phys. Rev. D 65 (2002) 054009. [arXiv:hep-ph/0109056](https://arxiv.org/abs/hep-ph/0109056), [doi:10.1103/PhysRevD.65.054009](https://doi.org/10.1103/PhysRevD.65.054009).
- [192] J. Nebreda, J. R. Pelaez., Strange and non-strange quark mass dependence of elastic light resonances from SU(3) Unitarized Chiral Perturbation Theory to one loop, Phys. Rev. D 81 (2010) 054035. [arXiv:1001.5237](https://arxiv.org/abs/1001.5237), [doi:10.1103/PhysRevD.81.054035](https://doi.org/10.1103/PhysRevD.81.054035).
- [193] J. A. Oller, E. Oset, Chiral symmetry amplitudes in the S wave isoscalar and isovector channels and the σ , $f_0(980)$, $a_0(980)$ scalar mesons, Nucl. Phys. A 620 (1997) 438–456, [Erratum: Nucl.Phys.A 652, 407–409 (1999)]. [arXiv:hep-ph/9702314](https://arxiv.org/abs/hep-ph/9702314), [doi:10.1016/S0375-9474\(97\)00160-7](https://doi.org/10.1016/S0375-9474(97)00160-7).
- [194] J. A. Oller, E. Oset, J. R. Pelaez, Meson meson interaction in a nonperturbative chiral approach, Phys. Rev. D 59 (1999) 074001, [Erratum: Phys.Rev.D 60, 099906 (1999), Erratum: Phys.Rev.D 75, 099903 (2007)]. [arXiv:hep-ph/9804209](https://arxiv.org/abs/hep-ph/9804209), [doi:10.1103/PhysRevD.59.074001](https://doi.org/10.1103/PhysRevD.59.074001).
- [195] S. Ceci, M. Döring, C. Hanhart, S. Krewald, U.-G. Meißner, A. Švarc, Relevance of complex branch points for partial wave analysis, Phys. Rev. C 84 (2011) 015205. [arXiv:1104.3490](https://arxiv.org/abs/1104.3490), [doi:10.1103/PhysRevC.84.015205](https://doi.org/10.1103/PhysRevC.84.015205).
- [196] Y. Ikeda, T. Sato, Strange dibaryon resonance in the $\bar{K}NN - \pi\Sigma N$ system, Phys. Rev. C 76 (2007) 035203. [arXiv:0704.1978](https://arxiv.org/abs/0704.1978),

- [doi:10.1103/PhysRevC.76.035203](https://doi.org/10.1103/PhysRevC.76.035203).
- [197] W. Glöckle, S-matrix pole trajectory in a three-neutron model, Phys. Rev. C 18 (1978) 564–572. [doi:10.1103/PhysRevC.18.564](https://doi.org/10.1103/PhysRevC.18.564).
- [198] J. A. Oller, Coupled-channel approach in hadron–hadron scattering, Prog. Part. Nucl. Phys. 110 (2020) 103728. [arXiv:1909.00370](https://arxiv.org/abs/1909.00370), [doi:10.1016/j.ppnp.2019.103728](https://doi.org/10.1016/j.ppnp.2019.103728).
- [199] M. Albaladejo, et al., Novel approaches in hadron spectroscopy, Prog. Part. Nucl. Phys. 127 (2022) 103981. [arXiv:2112.13436](https://arxiv.org/abs/2112.13436), [doi:10.1016/j.ppnp.2022.103981](https://doi.org/10.1016/j.ppnp.2022.103981).
- [200] M. Mai, Review of the $\Lambda(1405)$ A curious case of a strangeness resonance, Eur. Phys. J. ST 230 (6) (2021) 1593–1607. [arXiv:2010.00056](https://arxiv.org/abs/2010.00056), [doi:10.1140/epjs/s11734-021-00144-7](https://doi.org/10.1140/epjs/s11734-021-00144-7).
- [201] M. Mai, U.-G. Meißner, New insights into antikaon-nucleon scattering and the structure of the $\Lambda(1405)$, Nucl. Phys. A 900 (2013) 51 – 64. [arXiv:1202.2030](https://arxiv.org/abs/1202.2030), [doi:10.1016/j.nuclphysa.2013.01.032](https://doi.org/10.1016/j.nuclphysa.2013.01.032).
- [202] M. Mai, From meson-baryon scattering to meson photoproduction, Ph.D. thesis, Bonn U. (2013).
- [203] E. E. Salpeter, H. A. Bethe, A Relativistic equation for bound state problems, Phys. Rev. 84 (1951) 1232–1242. [doi:10.1103/PhysRev.84.1232](https://doi.org/10.1103/PhysRev.84.1232).
- [204] J. Nieves, E. Ruiz Arriola, Bethe-Salpeter approach for unitarized chiral perturbation theory, Nucl. Phys. A 679 (2000) 57–117. [arXiv:hep-ph/9907469](https://arxiv.org/abs/hep-ph/9907469), [doi:10.1016/S0375-9474\(00\)00321-3](https://doi.org/10.1016/S0375-9474(00)00321-3).
- [205] M. Mai, Theory of resonances (2 2025). [arXiv:2502.02654](https://arxiv.org/abs/2502.02654).
- [206] D. L. B. Sombillo, Y. Ikeda, T. Sato, A. Hosaka, Classifying the pole of an amplitude using a deep neural network, Phys. Rev. D 102 (1) (2020) 016024. [arXiv:2003.10770](https://arxiv.org/abs/2003.10770), [doi:10.1103/PhysRevD.102.016024](https://doi.org/10.1103/PhysRevD.102.016024).
- [207] J. Landay, M. Mai, M. Döring, H. Haberzettl, K. Nakayama, Towards the Minimal Spectrum of Excited Baryons, Phys. Rev. D 99 (1) (2019) 016001. [arXiv:1810.00075](https://arxiv.org/abs/1810.00075), [doi:10.1103/PhysRevD.99.016001](https://doi.org/10.1103/PhysRevD.99.016001).
- [208] L. Ng, L. Bibrzycki, J. Nys, C. Fernández-Ramírez, A. Pilloni, V. Mathieu, A. J. Rasmussen, A. P. Szczepaniak, Deep learning exotic hadrons, Phys. Rev. D 105 (9) (2022) L091501. [arXiv:2110.13742](https://arxiv.org/abs/2110.13742), [doi:10.1103/PhysRevD.105.L091501](https://doi.org/10.1103/PhysRevD.105.L091501).
- [209] C. Fernández-Ramírez, A. Pilloni, M. Albaladejo, A. Jackura, V. Mathieu, M. Mikhasenko, J. A. Silva-Castro, A. P. Szczepaniak, Interpretation of the LHCb $P_c(4312)^+$ Signal, Phys. Rev. Lett. 123 (9) (2019) 092001. [arXiv:1904.10021](https://arxiv.org/abs/1904.10021), [doi:10.1103/PhysRevLett.123.092001](https://doi.org/10.1103/PhysRevLett.123.092001).
- [210] D. L. B. Sombillo, Y. Ikeda, T. Sato, A. Hosaka, Model independent analysis of coupled-channel scattering: A deep learning approach, Phys. Rev. D 104 (3) (2021) 036001. [arXiv:2105.04898](https://arxiv.org/abs/2105.04898), [doi:10.1103/PhysRevD.104.036001](https://doi.org/10.1103/PhysRevD.104.036001).
- [211] L. M. Santos, V. A. A. Chavez, D. L. B. Sombillo, Pole structure of $P_\psi^N(4312)^+$ via machine learning and uniformized S-matrix, J. Phys. G 52 (1) (2025) 015104. [arXiv:2405.11906](https://arxiv.org/abs/2405.11906), [doi:10.1088/1361-6471/ad8ee3](https://doi.org/10.1088/1361-6471/ad8ee3).
- [212] L. Ng, L. Bibrzycki, J. Nys, C. Fernández-Ramírez, A. Pilloni, V. Mathieu, A. J. Rasmussen, A. P. Szczepaniak, Machine learning exotic hadrons, Nuovo Cim. C 47 (4) (2024) 207. [doi:10.1393/ncc/i2024-24207-8](https://doi.org/10.1393/ncc/i2024-24207-8).
- [213] D. Darulis, R. Tyson, D. G. Ireland, D. I. Glazier, B. McKinnon, P. Pauli, Machine Learned Particle Detector Simulations (7 2022). [arXiv:2207.11254](https://arxiv.org/abs/2207.11254).
- [214] T. Alghamdi, et al., Toward a generative modeling analysis of CLAS exclusive 2π photoproduction, Phys. Rev. D 108 (9) (2023) 094030. [arXiv:2307.04450](https://arxiv.org/abs/2307.04450), [doi:10.1103/PhysRevD.108.094030](https://doi.org/10.1103/PhysRevD.108.094030).
- [215] M. Malekhosseini, S. Rostami, A. R. Olamaei, R. Ostovar, K. Azizi, Meson mass and width: Deep learning approach, Phys. Rev. D 110 (5) (2024) 054011. [arXiv:2404.00448](https://arxiv.org/abs/2404.00448), [doi:10.1103/PhysRevD.110.054011](https://doi.org/10.1103/PhysRevD.110.054011).
- [216] D. A. O. Co, V. A. A. Chavez, D. L. B. Sombillo, Deep learning framework for disentangling triangle singularity and pole-based enhancements, Phys. Rev. D 110 (11) (2024) 114034. [arXiv:2403.18265](https://arxiv.org/abs/2403.18265), [doi:10.1103/PhysRevD.110.114034](https://doi.org/10.1103/PhysRevD.110.114034).
- [217] G. Aarts, K. Fukushima, T. Hatsuda, A. Ipp, S. Shi, L. Wang, K. Zhou, Physics-driven learning for inverse problems in quantum chromodynamics, Nature Rev. Phys. 7 (3) (2025) 154–163. [arXiv:2501.05580](https://arxiv.org/abs/2501.05580), [doi:10.1038/s42254-024-00798-x](https://doi.org/10.1038/s42254-024-00798-x).
- [218] L. De Cruz, J. Ryckebusch, T. Vrancx, P. Vancreyveld, A Bayesian analysis of kaon photoproduction with the Regge-plus-resonance model, Phys. Rev. C 86 (2012) 015212. [arXiv:1205.2195](https://arxiv.org/abs/1205.2195), [doi:10.1103/PhysRevC.86.015212](https://doi.org/10.1103/PhysRevC.86.015212).
- [219] L. De Cruz, T. Vrancx, P. Vancreyveld, J. Ryckebusch, Bayesian inference of the resonance content of $p(\gamma, K^+)\Lambda$, Phys. Rev. Lett. 108 (2012) 182002. [arXiv:1111.6511](https://arxiv.org/abs/1111.6511), [doi:10.1103/PhysRevLett.108.182002](https://doi.org/10.1103/PhysRevLett.108.182002).
- [220] J. Nys, J. Ryckebusch, D. G. Ireland, D. I. Glazier, Model discrimination in pseudoscalar-meson photoproduction, Phys. Lett. B 759 (2016) 260–265. [arXiv:1603.02001](https://arxiv.org/abs/1603.02001), [doi:10.1016/j.physletb.2016.05.069](https://doi.org/10.1016/j.physletb.2016.05.069).
- [221] B. Guegan, J. Hardin, J. Stevens, M. Williams, Model selection for amplitude analysis, JINST 10 (09) (2015) P09002. [arXiv:1505.05133](https://arxiv.org/abs/1505.05133), [doi:10.1088/1748-0221/10/09/P09002](https://doi.org/10.1088/1748-0221/10/09/P09002).
- [222] M. Williams, A novel approach to the bias-variance problem in bump hunting, JINST 12 (09) (2017) P09034. [arXiv:1705.03578](https://arxiv.org/abs/1705.03578), [doi:10.1088/1748-0221/12/09/P09034](https://doi.org/10.1088/1748-0221/12/09/P09034).
- [223] B. Ketzer, B. Grube, D. Ryabchikov, Light-Meson Spectroscopy with COMPASS, Prog. Part. Nucl. Phys. 113 (2020) 103755. [arXiv:1909.06366](https://arxiv.org/abs/1909.06366), [doi:10.1016/j.ppnp.2020.103755](https://doi.org/10.1016/j.ppnp.2020.103755).
- [224] X. Dong, C.-C. Pan, Y.-C. Sun, A.-Y. Cheng, A.-B. Wang, H. Cai, K. Zhu, Fraction constraint in partial wave analysis, Int. J. Mod. Phys. E 33 (01n02) (2024) 2450001. [arXiv:2309.14740](https://arxiv.org/abs/2309.14740), [doi:10.1142/S0218301324500010](https://doi.org/10.1142/S0218301324500010).
- [225] R. Tibshirani, Regression shrinkage and selection via the lasso: A retrospective, Journal of the Royal Statistical Society Series B: Statistical Methodology 73 (3) (2011) 273–282. [doi:10.1111/j.1467-9868.2011.00771.x](https://doi.org/10.1111/j.1467-9868.2011.00771.x).
URL <https://doi.org/10.1111/j.1467-9868.2011.00771.x>
- [226] T. Hastie, R. Tibshirani, J. Friedman, The Elements of Statistical Learning, Springer New York, 2009. [doi:10.1007/978-0-387-84858-7](https://doi.org/10.1007/978-0-387-84858-7).
URL <http://dx.doi.org/10.1007/978-0-387-84858-7>
- [227] J. Landay, M. Döring, C. Fernández-Ramírez, B. Hu, R. Molina, Model Selection for Pion Photoproduction, Phys. Rev. C 95 (1) (2017) 015203. [arXiv:1610.07547](https://arxiv.org/abs/1610.07547), [doi:10.1103/PhysRevC.95.015203](https://doi.org/10.1103/PhysRevC.95.015203).
- [228] P. Bydžovský, A. Cieplý, D. Petrellis, D. Skoupil, N. Zachariou, Model selection for $K^+\Sigma^-$ photoproduction within an isobar model, Phys. Rev. C 104 (6) (2021) 065202, [Erratum: Phys. Rev. C 110, 029901 (2024)]. [arXiv:2106.15199](https://arxiv.org/abs/2106.15199), [doi:10.1103/PhysRevC.104.065202](https://doi.org/10.1103/PhysRevC.104.065202).
- [229] D. Petrellis, D. Skoupil, Ridge regression for minimizing the couplings of hyperon resonances in $K+\Lambda$ photoproduction, Phys. Rev. C 107 (4) (2023) 045206. [arXiv:2212.14305](https://arxiv.org/abs/2212.14305), [doi:10.1103/PhysRevC.107.045206](https://doi.org/10.1103/PhysRevC.107.045206).
- [230] C. Fernández-Ramírez, E. Moya de Guerrra, A. Udiá, J. M. Udiá, Properties of Nucleon Resonances by means of a Genetic Algorithm, Phys. Rev. C 77 (2008) 065212. [arXiv:0805.4178](https://arxiv.org/abs/0805.4178), [doi:10.1103/PhysRevC.77.065212](https://doi.org/10.1103/PhysRevC.77.065212).
- [231] P. Bydzovsky, T. Mart, Analysis of the data consistency on kaon photoproduction with Lambda in the final state, Phys. Rev. C 76 (2007) 065202. [arXiv:nucl-th/0605014](https://arxiv.org/abs/nucl-th/0605014), [doi:10.1103/PhysRevC.76.065202](https://doi.org/10.1103/PhysRevC.76.065202).
- [232] G. D'Agostini, On the use of the covariance matrix to fit correlated data, Nucl. Instrum. Meth. A 346 (1994) 306–311. [doi:10.1016/0168-9002\(94\)90719-6](https://doi.org/10.1016/0168-9002(94)90719-6).
- [233] R. D. Ball, L. Del Debbio, S. Forte, A. Guffanti, J. I. Latorre, J. Rojo, M. Ubiali, Fitting Parton Distribution Data with Multiplicative Normalization Uncertainties, JHEP 05 (2010) 075. [arXiv:0912.2276](https://arxiv.org/abs/0912.2276), [doi:10.1007/JHEP05\(2010\)075](https://doi.org/10.1007/JHEP05(2010)075).

- [234] Z. Liu, M. Tegmark, Machine Learning Hidden Symmetries, Phys. Rev. Lett. 128 (18) (2022) 180201. [arXiv:2109.09721](https://arxiv.org/abs/2109.09721), doi:10.1103/PhysRevLett.128.180201.
- [235] R. Iten, T. Metger, H. Wilming, L. del Rio, R. Renner, Discovering Physical Concepts with Neural Networks, Phys. Rev. Lett. 124 (1) (2020) 010508. doi:10.1103/PhysRevLett.124.010508.
- [236] E. H. Müller, Exact conservation laws for neural network integrators of dynamical systems, J. Comput. Phys. 488 (2023) 112234. [arXiv:2209.11661](https://arxiv.org/abs/2209.11661), doi:10.1016/j.jcp.2023.112234.
- [237] M. Mattheakis, P. Protopapas, D. Sondak, M. Di Giovanni, E. Kaxiras, Physical Symmetries Embedded in Neural Networks (4 2019). [arXiv:1904.08991](https://arxiv.org/abs/1904.08991).
- [238] M. Lüscher, Volume Dependence of the Energy Spectrum in Massive Quantum Field Theories. 1. Stable Particle States, Commun. Math. Phys. 104 (1986) 177. doi:10.1007/BF01211589.
- [239] M. Lüscher, Volume Dependence of the Energy Spectrum in Massive Quantum Field Theories. 2. Scattering States, Commun. Math. Phys. 105 (1986) 153–188. doi:10.1007/BF01211097.
- [240] M. Lüscher, Two particle states on a torus and their relation to the scattering matrix, Nucl. Phys. B 354 (1991) 531–578. doi:10.1016/0550-3213(91)90366-6.
- [241] M. T. Hansen, S. R. Sharpe, Lattice QCD and Three-particle Decays of Resonances, Ann. Rev. Nucl. Part. Sci. 69 (2019) 65–107. [arXiv:1901.00483](https://arxiv.org/abs/1901.00483), doi:10.1146/annurev-nucl-101918-023723.
- [242] M. Mai, M. Döring, A. Rusetsky, Multi-particle systems on the lattice and chiral extrapolations: a brief review, Eur. Phys. J. ST 230 (6) (2021) 1623–1643. [arXiv:2103.00577](https://arxiv.org/abs/2103.00577), doi:10.1140/epjs/s11734-021-00146-5.
- [243] M. Döring, U.-G. Meißner, E. Oset, A. Rusetsky, Unitarized Chiral Perturbation Theory in a finite volume: Scalar meson sector, Eur. Phys. J. A 47 (2011) 139. [arXiv:1107.3988](https://arxiv.org/abs/1107.3988), doi:10.1140/epja/i2011-11139-7.
- [244] S. R. Beane, P. F. Bedaque, A. Parreno, M. J. Savage, Exploring hyperons and hypernuclei with lattice QCD, Nucl. Phys. A 747 (2005) 55–74. [arXiv:nucl-th/0311027](https://arxiv.org/abs/nucl-th/0311027), doi:10.1016/j.nuclphysa.2004.09.081.
- [245] S. He, X. Feng, C. Liu, Two particle states and the S-matrix elements in multi-channel scattering, JHEP 07 (2005) 011. [arXiv:hep-lat/0504019](https://arxiv.org/abs/hep-lat/0504019), doi:10.1088/1126-6708/2005/07/011.
- [246] M. Göckeler, R. Horsley, M. Lage, U.-G. Meißner, P. E. L. Rakow, A. Rusetsky, G. Schierholz, J. M. Zanotti, Scattering phases for meson and baryon resonances on general moving-frame lattices, Phys. Rev. D 86 (2012) 094513. [arXiv:1206.4141](https://arxiv.org/abs/1206.4141), doi:10.1103/PhysRevD.86.094513.
- [247] C. Morningstar, J. Bulava, B. Singha, R. Brett, J. Fallica, A. Hanlon, B. Hörrz, Estimating the two-particle K -matrix for multiple partial waves and decay channels from finite-volume energies, Nucl. Phys. B 924 (2017) 477–507. [arXiv:1707.05817](https://arxiv.org/abs/1707.05817), doi:10.1016/j.nuclphysb.2017.09.014.
- [248] M. Döring, U.-G. Meißner, E. Oset, A. Rusetsky, Scalar mesons moving in a finite volume and the role of partial wave mixing, Eur. Phys. J. A 48 (2012) 114. [arXiv:1205.4838](https://arxiv.org/abs/1205.4838), doi:10.1140/epja/i2012-12114-6.
- [249] F. X. Lee, C. Morningstar, A. Alexandru, Energy spectrum of two-particle scattering in a periodic box, Int. J. Mod. Phys. C 31 (09) (2020) 2050131. doi:10.1142/S0129183120501314.
- [250] C. S. Pelissier, A. Alexandru, F. X. Lee, ρ meson decay on asymmetrical lattices, PoS LATTICE2011 (2011) 134. [arXiv:1111.2314](https://arxiv.org/abs/1111.2314), doi:10.22323/1.139.0134.
- [251] C. Culver, M. Mai, A. Alexandru, M. Döring, F. X. Lee, Pion scattering in the isospin $I = 2$ channel from elongated lattices, Phys. Rev. D 100 (3) (2019) 034509. [arXiv:1905.10202](https://arxiv.org/abs/1905.10202), doi:10.1103/PhysRevD.100.034509.
- [252] F. X. Lee, A. Alexandru, Scattering phase-shift formulas for mesons and baryons in elongated boxes, Phys. Rev. D 96 (5) (2017) 054508. [arXiv:1706.00262](https://arxiv.org/abs/1706.00262), doi:10.1103/PhysRevD.96.054508.
- [253] M. Mai, M. Döring, Three-body Unitarity in the Finite Volume, Eur. Phys. J. A 53 (12) (2017) 240. [arXiv:1709.08222](https://arxiv.org/abs/1709.08222), doi:10.1140/epja/i2017-12440-1.
- [254] M. Döring, J. Haidenbauer, U.-G. Meißner, A. Rusetsky, Dynamical coupled-channel approaches on a momentum lattice, Eur. Phys. J. A 47 (2011) 163. [arXiv:1108.0676](https://arxiv.org/abs/1108.0676), doi:10.1140/epja/i2011-11163-7.
- [255] OEIS foundation, The On-Line Encyclopedia of Integer Sequences for the $\vartheta^{(P)}$ series and $\vartheta^{(A)}$ series, <http://oeis.org/A005875> and <http://oeis.org/A008443>.
- [256] M.-L. Du, A. Filin, V. Baru, X.-K. Dong, E. Epelbaum, F.-K. Guo, C. Hanhart, A. Nefediev, J. Nieves, Q. Wang, Role of Left-Hand Cut Contributions on Pole Extractions from Lattice Data: Case Study for $T_{cc}(3875)^+$, Phys. Rev. Lett. 131 (13) (2023) 131903. [arXiv:2303.09441](https://arxiv.org/abs/2303.09441), doi:10.1103/PhysRevLett.131.131903.
- [257] L. Meng, V. Baru, E. Epelbaum, A. A. Filin, A. M. Gasparyan, Solving the left-hand cut problem in lattice QCD: $T_{cc}(3875)^+$ from finite volume energy levels, Phys. Rev. D 109 (7) (2024) L071506. [arXiv:2312.01930](https://arxiv.org/abs/2312.01930), doi:10.1103/PhysRevD.109.L071506.
- [258] M. T. Hansen, F. Romero-López, S. R. Sharpe, Incorporating $DD\pi$ effects and left-hand cuts in lattice QCD studies of the $T_{cc}(3875)^+$, JHEP 06 (2024) 051. [arXiv:2401.06609](https://arxiv.org/abs/2401.06609), doi:10.1007/JHEP06(2024)051.
- [259] J. M. M. Hall, A. C. P. Hsu, D. B. Leinweber, A. W. Thomas, R. D. Young, Finite-volume matrix Hamiltonian model for a $\Delta \rightarrow N\pi$ system, Phys. Rev. D 87 (9) (2013) 094510. [arXiv:1303.4157](https://arxiv.org/abs/1303.4157), doi:10.1103/PhysRevD.87.094510.
- [260] J. M. M. Hall, W. Kamleh, D. B. Leinweber, B. J. Menadue, B. J. Owen, A. W. Thomas, R. D. Young, Lattice QCD Evidence that the $\Lambda(1405)$ Resonance is an Antikaon-Nucleon Molecule, Phys. Rev. Lett. 114 (13) (2015) 132002. [arXiv:1411.3402](https://arxiv.org/abs/1411.3402), doi:10.1103/PhysRevLett.114.132002.
- [261] Z.-W. Liu, W. Kamleh, D. B. Leinweber, F. M. Stokes, A. W. Thomas, J.-J. Wu, Hamiltonian effective field theory study of the $N^*(1535)$ resonance in lattice QCD, Phys. Rev. Lett. 116 (8) (2016) 082004. [arXiv:1512.00140](https://arxiv.org/abs/1512.00140), doi:10.1103/PhysRevLett.116.082004.
- [262] Z.-W. Liu, J. M. M. Hall, D. B. Leinweber, A. W. Thomas, J.-J. Wu, Structure of the $\Lambda(1405)$ from Hamiltonian effective field theory, Phys. Rev. D 95 (1) (2017) 014506. [arXiv:1607.05856](https://arxiv.org/abs/1607.05856), doi:10.1103/PhysRevD.95.014506.
- [263] J. Bulava, et al., Lattice QCD study of $\pi\Sigma\text{-}K^-\text{N}$ scattering and the $\Lambda(1405)$ resonance, Phys. Rev. D 109 (1) (2024) 014511. [arXiv:2307.13471](https://arxiv.org/abs/2307.13471), doi:10.1103/PhysRevD.109.014511.
- [264] J. Bulava, et al., Two-Pole Nature of the $\Lambda(1405)$ resonance from Lattice QCD, Phys. Rev. Lett. 132 (5) (2024) 051901. [arXiv:2307.10413](https://arxiv.org/abs/2307.10413), doi:10.1103/PhysRevLett.132.051901.
- [265] B. J. Menadue, W. Kamleh, D. B. Leinweber, M. S. Mahbub, Isolating the $\Lambda(1405)$ in Lattice QCD, Phys. Rev. Lett. 108 (2012) 112001. [arXiv:1109.6716](https://arxiv.org/abs/1109.6716), doi:10.1103/PhysRevLett.108.112001.
- [266] R. Molina, M. Döring, Pole structure of the $\Lambda(1405)$ in a recent QCD simulation, Phys. Rev. D 94 (5) (2016) 056010, [Addendum: Phys. Rev. D 94, 079901 (2016)]. [arXiv:1512.05831](https://arxiv.org/abs/1512.05831), doi:10.1103/PhysRevD.94.079901.
- [267] Z. Zhuang, R. Molina, J.-X. Lu, L.-S. Geng, Pole trajectories of the $\Lambda(1405)$ helps establish its dynamical nature (5 2024). [arXiv:2405.07686](https://arxiv.org/abs/2405.07686).
- [268] P. C. Bruns, A. Cieplý, Chirally motivated $\pi\Sigma - \bar{K}N$ model in a finite volume, Eur. Phys. J. A 61 (3) (2025) 44. [arXiv:2412.12977](https://arxiv.org/abs/2412.12977), doi:10.1140/epja/s10050-025-01519-3.

- [269] R. C. Brower, et al., Light scalar meson and decay constant in SU(3) gauge theory with eight dynamical flavors, Phys. Rev. D 110 (5) (2024) 054501. [arXiv:2306.06095](https://arxiv.org/abs/2306.06095), doi:[10.1103/PhysRevD.110.054501](https://doi.org/10.1103/PhysRevD.110.054501).
- [270] A. Rodas, J. J. Dudek, R. G. Edwards, Determination of crossing-symmetric $\pi\pi$ scattering amplitudes and the quark mass evolution of the σ constrained by lattice QCD, Phys. Rev. D 109 (3) (2024) 034513. [arXiv:2304.03762](https://arxiv.org/abs/2304.03762), doi:[10.1103/PhysRevD.109.034513](https://doi.org/10.1103/PhysRevD.109.034513).
- [271] A. Rodas, J. J. Dudek, R. G. Edwards, Quark mass dependence of $\pi\pi$ scattering in isospin 0, 1, and 2 from lattice QCD, Phys. Rev. D 108 (3) (2023) 034513. [arXiv:2303.10701](https://arxiv.org/abs/2303.10701), doi:[10.1103/PhysRevD.108.034513](https://doi.org/10.1103/PhysRevD.108.034513).
- [272] M. Mai, C. Culver, A. Alexandru, M. Döring, F. X. Lee, Cross-channel study of pion scattering from lattice QCD, Phys. Rev. D 100 (11) (2019) 114514. [arXiv:1908.01847](https://arxiv.org/abs/1908.01847), doi:[10.1103/PhysRevD.100.114514](https://doi.org/10.1103/PhysRevD.100.114514).
- [273] D. Guo, A. Alexandru, R. Molina, M. Mai, M. Döring, Extraction of isoscalar $\pi\pi$ phase-shifts from lattice QCD, Phys. Rev. D 98 (1) (2018) 014507. [arXiv:1803.02897](https://arxiv.org/abs/1803.02897), doi:[10.1103/PhysRevD.98.014507](https://doi.org/10.1103/PhysRevD.98.014507).
- [274] Z. Fu, X. Chen, $I = 0$ $\pi\pi$ s-wave scattering length from lattice QCD, Phys. Rev. D 98 (1) (2018) 014514. [arXiv:1712.02219](https://arxiv.org/abs/1712.02219), doi:[10.1103/PhysRevD.98.014514](https://doi.org/10.1103/PhysRevD.98.014514).
- [275] R. A. Briceño, J. J. Dudek, R. G. Edwards, D. J. Wilson, Isoscalar $\pi\pi$ scattering and the σ meson resonance from QCD, Phys. Rev. Lett. 118 (2) (2017) 022002. [arXiv:1607.05900](https://arxiv.org/abs/1607.05900), doi:[10.1103/PhysRevLett.118.022002](https://doi.org/10.1103/PhysRevLett.118.022002).
- [276] J. Haidenbauer, G. Krein, U.-G. Meißner, L. Tolos, DN interaction from meson exchange, Eur. Phys. J. A 47 (2011) 18. [arXiv:1008.3794](https://arxiv.org/abs/1008.3794), doi:[10.1140/epja/i2011-11018-3](https://doi.org/10.1140/epja/i2011-11018-3).
- [277] E. Oset, A. Ramos, Nonperturbative chiral approach to s wave $\bar{K}N$ interactions, Nucl. Phys. A 635 (1998) 99–120. [arXiv:nucl-th/9711022](https://arxiv.org/abs/nucl-th/9711022), doi:[10.1016/S0375-9474\(98\)00170-5](https://doi.org/10.1016/S0375-9474(98)00170-5).
- [278] G. Janssen, B. C. Pearce, K. Holinde, J. Speth, On the structure of the scalar mesons $f_0(975)$ and $a_0(980)$, Phys. Rev. D 52 (1995) 2690–2700. [arXiv:nucl-th/9411021](https://arxiv.org/abs/nucl-th/9411021), doi:[10.1103/PhysRevD.52.2690](https://doi.org/10.1103/PhysRevD.52.2690).
- [279] O. Krehl, R. Rapp, J. Speth, Meson-meson scattering: $K\bar{K}$ thresholds and $f_0(980)$ - $a_0(980)$ mixing, Phys. Lett. B 390 (1997) 23–28. [arXiv:nucl-th/9609013](https://arxiv.org/abs/nucl-th/9609013), doi:[10.1016/S0370-2693\(96\)01425-6](https://doi.org/10.1016/S0370-2693(96)01425-6).
- [280] J. A. Oller, U. G. Meißner, Chiral dynamics in the presence of bound states: Kaon nucleon interactions revisited, Phys. Lett. B 500 (2001) 263–272. [arXiv:hep-ph/0011146](https://arxiv.org/abs/hep-ph/0011146), doi:[10.1016/S0370-2693\(01\)00078-8](https://doi.org/10.1016/S0370-2693(01)00078-8).
- [281] D. Jido, J. A. Oller, E. Oset, A. Ramos, U.-G. Meißner, Chiral dynamics of the two $\Lambda(1405)$ states, Nucl. Phys. A 725 (2003) 181–200. [arXiv:nucl-th/0303062](https://arxiv.org/abs/nucl-th/0303062), doi:[10.1016/S0375-9474\(03\)01598-7](https://doi.org/10.1016/S0375-9474(03)01598-7).
- [282] V. Bernard, M. Lage, U.-G. Meißner, A. Rusetsky, Scalar mesons in a finite volume, JHEP 01 (2011) 019. [arXiv:1010.6018](https://arxiv.org/abs/1010.6018), doi:[10.1007/JHEP01\(2011\)019](https://doi.org/10.1007/JHEP01(2011)019).
- [283] M. Döring, M. Mai, U.-G. Meißner, Finite volume effects and quark mass dependence of the $N(1535)$ and $N(1650)$, Phys. Lett. B 722 (2013) 185–192. [arXiv:1302.4065](https://arxiv.org/abs/1302.4065), doi:[10.1016/j.physletb.2013.04.016](https://doi.org/10.1016/j.physletb.2013.04.016).
- [284] C. B. Lang, L. Leskovec, M. Padmanath, S. Prelovsek, Pion-nucleon scattering in the Roper channel from lattice QCD, Phys. Rev. D 95 (1) (2017) 014510. [arXiv:1610.01422](https://arxiv.org/abs/1610.01422), doi:[10.1103/PhysRevD.95.014510](https://doi.org/10.1103/PhysRevD.95.014510).
- [285] A. L. Kiratidis, W. Kamleh, D. B. Leinweber, Z.-W. Liu, F. M. Stokes, A. W. Thomas, Search for low-lying lattice QCD eigenstates in the Roper regime, Phys. Rev. D 95 (7) (2017) 074507. [arXiv:1608.03051](https://arxiv.org/abs/1608.03051), doi:[10.1103/PhysRevD.95.074507](https://doi.org/10.1103/PhysRevD.95.074507).
- [286] Z.-W. Liu, W. Kamleh, D. B. Leinweber, F. M. Stokes, A. W. Thomas, J.-J. Wu, Hamiltonian effective field theory study of the $N^*(1440)$ resonance in lattice QCD, Phys. Rev. D 95 (3) (2017) 034034. [arXiv:1607.04536](https://arxiv.org/abs/1607.04536), doi:[10.1103/PhysRevD.95.034034](https://doi.org/10.1103/PhysRevD.95.034034).
- [287] B. Hörl, A. Hanlon, Two- and three-pion finite-volume spectra at maximal isospin from lattice QCD, Phys. Rev. Lett. 123 (14) (2019) 142002. [arXiv:1905.04277](https://arxiv.org/abs/1905.04277), doi:[10.1103/PhysRevLett.123.142002](https://doi.org/10.1103/PhysRevLett.123.142002).
- [288] C. Culver, M. Mai, R. Brett, A. Alexandru, M. Döring, Three pion spectrum in the $I = 3$ channel from lattice QCD, Phys. Rev. D 101 (11) (2020) 114507. [arXiv:1911.09047](https://arxiv.org/abs/1911.09047), doi:[10.1103/PhysRevD.101.114507](https://doi.org/10.1103/PhysRevD.101.114507).
- [289] M. Fischer, B. Kostrzewa, L. Liu, F. Romero-López, M. Ueding, C. Urbach, Scattering of two and three physical pions at maximal isospin from lattice QCD, Eur. Phys. J. C 81 (5) (2021) 436. [arXiv:2008.03035](https://arxiv.org/abs/2008.03035), doi:[10.1140/epjc/s10052-021-09206-5](https://doi.org/10.1140/epjc/s10052-021-09206-5).
- [290] M. T. Hansen, R. A. Briceño, R. G. Edwards, C. E. Thomas, D. J. Wilson, Energy-Dependent $\pi^+\pi^+\pi^+$ Scattering Amplitude from QCD, Phys. Rev. Lett. 126 (2021) 012001. [arXiv:2009.04931](https://arxiv.org/abs/2009.04931), doi:[10.1103/PhysRevLett.126.012001](https://doi.org/10.1103/PhysRevLett.126.012001).
- [291] T. D. Blanton, A. D. Hanlon, B. Hörl, C. Morningstar, F. Romero-López, S. R. Sharpe, Interactions of two and three mesons including higher partial waves from lattice QCD, JHEP 10 (2021) 023. [arXiv:2106.05590](https://arxiv.org/abs/2106.05590), doi:[10.1007/JHEP10\(2021\)023](https://doi.org/10.1007/JHEP10(2021)023).
- [292] S. R. Beane, et al., Charged multihadron systems in lattice QCD+QED, Phys. Rev. D 103 (5) (2021) 054504. [arXiv:2003.12130](https://arxiv.org/abs/2003.12130), doi:[10.1103/PhysRevD.103.054504](https://doi.org/10.1103/PhysRevD.103.054504).
- [293] P. Bühlmann, U. Wenger, Finite-volume effects and meson scattering in the 2-flavour Schwinger model, PoS LATTICE2021 (2022) 463. [arXiv:2112.15228](https://arxiv.org/abs/2112.15228), doi:[10.22323/1.396.0463](https://doi.org/10.22323/1.396.0463).
- [294] S. M. Dawid, Z. T. Draper, A. D. Hanlon, B. Hörl, C. Morningstar, F. Romero-López, S. R. Sharpe, S. Skinner, Two- and three-meson scattering amplitudes with physical quark masses from lattice QCD (2025). [arXiv:2502.17976](https://arxiv.org/abs/2502.17976).
- [295] S. M. Dawid, F. Romero-López, S. R. Sharpe, Finite- and infinite-volume study of $DD\pi$ scattering, JHEP 01 (2025) 060. [arXiv:2409.17059](https://arxiv.org/abs/2409.17059), doi:[10.1007/JHEP01\(2025\)060](https://doi.org/10.1007/JHEP01(2025)060).
- [296] Z. T. Draper, S. R. Sharpe, Three-particle formalism for multiple channels: the $\eta\pi\pi + K\bar{K}\pi$ system in isosymmetric QCD, JHEP 07 (2024) 083. [arXiv:2403.20064](https://arxiv.org/abs/2403.20064), doi:[10.1007/JHEP07\(2024\)083](https://doi.org/10.1007/JHEP07(2024)083).
- [297] M. T. Hansen, S. R. Sharpe, Relativistic, model-independent, three-particle quantization condition, Phys. Rev. D 90 (11) (2014) 116003. [arXiv:1408.5933](https://arxiv.org/abs/1408.5933), doi:[10.1103/PhysRevD.90.116003](https://doi.org/10.1103/PhysRevD.90.116003).
- [298] P. F. Bedaque, H. W. Hammer, U. van Kolck, Renormalization of the three-body system with short range interactions, Phys. Rev. Lett. 82 (1999) 463–467. [arXiv:nucl-th/9809025](https://arxiv.org/abs/nucl-th/9809025), doi:[10.1103/PhysRevLett.82.463](https://doi.org/10.1103/PhysRevLett.82.463).
- [299] M. Döring, H. W. Hammer, M. Mai, J. Y. Pang, t. A. Rusetsky, J. Wu, Three-body spectrum in a finite volume: the role of cubic symmetry, Phys. Rev. D 97 (11) (2018) 114508. [arXiv:1802.03362](https://arxiv.org/abs/1802.03362), doi:[10.1103/PhysRevD.97.114508](https://doi.org/10.1103/PhysRevD.97.114508).
- [300] D. Severt, M. Mai, U.-G. Meißner, Particle-dimer approach for the Roper resonance in a finite volume, JHEP 04 (2023) 100. [arXiv:2212.02171](https://arxiv.org/abs/2212.02171), doi:[10.1007/JHEP04\(2023\)100](https://doi.org/10.1007/JHEP04(2023)100).
- [301] F. Gross, et al., 50 Years of Quantum Chromodynamics, Eur. Phys. J. C 83 (2023) 1125. [arXiv:2212.11107](https://arxiv.org/abs/2212.11107), doi:[10.1140/epjc/s10052-023-11949-2](https://doi.org/10.1140/epjc/s10052-023-11949-2).
- [302] A. Deur, S. J. Brodsky, C. D. Roberts, QCD running couplings and effective charges, Prog. Part. Nucl. Phys. 134 (2024) 104081. [arXiv:2303.00723](https://arxiv.org/abs/2303.00723), doi:[10.1016/j.ppnp.2023.104081](https://doi.org/10.1016/j.ppnp.2023.104081).
- [303] B. H. Bransden, R. G. Moorhouse, The Pion-nucleon system, Princeton Legacy Library, Princeton University Press, Princeton, NJ, 2015.
- [304] G. Höhler, F. Kaiser, R. Koch, E. Pietarinen, HANDBOOK OF PION NUCLEON SCATTERING, Vol. 12N1, 1979.
- [305] T. E. O. Ericson, W. Weise, Pions and Nuclei, Clarendon Press, Oxford, UK, 1988.
- [306] R. Levi-Setti, T. Lasinski, Strongly interacting particles [by] Riccardo Levi Setti [and] Thomas Lasinski., Chicago lectures in physics, University of Chicago Press, Chiago, 1973.

- [307] S. U. Chung, J. Brose, R. Hackmann, E. Klempt, S. Spanier, C. Strassburger, Partial wave analysis in K matrix formalism, Annalen Phys. 4 (1995) 404–430. [doi:10.1002/andp.19955070504](https://doi.org/10.1002/andp.19955070504).
- [308] R. H. Dalitz, Strange Particles and Strong Interactions, paperback Edition, Oxford University Press, 1962.
- [309] F. Close, S. Donnachie, G. Shaw (Eds.), Electromagnetic interactions and hadronic structure, Vol. 25, Cambridge University Press, 2009.
- [310] J. L. Rosner, The Classification and Decays of Resonant Particles, Phys. Rept. 11 (1974) 189–326. [doi:10.1016/0370-1573\(74\)90007-6](https://doi.org/10.1016/0370-1573(74)90007-6).
- [311] A. Donnachie, Partial wave analysis and baryon resonances (in meson-baryon scattering), Reports on Progress in Physics 36 (6) (1973) 695.
- [312] R. H. Dalitz, R. G. Moorhouse, What is resonance?, Proc. Roy. Soc. Lond. A 318 (1970) 279–298. [doi:10.1098/rspa.1970.0145](https://doi.org/10.1098/rspa.1970.0145).
- [313] E. Klempt, J.-M. Richard, Baryon spectroscopy, Rev. Mod. Phys. 82 (2010) 1095–1153. [arXiv:0901.2055](https://arxiv.org/abs/0901.2055), [doi:10.1103/RevModPhys.82.1095](https://doi.org/10.1103/RevModPhys.82.1095).
- [314] J.-M. Richard, An introduction to the quark model, in: Ferrara International School Niccolò Cabeo 2012: Hadronic spectroscopy, 2012. [arXiv:1205.4326](https://arxiv.org/abs/1205.4326).
- [315] G. Eichmann, Theory Introduction to Baryon Spectroscopy, Few Body Syst. 63 (3) (2022) 57. [arXiv:2202.13378](https://arxiv.org/abs/2202.13378), [doi:10.1007/s00601-022-01756-y](https://doi.org/10.1007/s00601-022-01756-y).
- [316] G. Eichmann, Hadron physics with functional methods (3 2025). [arXiv:2503.10397](https://arxiv.org/abs/2503.10397).
- [317] M. F. M. Lutz, et al., Resonances in QCD, Nucl. Phys. A 948 (2016) 93–105. [arXiv:1511.09353](https://arxiv.org/abs/1511.09353), [doi:10.1016/j.nuclphysa.2016.01.070](https://doi.org/10.1016/j.nuclphysa.2016.01.070).
- [318] N. Isgur, G. Karl, Hyperfine Interactions in Negative Parity Baryons, Phys. Lett. B 72 (1977) 109. [doi:10.1016/0370-2693\(77\)90074-0](https://doi.org/10.1016/0370-2693(77)90074-0).
- [319] N. Isgur, G. Karl, Positive Parity Excited Baryons in a Quark Model with Hyperfine Interactions, Phys. Rev. D 19 (1979) 2653, [Erratum: Phys.Rev.D 23, 817 (1981)]. [doi:10.1103/PhysRevD.19.2653](https://doi.org/10.1103/PhysRevD.19.2653).
- [320] S. Capstick, N. Isgur, Baryons in a relativized quark model with chromodynamics, Phys. Rev. D 34 (9) (1986) 2809–2835. [doi:10.1103/physrevd.34.2809](https://doi.org/10.1103/physrevd.34.2809).
- [321] M. Ferraris, M. M. Giannini, M. Pizzo, E. Santopinto, L. Tiator, A Three body force model for the baryon spectrum, Phys. Lett. B 364 (1995) 231–238. [doi:10.1016/0370-2693\(95\)01091-2](https://doi.org/10.1016/0370-2693(95)01091-2).
- [322] L. Y. Glozman, Z. Papp, W. Plessas, Light baryons in a constituent quark model with chiral dynamics, Phys. Lett. B 381 (1996) 311–316. [arXiv:hep-ph/9601353](https://arxiv.org/abs/hep-ph/9601353), [doi:10.1016/0370-2693\(96\)00610-7](https://doi.org/10.1016/0370-2693(96)00610-7).
- [323] L. Y. Glozman, W. Plessas, K. Varga, R. F. Wagenbrunn, Unified description of light and strange baryon spectra, Phys. Rev. D 58 (1998) 094030. [arXiv:hep-ph/9706507](https://arxiv.org/abs/hep-ph/9706507), [doi:10.1103/PhysRevD.58.094030](https://doi.org/10.1103/PhysRevD.58.094030).
- [324] S. Capstick, W. Roberts, Quark models of baryon masses and decays, Prog. Part. Nucl. Phys. 45 (2000) S241–S331. [arXiv:nucl-th/0008028](https://arxiv.org/abs/nucl-th/0008028), [doi:10.1016/S0146-6410\(00\)00109-5](https://doi.org/10.1016/S0146-6410(00)00109-5).
- [325] U. Loring, K. Kretzschmar, B. C. Metsch, H. R. Petry, Relativistic quark models of baryons with instantaneous forces: Theoretical background, Eur. Phys. J. A 10 (2001) 309–346. [arXiv:hep-ph/0103287](https://arxiv.org/abs/hep-ph/0103287), [doi:10.1007/s100500170117](https://doi.org/10.1007/s100500170117).
- [326] U. Loring, B. C. Metsch, H. R. Petry, The Light baryon spectrum in a relativistic quark model with instanton induced quark forces: The Nonstrange baryon spectrum and ground states, Eur. Phys. J. A 10 (2001) 395–446. [arXiv:hep-ph/0103289](https://arxiv.org/abs/hep-ph/0103289), [doi:10.1007/s100500170105](https://doi.org/10.1007/s100500170105).
- [327] U. Loring, B. C. Metsch, H. R. Petry, The Light baryon spectrum in a relativistic quark model with instanton induced quark forces: The Strange baryon spectrum, Eur. Phys. J. A 10 (2001) 447–486. [arXiv:hep-ph/0103290](https://arxiv.org/abs/hep-ph/0103290), [doi:10.1007/s100500170106](https://doi.org/10.1007/s100500170106).
- [328] M. Ronniger, B. C. Metsch, Effects of a spin-flavour dependent interaction on light-flavoured baryon helicity amplitudes, Eur. Phys. J. A 49 (2013) 8. [arXiv:1207.2640](https://arxiv.org/abs/1207.2640), [doi:10.1140/epja/i2013-13008-9](https://doi.org/10.1140/epja/i2013-13008-9).
- [329] E. Santopinto, An Interacting quark-diquark model of baryons, Phys. Rev. C 72 (2005) 022201. [arXiv:hep-ph/0412319](https://arxiv.org/abs/hep-ph/0412319), [doi:10.1103/PhysRevC.72.022201](https://doi.org/10.1103/PhysRevC.72.022201).
- [330] M. De Sanctis, J. Ferretti, E. Santopinto, A. Vassallo, Relativistic quark-diquark model of baryons with a spin-isospin transition interaction: Non-strange baryon spectrum and nucleon magnetic moments, Eur. Phys. J. A 52 (5) (2016) 121. [arXiv:1410.0590](https://arxiv.org/abs/1410.0590), [doi:10.1140/epja/i2016-16121-3](https://doi.org/10.1140/epja/i2016-16121-3).
- [331] E. Santopinto, J. Ferretti, Strange and nonstrange baryon spectra in the relativistic interacting quark-diquark model with a Gürsey and Radicati-inspired exchange interaction, Phys. Rev. C 92 (2) (2015) 025202. [arXiv:1412.7571](https://arxiv.org/abs/1412.7571), [doi:10.1103/PhysRevC.92.025202](https://doi.org/10.1103/PhysRevC.92.025202).
- [332] M. Y. Barabanyov, et al., Diquark correlations in hadron physics: Origin, impact and evidence, Prog. Part. Nucl. Phys. 116 (2021) 103835. [arXiv:2008.07630](https://arxiv.org/abs/2008.07630), [doi:10.1016/j.ppnp.2020.103835](https://doi.org/10.1016/j.ppnp.2020.103835).
- [333] M. M. Giannini, E. Santopinto, A. Vassallo, Hypercentral constituent quark model and isospin dependence, Eur. Phys. J. A 12 (2001) 447–452. [arXiv:nucl-th/0111073](https://arxiv.org/abs/nucl-th/0111073), [doi:10.1007/s10050-001-8668-y](https://doi.org/10.1007/s10050-001-8668-y).
- [334] M. M. Giannini, E. Santopinto, The hypercentral Constituent Quark Model and its application to baryon properties, Chin. J. Phys. 53 (2015) 020301. [arXiv:1501.03722](https://arxiv.org/abs/1501.03722), [doi:10.6122/CJP.20150120](https://doi.org/10.6122/CJP.20150120).
- [335] C. Menapara, Z. Shah, A. Kumar Rai, Spectroscopic properties of Δ baryons, Chin. Phys. C 45 (2) (2021) 023102. [arXiv:2010.04386](https://arxiv.org/abs/2010.04386), [doi:10.1088/1674-1137/abcc58](https://doi.org/10.1088/1674-1137/abcc58).
- [336] C. Menapara, A. K. Rai, Spectroscopy of light baryons: Δ resonances, Int. J. Mod. Phys. A 37 (27) (2022) 2250177. [arXiv:2204.08840](https://arxiv.org/abs/2204.08840), [doi:10.1142/S0217751X22501779](https://doi.org/10.1142/S0217751X22501779).
- [337] F. Gross, G. Ramalho, M. T. Peña, A Pure S-wave covariant model for the nucleon, Phys. Rev. C 77 (2008) 015202. [arXiv:nucl-th/0606029](https://arxiv.org/abs/nucl-th/0606029), [doi:10.1103/PhysRevC.77.015202](https://doi.org/10.1103/PhysRevC.77.015202).
- [338] G. Ramalho, M. T. Peña, F. Gross, A Covariant model for the nucleon and the Delta, Eur. Phys. J. A 36 (2008) 329–348. [arXiv:0803.3034](https://arxiv.org/abs/0803.3034), [doi:10.1140/epja/i2008-10599-0](https://doi.org/10.1140/epja/i2008-10599-0).
- [339] G. Ramalho, M. T. Peña, Valence quark contribution for the $\gamma N \rightarrow \Delta$ quadrupole transition extracted from lattice QCD, Phys. Rev. D 80 (2009) 013008. [arXiv:0901.4310](https://arxiv.org/abs/0901.4310), [doi:10.1103/PhysRevD.80.013008](https://doi.org/10.1103/PhysRevD.80.013008).
- [340] G. Ramalho, M. T. Peña, F. Gross, Electromagnetic form factors of the Delta with D-waves, Phys. Rev. D 81 (2010) 113011. [arXiv:1002.4170](https://arxiv.org/abs/1002.4170), [doi:10.1103/PhysRevD.81.113011](https://doi.org/10.1103/PhysRevD.81.113011).
- [341] G. Ramalho, M. T. Peña, A covariant model for the $\gamma N \rightarrow N(1535)$ transition at high momentum transfer, Phys. Rev. D 84 (2011) 033007. [arXiv:1105.2223](https://arxiv.org/abs/1105.2223), [doi:10.1103/PhysRevD.84.033007](https://doi.org/10.1103/PhysRevD.84.033007).
- [342] L. E. Marcucci, F. Gross, M. T. Peña, M. Piarulli, R. Schiavilla, I. Sick, A. Stadler, J. W. Van Orden, M. Viviani, Electromagnetic Structure of Few-Nucleon Ground States, J. Phys. G 43 (2016) 023002. [arXiv:1504.05063](https://arxiv.org/abs/1504.05063), [doi:10.1088/0954-3899/43/2/023002](https://doi.org/10.1088/0954-3899/43/2/023002).
- [343] G. Ramalho, M. T. Peña, J. Weil, H. van Hees, U. Mosel, Role of the pion electromagnetic form factor in the $\Delta(1232) \rightarrow \gamma^* N$ timelike transition, Phys. Rev. D 93 (3) (2016) 033004. [arXiv:1512.03764](https://arxiv.org/abs/1512.03764), [doi:10.1103/PhysRevD.93.033004](https://doi.org/10.1103/PhysRevD.93.033004).
- [344] G. Ramalho, M. T. Peña, Timelike $\gamma^* N \rightarrow \Delta$ form factors and Δ Dalitz decay, Phys. Rev. D 85 (2012) 113014. [arXiv:1205.2575](https://arxiv.org/abs/1205.2575), [doi:10.1103/PhysRevD.85.113014](https://doi.org/10.1103/PhysRevD.85.113014).
- [345] G. Eichmann, M. T. Peña, R. D. Torres, Five-body systems with Bethe-Salpeter equations (2 2025). [arXiv:2502.17944](https://arxiv.org/abs/2502.17944).

- [346] J. Vijande, F. Fernandez, A. Valcarce, Constituent quark model study of the meson spectra, *J. Phys. G* 31 (2005) 481. [arXiv:hep-ph/0411299](#), [doi:10.1088/0954-3899/31/5/017](#).
- [347] F. Huang, Z. Y. Zhang, Y. W. Yu, $N\phi$ state in chiral quark model, *Phys. Rev. C* 73 (2006) 025207. [arXiv:nucl-th/0512079](#), [doi:10.1103/PhysRevC.73.025207](#).
- [348] H. Garcilazo, J. Vijande, A. Valcarce, Faddeev study of heavy baryon spectroscopy, *J. Phys. G* 34 (2007) 961–976. [arXiv:hep-ph/0703257](#), [doi:10.1088/0954-3899/34/5/014](#).
- [349] P. Bicudo, M. Cardoso, F. J. Llanes-Estrada, T. Van Cauteren, Mapping chiral symmetry breaking in the excited baryon spectrum, *Phys. Rev. D* 94 (5) (2016) 054006. [arXiv:1605.05171](#), [doi:10.1103/PhysRevD.94.054006](#).
- [350] H.-H. Zhong, M.-S. Liu, R.-H. Ni, M.-Y. Chen, X.-H. Zhong, Q. Zhao, Unified study of nucleon and Δ baryon spectra and their strong decays with chiral dynamics, *Phys. Rev. D* 110 (11) (2024) 116034. [arXiv:2409.07998](#), [doi:10.1103/PhysRevD.110.116034](#).
- [351] G. Ramalho, M. T. Peña, Electromagnetic transition form factors of baryon resonances, *Prog. Part. Nucl. Phys.* 136 (2024) 104097. [arXiv:2306.13900](#), [doi:10.1016/j.ppnp.2024.104097](#).
- [352] G. Ramalho, Analytic parametrizations of the $\gamma^* N \rightarrow N(1440)$ form factors inspired by light-front holography, *Phys. Rev. D* 96 (5) (2017) 054021. [arXiv:1706.05707](#), [doi:10.1103/PhysRevD.96.054021](#).
- [353] G. Ramalho, Semirelativistic approximation to the $\gamma^* N \rightarrow N(1520)$ and $\gamma^* N \rightarrow N(1535)$ transition form factors, *Phys. Rev. D* 95 (5) (2017) 054008. [arXiv:1612.09555](#), [doi:10.1103/PhysRevD.95.054008](#).
- [354] X.-H. Zhong, Q. Zhao, η' photoproduction on the nucleons in the quark model, *Phys. Rev. C* 84 (2011) 065204. [arXiv:1110.5466](#), [doi:10.1103/PhysRevC.84.065204](#).
- [355] J. He, B. Saghai, Combined study of $\gamma p \rightarrow \eta p$ and $\pi^- p \rightarrow \eta n$ in a chiral constituent quark approach, *Phys. Rev. C* 80 (2009) 015207. [arXiv:0812.1617](#), [doi:10.1103/PhysRevC.80.015207](#).
- [356] B. Golli, S. Sirca, A Chiral quark model for meson electro-production in the S11 partial wave, *Eur. Phys. J. A* 47 (2011) 61. [arXiv:1101.5527](#), [doi:10.1140/epja/i2011-11061-0](#).
- [357] C. An, B. Saghai, Strong decay of low-lying S_{11} and D_{13} nucleon resonances to pseudoscalar mesons and octet baryons, *Phys. Rev. C* 84 (2011) 045204. [arXiv:1108.3282](#), [doi:10.1103/PhysRevC.84.045204](#).
- [358] B. Golli, S. Sirca, M. Fiolhais, Pion electro-production in the Roper region in chiral quark models, *Eur. Phys. J. A* 42 (2009) 185–193. [arXiv:0906.2066](#), [doi:10.1140/epja/i2009-10878-2](#).
- [359] B. Golli, S. Širca, A chiral quark model for meson electroproduction in the region of D-wave resonances, *Eur. Phys. J. A* 49 (2013) 111. [arXiv:1306.3330](#), [doi:10.1140/epja/i2013-13111-y](#).
- [360] B. Golli, S. Širca, Eta and kaon production in a chiral quark model, *Eur. Phys. J. A* 52 (9) (2016) 279. [arXiv:1604.01937](#), [doi:10.1140/epja/i2016-16279-6](#).
- [361] L.-Y. Xiao, F. Ouyang, K.-L. Wang, X.-H. Zhong, Combined analysis of the $\pi^- p \rightarrow K^0 \Lambda$, ηn reactions in a chiral quark model, *Phys. Rev. C* 94 (3) (2016) 035202. [arXiv:1602.04455](#), [doi:10.1103/PhysRevC.94.035202](#).
- [362] K. Bermuth, D. Drechsel, L. Tiator, J. B. Seaborn, Photoproduction of Δ and Roper Resonances in the Cloudy Bag Model, *Phys. Rev. D* 37 (1988) 89–100. [doi:10.1103/PhysRevD.37.89](#).
- [363] S. Scherer, D. Drechsel, L. Tiator, Photoproduction of Pions in Chiral Bag Models, *Phys. Lett. B* 193 (1987) 1–6. [doi:10.1016/0370-2693\(87\)90446-1](#).
- [364] E. E. Jenkins, R. F. Lebed, Baryon mass splittings in the $1/N(c)$ expansion, *Phys. Rev. D* 52 (1995) 282–294. [arXiv:hep-ph/9502227](#), [doi:10.1103/PhysRevD.52.282](#).
- [365] C. E. Carlson, C. D. Carone, J. L. Goity, R. F. Lebed, Operator analysis of $1 - 1$ baryon masses in large $N(c)$ QCD, *Phys. Rev. D* 59 (1999) 114008. [arXiv:hep-ph/9812440](#), [doi:10.1103/PhysRevD.59.114008](#).
- [366] C. E. Carlson, C. D. Carone, J. L. Goity, R. F. Lebed, Masses of orbitally excited baryons in large $N(c)$ QCD, *Phys. Lett. B* 438 (1998) 327–335. [arXiv:hep-ph/9807334](#), [doi:10.1016/S0370-2693\(98\)00992-7](#).
- [367] C. L. Schat, J. L. Goity, N. N. Scoccola, Masses of the 70- baryons in large $N(c)$ QCD, *Phys. Rev. Lett.* 88 (2002) 102002. [arXiv:hep-ph/0111082](#), [doi:10.1103/PhysRevLett.88.102002](#).
- [368] J. L. Goity, C. L. Schat, N. N. Scoccola, Negative parity 70-plet baryon masses in the $1/N(c)$ expansion, *Phys. Rev. D* 66 (2002) 114014. [arXiv:hep-ph/0209174](#), [doi:10.1103/PhysRevD.66.114014](#).
- [369] J. L. Goity, C. Schat, N. Scoccola, Decays of non-strange negative parity baryons in the $1/N(c)$ expansion, *Phys. Rev. D* 71 (2005) 034016. [arXiv:hep-ph/0411092](#), [doi:10.1103/PhysRevD.71.034016](#).
- [370] C. Garcia-Recio, J. Nieves, L. L. Salcedo, Large N_c Weinberg-Tomozawa interaction and negative parity s-wave baryon resonances, *Phys. Rev. D* 74 (2006) 036004. [arXiv:hep-ph/0605059](#), [doi:10.1103/PhysRevD.74.036004](#).
- [371] N. N. Scoccola, J. L. Goity, N. Matagne, Analysis of Negative Parity Baryon Photoproduction Amplitudes in the $1/N_c$ Expansion, *Phys. Lett. B* 663 (2008) 222–227. [arXiv:0711.4203](#), [doi:10.1016/j.physletb.2008.03.056](#).
- [372] A. Cherman, T. D. Cohen, R. F. Lebed, All you need is N : Baryon spectroscopy in two large N limits, *Phys. Rev. D* 80 (2009) 036002. [arXiv:0906.2400](#), [doi:10.1103/PhysRevD.80.036002](#).
- [373] N. Matagne, F. Stancu, Updated $1/N_c$ expansion analysis of $[56, 2^+]$ and $[70, \ell^+]$ baryon multiplets, *Phys. Rev. D* 93 (9) (2016) 096004. [arXiv:1604.07324](#), [doi:10.1103/PhysRevD.93.096004](#).
- [374] N. Matagne, F. Stancu, Highly excited negative parity baryons in the $1/N_c$ expansion, *Phys. Rev. D* 85 (2012) 116003. [arXiv:1205.5207](#), [doi:10.1103/PhysRevD.85.116003](#).
- [375] N. Matagne, F. Stancu, Baryon resonances in large N_c QCD, *Rev. Mod. Phys.* 87 (2015) 211–245. [arXiv:1406.1791](#), [doi:10.1103/RevModPhys.87.211](#).
- [376] I. G. Aznauryan, V. Burkert, Electroexcitation of nucleon resonances of the $[70, 1^-]$ multiplet in a light-front relativistic quark model, *Phys. Rev. C* 95 (6) (2017) 065207. [arXiv:1703.01751](#), [doi:10.1103/PhysRevC.95.065207](#).
- [377] I. G. Aznauryan, V. D. Burkert, Nucleon electromagnetic form factors and electroexcitation of low lying nucleon resonances in a light-front relativistic quark model, *Phys. Rev. C* 85 (2012) 055202. [arXiv:1201.5759](#), [doi:10.1103/PhysRevC.85.055202](#).
- [378] I. G. Aznauryan, et al., Studies of Nucleon Resonance Structure in Exclusive Meson Electroproduction, *Int. J. Mod. Phys. E* 22 (2013) 1330015. [arXiv:1212.4891](#), [doi:10.1142/S0218301313300154](#).
- [379] I. G. Aznauryan, et al., Electroexcitation of nucleon resonances from CLAS data on single pion electroproduction, *Phys. Rev. C* 80 (2009) 055203. [arXiv:0909.2349](#), [doi:10.1103/PhysRevC.80.055203](#).
- [380] I. G. Aznauryan, et al., Electroexcitation of nucleon resonances from CLAS data on single pion electroproduction, *Phys. Rev. C* 80 (2009) 055203. [arXiv:0909.2349](#), [doi:10.1103/PhysRevC.80.055203](#).
- [381] I. G. Aznauryan, V. D. Burkert, H. Egiyan, K. Joo, R. Minehart, L. C. Smith, Electroexcitation of the $P(33)(1232)$, $P(11)(1440)$, $D(13)(1520)$, $S(11)(1535)$ at $Q^2 = 0.4$ and 0.65 (GeV/c^2), *Phys. Rev. C* 71 (2005) 015201. [arXiv:nucl-th/0407021](#), [doi:10.1103/PhysRevC.71.015201](#).
- [382] I. G. Aznauryan, V. D. Burkert, Electroexcitation of nucleon resonances, *Prog. Part. Nucl. Phys.* 67 (2012) 1–54. [arXiv:1109.1720](#),

- [doi:10.1016/j.ppnp.2011.08.001](https://doi.org/10.1016/j.ppnp.2011.08.001).
- [383] D. S. Carman, R. W. Gothe, V. I. Mokeev, C. D. Roberts, Nucleon Resonance Electroexcitation Amplitudes and Emergent Hadron Mass, Particles 6 (1) (2023) 416–439. [arXiv:2301.07777](https://arxiv.org/abs/2301.07777), [doi:10.3390/particles6010023](https://doi.org/10.3390/particles6010023).
 - [384] V. I. Mokeev, D. S. Carman, Photo- and Electrocouplings of Nucleon Resonances, Few Body Syst. 63 (3) (2022) 59. [arXiv:2202.04180](https://arxiv.org/abs/2202.04180), [doi:10.1007/s00601-022-01760-2](https://doi.org/10.1007/s00601-022-01760-2).
 - [385] L.-Y. Dai, J. Haidenbauer, U.-G. Meißner, Electromagnetic Form Factors of Hyperons in the Timelike Region: A Short Review, Chin. Phys. Lett. 42 (3) (2025) 030202. [arXiv:2412.07543](https://arxiv.org/abs/2412.07543), [doi:10.1088/0256-307X/42/3/030202](https://doi.org/10.1088/0256-307X/42/3/030202).
 - [386] S. Diehl, et al., Exploring Baryon Resonances with Transition Generalized Parton Distributions: Status and Perspectives (5 2024). [arXiv:2405.15386](https://arxiv.org/abs/2405.15386).
 - [387] J. Erlich, An Introduction to Holographic QCD for Nonspecialists, Contemp. Phys. 56 (2) (2015) 159–171. [arXiv:1407.5002](https://arxiv.org/abs/1407.5002), [doi:10.1080/00107514.2014.942079](https://doi.org/10.1080/00107514.2014.942079).
 - [388] J. Erlich, E. Katz, D. T. Son, M. A. Stephanov, QCD and a holographic model of hadrons, Phys. Rev. Lett. 95 (2005) 261602. [arXiv:hep-ph/0501128](https://arxiv.org/abs/hep-ph/0501128), [doi:10.1103/PhysRevLett.95.261602](https://doi.org/10.1103/PhysRevLett.95.261602).
 - [389] G. F. de Teramond, S. J. Brodsky, Hadronic spectrum of a holographic dual of QCD, Phys. Rev. Lett. 94 (2005) 201601. [arXiv:hep-th/0501022](https://arxiv.org/abs/hep-th/0501022), [doi:10.1103/PhysRevLett.94.201601](https://doi.org/10.1103/PhysRevLett.94.201601).
 - [390] A. Karch, E. Katz, D. T. Son, M. A. Stephanov, Linear confinement and AdS/QCD, Phys. Rev. D 74 (2006) 015005. [arXiv:hep-ph/0602229](https://arxiv.org/abs/hep-ph/0602229), [doi:10.1103/PhysRevD.74.015005](https://doi.org/10.1103/PhysRevD.74.015005).
 - [391] G. F. de Teramond, S. J. Brodsky, Light-Front Holography: A First Approximation to QCD, Phys. Rev. Lett. 102 (2009) 081601. [arXiv:0809.4899](https://arxiv.org/abs/0809.4899), [doi:10.1103/PhysRevLett.102.081601](https://doi.org/10.1103/PhysRevLett.102.081601).
 - [392] H. Forkel, E. Klemt, Diquark correlations in baryon spectroscopy and holographic QCD, Phys. Lett. B 679 (2009) 77–80. [arXiv:0810.2959](https://arxiv.org/abs/0810.2959), [doi:10.1016/j.physletb.2009.07.008](https://doi.org/10.1016/j.physletb.2009.07.008).
 - [393] S. J. Brodsky, G. F. de Teramond, H. G. Dosch, J. Erlich, Light-Front Holographic QCD and Emerging Confinement, Phys. Rept. 584 (2015) 1–105. [arXiv:1407.8131](https://arxiv.org/abs/1407.8131), [doi:10.1016/j.physrep.2015.05.001](https://doi.org/10.1016/j.physrep.2015.05.001).
 - [394] P. Maris, C. D. Roberts, Dyson-Schwinger equations: A Tool for hadron physics, Int. J. Mod. Phys. E 12 (2003) 297–365. [arXiv:nucl-th/0301049](https://arxiv.org/abs/nucl-th/0301049), [doi:10.1142/S0218301303001326](https://doi.org/10.1142/S0218301303001326).
 - [395] C. D. Roberts, Hadron Properties and Dyson-Schwinger Equations, Prog. Part. Nucl. Phys. 61 (2008) 50–65. [arXiv:0712.0633](https://arxiv.org/abs/0712.0633), [doi:10.1016/j.ppnp.2007.12.034](https://doi.org/10.1016/j.ppnp.2007.12.034).
 - [396] M. Ding, C. D. Roberts, S. M. Schmidt, Emergence of Hadron Mass and Structure, Particles 6 (1) (2023) 57–120. [arXiv:2211.07763](https://arxiv.org/abs/2211.07763), [doi:10.3390/particles6010004](https://doi.org/10.3390/particles6010004).
 - [397] C. D. Roberts, D. G. Richards, T. Horn, L. Chang, Insights into the emergence of mass from studies of pion and kaon structure, Prog. Part. Nucl. Phys. 120 (2021) 103883. [arXiv:2102.01765](https://arxiv.org/abs/2102.01765), [doi:10.1016/j.ppnp.2021.103883](https://doi.org/10.1016/j.ppnp.2021.103883).
 - [398] V. D. Burkert, C. D. Roberts, Colloquium : Roper resonance: Toward a solution to the fifty year puzzle, Rev. Mod. Phys. 91 (1) (2019) 011003. [arXiv:1710.02549](https://arxiv.org/abs/1710.02549), [doi:10.1103/RevModPhys.91.011003](https://doi.org/10.1103/RevModPhys.91.011003).
 - [399] A. Bashir, L. Chang, I. C. Cloët, B. El-Bennich, Y.-X. Liu, C. D. Roberts, P. C. Tandy, Collective perspective on advances in Dyson-Schwinger Equation QCD, Commun. Theor. Phys. 58 (2012) 79–134. [arXiv:1201.3366](https://arxiv.org/abs/1201.3366), [doi:10.1088/0253-6102/58/1/16](https://doi.org/10.1088/0253-6102/58/1/16).
 - [400] H. L. L. Roberts, L. Chang, I. C. Cloët, C. D. Roberts, Masses of ground and excited-state hadrons, Few Body Syst. 51 (2011) 1–25. [arXiv:1101.4244](https://arxiv.org/abs/1101.4244), [doi:10.1007/s00601-011-0225-x](https://doi.org/10.1007/s00601-011-0225-x).
 - [401] C. Chen, L. Chang, C. D. Roberts, S. Wan, D. J. Wilson, Spectrum of hadrons with strangeness, Few Body Syst. 53 (2012) 293–326. [arXiv:1204.2553](https://arxiv.org/abs/1204.2553), [doi:10.1007/s00601-012-0466-3](https://doi.org/10.1007/s00601-012-0466-3).
 - [402] C. Chen, G. I. Krein, C. D. Roberts, S. M. Schmidt, J. Segovia, Spectrum and structure of octet and decuplet baryons and their positive-parity excitations, Phys. Rev. D 100 (5) (2019) 054009. [arXiv:1901.04305](https://arxiv.org/abs/1901.04305), [doi:10.1103/PhysRevD.100.054009](https://doi.org/10.1103/PhysRevD.100.054009).
 - [403] D. J. Wilson, I. C. Cloët, L. Chang, C. D. Roberts, Nucleon and Roper electromagnetic elastic and transition form factors, Phys. Rev. C 85 (2012) 025205. [arXiv:1112.2212](https://arxiv.org/abs/1112.2212), [doi:10.1103/PhysRevC.85.025205](https://doi.org/10.1103/PhysRevC.85.025205).
 - [404] C. Chen, Y. Lu, D. Binosi, C. D. Roberts, J. Rodríguez-Quintero, J. Segovia, Nucleon-to-Roper electromagnetic transition form factors at large Q^2 , Phys. Rev. D 99 (3) (2019) 034013. [arXiv:1811.08440](https://arxiv.org/abs/1811.08440), [doi:10.1103/PhysRevD.99.034013](https://doi.org/10.1103/PhysRevD.99.034013).
 - [405] Y. Lu, C. Chen, Z.-F. Cui, C. D. Roberts, S. M. Schmidt, J. Segovia, H. S. Zong, Transition form factors: $\gamma^* + p \rightarrow \Delta(1232), \Delta(1600)$, Phys. Rev. D 100 (3) (2019) 034001. [arXiv:1904.03205](https://arxiv.org/abs/1904.03205), [doi:10.1103/PhysRevD.100.034001](https://doi.org/10.1103/PhysRevD.100.034001).
 - [406] K. Raya, L. X. Gutiérrez-Guerrero, A. Bashir, L. Chang, Z.-F. Cui, Y. Lu, C. D. Roberts, J. Segovia, Dynamical diquarks in the $\gamma^{(*)} p \rightarrow N(1535)_{\frac{1}{2}}^-$ transition, Eur. Phys. J. A 57 (9) (2021) 266. [arXiv:2108.02306](https://arxiv.org/abs/2108.02306), [doi:10.1140/epja/s10050-021-00574-w](https://doi.org/10.1140/epja/s10050-021-00574-w).
 - [407] I. C. Cloët, C. D. Roberts, Explanation and Prediction of Observables using Continuum Strong QCD, Prog. Part. Nucl. Phys. 77 (2014) 1–69. [arXiv:1310.2651](https://arxiv.org/abs/1310.2651), [doi:10.1016/j.ppnp.2014.02.001](https://doi.org/10.1016/j.ppnp.2014.02.001).
 - [408] C. S. Fischer, Infrared properties of QCD from Dyson-Schwinger equations, J. Phys. G 32 (2006) R253–R291. [arXiv:hep-ph/0605173](https://arxiv.org/abs/hep-ph/0605173), [doi:10.1088/0954-3899/32/8/R02](https://doi.org/10.1088/0954-3899/32/8/R02).
 - [409] G. Eichmann, H. Sanchis-Alepuz, R. Williams, R. Alkofer, C. S. Fischer, Baryons as relativistic three-quark bound states, Prog. Part. Nucl. Phys. 91 (2016) 1–100. [arXiv:1606.09602](https://arxiv.org/abs/1606.09602), [doi:10.1016/j.ppnp.2016.07.001](https://doi.org/10.1016/j.ppnp.2016.07.001).
 - [410] G. Eichmann, C. S. Fischer, H. Sanchis-Alepuz, Light baryons and their excitations, Phys. Rev. D 94 (9) (2016) 094033. [arXiv:1607.05748](https://arxiv.org/abs/1607.05748), [doi:10.1103/PhysRevD.94.094033](https://doi.org/10.1103/PhysRevD.94.094033).
 - [411] H. Sanchis-Alepuz, C. S. Fischer, Octet and Decuplet masses: a covariant three-body Faddeev calculation, Phys. Rev. D 90 (9) (2014) 096001. [arXiv:1408.5577](https://arxiv.org/abs/1408.5577), [doi:10.1103/PhysRevD.90.096001](https://doi.org/10.1103/PhysRevD.90.096001).
 - [412] H. Sanchis-Alepuz, S. D. Kubrak, C. S. Fischer, Beyond Rainbow-Ladder in a covariant three-body Bethe-Salpeter approach: Baryons, EPJ Web Conf. 73 (2014) 04019. [arXiv:1402.1013](https://arxiv.org/abs/1402.1013), [doi:10.1051/epjconf/20147304019](https://doi.org/10.1051/epjconf/20147304019).
 - [413] G. Eichmann, R. Alkofer, A. Krassnigg, D. Nicmorus, Nucleon mass from a covariant three-quark Faddeev equation, Phys. Rev. Lett. 104 (2010) 201601. [arXiv:0912.2246](https://arxiv.org/abs/0912.2246), [doi:10.1103/PhysRevLett.104.201601](https://doi.org/10.1103/PhysRevLett.104.201601).
 - [414] C. Chen, C. S. Fischer, C. D. Roberts, Nucleon-to- Δ Axial and Pseudoscalar Transition Form Factors, Phys. Rev. Lett. 133 (13) (2024) 131901. [arXiv:2312.13724](https://arxiv.org/abs/2312.13724), [doi:10.1103/PhysRevLett.133.131901](https://doi.org/10.1103/PhysRevLett.133.131901).
 - [415] P.-L. Yin, C. Chen, C. S. Fischer, C. D. Roberts, Δ -Baryon axialvector and pseudoscalar form factors, and associated PCAC relations, Eur. Phys. J. A 59 (7) (2023) 163. [arXiv:2305.09831](https://arxiv.org/abs/2305.09831), [doi:10.1140/epja/s10050-023-01066-9](https://doi.org/10.1140/epja/s10050-023-01066-9).
 - [416] G. Eichmann, C. S. Fischer, Baryon Structure and Reactions, Few Body Syst. 60 (1) (2019) 2. [doi:10.1007/s00601-018-1469-5](https://doi.org/10.1007/s00601-018-1469-5).
 - [417] J. Segovia, B. El-Bennich, E. Rojas, I. C. Cloët, C. D. Roberts, S.-S. Xu, H.-S. Zong, Completing the picture of the Roper resonance, Phys. Rev. Lett. 115 (17) (2015) 171801. [arXiv:1504.04386](https://arxiv.org/abs/1504.04386), [doi:10.1103/PhysRevLett.115.171801](https://doi.org/10.1103/PhysRevLett.115.171801).
 - [418] A. Francis, P. de Forcrand, R. Lewis, K. Maltman, Shapes and sizes of diquarks in lattice QCD, PoS ICHEP2022 (2022) 795. [doi:10.22323/1.414.0795](https://doi.org/10.22323/1.414.0795).
 - [419] A. Francis, P. de Forcrand, R. Lewis, K. Maltman, Good and bad diquark properties and spatial correlations in lattice QCD, Rev. Mex. Fis. Suppl. 3 (3) (2022) 030802. [arXiv:2201.03332](https://arxiv.org/abs/2201.03332), [doi:10.31349/SuplRevMexFis.3.030802](https://doi.org/10.31349/SuplRevMexFis.3.030802).

- [420] S. Scherer, Chiral Perturbation Theory: Introduction and Recent Results in the One-Nucleon Sector, *Prog. Part. Nucl. Phys.* 64 (2010) 1–60. [arXiv:0908.3425](#), [doi:10.1016/j.ppnp.2009.08.002](#).
- [421] V. Pascalutsa, Quantization of an interacting spin-3/2 field and the Δ isobar, *Phys. Rev. D* 58 (1998) 096002. [arXiv:hep-ph/9802288](#), [doi:10.1103/PhysRevD.58.096002](#).
- [422] V. Pascalutsa, R. Timmermans, Field theory of nucleon to higher spin baryon transitions, *Phys. Rev. C* 60 (1999) 042201. [arXiv:nucl-th/9905065](#), [doi:10.1103/PhysRevC.60.042201](#).
- [423] N. Fettes, U.-G. Meißner, Pion nucleon scattering in chiral perturbation theory. II.: Fourth order calculation, *Nucl. Phys. A* 676 (2000) 311. [arXiv:hep-ph/0002162](#), [doi:10.1016/S0375-9474\(00\)00199-8](#).
- [424] N. Fettes, U.-G. Meißner, Pion - nucleon scattering in an effective chiral field theory with explicit spin 3/2 fields, *Nucl. Phys. A* 679 (2001) 629–670. [arXiv:hep-ph/0006299](#), [doi:10.1016/S0375-9474\(00\)00368-7](#).
- [425] N. Fettes, U.-G. Meißner, M. Mojžiš, S. Steininger, The Chiral effective pion nucleon Lagrangian of order p^4 , *Annals Phys.* 283 (2000) 273–302, [Erratum: *Annals Phys.* 288, 249–250 (2001)]. [arXiv:hep-ph/0001308](#), [doi:10.1006/aphy.2000.6059](#).
- [426] V. Pascalutsa, D. R. Phillips, Effective theory of the $\Delta(1232)$ resonance in Compton scattering off the nucleon, *Phys. Rev. C* 67 (2003) 055202. [arXiv:nucl-th/0212024](#), [doi:10.1103/PhysRevC.67.055202](#).
- [427] N. Fettes, U.-G. Meißner, Complete analysis of pion nucleon scattering in chiral perturbation theory to third order, *Nucl. Phys. A* 693 (2001) 693–709. [arXiv:hep-ph/0101030](#), [doi:10.1016/S0375-9474\(01\)00977-0](#).
- [428] B. Borasoy, P. C. Bruns, U.-G. Meißner, R. Lewis, Chiral corrections to the Roper mass, *Phys. Lett. B* 641 (2006) 294–300. [arXiv:hep-lat/0608001](#), [doi:10.1016/j.physletb.2006.08.057](#).
- [429] V. Pascalutsa, The $\Delta(1232)$ Resonance in Chiral Effective Field Theory, *Prog. Part. Nucl. Phys.* 61 (2008) 27–33. [arXiv:0712.3919](#), [doi:10.1016/j.ppnp.2007.12.023](#).
- [430] V. Baru, J. Haidenbauer, C. Hanhart, A. E. Kudryavtsev, V. Lensky, U.-G. Meißner, Role of the $\Delta(1232)$ in pion-deuteron scattering at threshold within chiral effective field theory, *Phys. Lett. B* 659 (2008) 184–191. [arXiv:0706.4023](#), [doi:10.1016/j.physletb.2007.10.063](#).
- [431] V. Bernard, D. Hoja, U.-G. Meißner, A. Rusetsky, The Mass of the Delta resonance in a finite volume: fourth-order calculation, *JHEP* 06 (2009) 061. [arXiv:0902.2346](#), [doi:10.1088/1126-6708/2009/06/061](#).
- [432] D. Siemens, V. Bernard, E. Epelbaum, H. Krebs, U.-G. Meißner, The reaction $\pi N \rightarrow \pi\pi N$ in chiral effective field theory with explicit $\Delta(1232)$ degrees of freedom, *Phys. Rev. C* 89 (6) (2014) 065211. [arXiv:1403.2510](#), [doi:10.1103/PhysRevC.89.065211](#).
- [433] J. Gegelia, U.-G. Meißner, D.-L. Yao, The width of the Roper resonance in baryon chiral perturbation theory, *Phys. Lett. B* 760 (2016) 736–741. [arXiv:1606.04873](#), [doi:10.1016/j.physletb.2016.07.068](#).
- [434] J. Gegelia, U.-G. Meißner, D. Siemens, D.-L. Yao, The width of the Δ -resonance at two loop order in baryon chiral perturbation theory, *Phys. Lett. B* 763 (2016) 1–8. [arXiv:1608.00517](#), [doi:10.1016/j.physletb.2016.10.017](#).
- [435] T. Vonk, F.-K. Guo, U.-G. Meißner, Pion axioproduction: The Δ resonance contribution, *Phys. Rev. D* 105 (5) (2022) 054029. [arXiv:2202.00268](#), [doi:10.1103/PhysRevD.105.054029](#).
- [436] H. Alharazin, E. Epelbaum, J. Gegelia, U.-G. Meißner, B. D. Sun, Gravitational form factors of the Delta resonance in chiral EFT, *Eur. Phys. J. C* 82 (10) (2022) 907. [arXiv:2209.01233](#), [doi:10.1140/epjc/s10052-022-10882-0](#).
- [437] V. Bernard, N. Kaiser, U.-G. Meißner, Chiral dynamics in nucleons and nuclei, *Int. J. Mod. Phys. E* 4 (1995) 193–346. [arXiv:hep-ph/9501384](#), [doi:10.1142/S0218301395000092](#).
- [438] V. Pascalutsa, M. Vanderhaeghen, S. N. Yang, Electromagnetic excitation of the $\Delta(1232)$ -resonance, *Phys. Rept.* 437 (2007) 125–232. [arXiv:hep-ph/0609004](#), [doi:10.1016/j.physrep.2006.09.006](#).
- [439] V. Bernard, Chiral Perturbation Theory and Baryon Properties, *Prog. Part. Nucl. Phys.* 60 (2008) 82–160. [arXiv:0706.0312](#), [doi:10.1016/j.ppnp.2007.07.001](#).
- [440] F.-K. Guo, C. Hanhart, U.-G. Meißner, Q. Wang, Q. Zhao, B.-S. Zou, Hadronic molecules, *Rev. Mod. Phys.* 90 (1) (2018) 015004, [Erratum: *Rev.Mod.Phys.* 94, 029901 (2022)]. [arXiv:1705.00141](#), [doi:10.1103/RevModPhys.90.015004](#).
- [441] A. Feijoo, M. Korwieser, L. Fabbietti, Relevance of the coupled channels in the ϕp and ρp correlation functions, *Phys. Rev. D* 111 (1) (2025) 014009. [arXiv:2407.01128](#), [doi:10.1103/PhysRevD.111.014009](#).
- [442] J. He, Nucleon resonances $N(1875)$ and $N(2100)$ as strange partners of LHCb pentaquarks, *Phys. Rev. D* 95 (7) (2017) 074031. [arXiv:1701.03738](#), [doi:10.1103/PhysRevD.95.074031](#).
- [443] J. He, Internal structures of the nucleon resonances $N(1875)$ and $N(2120)$, *Phys. Rev. C* 91 (1) (2015) 018201. [arXiv:1501.00522](#), [doi:10.1103/PhysRevC.91.018201](#).
- [444] L. Roca, M. Mai, E. Oset, U.-G. Meißner, Predictions for the $\Lambda_b \rightarrow J/\psi \Lambda(1405)$ decay, *Eur. Phys. J. C* 75 (5) (2015) 218. [arXiv:1503.02936](#), [doi:10.1140/epjc/s10052-015-3438-1](#).
- [445] E. J. Garzon, E. Oset, Mixing of pseudoscalar-baryon and vector-baryon in the $J^P = 1/2^-$ sector and the $N^*(1535)$ and $N^*(1650)$ resonances, *Phys. Rev. C* 91 (2) (2015) 025201. [arXiv:1411.3547](#), [doi:10.1103/PhysRevC.91.025201](#).
- [446] E. Oset, A. Ramos, E. J. Garzon, R. Molina, L. Tolos, C. W. Xiao, J. J. Wu, B. S. Zou, Interaction of vector mesons with baryons and nuclei, *Int. J. Mod. Phys. E* 21 (2012) 1230011. [arXiv:1210.3738](#), [doi:10.1142/S0218301312300111](#).
- [447] E. J. Garzon, E. Oset, Effects of pseudoscalar-baryon channels in the dynamically generated vector-baryon resonances, *Eur. Phys. J. A* 48 (2012) 5. [arXiv:1201.3756](#), [doi:10.1140/epja/i2012-12005-x](#).
- [448] K. P. Khemchandani, A. Martínez Torres, H. Kaneko, H. Nagahiro, A. Hosaka, Coupling vector and pseudoscalar mesons to study baryon resonances, *Phys. Rev. D* 84 (2011) 094018. [arXiv:1107.0574](#), [doi:10.1103/PhysRevD.84.094018](#).
- [449] J.-J. Xie, A. Martínez Torres, E. Oset, P. Gonzalez, Plausible explanation of the $\Delta_{5/2^+}(2000)$ puzzle, *Phys. Rev. C* 83 (2011) 055204. [arXiv:1101.1722](#), [doi:10.1103/PhysRevC.83.055204](#).
- [450] S. Sarkar, B.-X. Sun, E. Oset, M. J. Vicente Vacas, Dynamically generated resonances from the vector octet-baryon decuplet interaction, *Eur. Phys. J. A* 44 (2010) 431–443. [arXiv:0902.3150](#), [doi:10.1140/epja/i2010-10956-4](#).
- [451] J.-J. Xie, A. Martínez Torres, E. Oset, Faddeev fixed center approximation to the $N\bar{K}$ system and the signature of a $N^*(1920)(1/2^+)$ state, *Phys. Rev. C* 83 (2011) 065207. [arXiv:1010.6164](#), [doi:10.1103/PhysRevC.83.065207](#).
- [452] P. Gonzalez, E. Oset, J. Vijande, An Explanation of the $\Delta 5/2^-$ (1930) as a $\rho\Delta$ bound state, *Phys. Rev. C* 79 (2009) 025209. [arXiv:0812.3368](#), [doi:10.1103/PhysRevC.79.025209](#).
- [453] M. F. M. Lutz, E. E. Kolomeitsev, Baryon resonances from chiral coupled-channel dynamics, *Nucl. Phys. A* 755 (2005) 29–39. [arXiv:hep-ph/0501224](#), [doi:10.1016/j.nuclphysa.2005.03.110](#).
- [454] S. Sarkar, E. Oset, M. J. Vicente Vacas, Baryonic resonances from baryon decuplet-meson octet interaction, *Nucl. Phys. A* 750 (2005) 294–323, [Erratum: *Nucl.Phys.A* 780, 90–90 (2006)]. [arXiv:nucl-th/0407025](#), [doi:10.1016/j.nuclphysa.2005.01.006](#).
- [455] E. E. Kolomeitsev, M. F. M. Lutz, On baryon resonances and chiral symmetry, *Phys. Lett. B* 585 (2004) 243–252. [arXiv:nucl-th/0305101](#), [doi:10.1016/j.physletb.2004.01.066](#).
- [456] C. Garcia-Recio, M. F. M. Lutz, J. Nieves, Quark mass dependence of s wave baryon resonances, *Phys. Lett. B* 582 (2004) 49–54.

- [arXiv:nucl-th/0305100](https://arxiv.org/abs/nucl-th/0305100), doi:10.1016/j.physletb.2003.11.073.
- [457] J. Nieves, E. Ruiz Arriola, The S_{11} – $N(1535)$ and $-N(1650)$ resonances in meson baryon unitarized coupled channel chiral perturbation theory, Phys. Rev. D 64 (2001) 116008. [arXiv:hep-ph/0104307](https://arxiv.org/abs/hep-ph/0104307), doi:10.1103/PhysRevD.64.116008.
- [458] M. F. M. Lutz, E. E. Kolomeitsev, Covariant meson baryon scattering with chiral and large N_C constraints, Found. Phys. 31 (2001) 1671–1702. [arXiv:nucl-th/0105068](https://arxiv.org/abs/nucl-th/0105068), doi:10.1023/A:1012655116247.
- [459] M. F. M. Lutz, E. E. Kolomeitsev, Relativistic chiral SU(3) symmetry, large N_C sum rules and meson baryon scattering, Nucl. Phys. A 700 (2002) 193–308. [arXiv:nucl-th/0105042](https://arxiv.org/abs/nucl-th/0105042), doi:10.1016/S0375-9474(01)01312-4.
- [460] N. Kaiser, P. B. Siegel, W. Weise, Chiral dynamics and the S_{11} (1535) nucleon resonance, Phys. Lett. B 362 (1995) 23–28. [arXiv:nucl-th/9507036](https://arxiv.org/abs/nucl-th/9507036), doi:10.1016/0370-2693(95)01203-3.
- [461] D. Sadasivan, M. Mai, M. Döring, U.-G. Meißner, F. Amorim, J. P. Klucik, J.-X. Lu, L.-S. Geng, New insights into the pole parameters of the $\Lambda(1380)$, the $\Lambda(1405)$ and the $\Sigma(1385)$, Front. Phys. 11 (2023) 1139236. [arXiv:2212.10415](https://arxiv.org/abs/2212.10415), doi:10.3389/fphy.2023.1139236.
- [462] D. Sadasivan, M. Mai, M. Döring, S- and p-wave structure of $S = -1$ meson-baryon scattering in the resonance region, Phys. Lett. B 789 (2019) 329–335. [arXiv:1805.04534](https://arxiv.org/abs/1805.04534), doi:10.1016/j.physletb.2018.12.035.
- [463] A. Feijoo, V. Magas, A. Ramos, $S=-1$ meson-baryon interaction and the role of isospin filtering processes, Phys. Rev. C 99 (3) (2019) 035211. [arXiv:1810.07600](https://arxiv.org/abs/1810.07600), doi:10.1103/PhysRevC.99.035211.
- [464] K. P. Khemchandani, A. Martínez Torres, A. Hosaka, H. Nagahiro, F. S. Navarra, M. Nielsen, Why $\Xi(1690)$ and $\Xi(2120)$ are so narrow?, Phys. Rev. D 97 (3) (2018) 034005. [arXiv:1608.07086](https://arxiv.org/abs/1608.07086), doi:10.1103/PhysRevD.97.034005.
- [465] A. Ramos, A. Feijoo, V. K. Magas, The chiral $S = -1$ meson–baryon interaction with new constraints on the NLO contributions, Nucl. Phys. A 954 (2016) 58–74. [arXiv:1605.03767](https://arxiv.org/abs/1605.03767), doi:10.1016/j.nuclphysa.2016.05.006.
- [466] K. P. Khemchandani, A. Martínez Torres, H. Nagahiro, A. Hosaka, Role of vector and pseudoscalar mesons in understanding $1/2^- N^*$ and Δ resonances, Phys. Rev. D 88 (11) (2013) 114016. [arXiv:1307.8420](https://arxiv.org/abs/1307.8420), doi:10.1103/PhysRevD.88.114016.
- [467] S. X. Nakamura, D. Jido, Lambda (1405) photoproduction based on chiral unitary model, PTEP 2014 (2014) 023D01. [arXiv:1310.5768](https://arxiv.org/abs/1310.5768), doi:10.1093/ptep/ptt121.
- [468] C. García-Recio, J. Nieves, E. Ruiz Arriola, M. J. Vicente Vacas, $S = -1$ meson baryon unitarized coupled channel chiral perturbation theory and the S_{01} resonances $\Lambda(1405)$ and $\Lambda(1670)$, Phys. Rev. D 67 (2003) 076009. [arXiv:hep-ph/0210311](https://arxiv.org/abs/hep-ph/0210311), doi:10.1103/PhysRevD.67.076009.
- [469] E. Oset, A. Ramos, C. Bennhold, Low lying $S = -1$ excited baryons and chiral symmetry, Phys. Lett. B 527 (2002) 99–105, [Erratum: Phys.Lett.B 530, 260–260 (2002)]. [arXiv:nucl-th/0109006](https://arxiv.org/abs/nucl-th/0109006), doi:10.1016/S0370-2693(01)01523-4.
- [470] N. Kaiser, P. B. Siegel, W. Weise, Chiral dynamics and the low-energy kaon – nucleon interaction, Nucl. Phys. A 594 (1995) 325–345. [arXiv:nucl-th/9505043](https://arxiv.org/abs/nucl-th/9505043), doi:10.1016/0375-9474(95)00362-5.
- [471] J.-X. Lu, L.-S. Geng, M. Doering, M. Mai, Cross-Channel Constraints on Resonant Antikaon-Nucleon Scattering, Phys. Rev. Lett. 130 (7) (2023) 071902. [arXiv:2209.02471](https://arxiv.org/abs/2209.02471), doi:10.1103/PhysRevLett.130.071902.
- [472] S.-H. Kim, K. P. Khemchandani, A. Martínez Torres, S.-i. Nam, A. Hosaka, Photoproduction of Λ^* and Σ^* resonances with $J^P = 1/2^-$ off the proton, Phys. Rev. D 103 (11) (2021) 114017. [arXiv:2101.08668](https://arxiv.org/abs/2101.08668), doi:10.1103/PhysRevD.103.114017.
- [473] M. Mai, U.-G. Meißner, Constraints on the chiral unitary $\bar{K}N$ amplitude from $\pi\Sigma K^+$ photoproduction data, Eur. Phys. J. A 51 (3) (2015) 30. [arXiv:1411.7884](https://arxiv.org/abs/1411.7884), doi:10.1140/epja/i2015-15030-3.
- [474] N. Sharma, A. Martínez Torres, K. P. Khemchandani, H. Dahiya, Magnetic moments of the low-lying $1/2^-$ octet baryon resonances, Eur. Phys. J. A 49 (2013) 11. [arXiv:1207.3311](https://arxiv.org/abs/1207.3311), doi:10.1140/epja/i2013-13011-2.
- [475] A. Gasparyan, M. F. M. Lutz, Photon- and pion-nucleon interactions in a unitary and causal effective field theory based on the chiral Lagrangian, Nucl. Phys. A 848 (2010) 126–182. [arXiv:1003.3426](https://arxiv.org/abs/1003.3426), doi:10.1016/j.nuclphysa.2010.08.006.
- [476] B.-X. Sun, E. J. Garzon, E. Oset, Radiative decay into γ -baryon of dynamically generated resonances from the vector-baryon interaction, Phys. Rev. D 82 (2010) 034028. [arXiv:1003.4664](https://arxiv.org/abs/1003.4664), doi:10.1103/PhysRevD.82.034028.
- [477] M. Döring, E. Oset, U.-G. Meißner, Evaluation of the polarization observables I^S and I^C in the reaction $\gamma p \rightarrow \pi^0 \eta p$, Eur. Phys. J. A 46 (2010) 315–323. [arXiv:1003.0097](https://arxiv.org/abs/1003.0097), doi:10.1140/epja/i2010-11047-4.
- [478] M. Döring, D. Jido, E. Oset, Helicity Amplitudes of the $\Lambda(1670)$ and two $\Lambda(1405)$ as dynamically generated resonances, Eur. Phys. J. A 45 (2010) 319–333. [arXiv:1002.3688](https://arxiv.org/abs/1002.3688), doi:10.1140/epja/i2010-11015-0.
- [479] M. Döring, K. Nakayama, On the cross section ratio σ_n/σ_p in η photoproduction, Phys. Lett. B 683 (2010) 145–149. [arXiv:0909.3538](https://arxiv.org/abs/0909.3538), doi:10.1016/j.physletb.2009.12.029.
- [480] J. Ajaka, et al., Simultaneous photoproduction of η and π^0 mesons on the proton, Phys. Rev. Lett. 100 (2008) 052003. doi:10.1103/PhysRevLett.100.052003.
- [481] D. Jido, M. Doering, E. Oset, Transition form factors of the $N^*(1535)$ as a dynamically generated resonance, Phys. Rev. C 77 (2008) 065207. [arXiv:0712.0038](https://arxiv.org/abs/0712.0038), doi:10.1103/PhysRevC.77.065207.
- [482] L. S. Geng, E. Oset, M. Döring, The Radiative decay of the $\Lambda(1405)$ and its two-pole structure, Eur. Phys. J. A 32 (2007) 201–211. [arXiv:hep-ph/0702093](https://arxiv.org/abs/hep-ph/0702093), doi:10.1140/epja/i2007-10371-0.
- [483] M. Döring, Radiative decay of the $\Delta^*(1700)$, Nucl. Phys. A 786 (2007) 164–182. [arXiv:nucl-th/0701070](https://arxiv.org/abs/nucl-th/0701070), doi:10.1016/j.nuclphysa.2007.02.004.
- [484] L. Roca, C. Hanhart, E. Oset, U.-G. Meißner, Testing the nature of the $\Lambda(1520)$ resonance in proton-induced production, Eur. Phys. J. A 27 (2006) 373–380. [arXiv:nucl-th/0602016](https://arxiv.org/abs/nucl-th/0602016), doi:10.1140/epja/i2006-10009-9.
- [485] M. Döring, E. Oset, D. Strottman, Clues to the nature of the $\Delta^*(1700)$ resonance from pion- and photon-induced reactions, Phys. Lett. B 639 (2006) 59–67. [arXiv:nucl-th/0602055](https://arxiv.org/abs/nucl-th/0602055), doi:10.1016/j.physletb.2006.06.022.
- [486] M. Döring, E. Oset, S. Sarkar, Radiative decay of the $\Lambda(1520)$, Phys. Rev. C 74 (2006) 065204. [arXiv:nucl-th/0601027](https://arxiv.org/abs/nucl-th/0601027), doi:10.1103/PhysRevC.74.065204.
- [487] M. Döring, E. Oset, D. Strottman, Chiral dynamics in the $\gamma p \rightarrow \pi^0 \eta p$ and $\gamma p \rightarrow \pi^0 K^0 \Sigma^+$ reactions, Phys. Rev. C 73 (2006) 045209. [arXiv:nucl-th/0510015](https://arxiv.org/abs/nucl-th/0510015), doi:10.1103/PhysRevC.73.045209.
- [488] N. Kaiser, T. Waas, W. Weise, SU(3) chiral dynamics with coupled channels: Eta and kaon photoproduction, Nucl. Phys. A 612 (1997) 297–320. [arXiv:hep-ph/9607459](https://arxiv.org/abs/hep-ph/9607459), doi:10.1016/S0375-9474(96)00321-1.
- [489] K. P. Khemchandani, A. Martínez Torres, H. Nagahiro, A. Hosaka, Negative parity Λ and Σ resonances coupled to pseudoscalar and vector mesons, Phys. Rev. D 85 (2012) 114020. [arXiv:1203.6711](https://arxiv.org/abs/1203.6711), doi:10.1103/PhysRevD.85.114020.
- [490] L. S. Geng, E. Oset, B. S. Zou, M. Döring, The Role of the $N^*(1535)$ in the $J/\psi \rightarrow \bar{p}\eta p$ and $J/\psi \rightarrow \bar{p}K^+\Lambda$ reactions, Phys. Rev. C 79 (2009) 025203. [arXiv:0807.2913](https://arxiv.org/abs/0807.2913), doi:10.1103/PhysRevC.79.025203.
- [491] M. Döring, E. Oset, B. S. Zou, The Role of the $N^*(1535)$ resonance and the $\pi^- p \rightarrow KY$ amplitudes in the OZI forbidden $\pi N \rightarrow \phi N$ reaction, Phys. Rev. C 78 (2008) 025207. [arXiv:0805.1799](https://arxiv.org/abs/0805.1799), doi:10.1103/PhysRevC.78.025207.
- [492] B. B. Malabarba, K. P. Khemchandani, A. M. Torres, N^* states with hidden charm and a three-body nature, Eur. Phys. J. A 58 (2) (2022) 33. [arXiv:2103.09978](https://arxiv.org/abs/2103.09978), doi:10.1140/epja/s10050-022-00681-2.

- [493] K. P. Khemchandani, A. Martínez Torres, H. Nagahiro, A. Hosaka, Decay properties of N^* (1895), Phys. Rev. D 103 (1) (2021) 016015. [arXiv:2010.04584](#), [doi:10.1103/PhysRevD.103.016015](#).
- [494] A. Martínez Torres, D. Jido, $K\Lambda$ (1405) configuration of the $K\bar{K}N$ system, Phys. Rev. C 82 (2010) 038202. [arXiv:1008.0457](#), [doi:10.1103/PhysRevC.82.038202](#).
- [495] A. Martínez Torres, K. P. Khemchandani, U.-G. Meißner, E. Oset, Searching for signatures around 1920-MeV of a N^* state of three hadron nature, Eur. Phys. J. A 41 (2009) 361–368. [arXiv:0902.3633](#), [doi:10.1140/epja/i2009-10834-2](#).
- [496] A. Martínez Torres, K. P. Khemchandani, E. Oset, Solution to Faddeev equations with two-body experimental amplitudes as input and application to $J^P = 1/2^+$, $S = 0$ baryon resonances, Phys. Rev. C 79 (2009) 065207. [arXiv:0812.2235](#), [doi:10.1103/PhysRevC.79.065207](#).
- [497] A. M. Torres, K. P. Khemchandani, E. Oset, Three-body hadronic structure of low-lying $1/2^+$ Σ and Λ resonances, Eur. Phys. J. A 35 (2008) 295–297. [arXiv:0805.3641](#), [doi:10.1140/epja/i2007-10563-6](#).
- [498] K. P. Khemchandani, A. Martínez Torres, E. Oset, The $N^*(1710)$ as a resonance in the $\pi\pi N$ system, Eur. Phys. J. A 37 (2008) 233–243. [arXiv:0804.4670](#), [doi:10.1140/epja/i2008-10625-3](#).
- [499] A. Martínez Torres, K. P. Khemchandani, E. Oset, Three body resonances in two meson-one baryon systems, Phys. Rev. C 77 (2008) 042203. [arXiv:0706.2330](#), [doi:10.1103/PhysRevC.77.042203](#).
- [500] J. A. Oller, E. Oset, A. Ramos, Chiral unitary approach to meson meson and meson - baryon interactions and nuclear applications, Prog. Part. Nucl. Phys. 45 (2000) 157–242. [arXiv:hep-ph/0002193](#), [doi:10.1016/S0146-6410\(00\)00104-6](#).
- [501] E. Oset, et al., Weak decays of heavy hadrons into dynamically generated resonances, Int. J. Mod. Phys. E 25 (2016) 1630001. [arXiv:1601.03972](#), [doi:10.1142/S0218301316300010](#).
- [502] U.-G. Meißner, Two-pole structures in QCD: Facts, not fantasy!, Symmetry 12 (6) (2020) 981. [arXiv:2005.06909](#), [doi:10.3390/sym12060981](#).
- [503] T. Hyodo, D. Jido, The nature of the $\Lambda(1405)$ resonance in chiral dynamics, Prog. Part. Nucl. Phys. 67 (2012) 55–98. [arXiv:1104.4474](#), [doi:10.1016/j.ppnp.2011.07.002](#).
- [504] M. F. M. Lutz, C. L. Korpa, On coupled-channel dynamics in the presence of anomalous thresholds, Phys. Rev. D 98 (7) (2018) 076003. [arXiv:1808.08695](#), [doi:10.1103/PhysRevD.98.076003](#).
- [505] C. L. Korpa, M. F. M. Lutz, X.-Y. Guo, Y. Heo, Coupled-channel system with anomalous thresholds and unitarity, Phys. Rev. D 107 (3) (2023) L031505. [arXiv:2211.03508](#), [doi:10.1103/PhysRevD.107.L031505](#).
- [506] Y.-F. Wang, U.-G. Meißner, D. Rönchen, C.-W. Shen, Examination of the nature of the N^* and Δ resonances via coupled-channels dynamics, Phys. Rev. C 109 (1) (2024) 015202. [arXiv:2307.06799](#), [doi:10.1103/PhysRevC.109.015202](#).
- [507] T. Sekihara, Two-body wave functions and compositeness from scattering amplitudes. II. Application to the physical N^* and Δ^* resonances, Phys. Rev. C 104 (3) (2021) 035202. [arXiv:2104.01962](#), [doi:10.1103/PhysRevC.104.035202](#).
- [508] E. Wang, J.-J. Xie, W.-H. Liang, F.-K. Guo, E. Oset, Role of a triangle singularity in the $\gamma p \rightarrow K^+\Lambda(1405)$ reaction, Phys. Rev. C 95 (1) (2017) 015205. [arXiv:1610.07117](#), [doi:10.1103/PhysRevC.95.015205](#).
- [509] D. Samart, W.-h. Liang, E. Oset, Triangle mechanisms in the build up and decay of the $N^*(1875)$, Phys. Rev. C 96 (3) (2017) 035202. [arXiv:1703.09872](#), [doi:10.1103/PhysRevC.96.035202](#).
- [510] L. Roca, E. Oset, Role of a triangle singularity in the $\pi\Delta$ decay of the $N(1700)(3/2^-)$, Phys. Rev. C 95 (6) (2017) 065211. [arXiv:1702.07220](#), [doi:10.1103/PhysRevC.95.065211](#).
- [511] V. Metag, et al., Observation of a structure in the $M_{p\eta}$ invariant mass distribution near 1700 MeV/ c^2 in the $\gamma p \rightarrow p\pi^0\eta$ reaction, Eur. Phys. J. A 57 (12) (2021) 325. [arXiv:2110.05155](#), [doi:10.1140/epja/s10050-021-00634-1](#).
- [512] C. Ditsche, M. Hoferichter, B. Kubis, U.-G. Meißner, Roy-Steiner equations for pion-nucleon scattering, JHEP 06 (2012) 043. [arXiv:1203.4758](#), [doi:10.1007/JHEP06\(2012\)043](#).
- [513] M. Hoferichter, J. Ruiz de Elvira, B. Kubis, U.-G. Meißner, High-Precision Determination of the Pion-Nucleon σ Term from Roy-Steiner Equations, Phys. Rev. Lett. 115 (2015) 092301. [arXiv:1506.04142](#), [doi:10.1103/PhysRevLett.115.092301](#).
- [514] T. Khan, D. Richards, F. Winter, Positive-parity baryon spectrum and the role of hybrid baryons, Phys. Rev. D 104 (3) (2021) 034503. [arXiv:2010.03052](#), [doi:10.1103/PhysRevD.104.034503](#).
- [515] G. P. Engel, C. B. Lang, D. Mohler, A. Schäfer, QCD with Two Light Dynamical Chirally Improved Quarks: Baryons, Phys. Rev. D 87 (7) (2013) 074504. [arXiv:1301.4318](#), [doi:10.1103/PhysRevD.87.074504](#).
- [516] J. J. Dudek, R. G. Edwards, Hybrid Baryons in QCD, Phys. Rev. D 85 (2012) 054016. [arXiv:1201.2349](#), [doi:10.1103/PhysRevD.85.054016](#).
- [517] R. G. Edwards, J. J. Dudek, D. G. Richards, S. J. Wallace, Excited state baryon spectroscopy from lattice QCD, Phys. Rev. D 84 (2011) 074508. [arXiv:1104.5152](#), [doi:10.1103/PhysRevD.84.074508](#).
- [518] J. Bulava, R. G. Edwards, E. Engelson, B. Joo, H.-W. Lin, C. Morningstar, D. G. Richards, S. J. Wallace, Nucleon, Δ and Ω excited states in $N_f = 2 + 1$ lattice QCD, Phys. Rev. D 82 (2010) 014507. [arXiv:1004.5072](#), [doi:10.1103/PhysRevD.82.014507](#).
- [519] W. Melnitchouk, S. O. Bilson-Thompson, F. D. R. Bonnet, J. N. Hedditch, F. X. Lee, D. B. Leinweber, A. G. Williams, J. M. Zanotti, J. B. Zhang, Excited baryons in lattice QCD, Phys. Rev. D 67 (2003) 114506. [arXiv:hep-lat/0202022](#), [doi:10.1103/PhysRevD.67.114506](#).
- [520] J. Bulava, A. D. Hanlon, B. Hörz, C. Morningstar, A. Nicholson, F. Romero-López, S. Skinner, P. Vranas, A. Walker-Loud, Elastic nucleon-pion scattering at $m\pi=200$ MeV from lattice QCD, Nucl. Phys. B 987 (2023) 116105. [arXiv:2208.03867](#), [doi:10.1016/j.nuclphysb.2023.116105](#).
- [521] G. Silvi, et al., P -wave nucleon-pion scattering amplitude in the $\Delta(1232)$ channel from lattice QCD, Phys. Rev. D 103 (9) (2021) 094508. [arXiv:2101.00689](#), [doi:10.1103/PhysRevD.103.094508](#).
- [522] F. Pittler, C. Alexandrou, K. Hadjiantakou, G. Koutsou, S. Paul, M. Petschlies, A. Todaro, Elastic $\pi - N$ scattering in the $I = 3/2$ channel, PoS LATTICE2021 (2022) 226. [arXiv:2112.04146](#), [doi:10.22323/1.396.0226](#).
- [523] C. B. Lang, V. Verduci, Scattering in the πN negative parity channel in lattice QCD, Phys. Rev. D 87 (5) (2013) 054502. [arXiv:1212.5055](#), [doi:10.1103/PhysRevD.87.054502](#).
- [524] H.-W. Lin, S. D. Cohen, R. G. Edwards, D. G. Richards, First Lattice Study of the $N - P_{11}$ Transition Form Factors, Phys. Rev. D 78 (2008) 114508. [arXiv:0803.3020](#), [doi:10.1103/PhysRevD.78.114508](#).
- [525] S. Owa, D. B. Leinweber, A. W. Thomas, Nucleon resonance structure to 2 GeV and the nature of the Roper (3 2025). [arXiv:2503.09945](#).
- [526] Y. Zhuge, Z.-W. Liu, D. B. Leinweber, A. W. Thomas, Pion photoproduction of nucleon excited states with Hamiltonian effective field theory, Phys. Rev. D 110 (9) (2024) 094015. [arXiv:2407.05334](#), [doi:10.1103/PhysRevD.110.094015](#).
- [527] J.-J. Liu, Z.-W. Liu, K. Chen, D. Guo, D. B. Leinweber, X. Liu, A. W. Thomas, Structure of the $\Lambda(1670)$ resonance, Phys. Rev. D 109 (5) (2024) 054025. [arXiv:2312.13072](#), [doi:10.1103/PhysRevD.109.054025](#).
- [528] L. Hockley, W. Kamleh, D. Leinweber, A. Thomas, Searching for the first radial excitation of the $\Delta(1232)$ in lattice QCD, J. Phys. G 51 (6) (2024) 065106. [arXiv:2312.11574](#), [doi:10.1088/1361-6471/ad33e2](#).
- [529] C. D. Abell, D. B. Leinweber, Z.-W. Liu, A. W. Thomas, J.-J. Wu, Low-lying odd-parity nucleon resonances as quark-model-like states,

- Phys. Rev. D 108 (9) (2023) 094519. [arXiv:2306.00337](https://arxiv.org/abs/2306.00337), doi:[10.1103/PhysRevD.108.094519](https://doi.org/10.1103/PhysRevD.108.094519).
- [530] J.-j. Wu, D. B. Leinweber, Z.-w. Liu, A. W. Thomas, Structure of the Roper Resonance from Lattice QCD Constraints, Phys. Rev. D 97 (9) (2018) 094509. [arXiv:1703.10715](https://arxiv.org/abs/1703.10715), doi:[10.1103/PhysRevD.97.094509](https://doi.org/10.1103/PhysRevD.97.094509).
- [531] J.-J. Wu, H. Kamano, T. S. H. Lee, D. B. Leinweber, A. W. Thomas, Nucleon resonance structure in the finite volume of lattice QCD, Phys. Rev. D 95 (11) (2017) 114507. [arXiv:1611.05970](https://arxiv.org/abs/1611.05970), doi:[10.1103/PhysRevD.95.114507](https://doi.org/10.1103/PhysRevD.95.114507).
- [532] A. L. Kiratidis, W. Kamleh, D. B. Leinweber, B. J. Owen, Lattice baryon spectroscopy with multi-particle interpolators, Phys. Rev. D 91 (2015) 094509. [arXiv:1501.07667](https://arxiv.org/abs/1501.07667), doi:[10.1103/PhysRevD.91.094509](https://doi.org/10.1103/PhysRevD.91.094509).
- [533] J. Bulava, et al., Hadron Spectroscopy with Lattice QCD, in: Snowmass 2021, 2022. [arXiv:2203.03230](https://arxiv.org/abs/2203.03230).
- [534] M. Padmanath, Hadron Spectroscopy and Resonances: Review, PoS LATTICE2018 (2018) 013. [arXiv:1905.09651](https://arxiv.org/abs/1905.09651), doi:[10.22323/1.334.0013](https://doi.org/10.22323/1.334.0013).
- [535] M. F. M. Lutz, Y. Heo, R. J. Hudspith, QCD in the chiral SU(3) limit from baryon masses on lattice QCD ensembles, Phys. Rev. D 110 (9) (2024) 094046. [arXiv:2406.07442](https://arxiv.org/abs/2406.07442), doi:[10.1103/PhysRevD.110.094046](https://doi.org/10.1103/PhysRevD.110.094046).
- [536] R. J. Hudspith, M. F. M. Lutz, D. Mohler, Precise Omega baryons from lattice QCD (4 2024). [arXiv:2404.02769](https://arxiv.org/abs/2404.02769).
- [537] S. Aoki, et al., FLAG Review 2019: Flavour Lattice Averaging Group (FLAG), Eur. Phys. J. C 80 (2) (2020) 113. [arXiv:1902.08191](https://arxiv.org/abs/1902.08191), doi:[10.1140/epjc/s10052-019-7354-7](https://doi.org/10.1140/epjc/s10052-019-7354-7).
- [538] V. Crede, W. Roberts, Progress towards understanding baryon resonances, Rept. Prog. Phys. 76 (2013) 076301. [arXiv:1302.7299](https://arxiv.org/abs/1302.7299), doi:[10.1088/0034-4885/76/7/076301](https://doi.org/10.1088/0034-4885/76/7/076301).
- [539] A. Thiel, F. Afzal, Y. Wunderlich, Light Baryon Spectroscopy, Prog. Part. Nucl. Phys. 125 (2022) 103949. [arXiv:2202.05055](https://arxiv.org/abs/2202.05055), doi:[10.1016/j.ppnp.2022.103949](https://doi.org/10.1016/j.ppnp.2022.103949).
- [540] D. G. Ireland, E. Pasyuk, I. Strakovsky, Photoproduction Reactions and Non-Strange Baryon Spectroscopy, Prog. Part. Nucl. Phys. 111 (2020) 103752. [arXiv:1906.04228](https://arxiv.org/abs/1906.04228), doi:[10.1016/j.ppnp.2019.103752](https://doi.org/10.1016/j.ppnp.2019.103752).
- [541] B. Krusche, S. Schadmand, Study of nonstrange baryon resonances with meson photoproduction, Prog. Part. Nucl. Phys. 51 (2003) 399–485. [arXiv:nucl-ex/0306023](https://arxiv.org/abs/nucl-ex/0306023), doi:[10.1016/S0146-6410\(03\)90005-6](https://doi.org/10.1016/S0146-6410(03)90005-6).
- [542] J. Bijnens, G. Fäldt, B. M. K. Nefkens (Eds.), Production, interaction and decay of the eta meson. Proceedings, Workshop, Uppsala, Sweden, October 25-27, 2001, Vol. 99, 2002.
- [543] B. Krusche, C. Wilkin, Production of η and η' mesons on nucleons and nuclei, Prog. Part. Nucl. Phys. 80 (2015) 43–95. [arXiv:1410.7680](https://arxiv.org/abs/1410.7680), doi:[10.1016/j.ppnp.2014.10.001](https://doi.org/10.1016/j.ppnp.2014.10.001).
- [544] L. Álvarez-Ruso, On the nature of the Roper resonance, in: Mini-Workshop Bled 2010: Dressing Hadrons, 2010, pp. 1–8. [arXiv:1011.0609](https://arxiv.org/abs/1011.0609).
- [545] M. Ablikim, et al., Partial wave analyses of $\psi(3686) \rightarrow p\bar{p}\pi^0$ and $\psi(3686) \rightarrow p\bar{p}\eta$, Phys. Rev. D 111 (3) (2025) 032011. [arXiv:2412.06247](https://arxiv.org/abs/2412.06247), doi:[10.1103/PhysRevD.111.032011](https://doi.org/10.1103/PhysRevD.111.032011).
- [546] R. G. Ping, H. C. Chiang, B. S. Zou, A Study of the Roper resonance as a hybrid state from J/ψ decays, Nucl. Phys. A 743 (2004) 149–169. [arXiv:nucl-th/0408007](https://arxiv.org/abs/nucl-th/0408007), doi:[10.1016/j.nuclphysa.2004.07.004](https://doi.org/10.1016/j.nuclphysa.2004.07.004).
- [547] L. Álvarez-Ruso, The Role of the Roper resonance in $np \rightarrow d(\pi\pi)^0$, Phys. Lett. B 452 (1999) 207–213. [arXiv:nucl-th/9811058](https://arxiv.org/abs/nucl-th/9811058), doi:[10.1016/S0370-2693\(99\)00310-X](https://doi.org/10.1016/S0370-2693(99)00310-X).
- [548] D. Stamen, D. Winney, A. Rodas, C. Fernández-Ramírez, V. Mathieu, G. Montaña, A. Pilloni, A. P. Szczepaniak, Toward a unified description of hadron scattering at all energies, Phys. Rev. D 110 (11) (2024) 114023. [arXiv:2409.09172](https://arxiv.org/abs/2409.09172), doi:[10.1103/PhysRevD.110.114023](https://doi.org/10.1103/PhysRevD.110.114023).
- [549] J. A. Silva-Castro, C. Fernandez-Ramirez, M. Albaladejo, I. V. Danilkin, A. Jackura, V. Mathieu, J. Nys, A. Pilloni, A. P. Szczepaniak, G. Fox, Regge phenomenology of the N^* and Δ^* poles, Phys. Rev. D 99 (3) (2019) 034003. [arXiv:1809.01954](https://arxiv.org/abs/1809.01954), doi:[10.1103/PhysRevD.99.034003](https://doi.org/10.1103/PhysRevD.99.034003).
- [550] V. Mathieu, J. Nys, C. Fernández-Ramírez, A. Jackura, A. Pilloni, N. Sherrill, A. P. Szczepaniak, G. Fox, Vector Meson Photoproduction with a Linearly Polarized Beam, Phys. Rev. D 97 (9) (2018) 094003. [arXiv:1802.09403](https://arxiv.org/abs/1802.09403), doi:[10.1103/PhysRevD.97.094003](https://doi.org/10.1103/PhysRevD.97.094003).
- [551] V. Mathieu, J. Nys, C. Fernández-Ramírez, A. N. Hiller Blin, A. Jackura, A. Pilloni, A. P. Szczepaniak, G. Fox, Structure of Pion Photoproduction Amplitudes, Phys. Rev. D 98 (1) (2018) 014041. [arXiv:1806.08414](https://arxiv.org/abs/1806.08414), doi:[10.1103/PhysRevD.98.014041](https://doi.org/10.1103/PhysRevD.98.014041).
- [552] J. Nys, A. N. Hiller Blin, V. Mathieu, C. Fernández-Ramírez, A. Jackura, A. Pilloni, J. Ryckebusch, A. P. Szczepaniak, G. Fox, Global analysis of charge exchange meson production at high energies, Phys. Rev. D 98 (3) (2018) 034020. [arXiv:1806.01891](https://arxiv.org/abs/1806.01891), doi:[10.1103/PhysRevD.98.034020](https://doi.org/10.1103/PhysRevD.98.034020).
- [553] J. Nys, V. Mathieu, C. Fernández-Ramírez, A. N. Hiller Blin, A. Jackura, M. Mikhasenko, A. Pilloni, A. P. Szczepaniak, G. Fox, J. Ryckebusch, Finite-energy sum rules in eta photoproduction off a nucleon, Phys. Rev. D 95 (3) (2017) 034014. [arXiv:1611.04658](https://arxiv.org/abs/1611.04658), doi:[10.1103/PhysRevD.95.034014](https://doi.org/10.1103/PhysRevD.95.034014).
- [554] V. Mathieu, I. V. Danilkin, C. Fernández-Ramírez, M. R. Pennington, D. Schott, A. P. Szczepaniak, G. Fox, Toward Complete Pion Nucleon Amplitudes, Phys. Rev. D 92 (7) (2015) 074004. [arXiv:1506.01764](https://arxiv.org/abs/1506.01764), doi:[10.1103/PhysRevD.92.074004](https://doi.org/10.1103/PhysRevD.92.074004).
- [555] M. F. M. Lutz, E. E. Kolomeitsev, C. L. Korpa, Spectral representation for u- and t-channel exchange processes in a partial-wave decomposition, Phys. Rev. D 92 (1) (2015) 016003. [arXiv:1506.02375](https://arxiv.org/abs/1506.02375), doi:[10.1103/PhysRevD.92.016003](https://doi.org/10.1103/PhysRevD.92.016003).
- [556] I. V. Danilkin, A. M. Gasparian, M. F. M. Lutz, On causality, unitarity and perturbative expansions, Phys. Lett. B 697 (2011) 147–152. [arXiv:1009.5928](https://arxiv.org/abs/1009.5928), doi:[10.1016/j.physletb.2011.01.036](https://doi.org/10.1016/j.physletb.2011.01.036).
- [557] D.-L. Yao, L.-Y. Dai, H.-Q. Zheng, Z.-Y. Zhou, A review on partial-wave dynamics with chiral effective field theory and dispersion relation, Rept. Prog. Phys. 84 (7) (2021) 076201. [arXiv:2009.13495](https://arxiv.org/abs/2009.13495), doi:[10.1088/1361-6633/abfa6f](https://doi.org/10.1088/1361-6633/abfa6f).
- [558] J. Adamczewski-Musch, et al., $\Delta(1232)$ Dalitz decay in proton-proton collisions at $T=1.25$ GeV measured with HADES at GSI, Phys. Rev. C 95 (6) (2017) 065205. [arXiv:1703.07840](https://arxiv.org/abs/1703.07840), doi:[10.1103/PhysRevC.95.065205](https://doi.org/10.1103/PhysRevC.95.065205).
- [559] G. Agakishiev, et al., Baryon resonance production and dielectron decays in proton-proton collisions at 3.5 GeV, Eur. Phys. J. A 50 (2014) 82. [arXiv:1403.3054](https://arxiv.org/abs/1403.3054), doi:[10.1140/epja/i2014-14082-1](https://doi.org/10.1140/epja/i2014-14082-1).
- [560] G. Agakishiev, et al., Study of exclusive one-pion and one-eta production using hadron and dielectron channels in pp reactions at kinetic beam energies of 1.25 GeV and 2.2 GeV with HADES, Eur. Phys. J. A 48 (2012) 74. [arXiv:1203.1333](https://arxiv.org/abs/1203.1333), doi:[10.1140/epja/i2012-12074-9](https://doi.org/10.1140/epja/i2012-12074-9).
- [561] M. Röder, et al., Final-State Interactions in the Process $\bar{p}p \rightarrow pK^+\Lambda$, Eur. Phys. J. A 49 (2013) 157. [arXiv:1305.0451](https://arxiv.org/abs/1305.0451), doi:[10.1140/epja/i2013-13157-9](https://doi.org/10.1140/epja/i2013-13157-9).
- [562] M. Abdel-Bary, et al., The $pK^0\Sigma^+$ final state in proton-proton collisions, Eur. Phys. J. A 48 (2012) 23. [arXiv:1202.4108](https://arxiv.org/abs/1202.4108), doi:[10.1140/epja/i2012-12023-8](https://doi.org/10.1140/epja/i2012-12023-8).
- [563] S. Abd El-Samad, et al., Influence of N^* -resonances on hyperon production in the channel $pp \rightarrow K^+\Lambda p$ at 2.95, 3.20 and 3.30 GeV/c beam momentum, Phys. Lett. B 688 (2010) 142–149. [arXiv:1003.0603](https://arxiv.org/abs/1003.0603), doi:[10.1016/j.physletb.2010.03.076](https://doi.org/10.1016/j.physletb.2010.03.076).
- [564] G. Ramalho, M. T. Peña, $\gamma^*N \rightarrow N^*(1520)$ form factors in the timelike regime, Phys. Rev. D 95 (1) (2017) 014003. [arXiv:1610.08788](https://arxiv.org/abs/1610.08788), doi:[10.1103/PhysRevD.95.014003](https://doi.org/10.1103/PhysRevD.95.014003).

- [565] G. Agakishiev, et al., Analysis of pion production data measured by HADES in proton-proton collisions at 1.25 GeV, *Eur. Phys. J. A* 51 (10) (2015) 137. [arXiv:1703.08398](https://arxiv.org/abs/1703.08398), doi:10.1140/epja/i2015-15137-5.
- [566] K. N. Ermakov, V. I. Medvedev, V. A. Nikonorov, O. V. Rogachevsky, A. V. Sarantsev, V. V. Sarantsev, S. G. Sherman, The study of the proton-proton collisions at the beam momentum 1628 MeV/c, *Eur. Phys. J. A* 47 (2011) 159. [arXiv:1109.1111](https://arxiv.org/abs/1109.1111), doi:10.1140/epja/i2011-11159-3.
- [567] J.-J. Xie, H.-X. Chen, E. Oset, The $pp \rightarrow p\Lambda K^+$ and $pp \rightarrow p\Sigma^0 K^+$ reactions with chiral dynamics, *Phys. Rev. C* 84 (2011) 034004. [arXiv:1105.4791](https://arxiv.org/abs/1105.4791), doi:10.1103/PhysRevC.84.034004.
- [568] Y. Valdau, et al., The energy dependence of the $pp \rightarrow K^+ n\Sigma^+$ reaction close to threshold, *Phys. Rev. C* 81 (2010) 045208. [arXiv:1002.3459](https://arxiv.org/abs/1002.3459), doi:10.1103/PhysRevC.81.045208.
- [569] X. Cao, X.-G. Lee, Q.-W. Wang, Strangeness production process $pp \rightarrow nK^+\Sigma^+$ within resonance model, *Chin. Phys. Lett.* 25 (2008) 888–891. [arXiv:0711.3063](https://arxiv.org/abs/0711.3063), doi:10.1088/0256-307X/25/3/023.
- [570] J.-J. Xie, B.-S. Zou, The Role of $\Delta^{++}(1620)$ resonances in $pp \rightarrow nK^+\Sigma^+$ reaction and its important implications, *Phys. Lett. B* 649 (2007) 405–412. [arXiv:nucl-th/0701021](https://arxiv.org/abs/nucl-th/0701021), doi:10.1016/j.physletb.2007.04.035.
- [571] A. V. Anisovich, V. V. Anisovich, E. Klempert, V. A. Nikonorov, A. V. Sarantsev, Baryon-baryon and baryon-antibaryon interaction amplitudes in the spin-momentum operator expansion method, *Eur. Phys. J. A* 34 (2007) 129–152. doi:10.1140/epja/i2007-10499-9.
- [572] A. Sibirtsev, J. Haidenbauer, H. W. Hammer, U.-G. Meißner, The $pp \rightarrow K^+\Sigma^+n$ cross section from missing mass spectra, *Eur. Phys. J. A* 32 (2007) 229–241. [arXiv:hep-ph/0701269](https://arxiv.org/abs/hep-ph/0701269), doi:10.1140/epja/i2007-10370-1.
- [573] A. Sibirtsev, J. Haidenbauer, H. W. Hammer, U.-G. Meißner, Phenomenology of the Lambda/Sigma0 production ratio in pp collisions, *Eur. Phys. J. A* 29 (2006) 363–367. [arXiv:hep-ph/0608098](https://arxiv.org/abs/hep-ph/0608098), doi:10.1140/epja/i2006-10097-5.
- [574] A. Sibirtsev, J. Haidenbauer, H.-W. Hammer, S. Krewald, Resonances and final state interactions in the reaction $pp \rightarrow pK^+\Lambda$, *Eur. Phys. J. A* 27 (3) (2006) 269–285. [arXiv:nucl-th/0512059](https://arxiv.org/abs/nucl-th/0512059), doi:10.1140/epja/i2005-10268-x.
- [575] S. Teis, W. Cassing, M. Effenberger, A. Hombach, U. Mosel, G. Wolf, Pion production in heavy ion collisions at SIS energies, *Z. Phys. A* 356 (1997) 421–435. [arXiv:nucl-th/9609009](https://arxiv.org/abs/nucl-th/9609009), doi:10.1007/BF02769248.
- [576] A. Gasparian, J. Haidenbauer, C. Hanhart, L. Kondratyuk, J. Speth, The reactions $pp \rightarrow p\Lambda K^+$ and $pp \rightarrow p\Sigma^0 K^+$ near their thresholds, *Phys. Lett. B* 480 (2000) 273–279. [arXiv:nucl-th/9909017](https://arxiv.org/abs/nucl-th/9909017), doi:10.1016/S0370-2693(00)00412-3.
- [577] V. Baru, A. M. Gasparyan, J. Haidenbauer, C. Hanhart, A. E. Kudryavtsev, J. Speth, Production of η mesons in nucleon-nucleon collisions, *Phys. Rev. C* 67 (2003) 024002. [arXiv:nucl-th/0212014](https://arxiv.org/abs/nucl-th/0212014), doi:10.1103/PhysRevC.67.024002.
- [578] P. Salabura, J. Stroth, Dilepton radiation from strongly interacting systems, *Prog. Part. Nucl. Phys.* 120 (2021) 103869. [arXiv:2005.14589](https://arxiv.org/abs/2005.14589), doi:10.1016/j.ppnp.2021.103869.
- [579] J. M. Laget, Exclusive Meson Photo- and Electro-production, a Window on the Structure of Hadronic Matter, *Prog. Part. Nucl. Phys.* 111 (2020) 103737. [arXiv:1911.04825](https://arxiv.org/abs/1911.04825), doi:10.1016/j.ppnp.2019.103737.
- [580] H. Lenske, M. Dhar, T. Gaitanos, X. Cao, Baryons and baryon resonances in nuclear matter, *Prog. Part. Nucl. Phys.* 98 (2018) 119–206. doi:10.1016/j.ppnp.2017.09.001.
- [581] V. Metag, M. Nanova, E. Y. Paryev, Meson–nucleus potentials and the search for meson–nucleus bound states, *Prog. Part. Nucl. Phys.* 97 (2017) 199–260. [arXiv:1706.09654](https://arxiv.org/abs/1706.09654), doi:10.1016/j.ppnp.2017.08.002.
- [582] P. Moskal, M. Wolke, A. Khokhaz, W. Oelert, Close-to-threshold meson production in hadronic interactions, *Prog. Part. Nucl. Phys.* 49 (2002) 1. [arXiv:hep-ph/0208002](https://arxiv.org/abs/hep-ph/0208002), doi:10.1016/S0146-6410(02)00143-6.
- [583] P. Gonzalez, J. Vijande, A. Valcarce, Meson-baryon threshold effects in the light-quark baryon spectrum, *Phys. Rev. C* 77 (2008) 065213. [arXiv:0805.4677](https://arxiv.org/abs/0805.4677), doi:10.1103/PhysRevC.77.065213.
- [584] D. Drechsel, L. Tiator, Threshold pion photoproduction on nucleons, *J. Phys. G* 18 (1992) 449–497. doi:10.1088/0954-3899/18/3/004.
- [585] T. Hyodo, M. Niiyama, QCD and the strange baryon spectrum, *Prog. Part. Nucl. Phys.* 120 (2021) 103868. [arXiv:2010.07592](https://arxiv.org/abs/2010.07592), doi:10.1016/j.ppnp.2021.103868.
- [586] L. Tolos, L. Fabbietti, Strangeness in Nuclei and Neutron Stars, *Prog. Part. Nucl. Phys.* 112 (2020) 103770. [arXiv:2002.09223](https://arxiv.org/abs/2002.09223), doi:10.1016/j.ppnp.2020.103770.
- [587] R. E. Cutkosky, R. E. Hendrick, J. W. Alcock, Y. A. Chao, R. G. Lipes, J. C. Sandusky, R. L. Kelly, PION - NUCLEON PARTIAL WAVE ANALYSIS, *Phys. Rev. D* 20 (1979) 2804. doi:10.1103/PhysRevD.20.2804.
- [588] R. E. Cutkosky, C. P. Forsyth, R. E. Hendrick, R. L. Kelly, Pion - Nucleon Partial Wave Amplitudes, *Phys. Rev. D* 20 (1979) 2839. doi:10.1103/PhysRevD.20.2839.
- [589] R. Koch, E. Pietarinen, Low-Energy pi N Partial Wave Analysis, *Nucl. Phys. A* 336 (1980) 331–346. doi:10.1016/0375-9474(80)90214-6.
- [590] D. M. Manley, R. A. Arndt, Y. Goradia, V. L. Teplitz, An Isobar Model Partial Wave Analysis of $\pi N \rightarrow \pi\pi N$ in the Center-of-mass Energy Range 1320–1930 MeV, *Phys. Rev. D* 30 (1984) 904. doi:10.1103/PhysRevD.30.904.
- [591] D. M. Manley, E. M. Saleski, Multichannel resonance parametrization of πN scattering amplitudes, *Phys. Rev. D* 45 (1992) 4002–4033. doi:10.1103/PhysRevD.45.4002.
- [592] T. P. Vrana, S. A. Dytman, T. S. H. Lee, Baryon resonance extraction from pi N data using a unitary multichannel model, *Phys. Rept.* 328 (2000) 181–236. [arXiv:nucl-th/9910012](https://arxiv.org/abs/nucl-th/9910012), doi:10.1016/S0370-1573(99)00108-8.
- [593] M. Batinic, I. Slaus, A. Švarc, B. M. K. Nefkens, $\pi N \rightarrow \eta N$ and $\eta N \rightarrow \eta N$ partial wave T matrices in a coupled, three channel model, *Phys. Rev. C* 51 (1995) 2310–2325, [Erratum: Phys. Rev. C 57, 1004–1005 (1998)]. [arXiv:nucl-th/9501011](https://arxiv.org/abs/nucl-th/9501011), doi:10.1103/PhysRevC.57.1004.
- [594] M. Batinic, I. Dadić, I. Slaus, A. Švarc, B. M. K. Nefkens, T. S. H. Lee, Update of the $\pi N \rightarrow \eta N$ and $\eta N \rightarrow \eta N$ partial wave amplitudes (3 1997). [arXiv:nucl-th/9703023](https://arxiv.org/abs/nucl-th/9703023).
- [595] S. Ceci, A. Švarc, B. Zauner, $\pi N \rightarrow \eta N$ data require the existence of the $N(1710)P_{11}$ resonance reducing the 1700-MeV continuum ambiguity, *Phys. Rev. Lett.* 97 (2006) 062002. [arXiv:hep-ph/0603144](https://arxiv.org/abs/hep-ph/0603144), doi:10.1103/PhysRevLett.97.062002.
- [596] M. Batinic, S. Ceci, A. Švarc, B. Zauner, Poles of the Zagreb analysis partial-wave T matrices, *Phys. Rev. C* 82 (2010) 038203. doi:10.1103/PhysRevC.82.038203.
- [597] R. A. Arndt, J. M. Ford, L. D. Roper, Pion-nucleon partial-wave analysis to 1100-MeV, *Phys. Rev. D* 32 (1985) 1085. doi:10.1103/PhysRevD.32.1085.
- [598] R. A. Arndt, I. I. Strakovsky, R. L. Workman, M. M. Pavan, Updated analysis of πN elastic scattering data to 2.1-GeV: The Baryon spectrum, *Phys. Rev. C* 52 (1995) 2120–2130. [arXiv:nucl-th/9505040](https://arxiv.org/abs/nucl-th/9505040), doi:10.1103/PhysRevC.52.2120.
- [599] R. A. Arndt, A. M. Green, R. L. Workman, S. Wycech, Energies and residues of the nucleon resonances N(1535) and N(1650), *Phys. Rev. C* 58 (1998) 3636–3640. [arXiv:nucl-th/9807009](https://arxiv.org/abs/nucl-th/9807009), doi:10.1103/PhysRevC.58.3636.
- [600] M. Dugger, et al., π^0 photoproduction on the proton for photon energies from 0.675 to 2.875-GeV, *Phys. Rev. C* 76 (2007) 025211. [arXiv:0705.0816](https://arxiv.org/abs/0705.0816), doi:10.1103/PhysRevC.76.025211.
- [601] R. L. Workman, R. A. Arndt, M. W. Paris, Resonance parameters from K-matrix and T-matrix poles, *Phys. Rev. C* 79 (2009) 038201.

- [arXiv:0808.2176](#), [doi:10.1103/PhysRevC.79.038201](#).
- [602] R. Arndt, W. Briscoe, I. Strakovsky, R. Workman, Partial-wave analysis and baryon spectroscopy, *Eur. Phys. J. A* 35 (2008) 311–316. [doi:10.1140/epja/i2008-10572-y](#).
- [603] M. Dugger, et al., pi+ photoproduction on the proton for photon energies from 0.725 to 2.875-GeV, *Phys. Rev. C* 79 (2009) 065206. [arXiv:0903.1110](#), [doi:10.1103/PhysRevC.79.065206](#).
- [604] R. L. Workman, W. J. Briscoe, M. W. Paris, I. I. Strakovsky, Updated SAID analysis of pion photoproduction data, *Phys. Rev. C* 85 (2012) 025201. [arXiv:1109.0722](#), [doi:10.1103/PhysRevC.85.025201](#).
- [605] R. L. Workman, M. W. Paris, W. J. Briscoe, I. I. Strakovsky, Unified Chew-Mandelstam SAID analysis of pion photoproduction data, *Phys. Rev. C* 86 (2012) 015202. [arXiv:1202.0845](#), [doi:10.1103/PhysRevC.86.015202](#).
- [606] R. L. Workman, R. A. Arndt, W. J. Briscoe, M. W. Paris, I. I. Strakovsky, Parameterization dependence of T matrix poles and eigenphases from a fit to πN elastic scattering data, *Phys. Rev. C* 86 (2012) 035202. [arXiv:1204.2277](#), [doi:10.1103/PhysRevC.86.035202](#).
- [607] M. Dugger, et al., Beam asymmetry Σ for π^+ and π^0 photoproduction on the proton for photon energies from 1.102 to 1.862 GeV, *Phys. Rev. C* 88 (6) (2013) 065203, [Addendum: *Phys. Rev. C* 89, 029901 (2014)]. [arXiv:1308.4028](#), [doi:10.1103/PhysRevC.88.065203](#).
- [608] P. Adlarson, et al., Measurement of π^0 photoproduction on the proton at MAMI C, *Phys. Rev. C* 92 (2) (2015) 024617. [arXiv:1506.08849](#), [doi:10.1103/PhysRevC.92.024617](#).
- [609] S. Strauch, et al., First Measurement of the Polarization Observable E in the $\vec{p}(\vec{\gamma}, \pi^+)n$ Reaction up to 2.25 GeV, *Phys. Lett. B* 750 (2015) 53–58. [arXiv:1503.05163](#), [doi:10.1016/j.physletb.2015.08.053](#).
- [610] A. V. Anisovich, et al., The impact of new polarization data from Bonn, Mainz and Jefferson Laboratory on $\gamma p \rightarrow \pi N$ multipoles, *Eur. Phys. J. A* 52 (9) (2016) 284. [arXiv:1604.05704](#), [doi:10.1140/epja/i2016-16284-9](#).
- [611] V. L. Kashevarev, et al., Study of η and η' Photoproduction at MAMI, *Phys. Rev. Lett.* 118 (21) (2017) 212001. [arXiv:1701.04809](#), [doi:10.1103/PhysRevLett.118.212001](#).
- [612] D. Ho, et al., Beam-Target Helicity Asymmetry for $\vec{\gamma}\vec{n} \rightarrow \pi^- p$ in the N^* Resonance Region, *Phys. Rev. Lett.* 118 (24) (2017) 242002. [arXiv:1705.04713](#), [doi:10.1103/PhysRevLett.118.242002](#).
- [613] W. J. Briscoe, et al., Cross section for $\gamma n \rightarrow \pi^0 n$ at the Mainz A2 experiment, *Phys. Rev. C* 100 (6) (2019) 065205. [arXiv:1908.02730](#), [doi:10.1103/PhysRevC.100.065205](#).
- [614] W. J. Briscoe, A. E. Kudryavtsev, I. I. Strakovsky, V. E. Tarasov, R. L. Workman, Threshold π^- photoproduction on the neutron, *Eur. Phys. J. A* 56 (8) (2020) 218. [arXiv:2004.01742](#), [doi:10.1140/epja/s10050-020-00221-w](#).
- [615] I. Strakovsky, S. Sirca, W. J. Briscoe, A. Deur, A. Schmidt, R. L. Workman, Single-pion contribution to the Gerasimov-Drell-Hearn sum rule and related integrals, *Phys. Rev. C* 105 (4) (2022) 045202. [arXiv:2201.06495](#), [doi:10.1103/PhysRevC.105.045202](#).
- [616] W. J. Briscoe, A. Schmidt, I. Strakovsky, R. L. Workman, A. Svarc, Extended SAID partial-wave analysis of pion photoproduction, *Phys. Rev. C* 108 (6) (2023) 065205. [arXiv:2309.06631](#), [doi:10.1103/PhysRevC.108.065205](#).
- [617] W. R. Frazer, J. R. Fulco, Partial-Wave Dispersion Relations for Pion-Nucleon Scattering, *Phys. Rev.* 119 (1960) 1420–1426. [doi:10.1103/PhysRev.119.1420](#).
- [618] S. Mandelstam, Determination of the pion - nucleon scattering amplitude from dispersion relations and unitarity. General theory, *Phys. Rev.* 112 (1958) 1344–1360. [doi:10.1103/PhysRev.112.1344](#).
- [619] M. Döring, J. Revier, D. Rönchen, R. L. Workman, Correlations of πN partial waves for multireaction analyses, *Phys. Rev. C* 93 (6) (2016) 065205. [arXiv:1603.07265](#), [doi:10.1103/PhysRevC.93.065205](#).
- [620] W. J. Briscoe, M. Döring, H. Haberzettl, D. M. Manley, M. Naruki, I. I. Strakovsky, E. S. Swanson, Physics opportunities with meson beams, *Eur. Phys. J. A* 51 (10) (2015) 129. [arXiv:1503.07763](#), [doi:10.1140/epja/i2015-15129-5](#).
- [621] W. J. Briscoe, M. Döring, H. Haberzettl, D. M. Manley, M. Naruki, G. Smith, I. Strakovsky, E. S. Swanson, Physics Opportunities with Meson Beams for EIC (8 2021). [arXiv:2108.07591](#).
- [622] D. Drechsel, O. Hanstein, S. S. Kamalov, L. Tiator, A Unitary isobar model for pion photoproduction and electroproduction on the proton up to 1-GeV, *Nucl. Phys. A* 645 (1999) 145–174. [arXiv:nucl-th/9807001](#), [doi:10.1016/S0375-9474\(98\)00572-7](#).
- [623] A. Anisovich, E. Klempt, A. Sarantsev, U. Thoma, Partial wave decomposition of pion and photoproduction amplitudes, *Eur. Phys. J. A* 24 (2005) 111–128. [arXiv:hep-ph/0407211](#), [doi:10.1140/epja/i2004-10125-6](#).
- [624] D. Drechsel, S. S. Kamalov, L. Tiator, Unitary Isobar Model - MAID2007, *Eur. Phys. J. A* 34 (2007) 69–97. [arXiv:0710.0306](#), [doi:10.1140/epja/i2007-10490-6](#).
- [625] A. V. Anisovich, R. Beck, E. Klempt, V. A. Nikonorov, A. V. Sarantsev, U. Thoma, Properties of baryon resonances from a multichannel partial wave analysis, *Eur. Phys. J. A* 48 (2012) 15. [arXiv:1112.4937](#), [doi:10.1140/epja/i2012-12015-8](#).
- [626] Y.-F. Wang, M. Döring, J. Hergenrather, M. Mai, T. Mart, U.-G. Meißner, D. Rönchen, R. Workman, Global Data-Driven Determination of Baryon Transition Form Factors, *Phys. Rev. Lett.* 133 (10) (2024) 101901. [arXiv:2404.17444](#), [doi:10.1103/PhysRevLett.133.101901](#).
- [627] D. J. Candlin, et al., Differential Cross-section and Polarization for $\pi^+ p \rightarrow K^+ \Sigma^+$ at 26 Momenta Between 1.282-GeV/c and 2.473-GeV/c, *Nucl. Phys. B* 226 (1983) 1. [doi:10.1016/0550-3213\(83\)90461-3](#).
- [628] D. J. Candlin, et al., Measurement of the Spin Rotation Parameter, β , in the Reaction $\pi^+ p \rightarrow K^+ \Sigma^+$ at 1.60-GeV/c and 1.88-GeV/c, *Nucl. Phys. B* 311 (1989) 613–629. [doi:10.1016/0550-3213\(89\)90170-3](#).
- [629] Website with figures of JBW fits to pion- and photon-induced single-meson production data, including reference of all data, https://collaborations.fz-juelich.de/ikp/meson-baryon/juelich_amplitudes.html.
- [630] I. G. Alekseev, et al., High-precision measurements of πp elastic differential cross sections in the second resonance region, *Phys. Rev. C* 91 (2) (2015) 025205. [arXiv:1410.6418](#), [doi:10.1103/PhysRevC.91.025205](#).
- [631] K. Shirotori, et al., Search for the Θ^+ pentaquark via the $\pi^- p \rightarrow K^- X$ reaction at 1.92 GeV/c, *Phys. Rev. Lett.* 109 (2012) 132002. [arXiv:1203.3604](#), [doi:10.1103/PhysRevLett.109.132002](#).
- [632] H. Ohnishi, F. Sakuma, T. Takahashi, Hadron Physics at J-PARC, *Prog. Part. Nucl. Phys.* 113 (2020) 103773. [arXiv:1912.02380](#), [doi:10.1016/j.ppnp.2020.103773](#).
- [633] P. Salabura, J. Stroth, L. Fabbietti, The HADES Pion Beam Facility, *Nucl. Phys. News* 25 (2) (2015) 22–24. [doi:10.1080/10619127.2015.1035929](#).
- [634] H. Kamano, Impact of $\pi N \rightarrow \pi\pi N$ data on determining high-mass nucleon resonances, *Phys. Rev. C* 88 (2013) 045203. [arXiv:1305.6678](#), [doi:10.1103/PhysRevC.88.045203](#).
- [635] H. Sako, S. Hasegawa, K. Hosomi, Y. Ichikawa, K. Imai, K. Hicks, J. K. Ahn, S. Kim, J. Lee, S. Hwang, Baryon spectroscopy in $(\pi, 2\pi)$ reactions with 10^6 Hz pion beams at J-PARC, *Pos INPC2016* (2017) 266. [doi:10.22323/1.281.0266](#).
- [636] C. Gleason, Amplitude analysis of $\eta\pi$ final states at glueX, *Rev. Mex. Fis. Suppl.* 3 (3) (2022) 0308021. [doi:10.31349/SuplRevMexFis.3.0308021](#).
- [637] A. Rodas, et al., Determination of the pole position of the lightest hybrid meson candidate, *Phys. Rev. Lett.* 122 (4) (2019) 042002. [arXiv:1810.04171](#), [doi:10.1103/PhysRevLett.122.042002](#).

- [638] A. Jackura, et al., New analysis of $\eta\pi$ tensor resonances measured at the COMPASS experiment, Phys. Lett. B 779 (2018) 464–472. [arXiv:1707.02848](https://arxiv.org/abs/1707.02848), doi:10.1016/j.physletb.2018.01.017.
- [639] C. Adolph, et al., Odd and even partial waves of $\eta\pi^-$ and $\eta'\pi^-$ in $\pi^-p \rightarrow \eta^{(\prime)}\pi^-p$ at 191 GeV/c, Phys. Lett. B 740 (2015) 303–311, [Erratum: Phys.Lett.B 811, 135913 (2020)]. [arXiv:1408.4286](https://arxiv.org/abs/1408.4286), doi:10.1016/j.physletb.2014.11.058.
- [640] R. Arndt, Private communication.
- [641] K. Hicks, H. Sako et al., Measurement of $\pi N \rightarrow \pi\pi N$ and $\pi N \rightarrow KY$ at J-PARC (J-PARC E45), http://j-parc.jp/researcher/Hadron/en/pac_1207/pdf/P45_2012-3.pdf.
- [642] R. K. Bradford, et al., First measurement of beam-recoil observables C_x and C_z in hyperon photoproduction, Phys. Rev. C 75 (2007) 035205. [arXiv:nucl-ex/0611034](https://arxiv.org/abs/nucl-ex/0611034), doi:10.1103/PhysRevC.75.035205.
- [643] M. E. McCracken, et al., Differential cross section and recoil polarization measurements for the $\gamma p \rightarrow K^+\Lambda$ reaction using CLAS at Jefferson Lab, Phys. Rev. C 81 (2010) 025201. [arXiv:0912.4274](https://arxiv.org/abs/0912.4274), doi:10.1103/PhysRevC.81.025201.
- [644] I. Senderovich, et al., First measurement of the helicity asymmetry E in η photoproduction on the proton, Phys. Lett. B 755 (2016) 64–69. [arXiv:1507.00325](https://arxiv.org/abs/1507.00325), doi:10.1016/j.physletb.2016.01.044.
- [645] P. Collins, et al., Photon beam asymmetry Σ for η and η' photoproduction from the proton, Phys. Lett. B 771 (2017) 213–221. [arXiv:1703.00433](https://arxiv.org/abs/1703.00433), doi:10.1016/j.physletb.2017.05.045.
- [646] L. Clark, et al., Photoproduction of the Σ^+ hyperon using linearly polarized photons with CLAS, Phys. Rev. C 111 (2) (2025) 025204. [arXiv:2404.19404](https://arxiv.org/abs/2404.19404), doi:10.1103/PhysRevC.111.025204.
- [647] V. Crede, et al., Photoproduction of η mesons off protons for 0.75-GeV < E_γ < 3-GeV, Phys. Rev. Lett. 94 (2005) 012004. [arXiv:hep-ex/0311045](https://arxiv.org/abs/hep-ex/0311045), doi:10.1103/PhysRevLett.94.012004.
- [648] R. Castelijns, et al., Nucleon resonance decay by the K0 Sigma+ channel, Eur. Phys. J. A 35 (2008) 39–45. [arXiv:nucl-ex/0702033](https://arxiv.org/abs/nucl-ex/0702033), doi:10.1140/epja/i2007-10529-8.
- [649] I. Jaegle, et al., Quasi-free photoproduction of η mesons of the neutron, Phys. Rev. Lett. 100 (2008) 252002. [arXiv:0804.4841](https://arxiv.org/abs/0804.4841), doi:10.1103/PhysRevLett.100.252002.
- [650] V. Crede, et al., Photoproduction of η and η' mesons off protons, Phys. Rev. C 80 (2009) 055202. [arXiv:0909.1248](https://arxiv.org/abs/0909.1248), doi:10.1103/PhysRevC.80.055202.
- [651] A. Thiel, et al., Well-established nucleon resonances revisited by double-polarization measurements, Phys. Rev. Lett. 109 (2012) 102001. [arXiv:1207.2686](https://arxiv.org/abs/1207.2686), doi:10.1103/PhysRevLett.109.102001.
- [652] E. Gutz, et al., High statistics study of the reaction $\gamma p \rightarrow p\pi^0\eta$, Eur. Phys. J. A 50 (2014) 74. [arXiv:1402.4125](https://arxiv.org/abs/1402.4125), doi:10.1140/epja/i2014-14074-1.
- [653] F. Afzal, et al., Observation of the $p\eta'$ Cusp in the New Precise Beam Asymmetry Σ Data for $\gamma p \rightarrow p\eta$, Phys. Rev. Lett. 125 (15) (2020) 152002. [arXiv:2009.06248](https://arxiv.org/abs/2009.06248), doi:10.1103/PhysRevLett.125.152002.
- [654] E. O. Rosanowski, et al., $K^+\Lambda(1520)$ photoproduction at forward angles near threshold with the BGOOD experiment (6 2024). [arXiv:2406.01121](https://arxiv.org/abs/2406.01121).
- [655] A. J. C. Figueiredo, et al., Coherent $\pi^0\eta d$ photoproduction at forward deuteron angles measured at BGOOD (5 2024). [arXiv:2405.09392](https://arxiv.org/abs/2405.09392).
- [656] T. C. Jude, et al., Evidence of a dibaryon spectrum in coherent $\pi^0\pi^0d$ photoproduction at forward deuteron angles, Phys. Lett. B 832 (2022) 137277. [arXiv:2202.08594](https://arxiv.org/abs/2202.08594), doi:10.1016/j.physletb.2022.137277.
- [657] K. Kohl, et al., Measurement of the $\gamma n \rightarrow K^0\Sigma^0$ differential cross section over the K^* threshold, Eur. Phys. J. A 59 (11) (2023) 254. [arXiv:2108.13319](https://arxiv.org/abs/2108.13319), doi:10.1140/epja/s10050-023-01133-1.
- [658] G. Scheluchin, et al., Photoproduction of $K^+\Lambda(1405) \rightarrow K^+\pi^0\Sigma^0$ extending to forward angles and low momentum transfer, Phys. Lett. B 833 (2022) 137375. [arXiv:2108.12235](https://arxiv.org/abs/2108.12235), doi:10.1016/j.physletb.2022.137375.
- [659] S. Alef, et al., $K^+\Lambda$ photoproduction at forward angles and low momentum transfer, Eur. Phys. J. A 57 (2) (2021) 80. [arXiv:2006.12350](https://arxiv.org/abs/2006.12350), doi:10.1140/epja/s10050-021-00392-0.
- [660] T. C. Jude, et al., Observation of a cusp-like structure in the $\gamma p \rightarrow K^+\Sigma^0$ cross section at forward angles and low momentum transfer, Phys. Lett. B 820 (2021) 136559. [arXiv:2006.12437](https://arxiv.org/abs/2006.12437), doi:10.1016/j.physletb.2021.136559.
- [661] S. Alef, et al., The BGOOD experimental setup at ELSA, Eur. Phys. J. A 56 (4) (2020) 104. [arXiv:1910.11939](https://arxiv.org/abs/1910.11939), doi:10.1140/epja/s10050-020-00107-x.
- [662] T. C. Jude, et al., $K^+\Lambda$ and $K^+\Sigma^0$ photoproduction with fine center-of-mass energy resolution, Phys. Lett. B 735 (2014) 112–118. [arXiv:1308.5659](https://arxiv.org/abs/1308.5659), doi:10.1016/j.physletb.2014.06.015.
- [663] D. Werthmüller, et al., Quasifree photoproduction of η mesons off protons and neutrons, Phys. Rev. C 90 (1) (2014) 015205. [arXiv:1407.6974](https://arxiv.org/abs/1407.6974), doi:10.1103/PhysRevC.90.015205.
- [664] E. F. McNicoll, et al., Study of the $\gamma p \rightarrow \eta p$ reaction with the Crystal Ball detector at the Mainz Microtron(MAMI-C), Phys. Rev. C 82 (2010) 035208, [Erratum: Phys.Rev.C 84, 029901 (2011)]. [arXiv:1007.0777](https://arxiv.org/abs/1007.0777), doi:10.1103/PhysRevC.84.029901.
- [665] V. L. Kashevarov, et al., Photoproduction of $\pi^0\eta$ on protons and the $\Delta(1700)$ D_{33} resonance, Eur. Phys. J. A 42 (2009) 141–149. [arXiv:0901.3888](https://arxiv.org/abs/0901.3888), doi:10.1140/epja/i2009-10868-4.
- [666] J. Ahrens, et al., First measurement of the Gerasimov-Drell-Hearn integral for Hydrogen from 200 to 800 MeV, Phys. Rev. Lett. 87 (2001) 022003. [arXiv:hep-ex/0105089](https://arxiv.org/abs/hep-ex/0105089), doi:10.1103/PhysRevLett.87.022003.
- [667] H. Kohri, et al., Differential cross section and photon beam asymmetry for the $\bar{\gamma}p \rightarrow \pi^+$ reaction at forward π^+ angles at $E_\gamma = 1.5\text{--}2.95$ GeV, Phys. Rev. C 97 (1) (2018) 015205. [arXiv:1708.09574](https://arxiv.org/abs/1708.09574), doi:10.1103/PhysRevC.97.015205.
- [668] S. H. Shiu, et al., Photoproduction of Λ and Σ^0 hyperons off protons with linearly polarized photons at $E_\gamma = 1.5\text{--}3.0$ GeV, Phys. Rev. C 97 (1) (2018) 015208. [arXiv:1711.04996](https://arxiv.org/abs/1711.04996), doi:10.1103/PhysRevC.97.015208.
- [669] M. Sumihama, et al., Backward-angle η photoproduction from protons at $E_\gamma = 1.6\text{--}2.4$ GeV, Phys. Rev. C 80 (2009) 052201. [arXiv:0910.0900](https://arxiv.org/abs/0910.0900), doi:10.1103/PhysRevC.80.052201.
- [670] M. Sumihama, et al., The $\bar{\gamma}p \rightarrow K^+\Lambda$ and $\bar{\gamma}p \rightarrow K^+\Sigma^0$ reactions at forward angles with photon energies from 1.5-GeV to 2.4-GeV, Phys. Rev. C 73 (2006) 035214. [arXiv:hep-ex/0512053](https://arxiv.org/abs/hep-ex/0512053), doi:10.1103/PhysRevC.73.035214.
- [671] T. Ishikawa, et al., ωN scattering length from ω photoproduction on the proton near the threshold, Phys. Rev. C 101 (5) (2020) 052201. [arXiv:1904.02797](https://arxiv.org/abs/1904.02797), doi:10.1103/PhysRevC.101.052201.
- [672] A. Lleres, et al., Measurement of beam-recoil observables $O(x)$, $O(z)$ and target asymmetry for the reaction $\gamma p \rightarrow K^+\Lambda$, Eur. Phys. J. A 39 (2009) 149–161. [arXiv:0807.3839](https://arxiv.org/abs/0807.3839), doi:10.1140/epja/i2008-10713-4.
- [673] A. M. Sandorfi, B. Dey, A. Sarantsev, L. Tiator, R. Workman, A Rosetta Stone Relating Conventions In Photo-Meson Partial Wave Analyses, AIP Conf. Proc. 1432 (1) (2012) 219–222. [arXiv:1108.5411](https://arxiv.org/abs/1108.5411), doi:10.1063/1.3701216.
- [674] J. Ahrens, et al., Helicity dependence of $\gamma p \rightarrow N\pi$ below 450-MeV and contribution to the Gerasimov-Drell-Hearn sum rule, Phys. Rev. Lett. 84 (2000) 5950–5954. [arXiv:0003.05950](https://arxiv.org/abs/0003.05950), doi:10.1103/PhysRevLett.84.5950.
- [675] H. W. Griesshammer, J. A. McGovern, D. R. Phillips, G. Feldman, Using effective field theory to analyse low-energy Compton scattering data from protons and light nuclei, Prog. Part. Nucl. Phys. 67 (2012) 841–897. [arXiv:1203.6834](https://arxiv.org/abs/1203.6834), doi:10.1016/j.ppnp.2012.04.003.

- [676] J. A. McGovern, D. R. Phillips, H. W. Griesshammer, Compton scattering from the proton in an effective field theory with explicit Delta degrees of freedom, *Eur. Phys. J. A* 49 (2013) 12. [arXiv:1210.4104](https://arxiv.org/abs/1210.4104), [doi:10.1140/epja/i2013-13012-1](https://doi.org/10.1140/epja/i2013-13012-1).
- [677] V. Shklyar, H. Lenske, U. Mosel, η -photoproduction in the resonance energy region, *Phys. Lett. B* 650 (2007) 172–178. [arXiv:nucl-th/0611036](https://arxiv.org/abs/nucl-th/0611036), [doi:10.1016/j.physletb.2007.05.005](https://doi.org/10.1016/j.physletb.2007.05.005).
- [678] L. Witthauer, et al., Insight into the Narrow Structure in η Photoproduction on the Neutron from Helicity-Dependent Cross Sections, *Phys. Rev. Lett.* 117 (13) (2016) 132502. [arXiv:1702.01408](https://arxiv.org/abs/1702.01408), [doi:10.1103/PhysRevLett.117.132502](https://doi.org/10.1103/PhysRevLett.117.132502).
- [679] D. Diakonov, V. Petrov, M. V. Polyakov, Exotic anti-decuplet of baryons: Prediction from chiral solitons, *Z. Phys. A* 359 (1997) 305–314. [arXiv:hep-ph/9703373](https://arxiv.org/abs/hep-ph/9703373), [doi:10.1007/s002180050406](https://doi.org/10.1007/s002180050406).
- [680] A. V. Anisovich, V. Burkert, E. Klempert, V. A. Nikonov, A. V. Sarantsev, U. Thoma, Scrutinizing the evidence for N(1685), *Phys. Rev. C* 95 (3) (2017) 035211. [arXiv:1701.06387](https://arxiv.org/abs/1701.06387), [doi:10.1103/PhysRevC.95.035211](https://doi.org/10.1103/PhysRevC.95.035211).
- [681] V. Shklyar, H. Lenske, U. Mosel, η -meson production in the resonance-energy region, *Phys. Rev. C* 87 (1) (2013) 015201. [arXiv:1206.5414](https://arxiv.org/abs/1206.5414), [doi:10.1103/PhysRevC.87.015201](https://doi.org/10.1103/PhysRevC.87.015201).
- [682] A. Švarc, et al., Connection between angle-dependent phase ambiguities and the uniqueness of the partial-wave decomposition, *Phys. Rev. C* 97 (5) (2018) 054611. [arXiv:1706.03211](https://arxiv.org/abs/1706.03211), [doi:10.1103/PhysRevC.97.054611](https://doi.org/10.1103/PhysRevC.97.054611).
- [683] I. S. Barker, A. Donnachie, J. K. Storrow, Complete Experiments in Pseudoscalar Photoproduction, *Nucl. Phys. B* 95 (1975) 347–356. [doi:10.1016/0550-3213\(75\)90049-8](https://doi.org/10.1016/0550-3213(75)90049-8).
- [684] A. M. Sandorfi, S. Hoblit, H. Kamano, T. S. H. Lee, Determining pseudoscalar meson photo-production amplitudes from complete experiments, *J. Phys. G* 38 (2011) 053001. [arXiv:1010.4555](https://arxiv.org/abs/1010.4555), [doi:10.1088/0954-3899/38/5/053001](https://doi.org/10.1088/0954-3899/38/5/053001).
- [685] Y. Wunderlich, R. Beck, L. Tiator, The complete-experiment problem of photoproduction of pseudoscalar mesons in a truncated partial-wave analysis, *Phys. Rev. C* 89 (5) (2014) 055203. [arXiv:1312.0245](https://arxiv.org/abs/1312.0245), [doi:10.1103/PhysRevC.89.055203](https://doi.org/10.1103/PhysRevC.89.055203).
- [686] R. L. Workman, L. Tiator, Y. Wunderlich, M. Döring, H. Haberzettl, Amplitude reconstruction from complete photoproduction experiments and truncated partial-wave expansions, *Phys. Rev. C* 95 (1) (2017) 015206. [arXiv:1611.04434](https://arxiv.org/abs/1611.04434), [doi:10.1103/PhysRevC.95.015206](https://doi.org/10.1103/PhysRevC.95.015206).
- [687] Y. Wunderlich, New graphical criterion for the selection of complete sets of polarization observables and its application to single-meson photoproduction as well as electroproduction, *Phys. Rev. C* 104 (4) (2021) 045203. [arXiv:2106.00486](https://arxiv.org/abs/2106.00486), [doi:10.1103/PhysRevC.104.045203](https://doi.org/10.1103/PhysRevC.104.045203).
- [688] P. Kroenert, Y. Wunderlich, F. Afzal, A. Thiel, Truncated partial-wave analysis for η -photoproduction observables via Bayesian statistics, *Phys. Rev. C* 109 (4) (2024) 045206. [arXiv:2305.10367](https://arxiv.org/abs/2305.10367), [doi:10.1103/PhysRevC.109.045206](https://doi.org/10.1103/PhysRevC.109.045206).
- [689] P. Kroenert, Y. Wunderlich, F. Afzal, A. Thiel, Minimal complete sets for two pseudoscalar meson photoproduction, *Phys. Rev. C* 103 (1) (2021) 014607. [arXiv:2009.04356](https://arxiv.org/abs/2009.04356), [doi:10.1103/PhysRevC.103.014607](https://doi.org/10.1103/PhysRevC.103.014607).
- [690] L. Tiator, R. L. Workman, Y. Wunderlich, H. Haberzettl, Amplitude reconstruction from complete electroproduction experiments and truncated partial-wave expansions, *Phys. Rev. C* 96 (2) (2017) 025210. [arXiv:1702.08375](https://arxiv.org/abs/1702.08375), [doi:10.1103/PhysRevC.96.025210](https://doi.org/10.1103/PhysRevC.96.025210).
- [691] A. Švarc, Y. Wunderlich, L. Tiator, Amplitude- and truncated partial-wave analyses combined: A novel, almost theory-independent single-channel method for extracting photoproduction multipoles directly from measured data, *Phys. Rev. C* 102 (2020) 064609. [arXiv:2008.01355](https://arxiv.org/abs/2008.01355), [doi:10.1103/PhysRevC.102.064609](https://doi.org/10.1103/PhysRevC.102.064609).
- [692] A. Švarc, Complete set of observables in pseudo-scalar meson photoproduction – Controversy solved (2 2025). [arXiv:2502.08195](https://arxiv.org/abs/2502.08195).
- [693] Y. Wunderlich, F. Afzal, A. Thiel, R. Beck, Determining the dominant partial wave contributions from angular distributions of single- and double-polarization observables in pseudoscalar meson photoproduction, *Eur. Phys. J. A* 53 (5) (2017) 86. [arXiv:1611.01031](https://arxiv.org/abs/1611.01031), [doi:10.1140/epja/i2017-12255-0](https://doi.org/10.1140/epja/i2017-12255-0).
- [694] A. Švarc, R. L. Workman, Single-channel and single-energy partial-wave analysis with continuity improved through minimal phase constraints, *Phys. Rev. C* 110 (2) (2024) 024614. [arXiv:2404.11990](https://arxiv.org/abs/2404.11990), [doi:10.1103/PhysRevC.110.024614](https://doi.org/10.1103/PhysRevC.110.024614).
- [695] A. Švarc, Y. Wunderlich, L. Tiator, Application of the single-channel, single-energy amplitude and partial-wave analysis method to $K^+\Lambda$ photoproduction, *Phys. Rev. C* 105 (2) (2022) 024614. [arXiv:2111.09587](https://arxiv.org/abs/2111.09587), [doi:10.1103/PhysRevC.105.024614](https://doi.org/10.1103/PhysRevC.105.024614).
- [696] A. V. Anisovich, et al., Strong evidence for nucleon resonances near 1900 MeV, *Phys. Rev. Lett.* 119 (6) (2017) 062004. [arXiv:1712.07549](https://arxiv.org/abs/1712.07549), [doi:10.1103/PhysRevLett.119.062004](https://doi.org/10.1103/PhysRevLett.119.062004).
- [697] A. Švarc, M. Hadžimehmedović, H. Osmanović, J. Stahov, L. Tiator, R. L. Workman, Generalization of the model-independent Laurent–Pietarinen single-channel pole-extraction formalism to multiple channels, *Phys. Lett. B* 755 (2016) 452–455. [arXiv:1512.07403](https://arxiv.org/abs/1512.07403), [doi:10.1016/j.physletb.2016.02.058](https://doi.org/10.1016/j.physletb.2016.02.058).
- [698] A. Švarc, M. Hadžimehmedović, H. Osmanović, J. Stahov, L. Tiator, R. L. Workman, Pole positions and residues from pion photoproduction using the Laurent–Pietarinen expansion method, *Phys. Rev. C* 89 (6) (2014) 065208. [arXiv:1404.1544](https://arxiv.org/abs/1404.1544), [doi:10.1103/PhysRevC.89.065208](https://doi.org/10.1103/PhysRevC.89.065208).
- [699] H. Osmanović, M. Hadžimehmedović, R. Omerović, J. Stahov, V. Kashevarov, M. Ostrick, L. Tiator, A. Švarc, Single-energy partial-wave analysis for pion photoproduction with fixed-t analyticity, *Phys. Rev. C* 104 (3) (2021) 034605. [arXiv:2107.06513](https://arxiv.org/abs/2107.06513), [doi:10.1103/PhysRevC.104.034605](https://doi.org/10.1103/PhysRevC.104.034605).
- [700] H. Osmanović, M. Hadžimehmedović, R. Omerović, J. Stahov, M. Gorchtein, V. Kashevarov, K. Nikonov, M. Ostrick, L. Tiator, A. Švarc, Single-energy partial wave analysis for π^0 photoproduction on the proton with fixed- t analyticity imposed, *Phys. Rev. C* 100 (5) (2019) 055203. [arXiv:1908.05167](https://arxiv.org/abs/1908.05167), [doi:10.1103/PhysRevC.100.055203](https://doi.org/10.1103/PhysRevC.100.055203).
- [701] O. Morimatsu, K. Yamada, Renormalization of the unitarized Weinberg–Tomozawa interaction without on-shell factorization and $I=0$ $\bar{K}N - \pi\Sigma$ coupled channels, *Phys. Rev. C* 100 (2) (2019) 025201. [arXiv:1903.12380](https://arxiv.org/abs/1903.12380), [doi:10.1103/PhysRevC.100.025201](https://doi.org/10.1103/PhysRevC.100.025201).
- [702] R. A. Arndt, W. J. Briscoe, I. I. Strakovsky, R. L. Workman, Analysis of pion photoproduction data, *Phys. Rev. C* 66 (2002) 055213. [arXiv:nucl-th/0205067](https://arxiv.org/abs/nucl-th/0205067), [doi:10.1103/PhysRevC.66.055213](https://doi.org/10.1103/PhysRevC.66.055213).
- [703] W. J. Briscoe, A. E. Kudryavtsev, I. I. Strakovsky, V. E. Tarasov, R. L. Workman, On the photoproduction reactions $\gamma d \rightarrow \pi NN$, *Eur. Phys. J. A* 58 (2) (2022) 23. [arXiv:2112.08150](https://arxiv.org/abs/2112.08150), [doi:10.1140/epja/s10050-022-00671-4](https://doi.org/10.1140/epja/s10050-022-00671-4).
- [704] V. E. Tarasov, W. J. Briscoe, H. Gao, A. E. Kudryavtsev, I. I. Strakovsky, Extracting the photoproduction cross section off the neutron, via the $\gamma n \rightarrow \pi^- p$ reaction, from deuteron data with final-state interaction effects, *Phys. Rev. C* 84 (2011) 035203. [arXiv:1105.0225](https://arxiv.org/abs/1105.0225), [doi:10.1103/PhysRevC.84.035203](https://doi.org/10.1103/PhysRevC.84.035203).
- [705] V. E. Tarasov, W. J. Briscoe, M. Dieterle, B. Krusche, A. E. Kudryavtsev, M. Ostrick, I. I. Strakovsky, On the extraction of cross sections for π^0 and η photoproduction off neutrons from deuteron data, *Phys. Atom. Nucl.* 79 (2) (2016) 216–227. [arXiv:1503.06671](https://arxiv.org/abs/1503.06671), [doi:10.1134/S1063778816020186](https://doi.org/10.1134/S1063778816020186).
- [706] G. Knochlein, D. Drechsel, L. Tiator, Photoproduction and electroproduction of eta mesons, *Z. Phys. A* 352 (1995) 327–343. [arXiv:nucl-th/9506029](https://arxiv.org/abs/nucl-th/9506029), [doi:10.1007/BF01289506](https://doi.org/10.1007/BF01289506).
- [707] L. Tiator, C. Bennhold, S. S. Kamalov, The Eta N N coupling in eta photoproduction, *Nucl. Phys. A* 580 (1994) 455–474. [arXiv:nucl-th/9404013](https://arxiv.org/abs/nucl-th/9404013), [doi:10.1016/0375-9474\(94\)90909-1](https://doi.org/10.1016/0375-9474(94)90909-1).
- [708] O. Hanstein, D. Drechsel, L. Tiator, Multipole analysis of pion photoproduction based on fixed t dispersion relations and unitarity,

- Nucl. Phys. A 632 (1998) 561–606. [arXiv:nucl-th/9709067](#), doi:10.1016/S0375-9474(98)00818-5.
- [709] W.-T. Chiang, S.-N. Yang, L. Tiator, D. Drechsel, An Isobar model for η photoproduction and electroproduction on the nucleon, Nucl. Phys. A 700 (2002) 429–453. [arXiv:nucl-th/0110034](#), doi:10.1016/S0375-9474(01)01325-2.
- [710] W.-T. Chiang, S. N. Yang, L. Tiator, M. Vanderhaeghen, D. Drechsel, A Reggeized model for η and η' photoproduction, Phys. Rev. C 68 (2003) 045202. [arXiv:nucl-th/0212106](#), doi:10.1103/PhysRevC.68.045202.
- [711] F. X. Lee, T. Mart, C. Bennhold, L. E. Wright, Quasifree kaon photoproduction on nuclei, Nucl. Phys. A 695 (2001) 237–272. [arXiv:nucl-th/9907119](#), doi:10.1016/S0375-9474(01)01098-3.
- [712] C. Bennhold, H. Haberzettl, T. Mart, A New resonance in $K^+\Lambda$ electroproduction: The $D_{13}(1895)$ and its electromagnetic form-factors, in: 2nd ICTP International Conference on Perspectives in Hadronic Physics, 1999, pp. 328–337. [arXiv:nucl-th/9909022](#).
- [713] M. Hilt, S. Scherer, L. Tiator, Threshold π^0 photoproduction in relativistic chiral perturbation theory, Phys. Rev. C 87 (4) (2013) 045204. [arXiv:1301.5576](#), doi:10.1103/PhysRevC.87.045204.
- [714] M. Hilt, B. C. Lehnhart, S. Scherer, L. Tiator, Pion photo- and electroproduction in relativistic baryon chiral perturbation theory and the chiral MAID interface, Phys. Rev. C 88 (2013) 055207. [arXiv:1309.3385](#), doi:10.1103/PhysRevC.88.055207.
- [715] L. Tiator, M. Gorchtein, V. L. Kashevarov, K. Nikonov, M. Ostrick, M. Hadžimehmedović, R. Omerović, H. Osmanović, J. Stahov, A. Švarc, Eta and Etaprime Photoproduction on the Nucleon with the Isobar Model EtaMAID2018, Eur. Phys. J. A 54 (12) (2018) 210. [arXiv:1807.04525](#), doi:10.1140/epja/i2018-12643-x.
- [716] L. Tiator, The MAID Legacy and Future, Few Body Syst. 59 (3) (2018) 21. [arXiv:1801.04777](#), doi:10.1007/s00601-018-1343-5.
- [717] A. V. Anisovich, R. Beck, E. Klempert, V. A. Nikonov, A. V. Sarantsev, U. Thoma, Pion- and photo-induced transition amplitudes to ΛK , ΣK , and $N\eta$, Eur. Phys. J. A 48 (2012) 88. [arXiv:1205.2255](#), doi:10.1140/epja/i2012-12088-3.
- [718] A. Thiel, et al., Three-body nature of N^* and Δ^* resonances from sequential decay chains, Phys. Rev. Lett. 114 (9) (2015) 091803. [arXiv:1501.02094](#), doi:10.1103/PhysRevLett.114.091803.
- [719] M. Oberle, et al., Measurement of the beam-helicity asymmetry I^\odot in the photoproduction of π^0 -pairs off the proton and off the neutron, Phys. Lett. B 721 (2013) 237–243. [arXiv:1304.1919](#), doi:10.1016/j.physletb.2013.03.021.
- [720] W. A. Smith, et al., Ambiguities in partial wave analysis of two spinless meson photoproduction, Phys. Rev. D 108 (7) (2023) 076001. [arXiv:2306.17779](#), doi:10.1103/PhysRevD.108.076001.
- [721] V. Mathieu, M. Albaladejo, C. Fernández-Ramírez, A. W. Jackura, M. Mikhasenko, A. Pilloni, A. P. Szczepaniak, Moments of angular distribution and beam asymmetries in $\eta\pi^0$ photoproduction at GlueX, Phys. Rev. D 100 (5) (2019) 054017. [arXiv:1906.04841](#), doi:10.1103/PhysRevD.100.054017.
- [722] J. Nys, V. Mathieu, C. Fernández-Ramírez, A. Jackura, M. Mikhasenko, A. Pilloni, N. Sherrill, J. Ryckebusch, A. P. Szczepaniak, G. Fox, Features of $\pi\Delta$ Photoproduction at High Energies, Phys. Lett. B 779 (2018) 77–81. [arXiv:1710.09394](#), doi:10.1016/j.physletb.2018.01.075.
- [723] M. Battaglieri, et al., First measurement of direct $f_0(980)$ photoproduction on the proton, Phys. Rev. Lett. 102 (2009) 102001. [arXiv:0811.1681](#), doi:10.1103/PhysRevLett.102.102001.
- [724] H. Haberzettl, K. Nakayama, Y. Oh, Theory of two-meson photo- and electroproduction off the nucleon, Phys. Rev. D 99 (5) (2019) 053001. [arXiv:1811.01475](#), doi:10.1103/PhysRevD.99.053001.
- [725] J. C. Nacher, E. Oset, Study of polarization observables in double pion photoproduction on the proton, Nucl. Phys. A 697 (2002) 372–387. [arXiv:nucl-th/0106005](#), doi:10.1016/S0375-9474(01)01251-9.
- [726] J. C. Nacher, E. Oset, M. J. Vicente, L. Roca, The Role of $\Delta(1700)$ excitation and ρ production in double pion photoproduction, Nucl. Phys. A 695 (2001) 295–327. [arXiv:nucl-th/0012065](#), doi:10.1016/S0375-9474(01)01110-1.
- [727] J. C. Nacher, E. Oset, A Model for the $eN \rightarrow e\Delta\pi$ reaction, Nucl. Phys. A 674 (2000) 205–228. [arXiv:nucl-th/9804006](#), doi:10.1016/S0375-9474(00)00165-2.
- [728] J. A. Gomez Tejedor, E. Oset, Double pion photoproduction on the nucleon: Study of the isospin channels, Nucl. Phys. A 600 (1996) 413–435. [arXiv:hep-ph/9506209](#), doi:10.1016/0375-9474(95)00492-0.
- [729] A. V. Sarantsev, E. Klempert, K. V. Nikonov, T. Seifen, U. Thoma, Y. Wunderlich, P. Achenbach, V. D. Burkert, V. Mokeev, V. Crede, Decays of N^* and Δ^* resonances into $N\rho$, $\Delta\pi$, and $N\sigma$ (3 2025). [arXiv:2503.16636](#).
- [730] A. V. Anisovich, V. Burkert, E. Klempert, V. A. Nikonov, A. V. Sarantsev, U. Thoma, Helicity amplitudes for photoexcitation of nucleon resonances off neutrons, Eur. Phys. J. A 49 (2013) 67. [arXiv:1304.2177](#), doi:10.1140/epja/i2013-13067-x.
- [731] I. Denisenko, A. V. Anisovich, V. Crede, H. Eberhardt, E. Klempert, V. A. Nikonov, A. V. Sarantsev, H. Schmieden, U. Thoma, A. Wilson, N^* decays to $N\omega$ from new data on $\gamma p \rightarrow \omega p$, Phys. Lett. B 755 (2016) 97–101. [arXiv:1601.06092](#), doi:10.1016/j.physletb.2016.01.061.
- [732] A. Wilson, et al., Photoproduction of ω mesons off the proton, Phys. Lett. B 749 (2015) 407–413. [arXiv:1508.01483](#), doi:10.1016/j.physletb.2015.08.011.
- [733] A. V. Anisovich, V. Burkert, J. Hartmann, E. Klempert, V. A. Nikonov, E. Pasyuk, A. V. Sarantsev, S. Strauch, U. Thoma, Evidence for $\Delta(2200)7/2^-$ from photoproduction and consequence for chiral-symmetry restoration at high mass, Phys. Lett. B 766 (2017) 357–361. [arXiv:1503.05774](#), doi:10.1016/j.physletb.2016.12.014.
- [734] V. D. Burkert, H. Kamano, E. Klempert, D. Rönchen, A. V. Sarantsev, T. Sato, A. Švarc, L. Tiator, R. L. Workman, Status of some P-wave baryon resonances and importance of inelastic channels (11 2014). [arXiv:1412.0241](#).
- [735] A. V. Anisovich, E. Klempert, V. A. Nikonov, A. V. Sarantsev, U. Thoma, Sign ambiguity in the $K\Sigma$ channel, Eur. Phys. J. A 49 (2013) 158. [arXiv:1310.3610](#), doi:10.1140/epja/i2013-13158-8.
- [736] V. D. Burkert, Evidence of new nucleon resonances from electromagnetic meson production, EPJ Web Conf. 37 (2012) 01017. [arXiv:1209.2402](#), doi:10.1051/epjconf/20123701017.
- [737] A. V. Anisovich, E. Klempert, V. A. Nikonov, M. A. Matveev, A. V. Sarantsev, U. Thoma, Photoproduction of pions and properties of baryon resonances from a Bonn-Gatchina partial wave analysis, Eur. Phys. J. A 44 (2010) 203–220. [arXiv:0911.5277](#), doi:10.1140/epja/i2010-10950-x.
- [738] A. V. Sarantsev, V. A. Nikonov, A. V. Anisovich, E. Klempert, U. Thoma, Decays of baryon resonances into ΛK^+ , $\Sigma^0 K^+$ and $\Sigma^+ K^0$, Eur. Phys. J. A 25 (2005) 441–453. [arXiv:hep-ex/0506011](#), doi:10.1140/epja/i2005-10121-4.
- [739] A. V. Anisovich, A. Sarantsev, O. Bartholomy, E. Klempert, V. A. Nikonov, U. Thoma, Photoproduction of baryons decaying into $N\pi$ and $N\eta$, Eur. Phys. J. A 25 (2005) 427–439. [arXiv:hep-ex/0506010](#), doi:10.1140/epja/i2005-10120-5.
- [740] V. A. Nikonov, A. V. Anisovich, E. Klempert, A. V. Sarantsev, U. Thoma, Further evidence for $N(1900)P_{13}$ from photoproduction of hyperons, Phys. Lett. B 662 (2008) 245–251. [arXiv:0707.3600](#), doi:10.1016/j.physletb.2008.03.004.
- [741] V. Sokhoyan, et al., Data on I^s and I^c in $\bar{\gamma}p \rightarrow p\pi^0\pi^0$ reveal cascade decays of $N(1900)$ via $N(1520)\pi$, Phys. Lett. B 746 (2015) 127–131. doi:10.1016/j.physletb.2015.04.063.
- [742] A. V. Anisovich, E. Klempert, V. A. Nikonov, A. V. Sarantsev, U. Thoma, Nucleon resonances in the fourth resonance region, Eur. Phys. J. A 47 (2011) 153. [arXiv:1109.0970](#), doi:10.1140/epja/i2011-11153-9.

- [743] E. Klemt, Hadron Spectroscopy, Results and Ideas (7 2012). [arXiv:1207.1601](#).
- [744] V. Shklyar, H. Lenske, U. Mosel, 2π production in the Giessen coupled-channel model, Phys. Rev. C 93 (4) (2016) 045206. [arXiv:1409.7920](#), doi:10.1103/PhysRevC.93.045206.
- [745] X. Cao, V. Shklyar, H. Lenske, Coupled-channel analysis of $K\Sigma$ production on the nucleon up to 2.0 GeV, Phys. Rev. C 88 (5) (2013) 055204. [arXiv:1303.2604](#), doi:10.1103/PhysRevC.88.055204.
- [746] V. Shklyar, H. Lenske, U. Mosel, A Coupled-channel analysis of $K\Lambda$ production in the nucleon resonance region, Phys. Rev. C 72 (2005) 015210. [arXiv:nucl-th/0505010](#), doi:10.1103/PhysRevC.72.015210.
- [747] V. Shklyar, H. Lenske, U. Mosel, G. Penner, Coupled-channel analysis of the omega-meson production in pi N and gamma N reactions for c.m. energies up to 2-GeV, Phys. Rev. C 71 (2005) 055206, [Erratum: Phys.Rev.C 72, 019903 (2005)]. [arXiv:nucl-th/0412029](#), doi:10.1103/PhysRevC.72.019903.
- [748] G. Penner, U. Mosel, Vector meson production and nucleon resonance analysis in a coupled channel approach for energies $m_N < \sqrt{s} < 2$ GeV. II. Photon induced results, Phys. Rev. C 66 (2002) 055212. [arXiv:nucl-th/0207069](#), doi:10.1103/PhysRevC.66.055212.
- [749] G. Penner, U. Mosel, Vector meson production and nucleon resonance analysis in a coupled channel approach for energies $m_N < \sqrt{s} < 2$ GeV. I. Pion induced results and hadronic parameters, Phys. Rev. C 66 (2002) 055211. [arXiv:nucl-th/0207066](#), doi:10.1103/PhysRevC.66.055211.
- [750] M. Shrestha, D. M. Manley, Multichannel parametrization of πN scattering amplitudes and extraction of resonance parameters, Phys. Rev. C 86 (2012) 055203. [arXiv:1208.2710](#), doi:10.1103/PhysRevC.86.055203.
- [751] B. C. Hunt, D. M. Manley, Updated determination of N^* resonance parameters using a unitary, multichannel formalism, Phys. Rev. C 99 (5) (2019) 055205. [arXiv:1810.13086](#), doi:10.1103/PhysRevC.99.055205.
- [752] B. C. Hunt, D. M. Manley, Partial-Wave Analysis of $\gamma p \rightarrow K^+ \Lambda$ using a multichannel framework, Phys. Rev. C 99 (5) (2019) 055204. [arXiv:1804.07422](#), doi:10.1103/PhysRevC.99.055204.
- [753] M. Shrestha, D. M. M. Manley, Partial-Wave Analysis of $\pi^- p \rightarrow \eta n$ and $\pi^- p \rightarrow K^0 \Lambda$ Reactions, Phys. Rev. C 86 (2012) 045204. [arXiv:1205.5294](#), doi:10.1103/PhysRevC.86.045204.
- [754] A.-C. Wang, N.-C. Wei, F. Huang, Analysis of the $\gamma p \rightarrow K^+ \Sigma^0(1385)$, $\gamma n \rightarrow K^+ \Sigma^-(1385)$, and $\pi^+ p \rightarrow K^+ \Sigma^+(1385)$ reactions, Phys. Rev. D 111 (5) (2025) 054032. [arXiv:2503.02295](#), doi:10.1103/PhysRevD.111.054032.
- [755] A.-C. Wang, N.-C. Wei, F. Huang, Analysis of the data on differential cross sections and spin density matrix elements for $\gamma p \rightarrow p 0 p$, Phys. Rev. C 111 (2) (2025) 025205. [arXiv:2502.11499](#), doi:10.1103/PhysRevC.111.025205.
- [756] S.-H. Kim, Y. Oh, S. Son, S. Sakinah, M.-K. Cheoun, Effective Lagrangian for strong and electromagnetic interactions of high-spin resonances, Phys. Rev. D 111 (5) (2025) 054031. [arXiv:2412.18927](#), doi:10.1103/PhysRevD.111.054031.
- [757] N.-C. Wei, A.-C. Wang, F. Huang, Photoproduction of $\gamma p \rightarrow f_0(980)p$ in an effective Lagrangian approach, Phys. Rev. C 110 (2) (2024) 025207. [arXiv:2408.11352](#), doi:10.1103/PhysRevC.110.025207.
- [758] D. Petrellis, D. Skoupil, Photoproduction of $K^+ \Sigma^0$ within the isobar model, Phys. Rev. C 110 (6) (2024) 065204. doi:10.1103/PhysRevC.110.065204.
- [759] D. Ben, A.-C. Wang, F. Huang, B.-S. Zou, Effects of $N(2080)3/2^-$ and $N(2270)3/2^-$ molecules on $K^* \Sigma$ photoproduction, Phys. Rev. C 108 (6) (2023) 065201. [arXiv:2302.14308](#), doi:10.1103/PhysRevC.108.065201.
- [760] N.-C. Wei, A.-C. Wang, F. Huang, K. Nakayama, Nucleon and Δ resonances in $\gamma n \rightarrow K^+ \Sigma^-$ photoproduction, Phys. Rev. D 105 (9) (2022) 094017. [arXiv:2204.13922](#), doi:10.1103/PhysRevD.105.094017.
- [761] I. I. Strakovsky, W. J. Briscoe, O. C. Becerra, M. Dugger, G. Goldstein, V. L. Kashevarov, A. Schmidt, P. Solazzo, B.-G. Yu, Pseudoscalar and scalar meson photoproduction interpreted by Regge phenomenology, Phys. Rev. C 107 (1) (2023) 015203. [arXiv:2211.12029](#), doi:10.1103/PhysRevC.107.015203.
- [762] S. Clymton, T. Mart, Extracting the pole and Breit-Wigner properties of nucleon and Δ resonances from the $\gamma N \rightarrow K\Sigma$ photoproduction, Phys. Rev. D 104 (5) (2021) 056015. [arXiv:2104.10333](#), doi:10.1103/PhysRevD.104.056015.
- [763] N. H. Luthfiyah, T. Mart, Role of the high-spin nucleon and delta resonances in the $K\Lambda$ and $K\Sigma$ photoproduction off the nucleon, Phys. Rev. D 104 (2021) 076022. [arXiv:2110.01789](#), doi:10.1103/PhysRevD.104.076022.
- [764] N. C. Wei, F. Huang, K. Nakayama, D. M. Li, Nucleon resonances in $\gamma p \rightarrow \omega p$ reaction, Phys. Rev. D 100 (11) (2019) 114026. [arXiv:1908.01139](#), doi:10.1103/PhysRevD.100.114026.
- [765] T. Mart, M. J. Kholili, Partial wave analysis for $K\Sigma$ photoproduction on the nucleon valid from threshold up to $W = 2.8$ GeV, J. Phys. G 46 (10) (2019) 105112. doi:10.1088/1361-6471/ab34c6.
- [766] T. Mart, Coupled $K^+ \Lambda$ and $K^0 \Lambda$ photoproduction off the nucleon: Consequences from the recent CLAS and MAMI data and the $N(1680)P_{11}$ narrow state, Phys. Rev. D 100 (5) (2019) 056008. [arXiv:1909.02696](#), doi:10.1103/PhysRevD.100.056008.
- [767] P. Bydžovský, D. Skoupil, Photoproduction of $K^+ \Lambda$ with a Regge-plus-resonance model, Phys. Rev. C 100 (3) (2019) 035202. [arXiv:1903.02292](#), doi:10.1103/PhysRevC.100.035202.
- [768] D. Skoupil, P. Bydžovský, Photo- and electroproduction of $K^+ \Lambda$ with unitarity-restored isobar model, Phys. Rev. C 97 (2) (2018) 025202. [arXiv:1801.07466](#), doi:10.1103/PhysRevC.97.025202.
- [769] S. Clymton, T. Mart, Isobar model for kaon photoproduction with spin- $7/2$ and - $9/2$ nucleon resonances, Phys. Rev. D 96 (5) (2017) 054004. doi:10.1103/PhysRevD.96.054004.
- [770] A. C. Wang, W. L. Wang, F. Huang, H. Haberzettl, K. Nakayama, Nucleon resonances in $\gamma p \rightarrow K^{*+} \Lambda$, Phys. Rev. C 96 (2017) 035206. [arXiv:1704.04562](#), doi:10.1103/PhysRevC.96.035206.
- [771] D. Skoupil, P. Bydžovský, Photoproduction of $K\Lambda$ on the proton, Phys. Rev. C 93 (2) (2016) 025204. [arXiv:1601.03840](#), doi:10.1103/PhysRevC.93.025204.
- [772] T. Mart, S. Clymton, A. J. Arifi, Nucleon resonances with spin $3/2$ and $5/2$ in the isobar model for kaon photoproduction, Phys. Rev. D 92 (9) (2015) 094019. doi:10.1103/PhysRevD.92.094019.
- [773] X.-Y. Wang, J. He, H. Haberzettl, Analysis of recent CLAS data on $\Sigma^*(1385)$ photoproduction off a neutron target, Phys. Rev. C 93 (4) (2016) 045204. [arXiv:1511.04262](#), doi:10.1103/PhysRevC.93.045204.
- [774] T. Mart, Electromagnetic production of $K\Sigma$ on the nucleon near threshold, Phys. Rev. C 90 (6) (2014) 065202. [arXiv:1412.1555](#), doi:10.1103/PhysRevC.90.065202.
- [775] X. Cao, J.-J. Xie, Nucleon resonances in $\pi N \rightarrow \eta' N$ and $J/\psi \rightarrow p\bar{p}\eta^{**}$, Chin. Phys. C 40 (8) (2016) 083103. [arXiv:1411.1493](#), doi:10.1088/1674-1137/40/8/083103.
- [776] S.-H. Kim, A. Hosaka, H.-C. Kim, Effects of $N(2000)5/2^+$, $N(2060)5/2^-$, $N(2120)3/2^-$, and $N(2190)7/2^-$ on $K^* \Lambda$ photoproduction, Phys. Rev. D 90 (1) (2014) 014021. [arXiv:1402.1753](#), doi:10.1103/PhysRevD.90.014021.
- [777] J. He, $\Sigma(1385)$ photoproduciton from proton within a Regge-plus-resonance approach, Phys. Rev. C 89 (5) (2014) 055204. [arXiv:1311.0571](#), doi:10.1103/PhysRevC.89.055204.
- [778] J.-J. Xie, E. Wang, J. Nieves, Re-analysis of the $\Lambda(1520)$ photoproduction reaction, Phys. Rev. C 89 (1) (2014) 015203. [arXiv:1309.7135](#), doi:10.1103/PhysRevC.89.015203.

- [779] T. Mart, Coupling strength of the $N^*(1535)S_{11}$ to the $K^+\Lambda$ channel, Phys. Rev. C 87 (4) (2013) 042201. [arXiv:1303.6735](https://arxiv.org/abs/1303.6735), doi: [10.1103/PhysRevC.87.042201](https://doi.org/10.1103/PhysRevC.87.042201).
- [780] T. Mart, Constraining the mass and width of the $N^*(1685)$ resonance, Phys. Rev. D 88 (5) (2013) 057501. [arXiv:1309.5191](https://arxiv.org/abs/1309.5191), doi: [10.1103/PhysRevD.88.057501](https://doi.org/10.1103/PhysRevD.88.057501).
- [781] J.-J. Xie, J. Nieves, The role of the $N^*(2080)$ resonance in the $\bar{\gamma}p \rightarrow K^+\Lambda(1520)$ reaction, Phys. Rev. C 82 (2010) 045205. [arXiv:1007.3141](https://arxiv.org/abs/1007.3141), doi: [10.1103/PhysRevC.82.045205](https://doi.org/10.1103/PhysRevC.82.045205).
- [782] F. Huang, A. Sibirtsev, S. Krewald, C. Hanhart, J. Haidenbauer, U.-G. Meißner, Pion-nucleon charge-exchange amplitudes above 2 GeV, Eur. Phys. J. A 40 (2009) 77–87. [arXiv:0810.2680](https://arxiv.org/abs/0810.2680), doi: [10.1140/epja/i2008-10728-9](https://doi.org/10.1140/epja/i2008-10728-9).
- [783] T. Mart, A. Sulaksono, Kaon photoproduction in a multipole approach, Phys. Rev. C 74 (2006) 055203. [arXiv:nucl-th/0609077](https://arxiv.org/abs/nucl-th/0609077), doi: [10.1103/PhysRevC.74.055203](https://doi.org/10.1103/PhysRevC.74.055203).
- [784] T. Mart, C. Bennhold, Evidence for a missing nucleon resonance in kaon photoproduction, Phys. Rev. C 61 (2000) 012201. [arXiv:nucl-th/9906096](https://arxiv.org/abs/nucl-th/9906096), doi: [10.1103/PhysRevC.61.012201](https://doi.org/10.1103/PhysRevC.61.012201).
- [785] T. Mart, C. Bennhold, C. E. Hyde-Wright, Constraints on coupling constants through charged sigma photoproduction, Phys. Rev. C 51 (1995) R1074–R1077. [arXiv:nucl-th/9502016](https://arxiv.org/abs/nucl-th/9502016), doi: [10.1103/PhysRevC.51.R1074](https://doi.org/10.1103/PhysRevC.51.R1074).
- [786] F. Huang, H. Haberzettl, K. Nakayama, Combined analysis of η' production reactions: $\gamma N \rightarrow \eta'N$, $NN \rightarrow NN\eta'$, and $\pi N \rightarrow \eta'N$, Phys. Rev. C 87 (2013) 054004. [arXiv:1208.2279](https://arxiv.org/abs/1208.2279), doi: [10.1103/PhysRevC.87.054004](https://doi.org/10.1103/PhysRevC.87.054004).
- [787] H. Haberzettl, Using gauge invariance to symmetrize the energy-momentum tensor of electrodynamics (6 2024). [arXiv:2406.06785](https://arxiv.org/abs/2406.06785).
- [788] H. Haberzettl, Gauge invariance of meson photo- and electroproduction currents revisited, Phys. Rev. D 104 (5) (2021) 056001. [arXiv:2105.11554](https://arxiv.org/abs/2105.11554), doi: [10.1103/PhysRevD.104.056001](https://doi.org/10.1103/PhysRevD.104.056001).
- [789] G. Montana, et al., Revisiting gauge invariance and Reggeization of pion exchange, Phys. Rev. D 110 (11) (2024) 114012. [arXiv:2407.19577](https://arxiv.org/abs/2407.19577), doi: [10.1103/PhysRevD.110.114012](https://doi.org/10.1103/PhysRevD.110.114012).
- [790] H. Haberzettl, Model-independent form-factor constraints for electromagnetic spin-1 currents, Phys. Rev. D 100 (3) (2019) 036008. [arXiv:1905.06299](https://arxiv.org/abs/1905.06299), doi: [10.1103/PhysRevD.100.036008](https://doi.org/10.1103/PhysRevD.100.036008).
- [791] H. Haberzettl, C. Bennhold, T. Mart, T. Feuster, Gauge-invariant tree-level photoproduction amplitudes with form factors, Phys. Rev. C 58 (1) (1998) R40–R44. [arXiv:nucl-th/9804051](https://arxiv.org/abs/nucl-th/9804051), doi: [10.1103/PhysRevC.58.R40](https://doi.org/10.1103/PhysRevC.58.R40).
- [792] V. Mathieu, G. Fox, A. P. Szczepaniak, Neutral Pion Photoproduction in a Regge Model, Phys. Rev. D 92 (7) (2015) 074013. [arXiv:1505.02321](https://arxiv.org/abs/1505.02321), doi: [10.1103/PhysRevD.92.074013](https://doi.org/10.1103/PhysRevD.92.074013).
- [793] V. Mathieu, J. Nys, C. Fernández-Ramírez, A. Jackura, M. Mikhasenko, A. Pilloni, A. P. Szczepaniak, G. Fox, On the η and η' Photoproduction Beam Asymmetry at High Energies, Phys. Lett. B 774 (2017) 362–367. [arXiv:1704.07684](https://arxiv.org/abs/1704.07684), doi: [10.1016/j.physletb.2017.09.081](https://doi.org/10.1016/j.physletb.2017.09.081).
- [794] H. Al Ghoul, et al., Measurement of the beam asymmetry Σ for π^0 and η photoproduction on the proton at $E_\gamma = 9$ GeV, Phys. Rev. C 95 (4) (2017) 042201. [arXiv:1701.08123](https://arxiv.org/abs/1701.08123), doi: [10.1103/PhysRevC.95.042201](https://doi.org/10.1103/PhysRevC.95.042201).
- [795] T. H. Boyer, Conserved currents, renormalization, and the ward identity, Annals of Physics 44 (1) (1967) 1–10. doi: [https://doi.org/10.1016/0003-4916\(67\)90261-8](https://doi.org/10.1016/0003-4916(67)90261-8).
- [796] H. Haberzettl, Gauge invariant theory of pion photoproduction with dressed hadrons, Phys. Rev. C 56 (1997) 2041–2058. [arXiv:nucl-th/9704057](https://arxiv.org/abs/nucl-th/9704057), doi: [10.1103/PhysRevC.56.2041](https://doi.org/10.1103/PhysRevC.56.2041).
- [797] H. Haberzettl, K. Nakayama, S. Krewald, Gauge-invariant approach to meson photoproduction including the final-state interaction, Phys. Rev. C 74 (2006) 045202. [arXiv:nucl-th/0605059](https://arxiv.org/abs/nucl-th/0605059), doi: [10.1103/PhysRevC.74.045202](https://doi.org/10.1103/PhysRevC.74.045202).
- [798] H. Haberzettl, F. Huang, K. Nakayama, Dressing the electromagnetic nucleon current, Phys. Rev. C 83 (2011) 065502. [arXiv:1103.2065](https://arxiv.org/abs/1103.2065), doi: [10.1103/PhysRevC.83.065502](https://doi.org/10.1103/PhysRevC.83.065502).
- [799] S. Razavi, K. Nakayama, Complex phase structure of the meson-baryon T -matrix, Phys. Rev. D 100 (11) (2019) 114036. [arXiv:1909.00869](https://arxiv.org/abs/1909.00869), doi: [10.1103/PhysRevD.100.114036](https://doi.org/10.1103/PhysRevD.100.114036).
- [800] C. Hanhart, A New Parameterization for the Pion Vector Form Factor, Phys. Lett. B 715 (2012) 170–177. [arXiv:1203.6839](https://arxiv.org/abs/1203.6839), doi: [10.1016/j.physletb.2012.07.038](https://doi.org/10.1016/j.physletb.2012.07.038).
- [801] D. Morgan, M. R. Pennington, What Can We Learn From $\gamma\gamma \rightarrow \pi\pi$, $K\bar{K}$ in the Resonance Region, Z. Phys. C 37 (1988) 431, [Erratum: Z. Phys. C 39, 590 (1988)]. doi: [10.1007/BF01578139](https://doi.org/10.1007/BF01578139).
- [802] JBW Interactive Scattering Analysis website (under development), <https://JBW.phys.gwu.edu> (2021).
- [803] M. Ablikim, et al., Polarization and Entanglement in Baryon-Antibaryon Pair Production in Electron-Positron Annihilation, Nature Phys. 15 (2019) 631–634. [arXiv:1808.08917](https://arxiv.org/abs/1808.08917), doi: [10.1038/s41567-019-0494-8](https://doi.org/10.1038/s41567-019-0494-8).
- [804] D. G. Ireland, M. Döring, D. I. Glazier, J. Haidenbauer, M. Mai, R. Murray-Smith, D. Rönchen, Kaon Photoproduction and the Λ Decay Parameter α_- , Phys. Rev. Lett. 123 (18) (2019) 182301. [arXiv:1904.07616](https://arxiv.org/abs/1904.07616), doi: [10.1103/PhysRevLett.123.182301](https://doi.org/10.1103/PhysRevLett.123.182301).
- [805] C. A. Paterson, et al., Photoproduction of Λ and Σ^0 hyperons using linearly polarized photons, Phys. Rev. C 93 (6) (2016) 065201. [arXiv:1603.06492](https://arxiv.org/abs/1603.06492), doi: [10.1103/PhysRevC.93.065201](https://doi.org/10.1103/PhysRevC.93.065201).
- [806] M. Tanabashi, et al., Review of Particle Physics, Phys. Rev. D 98 (3) (2018) 030001. doi: [10.1103/PhysRevD.98.030001](https://doi.org/10.1103/PhysRevD.98.030001).
- [807] Website with results of ANL-Osaka fits to pion- and photon-induced reaction data, <https://www.rcnp.osaka-u.ac.jp/~anl-osc/>.
- [808] B. C. Liu, B. S. Zou, Mass and K Lambda coupling of $N^*(1535)$, Phys. Rev. Lett. 96 (4) (2006) 042002. [arXiv:nucl-th/0503069](https://arxiv.org/abs/nucl-th/0503069), doi: [10.1103/PhysRevLett.96.042002](https://doi.org/10.1103/PhysRevLett.96.042002).
- [809] A. Sibirtsev, J. Haidenbauer, U. G. Meißner, Comment on ‘Mass and K Lambda coupling of the $N^*(1535)$ ’, Phys. Rev. Lett. 98 (2007) 039101. [arXiv:hep-ph/0607212](https://arxiv.org/abs/hep-ph/0607212), doi: [10.1103/PhysRevLett.98.039101](https://doi.org/10.1103/PhysRevLett.98.039101).
- [810] Y.-F. Wang, D.-L. Yao, H.-Q. Zheng, New Insights on Low Energy πN Scattering Amplitudes, Eur. Phys. J. C 78 (7) (2018) 543. [arXiv:1712.09257](https://arxiv.org/abs/1712.09257), doi: [10.1140/epjc/s10052-018-6024-5](https://doi.org/10.1140/epjc/s10052-018-6024-5).
- [811] Y.-F. Wang, D.-L. Yao, H.-Q. Zheng, New insights on low energy πN scattering amplitudes: comprehensive analyses at $\mathcal{O}(p^3)$ level, Chin. Phys. C 43 (6) (2019) 064110. [arXiv:1811.09748](https://arxiv.org/abs/1811.09748), doi: [10.1088/1674-1137/43/6/064110](https://doi.org/10.1088/1674-1137/43/6/064110).
- [812] Z. Xiao, H. Q. Zheng, Left-hand singularities, hadron form-factors and the properties of the sigma meson, Nucl. Phys. A 695 (2001) 273–294. [arXiv:hep-ph/0011260](https://arxiv.org/abs/hep-ph/0011260), doi: [10.1016/S0375-9474\(01\)01100-9](https://doi.org/10.1016/S0375-9474(01)01100-9).
- [813] J. He, Z. Xiao, H. Q. Zheng, The Constraints of unitarity on $\pi\pi$ scattering dispersion relations, Phys. Lett. B 536 (2002) 59–66, [Erratum: Phys. Lett. B 549, 362–363 (2002)]. [arXiv:hep-ph/0201257](https://arxiv.org/abs/hep-ph/0201257), doi: [10.1016/S0370-2693\(02\)01811-7](https://doi.org/10.1016/S0370-2693(02)01811-7).
- [814] H. Q. Zheng, Z. Y. Zhou, G. Y. Qin, Z. Xiao, J. J. Wang, N. Wu, The κ resonance in s wave πK scatterings, Nucl. Phys. A 733 (2004) 235–261. [arXiv:hep-ph/0310293](https://arxiv.org/abs/hep-ph/0310293), doi: [10.1016/j.nuclphysa.2003.12.021](https://doi.org/10.1016/j.nuclphysa.2003.12.021).
- [815] Z. Y. Zhou, H. Q. Zheng, An improved study of the κ resonance and the non-exotic s wave πK scatterings up to $\sqrt{s} = 2.1$ GeV of LASS data, Nucl. Phys. A 775 (2006) 212–223. [arXiv:hep-ph/0603062](https://arxiv.org/abs/hep-ph/0603062), doi: [10.1016/j.nuclphysa.2006.06.170](https://doi.org/10.1016/j.nuclphysa.2006.06.170).
- [816] X.-H. Cao, Q.-Z. Li, H.-Q. Zheng, A possible subthreshold pole in S_{11} channel from πN Roy-Steiner equation analyses, JHEP 12 (2022) 073. [arXiv:2207.09743](https://arxiv.org/abs/2207.09743), doi: [10.1007/JHEP12\(2022\)073](https://doi.org/10.1007/JHEP12(2022)073).
- [817] X.-H. Cao, Y. Ma, H.-Q. Zheng, Dispersive analysis of low energy $\gamma^* N \rightarrow \pi N$ process, Phys. Rev. D 103 (11) (2021) 114007. [arXiv:2109.03887](https://arxiv.org/abs/2109.03887)

2101.12576, doi:10.1103/PhysRevD.103.114007.

- [818] Y. Ma, W.-Q. Niu, D.-L. Yao, H.-Q. Zheng, Dispersive analysis of low energy $\gamma N \rightarrow \pi N$ process and studies on the $N^*(890)$ resonance, Chin. Phys. C 45 (1) (2021) 014104. arXiv:2005.10695, doi:10.1088/1674-1137/abc169.
- [819] Q.-Z. Li, Z. Xiao, H.-Q. Zheng, On the pole trajectory of the subthreshold negative parity nucleon with varying pion masses (1 2025). arXiv:2501.01619.
- [820] L. D. Roper, Evidence for a P-11 Pion-Nucleon Resonance at 556 MeV, Phys. Rev. Lett. 12 (1964) 340–342. doi:10.1103/PhysRevLett.12.340.
- [821] L. Y. Glozman, D. O. Riska, The Spectrum of the nucleons and the strange hyperons and chiral dynamics, Phys. Rept. 268 (1996) 263–303. arXiv:hep-ph/9505422, doi:10.1016/0370-1573(95)00062-3.
- [822] B. Golli, H. Osmanović, S. Širca, A. Švarc, Genuine quark state versus dynamically generated structure for the Roper resonance, Phys. Rev. C 97 (3) (2018) 035204. arXiv:1709.09025, doi:10.1103/PhysRevC.97.035204.
- [823] B. Golli, The Roper resonance – a genuine three quark or a dynamically generated resonance?, Bled Workshops Phys. 18 (1) (2017) 76–81.
- [824] C. Alexandrou, T. Korzec, G. Koutsou, T. Leontiou, Nucleon Excited States in $N_f=2$ lattice QCD, Phys. Rev. D 89 (3) (2014) 034502. arXiv:1302.4410, doi:10.1103/PhysRevD.89.034502.
- [825] D. S. Roberts, W. Kamleh, D. B. Leinweber, Wave Function of the Roper from Lattice QCD, Phys. Lett. B 725 (2013) 164–169. arXiv:1304.0325, doi:10.1016/j.physletb.2013.06.056.
- [826] C. Alexandrou, T. Leontiou, C. N. Papanicolas, E. Stiliaris, Novel analysis method for excited states in lattice QCD: The nucleon case, Phys. Rev. D 91 (1) (2015) 014506. arXiv:1411.6765, doi:10.1103/PhysRevD.91.014506.
- [827] K.-F. Liu, Y. Chen, M. Gong, R. Sufian, M. Sun, A. Li, The Roper Puzzle, PoS LATTICE2013 (2014) 507. arXiv:1403.6847, doi:10.22323/1.187.0507.
- [828] N. Mathur, Y. Chen, S. J. Dong, T. Draper, I. Horvath, F. X. Lee, K. F. Liu, J. B. Zhang, Roper resonance and $S(11)(1535)$ from lattice QCD, Phys. Lett. B 605 (2005) 137–143. arXiv:hep-ph/0306199, doi:10.1016/j.physletb.2004.11.010.
- [829] M. Padmanath, C. B. Lang, L. Leskovec, S. Prelovsek, $N\pi$ scattering in the Roper channel, EPJ Web Conf. 175 (2018) 05004. arXiv:1711.06334, doi:10.1051/epjconf/201817505004.
- [830] L. Leskovec, C. B. Lang, M. Padmanath, S. Prelovsek, A lattice QCD study of pion-nucleon scattering in the Roper channel, Few Body Syst. 59 (5) (2018) 95. arXiv:1806.02363, doi:10.1007/s00601-018-1419-2.
- [831] D. Severt, U.-G. Meißner, The Roper Resonance in a finite volume, Commun. Theor. Phys. 72 (7) (2020) 075201. arXiv:2003.05745, doi:10.1088/1572-9494/ab8a24.
- [832] T. Burch, C. Gattringer, L. Y. Glozman, C. Hagen, D. Hierl, C. B. Lang, A. Schafer, Excited hadrons on the lattice: Baryons, Phys. Rev. D 74 (2006) 014504. arXiv:hep-lat/0604019, doi:10.1103/PhysRevD.74.014504.
- [833] G. P. Engel, C. B. Lang, M. Limmer, D. Mohler, A. Schafer, Meson and baryon spectrum for QCD with two light dynamical quarks, Phys. Rev. D 82 (2010) 034505. arXiv:1005.1748, doi:10.1103/PhysRevD.82.034505.
- [834] R. G. Edwards, N. Mathur, D. G. Richards, S. J. Wallace, Flavor structure of the excited baryon spectra from lattice QCD, Phys. Rev. D 87 (5) (2013) 054506. arXiv:1212.5236, doi:10.1103/PhysRevD.87.054506.
- [835] C. Alexandrou, J. W. Negele, M. Petschlies, A. Strelchenko, A. Tsapalis, Determination of Δ Resonance Parameters from Lattice QCD, Phys. Rev. D 88 (3) (2013) 031501. arXiv:1305.6081, doi:10.1103/PhysRevD.88.031501.
- [836] C. Alexandrou, J. W. Negele, M. Petschlies, A. V. Pochinsky, S. N. Syritsyn, Study of decuplet baryon resonances from lattice QCD, Phys. Rev. D 93 (11) (2016) 114515. arXiv:1507.02724, doi:10.1103/PhysRevD.93.114515.
- [837] F. M. Stokes, W. Kamleh, D. B. Leinweber, Elastic Form Factors of Nucleon Excitations in Lattice QCD, Phys. Rev. D 102 (1) (2020) 014507. arXiv:1907.00177, doi:10.1103/PhysRevD.102.014507.
- [838] G. S. Bali, S. Collins, P. Georg, D. Jenkins, P. Korcyl, A. Schäfer, E. E. Scholz, J. Simeth, W. Söldner, S. Weishäupl, Scale setting and the light baryon spectrum in $N_f = 2 + 1$ QCD with Wilson fermions, JHEP 05 (2023) 035. arXiv:2211.03744, doi:10.1007/JHEP05(2023)035.
- [839] R. Bijker, E. Santopinto, E. Santopinto, Unquenched quark model for baryons: Magnetic moments, spins and orbital angular momenta, Phys. Rev. C 80 (2009) 065210. arXiv:0912.4494, doi:10.1103/PhysRevC.80.065210.
- [840] M. Ronniger, B. C. Metsch, Effects of a spin-flavour dependent interaction on the baryon mass spectrum, Eur. Phys. J. A 47 (2011) 162. arXiv:1111.3835, doi:10.1140/epja/i2011-11162-8.
- [841] E. Klemp, B. C. Metsch, Multiplet classification of light-quark baryons, Eur. Phys. J. A 48 (2012) 127. doi:10.1140/epja/i2012-12127-1.
- [842] L. Liu, C. Chen, Y. Lu, C. D. Roberts, J. Segovia, Composition of low-lying $J=32\pm\Delta$ -baryons, Phys. Rev. D 105 (11) (2022) 114047. arXiv:2203.12083, doi:10.1103/PhysRevD.105.114047.
- [843] U.-G. Meißner, The Beauty of Spin, J. Phys. Conf. Ser. 295 (2011) 012001. arXiv:1012.0924, doi:10.1088/1742-6596/295/1/012001.
- [844] C. W. Andersen, J. Bulava, B. Hörrz, C. Morningstar, Elastic $I = 3/2$ p-wave nucleon-pion scattering amplitude and the $\Delta(1232)$ resonance from $N_f=2+1$ lattice QCD, Phys. Rev. D 97 (1) (2018) 014506. arXiv:1710.01557, doi:10.1103/PhysRevD.97.014506.
- [845] D. S. Carman, et al., First measurement of transferred polarization in the exclusive $\bar{e}p \rightarrow e'K^+\Lambda$ reaction, Phys. Rev. Lett. 90 (2003) 131804. arXiv:hep-ex/0212014, doi:10.1103/PhysRevLett.90.131804.
- [846] P. Ambrozewicz, et al., Separated structure functions for the exclusive electroproduction of $K^+\Lambda$ and $K^+\Sigma^0$ final states, Phys. Rev. C 75 (2007) 045203. arXiv:hep-ex/0611036, doi:10.1103/PhysRevC.75.045203.
- [847] R. Nasseripour, et al., Polarized Structure Function $\sigma_{LT'}$ for $p(\bar{e}, e'K^+)\Lambda$ in the Nucleon Resonance Region, Phys. Rev. C 77 (2008) 065208. arXiv:0801.4711, doi:10.1103/PhysRevC.77.065208.
- [848] D. S. Carman, et al., Beam-Recoil Polarization Transfer in the Nucleon Resonance Region in the Exclusive $\bar{e}p \rightarrow e'K^+\bar{\Lambda}$ and $\bar{e}p \rightarrow e'K^+\bar{\Sigma}^0$ Reactions at CLAS, Phys. Rev. C 79 (2009) 065205. arXiv:0904.3246, doi:10.1103/PhysRevC.79.065205.
- [849] S. Taylor, et al., Radiative decays of the $\Sigma^0(1385)$ and $\Lambda(1520)$ hyperons, Phys. Rev. C 71 (2005) 054609, [Erratum: Phys. Rev. C 72, 039902 (2005)]. arXiv:hep-ex/0503014, doi:10.1103/PhysRevC.71.054609.
- [850] D. S. Carman, et al., Separated Structure Functions for Exclusive $K^+\Lambda$ and $K^+\Sigma^0$ Electroproduction at 5.5 GeV with CLAS, Phys. Rev. C 87 (2) (2013) 025204. arXiv:1212.1336, doi:10.1103/PhysRevC.87.025204.
- [851] M. Gabrielyan, et al., Induced polarization of $\Lambda(1116)$ in kaon electroproduction, Phys. Rev. C 90 (3) (2014) 035202. arXiv:1406.4046, doi:10.1103/PhysRevC.90.035202.
- [852] D. S. Carman, K. Joo, V. I. Mokeev, Strong QCD Insights from Excited Nucleon Structure Studies with CLAS and CLAS12, Few Body Syst. 61 (3) (2020) 29. arXiv:2006.15566, doi:10.1007/s00601-020-01563-3.
- [853] S. J. Brodsky, et al., Strong QCD from Hadron Structure Experiments: Newport News, VA, USA, November 4-8, 2019, Int. J. Mod. Phys. E 29 (08) (2020) 2030006. arXiv:2006.06802, doi:10.1142/S0218301320300064.
- [854] V. I. Mokeev, et al., Evidence for the $N'(1720)3/2^+$ Nucleon Resonance from Combined Studies of CLAS $\pi^+\pi^-p$ Photo- and Electro-

- production Data, Phys. Lett. B 805 (2020) 135457. [arXiv:2004.13531](#), [doi:10.1016/j.physletb.2020.135457](#).
- [855] C. E. Carlson, M. Vanderhaeghen, Empirical transverse charge densities in the nucleon and the nucleon-to-Delta transition, Phys. Rev. Lett. 100 (2008) 032004. [arXiv:0710.0835](#), [doi:10.1103/PhysRevLett.100.032004](#).
- [856] V. Bernard, N. Kaiser, U.-G. Meißner, On the low-energy theorems for threshold pion electroproduction, Phys. Lett. B 282 (1992) 448–452. [doi:10.1016/0370-2693\(92\)90667-S](#).
- [857] V. Bernard, N. Kaiser, T. S. H. Lee, U.-G. Meißner, Chiral symmetry and threshold π^0 electroproduction, Phys. Rev. Lett. 70 (1993) 387–390. [doi:10.1103/PhysRevLett.70.387](#).
- [858] V. Bernard, N. Kaiser, T. S. H. Lee, U.-G. Meißner, Threshold pion electroproduction in chiral perturbation theory, Phys. Rept. 246 (1994) 315–363. [arXiv:hep-ph/9310329](#), [doi:10.1016/0370-1573\(94\)90088-4](#).
- [859] V. Bernard, N. Kaiser, U.-G. Meißner, Novel pion electroproduction low-energy theorems, Phys. Rev. Lett. 74 (1995) 3752–3755. [arXiv:hep-ph/9412282](#), [doi:10.1103/PhysRevLett.74.3752](#).
- [860] V. Bernard, N. Kaiser, U.-G. Meißner, Threshold neutral pion electroproduction in heavy baryon chiral perturbation theory, Nucl. Phys. A 607 (1996) 379–401, [Erratum: Nucl.Phys.A 633, 695–697 (1998)]. [arXiv:hep-ph/9601267](#), [doi:10.1016/0375-9474\(96\)00184-4](#).
- [861] S. Steininger, U.-G. Meißner, Threshold kaon photoproduction and electroproduction in SU(3) baryon chiral perturbation theory, Phys. Lett. B 391 (1997) 446–450. [arXiv:nucl-th/9609051](#), [doi:10.1016/S0370-2693\(96\)01490-6](#).
- [862] V. Bernard, N. Kaiser, U.-G. Meißner, The Pion charge radius from charged pion electroproduction, Phys. Rev. C 62 (2000) 028201. [arXiv:nucl-th/0003062](#), [doi:10.1103/PhysRevC.62.028201](#).
- [863] H. Krebs, V. Bernard, U.-G. Meißner, Improved analysis of neutral pion electroproduction off deuterium in chiral perturbation theory, Eur. Phys. J. A 22 (2004) 503–514. [arXiv:nucl-th/0405006](#), [doi:10.1140/epja/i2004-10052-6](#).
- [864] T. A. Gail, T. R. Hemmert, Signatures of chiral dynamics in the nucleon to delta transition, Eur. Phys. J. A 28 (2006) 91–105. [arXiv:nucl-th/0512082](#), [doi:10.1140/epja/i2006-10023-y](#).
- [865] T. Bauer, S. Scherer, L. Tiator, Electromagnetic transition form factors of the Roper resonance in effective field theory, Phys. Rev. C 90 (1) (2014) 015201. [arXiv:1402.0741](#), [doi:10.1103/PhysRevC.90.015201](#).
- [866] S. Capstick, Photoproduction and electroproduction of nonstrange baryon resonances in the relativized quark model, Phys. Rev. D 46 (1992) 2864–2881. [doi:10.1103/PhysRevD.46.2864](#).
- [867] D. Merten, U. Loring, K. Kretzschmar, B. Metsch, H. R. Petry, Electroweak form-factors of nonstrange baryons, Eur. Phys. J. A 14 (2002) 477–489. [arXiv:hep-ph/0204024](#), [doi:10.1140/epja/i2002-10009-9](#).
- [868] G. Ramalho, M. T. Peña, F. Gross, D-state effects in the electromagnetic $N\Delta$ transition, Phys. Rev. D 78 (2008) 114017. [arXiv:0810.4126](#), [doi:10.1103/PhysRevD.78.114017](#).
- [869] E. Santopinto, M. M. Giannini, Systematic study of longitudinal and transverse helicity amplitudes in the hypercentral constituent quark model, Phys. Rev. C 86 (2012) 065202. [arXiv:1506.01207](#), [doi:10.1103/PhysRevC.86.065202](#).
- [870] I. T. Obukhovsky, A. Fässler, D. K. Fedorov, T. Gutsche, V. E. Lyubovitskij, Transition form factors and helicity amplitudes for electroexcitation of negative- and positive parity nucleon resonances in a light-front quark model, Phys. Rev. D 100 (9) (2019) 094013. [arXiv:1909.13787](#), [doi:10.1103/PhysRevD.100.094013](#).
- [871] G. Ramalho, M. T. Peña, Covariant model for the Dalitz decay of the $N(1535)$ resonance, Phys. Rev. D 101 (11) (2020) 114008. [arXiv:2003.04850](#), [doi:10.1103/PhysRevD.101.114008](#).
- [872] R. A. Williams, C. R. Ji, S. R. Cotanch, Hyperon electroproduction in a crossing and duality constrained model, Phys. Rev. C 46 (1992) 1617–1635. [doi:10.1103/PhysRevC.46.1617](#).
- [873] T. D. Cohen, L. Y. Glozman, Does one observe chiral symmetry restoration in baryon spectrum?, Int. J. Mod. Phys. A 17 (2002) 1327–1354. [arXiv:hep-ph/0201242](#), [doi:10.1142/S0217751X02009679](#).
- [874] C. Jayalath, J. L. Goity, E. Gonzalez de Urreta, N. N. Scoccola, Negative parity baryon decays in the $1/N_c$ expansion, Phys. Rev. D 84 (2011) 074012. [arXiv:1108.2042](#), [doi:10.1103/PhysRevD.84.074012](#).
- [875] I. V. Anikin, V. M. Braun, N. Offen, Electroproduction of the $N^*(1535)$ nucleon resonance in QCD, Phys. Rev. D 92 (1) (2015) 014018. [arXiv:1505.05759](#), [doi:10.1103/PhysRevD.92.014018](#).
- [876] I. C. Cloët, G. Eichmann, B. El-Bennich, T. Klahn, C. D. Roberts, Survey of nucleon electromagnetic form factors, Few Body Syst. 46 (2009) 1–36. [arXiv:0812.0416](#), [doi:10.1007/s00601-009-0015-x](#).
- [877] J. Segovia, I. C. Cloët, C. D. Roberts, S. M. Schmidt, Nucleon and Δ elastic and transition form factors, Few Body Syst. 55 (2014) 1185–1222. [arXiv:1408.2919](#), [doi:10.1007/s00601-014-0907-2](#).
- [878] S.-X. Qin, C. D. Roberts, S. M. Schmidt, Spectrum of light- and heavy-baryons, Few Body Syst. 60 (2) (2019) 26. [arXiv:1902.00026](#), [doi:10.1007/s00601-019-1488-x](#).
- [879] A. Agadjanov, V. Bernard, U.-G. Meißner, A. Rusetsky, A framework for the calculation of the $\Delta N\gamma^*$ transition form factors on the lattice, Nucl. Phys. B 886 (2014) 1199–1222. [arXiv:1405.3476](#), [doi:10.1016/j.nuclphysb.2014.07.023](#).
- [880] A. Radhakrishnan, J. J. Dudek, R. G. Edwards, Radiative decay of the resonant K^* and the $\gamma K \rightarrow K\pi$ amplitude from lattice QCD, Phys. Rev. D 106 (11) (2022) 114513. [arXiv:2208.13755](#), [doi:10.1103/PhysRevD.106.114513](#).
- [881] L. Tiator, M. Döring, R. L. Workman, M. Hadžimehmedović, H. Osmanović, R. Omerović, J. Stahov, A. Švarc, Baryon transition form factors at the pole, Phys. Rev. C 94 (6) (2016) 065204. [arXiv:1606.00371](#), [doi:10.1103/PhysRevC.94.065204](#).
- [882] L. Tiator, D. Drechsel, S. Kamalov, M. M. Giannini, E. Santopinto, A. Vassallo, Electroproduction of nucleon resonances, Eur. Phys. J. A 19 (2004) 55–60. [arXiv:nucl-th/0310041](#), [doi:10.1140/epjad/s2004-03-009-9](#).
- [883] L. Tiator, D. Drechsel, S. S. Kamalov, M. Vanderhaeghen, Electromagnetic Excitation of Nucleon Resonances, Eur. Phys. J. ST 198 (2011) 141–170. [arXiv:1109.6745](#), [doi:10.1140/epjst/e2011-01488-9](#).
- [884] I. G. Aznauryan, V. D. Burkert, Extracting meson-baryon contributions to the electroexcitation of the $N(1675)\frac{5}{2}^-$ nucleon resonance, Phys. Rev. C 92 (1) (2015) 015203. [arXiv:1412.1296](#), [doi:10.1103/PhysRevC.92.015203](#).
- [885] I. G. Aznauryan, et al., Electroexcitation of the Roper resonance for $1.7 < Q^{**2} < 4.5$ GeV 2 in $e\pi^-p \rightarrow e\pi^-p'$, Phys. Rev. C 78 (2008) 045209. [arXiv:0804.0447](#), [doi:10.1103/PhysRevC.78.045209](#).
- [886] I. G. Aznauryan, Multipole amplitudes of pion photoproduction on nucleons up to 2-Gev within dispersion relations and unitary isobar model, Phys. Rev. C 67 (2003) 015209. [arXiv:nucl-th/0206033](#), [doi:10.1103/PhysRevC.67.015209](#).
- [887] V. I. Mokeev, P. Achenbach, V. D. Burkert, D. S. Carman, R. W. Gothe, A. N. Hiller Blin, E. L. Isupov, K. Joo, K. Neupane, A. Trivedi, First Results on Nucleon Resonance Electroexcitation Amplitudes from $e\pi^-p \rightarrow e\pi^+\pi^-p'$ Cross Sections at $W = 1.4\text{--}1.7$ GeV and $Q^2 = 2.0\text{--}5.0$ GeV 2 , Phys. Rev. C 108 (2) (2023) 025204. [arXiv:2306.13777](#), [doi:10.1103/PhysRevC.108.025204](#).
- [888] A. N. Hiller Blin, V. I. Mokeev, W. Melnitchouk, Resonant contributions to polarized proton structure functions, Phys. Rev. C 107 (3) (2023) 035202. [arXiv:2212.11952](#), [doi:10.1103/PhysRevC.107.035202](#).
- [889] A. N. Hiller Blin, et al., Nucleon resonance contributions to unpolarised inclusive electron scattering, Phys. Rev. C 100 (3) (2019) 035201. [arXiv:1904.08016](#), [doi:10.1103/PhysRevC.100.035201](#).
- [890] O. V. Maxwell, Electromagnetic production of Σ^0 from the proton: A new fit to recent data, Phys. Rev. C 93 (1) (2016) 014605.

[doi:10.1103/PhysRevC.93.014605](https://doi.org/10.1103/PhysRevC.93.014605).

- [891] O. V. Maxwell, New fit to the reaction $\gamma p \rightarrow K^+ \Sigma^0$, Phys. Rev. C 92 (4) (2015) 044614. [doi:10.1103/PhysRevC.92.044614](https://doi.org/10.1103/PhysRevC.92.044614).
- [892] O. V. Maxwell, Electromagnetic production of kaons from protons, and baryon electromagnetic form factors, Phys. Rev. C 85 (2012) 034611. [doi:10.1103/PhysRevC.85.034611](https://doi.org/10.1103/PhysRevC.85.034611).
- [893] G. Ramalho, Improved empirical parametrizations of the $\gamma^* N \rightarrow \Delta(1232)$ and $\gamma^* N \rightarrow N(1520)$ helicity amplitudes and the Siegert's theorem, Phys. Rev. D 93 (11) (2016) 113012. [arXiv:1602.03832](https://arxiv.org/abs/1602.03832), [doi:10.1103/PhysRevD.93.113012](https://doi.org/10.1103/PhysRevD.93.113012).
- [894] G. Ramalho, Combined parametrization of G_{En} and $\gamma^* N \rightarrow \Delta(1232)$ quadrupole form factors, Eur. Phys. J. A 55 (3) (2019) 32. [arXiv:1710.10527](https://arxiv.org/abs/1710.10527), [doi:10.1140/epja/i2019-12699-0](https://doi.org/10.1140/epja/i2019-12699-0).
- [895] G. Ramalho, Low- Q^2 empirical parametrizations of the N^* helicity amplitudes, Phys. Rev. D 100 (11) (2019) 114014. [arXiv:1909.00013](https://arxiv.org/abs/1909.00013), [doi:10.1103/PhysRevD.100.114014](https://doi.org/10.1103/PhysRevD.100.114014).
- [896] E. Golovatch, et al., First results on nucleon resonance photocouplings from the $\gamma p \rightarrow \pi^+ \pi^- p$ reaction, Phys. Lett. B 788 (2019) 371–379. [arXiv:1806.01767](https://arxiv.org/abs/1806.01767), [doi:10.1016/j.physletb.2018.10.013](https://doi.org/10.1016/j.physletb.2018.10.013).
- [897] G. V. Fedotov, et al., Measurements of the $\gamma_V p \rightarrow p' \pi^+ \pi^-$ cross section with the CLAS detector for $0.4 \text{ GeV}^2 < Q^2 < 1.0 \text{ GeV}^2$ and $1.3 \text{ GeV} < W < 1.825 \text{ GeV}$, Phys. Rev. C 98 (2) (2018) 025203. [arXiv:1804.05136](https://arxiv.org/abs/1804.05136), [doi:10.1103/PhysRevC.98.025203](https://doi.org/10.1103/PhysRevC.98.025203).
- [898] E. L. Isupov, et al., Measurements of $ep \rightarrow e' \pi^+ \pi^- p'$ Cross Sections with CLAS at $1.40 \text{ GeV} < W < 2.0 \text{ GeV}$ and $2.0 \text{ GeV}^2 < Q^2 < 5.0 \text{ GeV}^2$, Phys. Rev. C 96 (2) (2017) 025209. [arXiv:1705.01901](https://arxiv.org/abs/1705.01901), [doi:10.1103/PhysRevC.96.025209](https://doi.org/10.1103/PhysRevC.96.025209).
- [899] G. V. Fedotov, et al., Electroproduction of p pi+ pi- off protons at $0.2 < Q^{**2} < 0.6 \text{ GeV}^{**2}$ and $1.3 < W < 1.57 \text{ GeV}$ with CLAS, Phys. Rev. C 79 (2009) 015204. [arXiv:0809.1562](https://arxiv.org/abs/0809.1562), [doi:10.1103/PhysRevC.79.015204](https://doi.org/10.1103/PhysRevC.79.015204).
- [900] M. Ripani, et al., Measurement of $e p \rightarrow e' \pi^+ \pi^- p$ and baryon resonance analysis, Phys. Rev. Lett. 91 (2003) 022002. [arXiv:hep-ex/0210054](https://arxiv.org/abs/hep-ex/0210054), [doi:10.1103/PhysRevLett.91.022002](https://doi.org/10.1103/PhysRevLett.91.022002).
- [901] A. Trivedi, Measurement of New Observables from the $\pi^+ \pi^- p$ Electroproduction Off the Proton (11 2018). [doi:10.1007/s00601-018-1471-y](https://doi.org/10.1007/s00601-018-1471-y).
- [902] V. I. Mokeev, et al., Experimental Study of the $P_{11}(1440)$ and $D_{13}(1520)$ resonances from CLAS data on $ep \rightarrow e' \pi^+ \pi^- p'$, Phys. Rev. C 86 (2012) 035203. [arXiv:1205.3948](https://arxiv.org/abs/1205.3948), [doi:10.1103/PhysRevC.86.035203](https://doi.org/10.1103/PhysRevC.86.035203).
- [903] V. I. Mokeev, et al., New Results from the Studies of the $N(1440)1/2^+$, $N(1520)3/2^-$, and $\Delta(1620)1/2^-$ Resonances in Exclusive $ep \rightarrow e' p' \pi^+ \pi^-$ Electroproduction with the CLAS Detector, Phys. Rev. C 93 (2) (2016) 025206. [arXiv:1509.05460](https://arxiv.org/abs/1509.05460), [doi:10.1103/PhysRevC.93.025206](https://doi.org/10.1103/PhysRevC.93.025206).
- [904] V. Bernard, N. Kaiser, U.-G. Meißner, A. Schmidt, Threshold two pion photoproduction and electroproduction: More neutrals than expected, Nucl. Phys. A 580 (1994) 475–499. [arXiv:nucl-th/9403013](https://arxiv.org/abs/nucl-th/9403013), [doi:10.1016/0375-9474\(94\)90910-5](https://doi.org/10.1016/0375-9474(94)90910-5).
- [905] D. S. Carman, et al., The CLAS12 Forward Time-of-Flight system, Nucl. Instrum. Meth. A 960 (2020) 163629. [doi:10.1016/j.nima.2020.163629](https://doi.org/10.1016/j.nima.2020.163629).
- [906] T. Mart, C. Bennhold, H. Haberzettl, An isobar model for the photoproduction and electroproduction of kaons on the nucleon, PiN Newslett. 16 (2002) 86–91.
- [907] T. Corthals, T. Van Cauteren, P. Van Craeyveld, J. Ryckebusch, D. G. Ireland, Electroproduction of kaons from the proton in a Regge-plus-resonance approach, Phys. Lett. B 656 (2007) 186–192. [arXiv:0704.3691](https://arxiv.org/abs/0704.3691), [doi:10.1016/j.physletb.2007.09.036](https://doi.org/10.1016/j.physletb.2007.09.036).
- [908] D. S. Carman, CLAS \bar{N}^* Excitation Results from Pion and Kaon Electroproduction, Few Body Syst. 59 (5) (2018) 82. [doi:10.1007/s00601-018-1405-8](https://doi.org/10.1007/s00601-018-1405-8).
- [909] T. Mart, Photo- and electroproduction of the $K^0 \Lambda$ near threshold and effects of the K^0 electromagnetic form factor, Phys. Rev. C 83 (2011) 048203. [arXiv:1104.2393](https://arxiv.org/abs/1104.2393), [doi:10.1103/PhysRevC.83.048203](https://doi.org/10.1103/PhysRevC.83.048203).
- [910] A. N. H. Blin, W. Melnitchouk, V. I. Mokeev, V. D. Burkert, V. V. Chesnokov, A. Pilloni, A. P. Szczepaniak, Resonant contributions to inclusive nucleon structure functions from exclusive meson electroproduction data, Phys. Rev. C 104 (2) (2021) 025201. [arXiv:2105.05834](https://arxiv.org/abs/2105.05834), [doi:10.1103/PhysRevC.104.025201](https://doi.org/10.1103/PhysRevC.104.025201).
- [911] A. Accardi, et al., Strong interaction physics at the luminosity frontier with 22 GeV electrons at Jefferson Lab, Eur. Phys. J. A 60 (9) (2024) 173. [arXiv:2306.09360](https://arxiv.org/abs/2306.09360), [doi:10.1140/epja/s10050-024-01282-x](https://doi.org/10.1140/epja/s10050-024-01282-x).
- [912] I. Aznauryan, et al., Theory Support for the Excited Baryon Program at the Jlab 12- GeV Upgrade, in: Electromagnetic N-N* Transition Form Factors Workshop, 2009. [arXiv:0907.1901](https://arxiv.org/abs/0907.1901).
- [913] V. Klimenko, et al., Inclusive Electron Scattering in the Resonance Region off a Hydrogen Target with CLAS12 (1 2025). [arXiv:2501.14996](https://arxiv.org/abs/2501.14996).
- [914] D. S. Carman, et al., Beam-recoil transferred polarization in K+Y electroproduction in the nucleon resonance region with CLAS12, Phys. Rev. C 105 (6) (2022) 065201. [arXiv:2202.03398](https://arxiv.org/abs/2202.03398), [doi:10.1103/PhysRevC.105.065201](https://doi.org/10.1103/PhysRevC.105.065201).
- [915] C. Mertz, et al., Search for quadrupole strength in the electroexcitation of the $\Delta(1232)$, Phys. Rev. Lett. 86 (2001) 2963–2966. [arXiv:nucl-ex/9902012](https://arxiv.org/abs/nucl-ex/9902012), [doi:10.1103/PhysRevLett.86.2963](https://doi.org/10.1103/PhysRevLett.86.2963).
- [916] D. Elsner, et al., Measurement of the LT-asymmetry in π^0 electroproduction at the energy of the $\Delta(1232)$ resonance, Eur. Phys. J. A 27 (2006) 91–97. [arXiv:nucl-ex/0507014](https://arxiv.org/abs/nucl-ex/0507014), [doi:10.1140/epja/i2005-10212-2](https://doi.org/10.1140/epja/i2005-10212-2).
- [917] K. Joo, et al., Measurement of the polarized structure function $\sigma_{LT'}$ for $p(\bar{e}, e' p) \pi^0$ in the $\Delta(1232)$ resonance region, Phys. Rev. C 68 (2003) 032201. [arXiv:nucl-ex/0301012](https://arxiv.org/abs/nucl-ex/0301012), [doi:10.1103/PhysRevC.68.032201](https://doi.org/10.1103/PhysRevC.68.032201).
- [918] N. F. Sparveris, et al., Measurement of the R(LT) response function for pi0 electroproduction at $Q^{**2} = 0.070 \text{ (GeV/c)}^{**2}$ in the $N \rightarrow \Delta$ transition, Phys. Rev. C 67 (2003) 058201. [arXiv:nucl-ex/0212022](https://arxiv.org/abs/nucl-ex/0212022), [doi:10.1103/PhysRevC.67.058201](https://doi.org/10.1103/PhysRevC.67.058201).
- [919] J. J. Kelly, et al., Recoil polarization for Delta excitation in pion electroproduction, Phys. Rev. Lett. 95 (2005) 102001. [arXiv:nucl-ex/0505024](https://arxiv.org/abs/nucl-ex/0505024), [doi:10.1103/PhysRevLett.95.102001](https://doi.org/10.1103/PhysRevLett.95.102001).
- [920] P. Bartsch, et al., Measurement of the beam helicity asymmetry in the $p(\bar{e}, e' p) \pi^0$ reaction at the energy of the $\Delta(1232)$ resonance, Phys. Rev. Lett. 88 (2002) 142001. [arXiv:nucl-ex/0112009](https://arxiv.org/abs/nucl-ex/0112009), [doi:10.1103/PhysRevLett.88.142001](https://doi.org/10.1103/PhysRevLett.88.142001).
- [921] I. K. Bensafa, et al., Beam-helicity asymmetry in photon and pion electroproduction in the $\Delta(1232)$ resonance region at $Q^2 = 0.35 \text{ (GeV/c)}^2$, Eur. Phys. J. A 32 (2007) 69–75. [arXiv:hep-ph/0612248](https://arxiv.org/abs/hep-ph/0612248), [doi:10.1140/epja/i2006-10277-3](https://doi.org/10.1140/epja/i2006-10277-3).
- [922] K. Joo, et al., Measurement of the polarized structure function $\sigma_{LT'}$ for $p(\bar{e}, e' \pi^+) n$ in the $\Delta(1232)$ resonance region, Phys. Rev. C 70 (2004) 042201. [arXiv:nucl-ex/0407013](https://arxiv.org/abs/nucl-ex/0407013), [doi:10.1103/PhysRevC.70.042201](https://doi.org/10.1103/PhysRevC.70.042201).
- [923] K. Park, private communication (2007).
- [924] D. Gaskell, et al., Longitudinal electroproduction of charged pions from H-1, H-2, He-3, Phys. Rev. Lett. 87 (2001) 202301. [doi:10.1103/PhysRevLett.87.202301](https://doi.org/10.1103/PhysRevLett.87.202301).
- [925] G. Laveissière, et al., Backward electroproduction of π^0 mesons on protons in the region of nucleon resonances at four momentum transfer squared $Q^{**2} = 1.0 \text{ (GeV/c)}^{**2}$, Phys. Rev. C 69 (2004) 045203. [arXiv:nucl-ex/0308009](https://arxiv.org/abs/nucl-ex/0308009), [doi:10.1103/PhysRevC.69.045203](https://doi.org/10.1103/PhysRevC.69.045203).
- [926] M. Ungaro, et al., Measurement of the $N \rightarrow \Delta(1232)$ transition at high momentum transfer by pi0 electroproduction, Phys. Rev. Lett. 97 (2006) 112003. [arXiv:hep-ex/0606042](https://arxiv.org/abs/hep-ex/0606042), [doi:10.1103/PhysRevLett.97.112003](https://doi.org/10.1103/PhysRevLett.97.112003).
- [927] J. Gayler, Electroproduction of π^0 mesons in the region of $\Delta(1232)$ with momentum transfer $q^2 = 15 \text{ fm}^{-2}$, Tech. Rep. DESY-F21-71-2,

- DESY (4 1971).
- [928] J. May, Koinzidenzmessungen zur Untersuchung der Reaktion $ep \rightarrow ep\pi^0$ beim Impulsübertrag $q^2 \approx 1\text{GeV}^2$ im Massenbereich zwischen 1.136 und 1.316 GeV, Ph.D. thesis, Hamburg U. (1971).
- [929] V. V. Frolov, et al., Electroproduction of the Delta (1232) resonance at high momentum transfer, Phys. Rev. Lett. 82 (1999) 45–48. [arXiv:hep-ex/9808024](#), doi:10.1103/PhysRevLett.82.45.
- [930] C. T. Hill, Higgs Scalars and the Nonleptonic Weak Interactions, Other thesis, Caltech (5 1977).
- [931] K. Joo, et al., Q^{**2} dependence of quadrupole strength in the gamma* p \rightarrow Delta+(1232) \rightarrow p pi0 transition, Phys. Rev. Lett. 88 (2002) 122001. [arXiv:hep-ex/0110007](#), doi:10.1103/PhysRevLett.88.122001.
- [932] R. Siddle, et al., Coincidence π^0 electroproduction experiments in the first resonance region at momentum transfers of 0.3, 0.45, 0.60, 0.76 GeV/c^2 , Nucl. Phys. B 35 (1971) 93–119. doi:10.1016/0550-3213(71)90134-9.
- [933] R. Haidan, Elektroproduktion pseudoskalarer Mesonen im Resonanzgebiet bei großen Impulsüberträgen, Ph.D. thesis, Hamburg U. (1979). doi:10.3204/PUBDB-2017-12089.
- [934] F. Kalleicher, U. Dittmayer, R. W. Gothe, H. Putsch, T. Reichelt, B. Schoch, M. Wilhelm, The determination of sigma(LT)/sigma(TT) in electropion production in the Delta resonance region, Z. Phys. A 359 (1997) 201–204. doi:10.1007/s002180050387.
- [935] K. Baetzner, et al., π^0 electroproduction at the $\Delta(1236)$ resonance at a four-momentum transfer of $q^2 = 0.3(\text{gev}/c)^2$, Nucl. Phys. B 76 (1974) 1–14. doi:10.1016/0550-3213(74)90133-3.
- [936] A. Latham, et al., Coincidence electroproduction of single neutral pions in the resonance region at $q^2 = 0.5 (\text{GeV}/c)^2$, Nucl. Phys. B 156 (1979) 58–92. doi:10.1016/0550-3213(79)90494-2.
- [937] A. Latham, et al., Electroproduction of π^0 Mesons in the Resonance Region at $q^2 = 1.0\{\text{GeV}\}/c^2$, Nucl. Phys. B 189 (1981) 1–14. doi:10.1016/0550-3213(81)90078-X.
- [938] S. C. Stave, Lowest Q^2 Measurement of the $\gamma^* p \rightarrow \Delta$ Reaction: Probing the Pionic Contribution, Ph.D. thesis, MIT (2006). doi:10.2172/922278.
- [939] N. F. Sparveris, et al., Determination of quadrupole strengths in the $\gamma^* p \rightarrow \Delta(1232)$ transition at $Q^2 = 0.20 (\text{GeV}/c)^2$, Phys. Lett. B 651 (2007) 102–107. [arXiv:nucl-ex/0611033](#), doi:10.1016/j.physletb.2007.04.056.
- [940] J. C. Alder, F. W. Brasse, W. Fehrenbach, J. Gayler, S. P. Goel, R. Haidan, V. Korbel, J. May, M. Merkwitz, A. Nurimba, Electroproduction of neutral pions in the resonance region, Nucl. Phys. B 105 (1976) 253–271. doi:10.1016/0550-3213(76)90266-2.
- [941] N. G. Afanasev, A. S. Esaulov, A. M. Pilipenko, Y. I. Titov, Separation of Transversal and Longitudinal Components of Cross-Section of Pion Electroproduction on Proton Near the Threshold, Pisma Zh. Eksp. Teor. Fiz. 22 (1975) 400–402.
- [942] W. J. Shuttleworth, et al., Coincidence π^0 electroproduction in the second resonance region, Nucl. Phys. B 45 (1972) 428–448. doi:10.1016/0550-3213(72)90251-9.
- [943] H. Blume, R. Farber, N. Feldmann, K. Heinloth, D. Kramarczyk, F. Kuckelkorn, H. J. Michels, J. Pasler, J. P. Dowd, ELECTRO-PRODUCTION OF pi0 MESONS ON PROTONS AT W = 1400-MeV TO 2000-MeV, $q^{**2} = 0.01\text{-GeV}^{**2}$ TO 0.1- GeV^{**2} , AND $t = 0.6\text{-GeV}^{**2}$ TO 2.2- GeV^{**2} CORRESPONDING TO Theta (CM) $\pi = 145\text{-degrees}$ TO 180-degrees, Z. Phys. C 16 (1983) 283. doi:10.1007/BF01577095.
- [944] M. Rosenberg, Electroproduction of Neutral π Mesons in the Range of the Two Nucleon Resonance at 0.3 GeV^2/c^2 Momentum Transfer, Thesis, Bonn (8 1979).
- [945] V. Gerhardt, Pion-Elektroproduktion im Bereich der 2. und 3. Nukleonresonanz, Ph.D. thesis, Hamburg U. (1979).
- [946] MONTANA, "Pion electroproduction pi0p", Ph.D. thesis, Harvard (1971).
- [947] H. Egiyan, et al., Single π^+ electroproduction on the proton in the first and second resonance regions at $0.25\text{-GeV}^{**2} < Q^{**2} < 0.65\text{-GeV}^{**2}$ using CLAS, Phys. Rev. C 73 (2006) 025204. [arXiv:nucl-ex/0601007](#), doi:10.1103/PhysRevC.73.025204.
- [948] H. Breuker, et al., Forward π^+ Electroproduction in the First Resonance Region at Four Momentum Transfers $q^{**2} = 0.15\text{-}(\text{GeV}/c)^{**2}$ and $0.3\text{-}(\text{GeV}/c)^{**2}$, Nucl. Phys. B 146 (1978) 285–302. doi:10.1016/0550-3213(78)90069-X.
- [949] G. Bardin, J. Duclos, J. Julien, A. Magnon, B. Michel, J. C. Montret, A measurement of the longitudinal and transverse parts of the π^+ electroproduction cross-section at 1175 MeV pion-nucleon centre-of-mass energy., Lett. Nuovo Cim. 13 (1975) 485–488.
- [950] G. Bardin, J. Duclos, A. Magnon, B. Michel, J. C. Montret, A Transverse and Longitudinal Cross-Section Separation in a π^+ Electro-production Coincidence Experiment and the Pion Radius, Nucl. Phys. B 120 (1977) 45–61. doi:10.1016/0550-3213(77)90094-3.
- [951] M. Davenport, Electroproduction of neutral and positive pions between the first and second resonance regions., Ph.D. thesis, Lancaster (1980).
- [952] O. Vapenikova, et al., ELECTROPRODUCTION OF SINGLE CHARGED PIONS FROM DEUTERIUM AT Q^{**2} APPROXIMATELY 1- GeV^{**2} IN THE RESONANCE REGION, Z. Phys. C 37 (1988) 251–258. doi:10.1007/BF01579910.
- [953] J. C. Alder, H. Behrens, F. W. Brasse, W. Fehrenbach, J. Gayler, S. P. Goel, R. Haidan, V. Korbel, J. May, M. Merkwitz, Electroproduction of π^+ Mesons in the Resonance Region, Nucl. Phys. B 99 (1975) 1–12. doi:10.1016/0550-3213(75)90052-8.
- [954] E. Evangelides, et al., Electroproduction of π^+ mesons in the second and third resonance regions, Nucl. Phys. B 71 (1974) 381–394. doi:10.1016/0550-3213(74)90189-8.
- [955] H. Breuker, et al., Electroproduction of π^+ Mesons at Forward and Backward Direction in the Region of the D^- 13 (1520) and ${}^{15}\text{F}$ (1688) Resonances, Z. Phys. C 13 (1982) 113. doi:10.1007/BF01547674.
- [956] H. Breuker, et al., Backward Electroproduction of π^+ Mesons in the Second and Third Nucleon Resonance Region, Z. Phys. C 17 (1983) 121. doi:10.1007/BF01574177.
- [957] C. J. Bebek, C. N. Brown, M. Herzlinger, S. D. Holmes, C. A. Lichtenstein, F. M. Pipkin, S. Raither, L. K. Sisterson, Measurement of the pion form-factor up to $q^2 = 4\text{-GeV}^2$, Phys. Rev. D 13 (1976) 25. doi:10.1103/PhysRevD.13.25.
- [958] C. N. Brown, C. R. Canizares, W. E. Cooper, A. M. Eisner, G. J. Feldmann, C. A. Lichtenstein, L. Litt, W. Liceretz, V. B. Montana, F. M. Pipkin, Coincidence electroproduction of charged pions and the pion form-factor, Phys. Rev. D 8 (1973) 92–135. doi:10.1103/PhysRevD.8.92.
- [959] L. Litt, PI+ ELECTROPRODUCTION ALONG THE VIRTUAL PHOTON AT FIXED k^{**2} , Other thesis, unknown (4 1971).
- [960] C. S. Armstrong, et al., Electroproduction of the S(11)(1535) resonance at high momentum transfer, Phys. Rev. D 60 (1999) 052004. [arXiv:nucl-ex/9811001](#), doi:10.1103/PhysRevD.60.052004.
- [961] H. Denizli, et al., Q^{**2} dependence of the S(11)(1535) photocoupling and evidence for a P-wave resonance in eta electroproduction, Phys. Rev. C 76 (2007) 015204. [arXiv:0704.2546](#), doi:10.1103/PhysRevC.76.015204.
- [962] R. Thompson, et al., The e p \rightarrow e-prime p eta reaction at and above the S(11)(1535) baryon resonance, Phys. Rev. Lett. 86 (2001) 1702–1706. [arXiv:hep-ex/0011029](#), doi:10.1103/PhysRevLett.86.1702.
- [963] M. M. Dalton, et al., Electroproduction of Eta Mesons in the S(11)(1535) Resonance Region at High Momentum Transfer, Phys. Rev. C 80 (2009) 015205. [arXiv:0804.3509](#), doi:10.1103/PhysRevC.80.015205.
- [964] C. Kunz, et al., Measurement of the transverse longitudinal cross-sections in the p (polarized-e, e-prime p) pi0 reaction in the Delta region, Phys. Lett. B 564 (2003) 21–26. [arXiv:nucl-ex/0302018](#), doi:10.1016/S0370-2693(03)00675-0.

- [965] S. Stave, et al., Lowest Q^{**2} Measurement of the gamma* $p \rightarrow$ Delta Reaction: Probing the Pionic Contribution, *Eur. Phys. J. A* 30 (2006) 471–476. [arXiv:nucl-ex/0604013](https://arxiv.org/abs/nucl-ex/0604013), doi:10.1140/epja/i2006-10162-1.
- [966] N. F. Sparveris, et al., Investigation of the conjectured nucleon deformation at low momentum transfer, *Phys. Rev. Lett.* 94 (2005) 022003. [arXiv:nucl-ex/0408003](https://arxiv.org/abs/nucl-ex/0408003), doi:10.1103/PhysRevLett.94.022003.
- [967] G. A. Warren, et al., Induced proton polarization for pi0 electroproduction at $Q^{**2} = 0.126\text{-GeV}^{**2} / c^{**2}$ around the Delta (1232) resonance, *Phys. Rev. C* 58 (1998) 3722. [arXiv:nucl-ex/9901004](https://arxiv.org/abs/nucl-ex/9901004), doi:10.1103/PhysRevC.58.3722.
- [968] T. Pospischil, et al., Measurement of the recoil polarization in the $p(\bar{e}, e' \bar{p})\pi^0$ reaction at the $\Delta(1232)$ resonance, *Phys. Rev. Lett.* 86 (2001) 2959–2962. [arXiv:nucl-ex/0010020](https://arxiv.org/abs/nucl-ex/0010020), doi:10.1103/PhysRevLett.86.2959.
- [969] A. J. F. Siegert, Note on the interaction between nuclei and electromagnetic radiation, *Phys. Rev.* 52 (1937) 787–789. doi:10.1103/PhysRev.52.787.
- [970] L. Tiator, Pion Electroproduction and Siegert's Theorem, *Few Body Syst.* 57 (11) (2016) 1087–1093. doi:10.1007/s00601-016-1158-1.
- [971] L. Tiator, D. Drechsel, S. S. Kamalov, M. Vanderhaeghen, Baryon Resonance Analysis from MAID, *Chin. Phys. C* 33 (2009) 1069–1076. [arXiv:0909.2335](https://arxiv.org/abs/0909.2335), doi:10.1088/1674-1137/33/12/005.
- [972] L. Tiator, M. Vanderhaeghen, Empirical transverse charge densities in the nucleon-to-P(11)(1440) transition, *Phys. Lett. B* 672 (2009) 344–348. [arXiv:0811.2285](https://arxiv.org/abs/0811.2285), doi:10.1016/j.physletb.2009.01.048.
- [973] M. E. Christy, P. E. Bosted, Empirical fit to precision inclusive electron-proton cross- sections in the resonance region, *Phys. Rev. C* 81 (2010) 055213. [arXiv:0712.3731](https://arxiv.org/abs/0712.3731), doi:10.1103/PhysRevC.81.055213.
- [974] S. X. Nakamura, et al., Towards a Unified Model of Neutrino-Nucleus Reactions for Neutrino Oscillation Experiments, *Rept. Prog. Phys.* 80 (5) (2017) 056301. [arXiv:1610.01464](https://arxiv.org/abs/1610.01464), doi:10.1088/1361-6633/aa5e6c.
- [975] T. Sato, Electromagnetic Transition form Factor of Nucleon Resonances, *Few Body Syst.* 57 (10) (2016) 949–953. doi:10.1007/s00601-016-1132-y.
- [976] M. Osipenko, et al., The Proton structure function F(2) with CLAS (9 2003). [arXiv:hep-ex/0309052](https://arxiv.org/abs/hep-ex/0309052).
- [977] K. Abe, et al., The T2K Experiment, *Nucl. Instrum. Meth. A* 659 (2011) 106–135. [arXiv:1106.1238](https://arxiv.org/abs/1106.1238), doi:10.1016/j.nima.2011.06.067.
- [978] K. Abe, et al., Physics potentials with the second Hyper-Kamiokande detector in Korea, *PTEP* 2018 (6) (2018) 063C01. [arXiv:1611.06118](https://arxiv.org/abs/1611.06118), doi:10.1093/ptep/pty044.
- [979] R. Acciarri, et al., Long-Baseline Neutrino Facility (LBNF) and Deep Underground Neutrino Experiment (DUNE): Conceptual Design Report, Volume 2: The Physics Program for DUNE at LBNF (12 2015). [arXiv:1512.06148](https://arxiv.org/abs/1512.06148).
- [980] L. Alvarez-Ruso, et al., NuSTEC White Paper: Status and challenges of neutrino–nucleus scattering, *Prog. Part. Nucl. Phys.* 100 (2018) 1–68. [arXiv:1706.03621](https://arxiv.org/abs/1706.03621), doi:10.1016/j.ppnp.2018.01.006.
- [981] C. Andreopoulos, et al., Summary of the NuSTEC Workshop on Shallow- and Deep-Inelastic Scattering, in: NuSTEC Workshop on Shallow- and Deep-Inelastic Scattering, 2019. [arXiv:1907.13252](https://arxiv.org/abs/1907.13252).
- [982] L. Aliaga, et al., Summary of the NuSTEC Workshop on Neutrino-Nucleus Pion Production in the Resonance Region, in: NuSTEC Workshop on Neutrino-Nucleus Pion Production in the Resonance Region, 2020. [arXiv:2011.07166](https://arxiv.org/abs/2011.07166).
- [983] D. Rein, L. M. Sehgal, Neutrino Excitation of Baryon Resonances and Single Pion Production, *Annals Phys.* 133 (1981) 79–153. doi:10.1016/0003-4916(81)90242-6.
- [984] C. Berger, L. M. Sehgal, Lepton mass effects in single pion production by neutrinos, *Phys. Rev. D* 76 (2007) 113004. [arXiv:0709.4378](https://arxiv.org/abs/0709.4378), doi:10.1103/PhysRevD.76.113004.
- [985] C. H. Llewellyn Smith, Neutrino Reactions at Accelerator Energies, *Phys. Rept.* 3 (1972) 261–379. doi:10.1016/0370-1573(72)90010-5.
- [986] E. Hernandez, J. Nieves, M. Valverde, Weak Pion Production off the Nucleon, *Phys. Rev. D* 76 (2007) 033005. [arXiv:hep-ph/0701149](https://arxiv.org/abs/hep-ph/0701149), doi:10.1103/PhysRevD.76.033005.
- [987] E. Hernandez, J. Nieves, M. Valverde, M. J. Vicente Vacas, N-Delta(1232) axial form factors from weak pion production, *Phys. Rev. D* 81 (2010) 085046. [arXiv:1001.4416](https://arxiv.org/abs/1001.4416), doi:10.1103/PhysRevD.81.085046.
- [988] E. Hernández, J. Nieves, Neutrino-induced one-pion production revisited: the $\nu_\mu n \rightarrow \mu^- n \pi^+$ channel, *Phys. Rev. D* 95 (5) (2017) 053007. [arXiv:1612.02343](https://arxiv.org/abs/1612.02343), doi:10.1103/PhysRevD.95.053007.
- [989] L. Alvarez-Ruso, E. Hernández, J. Nieves, M. J. Vicente Vacas, Watson's theorem and the $N\Delta(1232)$ axial transition, *Phys. Rev. D* 93 (1) (2016) 014016. [arXiv:1510.06266](https://arxiv.org/abs/1510.06266), doi:10.1103/PhysRevD.93.014016.
- [990] T. Sato, Neutrino-nucleon reactions in resonance region, *Eur. Phys. J. ST* 230 (24) (2021) 4409–4418. doi:10.1140/epjs/s11734-021-00284-w.
- [991] R. González-Jiménez, N. Jachowicz, K. Niewczas, J. Nys, V. Pandey, T. Van Cuyck, N. Van Dessel, Electroweak single-pion production off the nucleon: from threshold to high invariant masses, *Phys. Rev. D* 95 (11) (2017) 113007. [arXiv:1612.05511](https://arxiv.org/abs/1612.05511), doi:10.1103/PhysRevD.95.113007.
- [992] T. Sato, D. Uno, T. S. H. Lee, Dynamical model of weak pion production reactions, *Phys. Rev. C* 67 (2003) 065201. [arXiv:nucl-th/0303050](https://arxiv.org/abs/nucl-th/0303050), doi:10.1103/PhysRevC.67.065201.
- [993] K. Matsui, T. Sato, T. S. H. Lee, Quark-hadron duality and parity violating asymmetry of electroweak reactions in the Delta region, *Phys. Rev. C* 72 (2005) 025204. [arXiv:nucl-th/0504051](https://arxiv.org/abs/nucl-th/0504051), doi:10.1103/PhysRevC.72.025204.
- [994] X.-L. Ren, E. Oset, L. Alvarez-Ruso, M. J. Vicente Vacas, Antineutrino induced $\Lambda(1405)$ production off the proton, *Phys. Rev. C* 91 (4) (2015) 045201. [arXiv:1501.04073](https://arxiv.org/abs/1501.04073), doi:10.1103/PhysRevC.91.045201.
- [995] S. J. Barish, et al., Study of Neutrino Interactions in Hydrogen and Deuterium: Inelastic Charged Current Reactions, *Phys. Rev. D* 19 (1979) 2521. doi:10.1103/PhysRevD.19.2521.
- [996] P. Rodrigues, C. Wilkinson, K. McFarland, Constraining the GENIE model of neutrino-induced single pion production using reanalyzed bubble chamber data, *Eur. Phys. J. C* 76 (8) (2016) 474. [arXiv:1601.01888](https://arxiv.org/abs/1601.01888), doi:10.1140/epjc/s10052-016-4314-3.
- [997] T. Kitagaki, et al., Charged Current Exclusive Pion Production in Neutrino Deuterium Interactions, *Phys. Rev. D* 34 (1986) 2554–2565. doi:10.1103/PhysRevD.34.2554.
- [998] J.-J. Wu, T. Sato, T. S. H. Lee, Incoherent pion production in neutrino-deuteron interactions, *Phys. Rev. C* 91 (3) (2015) 035203. [arXiv:1412.2415](https://arxiv.org/abs/1412.2415), doi:10.1103/PhysRevC.91.035203.
- [999] S. X. Nakamura, H. Kamano, T. Sato, Impact of final state interactions on neutrino-nucleon pion production cross sections extracted from neutrino-deuteron reaction data, *Phys. Rev. D* 99 (3) (2019) 031301. [arXiv:1812.00144](https://arxiv.org/abs/1812.00144), doi:10.1103/PhysRevD.99.031301.
- [1000] D. Allasia, et al., Investigation of exclusive channels in neutrino / anti-neutrino deuteron charged current interactions, *Nucl. Phys. B* 343 (1990) 285–309. doi:10.1016/0550-3213(90)90472-P.
- [1001] M. Amaryan, et al., Strange Hadron Spectroscopy with Secondary KL Beam in Hall D (8 2020). [arXiv:2008.08215](https://arxiv.org/abs/2008.08215).
- [1002] K. Aoki, et al., Extension of the J-PARC Hadron Experimental Facility: Third White Paper (10 2021). [arXiv:2110.04462](https://arxiv.org/abs/2110.04462).
- [1003] Proposals for Nuclear and Particle Physics Experiments at J-PARC, https://j-parc.jp/researcher/Hadron/en/Proposal_e.html.
- [1004] S. Aikawa, et al., Pole position of $\Lambda(1405)$ measured in $d(K-,n)\pi\Sigma$ reactions, *Phys. Lett. B* 837 (2023) 137637. [arXiv:2209.08254](https://arxiv.org/abs/2209.08254), doi:10.1016/j.physletb.2022.137637.

- [1005] Y. Ichikawa, et al., High resolution spectroscopy of the “ ΣN cusp” by using the $d(K^-, \pi^-)$ reaction, EPJ Web Conf. 271 (2022) 02012. [doi:10.1051/epjconf/202227102012](https://doi.org/10.1051/epjconf/202227102012).
- [1006] Tanida, K et al., Proposal to J-PARC, *Search for a narrow Λ^* resonance using the $p(K^-, \Lambda)\eta$ reaction with the hypTPC detector*, <https://j-parc.jp/researcher/Hadron/en/pac1801/pdf/P722018-9.pdf>.
- [1007] C. Quintans, The New AMBER Experiment at the CERN SPS, Few Body Syst. 63 (4) (2022) 72. [doi:10.1007/s00601-022-01769-7](https://doi.org/10.1007/s00601-022-01769-7).
- [1008] J. M. Friedrich, The AMBER Experiment at CERN, EPJ Web Conf. 303 (2024) 06001. [doi:10.1051/epjconf/202430306001](https://doi.org/10.1051/epjconf/202430306001).
- [1009] P. Spiller, et al., The FAIR Heavy Ion Synchrotron SIS100, JINST 15 (12) (2020) T12013. [doi:10.1088/1748-0221/15/12/T12013](https://doi.org/10.1088/1748-0221/15/12/T12013).
- [1010] K. Moriya, et al., Measurement of the $\Sigma\pi$ photoproduction line shapes near the $\Lambda(1405)$, Phys. Rev. C 87 (3) (2013) 035206. [arXiv:1301.5000](https://arxiv.org/abs/1301.5000), [doi:10.1103/PhysRevC.87.035206](https://doi.org/10.1103/PhysRevC.87.035206).
- [1011] M. Sumihama, et al., Observation of $\Xi(1620)^0$ and evidence for $\Xi(1690)^0$ in $\Xi_c^+ \rightarrow \Xi^-\pi^+\pi^+$ decays, Phys. Rev. Lett. 122 (7) (2019) 072501. [arXiv:1810.06181](https://arxiv.org/abs/1810.06181), [doi:10.1103/PhysRevLett.122.072501](https://doi.org/10.1103/PhysRevLett.122.072501).
- [1012] V. Crede, J. Yelton, 70 years of hyperon spectroscopy: a review of strange Ξ , Ω baryons, and the spectrum of charmed and bottom baryons, Rept. Prog. Phys. 87 (10) (2024) 106301. [arXiv:2502.08815](https://arxiv.org/abs/2502.08815), [doi:10.1088/1361-6633/ad7610](https://doi.org/10.1088/1361-6633/ad7610).
- [1013] S. Acharya, et al., Accessing the strong interaction between Λ baryons and charged kaons with the femtoscopy technique at the LHC, Phys. Lett. B 845 (2023) 138145. [arXiv:2305.19093](https://arxiv.org/abs/2305.19093), [doi:10.1016/j.physletb.2023.138145](https://doi.org/10.1016/j.physletb.2023.138145).
- [1014] E. Epelbaum, S. Heihoff, U.-G. Meißner, A. Tscherwon, Can the strong interactions between hadrons be determined using femtoscopy? (4 2025). [arXiv:2504.08631](https://arxiv.org/abs/2504.08631).
- [1015] E. Wang, L.-S. Geng, J.-J. Wu, J.-J. Xie, B.-S. Zou, Review of the Low-Lying Excited Baryons $\Sigma^*(1/2^-)$, Chin. Phys. Lett. 41 (10) (2024) 101401. [arXiv:2406.07839](https://arxiv.org/abs/2406.07839), [doi:10.1088/0256-307X/41/10/101401](https://doi.org/10.1088/0256-307X/41/10/101401).
- [1016] Y. Qiang, Y. I. Azimov, I. I. Strakovsky, W. J. Briscoe, H. Gao, D. W. Higinbotham, V. V. Nelyubin, Properties of the $\Lambda(1520)$ Resonance from High-Precision Electroproduction Data, Phys. Lett. B 694 (2011) 123–128. [arXiv:1003.5612](https://arxiv.org/abs/1003.5612), [doi:10.1016/j.physletb.2010.09.052](https://doi.org/10.1016/j.physletb.2010.09.052).
- [1017] H. Zhang, J. Tulpan, M. Shrestha, D. M. Manley, Partial-wave analysis of $\bar{K}N$ scattering reactions, Phys. Rev. C 88 (3) (2013) 035204. [arXiv:1305.3598](https://arxiv.org/abs/1305.3598), [doi:10.1103/PhysRevC.88.035204](https://doi.org/10.1103/PhysRevC.88.035204).
- [1018] H. Zhang, J. Tulpan, M. Shrestha, D. M. Manley, Multichannel parametrization of $\bar{K}N$ scattering amplitudes and extraction of resonance parameters, Phys. Rev. C 88 (3) (2013) 035205. [arXiv:1305.4575](https://arxiv.org/abs/1305.4575), [doi:10.1103/PhysRevC.88.035205](https://doi.org/10.1103/PhysRevC.88.035205).
- [1019] C. Fernandez-Ramirez, I. V. Danilkin, D. M. Manley, V. Mathieu, A. P. Szczepaniak, Coupled-channel model for $\bar{K}N$ scattering in the resonant region, Phys. Rev. D 93 (3) (2016) 034029. [arXiv:1510.07065](https://arxiv.org/abs/1510.07065), [doi:10.1103/PhysRevD.93.034029](https://doi.org/10.1103/PhysRevD.93.034029).
- [1020] A. V. Anisovich, A. V. Sarantsev, V. A. Nikonov, V. Burkert, R. A. Schumacher, U. Thoma, E. Klempt, Hyperon III: $K^- p - \pi\Sigma$ coupled-channel dynamics in the $\Lambda(1405)$ mass region, Eur. Phys. J. A 56 (5) (2020) 139. [doi:10.1140/epja/s10050-020-00142-8](https://doi.org/10.1140/epja/s10050-020-00142-8).
- [1021] A. V. Sarantsev, M. Matveev, V. A. Nikonov, A. V. Anisovich, U. Thoma, E. Klempt, Hyperon II: Properties of excited hyperons, Eur. Phys. J. A 55 (10) (2019) 180. [arXiv:1907.13387](https://arxiv.org/abs/1907.13387), [doi:10.1140/epja/i2019-12880-5](https://doi.org/10.1140/epja/i2019-12880-5).
- [1022] M. Matveev, A. V. Sarantsev, V. A. Nikonov, A. V. Anisovich, U. Thoma, E. Klempt, Hyperon I: Partial-wave amplitudes for $K^- p$ scattering, Eur. Phys. J. A 55 (10) (2019) 179. [arXiv:1907.03645](https://arxiv.org/abs/1907.03645), [doi:10.1140/epja/i2019-12878-y](https://doi.org/10.1140/epja/i2019-12878-y).
- [1023] R. Buettgen, K. Holinde, A. Mueller-Groeling, J. Speth, P. Wyborny, A Meson Exchange Model for the $K^+ N$ Interaction, Nucl. Phys. A 506 (1990) 586–614. [doi:10.1016/0375-9474\(90\)90205-Z](https://doi.org/10.1016/0375-9474(90)90205-Z).
- [1024] M. Hoffmann, J. W. Durso, K. Holinde, B. C. Pearce, J. Speth, Role of correlated two pion exchange in $K^+ N$ scattering, Nucl. Phys. A 593 (1995) 341–361. [arXiv:nucl-th/9504029](https://arxiv.org/abs/nucl-th/9504029), [doi:10.1016/0375-9474\(95\)00320-Z](https://doi.org/10.1016/0375-9474(95)00320-Z).
- [1025] H. Kamano, T. S. H. Lee, Toward establishing low-lying Λ and Σ hyperon resonances with the $\bar{K} + d \rightarrow \pi + Y + N$ reaction, Phys. Rev. C 94 (6) (2016) 065205. [arXiv:1608.03470](https://arxiv.org/abs/1608.03470), [doi:10.1103/PhysRevC.94.065205](https://doi.org/10.1103/PhysRevC.94.065205).
- [1026] M. Alekseev, et al., Observation of a $J^{**}PC = 1+-$ exotic resonance in diffractive dissociation of 190-GeV/c pi- into pi- pi- pi+, Phys. Rev. Lett. 104 (2010) 241803. [arXiv:0910.5842](https://arxiv.org/abs/0910.5842), [doi:10.1103/PhysRevLett.104.241803](https://doi.org/10.1103/PhysRevLett.104.241803).
- [1027] M. G. Alexeev, et al., Exotic meson $\pi_1(1600)$ with $J^{PC} = 1^{-+}$ and its decay into $\rho(770)\pi$, Phys. Rev. D 105 (1) (2022) 012005. [arXiv:2108.01744](https://arxiv.org/abs/2108.01744), [doi:10.1103/PhysRevD.105.012005](https://doi.org/10.1103/PhysRevD.105.012005).
- [1028] H.-X. Chen, W. Chen, X. Liu, Y.-R. Liu, S.-L. Zhu, An updated review of the new hadron states, Rept. Prog. Phys. 86 (2) (2023) 026201. [arXiv:2204.02649](https://arxiv.org/abs/2204.02649), [doi:10.1088/1361-6633/aca3b6](https://doi.org/10.1088/1361-6633/aca3b6).
- [1029] M.-Z. Liu, Y.-W. Pan, Z.-W. Liu, T.-W. Wu, J.-X. Lu, L.-S. Geng, Three ways to decipher the nature of exotic hadrons: Multiplets, three-body hadronic molecules, and correlation functions, Phys. Rept. 1108 (2025) 1–108. [arXiv:2404.06399](https://arxiv.org/abs/2404.06399), [doi:10.1016/j.physrep.2024.12.001](https://doi.org/10.1016/j.physrep.2024.12.001).
- [1030] V. Baru, A. A. Filin, C. Hanhart, Y. S. Kalashnikova, A. E. Kudryavtsev, A. V. Nefediev, Three-body $D\bar{D}\pi$ dynamics for the $X(3872)$, Phys. Rev. D 84 (2011) 074029. [arXiv:1108.5644](https://arxiv.org/abs/1108.5644), [doi:10.1103/PhysRevD.84.074029](https://doi.org/10.1103/PhysRevD.84.074029).
- [1031] M. Cleven, Q. Wang, F.-K. Guo, C. Hanhart, U.-G. Meißner, Q. Zhao, $Y(4260)$ as the first S -wave open charm vector molecular state?, Phys. Rev. D 90 (7) (2014) 074039. [arXiv:1310.2190](https://arxiv.org/abs/1310.2190), [doi:10.1103/PhysRevD.90.074039](https://doi.org/10.1103/PhysRevD.90.074039).
- [1032] M.-L. Du, V. Baru, X.-K. Dong, A. Filin, F.-K. Guo, C. Hanhart, A. Nefediev, J. Nieves, Q. Wang, Coupled-channel approach to $Tcc+$ including three-body effects, Phys. Rev. D 105 (1) (2022) 014024. [arXiv:2110.13765](https://arxiv.org/abs/2110.13765), [doi:10.1103/PhysRevD.105.014024](https://doi.org/10.1103/PhysRevD.105.014024).
- [1033] Z.-Y. Lin, J.-B. Cheng, S.-L. Zhu, $Tcc+$ and $\chi c1(3872)$ with the complex scaling method and $DD(D^-)\pi$ three-body effect, Phys. Rev. D 110 (5) (2024) 054008. [arXiv:2205.14628](https://arxiv.org/abs/2205.14628), [doi:10.1103/PhysRevD.110.054008](https://doi.org/10.1103/PhysRevD.110.054008).
- [1034] A. Jackura, C. Fernández-Ramírez, V. Mathieu, M. Mikhasenko, J. Nys, A. Pilloni, K. Saldaña, N. Sherrill, A. P. Szczepaniak, Phenomenology of Relativistic $3 \rightarrow 3$ Reaction Amplitudes within the Isobar Approximation, Eur. Phys. J. C 79 (1) (2019) 56. [arXiv:1809.10523](https://arxiv.org/abs/1809.10523), [doi:10.1140/epjc/s10052-019-6566-1](https://doi.org/10.1140/epjc/s10052-019-6566-1).
- [1035] A. W. Jackura, S. M. Dawid, C. Fernández-Ramírez, V. Mathieu, M. Mikhasenko, A. Pilloni, S. R. Sharpe, A. P. Szczepaniak, Equivalence of three-particle scattering formalisms, Phys. Rev. D 100 (3) (2019) 034508. [arXiv:1905.12007](https://arxiv.org/abs/1905.12007), [doi:10.1103/PhysRevD.100.034508](https://doi.org/10.1103/PhysRevD.100.034508).
- [1036] M. Albaladejo, D. Winney, I. V. Danilkin, C. Fernández-Ramírez, V. Mathieu, M. Mikhasenko, A. Pilloni, J. A. Silva-Castro, A. P. Szczepaniak, Khuri-Treiman equations for 3π decays of particles with spin, Phys. Rev. D 101 (5) (2020) 054018. [arXiv:1910.03107](https://arxiv.org/abs/1910.03107), [doi:10.1103/PhysRevD.101.054018](https://doi.org/10.1103/PhysRevD.101.054018).
- [1037] A. W. Jackura, R. A. Briceño, S. M. Dawid, M. H. E. Islam, C. McCarty, Solving relativistic three-body integral equations in the presence of bound states, Phys. Rev. D 104 (1) (2021) 014507. [arXiv:2010.09820](https://arxiv.org/abs/2010.09820), [doi:10.1103/PhysRevD.104.014507](https://doi.org/10.1103/PhysRevD.104.014507).
- [1038] A. Martínez Torres, K. P. Khemchandani, L. Roca, E. Oset, Few-body systems consisting of mesons, Few Body Syst. 61 (4) (2020) 35. [arXiv:2005.14357](https://arxiv.org/abs/2005.14357), [doi:10.1007/s00601-020-01568-y](https://doi.org/10.1007/s00601-020-01568-y).
- [1039] A. W. Jackura, R. A. Briceño, Partial-wave projection of the one-particle exchange in three-body scattering amplitudes, Phys. Rev. D 109 (9) (2024) 096030. [arXiv:2312.00625](https://arxiv.org/abs/2312.00625), [doi:10.1103/PhysRevD.109.096030](https://doi.org/10.1103/PhysRevD.109.096030).
- [1040] X. Zhang, Relativistic three-body scattering and the $D0D^*+D+D^*0$ system, Phys. Rev. D 109 (9) (2024) 094010. [arXiv:2402.02151](https://arxiv.org/abs/2402.02151), [doi:10.1103/PhysRevD.109.094010](https://doi.org/10.1103/PhysRevD.109.094010).

- [1041] S. Leupold, M. F. M. Lutz, Hadronic three-body decays of light vector mesons, *Eur. Phys. J. A* 39 (2009) 205–212. [arXiv:0807.4686](#), [doi:10.1140/epja/i2008-10707-2](#).
- [1042] S. X. Nakamura, Q. Huang, J. J. Wu, H. P. Peng, Y. Zhang, Y. C. Zhu, Three-body unitary coupled-channel approach to radiative J/ψ decays and $\eta(1405/1475)$, *Phys. Rev. D* 109 (1) (2024) 014021. [arXiv:2311.05391](#), [doi:10.1103/PhysRevD.109.014021](#).
- [1043] H. Kamano, S. X. Nakamura, T. S. H. Lee, T. Sato, Unitary coupled-channels model for three-mesons decays of heavy mesons, *Phys. Rev. D* 84 (2011) 114019. [arXiv:1106.4523](#), [doi:10.1103/PhysRevD.84.114019](#).
- [1044] S. X. Nakamura, H. Kamano, T. S. H. Lee, T. Sato, Extraction of Meson Resonances from Three-pions Photo-production Reactions, *Phys. Rev. D* 86 (2012) 114012. [arXiv:1209.3402](#), [doi:10.1103/PhysRevD.86.114012](#).
- [1045] R. Pasquier, J. Y. Pasquier, Khuri-Treiman-Type Equations for Three-Body Decay and Production Processes, *Phys. Rev.* 170 (1968) 1294–1309. [doi:10.1103/PhysRev.170.1294](#).
- [1046] I. J. R. Aitchison, Relativistic Three Pion Dynamics Generated by Two-Body Unitarity and Analyticity, *J. Phys. G* 3 (1977) 121. [doi:10.1088/0305-4616/3/2/006](#).
- [1047] G. Colangelo, S. Lanz, E. Passemar, A New Dispersive Analysis of $\eta \rightarrow 3\pi$, *PoS CD09* (2009) 047. [arXiv:0910.0765](#), [doi:10.22323/1.086.0047](#).
- [1048] B. Kubis, S. P. Schneider, The Cusp effect in η' — $\eta\pi\pi$ decays, *Eur. Phys. J. C* 62 (2009) 511–523. [arXiv:0904.1320](#), [doi:10.1140/epjc/s10052-009-1054-7](#).
- [1049] S. P. Schneider, B. Kubis, C. Ditsche, Rescattering effects in $\eta \rightarrow 3\pi$ decays, *JHEP* 02 (2011) 028. [arXiv:1010.3946](#), [doi:10.1007/JHEP02\(2011\)028](#).
- [1050] K. Kampf, M. Knecht, J. Novotny, M. Zdrahal, Analytical dispersive construction of $\eta \rightarrow 3\pi$ amplitude: first order in isospin breaking, *Phys. Rev. D* 84 (2011) 114015. [arXiv:1103.0982](#), [doi:10.1103/PhysRevD.84.114015](#).
- [1051] F. Niecknig, B. Kubis, S. P. Schneider, Dispersive analysis of $\omega \rightarrow 3\pi$ and $\phi \rightarrow 3\pi$ decays, *Eur. Phys. J. C* 72 (2012) 2014. [arXiv:1203.2501](#), [doi:10.1140/epjc/s10052-012-2014-1](#).
- [1052] P. Guo, R. Mitchell, M. Shepherd, A. P. Szczepaniak, Amplitudes for the analysis of the decay $J/\psi \rightarrow K^+K^-\pi^0$, *Phys. Rev. D* 85 (2012) 056003. [arXiv:1112.3284](#), [doi:10.1103/PhysRevD.85.056003](#).
- [1053] I. V. Danilkin, C. Fernández-Ramírez, P. Guo, V. Mathieu, D. Schott, M. Shi, A. P. Szczepaniak, Dispersive analysis of $\omega/\phi \rightarrow 3\pi/\pi\gamma^*$, *Phys. Rev. D* 91 (9) (2015) 094029. [arXiv:1409.7708](#), [doi:10.1103/PhysRevD.91.094029](#).
- [1054] P. Guo, I. V. Danilkin, A. P. Szczepaniak, Dispersive approaches for three-particle final state interaction, *Eur. Phys. J. A* 51 (10) (2015) 135. [arXiv:1409.8652](#), [doi:10.1140/epja/i2015-15135-7](#).
- [1055] P. Guo, I. V. Danilkin, D. Schott, C. Fernández-Ramírez, V. Mathieu, A. P. Szczepaniak, Three-body final state interaction in $\eta \rightarrow 3\pi$, *Phys. Rev. D* 92 (5) (2015) 054016. [arXiv:1505.01715](#), [doi:10.1103/PhysRevD.92.054016](#).
- [1056] J. T. Daub, C. Hanhart, B. Kubis, A model-independent analysis of final-state interactions in $\bar{B}_{d/s}^0 \rightarrow J/\psi\pi\pi$, *JHEP* 02 (2016) 009. [arXiv:1508.06841](#), [doi:10.1007/JHEP02\(2016\)009](#).
- [1057] F. Niecknig, B. Kubis, Dispersion-theoretical analysis of the $D^+ \rightarrow K^-\pi^+\pi^+$ Dalitz plot, *JHEP* 10 (2015) 142. [arXiv:1509.03188](#), [doi:10.1007/JHEP10\(2015\)142](#).
- [1058] P. Guo, I. V. Danilkin, C. Fernández-Ramírez, V. Mathieu, A. P. Szczepaniak, Three-body final state interaction in $\eta \rightarrow 3\pi$ updated, *Phys. Lett. B* 771 (2017) 497–502. [arXiv:1608.01447](#), [doi:10.1016/j.physletb.2017.05.092](#).
- [1059] T. Isken, B. Kubis, S. P. Schneider, P. Stoffer, Dispersion relations for $\eta' \rightarrow \eta\pi\pi$, *Eur. Phys. J. C* 77 (7) (2017) 489. [arXiv:1705.04339](#), [doi:10.1140/epjc/s10052-017-5024-1](#).
- [1060] M. Albaladejo, B. Moussallam, Extended chiral Khuri-Treiman formalism for $\eta \rightarrow 3\pi$ and the role of the $a_0(980)$, $f_0(980)$ resonances, *Eur. Phys. J. C* 77 (8) (2017) 508. [arXiv:1702.04931](#), [doi:10.1140/epjc/s10052-017-5052-x](#).
- [1061] F. Niecknig, B. Kubis, Consistent Dalitz plot analysis of Cabibbo-favored $D^+ \rightarrow \bar{K}\pi\pi^+$ decays, *Phys. Lett. B* 780 (2018) 471–478. [arXiv:1708.00446](#), [doi:10.1016/j.physletb.2018.03.048](#).
- [1062] M. Dax, T. Isken, B. Kubis, Quark-mass dependence in $\omega \rightarrow 3\pi$ decays, *Eur. Phys. J. C* 78 (10) (2018) 859. [arXiv:1808.08957](#), [doi:10.1140/epjc/s10052-018-6346-3](#).
- [1063] J. Gasser, A. Rusetsky, Solving integral equations in $\eta \rightarrow 3\pi$, *Eur. Phys. J. C* 78 (11) (2018) 906. [arXiv:1809.06399](#), [doi:10.1140/epjc/s10052-018-6378-8](#).
- [1064] M. Mikhasenko, et al., Dalitz-plot decomposition for three-body decays, *Phys. Rev. D* 101 (3) (2020) 034033. [arXiv:1910.04566](#), [doi:10.1103/PhysRevD.101.034033](#).
- [1065] H. Akdag, T. Isken, B. Kubis, Patterns of C- and CP-violation in hadronic η and η' three-body decays, *JHEP* 02 (2022) 137, [Erratum: *JHEP* 12, 156 (2022)]. [arXiv:2111.02417](#), [doi:10.1007/JHEP02\(2022\)137](#).
- [1066] A. Martínez Torres, K. P. Khemchandani, D. Jido, A. Hosaka, Theoretical support for the $\pi(1300)$ and the recently claimed $f_0(1790)$ as molecular resonances, *Phys. Rev. D* 84 (2011) 074027. [arXiv:1106.6101](#), [doi:10.1103/PhysRevD.84.074027](#).
- [1067] P. C. Magalhaes, M. R. Robilotta, K. S. F. F. Guimaraes, T. Frederico, W. de Paula, I. Bediaga, A. C. d. Reis, C. M. Maekawa, G. R. S. Zarnauskas, Towards three-body unitarity in $D^+ \rightarrow K^-\pi^+\pi^+$, *Phys. Rev. D* 84 (2011) 094001. [arXiv:1105.5120](#), [doi:10.1103/PhysRevD.84.094001](#).
- [1068] P. C. Magalhaes, M. R. Robilotta, $D^+ \rightarrow K^-\pi^+\pi^+$ - the weak vector current, *Phys. Rev. D* 92 (9) (2015) 094005. [arXiv:1504.06346](#), [doi:10.1103/PhysRevD.92.094005](#).
- [1069] R. T. Aoude, P. C. Magalhaes, A. C. Dos Reis, M. R. Robilotta, Multimeson model for the $D^+ \rightarrow K^+K^-K^+$ decay amplitude, *Phys. Rev. D* 98 (5) (2018) 056021. [arXiv:1805.11764](#), [doi:10.1103/PhysRevD.98.056021](#).
- [1070] I. J. R. Aitchison, Unitarity, Analyticity and Crossing Symmetry in Two- and Three-hadron Final State Interactions (7 2015). [arXiv:1507.02697](#).
- [1071] I. J. R. Aitchison, R. Pasquier, Three-Body Unitarity and Khuri-Treiman Amplitudes, *Phys. Rev.* 152 (4) (1966) 1274. [doi:10.1103/PhysRev.152.1274](#).
- [1072] D. Stamen, T. Isken, B. Kubis, M. Mikhasenko, M. Niehus, Analysis of rescattering effects in 3π final states, *Eur. Phys. J. C* 83 (6) (2023) 510, [Erratum: *Eur.Phys.J.C* 83, 586 (2023)]. [arXiv:2212.11767](#), [doi:10.1140/epjc/s10052-023-11665-x](#).
- [1073] M. Aghasyan, et al., Light isovector resonances in $\pi^-p \rightarrow \pi^-\pi^-\pi^+p$ at 190 GeV/c, *Phys. Rev. D* 98 (9) (2018) 092003. [arXiv:1802.05913](#), [doi:10.1103/PhysRevD.98.092003](#).
- [1074] M. Albrecht, et al., Coupled channel analysis of $\bar{p}p \rightarrow \pi^0\pi^0\eta$, $\pi^0\eta\eta$ and $K^+K^-\pi^0$ at 900 MeV/c and of $\pi\pi$ -scattering data, *Eur. Phys. J. C* 80 (5) (2020) 453. [arXiv:1909.07091](#), [doi:10.1140/epjc/s10052-020-7930-x](#).
- [1075] M. Ablikim, et al., Amplitude analysis and branching fraction measurement of the decay $D^+ \rightarrow K_S^0\pi^+\pi^0\pi^0$, *JHEP* 09 (2023) 077. [arXiv:2305.15879](#), [doi:10.1007/JHEP09\(2023\)077](#).
- [1076] A. Rabusov, D. Greenwald, S. Paul, Partial wave analysis of $\tau^- \rightarrow \pi^-\pi^+\pi^-\nu_\tau$ at Belle, *PoS ICHEP2022* (2022) 1034. [arXiv:2211.11696](#), [doi:10.22323/1.414.1034](#).
- [1077] R. Aaij, et al., Amplitude analysis of the $D^+ \rightarrow \pi^-\pi^+\pi^+$ decay and measurement of the $\pi^-\pi^+$ S-wave amplitude, *JHEP* 06 (2023) 044.

[arXiv:2208.03300](https://arxiv.org/abs/2208.03300), doi:10.1007/JHEP06(2023)044.

- [1078] F. Krinner, D. Greenwald, D. Ryabchikov, B. Grube, S. Paul, Ambiguities in model-independent partial-wave analysis, Phys. Rev. D 97 (11) (2018) 114008. [arXiv:1710.09849](https://arxiv.org/abs/1710.09849), doi:10.1103/PhysRevD.97.114008.
- [1079] T. D. Blanton, S. R. Sharpe, Equivalence of relativistic three-particle quantization conditions, Phys. Rev. D 102 (5) (2020) 054515. [arXiv:2007.16190](https://arxiv.org/abs/2007.16190), doi:10.1103/PhysRevD.102.054515.
- [1080] T. D. Blanton, F. Romero-López, S. R. Sharpe, Implementing the three-particle quantization condition including higher partial waves, JHEP 03 (2019) 106. [arXiv:1901.07095](https://arxiv.org/abs/1901.07095), doi:10.1007/JHEP03(2019)106.
- [1081] M. T. Hansen, F. Romero-López, S. R. Sharpe, Generalizing the relativistic quantization condition to include all three-pion isospin channels, JHEP 07 (2020) 047, [Erratum: JHEP 02, 014 (2021)]. [arXiv:2003.10974](https://arxiv.org/abs/2003.10974), doi:10.1007/JHEP07(2020)047.
- [1082] T. D. Blanton, S. R. Sharpe, Relativistic three-particle quantization condition for nondegenerate scalars, Phys. Rev. D 103 (5) (2021) 054503. [arXiv:2011.05520](https://arxiv.org/abs/2011.05520), doi:10.1103/PhysRevD.103.054503.
- [1083] M. Mikhasenko, A. Pilloni, M. Albaladejo, C. Fernández-Ramírez, A. Jackura, V. Mathieu, J. Nys, A. Rodas, B. Ketzer, A. P. Szczepaniak, Pole position of the $a_1(1260)$ from τ -decay, Phys. Rev. D 98 (9) (2018) 096021. [arXiv:1810.00016](https://arxiv.org/abs/1810.00016), doi:10.1103/PhysRevD.98.096021.
- [1084] R. Molina, M. Döring, W. H. Liang, E. Oset, The $\pi f_0(500)$ decay of the $a_1(1260)$, Eur. Phys. J. C 81 (9) (2021) 782. [arXiv:2107.07439](https://arxiv.org/abs/2107.07439), doi:10.1140/epjc/s10052-021-09574-y.
- [1085] M. Wagner, S. Leupold, Information on the structure of the $a(1)$ from tau decay, Phys. Rev. D 78 (2008) 053001. [arXiv:0801.0814](https://arxiv.org/abs/0801.0814), doi:10.1103/PhysRevD.78.053001.
- [1086] J. Kuhn, et al., Exotic meson production in the $f(1)(1285)$ pi- system observed in the reaction $\pi^- p \rightarrow \eta \pi^+ \pi^- \pi^+$ at 18-GeV/c, Phys. Lett. B 595 (2004) 109–117. [arXiv:hep-ex/0401004](https://arxiv.org/abs/hep-ex/0401004), doi:10.1016/j.physletb.2004.05.032.
- [1087] M. Davier, A. Höcker, B. Malaescu, C.-Z. Yuan, Z. Zhang, Update of the ALEPH non-strange spectral functions from hadronic τ decays, Eur. Phys. J. C 74 (3) (2014) 2803. [arXiv:1312.1501](https://arxiv.org/abs/1312.1501), doi:10.1140/epjc/s10052-014-2803-9.
- [1088] S. Coleman, R. E. Norton, Singularities in the physical region, Nuovo Cim. 38 (1965) 438–442. doi:10.1007/BF02750472.
- [1089] R. Karplus, C. M. Sommerfield, E. H. Wichmann, Spectral Representations in Perturbation Theory. 1. Vertex Function, Phys. Rev. 111 (1958) 1187–1190. doi:10.1103/PhysRev.111.1187.
- [1090] L. D. Landau, On analytic properties of vertex parts in quantum field theory, Nucl. Phys. 13 (1) (1959) 181–192. doi:10.1016/B978-0-08-010586-4.50103-6.
- [1091] N. E. Booth, A. Abashian, K. M. Crowe, Anomaly in Meson Production in p+d Collisions, Phys. Rev. Lett. 7 (1961) 35–39. doi:10.1103/PhysRevLett.7.35.
- [1092] V. V. Anisovich, L. G. Dakho, Logarithmic singularities in the reactions $\pi^- + p \rightarrow n + \pi^- + \pi^+$ and $p + d \rightarrow He\ 3 + 2\pi$, Phys. Lett. 10 (2) (1964) 221–224. doi:10.1016/0031-9163(64)90176-3.
- [1093] X.-H. Liu, M. Oka, Q. Zhao, Searching for observable effects induced by anomalous triangle singularities, Phys. Lett. B 753 (2016) 297–302. [arXiv:1507.01674](https://arxiv.org/abs/1507.01674), doi:10.1016/j.physletb.2015.12.027.
- [1094] M. Bayar, F. Aceti, F.-K. Guo, E. Oset, A Discussion on Triangle Singularities in the $\Lambda_b \rightarrow J/\psi K^- p$ Reaction, Phys. Rev. D 94 (7) (2016) 074039. [arXiv:1609.04133](https://arxiv.org/abs/1609.04133), doi:10.1103/PhysRevD.94.074039.
- [1095] M. Mikhasenko, B. Ketzer, A. Sarantsev, Nature of the $a_1(1420)$, Phys. Rev. D 91 (9) (2015) 094015. [arXiv:1501.07023](https://arxiv.org/abs/1501.07023), doi:10.1103/PhysRevD.91.094015.
- [1096] G. D. Alexeev, et al., Triangle Singularity as the Origin of the $a_1(1420)$, Phys. Rev. Lett. 127 (8) (2021) 082501. [arXiv:2006.05342](https://arxiv.org/abs/2006.05342), doi:10.1103/PhysRevLett.127.082501.
- [1097] V. R. Debastiani, S. Sakai, E. Oset, Considerations on the Schmid theorem for triangle singularities, Eur. Phys. J. C 79 (1) (2019) 69. [arXiv:1809.06890](https://arxiv.org/abs/1809.06890), doi:10.1140/epjc/s10052-019-6558-1.
- [1098] T. Isken, X.-Y. Guo, Y. Heo, C. L. Korpa, M. F. M. Lutz, Triangle and box diagrams in coupled-channel systems from the chiral Lagrangian, Phys. Rev. D 109 (3) (2024) 034032. [arXiv:2309.09695](https://arxiv.org/abs/2309.09695), doi:10.1103/PhysRevD.109.034032.
- [1099] L. R. Dai, Q. X. Yu, E. Oset, Triangle singularity in $\tau^- \rightarrow \nu_\tau \pi^- f_0(980)$ ($a_0(980)$) decays, Phys. Rev. D 99 (1) (2019) 016021. [arXiv:1809.11007](https://arxiv.org/abs/1809.11007), doi:10.1103/PhysRevD.99.016021.
- [1100] W.-H. Liang, H.-X. Chen, E. Oset, E. Wang, Triangle singularity in the $J/\psi \rightarrow K^+ K^- f_0(980)$ ($a_0(980)$) decays, Eur. Phys. J. C 79 (5) (2019) 411. [arXiv:1903.01252](https://arxiv.org/abs/1903.01252), doi:10.1140/epjc/s10052-019-6928-8.
- [1101] H.-J. Jing, S. Sakai, F.-K. Guo, B.-S. Zou, Triangle singularities in $J/\psi \rightarrow \eta \pi^0 \phi$ and $\pi^0 \pi^0 \phi$, Phys. Rev. D 100 (11) (2019) 114010. [arXiv:1907.12719](https://arxiv.org/abs/1907.12719), doi:10.1103/PhysRevD.100.114010.
- [1102] F.-K. Guo, Novel Method for Precisely Measuring the $X(3872)$ Mass, Phys. Rev. Lett. 122 (20) (2019) 202002. [arXiv:1902.11221](https://arxiv.org/abs/1902.11221), doi:10.1103/PhysRevLett.122.202002.
- [1103] R. Molina, E. Oset, Triangle singularity in $B^- \rightarrow K^- X(3872); X \rightarrow \pi^0 \pi^+ \pi^-$ and the $X(3872)$ mass, Eur. Phys. J. C 80 (5) (2020) 451. [arXiv:2002.12821](https://arxiv.org/abs/2002.12821), doi:10.1140/epjc/s10052-020-8014-7.
- [1104] J. C. Polkinghorne, G. R. Scream, The analytic properties of perturbation theory — I, Nuovo Cim. 15 (2) (1960) 289–300. doi:10.1007/bf02860252.
- [1105] J. C. Polkinghorne, G. R. Scream, The analytic properties of perturbation theory — II, Nuovo Cim. 15 (6) (1960) 925–931. doi:10.1007/bf02860197.
- [1106] C. Hanhart, Meson production in nucleon-nucleon collisions close to the threshold, Phys. Rept. 397 (2004) 155–256. [arXiv:hep-ph/0311341](https://arxiv.org/abs/hep-ph/0311341), doi:10.1016/j.physrep.2004.03.007.
- [1107] H. Garcilazo, T. Mizutani, pi N N systems, World Scientific, Singapore, 1990.
- [1108] B. Blankleider, Theory of the coupled N N - pi N N system, Nucl. Phys. A 543 (1992) 163C–182C. doi:10.1016/0375-9474(92)90417-I.
- [1109] E. L. Lomon, Coupled Channel Interaction for Intermediate-energy Nucleon-nucleon Reactions, Phys. Rev. D 26 (1982) 576. doi:10.1103/PhysRevD.26.576.
- [1110] E. E. van Faassen, J. A. Tjon, Relativistic NN Scattering Calculations With Δ Degrees of Freedom, Phys. Rev. C 30 (1984) 285. doi:10.1103/PhysRevC.30.285.
- [1111] R. B. Wiringa, R. A. Smith, T. L. Ainsworth, Nucleon Nucleon Potentials with and Without Delta (1232) Degrees of Freedom, Phys. Rev. C 29 (1984) 1207–1221. doi:10.1103/PhysRevC.29.1207.
- [1112] J. Haidenbauer, K. Holinde, M. B. Johnson, A Coupled channel potential for nucleons and deltas, Phys. Rev. C 48 (1993) 2190–2200. doi:10.1103/PhysRevC.48.2190.
- [1113] G. Cattapan, L. S. Ferreira, The role of the Delta in nuclear physics, Phys. Rept. 362 (2002) 303–407. doi:10.1016/S0370-1573(01)00093-X.
- [1114] C. Elster, K. Holinde, D. Schütte, R. Machleidt, Extension of the Bonn Meson Exchange NN Potential Above Pion Production Threshold: Role of the Δ Isobar, Phys. Rev. C 38 (1988) 1828–1842. doi:10.1103/PhysRevC.38.1828.
- [1115] C. Ordóñez, L. Ray, U. van Kolck, The Two nucleon potential from chiral Lagrangians, Phys. Rev. C 53 (1996) 2086–2105. [arXiv:1115.00001](https://arxiv.org/abs/1115.00001).

[hep-ph/9511380](#), doi:10.1103/PhysRevC.53.2086.

- [1116] N. Kaiser, S. Gerstendorfer, W. Weise, Peripheral NN scattering: Role of delta excitation, correlated two pion and vector meson exchange, Nucl. Phys. A 637 (1998) 395–420. [arXiv:nucl-th/9802071](#), doi:10.1016/S0375-9474(98)00234-6.
- [1117] H. Krebs, E. Epelbaum, U.-G. Meißner, Nuclear forces with Delta-excitations up to next-to-next-to-leading order. I. Peripheral nucleon-nucleon waves, Eur. Phys. J. A 32 (2007) 127–137. [arXiv:nucl-th/0703087](#), doi:10.1140/epja/i2007-10372-y.
- [1118] J. J. de Swart, C. Dullemond, Effective range theory and the low energy hyperon-nucleon interactions, Annals Phys. 19 (1962) 458. doi:10.1016/0003-4916(62)90185-9.
- [1119] J. J. De Swart, M. M. Nagels, T. A. Rijken, P. A. Verhoeven, Hyperon-nucleon interaction, Springer Tracts Mod. Phys. 60 (1971) 138–203.
- [1120] T. A. Rijken, M. M. Nagels, Y. Yamamoto, Baryon-baryon interactions: Nijmegen extended-soft-core models, Prog. Theor. Phys. Suppl. 185 (2010) 14–71. doi:10.1143/PTPS.185.14.
- [1121] S. Petschauer, J. Haidenbauer, N. Kaiser, U.-G. Meißner, W. Weise, Hyperon-nuclear interactions from SU(3) chiral effective field theory, Front. in Phys. 8 (2020) 12. [arXiv:2002.00424](#), doi:10.3389/fphy.2020.00012.
- [1122] R. L. Jaffe, Perhaps a Stable Dihyperon, Phys. Rev. Lett. 38 (1977) 195–198, [Erratum: Phys. Rev. Lett. 38, 617 (1977)]. doi:10.1103/PhysRevLett.38.195.
- [1123] P. Adlarson, et al., ABC Effect in Basic Double-Pionic Fusion — Observation of a new resonance?, Phys. Rev. Lett. 106 (2011) 242302. [arXiv:1104.0123](#), doi:10.1103/PhysRevLett.106.242302.
- [1124] H. Clement, On the History of Dibaryons and their Final Observation, Prog. Part. Nucl. Phys. 93 (2017) 195. [arXiv:1610.05591](#), doi:10.1016/j.ppnp.2016.12.004.
- [1125] E. Epelbaum, H.-W. Hammer, U.-G. Meißner, Modern Theory of Nuclear Forces, Rev. Mod. Phys. 81 (2009) 1773–1825. [arXiv:0811.1338](#), doi:10.1103/RevModPhys.81.1773.
- [1126] R. Machleidt, D. R. Entem, Chiral effective field theory and nuclear forces, Phys. Rept. 503 (2011) 1–75. [arXiv:1105.2919](#), doi:10.1016/j.physrep.2011.02.001.
- [1127] P. Reinert, H. Krebs, E. Epelbaum, Semilocal momentum-space regularized chiral two-nucleon potentials up to fifth order, Eur. Phys. J. A 54 (5) (2018) 86. [arXiv:1711.08821](#), doi:10.1140/epja/i2018-12516-4.
- [1128] D. R. Entem, R. Machleidt, Y. Nosyk, High-quality two-nucleon potentials up to fifth order of the chiral expansion, Phys. Rev. C 96 (2) (2017) 024004. [arXiv:1703.05454](#), doi:10.1103/PhysRevC.96.024004.
- [1129] J. Haidenbauer, U.-G. Meißner, A. Nogga, H. Le, Hyperon-nucleon interaction in chiral effective field theory at next-to-next-to-leading order, Eur. Phys. J. A 59 (3) (2023) 63. [arXiv:2301.00722](#), doi:10.1140/epja/s10050-023-00960-6.
- [1130] H. Polinder, J. Haidenbauer, U.-G. Meißner, Hyperon-nucleon interactions: A Chiral effective field theory approach, Nucl. Phys. A 779 (2006) 244–266. [arXiv:nucl-th/0605050](#), doi:10.1016/j.nuclphysa.2006.09.006.
- [1131] J. Haidenbauer, U.-G. Meißner, A. Nogga, H. Polinder, The Hyperon-nucleon interaction: Conventional versus effective field theory approach, Lect. Notes Phys. 724 (2007) 113–140. [arXiv:nucl-th/0702015](#), doi:10.1007/978-3-540-72039-3_4.
- [1132] J. Haidenbauer, S. Petschauer, N. Kaiser, U.-G. Meißner, A. Nogga, W. Weise, Hyperon-nucleon interaction at next-to-leading order in chiral effective field theory, Nucl. Phys. A 915 (2013) 24–58. [arXiv:1304.5339](#), doi:10.1016/j.nuclphysa.2013.06.008.
- [1133] E. Epelbaum, W. Glöckle, U.-G. Meißner, Nuclear forces from chiral Lagrangians using the method of unitary transformation. 1. Formalism, Nucl. Phys. A 637 (1998) 107–134. [arXiv:nucl-th/9801064](#), doi:10.1016/S0375-9474(98)00220-6.
- [1134] E. Epelbaum, W. Glöckle, U.-G. Meißner, The Two-nucleon system at next-to-next-to-next-to-leading order, Nucl. Phys. A 747 (2005) 362–424. [arXiv:nucl-th/0405048](#), doi:10.1016/j.nuclphysa.2004.09.107.
- [1135] B. Holzenkamp, K. Holinde, J. Speth, A Meson Exchange Model for the Hyperon Nucleon Interaction, Nucl. Phys. A 500 (1989) 485–528. doi:10.1016/0375-9474(89)90223-6.
- [1136] H. Le, J. Haidenbauer, U.-G. Meißner, A. Nogga, $A = 4 - 7\Xi$ hypernnuclei based on interactions from chiral effective field theory, Eur. Phys. J. A 57 (12) (2021) 339. [arXiv:2109.06648](#), doi:10.1140/epja/s10050-021-00653-y.
- [1137] H. Le, J. Haidenbauer, U.-G. Meißner, A. Nogga, Separation energies of light Λ hypernnuclei and their theoretical uncertainties, Eur. Phys. J. A 60 (1) (2024) 3. [arXiv:2308.01756](#), doi:10.1140/epja/s10050-023-01219-w.
- [1138] H. Le, J. Haidenbauer, U.-G. Meißner, A. Nogga, Light Λ Hypernnuclei Studied with Chiral Hyperon-Nucleon and Hyperon-Nucleon Forces, Phys. Rev. Lett. 134 (7) (2025) 072502. [arXiv:2409.18577](#), doi:10.1103/PhysRevLett.134.072502.
- [1139] J. Haidenbauer, U.-G. Meißner, A study of hyperons in nuclear matter based on chiral effective field theory, Nucl. Phys. A 936 (2015) 29–44. [arXiv:1411.3114](#), doi:10.1016/j.nuclphysa.2015.01.005.
- [1140] S. Petschauer, J. Haidenbauer, N. Kaiser, U.-G. Meißner, W. Weise, Hyperons in nuclear matter from SU(3) chiral effective field theory, Eur. Phys. J. A 52 (1) (2016) 15. [arXiv:1507.08808](#), doi:10.1140/epja/i2016-16015-4.
- [1141] C. L. Korpa, A. E. L. Dieperink, R. G. E. Timmermans, Hyperon nucleon scattering and hyperon masses in the nuclear medium, Phys. Rev. C 65 (2002) 015208. [arXiv:nucl-th/0109072](#), doi:10.1103/PhysRevC.65.015208.
- [1142] D. B. Kaplan, M. J. Savage, M. B. Wise, Two nucleon systems from effective field theory, Nucl. Phys. B 534 (1998) 329–355. [arXiv:nucl-th/9802075](#), doi:10.1016/S0550-3213(98)00440-4.
- [1143] K.-W. Li, X.-L. Ren, L.-S. Geng, B. Long, Strangeness $S = -1$ hyperon-nucleon scattering in covariant chiral effective field theory, Phys. Rev. D 94 (1) (2016) 014029. [arXiv:1603.07802](#), doi:10.1103/PhysRevD.94.014029.
- [1144] X. L. Ren, E. Epelbaum, J. Gegelia, Λ -nucleon scattering in baryon chiral perturbation theory, Phys. Rev. C 101 (3) (2020) 034001. [arXiv:1911.05616](#), doi:10.1103/PhysRevC.101.034001.
- [1145] J. Song, Z.-W. Liu, K.-W. Li, L.-S. Geng, Test of the hyperon-nucleon interaction within leading order covariant chiral effective field theory, Phys. Rev. C 105 (3) (2022) 035203. [arXiv:2107.04742](#), doi:10.1103/PhysRevC.105.035203.
- [1146] A. Reuber, K. Holinde, J. Speth, Meson exchange hyperon - nucleon interactions in free scattering and nuclear matter, Nucl. Phys. A 570 (1994) 543–579. doi:10.1016/0375-9474(94)90073-6.
- [1147] J. Haidenbauer, U.-G. Meißner, The Jülich hyperon-nucleon model revisited, Phys. Rev. C 72 (2005) 044005. [arXiv:nucl-th/0506019](#), doi:10.1103/PhysRevC.72.044005.
- [1148] T. A. Rijken, V. G. J. Stoks, Y. Yamamoto, Soft core hyperon - nucleon potentials, Phys. Rev. C 59 (1999) 21–40. [arXiv:nucl-th/9807082](#), doi:10.1103/PhysRevC.59.21.
- [1149] M. M. Nagels, T. A. Rijken, Y. Yamamoto, Extended-soft-core baryon-baryon model ESC16. II. Hyperon-nucleon interactions, Phys. Rev. C 99 (4) (2019) 044003. [arXiv:1501.06636](#), doi:10.1103/PhysRevC.99.044003.
- [1150] K. Tominaga, T. Ueda, M. Yamaguchi, N. Kijima, D. Okamoto, K. Miyagawa, T. Yamada, A one-boson-exchange potential for Lambda N, Lambda Lambda and Xi N systems and hypernnuclei, Nucl. Phys. A 642 (1998) 483–505. doi:10.1016/S0375-9474(98)00485-0.
- [1151] K. Tominaga, T. Ueda, Effective one-boson-exchange potential for Lambda N and Sigma N systems and hypertriton, Nucl. Phys. A 693 (2001) 731–754. doi:10.1016/S0375-9474(01)00882-X.
- [1152] W. R. Greenberg, E. L. Lomon, The Lambda N - Sigma N interaction with isobar coupling, Phys. Rev. D 47 (1993) 2703–2721.

[arXiv:nucl-th/9212004](https://arxiv.org/abs/nucl-th/9212004), doi:10.1103/PhysRevD.47.2703.

- [1153] J. R. Pelaez, From controversy to precision on the sigma meson: a review on the status of the non-ordinary $f_0(500)$ resonance, Phys. Rept. 658 (2016) 1. [arXiv:1510.00653](https://arxiv.org/abs/1510.00653), doi:10.1016/j.physrep.2016.09.001.
- [1154] A. Reuber, K. Holinde, H.-C. Kim, J. Speth, Correlated pi pi and K anti-K exchange in the baryon baryon interaction, Nucl. Phys. A 608 (1996) 243–304. [arXiv:nucl-th/9511011](https://arxiv.org/abs/nucl-th/9511011), doi:10.1016/0375-9474(96)00256-4.
- [1155] Y. Fujiwara, Y. Suzuki, C. Nakamoto, Baryon-baryon interactions in the SU(6) quark model and their applications to light nuclear systems, Prog. Part. Nucl. Phys. 58 (2007) 439–520. [arXiv:nucl-th/0607013](https://arxiv.org/abs/nucl-th/0607013), doi:10.1016/j.ppnp.2006.08.001.
- [1156] J. Haidenbauer, U.-G. Meißner, A. Nogga, Hyperon-nucleon interaction within chiral effective field theory revisited, Eur. Phys. J. A 56 (3) (2020) 91. [arXiv:1906.11681](https://arxiv.org/abs/1906.11681), doi:10.1140/epja/s10050-020-00100-4.
- [1157] J. A. Kadyk, G. Alexander, J. H. Chan, P. Gaposchkin, G. H. Trilling, Lambda p interactions in momentum range 300 to 1500 mev/c, Nucl. Phys. B 27 (1971) 13–22. doi:10.1016/0550-3213(71)90076-9.
- [1158] S. Acharya, et al., Investigation of the p- Σ 0 interaction via femtoscopy in pp collisions, Phys. Lett. B 805 (2020) 135419. [arXiv:1910.14407](https://arxiv.org/abs/1910.14407), doi:10.1016/j.physletb.2020.135419.
- [1159] T. H. Tan, A STUDY OF HYPERON - NUCLEON INTERACTION IN THE REACTION anti-K D \rightarrow pi- p LAMBDA AT REST, Phys. Rev. Lett. 23 (1969) 395–398. doi:10.1103/PhysRevLett.23.395.
- [1160] S. Abd El-Samad, et al., On the ΣN cusp in the $pp \rightarrow pK^+\Lambda$ reaction, Eur. Phys. J. A 49 (2013) 41. [arXiv:1206.0426](https://arxiv.org/abs/1206.0426), doi:10.1140/epja/i2013-13041-8.
- [1161] S. Acharya, et al., Exploring the NA- \bar{N} coupled system with high precision correlation techniques at the LHC, Phys. Lett. B 833 (2022) 137272. [arXiv:2104.04427](https://arxiv.org/abs/2104.04427), doi:10.1016/j.physletb.2022.137272.
- [1162] O. I. Dahl, N. Horwitz, D. H. Miller, J. J. Murray, P. G. White, Influence of the Lambdapi Resonance on Correlations in the Reaction K-+d \rightarrow Lambda+pi+p, Phys. Rev. Lett. 6 (1961) 142–144. doi:10.1103/PhysRevLett.6.142.
- [1163] R. H. Dalitz, C. R. Hemming, E. J. Morris, THE (K-,pi-) STRANGENESS EXCHANGE REACTIONS ON DEUTERIUM, Nukleonika 26 (1980) 1555.
- [1164] H. Machner, J. Haidenbauer, F. Hinterberger, A. Magiera, J. A. Niskanen, J. Ritman, R. Siudak, Study of the Λp Interaction Close to the $\Sigma^+ n$ and $\Sigma^0 p$ Thresholds, Nucl. Phys. A 901 (2013) 65–88. [arXiv:1301.6089](https://arxiv.org/abs/1301.6089), doi:10.1016/j.nuclphysa.2013.01.031.
- [1165] F. Hauenstein, et al., First Model-Independent Measurement of the Spin Triplet $p\Lambda$ Scattering Length from Final State Interaction in the $\bar{p}p \rightarrow pK^+\Lambda$ Reaction, Phys. Rev. C 95 (3) (2017) 034001. [arXiv:1607.04783](https://arxiv.org/abs/1607.04783), doi:10.1103/PhysRevC.95.034001.
- [1166] H. G. Dosch, V. Hepp, Analysis of the Lambda p Enhancement at 2.129-GeV in the Reaction K- d \rightarrow pi- Lambda p, Phys. Rev. D 18 (1978) 4071. doi:10.1103/PhysRevD.18.4071.
- [1167] H. G. Dosch, I. O. Stamatescu, A Pole in the Triplet S Wave Hyperon - Nucleon Scattering Amplitudes, Z. Phys. C 3 (1980) 249. doi:10.1007/BF01577424.
- [1168] G. Toker, A. Gal, J. M. Eisenberg, The K- d \rightarrow pi- Λ p reaction at low energies in the faddeev formalism, Phys. Lett. B 88 (1979) 235–238. doi:10.1016/0370-2693(79)90455-6.
- [1169] G. Toker, A. Gal, J. M. Eisenberg, The Y N Interactions and K^- Reactions on Deuterium at Low-energies, Nucl. Phys. A 362 (1981) 405–430. doi:10.1016/0375-9474(81)90502-9.
- [1170] R. H. Dalitz, A. Deloff, The Strangeness Exchange Reaction $K^-d \rightarrow \Lambda p\pi^-$ in Flight, Austral. J. Phys. 36 (1983) 617–631. doi:10.1071/PH830617.
- [1171] M. Torres, R. H. Dalitz, A. Deloff, K^- Absorption Reactions From Rest in Deuterium, Phys. Lett. B 174 (1986) 213–218. doi:10.1016/0370-2693(86)90744-6.
- [1172] A. Deloff, THE K- DEUTERON INTERACTION BELOW 1-GEV/C, Nuovo Cim. A 102 (1989) 217–236. doi:10.1007/BF02735108.
- [1173] M. M. Nagels, T. A. Rijken, J. J. de Swart, Baryon Baryon Scattering in a One Boson Exchange Potential Approach. 2. Hyperon-Nucleon Scattering, Phys. Rev. D 15 (1977) 2547. doi:10.1103/PhysRevD.15.2547.
- [1174] M. M. Nagels, T. A. Rijken, J. J. de Swart, Baryon Baryon Scattering in a One Boson Exchange Potential Approach. 3. A Nucleon-Nucleon and Hyperon - Nucleon Analysis Including Contributions of a Nonet of Scalar Mesons, Phys. Rev. D 20 (1979) 1633. doi:10.1103/PhysRevD.20.1633.
- [1175] C. B. Dover, H. Feshbach, Unitary symmetry in baryon baryon scattering. 2., Annals Phys. 217 (1992) 51–65. doi:10.1016/0003-4916(92)90338-M.
- [1176] B. C. Pearce, B. F. Gibson, Observable Effects of Poles and Shadow Poles in Coupled Channel Systems, Phys. Rev. C 40 (1989) 902–911. doi:10.1103/PhysRevC.40.902.
- [1177] V. Hepp, H. Schleich, A New Determination of the Capture Ratio $r(c) = \text{Sigma- } p \rightarrow \text{Sigma0 } n / (\text{Sigma- } p \rightarrow \text{Sigma0 } n) + (\text{Sigma- } p \rightarrow \text{Lambda } n)$, the Lambda0-Lifetime and Sigma- Lambda0 Mass Difference, Z. Phys. 214 (1968) 71. doi:10.1007/BF01380085.
- [1178] D. Stephen, Study of $\Sigma^- p$ inelastic interaction with Σ^- momentum from 0 to 650 MeV/c, Ph.D. thesis, University of Massachusetts (1970).
- [1179] R. G. Newton, Scattering theory of waves and particles [by] Roger G. Newton., International series in pure and applied physics, McGraw-Hill, New York, 1966.
- [1180] J. Haidenbauer, U.-G. Meißner, S. Petschauer, Strangeness $S = -2$ baryon-baryon interaction at next-to-leading order in chiral effective field theory, Nucl. Phys. A 954 (2016) 273–293. [arXiv:1511.05859](https://arxiv.org/abs/1511.05859), doi:10.1016/j.nuclphysa.2016.01.006.
- [1181] L. Adamczyk, et al., $\Lambda\Lambda$ Correlation Function in Au+Au collisions at $\sqrt{s_{NN}} = 200$ GeV, Phys. Rev. Lett. 114 (2) (2015) 022301. [arXiv:1408.4360](https://arxiv.org/abs/1408.4360), doi:10.1103/PhysRevLett.114.022301.
- [1182] S. Acharya, et al., Study of the $\Lambda\Lambda$ interaction with femtoscopy correlations in pp and p-Pb collisions at the LHC, Phys. Lett. B 797 (2019) 134822. [arXiv:1905.07209](https://arxiv.org/abs/1905.07209), doi:10.1016/j.physletb.2019.134822.
- [1183] S. Acharya, et al., First Observation of an Attractive Interaction between a Proton and a Cascade Baryon, Phys. Rev. Lett. 123 (11) (2019) 112002. [arXiv:1904.12198](https://arxiv.org/abs/1904.12198), doi:10.1103/PhysRevLett.123.112002.
- [1184] Alice Collaboration, Unveiling the strong interaction among hadrons at the LHC, Nature 588 (2020) 232–238, [Erratum: Nature 590, E13 (2021)]. [arXiv:2005.11495](https://arxiv.org/abs/2005.11495), doi:10.1038/s41586-020-3001-6.
- [1185] B. Fu, Measurement of $p - \Xi^-$ ($\bar{p} - \Xi^+$) Correlation Function in Isobar and Au+Au Collisions at $\sqrt{s_{NN}} = 200$ GeV with the STAR Detector, EPJ Web Conf. 316 (2025) 03010. [arXiv:2412.00485](https://arxiv.org/abs/2412.00485), doi:10.1051/epjconf/202531603010.
- [1186] G. R. Farrar, A stable H dibaryon: Dark matter candidate within QCD?, Int. J. Theor. Phys. 42 (2003) 1211–1218. doi:10.1023/A:1025702431127.
- [1187] M. Doser, G. Farrar, G. Kornakov, Searching for a dark matter particle with anti-protonic atoms, Eur. Phys. J. C 83 (12) (2023) 1149. [arXiv:2302.00759](https://arxiv.org/abs/2302.00759), doi:10.1140/epjc/s10052-023-12319-8.
- [1188] C. J. Yoon, et al., Search for the H-dibaryon resonance in C-12 (K-, K+ Lambda Lambda X), Phys. Rev. C 75 (2007) 022201. doi:10.1103/PhysRevC.75.022201.
- [1189] S. R. Beane, et al., Evidence for a Bound H-dibaryon from Lattice QCD, Phys. Rev. Lett. 106 (2011) 162001. [arXiv:1012.3812](https://arxiv.org/abs/1012.3812),

[doi:10.1103/PhysRevLett.106.162001](https://doi.org/10.1103/PhysRevLett.106.162001).

- [1190] T. Inoue, N. Ishii, S. Aoki, T. Doi, T. Hatsuda, Y. Ikeda, K. Murano, H. Nemura, K. Sasaki, Bound H-dibaryon in Flavor SU(3) Limit of Lattice QCD, Phys. Rev. Lett. 106 (2011) 162002. [arXiv:1012.5928](https://arxiv.org/abs/1012.5928), [doi:10.1103/PhysRevLett.106.162002](https://doi.org/10.1103/PhysRevLett.106.162002).
- [1191] T. Inoue, S. Aoki, T. Doi, T. Hatsuda, Y. Ikeda, N. Ishii, K. Murano, H. Nemura, K. Sasaki, Two-Baryon Potentials and H-Dibaryon from 3-flavor Lattice QCD Simulations, Nucl. Phys. A 881 (2012) 28–43. [arXiv:1112.5926](https://arxiv.org/abs/1112.5926), [doi:10.1016/j.nuclphysa.2012.02.008](https://doi.org/10.1016/j.nuclphysa.2012.02.008).
- [1192] J. R. Green, A. D. Hanlon, P. M. Junnarkar, H. Wittig, Weakly bound H dibaryon from SU(3)-flavor-symmetric QCD, Phys. Rev. Lett. 127 (24) (2021) 242003. [arXiv:2103.01054](https://arxiv.org/abs/2103.01054), [doi:10.1103/PhysRevLett.127.242003](https://doi.org/10.1103/PhysRevLett.127.242003).
- [1193] K. Sasaki, et al., $\Lambda\Lambda$ and $N\Xi$ interactions from lattice QCD near the physical point, Nucl. Phys. A 998 (2020) 121737. [arXiv:1912.08630](https://arxiv.org/abs/1912.08630), [doi:10.1016/j.nuclphysa.2020.121737](https://doi.org/10.1016/j.nuclphysa.2020.121737).
- [1194] S. R. Beane, et al., Present Constraints on the H-dibaryon at the Physical Point from Lattice QCD, Mod. Phys. Lett. A 26 (2011) 2587–2595. [arXiv:1103.2821](https://arxiv.org/abs/1103.2821), [doi:10.1142/S0217732311036978](https://doi.org/10.1142/S0217732311036978).
- [1195] P. E. Shanahan, A. W. Thomas, R. D. Young, Mass of the H-dibaryon, Phys. Rev. Lett. 107 (2011) 092004. [arXiv:1106.2851](https://arxiv.org/abs/1106.2851), [doi:10.1103/PhysRevLett.107.092004](https://doi.org/10.1103/PhysRevLett.107.092004).
- [1196] J. Haidenbauer, U.-G. Meißner, To bind or not to bind: The H-dibaryon in light of chiral effective field theory, Phys. Lett. B 706 (2011) 100–105. [arXiv:1109.3590](https://arxiv.org/abs/1109.3590), [doi:10.1016/j.physletb.2011.10.070](https://doi.org/10.1016/j.physletb.2011.10.070).
- [1197] J. Haidenbauer, U.-G. Meißner, Exotic bound states of two baryons in light of chiral effective field theory, Nucl. Phys. A 881 (2012) 44–61. [arXiv:1111.4069](https://arxiv.org/abs/1111.4069), [doi:10.1016/j.nuclphysa.2012.01.021](https://doi.org/10.1016/j.nuclphysa.2012.01.021).
- [1198] J. Haidenbauer, U.-G. Meißner, In-medium properties of a ΞN interaction derived from chiral effective field theory, Eur. Phys. J. A 55 (2) (2019) 23. [arXiv:1810.04883](https://arxiv.org/abs/1810.04883), [doi:10.1140/epja/i2019-12689-2](https://doi.org/10.1140/epja/i2019-12689-2).
- [1199] J. Haidenbauer, U.-G. Meißner, S. Petschauer, Do $\Xi\Xi$ bound states exist?, Eur. Phys. J. A 51 (2) (2015) 17. [arXiv:1412.2991](https://arxiv.org/abs/1412.2991), [doi:10.1140/epja/i2015-15017-0](https://doi.org/10.1140/epja/i2015-15017-0).
- [1200] M. Ablikim, et al., First Study of Reaction $\Xi(0^-)\rightarrow\Xi^- p$ Using $\Xi(0^-)$ -Nucleus Scattering at an Electron-Positron Collider, Phys. Rev. Lett. 130 (25) (2023) 251902. [arXiv:2304.13921](https://arxiv.org/abs/2304.13921), [doi:10.1103/PhysRevLett.130.251902](https://doi.org/10.1103/PhysRevLett.130.251902).
- [1201] J. K. Ahn, et al., Measurement of the $\Xi^- p$ scattering cross sections at low energy, Phys. Lett. B 633 (2006) 214–218. [arXiv:nucl-ex/0502010](https://arxiv.org/abs/nucl-ex/0502010), [doi:10.1016/j.physletb.2005.12.057](https://doi.org/10.1016/j.physletb.2005.12.057).
- [1202] S. Aoki, et al., Quasifree $p(K^-K^+)\Xi^-$ reaction in nuclear emulsion, Nucl. Phys. A 644 (1998) 365–385. [doi:10.1016/S0375-9474\(98\)00596-X](https://doi.org/10.1016/S0375-9474(98)00596-X).
- [1203] J. Haidenbauer, Coupled-channel effects in hadron–hadron correlation functions, Nucl. Phys. A 981 (2019) 1–16. [arXiv:1808.05049](https://arxiv.org/abs/1808.05049), [doi:10.1016/j.nuclphysa.2018.10.090](https://doi.org/10.1016/j.nuclphysa.2018.10.090).
- [1204] Y. Kamiya, K. Sasaki, T. Fukui, T. Hyodo, K. Morita, K. Ogata, A. Ohnishi, T. Hatsuda, Femtoscopic study of coupled-channels $N\Xi$ and $\Lambda\Lambda$ interactions, Phys. Rev. C 105 (1) (2022) 014915. [arXiv:2108.09644](https://arxiv.org/abs/2108.09644), [doi:10.1103/PhysRevC.105.014915](https://doi.org/10.1103/PhysRevC.105.014915).
- [1205] Z.-W. Liu, K.-W. Li, L.-S. Geng, Strangeness $S = -2$ baryon–baryon interactions and femtoscopic correlation functions in covariant chiral effective field theory*, Chin. Phys. C 47 (2) (2023) 024108. [arXiv:2201.04997](https://arxiv.org/abs/2201.04997), [doi:10.1088/1674-1137/ac988a](https://doi.org/10.1088/1674-1137/ac988a).
- [1206] M. M. Nagels, T. A. Rijken, Y. Yamamoto, Extended-soft-core baryon–baryon model ESC16. IV. $S = -3$ and $S = -4$ hyperon–hyperon interactions, Phys. Rev. C 108 (2) (2023) 024003. [doi:10.1103/PhysRevC.108.024003](https://doi.org/10.1103/PhysRevC.108.024003).
- [1207] J. Haidenbauer, U. G. Meißner, Predictions for the strangeness $S = -3$ and -4 baryon–baryon interactions in chiral effective field theory, Phys. Lett. B 684 (2010) 275–280. [arXiv:0907.1395](https://arxiv.org/abs/0907.1395), [doi:10.1016/j.physletb.2010.01.031](https://doi.org/10.1016/j.physletb.2010.01.031).
- [1208] Z.-W. Liu, J. Song, K.-W. Li, L.-S. Geng, Strangeness $S = -3$ and $S = -4$ baryon–baryon interactions in relativistic chiral effective field theory, Phys. Rev. C 103 (2) (2021) 025201. [arXiv:2011.05510](https://arxiv.org/abs/2011.05510), [doi:10.1103/PhysRevC.103.025201](https://doi.org/10.1103/PhysRevC.103.025201).
- [1209] S. Acharya, et al., First measurement of the $\Lambda\Xi$ interaction in proton–proton collisions at the LHC, Phys. Lett. B 844 (2023) 137223. [arXiv:2204.10258](https://arxiv.org/abs/2204.10258), [doi:10.1016/j.physletb.2022.137223](https://doi.org/10.1016/j.physletb.2022.137223).
- [1210] N. Ishii, et al., Baryon interactions from lattice QCD with physical masses — $S = -3$ sector: $\Xi\Sigma$ and $\Xi\Sigma-\Lambda\Sigma-$, EPJ Web Conf. 175 (2018) 05013. [doi:10.1051/epjconf/201817505013](https://doi.org/10.1051/epjconf/201817505013).
- [1211] T. Iritani, et al., $N\Omega$ dibaryon from lattice QCD near the physical point, Phys. Lett. B 792 (2019) 284–289. [arXiv:1810.03416](https://arxiv.org/abs/1810.03416), [doi:10.1016/j.physletb.2019.03.050](https://doi.org/10.1016/j.physletb.2019.03.050).
- [1212] J. Adam, et al., The Proton- Ω correlation function in Au+Au collisions at $\sqrt{s_{NN}}=200$ GeV, Phys. Lett. B 790 (2019) 490–497. [arXiv:1808.02511](https://arxiv.org/abs/1808.02511), [doi:10.1016/j.physletb.2019.01.055](https://doi.org/10.1016/j.physletb.2019.01.055).
- [1213] T. Miyamoto, et al., $\Lambda_c N$ interaction from lattice QCD and its application to Λ_c hypernuclei, Nucl. Phys. A 971 (2018) 113–129. [arXiv:1710.05545](https://arxiv.org/abs/1710.05545), [doi:10.1016/j.nuclphysa.2018.01.015](https://doi.org/10.1016/j.nuclphysa.2018.01.015).
- [1214] T. Miyamoto, Coupled-channel $\Lambda_c N - \Sigma_c N$ interaction from lattice QCD, PoS Hadron2017 (2018) 146. [doi:10.22323/1.310.0146](https://doi.org/10.22323/1.310.0146).
- [1215] J. Haidenbauer, G. Krein, Scattering of charmed baryons on nucleons, Eur. Phys. J. A 54 (11) (2018) 199. [arXiv:1711.06470](https://arxiv.org/abs/1711.06470), [doi:10.1140/epja/i2018-12638-7](https://doi.org/10.1140/epja/i2018-12638-7).
- [1216] J. Song, Y. Xiao, Z.-W. Liu, C.-X. Wang, K.-W. Li, L.-S. Geng, $\Lambda_c N$ interaction in leading-order covariant chiral effective field theory, Phys. Rev. C 102 (6) (2020) 065208. [arXiv:2010.06916](https://arxiv.org/abs/2010.06916), [doi:10.1103/PhysRevC.102.065208](https://doi.org/10.1103/PhysRevC.102.065208).
- [1217] J. Haidenbauer, G. Krein, Comment on " $\Lambda_c N$ interaction in leading order covariant chiral effective field theory" (1 2021). [arXiv:2101.07160](https://arxiv.org/abs/2101.07160).
- [1218] Y.-R. Liu, M. Oka, $\Lambda_c N$ bound states revisited, Phys. Rev. D 85 (2012) 014015. [arXiv:1103.4624](https://arxiv.org/abs/1103.4624), [doi:10.1103/PhysRevD.85.014015](https://doi.org/10.1103/PhysRevD.85.014015).
- [1219] I. Vidaña, A. Ramos, C. E. Jimenez-Tejero, Charmed nuclei within a microscopic many-body approach, Phys. Rev. C 99 (4) (2019) 045208. [arXiv:1901.09644](https://arxiv.org/abs/1901.09644), [doi:10.1103/PhysRevC.99.045208](https://doi.org/10.1103/PhysRevC.99.045208).
- [1220] K. W. Edwards, et al., Observation of excited baryon states decaying to Lambda(c)+ pi+ pi-, Phys. Rev. Lett. 74 (1995) 3331–3335. [doi:10.1103/PhysRevLett.74.3331](https://arxiv.org/abs/10.1103/PhysRevLett.74.3331).
- [1221] P. L. Frabetti, et al., Study of higher mass charm baryons decaying to Lambda(c)+, Phys. Lett. B 365 (1996) 461–469. [doi:10.1016/0370-2693\(95\)01458-6](https://arxiv.org/abs/10.1016/0370-2693(95)01458-6).
- [1222] H. Albrecht, et al., Evidence for Lambda(c)+ (2593) production, Phys. Lett. B 402 (1997) 207–212. [doi:10.1016/S0370-2693\(97\)00503-0](https://arxiv.org/abs/10.1016/S0370-2693(97)00503-0).
- [1223] T. Aaltonen, et al., Measurements of the properties of $\Lambda_c(2595)$, $\Lambda_c(2625)$, $\Sigma_c(2455)$, and $\Sigma_c(2520)$ baryons, Phys. Rev. D 84 (2011) 012003. [arXiv:1105.5995](https://arxiv.org/abs/1105.5995), [doi:10.1103/PhysRevD.84.012003](https://doi.org/10.1103/PhysRevD.84.012003).
- [1224] J.-X. Lu, Y. Zhou, H.-X. Chen, J.-J. Xie, L.-S. Geng, Dynamically generated $J^P = 1/2^- (3/2^-)$ singly charmed and bottom heavy baryons, Phys. Rev. D 92 (1) (2015) 014036. [arXiv:1409.3133](https://arxiv.org/abs/1409.3133), [doi:10.1103/PhysRevD.92.014036](https://doi.org/10.1103/PhysRevD.92.014036).
- [1225] W. H. Liang, T. Uchino, C. W. Xiao, E. Oset, Baryon states with open charm in the extended local hidden gauge approach, Eur. Phys. J. A 51 (2) (2015) 16. [arXiv:1402.5293](https://arxiv.org/abs/1402.5293), [doi:10.1140/epja/i2015-15016-1](https://doi.org/10.1140/epja/i2015-15016-1).
- [1226] J. Hofmann, M. F. M. Lutz, Coupled-channel study of crypto-exotic baryons with charm, Nucl. Phys. A 763 (2005) 90–139. [arXiv:hep-ph/0507071](https://arxiv.org/abs/hep-ph/0507071), [doi:10.1016/j.nuclphysa.2005.08.022](https://doi.org/10.1016/j.nuclphysa.2005.08.022).
- [1227] C. Garcia-Recio, V. K. Magas, T. Mizutani, J. Nieves, A. Ramos, L. L. Salcedo, L. Tolos, The s-wave charmed baryon resonances from

- a coupled-channel approach with heavy quark symmetry, Phys. Rev. D 79 (2009) 054004. [arXiv:0807.2969](https://arxiv.org/abs/0807.2969), doi:10.1103/PhysRevD.79.054004.
- [1228] M. F. M. Lutz, E. E. Kolomeitsev, On charm baryon resonances and chiral symmetry, Nucl. Phys. A 730 (2004) 110–120. [arXiv:hep-ph/0307233](https://arxiv.org/abs/hep-ph/0307233), doi:10.1016/j.nuclphysa.2003.10.012.
- [1229] T. Mizutani, A. Ramos, D mesons in nuclear matter: A DN coupled-channel equations approach, Phys. Rev. C 74 (2006) 065201. [arXiv:hep-ph/0607257](https://arxiv.org/abs/hep-ph/0607257), doi:10.1103/PhysRevC.74.065201.
- [1230] M. F. M. Lutz, C. L. Korpa, Open-charm systems in cold nuclear matter, Phys. Lett. B 633 (2006) 43–48. [arXiv:nucl-th/0510006](https://arxiv.org/abs/nucl-th/0510006), doi:10.1016/j.physletb.2005.11.046.
- [1231] C. E. Jimenez-Tejero, A. Ramos, L. Tolos, I. Vidaña, Open charm meson in nuclear matter at finite temperature beyond the zero range approximation, Phys. Rev. C 84 (2011) 015208. [arXiv:1102.4786](https://arxiv.org/abs/1102.4786), doi:10.1103/PhysRevC.84.015208.
- [1232] O. Romanets, L. Tolos, C. Garcia-Recio, J. Nieves, L. L. Salcedo, R. G. E. Timmermans, Charmed and strange baryon resonances with heavy-quark spin symmetry, Phys. Rev. D 85 (2012) 114032. [arXiv:1202.2239](https://arxiv.org/abs/1202.2239), doi:10.1103/PhysRevD.85.114032.
- [1233] Z.-Y. Wang, J.-J. Qi, X.-H. Guo, K.-W. Wei, Study of molecular ND bound states in the Bethe-Salpeter equation approach, Phys. Rev. D 97 (9) (2018) 094025. doi:10.1103/PhysRevD.97.094025.
- [1234] B. Wang, L. Meng, S.-L. Zhu, $D^{(*)}N$ interaction and the structure of $\Sigma_c(2800)$ and $\Lambda_c(2940)$ in chiral effective field theory, Phys. Rev. D 101 (9) (2020) 094035. [arXiv:2003.05688](https://arxiv.org/abs/2003.05688), doi:10.1103/PhysRevD.101.094035.
- [1235] M.-L. Du, E. Hernández, J. Nieves, Is the $\Lambda_c(2625)^+$ the heavy quark spin symmetry partner of the $\Lambda_c(2595)^+?$, Phys. Rev. D 106 (11) (2022) 114020. [arXiv:2207.02109](https://arxiv.org/abs/2207.02109), doi:10.1103/PhysRevD.106.114020.
- [1236] J. Zheng, Studies of charmed baryons decaying to $\lambda_c^+(n\pi)$, Ph.D. thesis, University of Florida (1999). URL <http://www.lns.cornell.edu/public/THESIS1999/1999/THESIS99-4/JiuZheng.ps>
- [1237] Z.-H. Guo, J. A. Oller, Resonance on top of thresholds: the $\Lambda_c(2595)^+$ as an extremely fine-tuned state, Phys. Rev. D 93 (5) (2016) 054014. [arXiv:1601.00862](https://arxiv.org/abs/1601.00862), doi:10.1103/PhysRevD.93.054014.
- [1238] J. Nieves, A. Feijoo, M. Albaladejo, M.-L. Du, Lowest-lying 12- and 32- ΔQ resonances: From the strange to the bottom sectors, Prog. Part. Nucl. Phys. 137 (2024) 104118. [arXiv:2402.12726](https://arxiv.org/abs/2402.12726), doi:10.1016/j.ppnp.2024.104118.
- [1239] R. Aaij, et al., Study of the $D^0 p$ amplitude in $\Lambda_b^0 \rightarrow D^0 p \pi^-$ decays, JHEP 05 (2017) 030. [arXiv:1701.07873](https://arxiv.org/abs/1701.07873), doi:10.1007/JHEP05(2017)030.
- [1240] S. Sakai, F.-K. Guo, B. Kubis, Extraction of ND scattering lengths from the $\Lambda_b \rightarrow \pi^- p D^0$ decay and properties of the $\Sigma_c(2800)^+$, Phys. Lett. B 808 (2020) 135623. [arXiv:2004.09824](https://arxiv.org/abs/2004.09824), doi:10.1016/j.physletb.2020.135623.
- [1241] R. F. Lebed, R. E. Mitchell, E. S. Swanson, Heavy-Quark QCD Exotica, Prog. Part. Nucl. Phys. 93 (2017) 143–194. [arXiv:1610.04528](https://arxiv.org/abs/1610.04528), doi:10.1016/j.ppnp.2016.11.003.
- [1242] A. Esposito, A. Pilloni, A. D. Polosa, Multiquark Resonances, Phys. Rept. 668 (2017) 1–97. [arXiv:1611.07920](https://arxiv.org/abs/1611.07920), doi:10.1016/j.physrep.2016.11.002.
- [1243] A. Ali, J. S. Lange, S. Stone, Exotics: Heavy Pentaquarks and Tetraquarks, Prog. Part. Nucl. Phys. 97 (2017) 123–198. [arXiv:1706.00610](https://arxiv.org/abs/1706.00610), doi:10.1016/j.ppnp.2017.08.003.
- [1244] C. S. Akondi, et al., Experimental study of the $\gamma p \rightarrow K^0 \Sigma^+$, $\gamma n \rightarrow K^0 \Lambda$, and $\gamma n \rightarrow K^0 \Sigma^0$ reactions at the Mainz Microtron, Eur. Phys. J. A 55 (11) (2019) 202. [arXiv:1811.05547](https://arxiv.org/abs/1811.05547), doi:10.1140/epja/i2019-12924-x.
- [1245] S. L. Olsen, T. Skwarnicki, D. Ziemska, Nonstandard heavy mesons and baryons: Experimental evidence, Rev. Mod. Phys. 90 (1) (2018) 015003. [arXiv:1708.04012](https://arxiv.org/abs/1708.04012), doi:10.1103/RevModPhys.90.015003.
- [1246] Y.-R. Liu, H.-X. Chen, W. Chen, X. Liu, S.-L. Zhu, Pentaquark and Tetraquark states, Prog. Part. Nucl. Phys. 107 (2019) 237–320. [arXiv:1903.11976](https://arxiv.org/abs/1903.11976), doi:10.1016/j.ppnp.2019.04.003.
- [1247] N. Brambilla, S. Eidelman, C. Hanhart, A. Nefediev, C.-P. Shen, C. E. Thomas, A. Vairo, C.-Z. Yuan, The XYZ states: experimental and theoretical status and perspectives, Phys. Rept. 873 (2020) 1–154. [arXiv:1907.07583](https://arxiv.org/abs/1907.07583), doi:10.1016/j.physrep.2020.05.001.
- [1248] X.-K. Dong, F.-K. Guo, B.-S. Zou, A survey of heavy-heavy hadronic molecules, Commun. Theor. Phys. 73 (12) (2021) 125201. [arXiv:2108.02673](https://arxiv.org/abs/2108.02673), doi:10.1088/1572-9494/ac27a2.
- [1249] L. Meng, B. Wang, G.-J. Wang, S.-L. Zhu, Chiral perturbation theory for heavy hadrons and chiral effective field theory for heavy hadronic molecules, Phys. Rept. 1019 (2023) 1–149. [arXiv:2204.08716](https://arxiv.org/abs/2204.08716), doi:10.1016/j.physrep.2023.04.003.
- [1250] S. K. Choi, et al., Observation of a narrow charmonium-like state in exclusive $B^\pm \rightarrow K^\pm \pi^\pm \pi^- J/\psi$ decays, Phys. Rev. Lett. 91 (2003) 262001. [arXiv:hep-ex/0309032](https://arxiv.org/abs/hep-ex/0309032), doi:10.1103/PhysRevLett.91.262001.
- [1251] I. Matuschek, V. Baru, F.-K. Guo, C. Hanhart, On the nature of near-threshold bound and virtual states, Eur. Phys. J. A 57 (3) (2021) 101. [arXiv:2007.05329](https://arxiv.org/abs/2007.05329), doi:10.1140/epja/s10050-021-00413-y.
- [1252] X.-K. Dong, F.-K. Guo, B.-S. Zou, Explaining the Many Threshold Structures in the Heavy-Quark Hadron Spectrum, Phys. Rev. Lett. 126 (15) (2021) 152001. [arXiv:2011.14517](https://arxiv.org/abs/2011.14517), doi:10.1103/PhysRevLett.126.152001.
- [1253] M. Neubert, Heavy quark symmetry, Phys. Rept. 245 (1994) 259–396. [arXiv:hep-ph/9306320](https://arxiv.org/abs/hep-ph/9306320), doi:10.1016/0370-1573(94)90091-4.
- [1254] R. Aaij, et al., Observation of $J/\psi p$ Resonances Consistent with Pentaquark States in $\Lambda_b^0 \rightarrow J/\psi K^- p$ Decays, Phys. Rev. Lett. 115 (2015) 072001. [arXiv:1507.03414](https://arxiv.org/abs/1507.03414), doi:10.1103/PhysRevLett.115.072001.
- [1255] R. Aaij, et al., Observation of a narrow pentaquark state, $P_c(4312)^+$, and of two-peak structure of the $P_c(4450)^+$, Phys. Rev. Lett. 122 (22) (2019) 222001. [arXiv:1904.03947](https://arxiv.org/abs/1904.03947), doi:10.1103/PhysRevLett.122.222001.
- [1256] R. Aaij, et al., Evidence for a new structure in the $J/\psi p$ and $J/\psi \bar{p}$ systems in $B_s^0 \rightarrow J/\psi p \bar{p}$ decays, Phys. Rev. Lett. 128 (6) (2022) 062001. [arXiv:2108.04720](https://arxiv.org/abs/2108.04720), doi:10.1103/PhysRevLett.128.062001.
- [1257] B. Wang, L. Meng, S.-L. Zhu, Hidden-charm and hidden-bottom molecular pentaquarks in chiral effective field theory, JHEP 11 (2019) 108. [arXiv:1909.13054](https://arxiv.org/abs/1909.13054), doi:10.1007/JHEP11(2019)108.
- [1258] T. J. Burns, E. S. Swanson, Molecular interpretation of the $P_c(4440)$ and $P_c(4457)$ states, Phys. Rev. D 100 (11) (2019) 114033. [arXiv:1908.03528](https://arxiv.org/abs/1908.03528), doi:10.1103/PhysRevD.100.114033.
- [1259] N. Yalikun, Y.-H. Lin, F.-K. Guo, Y. Kamiya, B.-S. Zou, Coupled-channel effects of the $\Sigma c^{(*)} D^{(*)} - \Lambda c(2595) D^-$ system and molecular nature of the P_c pentaquark states from one-boson exchange model, Phys. Rev. D 104 (9) (2021) 094039. [arXiv:2109.03504](https://arxiv.org/abs/2109.03504), doi:10.1103/PhysRevD.104.094039.
- [1260] J.-Z. Wu, J.-Y. Pang, J.-J. Wu, $P_c(4457)$ Interpreted as a $JP = 1/2^+$ State by $D^- 0 \Lambda c + (2595) - \pi^0 P_c(4312)$, Chin. Phys. Lett. 41 (9) (2024) 091201. [arXiv:2407.05743](https://arxiv.org/abs/2407.05743), doi:10.1088/0256-307X/41/9/091201.
- [1261] U.-G. Meißner, J. A. Oller, Testing the $\chi_{c1} p$ composite nature of the $P_c(4450)$, Phys. Lett. B 751 (2015) 59–62. [arXiv:1507.07478](https://arxiv.org/abs/1507.07478), doi:10.1016/j.physletb.2015.10.015.
- [1262] M.-L. Du, V. Baru, F.-K. Guo, C. Hanhart, U.-G. Meißner, J. A. Oller, Q. Wang, Interpretation of the LHCb P_c States as Hadronic Molecules and Hints of a Narrow $P_c(4380)$, Phys. Rev. Lett. 124 (7) (2020) 072001. [arXiv:1910.11846](https://arxiv.org/abs/1910.11846), doi:10.1103/PhysRevLett.124.072001.
- [1263] M.-L. Du, V. Baru, F.-K. Guo, C. Hanhart, U.-G. Meißner, J. A. Oller, Q. Wang, Revisiting the nature of the P_c pentaquarks, JHEP

08 (2021) 157. [arXiv:2102.07159](#), [doi:10.1007/JHEP08\(2021\)157](#).

- [1264] W. Detmold, C. J. D. Lin, S. Meinel, Calculation of the heavy-hadron axial couplings g_1 , g_2 and g_3 using lattice QCD, Phys. Rev. D 85 (2012) 114508. [arXiv:1203.3378](#), [doi:10.1103/PhysRevD.85.114508](#).
- [1265] Q. Wang, V. Baru, A. A. Filin, C. Hanhart, A. V. Nefediev, J. L. Wynen, Line shapes of the $Z_b(10610)$ and $Z_b(10650)$ in the elastic and inelastic channels revisited, Phys. Rev. D 98 (7) (2018) 074023. [arXiv:1805.07453](#), [doi:10.1103/PhysRevD.98.074023](#).
- [1266] V. Baru, E. Epelbaum, A. A. Filin, C. Hanhart, A. V. Nefediev, Q. Wang, Spin partners W_{bJ} from the line shapes of the $Z_b(10610)$ and $Z_b(10650)$, Phys. Rev. D 99 (9) (2019) 094013. [arXiv:1901.10319](#), [doi:10.1103/PhysRevD.99.094013](#).
- [1267] M.-Z. Liu, Y.-W. Pan, F.-Z. Peng, M. Sánchez Sánchez, L.-S. Geng, A. Hosaka, M. Pavon Valderrama, Emergence of a complete heavy-quark spin symmetry multiplet: seven molecular pentaquarks in light of the latest LHCb analysis, Phys. Rev. Lett. 122 (24) (2019) 242001. [arXiv:1903.11560](#), [doi:10.1103/PhysRevLett.122.242001](#).
- [1268] J.-J. Wu, R. Molina, E. Oset, B. S. Zou, Dynamically generated N^* and Λ^* resonances in the hidden charm sector around 4.3 GeV, Phys. Rev. C 84 (2011) 015202. [arXiv:1011.2399](#), [doi:10.1103/PhysRevC.84.015202](#).
- [1269] L. Meng, B. Wang, G.-J. Wang, S.-L. Zhu, The hidden charm pentaquark states and $\Sigma_c \bar{D}^{(*)}$ interaction in chiral perturbation theory, Phys. Rev. D 100 (1) (2019) 014031. [arXiv:1905.04113](#), [doi:10.1103/PhysRevD.100.014031](#).
- [1270] C. W. Xiao, J. Nieves, E. Oset, Heavy quark spin symmetric molecular states from $\bar{D}^{(*)}\Sigma_c^{(*)}$ and other coupled channels in the light of the recent LHCb pentaquarks, Phys. Rev. D 100 (1) (2019) 014021. [arXiv:1904.01296](#), [doi:10.1103/PhysRevD.100.014021](#).
- [1271] J.-J. Wu, T.-S. H. Lee, B.-S. Zou, Nucleon resonances with hidden charm in γp reactions, Phys. Rev. C 100 (3) (2019) 035206. [arXiv:1906.05375](#), [doi:10.1103/PhysRevC.100.035206](#).
- [1272] X. Zhang, Pentaquarks P_c in a dynamical coupled-channel approach of $\gamma p \rightarrow J/\psi p$ reaction (10 2024). [arXiv:2410.10154](#).
- [1273] J.-T. Zhu, S.-Y. Kong, Y. Liu, J. He, Hidden-bottom molecular states from $\Sigma_b^{(*)} B^{(*)} - \Lambda_b B^{(*)}$ interaction, Eur. Phys. J. C 80 (11) (2020) 1016. [arXiv:2007.07596](#), [doi:10.1140/epjc/s10052-020-8410-z](#).
- [1274] R. Aaij, et al., Evidence of a $J/\psi \Lambda$ structure and observation of excited Ξ^- states in the $\Xi_b^- \rightarrow J/\psi \Lambda K^-$ decay, Sci. Bull. 66 (2021) 1278–1287. [arXiv:2012.10380](#), [doi:10.1016/j.scib.2021.02.030](#).
- [1275] R. Aaij, et al., Observation of a $J/\psi \Lambda$ Resonance Consistent with a Strange Pentaquark Candidate in $B \rightarrow J/\psi \Lambda p^-$ Decays, Phys. Rev. Lett. 131 (3) (2023) 031901. [arXiv:2210.10346](#), [doi:10.1103/PhysRevLett.131.031901](#).
- [1276] I. Adachi, et al., Evidence of the $P_{ccs}(4459)^0$ in $\Upsilon(1S, 2S)$ inclusive decays at Belle (2 2025). [arXiv:2502.09951](#).
- [1277] B. Wang, L. Meng, S.-L. Zhu, Spectrum of the strange hidden charm molecular pentaquarks in chiral effective field theory, Phys. Rev. D 101 (3) (2020) 034018. [arXiv:1912.12592](#), [doi:10.1103/PhysRevD.101.034018](#).
- [1278] M.-L. Du, Z.-H. Guo, J. A. Oller, Insights into the nature of the $P_{cs}(4459)$, Phys. Rev. D 104 (11) (2021) 114034. [arXiv:2109.14237](#), [doi:10.1103/PhysRevD.104.114034](#).
- [1279] J.-T. Zhu, S.-Y. Kong, J. He, $P\psi\Lambda(4459)$ and $P\psi\Lambda(4338)$ as molecular states in $J/\psi \Lambda$ invariant mass spectra, Phys. Rev. D 107 (3) (2023) 034029. [arXiv:2211.06232](#), [doi:10.1103/PhysRevD.107.034029](#).
- [1280] K. M. Watson, The Effect of final state interactions on reaction cross-sections, Phys. Rev. 88 (1952) 1163–1171. [doi:10.1103/PhysRev.88.1163](#).
- [1281] A. B. Migdal, The theory of nuclear reactions with production of slow particles, Sov. Phys. JETP 1 (1955) 2.
- [1282] R. Chen, X. Liu, Mass behavior of hidden-charm open-strange pentaquarks inspired by the established P_c molecular states, Phys. Rev. D 105 (1) (2022) 014029. [arXiv:2201.07603](#), [doi:10.1103/PhysRevD.105.014029](#).
- [1283] S. Clymton, H.-C. Kim, T. Mart, Molecular nature of hidden-charm pentaquark states $P_{c\bar{c}s}$ with strangeness $S = -1$ (4 2025). [arXiv:2504.07693](#).
- [1284] A. Feijoo, W.-F. Wang, C.-W. Xiao, J.-J. Wu, E. Oset, J. Nieves, B.-S. Zou, A new look at the P_{cs} states from a molecular perspective, Phys. Lett. B 839 (2023) 137760. [arXiv:2212.12223](#), [doi:10.1016/j.physletb.2023.137760](#).
- [1285] R. Aaij, et al., Observation of an exotic narrow doubly charmed tetraquark, Nature Phys. 18 (7) (2022) 751–754. [arXiv:2109.01038](#), [doi:10.1038/s41567-022-01614-y](#).
- [1286] A. Bondar, et al., Observation of two charged bottomonium-like resonances in $\Upsilon(5S)$ decays, Phys. Rev. Lett. 108 (2012) 122001. [arXiv:1110.2251](#), [doi:10.1103/PhysRevLett.108.122001](#).
- [1287] V. Baru, E. Epelbaum, A. A. Filin, C. Hanhart, A. V. Nefediev, Spin partners of the $Z_b(10610)$ and $Z_b(10650)$ revisited, JHEP 06 (2017) 158. [arXiv:1704.07332](#), [doi:10.1007/JHEP06\(2017\)158](#).
- [1288] R. Aaij, et al., Observation of structure in the J/ψ -pair mass spectrum, Sci. Bull. 65 (23) (2020) 1983–1993. [arXiv:2006.16957](#), [doi:10.1016/j.scib.2020.08.032](#).
- [1289] X.-K. Dong, V. Baru, F.-K. Guo, C. Hanhart, A. Nefediev, Coupled-Channel Interpretation of the LHCb Double- J/ψ Spectrum and Hints of a New State Near the $J/\psi J/\psi$ Threshold, Phys. Rev. Lett. 126 (13) (2021) 132001, [Erratum: Phys. Rev. Lett. 127, 119901 (2021)]. [arXiv:2009.07795](#), [doi:10.1103/PhysRevLett.127.119901](#).
- [1290] Y.-L. Song, Y. Zhang, V. Baru, F.-K. Guo, C. Hanhart, A. Nefediev, Toward a precision determination of the $X(6200)$ parameters from data, Phys. Rev. D 111 (3) (2025) 034038. [arXiv:2411.12062](#), [doi:10.1103/PhysRevD.111.034038](#).
- [1291] G. Aad, et al., Observation of an Excess of Dicharmonium Events in the Four-Muon Final State with the ATLAS Detector, Phys. Rev. Lett. 131 (15) (2023) 151902. [arXiv:2304.08962](#), [doi:10.1103/PhysRevLett.131.151902](#).
- [1292] A. Hayrapetyan, et al., New Structures in the $J/\psi J/\psi$ Mass Spectrum in Proton-Proton Collisions at $s=13$ TeV, Phys. Rev. Lett. 132 (11) (2024) 111901. [arXiv:2306.07164](#), [doi:10.1103/PhysRevLett.132.111901](#).